



DEPARTMENT OF THE NAVY
NAVAL INTELLIGENCE SUPPORT CENTER
TRANSLATION DIVISION
4301 SUITLAND ROAD
WASHINGTON, D.C. 20390

(3) FC

AD A032120

CLASSIFICATION: UNCLASSIFIED

APPROVED FOR PUBLIC RELEASE, DISTRIBUTION UNLIMITED

TITLE:

(6) The Hydrodynamics of High-Speed Craft
(Gidrodinamika Bystrokhodnykh Sudov)

AUTHOR: I.T. / Yegorov, I.T., and Sokolov, V.T.

PAGES: 21 374

SOURCE: Trans. from Sudostroveniy Publishing House, Leningrad, 1971 p3-352 / 1971.
Pages 3-352

(10) Ivan Timofeyevich / Yegorov
Vitaliy Timofeyevich / Sokolov

(USSR)

DDC

NOV 17 1976

ORIGINAL LANGUAGE: Russian

TRANSLATOR: C

NISC TRANSLATION NO. 3834

APPROVED P.T.K.

DATE 12 August 1976

14 NISC-Trans-3834

11

12 379p.

407 682
bpg

Translation of

THE HYDRODYNAMICS OF HIGH-SPEED CRAFT

By Ivan Timofeyevich Yegorov and Vitaliy Timofeyevich Sokolov

Published in Leningrad by Sudostroyeniye, 1971, 424 pages, 2nd ed.

The book presents the results of theoretical research into the hydrodynamics of planing, hydrofoil, and air-cushion craft. Primary attention is devoted to methods of calculating the hydrodynamic characteristics of the lifting surfaces of these craft and also to methods of determining their seakeeping characteristics.

The book is intended for scientific workers, design engineers, and also graduate students specializing in the field of ship hydrodynamics.

ADDITION for	
NTIS	White Section <input checked="" type="checkbox"/>
DIC	Dist Section <input type="checkbox"/>
UNANNOUNCED	<input type="checkbox"/>
JUSTIFICATION	
BY	
DISTRIBUTION/AVAILABILITY	
Dist.	Avail. and/or
A	

TABLE OF CONTENTS

Foreword	1
Chapter I. Stationary hydrodynamic characteristics of a hydrofoil	4
§1. Forces acting on a hydrofoil and methods of determining them	4
§2. Hydrodynamic characteristics of hydrofoil profiles and their dependence on geometric parameters	8
§3. Formulation of the problem of foil movement beneath the free surface of a liquid. Analysis of boundary conditions	21
§4. Principal results from the theory of a foil moving beneath the surface of a heavy liquid	23
§5. Lift produced by a foil of finite span moving beneath the surface of a liquid at great relative velocity	28
§6. Hydrodynamic calculations for a hydrofoil of any arbitrary planform moving at a great relative velocity	38
§7. Hydrodynamical calculations of a V-shaped surface piercing foil	56
§8. Hydrodynamical calculations of a flat foil with vertical struts and a foil with inclined stabilizers	61
§9. Calculating the velocity corresponding to the limit of subcavitating flow around a hydrofoil	67
§10. Recommendations as to selection of profile and area of a hydrofoil	79
§11. The effect of sweepback on lift and velocity of subcavitating flow around a hydrofoil	85
§12. Some data on the hydrodynamic characteristics of supercavitating and ventilating profiles	96
References	101
Chapter II. Nonstationary hydrodynamic characteristics of hydrofoils	103
A. Some results from the theory of a nonstationarily moving thin foil	103
§13. Hydrodynamic patterns of movement of a liquid and hydrodynamic forces acting on a foil during unsteady movement	103
§14. Extending the methods and results of the theory of a thin foil to planing and impact	113
§15. Hydrodynamic forces during arbitrary unsteady movement of a foil in an unbounded liquid	117
B. Hydrodynamic forces acting on a hydrofoil during unsteady movement	139

§16.	Formulation of the problem and derivation of integral equation for determining the intensity of the vortex sheet of a foil moving close to the water's surface	139
§17.	Solution to an integral equation for a hydrofoil. Hydrodynamic forces in the general case of unsteady movement of a profile close to the free surface of the water	146
§18.	Experimental investigation of unsteady movement of a hydrofoil	153
§19.	Unsteady movement of a system of thin profiles	158
§20.	Method for calculating external forces acting on a hydrofoil in a regular seaway	166
§21.	Effect of nonstationarity of movement on lift and restoring moment when a craft rises on its foils	193
	References	199
	Chapter III. Nonstationary hydrodynamic forces in interaction between the lift surfaces of craft and the free surface of the water	200
A.	Hydrodynamic forces during impact	200
§22.	Hydrodynamic forces and movement during impact of bodies moving on the surface of the water	201
§23.	Some information about hydrodynamic forces which arise when bodies fall on the surface of a liquid	228
§24.	Nonstationary forces acting on lift foils of high-speed craft during impact against waves	235
	Planing in a seaway	242
§25.	Hydrodynamic forces during unsteady planing	242
§26.	Differential equations describing movement of a planing craft in a seaway	244
§27.	Main modes of movement of a planing craft in a seaway	247
	References	251
	Chapter IV. Hydrodynamic calculations for a hydrofoil craft	253
A.	Hydrodynamic calculations for foil systems	253
§28.	Foil arrangements along the length and width of a craft. Distribution of load between bow- and sternfoils	253
§29.	Waves excited by a hydrofoil of finite span. Effect of interaction in tandem systems	255
§30.	Practical calculations of hydrodynamic characteristics of foils of finite span in a tandem system	250
§31.	Comparative description of main patterns of foil arrangement	268
B.	Drag and attitude of hydrofoil craft	272
§32.	Modes of movement of hydrofoil craft. Components of craft drag	272

§33. Distinguishing aspects of the hydrodynamics of hydrofoil craft in the transitional mode	276
§34. Calculating the attitude of a hydrofoil craft	282
§35. Method of calculating the components of drag on a hydrofoil craft	290
§36. Methods of determining drag on a hydrofoil craft experimentally	293
C. Transverse stability of hydrofoil craft	294
§37. Hydrodynamic forces, attitude, and drift of a banked hydrofoil craft	295
§38. Determination of restoring moment and conditional metacentric height of a hydrofoil craft	300
§39. Problems in standardizing the stability of a hydrofoil craft. Results of calculations and experiments	304
D. Translational and rotational motion of hydrofoil craft in an irregular seaway	307
§40. Investigation into statistical characteristics of translational and rotational motion of hydrofoil craft	307
§41. Approximate method of making practical calculations of pitching and heaving of hydrofoil craft	319
References	326
Chapter V. Distinguishing features of the way-making ability of high-speed craft	328
§42. Action of a blade element on a cavitating propeller	
§43. Solution to the problem of cavitation flow around a flat profile array	333
§44. Verifying calculations of cavitating propellers	337
§45. Hydrodynamic characteristics of cavitating propellers working in a uniformly skewed flow	342
§46. Hydrodynamic characteristics of propellers piercing the free surface of the water	354
§47. Calculation of the way-making ability of planing and hydrofoil craft	359
References	373
Chapter VI. (Not included in translation.)	

A main distinguishing feature in the development of modern shipbuilding is the increase in ship speed due to the greater power of power plants and also the improved design of hull lines and lifting surfaces. In the last few years hydrofoil and air-cushion craft and others have been added to those with planing hulls.

As the speed of movement of displacement and planing craft increases the contribution made by hydrodynamic forces to their seakeeping characteristics also increases. At slow speeds buoyancy is due to hydrostatic forces but at higher speeds hydrodynamic forces become dominant. This causes redistribution of the pressures acting on a craft's hull and, consequently, a change in its attitude and also its behavior during rolling, heaving, pitching, turning about, and other modes of movement.

In hydrofoil and air-cushion craft hydrodynamic forces are dominant in all the main modes of movement. This requires a comprehensive study of hydrodynamic forces and their influence on craft behavior and also development of practical methods for calculating the forces which arise on the lifting surfaces of high-speed craft and the kind of movement caused by them.

The authors assumed the task of identifying the main problems in the hydrodynamics of high-speed craft, establishing a theoretical basis for studying them, and generalizing the data needed by ship designers and builders.

The area of ship fluid mechanics under discussion is relatively new. Naturally therefore the reader will not find in this book exhaustive answers to all questions which arise in practice. Some of the problems encountered in the hydrodynamics of high-speed craft are discussed in detail, others are only mentioned in passing, and yet others, for example steerability of hydrofoil and air-cushion craft, are not mentioned at all. Nevertheless, the data contained in the book can serve as a basis for developing further the methods used to calculate the seakeeping characteristics of high-speed craft. There is no discussion here of the hydrodynamics involved in steady-state planing since this subject is well covered in the literature.

The first chapter deals with the theoretical methods used to calculate stationary hydrodynamic characteristics of hydrofoils of different two- and three-dimensional shapes and also with the hydrodynamics of supercavitating and ventilating foils.

* The numbers in the right margin indicate pagination in the original text.

The second and third chapters deal with methods for calculating nonstationary hydrodynamic forces arising on hydrofoils and other lifting surfaces of high-speed craft during interaction with a free water surface and unsteady movement close to the surface. [4]

The fourth chapter deals with methods of calculating the hydrodynamic characteristics of foil systems and the attitude of hydrofoil craft and also with methods for determining the drag and stability of this type craft.

The fifth chapter deals with distinguishing aspects of calculating the way-making ability of planing and hydrofoil craft.

The sixth chapter deals with general principles governing the movement of air-cushion craft, approximate methods for calculating lift and drag, and also principles governing the functioning of flexible skirts and calculation of them. The end of the chapter is devoted to the aerodynamic characteristics of above-water foils.

The references employed by the authors follow each chapter.

During the five years which have passed since publication of the first edition a great deal of work has been done on the hydrodynamics of high-speed craft and this has led to the need for a second edition.

In accordance with the expressed desires of shipbuilding specialists the authors incorporated corrections aimed at improving the content of the book. They also added the following new sections:

1. Section D of Chapter IV "Translational and Rotational Motion of Hydrofoil Craft in an Irregular Seaway" consisting of §40-41.
2. §52 "Calculating the Flexible Skirts of Air-Cushion Craft."
3. §53 "Aerohydrodynamic Characteristics of Above-Water Foils."

The first chapter and §28-36 of the fourth were written by V. T. Sokolov and the second and third chapters and also §37-39 of the fourth by I. T. Yegorov. I. T. Yegorov exercised overall supervision over the book.

The fifth and sixth chapters were based on materials which Yu. M. Sadovnikov and S. D. Prokhorov were kind enough to provide. Materials provided by A. B. Lukashevich, M. A. Basin, and Ye. A. Kramarev were incorporated in §5-8, 11, and 12. V. A. Abramovskiy, V. V. Klichko, and V. P. Shadrin helped

prepare the new sections of the book (§40-41, 52, 53) for printing.

The authors wish to express their indebtedness to these comrades. The authors also express their thanks to Ye. V. Vecherov and N. A. Koryukhin for their help in preparing the manuscript.

CHAPTER I. Stationary hydrodynamic characteristics of a hydrofoil

15

In order to support movement of a craft at a given height above the water a foil system must contain some provision for "regulating" the lifting force. The lifting force can be regulated as foil depth changes by:

- 1) using foils whose lifting area varies with depth of immersion;
- 2) utilizing the drop in lifting force which occurs as a foil approaches the free surface of the water;
- 3) changing the angle of attack of a foil, thereby changing the lift coefficient.

The following foil types can be distinguished based on the above regulating principles:

- 1) V- or arc-shaped surface-piercing foils which have a smoothly changing lifting surface and also ladder foils whose lifting surface changes in steps;
- 2) depth-effect foils;
- 3) automatically controlled submerged foils whose angle of attack (or angle at which flaps are set) is regulated automatically by a control system incorporating a sensor for maintaining the required height of hull above the water.

In actual practice use is made of more complex foils which combine elements of the simplest types, including trapezoidal (from configuration of foil projection on athwartship plane), fully submerged dihedral, and variable dihedral. Based on their planform foils are distinguished as having a constant or variable chord along the span and also as having a straight or sweptback axis.

This chapter will cover stationary hydrodynamic characteristics of hydrofoils of the following types:

- a) flat hydrofoil with any planform (with a straight axis);
- b) fully submerged dihedral foil;
- c) V-shaped surface-piercing foil;
- d) sweptback foil;
- e) complex foil consisting of horizontal and inclined elements with their struts (Fig. 1).

§1. Forces acting on a hydrofoil and methods of determining them

A hydrofoil is a lifting surface which, when it moves through the water, creates a lift for supporting a hydrofoil craft. As the foil moves through the water a drag is also created. The lift and the drag of the foil both are projections of the principal vector of the total hydrodynamic force which is the resultant of all forces exerted over the entire surface

of the foil by the liquid. These forces consist of a hydrodynamic pressure p acting perpendicularly to the foil's surface and a tangential stress τ due to the force of friction.

These surface forces yield the principal vector of hydrodynamic forces

$$\bar{A} = \int_S (\bar{p} + \bar{\tau}) dS$$

and the principal moment

$$\bar{M}_A = \int_S [(\bar{p} + \bar{\tau}) \times \bar{r}] dS,$$

where \bar{r} is the radius vector of the center of area dS with respect to the selected point of application of the moment. [7]

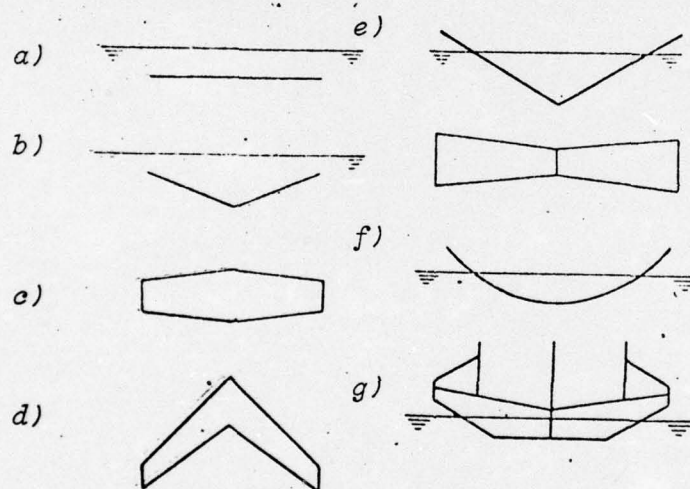


Fig. 1. Main types of hydrofoils: a--flat; b--submerged dihedral; c--straight; d--sweptback; e--V-shaped; f--arc-shaped; g--complex foil system.

Drag and lift are the projections of the principal vector in the direction of movement (x axis) and perpendicular to it (y axis) respectively

$$\left. \begin{aligned} R &= X = A \sin(A, x), \\ Y &= A \cos(A, y). \end{aligned} \right\} \quad (I.1)$$

The magnitudes of R and Y depend on the physical properties of the liquid* which include the mass density ρ , dynamic

* Surface tension which affects spray formation of very small dells is not included among these physical properties.

coefficient of viscosity μ , acceleration due to gravity g , and the saturated vapor pressure p_d and also on the speed of movement, the size and shape of the foil (chord b), orientation of the foil with respect to the direction of movement (angle of attack α), and location of the foil with respect to the surface of the water (depth of immersion h), that is:

$$\begin{aligned} R &= f_2(\text{shape}, b, \alpha, h, v, \rho, \mu, g, p_d), \\ Y &= f_1(\text{shape}, b, \alpha, h, v, \rho, \mu, g, p_d). \end{aligned} \quad (I.2)$$

According to the methods of similitude theory these relations can be expressed in dimensionless form.

The lift coefficient of a foil is

$$C_y = \frac{Y}{\frac{\rho v^2}{2} S} = f_1(\text{shape}, \lambda, \alpha, \bar{h}, Re, Fr, \chi). \quad (I.3a)$$

and the drag coefficient

$$C_x = \frac{R}{\frac{\rho v^2}{2} S} = f_2(\text{shape}, \lambda, \alpha, \bar{h}, Re, Fr, \chi). \quad (I.3b)$$

In these formulas $\lambda = l^2/S$ is the aspect ratio of the foil; $\bar{h} = h/b$ the relative depth of immersion; $Re = \frac{vb}{\mu} = \frac{vb}{\nu}$ the Reynolds number; $Fr = \frac{v}{\sqrt{gb}}$ the Froude number; and $\chi = \frac{p - p_d}{\frac{\rho v^2}{2}}$ the cavitation number.

It follows from (I.3a) and (I.3b) that geometrically similar foils (for example, those of a model and a prototype) when the angles of attack; relative depths of immersion; and criteria of similitude Fr , Re , and χ are the same will have the same C_y and C_x .

If the dependence of C_y and C_x on dimensionless criteria Fr , Re , and χ is known for a foil of any given shape, the lift and drag of a geometrically similar foil of any size traveling at any speed can be determined from the formulas: [8

$$\left. \begin{aligned} Y &= C_y \frac{\rho v^2}{2} S, \\ R &= C_x \frac{\rho v^2}{2} S. \end{aligned} \right\} \quad (I.4)$$

Determining the dependence of the lift and drag coefficients of a hydrofoil on its shape, angle of attack, relative depth of immersion, and criteria of similitude Fr , Re , and χ constitutes the fundamental problem in the hydrodynamics of a foil. Solving the problem completely presupposes a known law governing the distribution of forces over a foil's surface.

In the hydrodynamics of a hydrofoil the principle of separate determination of forces depending on their physical nature is applied, that is, the forces due to mass and depending on Fr and the forces due to viscosity and depending on Re are determined separately based on the assumption that there is no connection between the forces in the liquid attributable to mass and those attributable to viscosity. The total drag on a hydrofoil is found as the sum of the profile (R_{pr}), wave (R_w), and induced (R_i) drags and the coefficient of total drag as the sum of the coefficients of the corresponding drag components, that is,

$$\begin{aligned} R_f &= R_{pr} + R_w + R_i, \\ C_{xf} &= C_{xpr} + C_{xw} + C_{xi}. \end{aligned} \quad (I.5)$$

It is assumed in this process that the effect of viscosity on foil drag is taken completely into account in profile drag and that the induced and wave-making components do not depend on viscosity.

Foil lift is determined as an integral of the forces of hydrodynamic pressure (forces of friction are neglected).

Coefficients of hydrodynamic forces of a foil C_y , C_{xw} , and C_{xi} which are due to normal pressures are found from a theoretical solution to the problem of potential flow around a foil as it moves beneath the surface of an ideal (inviscid) heavy liquid. The effect of viscosity on C_y is taken into account by introducing an experimental correction in the angle of zero lift and the derivative of C_y with respect to α . The correction coefficients which are introduced are the same as for an unbounded liquid, that is, the correction for viscosity is determined without taking the free surface into account.

Drag coefficients C_{xw} and C_{xi} are determined entirely from calculations. The separation between these coefficients is made arbitrarily. It is impossible to make a direct experimental determination of them.

Wave drag is determined by solving a two-dimensional problem, that is, the wave drag coefficient $C_{xw\lambda}$ of a foil of finite span is set equal to the wave drag coefficient $C_{xw\infty}$ of a foil of infinite span. The effect of finiteness of span on foil drag is included entirely in induced drag.

The profile drag coefficient C_{xpr} is determined from calculations, the flow in the boundary layer being based on calculated and experimental pressure distribution curves and data on the point at which laminar flow becomes turbulent. An exact determination is then made later based on data from tests of full-scale series-produced foils. The effect of the free surface of the water and the Froude number on C_{xpr} is

taken into account by introducing into the calculations actual curves for pressure distribution over a profile which are drawn for movement of a foil beneath a free surface.

Hence, the stationary lift coefficient and drag component coefficients of a subcavitating hydrofoil are finally determined as functions of the following dimensionless parameters:

$$\begin{aligned} C_{yh} &= f_1(\text{shape}, \lambda, \alpha, \bar{h}, Fr), \\ C_{xpr} &= f_2(\text{shape}, \alpha, \bar{h}, Re), \\ C_{xw} &= f_3(C_{yh}, \bar{h}, Fr), \\ C_{xi} &= f_4(\text{shape}, C_{yh}, \bar{h}, \lambda, Fr). \end{aligned} \quad (I.6)$$

Included in functions f_3 and f_4 in place of α is the coefficient C_{yh} since C_{xw} and C_{xi} depend directly on the intensity of circulation around the foil which is proportional to C_{yh} .

§2. Hydrodynamic characteristics of hydrofoil profiles and their dependence on geometric parameters

The hydrodynamic characteristics of a foil depend on the shape of its transverse sections and the ratios between the geometric dimensions of their profiles. The specific conditions under which a hydrofoil is used, that is, the possibility that cavitation and stalled flow (ventilation) will occur under certain conditions has led to the use of special profiles different from airplane profiles which avoid these harmful phenomena or allow for them in the best way possible.

In subcavitating hydrofoils the profiles have their maximum thickness at chord midpoint or slightly forward of it and they exhibit a smooth pressure gradient curve on the low-pressure side. Such profiles include sharp-edged plano-convex segments and profiles with a rounded leading edge. Sharp-edged profiles with a slightly concave or convex lower side are also used.

The following geometric parameters have the greatest effect [10] on the hydrodynamic characteristics of a profile (Fig. 2):

$\bar{c} = c/b$	--relative thickness;
$\bar{x}_c = x_c/b$	--location of maximum thickness;
$\bar{f} = f/b$	--profile curvature, or the ratio between maximum depth of camber line and chord;
$\bar{x}_f = x_f/b$	--location of maximum curvature.

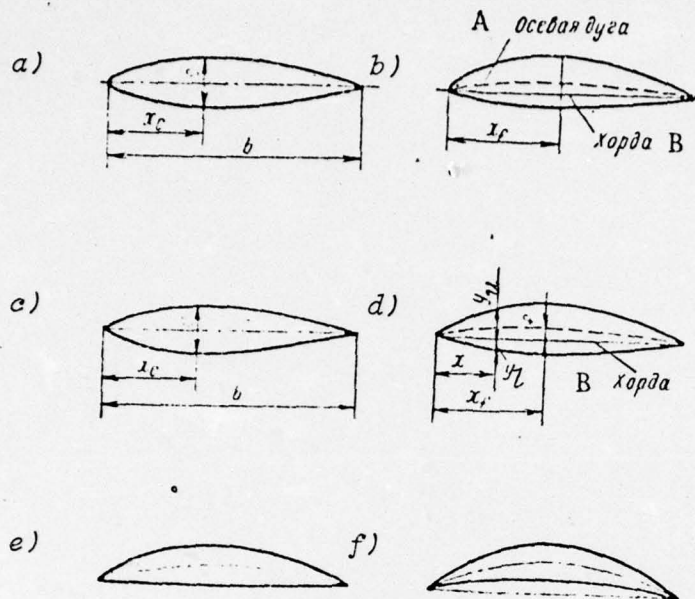


Fig. 2. Shape of profiles and their main geometric elements. Aviation profiles with rounded nose: a--symmetrical; b--convex on both sides. Sharp-edged profiles: c--symmetrical; d--convex on both sides; e--plano-convex; f--concave-convex (quarter moon).

KEY: A--camber line; B--chord.

A chord is the conventional base line of a profile from which profile coordinates and "geometric" angles of attack are measured. Usually it is a straight line segment joining the two extreme points of the profile. Sometimes a chord is defined differently. For example, the chord of a plano-convex sharp-edged profile and that of a profile with a rounded nose is a segment which coincides with the flat lower side of the profile and is delimited by a perpendicular tangent to the nose.

The main geometric parameters of the most common profiles [11] which are formed by the arcs of circles are related as follows (Fig. 3).

Half of the central angle of the upper and lower sides and the camber line is

$$\left. \begin{aligned} \varphi_1 &= 2 \operatorname{arctg} 2 \left(\bar{f} + \frac{\bar{c}}{2} \right) \approx 4 \bar{f}_1, \\ \varphi_2 &= 2 \operatorname{arctg} 2 \left(\bar{f} - \frac{\bar{c}}{2} \right) \approx 4 \bar{f}_2, \\ \varphi &= 2 \operatorname{arctg} 2 \bar{f} \approx 4 \bar{f}. \end{aligned} \right\} \quad (1.7)$$

The arc radii are

$$r_1 = \frac{b}{2 \sin \varphi_1}, \quad r_2 = \frac{b}{2 \sin \varphi_2}, \quad r = \frac{b}{2 \sin \varphi}. \quad (\text{I.8})$$

Angle of taper of the edges

$$\tau = \varphi_1 - \varphi_2 \approx 4\bar{c}. \quad (\text{I.9})$$

For a plano-convex segment

$$\varphi_1 = 2 \operatorname{arctg} 2\bar{c} \approx 4\bar{c}. \quad (\text{I.10})$$

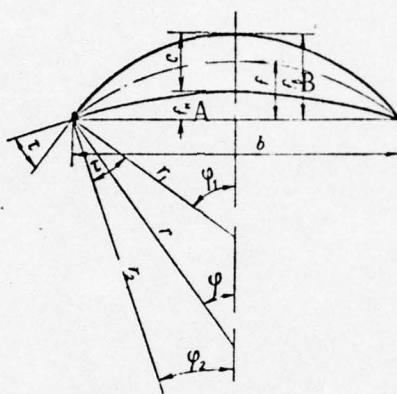


Fig. 3. Geometric elements of a profile formed by the arcs of circles.

EY: A-- f_l ; B-- f_u .

The hydrodynamic characteristics of hydrofoil profiles cannot be determined only theoretically, the results of experiments must also be used.

When determining the hydrodynamic characteristics of hydrofoils the initial characteristics used are those of profiles in an unbounded liquid.

The hydrodynamic characteristics of foil profiles are usually presented in the form of:

- curves of pressure distribution on the upper (low-pressure) and lower (high-pressure) sides;
- a graph showing the relation between the lift coefficient and the angle of attack $C_y(\alpha)$;
- a polar (first order), or a curve in C_y -- C_x coordinates;
- a graph of the moment coefficient $C_m = f(\alpha)$ or coefficient of the center of pressure $C_{press} = f(\alpha)$;
- a curve of the lift-drag ratio $k = C_y/C_x$ or a curve of the drag-lift ratio $\epsilon = C_x/C_y$.

The pressure distribution over a profile and also the lift and moment coefficients can be obtained by solving a two-dimen-

sional problem for the potential flow of an ideal liquid around a foil of infinite span. Such solutions have been found by the [12] method of conformal mapping for quarter-moon profiles formed by circle arcs. A special case of quarter moon is a plano-convex segment. Because of the uniformity among hydrofoil profiles the results found for a plano-convex circular segment can in most cases be extended to other plano-convex profiles. The following formulas have been obtained for the ordinate of maximum pressure gradient ξ_{max} and lift coefficient on the upper side of a profile C_{yu} based on the results of calculations made of potential flow with the introduction of a correction factor for viscosity:

$$\xi_{max} = 4.85\bar{c} + 0.42C_y, \quad (I.11)$$

$$C_{yu} = 2.25\bar{c} + (0.5 + \bar{c})C_y. \quad (I.12)$$

The formula for ξ_{max} holds for angles of attack corresponding to shock-free angles of entry when the maximum of the pressure gradient curve is in the area of maximum profile thickness.

Theory prescribes an almost linear relation between lift coefficient and angle of attack in the form of the expression

$$C_y = -\frac{2\pi}{1 - \frac{2c}{\pi}} (\alpha + \bar{f}). \quad (I.13)$$

Two magnitudes, the derivative $\partial C_y / \partial \alpha$ and the zero lift angle α_0 , determine the linear function $C_y(\alpha)$. Therefore the lift coefficient is usually presented in the form

$$C_y = \frac{\partial C_y}{\partial \alpha} (\alpha + \alpha_0). \quad (I.14)$$

For an ideal liquid

$$\alpha_{0id} = \left(\frac{\partial C_y}{\partial \alpha} \right)_{\lambda \rightarrow \infty} i d = \frac{2\pi}{1 - \frac{2c}{\pi}} \quad (I.15)$$

and

$$\alpha_{0id} = 2\bar{f} \text{ (radians),}$$

or

$$\alpha_{0id} = 114\bar{f} \text{ (degrees).} \quad (I.16)$$

Extensive experimental data reveals that the relation between C_y and the angle of attack is indeed close to linear but the numerical values of the zero lift angle α_0 and especially the derivative $\partial C_y / \partial \alpha$ differ markedly from those obtained theoretically for an ideal liquid. These values depend

on the Reynolds number, angle of taper at the trailing edge, and the condition of the foil surface, that is, on parameters determining the characteristics of the boundary layer which forms on the foil.

On the basis of experimental data Ye. A. Kramarev proposed [13] that α_0 be determined from the following empirical formula:

$$\alpha_0 \approx 110\bar{f} - 0.1\tau(6.3 - \lg Re), \quad (I.17)$$

where τ is the angle of taper at the trailing edge.

It follows from (I.17) that when $Re = 2.3 \cdot 10^6$

$$\alpha_0^* = 110\bar{f}. \quad (I.18)$$

The simpler formula (I.18) can be used for calculating α_0 for full-scale foils.

Since with an increasing Reynolds number the angle of zero lift decreases and the derivative $\partial C_y / \partial \alpha$ increases, the lift decreases at small angles of attack and increases at large angles of attack. This scale effect is not manifest at working angles of attack which for hydrofoils are about 1° .

Therefore $\partial C_y / \partial \alpha$ for a profile around which a viscous liquid flows can be assumed to be constant and, as follows from experimental data, is equal to

$$\alpha_\infty = 5.5 \text{ (}\alpha \text{ in radians)},$$

or

$$(I.19)$$

$$\alpha_\infty = 0.096 \text{ (}\alpha \text{ in degrees)}.$$

The derivative of C_y with respect to α is practically the same for all profiles, that is, it does not depend on profile shape or thickness. The individual distinguishing feature in the geometry of a profile--its curvature--is reflected in the hydrodynamic characteristics through the angle of zero lift. Formula (I.18) can be used for making an approximate determination of α_0 for hydrofoil profiles other than segmental.

The polar of a profile shows how the drag coefficient varies with the lift coefficient $C_x = f(C_y)$ and makes it possible to determine the lift-drag ratio $k = C_y / C_x$. A polar has two characteristic points: a point of minimum profile drag $C_{xpr \min}$ and a point of maximum lift-drag ratio (in Fig. 4 points P and K).

Point $C_{xpr \min}$ for plano-convex hydrofoil profiles corresponds to the zero geometric angle of attack. C_{xpr} increases as

the angle of attack either increases or decreases.

The maximum lift-drag ratio occurs at a certain positive angle of attack. On the polar this point lies at the point of tangency of a ray drawn from the origin of the coordinates.

Profile drag depends on the viscosity of a liquid (equal to zero in an inviscid liquid). It consists of friction drag and pressure drag, also called form drag. At small geometric angles of attack friction drag, constituting up to 90% of the total drag, predominates. At large angles of attack pressure drag increases by several times and total profile drag increases correspondingly. [14]

For bodies which are greatly elongated in the direction of flow friction drag usually differs very little from the drag of an equivalent flat plate. This is not true of hydrofoils. For even very thin hydrofoils friction drag differs markedly from that of a flat plate. The friction drag of foils ($\bar{c} = 0.05--0.1$) may exceed that of a plate by 10--20%. This difference is due to the fact that for foils which develop a lift the circulation component of induced velocity usually greatly exceeds the remaining components of the induced velocities of potential flow, the magnitude of which are of the same order as the velocity induced by elongated bodies not giving rise to a lifting force.

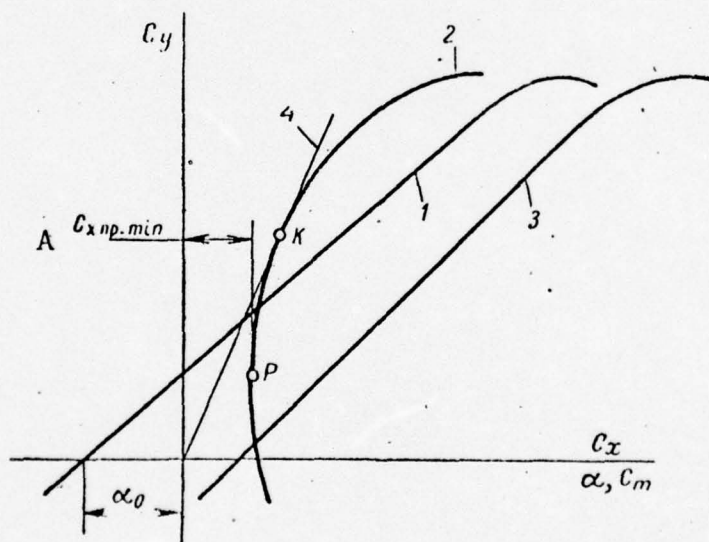


Fig. 4. Hydrodynamic characteristics of a profile.
1--curve of lift coefficient $C_y(\alpha)$; 2--polar of first order;
3--curve of moment coefficient $C_m(\alpha)$; 4--tangent to polar
drawn from origin of coordinates. Point K corresponds to the
maximum lift-drag ratio of the profile.

KEY: A-- $C_{xpr\ min}$.

Existing methods of calculating friction drag are suitable for calculating the drag on foils. However, in order to use them effectively experimental data on the location of the points where laminar flow becomes turbulent must be available.

When calculating foil friction drag the pressure gradient must be taken into account. However, taking the pressure gradient into strict account entails rather laborious calculations [15] and since these calculations are based on an approximate determination of the points of transition from laminar to turbulent flow, the results cannot be regarded as accurate. It is recommended that foil profile drag be calculated by Ye. A. Kramarev's simplified method which, however, necessitates taking into account foil-induced velocities.

In calculating friction drag from formulas for a flat plate we take as calculated velocity not that of the oncoming flow but one differing from it \bar{v}_{cal} . Based on the fact that the relation between friction drag and velocity is close to quadratic for bodies of any shape and the tangential stress at any point on the surface is approximately proportional to the square of the velocity at this point, the calculated velocity used is the easily determined approximately mean-square velocity of potential flow on the profile whose magnitude depends primarily on circulation flow. Thus, if R_f is the friction drag of a foil, ζ_{pl} the friction drag of an equivalent flat plate, and Ω its wetted surface, then

$$R_f = \zeta_{pl} \frac{\rho \bar{v}_{cal}^2}{2} \Omega,$$

$$C_{xf} = \frac{R_f}{\frac{\rho \bar{v}_0^2}{2} S} = 2 \zeta_{pl} \frac{\bar{v}_{cal}^2}{\bar{v}_0^2},$$

where

$$\bar{v}_{cal} = \frac{\bar{v}_{cal}}{\bar{v}_0}.$$

The factor 2 in the preceding formula occurs because the wetted surface of the foil is double the area of its projection S . The magnitude of ζ_{pl} for an aerodynamically smooth foil can be determined by one of several known methods.

When there is a turbulent boundary layer the friction coefficient ζ_{pl} of a hydrodynamically smooth plate can be determined by integrating the Prandtl-Schlikhting formula

$$\zeta_{pl} = 0.455 / (\lg Re)^{2.58}.$$

The friction drag coefficient of smooth plates as a function of the Reynolds number is shown in Fig. 5.

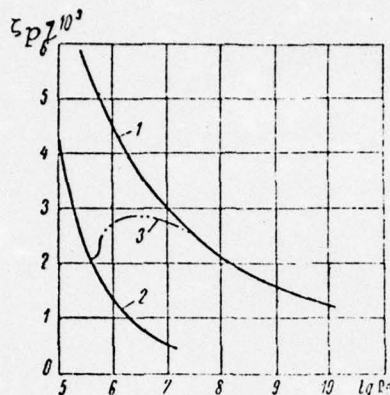


Fig. 5. Friction drag coefficient of smooth plates: 1--based on the Schlikhting formula for turbulent flow $\zeta_{pL} = 0.455 / (\lg Re)^{2.58}$; 2--laminar flow; 3--mixed boundary layer (experiment).

The formula proposed by L. G. Loytsyanskiy can be used in [16] the case of a mixed laminar-turbulent boundary layer for the purpose of calculating the friction drag on a plate:

$$\zeta_{pL} = 1.32 \sqrt{\frac{\bar{x}_l}{Re} + \frac{2}{Re} \left[0.00764 Re (1 - \bar{x}_l) + Re^{**7/6} |^{6/7} - Re_l^{**} \right]},$$

where $Re_l^{**} \approx \sqrt{0.44 x_l} Re$ and $\bar{x}_l = \frac{x_l}{b}$ is the relative length of the laminar sector.

In order to use this formula for making calculations the point of transition from laminar flow to turbulent must be known. If the surface of foils is insufficiently smooth, when $k_b Re/b < 70$, where k_b is the height of roughness elements, the foil cannot be considered to be hydrodynamically smooth; and in order to calculate the drag coefficient of an equivalent plate it is necessary to use formulas for determining the friction of rough surfaces.

The calculated velocity, which is taken to be the mean-square velocity, is

$$\bar{v}_{cal} = \sqrt{\frac{1}{2} \left(\int_0^1 \bar{v}_u^2(\bar{x}) d\bar{x} + \int_0^1 \bar{v}_l^2(\bar{x}) d\bar{x} \right)}$$

(v_u and v_l are the potential velocities on the upper and lower surfaces respectively of the profile) can be expressed in

terms of pressure coefficients on these surfaces

$$v_{cal} = \sqrt{1 - \frac{1}{2} \left(\int_0^1 \bar{p}_u(\bar{x}) d\bar{x} + \int_0^1 \bar{p}_l(\bar{x}) d\bar{x} \right)}.$$

An inspection of pressure distribution curves obtained for several profiles by calculating potential flow shows that at small positive angles of attack the expression

$$\frac{\int_0^1 \bar{p}_u(\bar{x}) d\bar{x}}{C_y} + \frac{\int_0^1 \bar{p}_l(\bar{x}) d\bar{x}}{C_y},$$

in which the modulus of the first term represents the share of the lifting force created by the upper side and the modulus of the second that of the lower side, depends little on the relative thickness and the angle of attack of profiles, that is, it is close to a certain constant magnitude which can be designated $2m_f$.

Thus,

$$\begin{aligned} \bar{v}_{cal} &= \sqrt{1 + m_f C_y}, \\ C_{xf} &= 2\zeta_p l (1 + m_f C_y). \end{aligned} \quad (I.20)$$

It has been found as a result of numerical integration of pressure distribution curves that for values of C_y between 0.2 and 0.6 coefficient m_f falls between 0.25 and 0.30, the smaller values of C_y corresponding to the smaller values of m_f . [17]

When using formula (I.20) it must be borne in mind that it is suitable only for small positive angles of attack in the range 0--2 degrees corresponding to shock-free entry. Furthermore, the formula holds only for large Reynolds numbers at which the laminar sector of the boundary layer on the foil is small. If the Reynolds number is less than 10^7 it is necessary to find the mean-square velocity and the drag coefficient of an equivalent plate corresponding to the low- and high-pressure sides of the foil separately, taking into account the locations of the transition points on each of the sides.

A formula similar to (I.20) for C_{xf} but more approximate can be used to determine the profile drag of foils:

$$C_{xpr} = 2\zeta_p l (1 + m_p C_u). \quad (I.21)$$

Coefficient m_p in the formula is determined based on coincidence between profile drag as calculated with this approximate formula and that calculated with the Squire-Young formula.

Coefficient m_p in the approximate formula for profile drag varies within the limits 0.5--0.75. Its smaller values correspond to $C_y = 0.15$ --0.20 and its larger to $C_y = 0.5$ --0.6. The formula presented holds for the same conditions as the approximate formula for friction drag.

Both approximate formulas were obtained for foils moving in an unbounded liquid. When applied to actual hydrofoils they can be used for a relative depth of immersion of $\bar{h} > 3$. Usually the relative depth of immersion is less and the free surface serves to reduce profile drag.

From the formula for friction drag of a foil in an unbounded liquid (I.20) we can obtain a similar expression for the friction drag of hydrofoils in the form

$$C_{xfh} = 2\zeta_p l (1 + m_{fh} C_{yh}), \quad (I.22)$$

but the magnitude of

$$m_{fh} = - \frac{\int_0^1 \bar{p}_u(\bar{x}) d\bar{x} + \int_0^1 \bar{p}_l(\bar{x}) d\bar{x}}{2C_{yh}} = \frac{(C_{yuh} - C_{ylh})}{2C_{yh}}$$

in it depends on the relative depth of immersion of the foils (see §5). When determining this magnitude we set $C_{ylh} = C_{yl}$, that is, the free surface does not affect the lifting force on the high-pressure side of the foil, and we also set [18]

$$\frac{C_{yh}}{C_y} \approx k_\psi \quad \text{and} \quad C_{yuh}/C_{yu} = \phi,$$

where k_ψ and ϕ are functions which take into account the effect of the free surface on the lifting force of the entire foil and of its upper surface (see §5, this chapter).

After making substitutions and the necessary transformations we obtain the following formulas:

$$m_{fh} = (m_l + 0.5) \frac{\eta}{k_\psi} - 0.5, \\ C_{xfh} = 2\zeta_p l \left\{ 1 + \left[(m_l + 0.5) \frac{\eta}{k_\psi} - 0.5 \right] C_{yh} \right\}. \quad (I.23)$$

It is important to note that when the relative depth of immersion of the foil is $\bar{h} = 0.2$ the friction drag no longer by 9% as in an unbounded liquid but by only 1.5% exceeds the drag of an equivalent flat plate and at smaller relative depths of immersion this difference diminishes even more markedly. Hence, nearness of a free surface causes a noticeable drop in the friction drag of foils.

The following formula, which is similar to the formula for C_{xfh} , can be used for determining the profile drag of a foil moving near a free surface:

$$C_{xhpr} = 2\zeta_p \left\{ 1 + \left[(m_p + 0.5) \frac{\eta}{k_q} - 0.5 \right] C_{yh} \right\}. \quad (I.24)$$

Coefficient m_p in this formula is the same as in the case of an unbounded liquid.

The approximate formulas presented above cannot be considered as relations between friction or profile drag and C_y or, implicitly, the angle of attack of one and the same foil. Since they hold only for the range of angles at which shock-free entry occurs, that is, for angles of attack of $0-2^\circ$ at which hydrofoils usually work, the included values of C_{yh} consequently allow for the geometric characteristics of profiles.

A profile polar for large angles of attack can be drawn using the method of E. E. Pappel' or by correcting an experimental polar for a foil model. In the latter case the entire polar should be shifted along the x axis so that at small angles it coincides with the point calculated from formula (I.24).

The curve of the moment coefficient makes it possible to determine the location of the center of pressure, that is, the point where the hydrodynamic force is considered to be applied along the length of a chord from the nose. The coefficient of the center of pressure $C_{press} = x_{cp}/b$ can be determined from the formula

$$C_{press} = \frac{M}{Nb} = \frac{C_m}{C_y \cos \alpha + C_x \sin \alpha} \approx \frac{C_m}{C_y}. \quad (I.25)$$

The coefficient of moment with respect to the nose of the profile is [19]

$$C_m = \frac{M}{\rho \frac{v^3}{2} Sb} = C_{m0} + \frac{\partial C_m}{\partial C_y} C_y$$

and with respect to any point T lying on the chord of the profile at a distance of x_T from the nose

$$C_{mT} = C_{m0} + \frac{\partial C_m}{\partial C_y} C_y + \frac{x_T}{b} C_y.$$

There is a point with respect to which the moment does not depend on C_y , that is, on the angle of attack. This point is called the focal point of the profile. The location of the focal point on a profile chord can be determined from the expression

whence

$$\frac{\partial C_m}{\partial C_y} C_y + \frac{x_F}{b} C_y = 0,$$

$$\bar{x}_F = \frac{x_F}{b} = -\frac{\partial C_m}{\partial C_y}.$$

With respect to the focal point $C_m = C_{m0} = \text{const}$, that is, the added hydrodynamic forces which depend on the angle of attack are applied at the focal point.

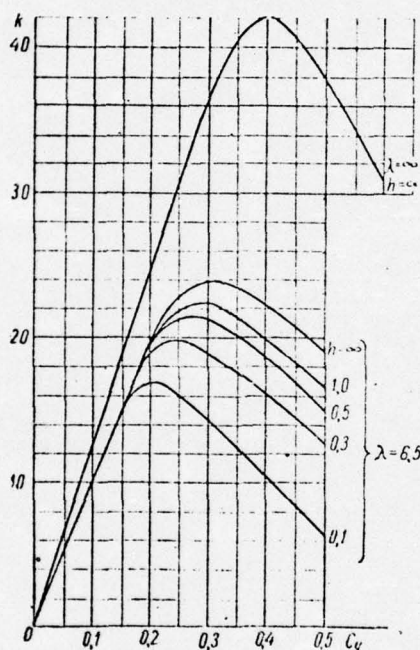


Fig. 6. Influence of free surface on lift-drag ratio of foil of finite span.

A curve of the lift-drag ratio $k = C_y/C_x$ drawn as a function of C_y or α conveniently and clearly describes the hydrodynamic picture of a profile or foil of finite span. Fig. 6 shows curves for the lift-drag ratio of a profile and foil of finite span in an unbounded liquid and beneath the surface of the water based on data obtained from tests of a model. As can be seen in the graph, the lift-drag ratio becomes very great, however, using hydrofoils at maximum ratios is in practice precluded because the relative profile thickness and working angle of attack must be selected based on the need for cavitation-free flow.

An idea of the actually achievable lift-drag ratios for

hydrofoils depending on relative thickness can be gained from the graph in Fig. 7 which is drawn from data obtained by calculating the lift-drag ratio of a flat isolated hydrofoil with a segmental profile. [21]

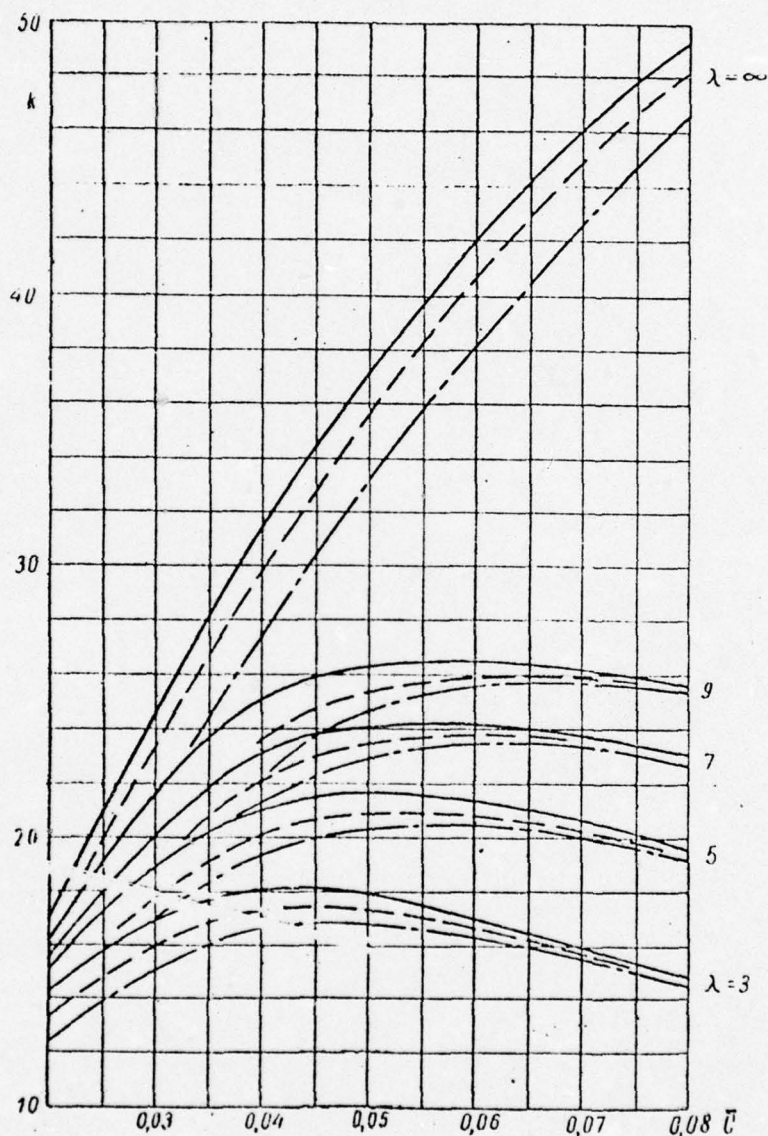


Fig. 7. Lift-drag ratio of a segmental hydrofoil as a function of relative thickness, depth of immersion, and aspect ratio. For the calculations $Re = 5 \cdot 10^7$, $Fr = 6.75$, and $C_y = 5\bar{c}$; — $\bar{h} = 0.5$; - - - $\bar{h} = 0.3$; - . - $\bar{h} = 0.15$.

The calculations were performed for Reynolds ($5 \cdot 10^7$) and

Broude (6.75) numbers characteristic of full-scale foils at relative depths of immersion of 0.15, 0.30, and 0.50. The values of lift coefficient required for determining the lift-drag ratio were found from the formula $C_y = 5\alpha$ which gives the most favorable magnitudes of C_y from the standpoint of preventing cavitation since in this way the angle of attack corresponds to the midpoint in the range of angles of cavitation-free flow around the foils under consideration. Profile, induced, and wave drag were taken into account in the calculations. As can be seen from the graph, the relative foil thickness which is optimal from the standpoint of lift-drag ratio depends on the aspect ratio and the relative depth of immersion.

§3. Formulation of the problem of foil movement beneath the free surface of a liquid. Analysis of boundary conditions

In the study of hydrofoil movement an actual viscous liquid is replaced with an ideal (inviscid) liquid. The foil is also replaced with a hydrodynamic model in the form of a system of singularities (vortices, sources, doublets) which create in the liquid outside a foil a flow equivalent to that created by the foil. The hydrodynamic model of a foil used in arriving at a theoretical solution is selected based on the purpose behind solving a particular problem.

A foil of finite span can best be modeled by a system of vortex sources distributed over the surface of the foil. For a foil moving at great velocity (theoretically when $Fr \rightarrow \infty$) when the effect of the liquid's mass on the lifting force can be neglected, a foil of finite span can be modeled by a Chaplygin-Prandtl vortex system which consists of an adjoining vortex (lift line) of variable intensity and a sheet of free vortices trailing from it. With a foil modeled in this way, according to the hypothesis of flat sections, the characteristics of the profile can be found from the solution to a two-dimensional problem.

In the two-dimensional problem of a foil of finite span in its most general formulation the movement is considered to be that of a solid profile beneath a free surface which is modeled by a system of vortices and sources distributed over its contour. Only by this approach to the problem is it possible to find the effect of a free surface on the flow around a solid profile and, specifically, the effect of thickness and curvature of a profile on the lifting force generated by a hydrofoil.

A vortex layer which is distributed along the camber line of a profile and is equivalent to an infinitesimally thin foil constitutes a simpler hydrodynamic model of a foil of infinite span. This kind of model makes it possible to determine the [22]

Effect of curvature, the angle of attack of a profile, and the finiteness of a chord but it is unsuitable for determining the characteristics of a solid profile of a hydrofoil. A flat plate is a special case of this model.

The simplest model of a foil of infinite span is a rectilinear infinite lifting vortex. The results obtained by solving the problem of vortex movement can be used to study the flow far to the rear of a foil, for example, when determining waves and wave drag.

In theoretical solutions the liquid used is ideal, incompressible, homogeneous, and subjected to the force of gravity. The foil moves uniformly and in a straight line parallel to the undisturbed surface of the liquid at depth h and velocity v . The axes of the coordinates are oriented on the foil. The x and z axes lie in the plane of the undisturbed liquid, the x axis being directed opposite to the direction of movement. The y axis is directed upward. Movement of the liquid outside the foil is irrotational (vortex-free). Due to the movement of the foil waves form on the surface of the liquid and move together with the foil at velocity v . It is assumed that the wave amplitude is small, making it possible to neglect the squares of the velocities induced on the surface of the liquid.

Mathematically the problem amounts to seeking the velocity potential $\phi(x, y, z)$ of absolute movement, knowing which a determination can be made of the induced velocity field, the ordinates of the wave surface, and the forces acting on a foil. The velocity potential must satisfy the Laplace equation (I.26) and the boundary conditions at the free surface (I.27), around the contour of the foil (I.28), and, in the case of a restricted channel, at fixed walls (I.29).

The Laplace equation expresses a condition of uninterrupted potential flow and for an incompressible liquid assumes the form

$$\Delta\phi = \frac{\partial^2\phi}{\partial x^2} + \frac{\partial^2\phi}{\partial y^2} + \frac{\partial^2\phi}{\partial z^2} = 0. \quad (I.26)$$

The boundary condition at the free surface amounts to constancy of pressure ($p = p_0 = \text{const}$). The waves are assumed to be small and therefore it can be considered that this condition is met at the level of an undisturbed surface. Neglecting the squares of the induced velocities makes it possible to linearize conditions at the free surface.

In view of these assumptions the boundary condition takes the form

or

$$v \frac{\partial \varphi}{\partial x} - gy = 0 \quad (I.27)$$

$$v^2 \frac{\partial^2 \varphi}{\partial x^2} + g \frac{\partial \varphi}{\partial y} = 0 \text{ when } y = 0.$$

It is easy to see that in the case of low velocities, when $v \rightarrow 0$ and $Fr \rightarrow 0$, $\partial \phi / \partial y = 0$, that is, the induced vertical velocities are equal to zero and the free surface remains flat. [23] This case is similar to movement of a foil near a solid wall.

In the case of high velocities when $Fr \rightarrow \infty$, then $\phi = \text{const}$ and $\partial \phi / \partial x \rightarrow 0$ when $y = 0$, that is, the velocity potential when $y = 0$ is constant and the horizontal induced velocity is equal to zero.

The boundary condition $\partial \phi / \partial x = 0$ for high velocities (theoretically when $Fr \rightarrow \infty$ and in practice when $Fr > 4-5$) has great applied importance since it becomes possible to reduce the problem of a hydrofoil to that of a biplane in an unbounded liquid.

The boundary condition at the surface of a foil expresses the condition of no flow, that is, the liquid has no velocity with respect to the foil in a direction normal to its surface:

$$\frac{\partial \varphi}{\partial n} = u_n = v \cos(n, x). \quad (I.28)$$

At fixed walls the condition of no flow assumes the form

$$\frac{\partial \varphi}{\partial n} = 0. \quad (I.29)$$

§4. Principal results from the theory of a foil moving beneath the surface of a heavy liquid

We will now present the solution to a two-dimensional problem in movement of a vortex beneath the surface of a liquid. This problem was solved by M. V. Keldysh and M. A. Lavrent'yev [1] and can be viewed as a special case of the general solution obtained later by N. Ye. Kochin [2].

In these solutions movement at velocity v of a vortex of intensity Γ at depth h beneath a free surface is considered. The coordinate axes are oriented on the vortex. The x axis lies in the plane of the undisturbed surface and is directed opposite to the movement of the vortex and the y axis is directed upward (Fig. 8). The figure depicts relative movement, that is, the vortex is fixed and the flow passes it at velocity v . In this system of coordinates movement of the liquid will be steady.

It is assumed that far to the front of the vortex the liquid is at rest and behind the vortex waves form.

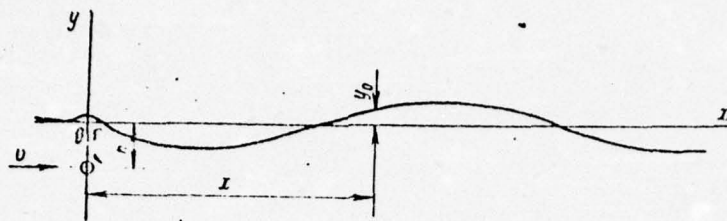


Fig. 8. Movement of a vortex beneath the surface of a heavy liquid.

The solution is found through functions of a complex variable and therefore we introduce the complex potential

$$W(z) = \varphi(x, y) + i\psi(x, y),$$

where $z = x + iy$ is a complex coordinate and $\psi(x, y)$ is a function of current.

The ordinates of the waves which form can be determined from the relation

$$y = -\frac{v}{g} \operatorname{Real} \left[\frac{dW}{dz} \right]_{y=0},$$

and the lifting force and the wave drag from the Chaplygin-Blasius formula

[24]

$$Y - iR_w = \int_C \left[\frac{dW}{dz} - v \right]^2 dx,$$

where C is a contour encompassing the vortex.

Below we present final formulas for calculating the surface ordinates, lift, and wave drag of a vortex. Sinusoidal waves which are described by the following formula form behind the vortex (when $x \rightarrow +\infty$):

$$y_0 = -\frac{2\Gamma}{v} e^{-\frac{gh}{v^2}} \sin \frac{gx}{v^2}. \quad (I.30)$$

$$\text{Vortex lift is: } Y = \rho v \Gamma - \rho l^2 \left[\frac{1}{4\pi h} - \frac{g}{\pi v^2} e^{-\frac{2gh}{v^2}} Ei_1 \left(\frac{2gh}{v^2} \right) \right]. \quad (I.31)$$

Wave drag is:

$$R_w = \rho g \left(\frac{\Gamma}{v} \right)^2 e^{-\frac{2gh}{v^2}}. \quad (I.32)$$

In (I.31) $Ei_1(2gh/v^2)$ is an integral exponential function. The first term expresses vortex lift in an unbounded liquid and the second term, which depends on the Froude number and on the depth of immersion, expresses completely the effect of the free surface on vortex lift. The sign of this additional lift ΔY_h depends only on the sign of the sum in the parentheses and does not depend on the sign of the circulation. As analysis

[3] shows, when the depth of immersion is small the additional lift is negative (directed downward) and as the vortex approaches the free surface it increases in absolute value without limit. As the depth of immersion increases this negative increment decreases in magnitude and then changes sign. Following the formation of a positive maximum it approaches zero asymptotically at very great depths.

The wave drag of the vortex $\Gamma = \text{const}$ has a maximum whose location is determined from the relation [25]

$$v = \sqrt{2gh}. \quad (I.33)$$

Figs. 9 and 10 show the change in added lift $\Delta Y_h / \alpha \rho \Gamma v$ due to the free surface and the wave drag coefficient C_{xw} . The vortex is replaced with a lifting foil with a chord of b and with the same circulation Γ as the vortex. The following dimensionless characteristics are introduced: the relative depth of immersion h/b (Fig. 9), inverse relative depth of immersion b/h (Fig. 10), Froude number $v/\sqrt{2gb}$, and angle of attack of the foil α .

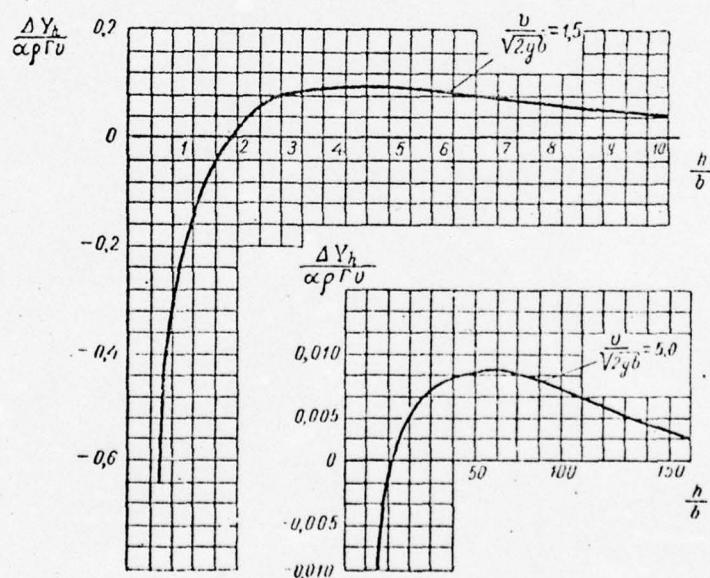


Fig. 9. Additional vortex lift due to free surface effect.

The problem of movement of an infinitesimally thin foil beneath a free surface was also solved by M. V. Keldysh and M. A. Lavrent'yev [1]. They replaced the foil with a vortex layer distributed over the camber line of an infinitesimally thin foil. Solving the problem amounts to determining the

vortex distribution density $\gamma(s)$ which is found from the boundary condition on the contour of the thin foil. The results of the preceding problem are used to write an expression for velocity potential. By assuming the curvature of the camber line to be slight and relating the effective curvilinear vortex distribution to a horizontal projection of the chord, the condition on the contour can be linearized and represented in the form of an integral equation whose solution yields an intensity of the vortex layer $\gamma(s)$. The integral equation is solved by expanding into a series to powers of the parameter [26]

$$\tau = \frac{b}{4h} = \frac{1}{4\bar{h}},$$

where $\bar{h} = h/b$ is the relative depth of immersion. The final formulas for lift and wave drag obtained by solving the problem (see formulas (19) and (20) in [3]) after reduction to dimensionless form are:

$$\begin{aligned} C_{yH} = C_{y\infty} & \left\{ 1 - \frac{\pi}{Fr^2} e^{-\frac{2\bar{h}}{Fr^2}} - \frac{1}{16\bar{h}^2} - \frac{1}{4Fr^2\bar{h}} + \right. \\ & + \frac{\pi}{Fr^4} e^{-\frac{4\bar{h}}{Fr^2}} + \frac{1}{Fr^4} e^{-\frac{2\bar{h}}{Fr^2}} Ei_1\left(\frac{2\bar{h}}{Fr^2}\right) \\ & - \alpha \left[\frac{1}{2\bar{h}} - \frac{2}{Fr^2} e^{-\frac{2\bar{h}}{Fr^2}} Ei_1\left(\frac{2\bar{h}}{Fr^2}\right) - \frac{\pi}{4Fr^2\bar{h}} \left(4 + \frac{2\bar{h}}{Fr^2}\right) e^{-\frac{2\bar{h}}{Fr^2}} + \right. \\ & \left. \left. + \frac{4\pi}{Fr^4} e^{-\frac{4\bar{h}}{Fr^2}} Ei_1\left(\frac{2\bar{h}}{Fr^2}\right) \right] \right\}, \end{aligned} \quad (I.34)$$

[27]

$$\begin{aligned} C_{xw} &= \frac{C_{y\infty}^2}{2Fr^2} e^{-\frac{2\bar{h}}{Fr^2}} \left\{ 1 - \frac{2\pi}{Fr^2} e^{-\frac{2\bar{h}}{Fr^2}} + \right. \\ & \left. + \alpha \left[\frac{1}{2Fr^2} - \frac{1}{2\bar{h}} + \frac{2}{Fr^2} e^{-\frac{2\bar{h}}{Fr^2}} Ei_1\left(\frac{2\bar{h}}{Fr^2}\right) \right] \right\}. \end{aligned} \quad (I.35)$$

After dropping the small terms in (I.35) we obtain a simplified formula for the wave drag of a foil:

$$C_{xw} \approx \frac{C_{y\infty}^2}{2Fr^2} e^{-\frac{2\bar{h}}{Fr^2}} \left(1 - \frac{2\pi}{Fr^2} e^{-\frac{2\bar{h}}{Fr^2}} \right). \quad (I.36)$$

The resulting formulas are approximate and cannot serve as a basis for developing a practical method for calculating the lift of a hydrofoil over the entire range of possible depths of immersion since they are based on great depths of immersion only. This is plainly evident in the attempt made by A. N. Vladimirov to use formula (I.34) to calculate lift and a simplified formula coinciding with the wave drag formula for an iso-

ated vortex to determine wave drag.

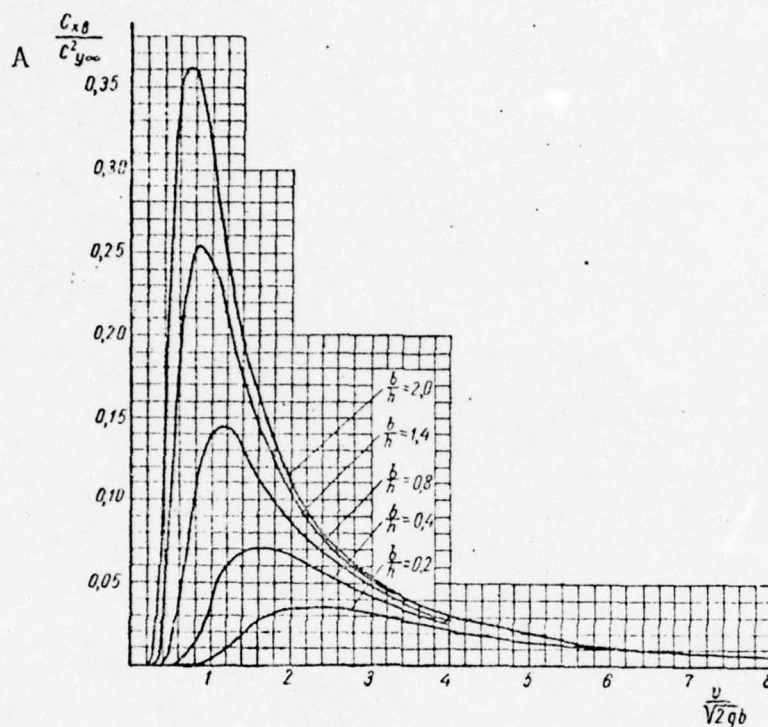


Fig. 10. Wave drag coefficient of a foil of infinite span as a function of the relative velocity.

KEY: A-- $C_{xw}/C_{y\infty}^2$.

A. N. Vladimirov [3] reduces the formulas for the lift coefficient (I.34) and wave drag coefficient (I.35) to the form

$$\left. \begin{aligned} C_{yh} &= \pi\alpha (M - N\alpha), \\ C_{xw} &= \pi^2\alpha^2 \frac{gb}{V^3} e^{-\frac{2gh}{v^2}}. \end{aligned} \right\} \quad (\text{I.37})$$

The magnitudes of M and N which appear in (I.37) were calculated by him and presented in the form of graphs. The value of C_{yh} found by means of formula (I.34) at relative depths of immersion less than 0.5--0.7 differ sharply from experimental data and, as a consequence, this formula is regarded as unsuitable for determining C_{yh} for depth-effect foils.

At first glance the obvious reason for the divergence between theory and experiment at small depths of immersion would seem to be linearization of the boundary conditions at the surface of the liquid, that is, the assumption that wave amplitude is small. This was pointed out by N. Ye. Kochin [2] in his article "Conference on Wave Drag": "...a foil is considered to be immersed sufficiently deeply so that the waves

forming on the surface can be considered small." However, this is in fact not quite accurate, in any case for the high velocities (when $Fr > 4-5$) at which A. N. Vladimirov compared theory with experiment. Linearization of a hydrofoil problem involving high Froude numbers is used effectively in developing methods presently used for practical calculations of which yield good agreement with experiment.

The main reason for unsuitability of the formulas obtained above for calculating depth-effect foils is the unfortunate choice of the parameter for expansion of the intensity of the vortex layer $\tau = b/4h = 1/4h$, since this parameter is small in magnitude only at great depths of foil immersion. [28]

However, it must be stressed that even an exact solution to the problem of movement of an infinitesimally thin foil beneath the surface of a liquid is inadequate for calculating the hydrodynamic characteristics of an actual foil since the effect of a free surface on the flow around a profile depends on its thickness and curvature.

A solution to the problem of movement of a foil of infinite span beneath the surface of the water with any arbitrary profile was found in completely general form (for any Froude number) by N. Ye. Kochin [2]. At the basis of his method is a special "N. Ye. Kochin function" $H(\lambda)$ which was introduced to express directly the drag of a foil as well as the lift. The N. Ye. Kochin function is a generalization of the concept of circulation and is defined in terms of the complex flow potential $W(z)$ caused by movement of a foil in a liquid when there is a free surface,

$$H(\lambda) = \int_{C_1} e^{-i\lambda} \frac{dW}{dz} dz,$$

where C_1 is an arbitrary contour encompassing the contour of the foil. For an unbounded liquid $H(0) = \Gamma$.

The formulas obtained by N. Ye. Kochin are complex and cannot in general form be solved in quadrature. Ye. N. Kochin solved in final form only a few special problems, including problems for a vortex and a thin foil. For a profile of arbitrary form forces are expressed in terms of the unknown function $H(\lambda)$. Nevertheless, N. Ye. Kochin's solution has great theoretical importance and, as investigations carried out by A. N. Panchenkov [4] show, can serve as a basis for obtaining practical results applicable to some actual profiles.

§5. Lift produced by a foil of infinite span moving beneath the surface of a liquid at great relative velocity

Since it is difficult to derive formulas for making practical calculations from a general theoretical solution for any arbitrary Froude number, in the hydrodynamics of hydrofoils extensive use is made of methods of making hydrodynamic calculations for high speeds of movement (the limiting case of an infinitely large Froude number).

It is apparent from formula (I.34) for lift that when $Fr \rightarrow \infty$ the terms containing Fr are equal to zero and, consequently, the lift of a hydrofoil does not depend on Fr . Numerous experiments in determining lift and drag and also in measuring the pressure over a foil profile close to a free surface show that a mode of self-similarity, when the lift and drag cease to depend on the Froude number, occurs for all practical purposes when $Fr > 4-5$. Inasmuch as under actual conditions a hydrofoil craft moves at $Fr > 4$, the solution to the problem of movement of a hydrofoil at great speeds is in complete keeping with practical purposes. [29]

In the following discussion we will consider the movement of a foil at great speed at which the boundary condition on the free surface requires that the horizontal induced velocities be equal to zero (see §3). Thus a hydrofoil is considered to be moving in an unbounded liquid. In order to satisfy the boundary conditions the effect of the free surface on the vertical induced velocities is replaced with the effect of a fictitious vortex system which is located above the actual system symmetrically with respect to the plane of the undisturbed surface of the water and whose vortices rotate in the same direction (Fig. 11). Hence, the problem of foil movement beneath the surface becomes one of determining the characteristics of the lower foil of a biplane with a distance between foils of $2h$ around which an unbounded liquid flows.

The device of replacing the effect of a free surface with the effect of the upper foil of a fictitious biplane makes it possible to develop sufficiently accurate and at the same time simple and practical methods for making calculations for a hydrofoil of finite span with an arbitrary planform, whether completely immersed in the water or piercing the free surface. When solving the problem of a hydrofoil as formulated here, use is made of the results and methods for solving problems of a biplane in an unbounded fluid and also the hypothesis of flat sections widely used in airfoil theory. Applying this hypothesis to a hydrofoil means assuming that any element of a hydrofoil of finite span experiences the same effect due to a free surface as an element of a foil of infinite span having the same section profile. It is assumed that their true angles of attack are the same and the relative depth of immersion of the foil of infinite span is equal to the relative depth of immersion of an element of the foil of finite span

under consideration.

Inasmuch as in the following discussion use is made of the hypothesis of flat sections the characteristics of a profile which are essential for making hydrodynamic calculations of a hydrofoil of finite span are determined from a solution to the two-dimensional problem of movement beneath a free surface of a foil of infinite span which for large Froude numbers is modeled by a biplane of infinite span in an unbounded liquid.

As experiments show, the effect of a free surface on the lift of a hydrofoil depends largely on the relative thickness and camber line curvature of a profile. Therefore, in determining the hydrodynamic characteristics of a hydrofoil profile, substituting a simplified hydrodynamic model is impermissible.

The problem of flow around a profile of arbitrary form is [30] very complex and the solution cannot serve as a basis for working out practical methods for making hydrodynamic calculations of a hydrofoil. The attempt made by T. Nishiyama [5] to obtain a simplified solution was not successful inasmuch as his calculations reflect impermissible discrepancies between theory and experiment. Therefore, when making practical calculations only total lift of a profile is taken from theoretical calculations and pressure distribution over the profile is based [31] on measurements of pressure made beneath the water's surface.

Good results agreeing with experiment can be obtained with A. B. Lukashevich's method for approximate theoretical determination of lift of a solid profile of a hydrofoil. The solution is reached for a high speed of movement on the assumption that the profile is thin, slightly curved, has a sharp leading edge, and the angles of attack are small. Therefore, its upper $y_1(x)$ and lower $y_2(x)$ sides can be considered to be given on a segment of the horizontal projection of the chord (Fig. 12). On this segment a vortex layer of intensity $\gamma(x)$ and a system of sources of intensity $q(x)$ are so located as to satisfy the boundary conditions on the surface of the profile. An unbounded liquid flows around this system which models a hydrofoil and the effect of the free surface on the flow around the profile is replaced with the effect of a fictitious system of singularities distributed over a horizontal segment equal to the chord and located above the main system at a height equal to twice the depth of immersion of the foil profile. The vortex layer has the same intensity and the same sign and the system of sources the same intensity and opposite sign (sinks) as the main system of singularities.

In order to determine the intensity of vortices and sources integral equations are written to express the equality between the vertical velocities induced jointly by the main and

fictitious singularity systems and the vertical projections of total velocities of flow around the upper and lower sides of the profile respectively.

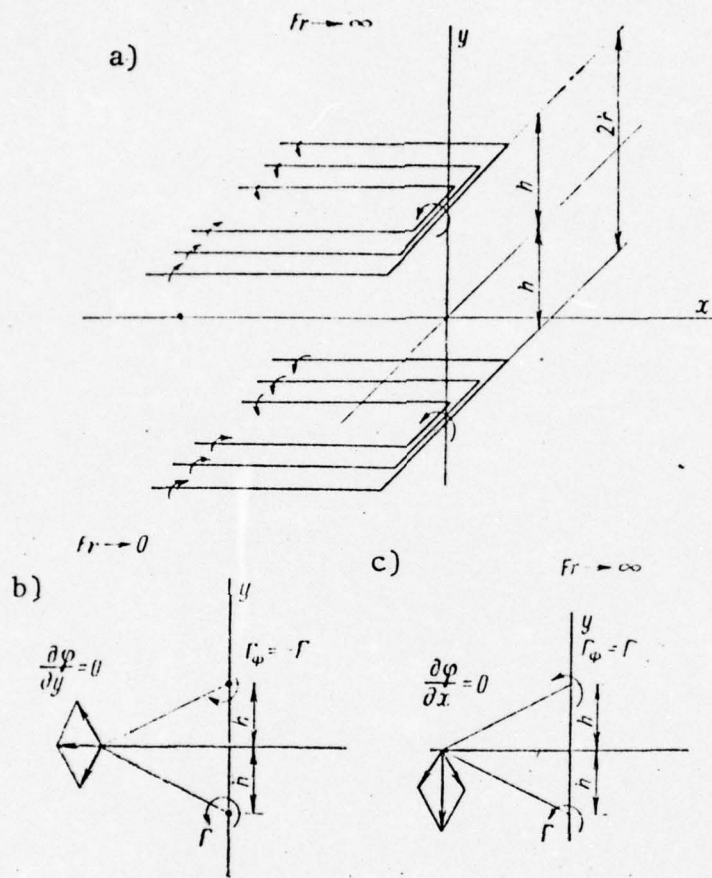


Fig. 11. Hydrodynamic model of a hydrofoil of finite span: a--the vortex system of a fictitious biplane in an unbounded fluid models a hydrofoil when $Fr \rightarrow \infty$; b--when $Fr \rightarrow 0$ vertical induced velocities are equal to zero (the "solid wall" effect) and the fictitious vortex has an opposite rotation; c--when $Fr \rightarrow \infty$ the horizontal induced velocities are equal to zero and the fictitious vortex rotates in the same direction as the main one.

The additional velocities which are induced by the fictitious vortex system of singularities and which express the effect of the free surface on the flow around the foil are represented as the sum of three components which depend on the angle of attack, relative thickness, and curvature of the camber line. These components are considered not to depend on one another and are taken into account in the final analysis by individual corrections. By using the methods of

[32]

conformal mapping, making the simplifying replacement of the fictitious system of singularities with discrete singularities, the following formula is obtained for the lift coefficient of a hydrofoil:

$$C_y = [K + 2L (\Delta\alpha_0 - \Delta\alpha_1)] (\alpha_1 - \Delta\alpha_0) + L (\alpha_1 - \Delta\alpha_0)^2, \quad (I.38)$$

where α_1 is the hydrodynamic angle of attack of a profile in an unbounded liquid measured from the axis of zero lift; $\Delta\alpha_1 = v_{c0}(\bar{h}) 8c / (1 + \bar{c}^2)$ the reduction in hydrodynamic angle of attack of a solid symmetrical profile beneath a free surface; and

$$\Delta\alpha_0 = \Delta\alpha_1 - \frac{K}{2L} \sqrt{\frac{K^2}{4L^2} - \frac{M}{L}}. \quad (I.39)$$

The coefficients K , L , and M are complex functions of the depth of immersion of a profile and its geometric parameters.

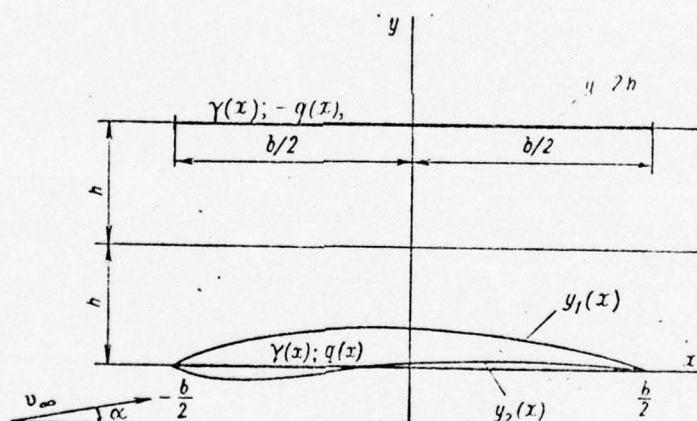


Fig. 12. Hydrodynamic model of a hydrofoil profile.

As formula (I.38) shows, the lift coefficient of a hydrofoil is not a linear function of the angle of attack, although the deviation from linearity is small.

Using (I.38) and (I.39) for practical determination of profile lift beneath a free surface is inconvenient since cumbersome calculations are needed to compute K , L , and M .

Ancillary graphs drawn from lift calculations for a large series of profiles of varying thickness and shape make it possible to determine easily and quickly the lift coefficient of a hydrofoil, using the following generally accepted formula:

$$C_{yh} = \gamma(\bar{h}) a_\infty (\alpha + \alpha_0 - \Delta\alpha_0), \quad (I.40)$$

where $\gamma(\bar{h}) = a_{h\infty}/a_\infty$ is a function describing the effect of the free surface of a liquid on the derivative $\partial C_y/\partial \alpha$ for a profile (a graph of $\gamma(\bar{h})$ is shown in Fig. 13); a_∞ and $a_{h\infty}$ are derivatives of the lift coefficient with respect to the angle of attack of a profile when $\alpha = \infty$ in an unbounded liquid and beneath a free surface; α is the geometric angle of attack; α_0 is the angle of zero lift of a profile around which an unbounded liquid flows; $\Delta\alpha_0$ is the change in angle of zero lift of a solid profile caused by the effect of a free surface,

$$\Delta\alpha_0 = \vartheta_{\alpha_0}(\bar{h}) \frac{8\bar{c}}{1+\bar{c}^2} - \vartheta_I(\bar{h}) \alpha_0. \quad (I.41)$$

The functions $\vartheta_{\alpha_0}(\bar{h})$ and $\vartheta_I(\bar{h})$ are shown graphically in Figs. 14 and 15. [33]

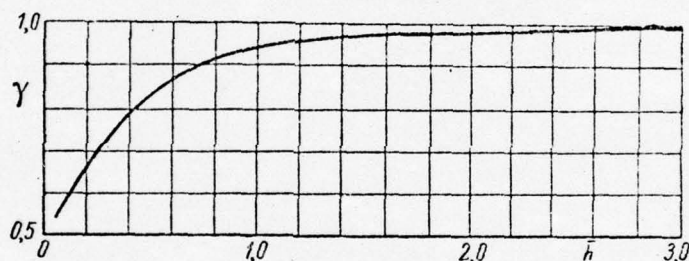


Fig. 13. Graph of the function $\gamma(\bar{h})$.

The simplified formula (I.40) expresses a linear relation between C_y and α and makes it possible to determine with sufficient accuracy the lift of a profile moving close to a free surface.

The results obtained show that as a consequence of the free surface effect a change occurs in both characteristics which determine the magnitude of profile lift--the derivative of the lift coefficient with respect to the angle of attack $\partial C_y/\partial \alpha$ and the angle of zero lift α_0 . As the results of calculations and experiment show, the magnitude of $\partial C_y/\partial \alpha$ of a profile depends almost not at all on its shape but is a function of only the relative depth of immersion. The effect on the lift of a hydrofoil of solidity of a profile and curvature of its camber line leads to a change only in the angle of zero lift of the profile (on $\Delta\alpha_0$). An examination of (I.41) shows that, all other conditions remaining equal, an increase in relative thickness of a profile leads to a decrease in the angle of zero lift and an increase in the curvature of the camber line leads to an increase in this angle as compared with its value in an unbounded flow. As calculations of the angle

of zero lift for segmental profiles show, because of the effect of thickness and curvature which varies in sign, $\Delta\alpha_0(\bar{h})$ changes not only in magnitude but also in sign (Fig. 16). At large relative depths of immersion $\Delta\alpha_0 < 0$, then, changing monotonically at $\bar{h} \approx 0.35$, the curve of $\Delta\alpha_0(\bar{h})$ cuts the \bar{h} axis, that is, $\Delta\alpha_0 = 0$. With further reduction in depth of immersion $\Delta\alpha_0$, remaining positive, increases abruptly in magnitude. As can be seen in Fig. 16, the absolute magnitude of negative values of $\Delta\alpha_0$ is very small and in practical calculations these negative values should be neglected.

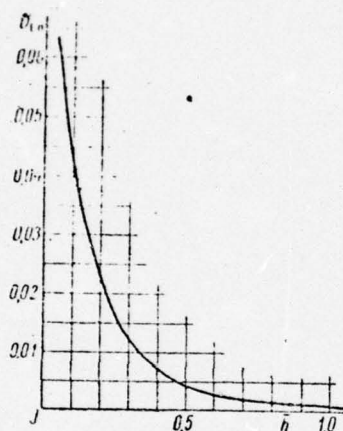


Fig. 14. Graph of function $v_{c0}(\bar{h})$.

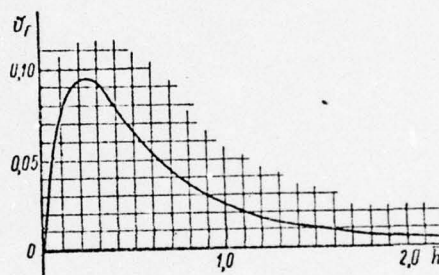


Fig. 15. Graph of function $v_f(\bar{h})$.

The function $\gamma(\bar{h})$ varies within the limits $0.5 \leq \gamma(\bar{h}) \leq 1$ as the depth of immersion of the foil varies within the limits $0 \leq \bar{h} \leq \infty$. When $\bar{h} = 3$ $\gamma(\bar{h})$ is for all practical purposes equal to about unity, that is, there is no free surface effect on lift. When \bar{h} diminishes to unity $\gamma(\bar{h})$ decreases by only 5% and with further decrease in \bar{h} $\gamma(\bar{h})$ diminishes sharply.

[35]

The decrease in lift of a hydrofoil of infinite span established theoretically can be explained by the change in physical picture of the flow around the profile of a foil moving beneath the surface of a liquid which can be traced by the nature of the change in pressure distribution over the profile.

Experimental investigation shows that the effect of a free surface on the flow around a profile moving at small angles of attack at a great relative speed ($Fr > 4$) is manifest for all practical purposes in a decrease in the pressure drop on the upper side only, the pressure on the lower side remaining almost unchanged. The decrease in pressure drop proves to be practically the same at all points on a profile regardless of its shape and angle of attack. It is a function

of the relative depth of immersion only, that is

$$\frac{\xi_h}{\xi_\infty} = \varphi(\bar{h}), \quad (I.42)$$

where ξ_h is the dimensionless pressure drop at a certain point on the upper side of the profile beneath a free surface; ξ_∞ the pressure drop at the same point in an unbounded liquid; $\varphi(\bar{h})$ varies from 1 to 0 as \bar{h} varies from ∞ to 0; and when $\frac{\phi}{h} = \text{const}$, $\varphi(\bar{h}) = \text{const}$.

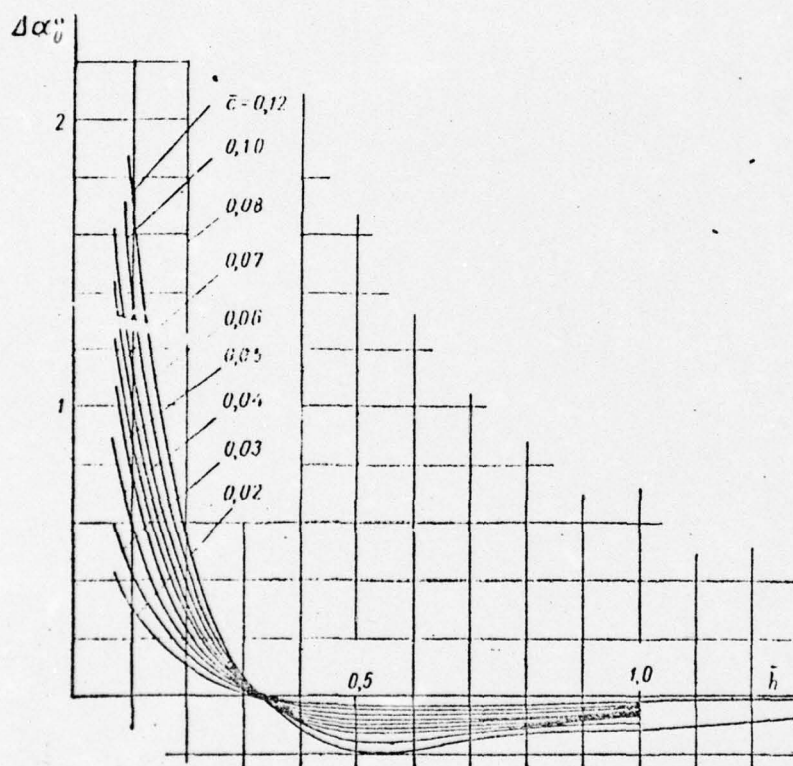


Fig. 16. Graph of angle of zero lift of plano-convex segmental profiles as a function of relative depth of immersion and relative thickness.

Fig. 17 shows an experimental curve for $\varphi(\bar{h})$ obtained by V. T. Sokolov which is well approximated by the formula

$$\varphi = 1 - e^{-2(\bar{h})^{0.6}}. \quad (I.43)$$

In actual fact the pressure also changes slightly on the lower side even at small angles of attack. Specifically, a free surface has an effect on the flow around the leading

edge of segmental profiles at angles of attack differing from angles of shock-free entry. Nevertheless, assuming absence of free-surface effect on the flow around the lower side of a profile to express independence of flow between the upper and lower sides of a profile which is an established principle in applied hydrodynamics reflects actual phenomena rather well. S. D. Chudinov, who worked out an approximate method for making the hydrodynamic calculations for a hydrofoil of finite span, [36] was the first to apply to a hydrofoil the principle of independence between the flows along the upper and lower sides of a profile (the Wagner analogy) [7].

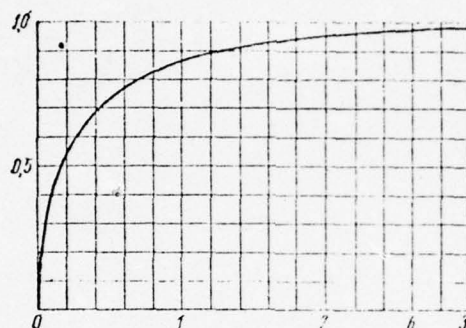


Fig. 17. Experimental curve of the function $\phi(\bar{h}) = \xi_h / \xi_\infty$.

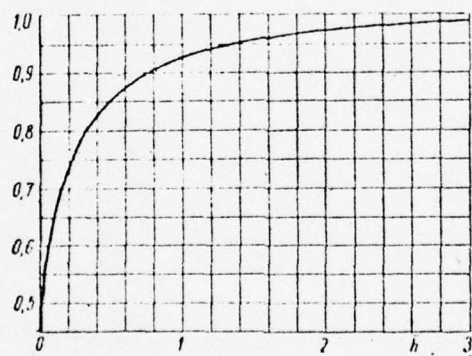


Fig. 18. Curve of the function $k_\phi = a_{h\infty} / a_\infty$.

S. D. Chudinov determined theoretically the pressure drop on the upper side of a profile by comparing the flow over the upper side of a profile with the flow over the upper side of an infinitesimally thin profile of the same curvature.

A practical method for calculating the lift coefficient of a hydrofoil profile based on assumed absence of the free-surface effect on the flow over the lower side of the profile and use of the experimental coefficient $\phi(\bar{h})$ for the pressure

drop on its upper side is described below.

In fact, in accordance with the stated assumption

$$\begin{aligned}\xi_h &= \phi \xi_\infty, \\ \bar{p}_{zh} &= \bar{p}_{z\infty}.\end{aligned}$$

Then

$$C_{yh} = C_{yl} + \phi C_{yu}, \quad (\text{I.44})$$

where the subscript "l" refers to the lower side of a profile and "u" to the upper.

Theoretical calculations for an unbounded liquid flowing around a plano-convex segmental profile leads to the following formula for the lift coefficient of the upper side of a profile:

$$C_{yu} = 1,25\bar{c} + (0,5 + \bar{c}) C_\psi, \quad (\text{I.45})$$

where \bar{c} is the relative thickness of the profile.

After substituting C_{yu} into (I.44) and making the required transformations, we arrive at an approximate formula similar to (I.40) for the lift coefficient of a profile of a hydrofoil ($\lambda = \infty$):

$$C_{yh} = k_\psi a_m (\alpha + \alpha_0 - \Delta\alpha_0), \quad (\text{I.46})$$

where

$$k_\psi = 1 - (0,5 + \bar{c}) e^{-2(\bar{h})^{0,6}}, \quad (\text{I.47})$$

$$\Delta\alpha_0 \approx 0,5 \left(\frac{1}{k_\psi} - 1 \right) \bar{c}; \quad (\text{I.48})$$

and k_ψ varies from 1 to 0.5 when $\infty \leq \bar{h} \leq 0$.

A graph of k_ψ is shown in Fig. 18.

A comparison of the lift of a hydrofoil profile calculated [37] according to this approximate method and the results of an experiment has showed satisfactory accuracy.

What distinguishes the last two methods from that of A. B. Lukashevich which was presented earlier is that they fail to take into account the effect of curvature of a profile on the angle of zero lift. Inasmuch as the absolute magnitude of the total correction $\Delta\alpha_0$ is small, the actual relative error in determining it does not result in any sig-

ificant error in the final result, especially since the corrections are greatest when $C_y = 0$, that is, at inoperative angles of attack of a foil. Therefore, practicable methods developed by failing to observe strictly independence between the flows over the upper and lower sides yield results which agree well with experiment.

§6. Hydrodynamic calculations for a hydrofoil of any arbitrary planform moving at a great relative velocity

The purpose of making hydrodynamic calculations for a foil of finite span is to determine the lift, induced drag, and the load distribution over the span of the foil.

We will investigate a foil of any arbitrary planform with an arbitrary dihedral β (but without sweepback) moving beneath the surface of an ideal liquid at a great relative velocity. The root section of the foil is at depth h_0 and forms angle of attack α with the direction of movement. The subject hydrofoil is replaced with main and fictitious vortex systems in an unbounded liquid, each of which consists of a V-shaped adjoining vortex of variable intensity $\Gamma(\xi)$ and a sheet of free vortices of intensity $d\Gamma/d\xi$ trailing to infinity so as to form a plano-dihedral surface situated horizontally. The configuration of the fictitious vortex system is a mirror image of the main system with respect to the undisturbed surface, and the direction of rotation of the vortices of the fictitious system coincides with that of the vortices in the main system.

The foil and the main vortex system modeling it are shown in Fig. 19.

Inasmuch as the aspect ratio of the foil is rather great, we will use the hypothesis of flat sections, that is, we will consider that the flow around each element of a hydrofoil of finite span is like that around an element of a foil of infinite span which has the same chord and depth of immersion at an angle of attack equal to the effective angle of attack of the given element as determined by taking into account the induced downwash of the flow caused by the free vortices. Then the lift coefficient of an element of a foil of finite span can be expressed in terms of the profile characteristics and the induced downwash in the following form: [38]

$$C_{yh} \sec = \gamma(\bar{h}) a_\infty (\alpha - \alpha_u), \quad (1.49)$$

where $\alpha = \alpha_u + \alpha_0 - \Delta\alpha_0$ is the hydrodynamic angle of attack of the hydrofoil profile.

We will note in passing that the above formula also holds for a foil as a whole when the downwash is constant along the

entire span.

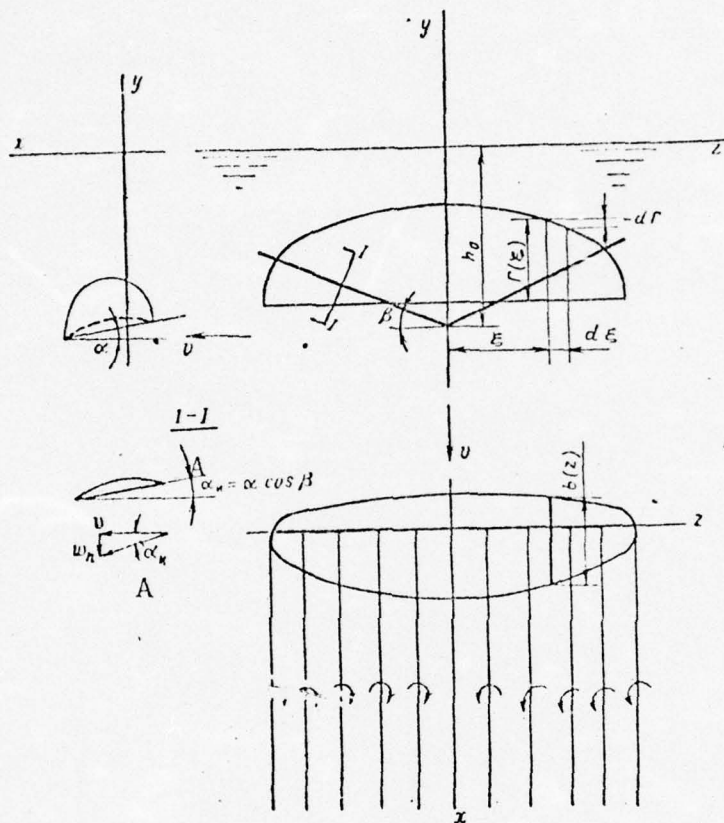


Fig. 19. Vortex system of a dihedral hydrofoil.
KEY: A-- α_i .

Applying N. Ye. Zhukovskiy's lift theorem to an element of the hydrofoil, we can write

$$dY = \rho v \Gamma(z) dz.$$

Then considering that

[39]

$$dY = \frac{1}{2} C_y \rho v^2 b(z) dz,$$

we obtain an equation relating the circulation to the hydrodynamic characteristics of the profile

$$\Gamma(z) = \frac{1}{2} C_y v b(z). \quad (I.50)$$

After substituting for C_y from (I.49) and transforming, we obtain the coupling equation in the form

$$\frac{2\Gamma(z)}{a_{\infty}V(h)vb(z)} = \alpha - \alpha_i. \quad (I.51)$$

All the variables in (I.51) pertain to the element being examined which is removed from the midpoint of the foil by a distance z (Fig. 20).

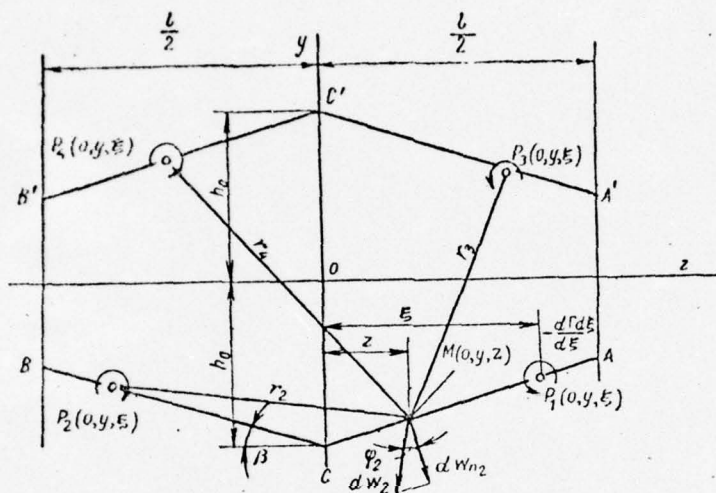


Fig. 20. Configuration of a system of lift vortices of a hydrodynamic model for an immersed dihedral hydrofoil moving at great relative velocity and a diagram for determining the induced velocities.

The hydrodynamic angle of attack of the foil element α and all its components and also the angle of induced downwash α_i entering into this formula are measured in a plane perpendicular to the halfspan of the foil. The "normal" geometric angle of attack α_n is related to the angle of attack of the foil's root section by

$$\alpha_n = \alpha \cos \beta. \quad (I.52)$$

The induced downwash can be expressed in terms of the induced velocities by the formula

$$\alpha_i = \lg \frac{w_n}{v} \approx \frac{w_n}{v}, \quad (I.53)$$

where w_n is the induced velocity on the line of an adjoining vortex normal to a halfspan of the foil (Fig. 20).

We will determine the induced velocity at an arbitrary point $M(0, y, z)$ of the lift vortex vortex of the lower foil. Inasmuch as the adjoining vortices do not create any downwash on the line of the lift vortex, it is caused entirely by the

effect of the free vortices.

An elementary semi-infinite vortex of intensity $d\Gamma/d\xi$ $d\xi$ originating at point $P_i(0, y, \xi)$ and lying at a distance r_i from point M induces at the given point a velocity which can be determined from the known hydrodynamical formula

$$dw_i = \frac{\frac{d\Gamma}{d\xi} d\xi}{4\pi r_i}.$$

The sought normal component of this velocity (in Fig. 20 the elementary induced velocity dw_2 and its normal projection

dw_{n2} are shown) is $dw_n = \sum_{i=1}^4 dw_i \cos \phi_i$, where ϕ_i is the angle between dw_i and the normal to the lift vortex. The cosine of this angle is determined geometrically. The total velocity w_n at point M induced by all free vortices is found by integrating along the span of the lift vortices. Integration is performed separately for each of the four straight sectors of the lift line of the main and fictitious vortex systems. [40]

The final expression for induced velocity in dimensionless form is

$$\frac{w_n(z)}{v} = \frac{\cos \beta}{2\pi} \int_{-1}^1 G'(\xi) L(\bar{z}, \xi) d\xi + \frac{\cos \beta}{2\pi} \int_{-1}^1 \frac{G'(\xi) d\xi}{\bar{z} - \xi}, \quad (\text{I.54})$$

where

$$L(\bar{z}, \xi) = \begin{cases} \frac{(\bar{z} + \xi) \operatorname{tg}^2 \beta - \frac{(\bar{z} + \xi)^2}{(\bar{z} - \xi)} \operatorname{tg}^2 \beta}{(\bar{z} - \xi)^2 + (\bar{z} + \xi)^2 \operatorname{tg}^2 \beta} + \\ + \frac{(\bar{z} - \xi) (1 + \operatorname{tg}^2 \beta) - 4 \frac{\bar{h}_0}{\lambda} \operatorname{tg} \beta}{\left[4 \frac{\bar{h}_0}{\lambda} - (\bar{z} - \xi) \operatorname{tg} \beta \right]^2 + (\bar{z} - \xi)^2} \quad \text{при } \bar{\xi} \leq 0, \\ \frac{(\bar{z} + \xi) \operatorname{tg}^2 \beta + (\bar{z} - \xi) - 4 \frac{\bar{h}_0}{\lambda} \operatorname{tg} \beta}{\left[4 \frac{\bar{h}_0}{\lambda} - (\bar{z} + \xi) \operatorname{tg} \beta \right]^2 + (\bar{z} - \xi)^2} \quad \text{при } \bar{\xi} \geq 0. \end{cases}$$

The dimensionless variables in formulas (I.54) and (I.55) stand for:

$$\bar{z} = \frac{2z}{l}, \quad \bar{\xi} = \frac{2\xi}{l}, \quad \lambda(\bar{z}) = \frac{l}{b(\bar{z})}, \quad \bar{h}_0 = \frac{h_0}{b_m} = \frac{h_0 \lambda}{l}, \quad (\text{I.56})$$

$$\lambda = \frac{l}{b_m}, \quad G(\bar{\xi}) = \frac{\Gamma(\bar{\xi})}{v l}, \quad G'(\bar{\xi}) = \frac{dG(\bar{\xi})}{d\bar{\xi}}.$$

After expressing the downwash in terms of the induced velocity found and substituting it into (I.51) we obtain the main integro-differential equation for a hydrofoil of finite span

$$\frac{2\lambda(\bar{z})}{a_{\infty}\gamma(\bar{h}_z)} G(\bar{z}) - \alpha \cos \beta = -\frac{\cos \beta}{2\pi} \int_{-1}^1 G'(\bar{\xi}) L(\bar{z}, \bar{\xi}) d\bar{\xi} - \frac{\cos \beta}{2\pi} \int_{-1}^1 \frac{G'(\bar{\xi}) d\bar{\xi}}{\bar{z} - \bar{\xi}}. \quad (\text{I.57})$$

If we set $\beta = 0$ in equation (I.57) it becomes the integro-differential equation for a flat hydrofoil. The function $L(\bar{z}, \bar{\xi})$ is simplified and assumes the form

$$L(\bar{z}, \bar{\xi}) = \frac{\bar{z} - \bar{\xi}}{16 \left(\frac{\bar{h}}{\lambda f} \right)^2 + (\bar{z} - \bar{\xi})^2}. \quad (\text{I.58})$$

In that case when $\bar{h} \rightarrow \infty$ function $L(\bar{z}, \bar{\xi}) \rightarrow 0$ and $\gamma(\bar{h}) \rightarrow 1$ and then equation (I.57) will become the integro-differential equation for a flat foil in an unbounded liquid. Thus, function $L(\bar{z}, \bar{\xi})$ describes the free surface effect on the circulation of a foil which is additional for a foil in an unbounded liquid. This function is determined by the configuration of the foil and the ratio $\bar{h}_0/\bar{l} = \bar{h}_0/\lambda$.

The solution to the integro-differential equation yields the distribution of circulation over the span of the foil, which when known makes it a simple matter to find the lift of the foil.

The integro-differential equation can be solved by the Multhopp approximate method [8]. A new independent variable θ is introduced which is related to $\bar{\xi}$ by $\bar{\xi} = \cos \theta$. The variable θ varies in an interval from 0 to π . This interval is broken down into $m + 1$ equal parts, m being odd. For a foil without a stepped change in geometric parameters it suffices to break the interval π down into eight parts, that is, to set $m = 7$ (Fig. 21).

One value of $\bar{z}_n = \cos \theta_n$ corresponds to each value of $\theta_n = \pi/(m + 1)$. [42]

The dimensionless circulation at any point on the span of a foil can be expressed by m values of $G(\bar{z}_n)$ at selected points by means of the interpolation polynomial

$$G(\bar{z}) = \sum_{n=1}^m G(\bar{z}_n) \frac{(-1)^{n+1} \sin(m+1)\theta \sin \theta_n}{(m+1)(\cos \theta - \cos \theta_n)}. \quad (\text{I.59})$$

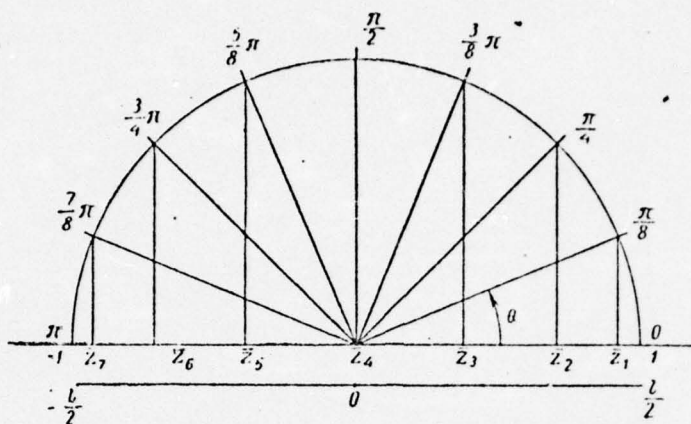


Fig. 21. Geometric interpretation of the relation between the variables z and θ .

Using an expansion into a series

$$\frac{\sin(m+1)\theta}{\cos\theta - \cos\theta_n} = \sum_{\mu=1}^m \frac{2(-1)^{\mu+1} \sin\mu\theta_n \sin\mu\theta}{\sin\theta_n}, \quad (\text{I.60})$$

the dimensionless circulation can be represented in the form of the trigonometric polynomial

$$G(\theta) = \frac{2}{m+1} \sum_{n=1}^m G(\theta_n) \sum_{\mu=1}^m \sin\mu\theta_n \sin\mu\theta. \quad (\text{I.61})$$

The relation expressed in (I.61) is basic for the calculations which follow. After substituting $z = z_n$ in (I.59) or $\theta = \theta_n$ in (I.61), these expressions yield values for circulation G at points z_n or θ_n .

In the following discussion we will indicate the sought values of circulation in the main equation (I.57) when $z = z_v$ by the subscript v . We will indicate foil parameters and depth of immersion in the same way, namely,

$$G_v = G(\bar{z}_v), \quad \alpha_v = \alpha(\bar{z}_v), \\ \lambda_v = \lambda(\bar{z}_v), \quad \gamma_v = \gamma(\bar{z}_v, \bar{h}_v).$$

By differentiating (I.61) we find $G'(\theta)$ which we substitute behind the integration sign in equation (I.57). The first integral can be determined in final form and the second [43] approximately using the rule of trapezoids.

By substituting the transformed integral equations into equation (I.57) we obtain a final expression for the integro-differential equation of a hydrofoil for symmetrical distribution of circulation in the form of the following linear system of algebraic equations:

$$\left(\frac{2\lambda_v}{\gamma_v a_\infty \cos \beta} - \bar{b}_{vv} \right) G_v = \alpha_v + \sum_{n=1}^{\frac{m+1}{2}} \bar{b}_{vn} G_n, \quad (I.62)$$

where \sum' is an incomplete sum, lacking terms with the same values of v and n .

The coefficients included in (I.62) can be determined from the following formulas:

$$\left. \begin{aligned} \bar{b}_{vv} &= B_{vv} + g_{vv}, \\ \bar{b}_{vn} &= B_{vn} - g_{vn}, \end{aligned} \right\} \quad (I.63)$$

$$\left. \begin{aligned} g_{vn} &= -\frac{1}{2(m+1)} \sum_{\mu=0}^{\frac{m-1}{2}} L_{v\mu} f_{n\mu}, \\ L_{v\mu} &= L_{v\mu} - L_{v, m+1-\mu}. \end{aligned} \right\} \quad (I.64)$$

For a dihedral foil

$$\begin{aligned} L(\bar{z}_v, \bar{\xi}_\mu) &= \\ = L_{v,\mu} &= \begin{cases} \frac{(\bar{z}_v + \bar{\xi}_\mu) \operatorname{tg}^2 \beta - \frac{(\bar{z}_v + \bar{\xi}_\mu)^2}{(\bar{z}_v - \bar{\xi}_\mu)} \operatorname{tg}^2 \beta}{(\bar{z}_v - \bar{\xi}_\mu)^2 + (\bar{z}_v + \bar{\xi}_\mu)^2 \operatorname{tg}^2 \beta} + \\ + \frac{(\bar{z}_v - \bar{\xi}_\mu) (1 + \operatorname{tg}^2 \beta) - 4 \frac{\bar{h}_0}{\lambda} \operatorname{tg} \beta}{\left[4 \frac{\bar{h}_0}{\lambda} - (\bar{z}_v - \bar{\xi}_\mu) \operatorname{tg} \beta \right]^2 + (\bar{z}_v - \bar{\xi}_\mu)^2} \xi \leq 0, \\ \frac{(\bar{z}_v + \bar{\xi}_\mu) \operatorname{tg}^2 \beta + (\bar{z}_v - \bar{\xi}_\mu) - 4 \frac{\bar{h}_0}{\lambda} \operatorname{tg} \beta}{\left[4 \frac{\bar{h}_0}{\lambda} - (\bar{z}_v + \bar{\xi}_\mu) \operatorname{tg} \beta \right]^2 + (\bar{z}_v - \bar{\xi}_\mu)^2} \xi \geq 0. \end{cases} \end{aligned} \quad (I.65)$$

For a flat foil

$$L(\bar{z}_v, \bar{\xi}_\mu) = L_{v\mu} = \frac{\bar{z}_v - \bar{\xi}_\mu}{16 \left(\frac{\bar{h}_0}{\lambda} \right)^2 + (\bar{z}_v - \bar{\xi}_\mu)^2}. \quad (I.66)$$

Coefficients B_{vn} and $f_{n\mu}^*$ for each fixed number m can be calculated ahead of time since they do not depend on foil parameters. These coefficients are presented in Tables 1, 2, and 3 for $m = 7$. The function $L_{v\mu}$ allows for the effect [45] on downwash of the upper (fictitious) biplane foil depending on its dihedral and the ratio between the depth of immersion of the root section and the span of the foil $\bar{h}_0/l = \bar{h}_0/\lambda$.

TABLE 1

Numerical Values of
Coefficients $B_{\nu n}$

n	$\nu = 1$	$\nu = 2$	$\nu = 3$	$\nu = 4$
1	5.2262	1.0360	0	0.1120
2	1.9142	2.8284	0.912	0
3	0	1.1945	2.1648	1.5774
4	0.1464	0	0.6536	2.0000

TABLE 2

Numerical Values of
Coefficients $f_{\mu n}^*$

μ	$n = 1$	$n = 2$	$n = 3$	$n = 4$
0	2.6131	-1.4142	1.0824	0.5
1	-1.4142	3.6955	-2.4112	1.0824
2	-1.5307	-1.0000	3.6955	-1.4142
3	0.4142	-1.5307	-1.4142	2.6131

TABLE 3

Numerical Values of the Difference $\bar{z}_\nu - \bar{\xi}_\mu$

μ	$\nu = 1$	$\nu = 2$	$\nu = 3$	$\nu = 4$	μ	$\nu = 1$	$\nu = 2$	$\nu = 3$	$\nu = 4$
0	-0.0761	-0.2929	-0.6173	-1.0000	5	1.3066	1.0898	0.7654	0.3827
1	0	-0.2168	-0.5412	-0.9239	6	1.6310	1.4142	1.0898	0.7071
2	0.2168	0	-0.3244	-0.7071	7	1.8478	1.6310	1.3066	0.9239
3	0.5412	0.3244	0	-0.3827	8	1.9239	1.7071	1.3827	1.0000
4	0.9239	0.7071	0.3827	0					

The term $2\lambda_v/\gamma_v a_\infty \cos \beta$ takes into account the effect of the foil planform by means of $\lambda_v = b_v/l$ and the hydrodynamic characteristics depending on h_v and b_v of a given foil element when the flow around it close to a free surface is plane-parallel by means of the function $\gamma_v(\bar{h}_v) = \gamma_v(h_v/b_v)$. In general form the true angle of attack of a section of a hydrofoil can be represented as the sum

$$\alpha_{tr}(\theta_v) = \alpha_{pl} + \alpha_{tw}(\theta_v) - \Delta\alpha_0(\theta_v), \quad (I.67)$$

where α_{pl} is the hydrodynamic angle of attack of a flat foil measured at the central section of an actual foil from the line of zero lift; $\alpha_{tw}(\theta_v)$ is the change in angle of attack of a given section compared with the central one due to aerodynamic or geometric twist; and $\Delta\alpha_0(\theta_v)$ is the change in angle of zero lift due to the free surface effect:

Therefore, due to the linearity of the main equation of the foil (I.62) the total circulation can be written as the following sum:

$$G = G_{pl} + G_{tw} + G_\Delta, \quad (I.68)$$

where G_{pl} is the circulation of a flat foil without any twist; G_{tw} the additional circulation due to twist in the foil; and G_Δ the added circulation due to the free-surface effect on the angle of zero lift of the profile.

Hence, for determining the separate components of circulation we have the following system of equations:

$$\left(\frac{2\lambda_v}{\gamma_v a_\infty \cos \beta} + \bar{b}_{vv} \right) G_{pl} = \alpha_v + \sum_{n=1}^{\frac{m+1}{2}} \bar{b}_{vn} G_{npl}; \quad (I.69)$$

$$\left(\frac{2\lambda_v}{\gamma_v a_\infty \cos \beta} + \bar{b}_{vv} \right) G_{tw} = \frac{\alpha_{vtw}}{\cos \beta} + \sum_{n=1}^{\frac{m+1}{2}} \bar{b}_{vn} G_{n tw}; \quad (I.70)$$

$$\left(\frac{2\lambda_v}{\gamma_v a_\infty \cos \beta} + \bar{b}_{vv} \right) G_\Delta = -\frac{\Delta\alpha_{0v}}{\cos \beta} + \sum_{n=1}^{\frac{m+1}{2}} \bar{b}_{vn} G_{n\Delta}. \quad (I.71)$$

Equations (I.69) and (I.71) differ only in the first term on the right side.

As a consequence of the fact that the circulation for a foil containing no twist is proportional to the hydrodynamical angle of attack, that is, since $G_{pl} = \bar{G}_{pl}\alpha$, the initial equation can be written in the form (subscript "pl" omitted) [46]

$$\left(\frac{2\lambda_v}{v_\infty \cos \beta} + \bar{b}_{vv}^*\right) \bar{G}_v = 1 + \sum_{n=1}^{m+1} \bar{b}_{vn}^* \bar{G}_n. \quad (I.72)$$

As a result of solving this equation we obtain the circulation distribution over the span of an untwisted hydrofoil.

Using the coupling equation we find the distribution of $C_{y \text{ sec}}$ over the span of an untwisted hydrofoil:

$$C_{y \text{ sec}}(\bar{z}_v) = \frac{2\Gamma(\bar{z}_v)}{b(\bar{z}_v)v} = \frac{2l}{b(\bar{z}_v)} G_v \alpha. \quad (I.73)$$

The lift coefficient of the foil is

$$C_{yf} = \lambda_f \int_{-1}^1 G(\bar{z}) d\bar{z}. \quad (I.74)$$

Using (I.43) we obtain for a symmetrical foil

$$C_{yf} = 2\pi\lambda_f/(m+1) \left(\frac{1}{2} G_{\frac{m+1}{2}} + \sum_{n=1}^{\frac{m-1}{2}} G_n \sin \theta_n \right), \quad (I.75)$$

whence

$$\frac{\partial C_{yf}}{\partial \alpha} = \frac{2\pi\lambda_f}{m+1} \left(\frac{1}{2} \bar{G}_{\frac{m+1}{2}} + \sum_{n=1}^{\frac{m-1}{2}} \bar{G}_n \sin \theta_n \right). \quad (I.76)$$

Dividing (I.73) by (I.75) we obtain the distribution of the lift coefficient along the span of the foil when $C_{yf} = 1$, that is,

$$C'_{y \text{ sec}} = C_{y \text{ sec}}(\bar{z}_v)/C_{yf} = \frac{(m+1)b_m}{ab_v} \cdot \frac{\bar{G}_v}{\frac{1}{2} \bar{G}_{\frac{m+1}{2}} + \sum_{n=1}^{\frac{m-1}{2}} \bar{G}_n \sin \theta_n}. \quad (I.77)$$

It should be stressed that the change in the angle of zero lift $\Delta\alpha_0$ along the span of a foil as a consequence of the effect of the free surface and also the twist in the foil are not reflected in the derivative $\partial C_{yf}/\partial \alpha$ inasmuch as these additions remain constant at all angles of attack. Hence, formula (I.75) holds for hydrofoils of any planform and any dihedral. The variability in $\Delta\alpha_0$ and the twist in the foil are reflected only in the load distribution over the span and in the angle of zero lift of the foil as a whole.

The distribution of the added load over the span due to twist in the foil is calculated from the formula [47]

$$C_{vtw}(\bar{z}_v) = 2\lambda_v \left(\frac{G_{vtw} - \bar{G}_v}{\frac{1}{2} \bar{G}_{\frac{m+1}{2}} + \sum_{n=1}^{\frac{m-1}{2}} \bar{G}_n \sin \theta_n} \right), \quad (I.78)$$

where G_{vtw} is the added circulation due to the twist in the foil as determined from formula (I.70) and \bar{G}_v is the circulation of a flat foil.

The added load due to the effect of the free surface on the angle of zero lift of the foil profile can be found from the formula

$$C_{v\Delta}(\bar{z}_v) = 2\lambda_v \left(\frac{G_{v\Delta} - \bar{G}_v}{\frac{1}{2} \bar{G}_{\frac{m+1}{2}} + \sum_{n=1}^{\frac{m-1}{2}} \bar{G}_n \sin \theta_n} \right), \quad (I.79)$$

where $G_{v\Delta}$ is the added circulation determined from formula (I.71).

Hydrodynamical calculations of a hydrofoil using the Multhopp method are basically simple but require lengthy numerical work. A simple approximate method which calls for precise calculations only in an unbounded liquid can be recommended for determining circulation distribution over a span and the hydrodynamic characteristics of a hydrofoil. The effect of a free surface on the magnitude of circulation at a particular section of a hydrofoil is taken into account by the introduction of a certain function which depends on the aspect ratio and depth of immersion of the foil and the location of the section along the span.

After solving equation (I.51) with respect to $r(\bar{z})$ and introducing the dimensionless magnitudes indicated in (I.56) we obtain another form of the main equation for a foil of finite span moving near a free surface

$$\begin{aligned} G(\bar{z}) &= \frac{\gamma(\bar{h}) a_\infty}{2\lambda(\bar{z})} [\alpha - \alpha_i(\bar{z}, \lambda, \bar{h})] = \\ &= \frac{\gamma(\bar{h}) a_\infty \alpha}{2\lambda(\bar{z})} [1 - \bar{\alpha}_i(\bar{z}, \lambda, \bar{h})], \end{aligned} \quad (I.80)$$

where $\alpha_i(\bar{z}, \lambda, \bar{h}) = \alpha_i(\bar{z}, \lambda, \bar{h})\alpha$ is the value of the induced angle of downwash at the particular foil section.

We will introduce the function

$$\psi(\bar{z}, \lambda, \bar{h}) = \frac{\bar{G}(\bar{z}, \lambda, \bar{h})}{\bar{G}_\infty(\bar{z}, \lambda)}.$$

In the above formula $G_\infty(\bar{z}, \lambda)$ stands for dimensionless circulation at a particular section as the foil moves in an unbounded liquid. Using (I.80) we obtain

[48]

$$\psi(\bar{z}, \lambda, \bar{h}) = \gamma(\bar{h}) \cdot \frac{1 - \bar{\alpha}_j(\bar{z}, \lambda, \bar{h})}{1 - \bar{\alpha}_{j\infty}(\bar{z}, \lambda)}.$$

In a foil whose planform varies from rectangular or in a banked rectangular foil the magnitude of $\partial C_{y h_\infty} / \partial \alpha$ will vary for sections over a span due to the effect of the free surface of the water. In the first approximation the induced angle of downwash at a certain section \bar{z}_v is the same as in an optimal hydrofoil along whose span the derivative of the lift coefficient of sections with respect to the angle of attack is constant and equal to its value at section \bar{z}_v , that is, it is equal to $\partial C_{y h_\infty} / \partial \alpha$. We will also set in the first approximation $\psi(\bar{z}_v) \approx \psi_0$ where ψ_0 is the function ψ calculated for the indicated optimal foil. According to data presented by T. Nishiyama [5] the planform of an optimal hydrofoil differs only slightly from elliptical. Neglecting this difference and using the solution to the problem of a foil and biplane with an optimal circulation distribution over the span [9], we obtain the following expression for determining function ψ at a particular hydrofoil section \bar{z}_v :

$$\psi_v = \gamma(\bar{h}_v) \frac{1 - \bar{\alpha}_{0v}}{1 - \bar{\alpha}_{0\infty}}, \quad (I.81)$$

where

$$\bar{\alpha}_{0\infty} = \frac{a_\infty}{\pi \lambda_f + a_\infty}; \quad (I.82)$$

$$\bar{\alpha}_{0v} = \frac{2}{\pi} \cdot \frac{\gamma(\bar{h}_v) a_\infty}{\pi \lambda_f + \frac{2}{\pi} \gamma(\bar{h}_v) a_\infty}; \quad (I.83)$$

$$\lambda_f = \frac{P}{S};$$

$\chi = f(\bar{h}_m / \lambda_f)$ is read from the graph in Fig. 22; and $\bar{h}_m = h_m / b_m$ is the mean relative depth of immersion of the foil as determined from the depth of immersion of the center of gravity of the foil area.

We find the circulation at section \bar{z}_v from the formula [49]

$$\bar{G}_v = \psi_v \bar{G}_\infty(\bar{z}_v). \quad (I.84)$$

The circulation distribution over the span of a particular

foil moving in an unbounded liquid $\bar{G}(\bar{z}_v)$ can be determined by the Multhopp method mentioned above or taken from reference books on the aerodynamics of a foil. The circulation distribution over the span of a flat foil in an unbounded liquid, either straight or with a varying degree of taper, is shown in Fig. 23 which is recommended as an aid for calculating flat foils.

When the circulation distribution over the span of a hydrofoil is known the lift can be found from formulas (I.75) and (I.76) and the restoring moment with respect to the midpoint of the foil can be determined from the following expressions:

$$\left. \begin{aligned} C_{m0} &= \frac{\partial C_{m0}}{\partial \alpha} (\alpha + \alpha_0 + \Delta \alpha_{m0}), \\ \frac{\partial C_{m0}}{\partial \alpha} &= \frac{\lambda c}{2} \int_{-1}^1 \bar{G}(\bar{z}_v) \bar{z}_v d\bar{z}_v, \\ \Delta \alpha_{m0} &= \frac{\Delta C_{m0}}{\frac{\partial C_{m0}}{\partial \alpha}}, \\ \Delta C_{m0} &= -\frac{\lambda c}{2} \int_{-1}^1 \bar{G}(\bar{z}_v) \Delta \alpha_0(\bar{z}_v) d\bar{z}_v. \end{aligned} \right\} \quad (I.85)$$

Approximate formulas ensuring adequate accuracy which were derived based on the following thinking can be recommended for making practical calculations of the total coefficients of lift and induced drag of a flat hydrofoil.

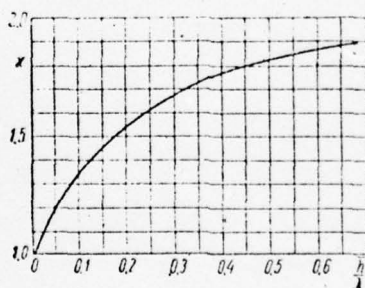


Fig. 22. Graph of the function $\chi(\bar{h}/\lambda)$.

The induced downwash of a hydrofoil can be expressed in terms of the induced downwash in an unbounded liquid with a correctional factor allowing for the effect of the free surface

$$\alpha_{ch} = \alpha_{c0} \chi\left(\frac{\bar{h}}{\lambda}\right) = \frac{C_{ph}}{\pi \lambda} (1 + \tau) \chi\left(\frac{\bar{h}}{\lambda}\right), \quad (I.86)$$

here τ is the Glauert correction for the effect of the plan-form which is determined from the curve in Fig. 24 and $\zeta(\bar{h}/\lambda)$ is a function of the \bar{h}/λ ratio of a hydrofoil.

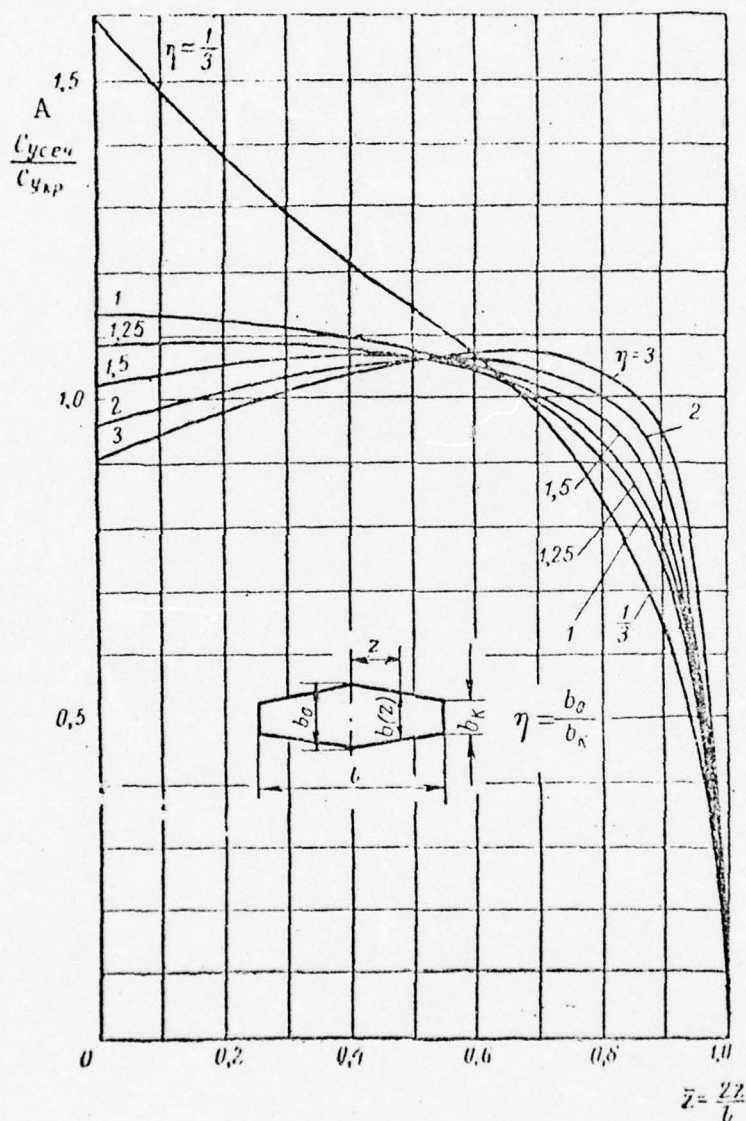


Fig. 23. Diagram of lift coefficient distribution over a half-span of a flat foil with a straight axis in an unbounded liquid.

KEY: $A = C_{ysec}/C_{yfp}$.

A graph of ζ as a function of \bar{h}/λ drawn from data for a flat foil as calculated by the Multhopp method is shown in Fig. 25.

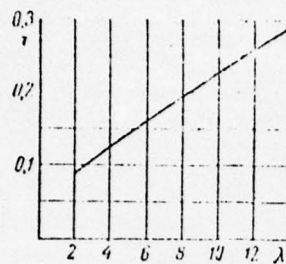


Fig. 24. Graph of correctional factor for the planform of a foil.

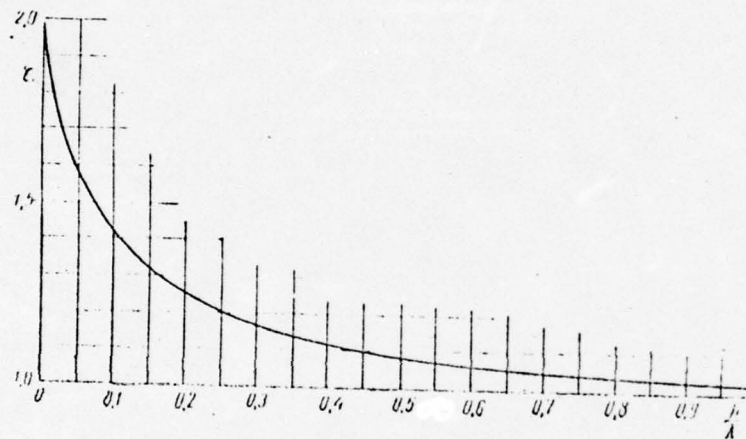


Fig. 25. Graph of the function $\xi(\bar{h}/\lambda)$.

With an optimal circulation distribution over the span of a hydrofoil when $\alpha_{i\bar{h}} = \text{const}$ use can be made of the solution for an optimal biplane in an unbounded liquid [9] from which it follows that

$$\alpha_{i\bar{h}} = \frac{C_{yh}}{\pi\lambda} \frac{2}{\chi}, \quad (I.87)$$

where $\chi = f(\bar{h}/\lambda)$ (see Fig. 22).

A comparison shows that $z \approx 2/\chi$.

Substituting the expression for $\alpha_{i\bar{h}}$ as written in (I.86) into formula (I.49) and transforming, we obtain an approximate formula for calculating C_{yh} for a flat hydrofoil

$$C_{yh} = \frac{\gamma(\bar{h}) a_\infty}{1 + \frac{\gamma(\bar{h}) a_\infty}{\pi\lambda} (1 + \tau) \zeta\left(\frac{\bar{h}}{\lambda}\right)} (\alpha + \alpha_0 - \Delta\alpha_0). \quad (I.88)$$

The induced drag is a projection onto the direction of movement of a lift vector which is deflected from the vertical

by the angle of downwash. Therefore, the coefficient of induced drag can be found from the relation

$$C_{x2} = \alpha_z C_{yh} = \frac{C_{yh}^2}{\pi \lambda} (1 + \delta) \zeta \left(\frac{h}{\lambda} \right), \quad (I.89)$$

where δ is a coefficient allowing for the effect of the planform as determined from the graph in Fig. 26.

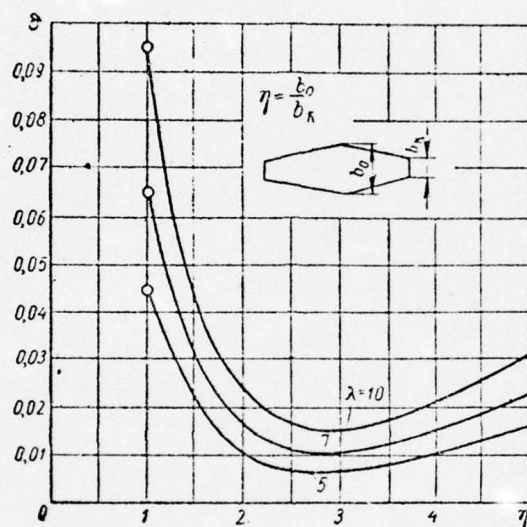


Fig. 26. Graph of correctional coefficient δ as a function of aspect ratio and taper of a foil.

For approximate calculations use can be made of the graph in Fig. 27 showing values of the derivative $\partial C_{yh} / \partial \alpha$ for a rectangular hydrofoil plotted as a function of the depth of immersion and aspect ratio as calculated from the formula

$$\frac{\partial C_{yh}}{\partial \alpha} = \frac{k_q a_\infty}{1 + \frac{k_q a_\infty}{\pi \lambda} (1 + \tau) \zeta \left(\frac{h}{\lambda} \right)}. \quad (I.90)$$

In many practical problems the load over the span of a flat hydrofoil can be determined in a simplified fashion by considering it to be the same as that of a foil in an unbounded liquid and using the diagram shown in Fig. 23. The basis for this is the weak effect nearness of a free surface has on the nature of load distribution over the span of a flat rectangular hydrofoil as established by calculations and confirmed by experiment [6]. In most actual foils foils differ little in form from a flat rectangular foil. [54]

All recommendations made for calculating flat foils pertain in full measure to foils with slight dihedral whose

dihedral angle is not greater than 6--8%. For all practical purposes the dihedral angle of all depth effect foils never exceeds the indicated range.

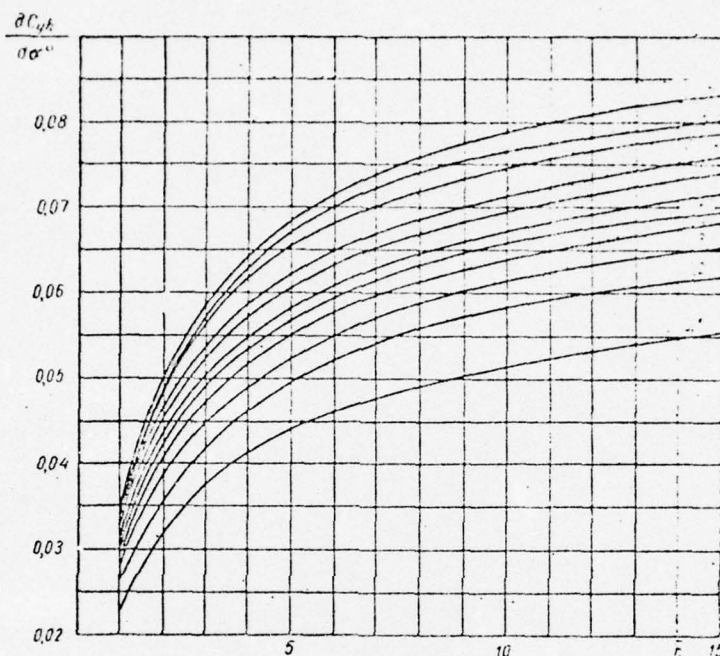


Fig. 27. Diagram of the derivative $\partial C_{yh}/\partial \alpha^\circ$ of a flat rectangular hydrofoil plotted as a function of relative depth of immersion and aspect ratio.

I. I. Isayev carried out calculations for dihedral foils using the Multhopp method, taking dihedral completely into account. He identified the error in determining lift which results from calculating a dihedral foil from the formulas for a flat foil. A graph of the error made in this way in the form of the ratio

$$\delta = \frac{\left(\frac{\partial C_{yh}}{\partial \alpha}\right)_\beta - \left(\frac{\partial C_{yh}}{\partial \alpha}\right)_\beta}{\left(\frac{\partial C_{yh}}{\partial \alpha}\right)_\beta} \cdot 100\%$$

for a foil with a straight planform and an aspect ratio of $\lambda = 6$ is shown in Fig. 28.

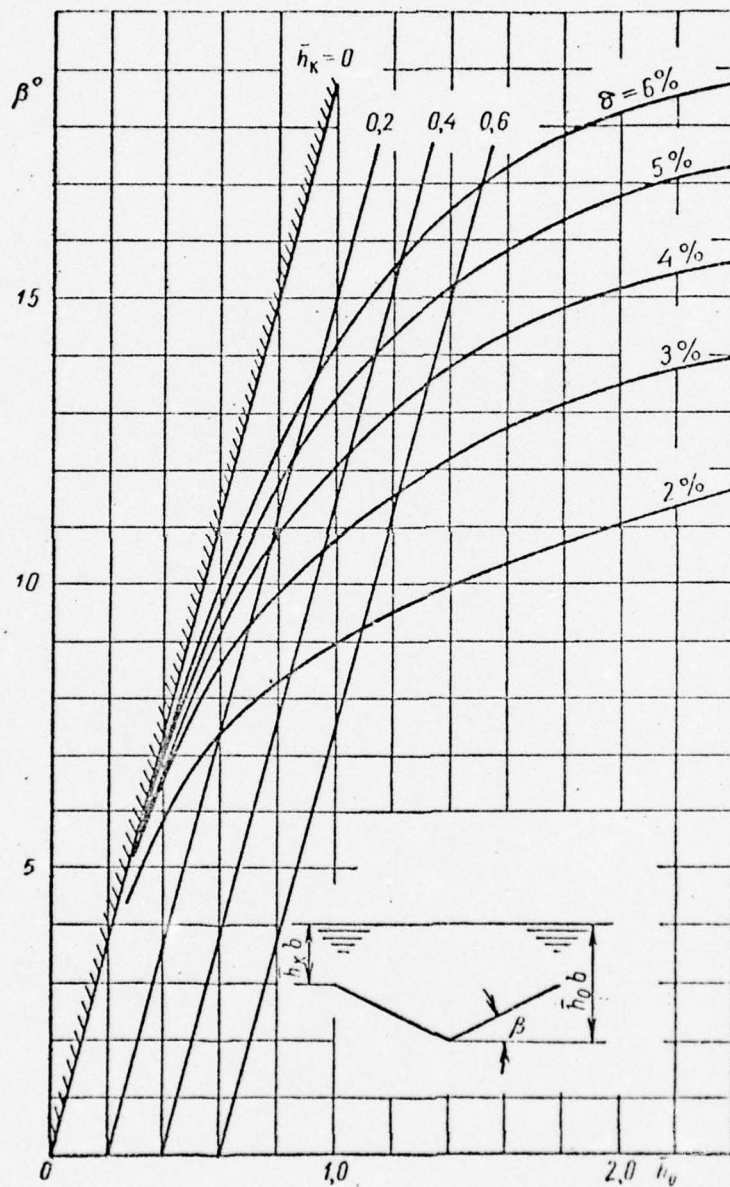


Fig. 28. Graph of error in determining the derivative of a dihedral foil from formulas for a flat foil.

3/. Hydrodynamical calculations of a V-shaped surface-piercing foil

For large relative speeds of movement determining the characteristics of a V-shaped surface-piercing foil (Fig. 29) amounts to calculating the characteristics of a lift system with the configuration shown in Fig. 30.

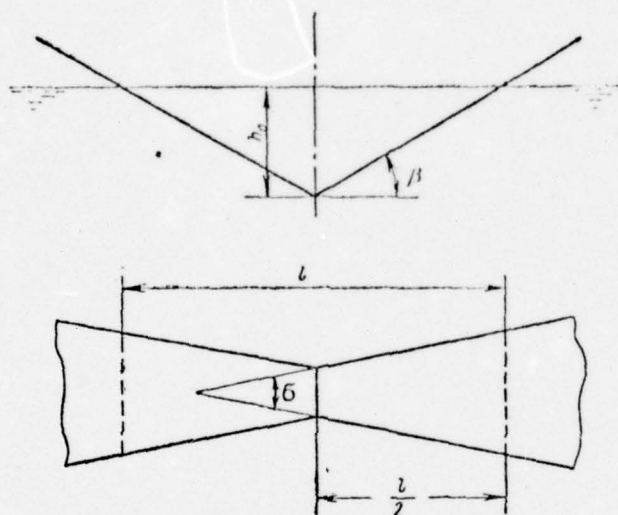


Fig. 29. Geometry of a V-shaped foil.

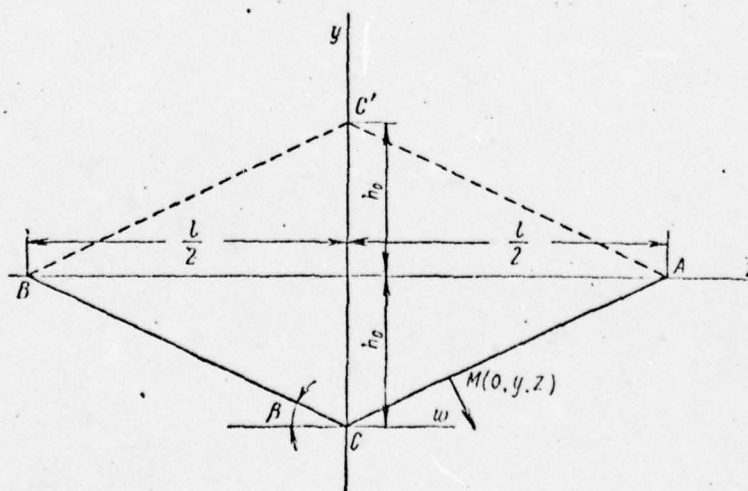


Fig. 30. Configuration of a system of lift vortices of a hydrodynamic model of a V-shaped surface-piercing foil.

The main integro-differential equation of a surface-piercing V-shaped foil is completely identical in outward

appearance to equation (I.57) which is for a completely immersed dihedral foil. All the variables in this equation have the same meaning for a V-shaped foil and the function $L(\bar{z}, \bar{\xi})$ is a limiting case of a similar function for a dihedral foil and can be obtained from formula (I.55) by substituting in it an expression for the depth of immersion of the root section of a dihedral foil in terms of the dihedral angle $h_0 = 2 \operatorname{tg} \beta / 2$.

For a V-shaped foil function $L(\bar{z}, \bar{\xi})$ takes the form [56]

$$L(\bar{z}, \bar{\xi}) = \begin{cases} \frac{(\bar{z} + \bar{\xi}) \operatorname{tg}^2 \beta - \frac{(\bar{z} + \bar{\xi})^2}{2 - \bar{\xi}} \operatorname{tg}^2 \beta}{(\bar{z} - \bar{\xi})^2 + (\bar{z} + \bar{\xi})^2 \operatorname{tg}^2 \beta} + \\ + \frac{(\bar{z} - \bar{\xi}) (1 + \operatorname{tg}^2 \beta) - 2 \operatorname{tg}^2 \beta}{[(\bar{z} - \bar{\xi}) - 2]^2 \operatorname{tg}^2 \beta + (\bar{z} - \bar{\xi})^2} & \bar{\xi} \leq 0, \\ \frac{(\bar{z} + \bar{\xi}) \operatorname{tg}^2 \beta - 2 \operatorname{tg}^2 \beta + (\bar{z} - \bar{\xi})}{[(\bar{z} + \bar{\xi}) - 2]^2 \operatorname{tg}^2 \beta + (\bar{z} - \bar{\xi})^2} & \bar{\xi} \geq 0. \end{cases} \quad (\text{I.91})$$

The integro-differential equation for a V-shaped foil can be solved and its characteristics determined from the formulas in §6.

Coefficients B_{vn} which do not depend on the specific distinguishing features of a foil are determined from Table 1. Coefficients g_{vn}^* depend not only on the number of points m at which circulation is calculated but also on function $L(\bar{z}, \bar{\xi})$. Since function L depends only on the dihedral angle β , coefficients \bar{b}_{vn}^* and \bar{b}_{vn}^* depend only on this parameter.

TABLE 4
Numerical Values of Coefficients \bar{b}_{vn}^* and \bar{b}_{vn}^* for a V-Shaped Foil

v = 1				v = 2			
β°	15	30	45	β°	15	30	45
\bar{b}_{11}^*	7.15	6.25	6.75	\bar{b}_{21}^*	1.0	1.0	0.9
\bar{b}_{12}^*	1.5	1.5	1.65	\bar{b}_{22}^*	3.7	3.3	3.15
\bar{b}_{13}^*	0.6	0.25	0.085	\bar{b}_{23}^*	1.05	1.05	1.1
\bar{b}_{14}^*	0.015	0.065	0.16	\bar{b}_{24}^*	0.12	0.045	0.085
v = 3				v = 4			
\bar{b}_{31}^*	0.105	0.025	0.045	\bar{b}_{41}^*	0.136	0.108	0.085
\bar{b}_{32}^*	0.9	0.85	0.8	\bar{b}_{42}^*	0.07	0.14	0.24
\bar{b}_{33}^*	2.5	2.35	2.2	\bar{b}_{43}^*	1.41	1.45	1.50
\bar{b}_{34}^*	0.7	0.75	0.8	\bar{b}_{44}^*	2.2	1.88	1.69

Table 4 gives values for the indicated coefficients as a function of the dihedral angle of a foil for $m = 7$.

After establishing the values of circulation G_v at m [57] points along the span of a foil, formula (1.76) is used to determine $\partial C_{yf} / \partial \alpha$ for a V-shaped foil. Based on the values of the added circulation $G_{v\Delta}$ due to the free surface effect on the angle of zero lift of foil sections the added lift coefficient is found to be

$$C_{y\Delta} = \lambda_f \int_{-1}^1 G_{v\Delta} d\bar{z}_v.$$

This force is a negative one, that is, it leads to a decrease in the angle of zero lift of the foil by

$$\Delta \alpha_{0f} = \frac{C_{y\Delta}}{\frac{\partial C_{yf}}{\partial \alpha}}. \quad (1.92)$$

A similar correction is made in the angle of zero lift when the foil has an angle of twist.

The lift coefficient of a foil is determined by substituting the magnitudes found into the equation

$$C_{yf} = \frac{\partial C_{yf}}{\partial \alpha} \left(\alpha + \frac{\alpha_0}{\cos \beta} - \Delta \alpha_{0f} \right). \quad (1.93)$$

This method was used to calculate a series of V-shaped foils differing in dihedral angle, planform, and depth of immersion at the root section. The curves drawn from the results of calculations (Figs. 31--34) make it possible to establish in general form the effect of dihedral β , wetted aspect ratio $\lambda = l : b_m$, relative depth of immersion of root section $\bar{h}_0 = h_0 : b_0$, and taper angle σ (the angle between the leading and trailing edges measured in the plane of a half-foil) on the hydrodynamic characteristics of V-shaped foils. They can be used for selecting the geometric parameters of foils and determining their hydrodynamic characteristics.

It follows directly from an examination of the graphs that a decrease in dihedral and increase in aspect ratio contribute to equalizing the load distribution over the span. However, the relative effect of dihedral (Fig. 31) and aspect ratio (Fig. 32) on the distribution of C_{ysec} of a straight V-shaped foil as well as of one widening toward the tips is not great. Widening a foil has a greater effect. It leads to an increase in C_{ysec} in the midpart and a decrease at the tips of a foil. The derivative $\partial C_{yf} / \partial \alpha$ (Fig. 33) increases sharply with an increase in the aspect ratio and depends little on dihedral. At large aspect ratios an increase in dihedral leads to a reduction in $\partial C_{yf} / \partial \alpha$. Within the limits $\beta = 15--30^\circ$ it

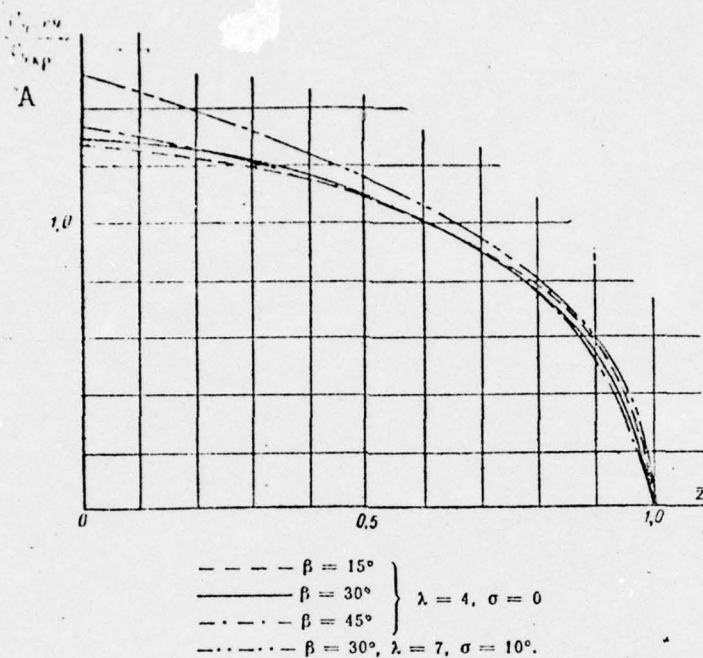


Fig. 31. Effect of dihedral and taper on lift coefficient distribution along a half-span of a V-shaped foil.
KEY: A-- C_{ysec}/C_{yf} .

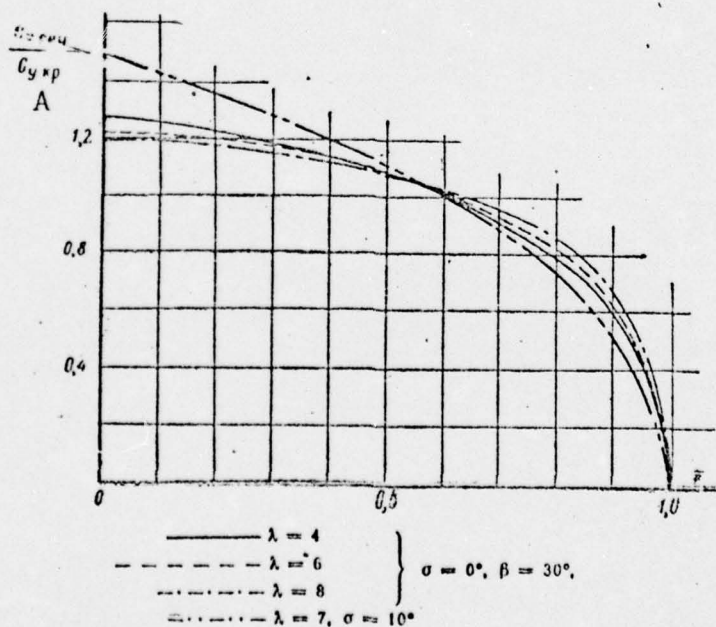


Fig. 32. Effect of relative (wetted) aspect ratio and dihedral of a V-shaped foil on lift coefficient distribution.
KEY: A-- C_{ysec}/C_{yf} .

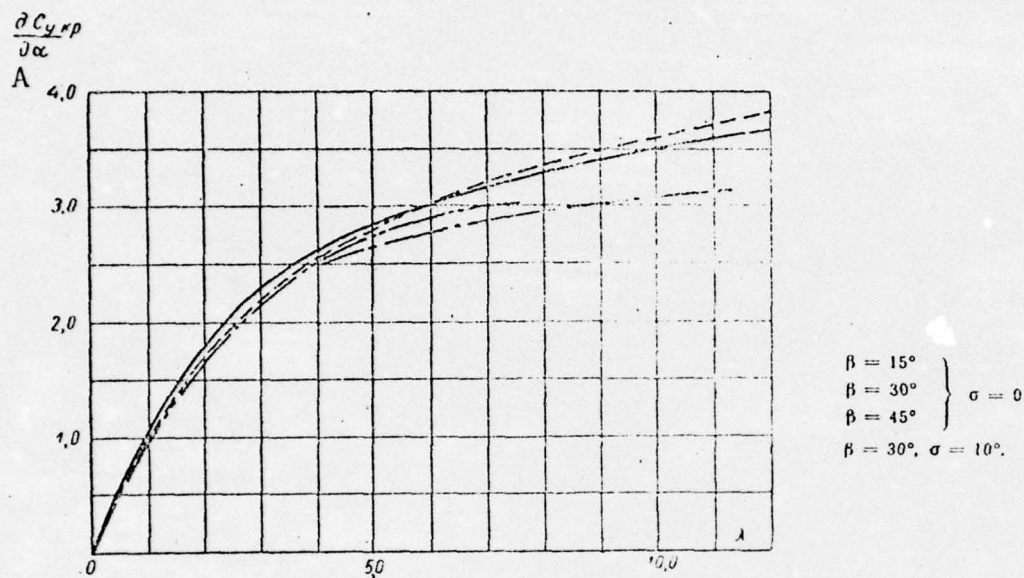


Fig. 33. Graph of derivative $\partial C_{yfp} / \partial \alpha$ of a V-shaped foil as a function of relative aspect ratio and dihedral.
KEY: A-- $\partial C_{yfp} / \partial \alpha$.

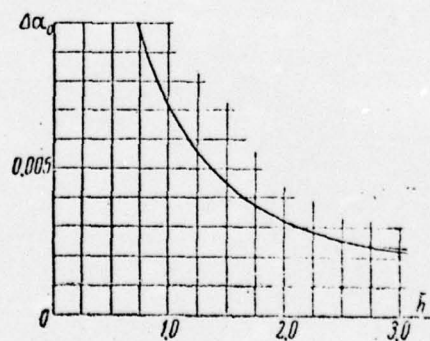


Fig. 34. Graph of change in angle of zero lift of a V-shaped foil with a segmental profile whose relative thickness is $c = 0.06$.

is not great and becomes more manifest when the dihedral reaches 45° . At small aspect ratios corresponding to small depths of immersion the effect of dihedral is the reverse, that is, an increase in it is accompanied by an increase in $\partial C_{yf}/\partial \alpha$.

It is easy to employ the graphs presented to determine the lift coefficient of a V-shaped foil. For this purpose the graph in Fig. 33 can be used to determine $\partial C_{yf}/\partial \alpha$ and that in Fig. 34 to find $\Delta \alpha_0$. Substituting the data found into formula (I.93) makes it possible to determine the lift coefficient of a V-shaped foil. [60]

§8. Hydrodynamical calculations of a flat foil with vertical struts and a foil with inclined stabilizers

Foil systems on craft may be complex in form, having horizontal lift foils combined with vertical or inclined supporting struts and with inclined lift elements (stabilizers, takeoff foils, etc.). One possible design for a foil system is shown in Fig. 88. The simplest hydrofoil system consists of a flat foil supported by one or two vertical surface-piercing struts.

If a flat foil of finite span has vertical surface-piercing struts, they cause a change in the induced downwash and a corresponding change in the lift and induced drag. For large speeds of movement ($Fr > 4-5$) the induced downwash of a flat hydrofoil with vertical struts can be found by solving the problem of movement in an unbounded liquid of a biplane consisting of foils with the same lift connected by two struts. The height of the biplane (distance between upper and lower foils) is equal to double the depth of immersion $2h$ of the hydrofoil. After making the additional assumption of constancy of the angle of downwash over the span, that is, assuming optimal (elliptical) circulation distribution over the foil, A. B. Lukashevich, using methods from the theory of a foil of finite span [9], determined the coefficient χ by substituting which in formula (I.87) he was able to find the induced downwash of a rectangular foil with vertical struts. The values of χ as a function of h/l and a/l are shown graphically in Fig. 35 where h is the depth of immersion of the foil, a the distance between struts, and l the foil span.

The lift coefficient is determined from formula (I.88) in which coefficient τ is replaced with $2/\chi$. The derivative of the lift coefficient is accordingly expressed by the formula

$$\frac{\partial C_{yh}}{\partial \alpha} = \frac{k_q a_\infty}{1 + \frac{k_q a_\infty}{\pi \lambda} (1 + \tau) \frac{2}{\chi}} \quad (I.94)$$

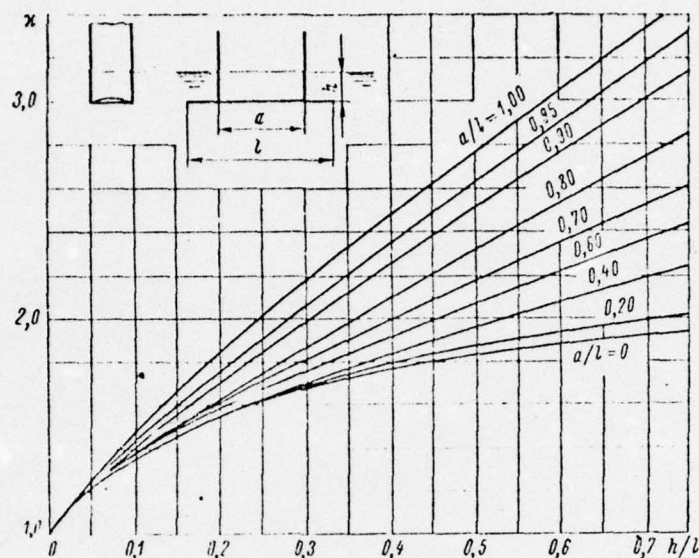


Fig. 35. Coefficient χ for the effect of the struts of a hydrofoil on induced downwash as a function of h/l and a/l .

It is apparent from Fig. 35 that the existence of vertical struts entails an increase in χ and, consequently, a decrease in the induced downwash. The struts are more effective when the depth of immersion of the foil is greater and when the struts are located right at the tips of the foil. When $a/l = 0$, that is, for a foil with one strut in a plane of symmetry, a strut has no effect and χ coincides with the χ in Fig. 22. [61]

As calculations show $\partial C_y / \partial \alpha$ for depth-effect foils ($\bar{h} = 0.15 - 0.30$) is not great and even when the struts are located at the tips does not exceed 1%. Beginning with a depth of immersion of $\bar{h} = 1$ $\partial C_y / \partial \alpha$ reaches 5% when the struts are located at the tips. When the struts are closer together their effect rapidly diminishes and it disappears completely at $\bar{h} = 0.375$ when $a/l = 0.9$ and at $\bar{h} = 1$ when $a/l = 0.7$.

These conclusions pertain to struts whose chord is equal to that of the foil and which extend over the entire width of the foil.

An approximate method similar to that described in §6 can be recommended for calculating the hydrodynamic characteristics of a hydrofoil with inclined stabilizers. This is true because the horizontal flat foil generates most of the lift in the main mode of movement and the inclined stabilizers contribute little.

In our investigation of the characteristics of a foil with inclined stabilizers we will consider only the horizontal projection of the system. This is similar to taking into account only the vertical components of lifting forces developed on the different elements of a hydrofoil with inclined stabilizers and lying perpendicular to the plane of the given elements. The horizontal components of the lifting forces are of no practical interest in an investigation of a ship's behavior in a vertical plane since their total effect on the characteristics of a foil is small. [62]

As a rule, the midpart of a foil (horizontal flat foil) is rectangular in the plan and the inclined stabilizers are either rectangular or widen toward the ends.

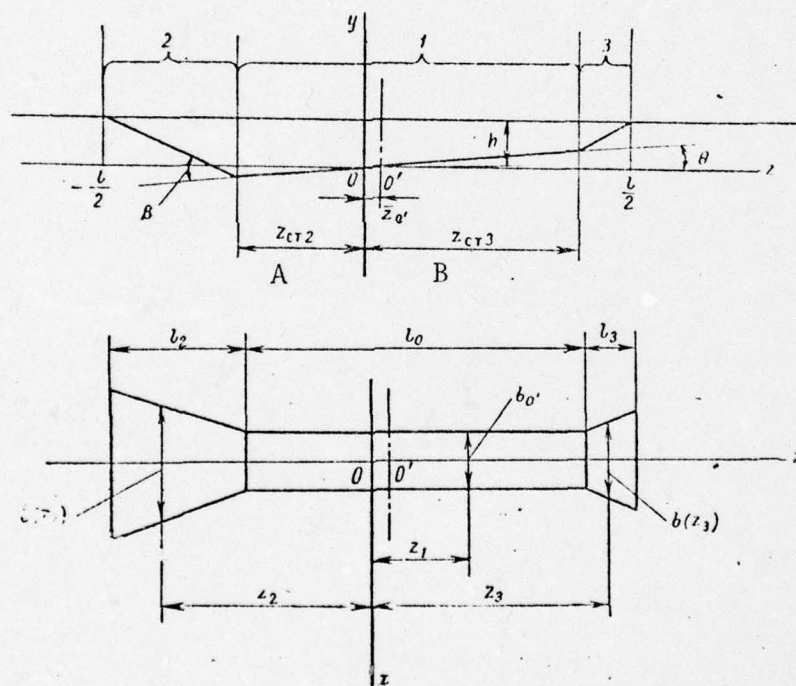


Fig. 36. Geometry of banked trapezoidal foil with inclined stabilizers.

KEY: A-- z_{st2} ; B-- z_{st3} .

We will now examine the geometric characteristics of a foil, knowledge of which is essential for calculating circulation distribution over the span. We will derive formulas for determining the indicated characteristics in the most general case, that of a foil banked at an angle of θ with widening inclined stabilizers piercing the water's surface.

We will subdivide the foil (Fig. 36) into three sectors:
 1--the foil's midpart; 2--the stabilizer which enters the water during a bank; and 3--the stabilizer which leaves the water during a bank.

As indicated above, the midpart of the foil is in the form of a foil with a rectangular planform. We will designate the length of this sector l_0 . When a foil is mounted on a craft the midsection of sector 1 will coincide with the centerline plane of the craft. We will regard this section (point O') as initial, relative to which the depth of immersion of the foil h is given. The horizontal z axis of a fixed system of coordinates passes through point O' and the y axis passes through the midpoint of the span l of the foil's projection. Let $z_{O'}$ be the distance of the midpoint of sector 1 from the origin of the coordinates and $b_{O'}$ the chord of this foil sector. Introducing the dimensionless magnitude $\bar{z} = 2z/l$ for the purpose of determining $z_{O'} = 2z_{O'}/l$ and local aspect ratio $\lambda(\bar{z}_{O'}) = l/b_{O'}$ for the midsection of the foil, we obtain the following formulas:

$$\begin{aligned}\lambda(\bar{z}_{O'}) &= \lambda_0 \cos \theta + \left(\bar{h} + \frac{\lambda_0}{2} \sin \theta \right) \operatorname{ctg}(\beta - \theta) + \\ &\quad + \left(\bar{h} - \frac{\lambda_0}{2} \sin \theta \right) \operatorname{ctg}(\beta + \theta), \\ \bar{z}_{O'} &= \frac{1}{\lambda(\bar{z}_{O'})} \left[\left(\bar{h} + \frac{\lambda_0}{2} \sin \theta \right) \operatorname{ctg}(\beta - \theta) - \right. \\ &\quad \left. - \left(\bar{h} - \frac{\lambda_0}{2} \sin \theta \right) \operatorname{ctg}(\beta + \theta) \right],\end{aligned}$$

where $\lambda_0 = l_0/b_{O'}$ is the aspect ratio of the midsection of the foil and $\bar{h} = h/b_{O'}$ the set relative depth of immersion of the section corresponding to the midpoint of sector 1.

The locations of the start of stabilizers 2 and 3 along the span of the foil \bar{z}_{st2} and \bar{z}_{st3} are determined from the formulas:

$$\begin{aligned}\bar{z}_{st2} &= - \left[\frac{\lambda_0 \cos \theta}{\lambda(\bar{z}_{O'})} - \bar{z}_{O'} \right], \\ \bar{z}_{st3} &= \frac{\lambda_0 \cos \theta}{\lambda(\bar{z}_{O'})} + \bar{z}_{O'}.\end{aligned}$$

For local aspect ratio corresponding to a section of any stabilizer we obtain

$$\lambda(\bar{z}) = \frac{l}{b(\bar{z})} = \frac{b_{O'}}{b(\bar{z})} \lambda(\bar{z}_{O'}),$$

here

$$\frac{b(\bar{z}_2)}{b_{0'}} = 1 + \frac{\lambda(\bar{z}_{0'}) (|\bar{z}_2| + \bar{z}_{0'}) - \lambda_0 \cos \theta}{\cos(\beta - \theta)} \operatorname{tg} \frac{\sigma}{2};$$

$$\frac{b(\bar{z}_3)}{b_{0'}} = 1 + \frac{\lambda(\bar{z}_{0'}) (\bar{z}_3 - \bar{z}_{0'}) - \lambda_0 \cos \theta}{\cos(\beta + \theta)} \operatorname{tg} \frac{\sigma}{2};$$

and σ is the taper angle of the stabilizers.

The foil aspect ratio is

[64

$$\lambda_f = \frac{b_{0'}}{b_m} \lambda(\bar{z}_{0'}),$$

where

$$\frac{b_m}{b_{0'}} = 1 + \frac{\operatorname{tg} \frac{\sigma}{2}}{2} \left\{ \left(\bar{h} + \frac{\lambda_0}{2} \sin \theta \right) \left[1 + \bar{z}_{0'} - \frac{\lambda_0 \cos \theta}{\lambda(\bar{z}_{0'})} \right] \frac{1}{\sin(\beta - \theta)} + \left(\bar{h} - \frac{\lambda_0}{2} \sin \theta \right) \left[1 - \bar{z}_{0'} - \frac{\lambda_0 \cos \theta}{\lambda(\bar{z}_{0'})} \right] \frac{1}{\sin(\beta + \theta)} \right\}.$$

Finally, local depths of immersion corresponding to the first, second, and third sectors of the foil and the mean depth of immersion can be found from the formulas

$$\bar{h}(\bar{z}_1) = \bar{h} - \frac{\lambda(\bar{z}_{0'}) \operatorname{tg} \theta}{2} (\bar{z} - \bar{z}_{0'});$$

$$\bar{h}(\bar{z}_2) = \bar{h} + \frac{\lambda_0}{2} \sin \theta - \frac{\operatorname{tg}(\beta - \theta)}{2} [\lambda(\bar{z}_{0'}) (|\bar{z}_2| + \bar{z}_{0'}) - \lambda_0 \cos \theta];$$

$$\bar{h}(\bar{z}_3) = \bar{h} - \frac{\lambda_0}{2} \sin \theta - \frac{\operatorname{tg}(\beta + \theta)}{2} [\lambda(\bar{z}_{0'}) (\bar{z}_3 - \bar{z}_{0'}) - \lambda_0 \cos \theta];$$

$$\bar{h}_m = \frac{1}{4} \frac{b_{0'}}{b_m} \left\{ 4 \frac{\lambda_0 \cos \theta}{\lambda(\bar{z}_{0'})} \bar{h} + \left[1 + \frac{b(-1)}{b_{0'}} \right] (1 - \bar{z}_s t_2) \bar{h}(\bar{z}_{m2}) + \left[1 + \frac{b(+1)}{b_{0'}} \right] (1 - \bar{z}_s t_3) \bar{h}(\bar{z}_{m3}) \right\},$$

where

$$\bar{z}_{m2} = \bar{z}_s t_2 - \frac{1 - |\bar{z}_s t_2|}{3} \frac{1 + 2 \frac{b(-1)}{b_{0'}}}{1 + \frac{b(-1)}{b_{0'}}};$$

$$\bar{z}_{m3} = \bar{z}_s t_3 - \frac{1 - \bar{z}_s t_3}{3} \frac{1 + 2 \frac{b(+1)}{b_{0'}}}{1 + \frac{b(+1)}{b_{0'}}}.$$

The value of dimensionless circulation $\bar{G}(\bar{z}_v)$ at sections of a foil with inclined stabilizers can be determined from formulas (I.84) and (I.81). If angles of attack are measured relative to an axis perpendicular to the direction of movement and lying in the plane of the middle sector of the foil, in order to take into account the effect of the angle of inclination of the stabilizer on the hydrodynamic characteristics of the foil the derivative of the coefficient of lift with respect to the angle of attack (or the magnitude of dimensionless circulation \bar{G}) of a section corresponding to the inclined stabilizer should [65 be multiplied by $\cos \beta$ and the angle of zero lift divided by $\cos \beta$.

The coefficients of lift, induced drag, and restoring moment calculated with respect to the origin of the coordinates can be determined from the formulas:

$$\left. \begin{aligned} C_{yf} &= \frac{\partial C_{yf}}{\partial \alpha} (\alpha + \alpha_{0f}), \\ \frac{\partial C_{yf}}{\partial \alpha} &= \lambda_f \int_{-1}^1 \bar{G}(\bar{z}) d\bar{z}, \\ \alpha_{0f} &= \frac{\int_{-1}^1 \bar{G}(\bar{z}) \alpha_0(\bar{z}) d\bar{z}}{\int_{-1}^1 \bar{G}(\bar{z}) d\bar{z}}, \\ \alpha_0(\bar{z}) &= \alpha_{0\infty}(\bar{z}) - \Delta \alpha_0(\bar{z}), \\ C_{xi} &= \frac{C_y^2}{\pi \lambda} \xi, \end{aligned} \right\} \quad (I.95)$$

$$\left. \begin{aligned} C_{m0} &= \frac{\partial C_{m0}}{\partial \alpha} (\alpha + \alpha_{m0}), \\ \frac{\partial C_{m0}}{\partial \alpha} &= \frac{M_0}{\rho \frac{v^2}{2} \cdot S_f l_f} = \frac{\lambda_f}{2} \int_{-1}^1 \bar{G}(\bar{z}) \bar{z} d\bar{z}, \\ \alpha_{m0} &= \frac{\Delta C_{m0}}{\frac{\partial C_{m0}}{\partial \alpha}}, \\ \Delta C_{m0} &= \frac{\lambda_f}{2} \int_{-1}^1 \bar{G}(\bar{z}) \alpha_0(\bar{z}) \bar{z} d\bar{z}. \end{aligned} \right\} \quad (I.96)$$

The system of forces can be referred more conveniently not to the origin of the fixed system of coordinates but to point O' (to the midpoint of sector 1). In this case

$$\left. \begin{aligned}
C_{m0}' &= C_{m0} - \frac{\bar{z}_0' \partial C_{yf}}{\partial \alpha} (\alpha + \alpha_0 f) = \frac{\partial C_{m0}'}{\partial \alpha} (\alpha + \alpha_{m0}'), \\
\frac{\partial C_{m0}'}{\partial \alpha} &= \frac{\partial C_{m0}}{\partial \alpha} - \frac{\bar{z}_0' \partial C_{yf}}{\partial \alpha}, \\
\alpha_{m0}' &= \frac{\frac{\partial C_{m0}}{\partial \alpha} \alpha_{m0} - \frac{\bar{z}_0' \partial C_{yf}}{\partial \alpha} \alpha_0 f}{\frac{\partial C_{m0}}{\partial \alpha} - \frac{\bar{z}_0' \partial C_{yf}}{\partial \alpha}}.
\end{aligned} \right\} \quad (I.97)$$

§9. Calculating the velocity corresponding to the limit of subcavitating flow around a hydrofoil [66]

When designing hydrofoils it must be borne in mind that under certain conditions a cavitation cavity will form in the liquid flowing around a foil and this will disrupt continuity of flow. Cavitation can lead to undesirable consequences such as loss of lift, shift in center of pressure, reduction in lift-drag ratio, and also foil erosion damage.

Significant reduction in the lift-drag ratio of a foil occurs only with strongly developed cavitation when the cavitation cavity extends beyond the limits of a foil profile. In the initial stage when the cavity is confined to the profile the foil lift is not reduced but if the velocity field is variable erosion damage to the foil can occur. Cavitation on a foil of ordinary (streamlined) profile is generally considered to be impermissible and, if it cannot be avoided, the foil should be made supercavitating, utilizing for this purpose special profiles over the entire upper side of which the flow separates.

For depth-effect foils cavitation is impermissible in principle. A depth-effect foil which cavitates along its entire upper side loses its main property of automatic stabilization since as it approaches the free surface its lift will increase whereas the lift of a subcavitating depth-effect foil will decrease.

Determining the limiting velocity of subcavitating flow and finding ways to avoid the onset of cavitation are of practical interest.

Cavitation is usually considered to begin when the pressure at a given point on a profile reaches saturation vapor pressure, that is,

$$p = p_d.$$

In this event the dimensionless overpressure can be expressed by the formula

$$p = \frac{p_d - p_0}{\frac{1}{2} \rho v^2} = \frac{p_d - (p_0 + \gamma h)}{\frac{1}{2} \rho v^2}.$$

Designating a negative pressure the coefficient of pressure drop $\xi = -p$, we obtain the condition for onset of cavitation in the form

$$\xi_{\max} = \frac{p_a - p_d + \gamma h}{\frac{1}{2} \rho v_k^2}, \quad (I.98)$$

where ξ is the maximum ordinate of pressure drop on a profile at a given angle of attack and v_k is the velocity of onset of cavitation.

Considering that $\kappa = \frac{p_a - p_d}{\frac{1}{2} \rho v^2}$ and comparing it with the [67] expression for \bar{p} , we obtain the condition for onset of cavitation in another form:

$$\xi_{\max} = \kappa, \quad (I.98a)$$

that is, cavitation begins when the coefficient of pressure drop at any point on a profile becomes equal to the cavitation number κ . Solving equation (I.98) for v_k , we obtain a formula for determining the velocity at which cavitation begins on a profile

$$v_k = \sqrt{\frac{p_a - p_d + \gamma h}{\frac{1}{2} \rho \xi_{\max}}}. \quad (I.99)$$

Hence, armed with the curve of pressure distribution over a profile we can find the place where cavitation begins for a given angle of attack and also determine the velocity at which it begins.

Depending on the nature of the flow around the leading edge of a profile and the place where the cavitation cavity for forms, the following types of cavitation can be distinguished (Fig 37):

a) cavitation on the upper (low-pressure) side of a profile beginning at the nose and occurring at rather large positive angles of attack when the zero line of the flow touches the lower side of the profile and the liquid flows around the nose from the bottom upward at great speed;

b) cavitation on the upper side beginning on the back of a profile at the point of greatest thickness and occurring in "shock-free" entry, that is, when the zero line of flow coincides with the entering edge;

c) cavitation on the lower (high-pressure) side of a profile beginning at the entering edge and occurring at negative angles of attack when the zero line of flow touches the upper side and the liquid flows around the nose from the top downward;

d) concurrent cavitation types b and c. Such cavitation occurs at small negative angles of attack.

The boundary separating the zone of subcavitating flow from the cavitation zone, that is, a curve drawn in cavitation number--angle of attack coordinates, has the form shown in Fig. 37. Curve sector AB corresponds to the start of cavitation of type a, sector BC marks the boundary of onset of type b, and curve CD the boundary of onset of type c.

Determining the boundary of cavitation of types a and c which begins at the nose of a profile based on the relation $\xi_{max} = \chi$ is very difficult since measuring or calculating the magnitude of pressure drop right at the leading edge is very complex. Determining the pressure drop ξ_{max} on the back of a profile and the velocity corresponding to onset of cavitation of type b doesn't entail any particular difficulty. It is just this case wherein a foil moves at angles of attack within the shock-free [69] entry range, making it possible to achieve the greatest velocity in subcavitating flow, that is of the greatest practical interest.

The pressure drop in an unbounded liquid which is required for calculating the velocity of onset of cavitation can be calculated, however, more complete data on the onset and development of cavitation are yielded by cavitation diagrams which are based on direct observations of the flow around profiles in cavitation tunnels. It is difficult under laboratory conditions to model cavitation on hydrofoils and observe it directly and, therefore, it is recommended that the effect of a free surface on the boundary of subcavitating flow be calculated based on an empirical relation between pressure drop and relative depth of immersion.

Fig. 38 presents cavitation diagrams of the most widely used hydrofoil profiles: two segmental profiles with relative thicknesses of 0.0385 and 0.0735, and Fig. 39 presents Falkner profile diagrams Nos. 10 and 11 which were based on the results of observations of the development of cavitation in an unbounded liquid. The contours of these profiles are shown in Fig. 40. The cavitation diagrams are drawn in the form of the relation $\alpha_{\infty} = f(\chi)$ where α_{∞} is the angle of attack of a profile of a foil of infinite span in an unbounded liquid. The upper curve, which is designated $\chi = 0$, represents a cavitation boundary of type b, the curve $\chi = 0.5$ which goes downward a boundary of type b, and the lower curve $\chi = 0$ a boundary of type c. Within these curves is a zone of subcavitating flow and outside them a cavitation zone. Within the cavitation zone are curves designated by the numbers 25, 50, 75, and 100 indicating a length of cavity along the profile equal respectively to 25, 50, 75, and 100% of profile chord..

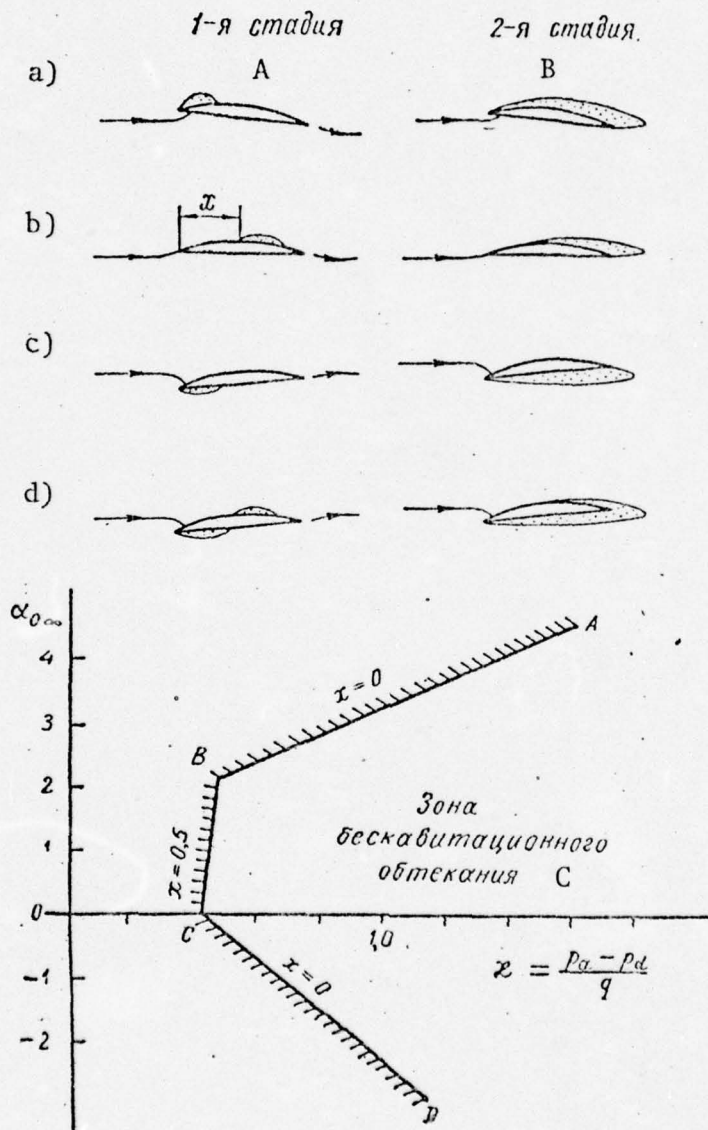


Fig. 37. Types of cavitation (a--d) and corresponding boundaries of subcavitating flow.

KEY: A--1st stage; B--2nd stage; C--zone of subcavitating flow.

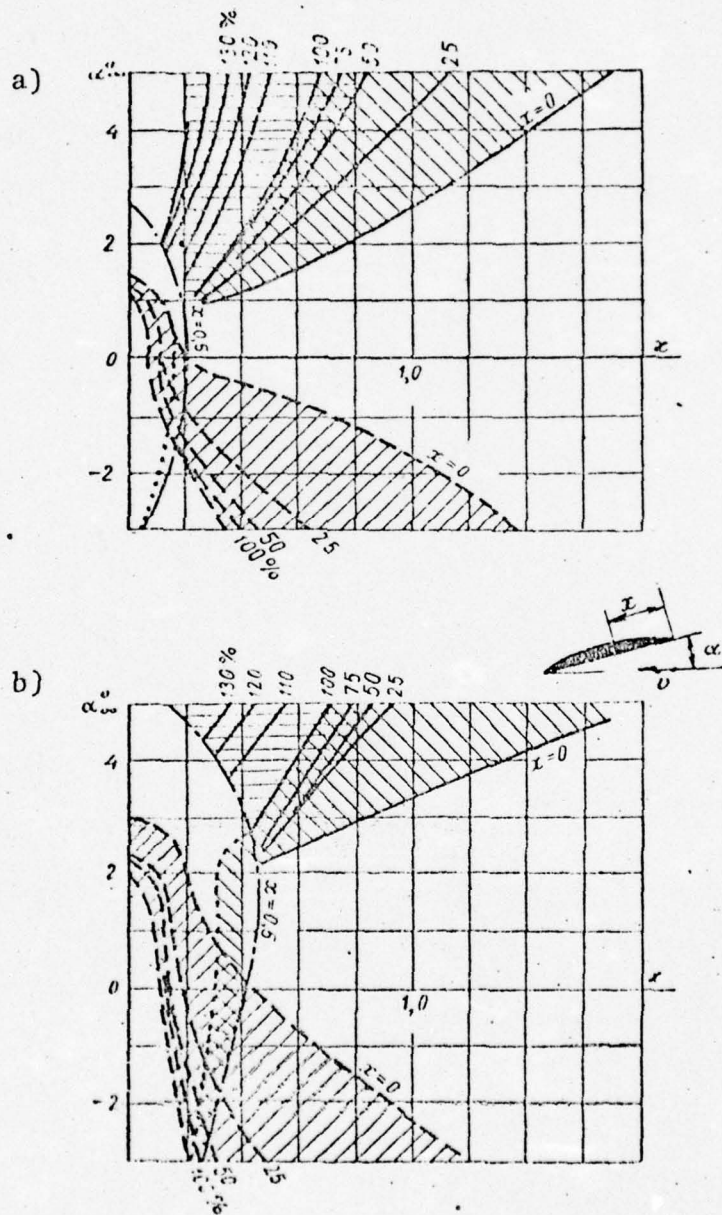


Fig. 38. Cavitation diagrams of segmental profiles:
a-- $\bar{e} = 0.0385$; b-- $\bar{e} = 0.0735$.

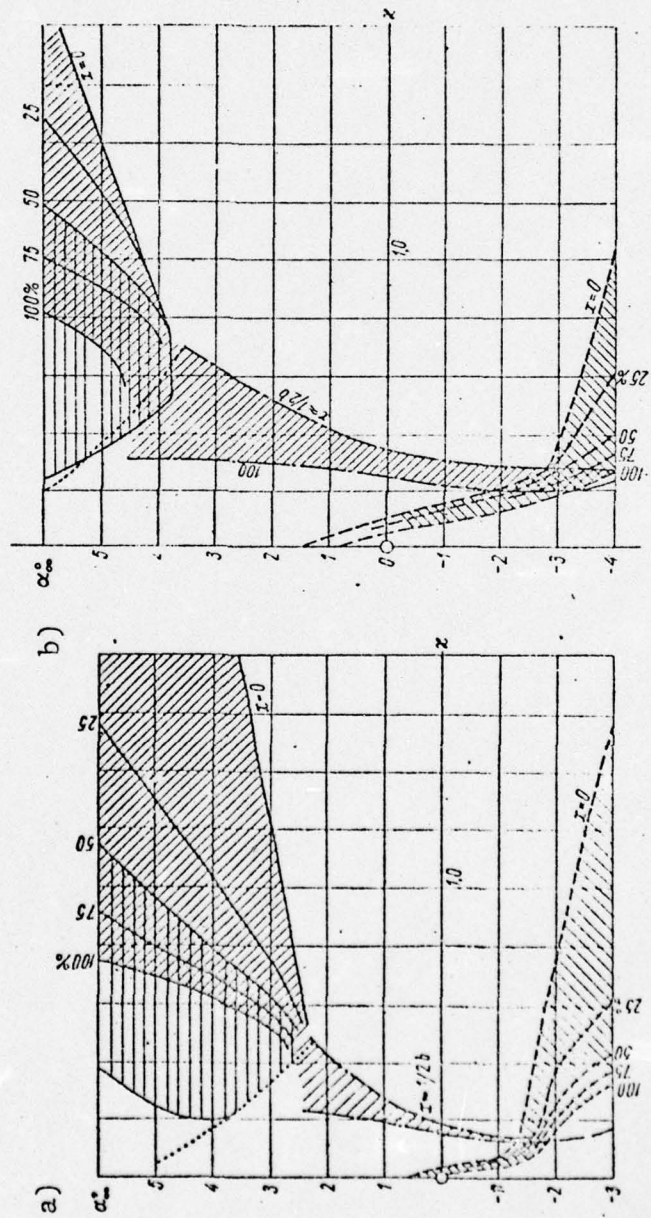


Fig. 39. Cavitation diagrams of Falkner profiles: a--No. 10, $\bar{c} = 0.0385$;
b--No. 11, $\bar{c} = 0.075$.

The velocity corresponding to the onset of cavitation in an unbounded liquid is determined from the following formula which can be derived directly from the expression for cavitation number:

$$v_k = \sqrt{\frac{p - p_d}{\frac{1}{2} \rho v_k^2}} \quad (\text{I.100})$$

Fig. 41 shows a diagram of the velocity corresponding to the onset of cavitation as determined from formula (I.100) as a function of the angle of attack for two segmental profiles and four Falkner profiles in an unbounded liquid at atmospheric pressure.

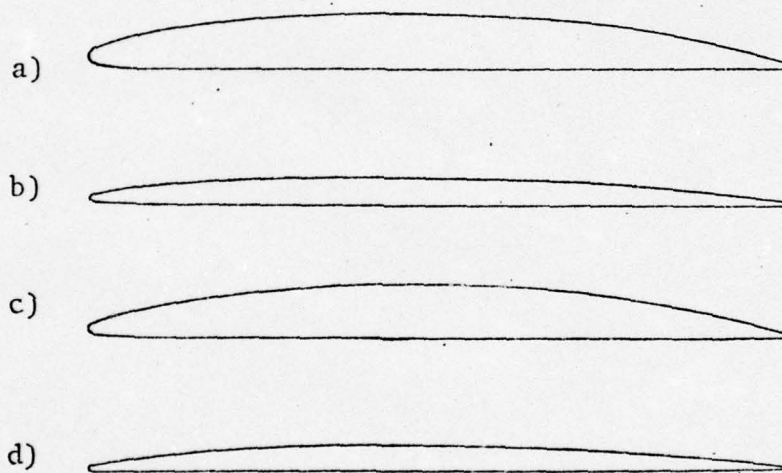


Fig. 40. Contours of Falkner profiles: a--No. 11, $\bar{c} = 0.0745$; b--No. 10, $\bar{c} = 0.0385$; c--No. 6, $\bar{c} = 0.075$; d--No. 5, $\bar{c} = 0.037$.

For analysis and convenience in use, the individual cavitation diagrams for each profile can easily be drawn in C_y/\bar{c} -- x/\bar{c} coordinates on one general diagram. Fig. 42 shows such a diagram for segmental and Falkner diagrams. It is apparent from the diagram that the Falkner and segmental profiles show practically coinciding boundaries for the onset of cavitation of type b. At the same time the range of C_y/\bar{c} between the boundaries for cavitation of types a and c is much greater for Falkner profiles than for segmental profiles. [72]

Hence, the shape of the profiles discussed here has an effect only on the range of shock-free angles of attack. The velocity of subcavitating flow corresponding to the onset of type b cavitation depends practically not at all on the shape of the profile but is determined entirely by relative thickness.

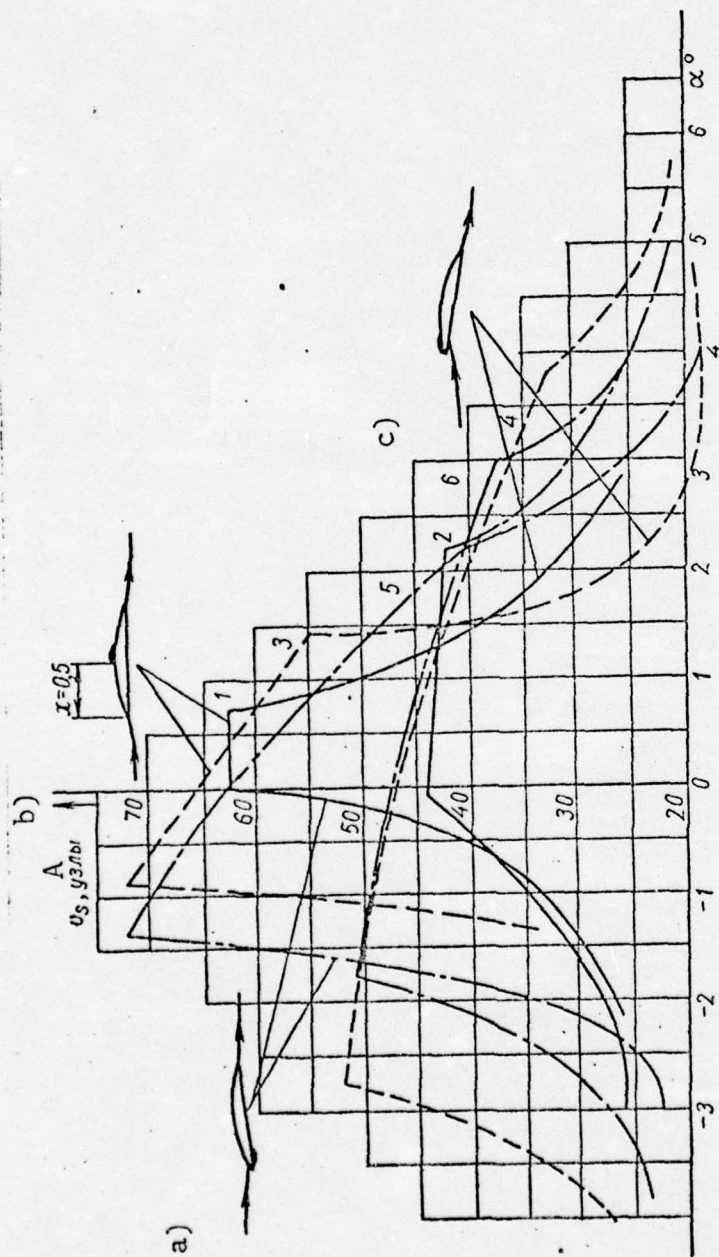


Fig. 41. Velocity corresponding to the onset of cavitation on profiles in an unbounded liquid: a--cavitation on pressure side beginning at the nose; b--cavitation on pressure drop side beginning at point of maximum thickness; c--cavitation on pressure drop side starting at nose.
Circular segment: 1-- $\bar{c} = 0.0385$; 2-- $\bar{c} = 0.0735$; 3--Falkner profile No. 5, $\bar{c} = 0.037$; 4--Falkner profile No. 6, $\bar{c} = 0.075$; 5--Falkner profile No. 10, $\bar{c} = 0.0385$; 6--Falkner profile No. 11, $\bar{c} = 0.0745$. KEY: A--knots.

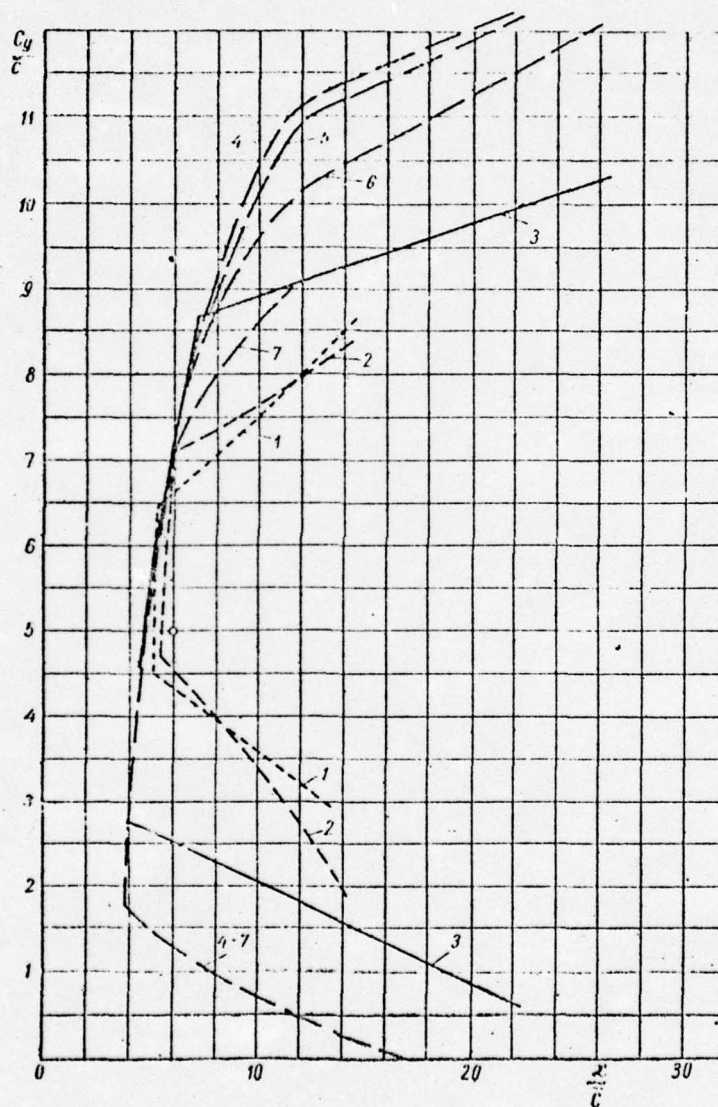


Fig. 42. General cavitation diagram.
 1--segment $\bar{\sigma} = 0.0385$; 2--segment $\bar{\sigma} = 0.0735$; 3--Falkner profiles
 Nos. 5--8; 4--7--Falkner profiles Nos. 9--13; Circle is point
 where $C_y/\bar{\sigma} = 5$ and $x/\bar{\sigma} = 6$.

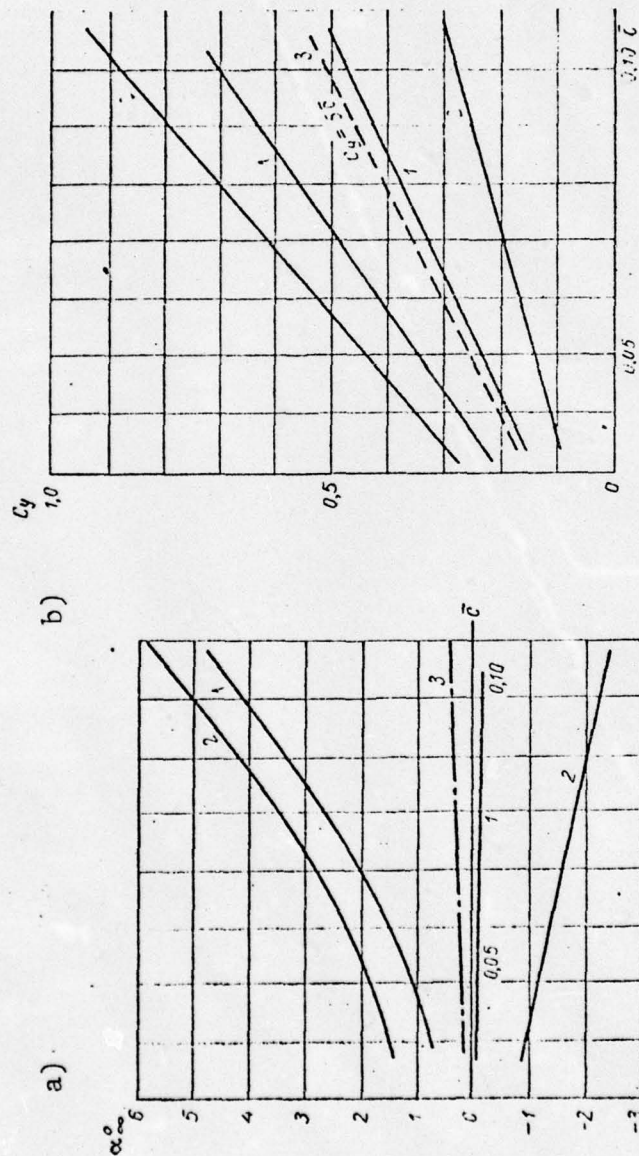


Fig. 43. Range of angles of attack for subcavitating flow around profiles when $\lambda = \infty$ (a) and corresponding values of c_y (b) as a function of c for an unbounded liquid. 1--circular segment; 2--Falkner profiles Nos. 5--8; 3--calculated $c_y = 5$.

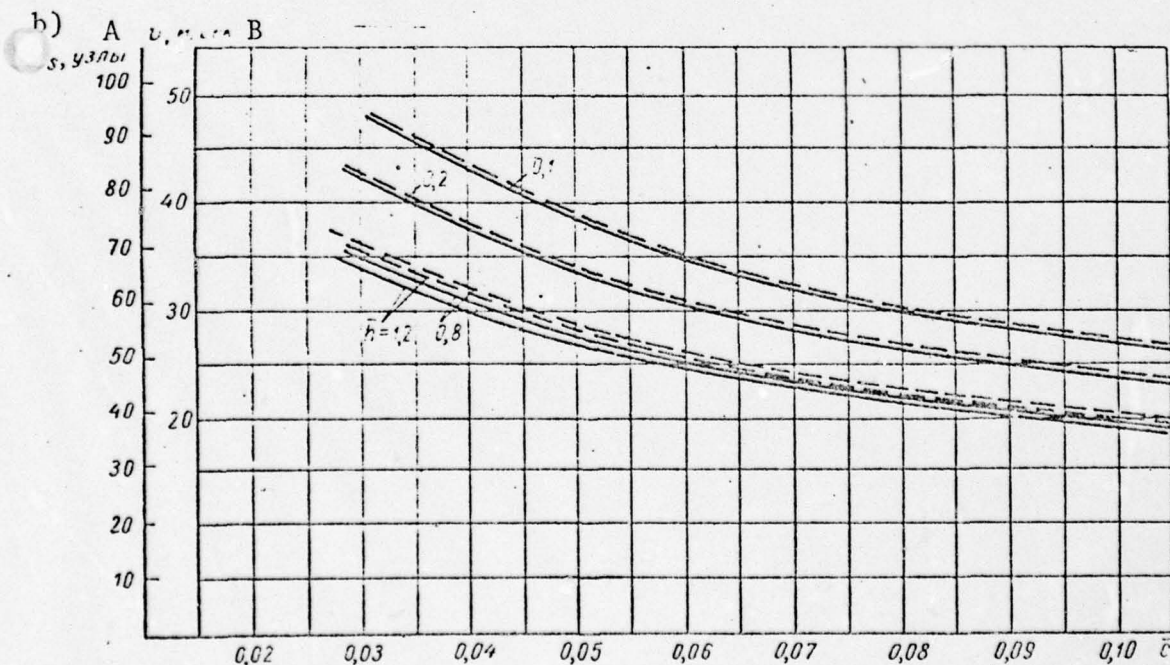
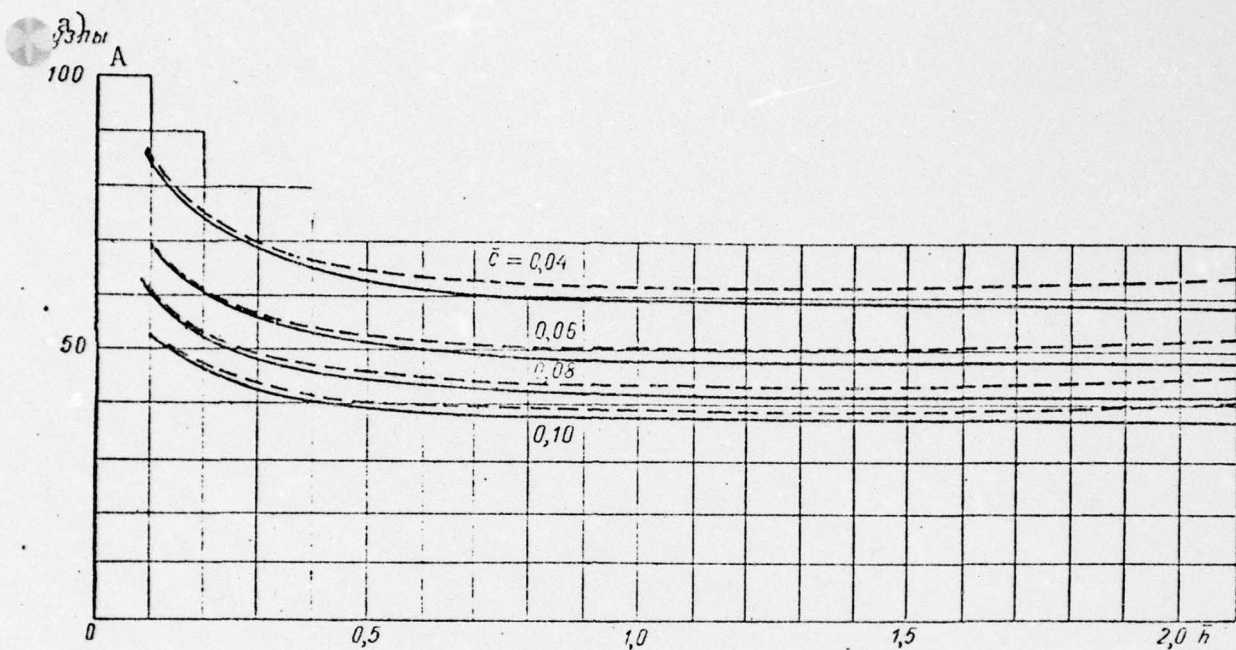


Fig. 44. Velocity of onset of cavitation at midspan of a rectangular hydrofoil: a--as a function of relative depth of immersion; b--as a function of relative foil thickness. Calculated from formula (I.104): Solid line $b = 1 \text{ m}$; broken line $b = 2 \text{ m}$. KEY: A--knots; B--m/sec.

From the data presented we can graph (Fig. 43a) the range of angles of attack of shock-free entry of a profile as a function of relative thickness for segmental and Falkner profiles. The lift coefficient at these angles of attack as a function of relative thickness is plotted in the $C_y(\alpha)$ graph shown in Fig. 43b.

It is apparent from a consideration of the general cavitation diagram in Fig. 42 that one and the same point with the following coordinates can be used for all profiles for the purpose of determining the velocity of onset of cavitation and finding the lift coefficient of a profile as a function of thickness:

$$\frac{C_y}{c} = 5; \quad \frac{\chi_k}{c} = 6. \quad (I.101)$$

Up to now we have been considering the cavitation characteristics of profiles, that is, foils of finite span under conditions of flow in an unbounded liquid. When a foil moves beneath a free surface the velocity of subcavitating flow increases and the lift coefficient generated by the foil decreases. [78]

The effect of the free surface is taken into consideration by assuming that the range of angles of shock-free entry of a foil profile beneath the free surface remains the same as in an unbounded liquid and, according to formula (I.42) the pressure drop on the upper side decreases proportionally to

$$\xi_{hmax} = \phi \xi_{\infty max}.$$

Since the pressure drop coefficient and cavitation number are equal, the value of χ_k for a hydrofoil profile at a fixed angle of attack corresponding to a cavitation boundary of type b also decreases proportionally to ϕ , that is,

$$\chi_{kh} = \phi \chi_{k\infty}. \quad (I.102)$$

By substituting χ_k from formulas (I.101) and (I.102) into (I.100) and taking into account the height of a column of water above the foil, we obtain the following approximate formula for calculating the velocity of onset of cavitation on a profile (of a foil of finite span) beneath a free surface:

$$v_{kh} = \sqrt{\frac{p_a - p_d + \gamma h_b}{0.5 \rho \cdot 6 \epsilon \eta}} \quad m/sec. \quad (I.103)$$

Furthermore, for a foil of finite span uniformity of lift distribution over the span should be taken into account. The greatest local value of the lift coefficient of a rectangular foil lies at the midpoint of the span and is equal to

$C_{ysec} = 1.14C_{yf}$ (see Fig. 17). Assuming that the local value of ξ_{max} increases in the same ratio, we obtain the formula for calculating v_{kh} for a rectangular foil in the form

$$v_{kh} = \sqrt{\frac{p_a - p_d + \gamma h b}{0.5\rho \cdot 1.14\phi \cdot 6c}} \text{ m/sec.} \quad (I.104)$$

In Fig. 44 a and b are diagrams of the velocity of onset of cavitation for a rectangular hydrofoil which are based on calculations made with formula (I.104) for two values of foil chord, 1 m and 2 m. By using these diagrams we can evaluate approximately the velocity of onset of cavitation on a foil for a given relative thickness and, conversely, we can determine the permissible relative thickness necessary for ensuring subcavitating flow around a hydrofoil at a given maximum velocity.

As can be seen in Fig. 44 at small relative depths of immersion the velocity of onset of cavitation rises sharply. The use of depth-effect foils ($\bar{h} = 0.1--0.2$) makes it possible to delay the velocity of onset of cavitation by up to 20 knots.

§10. Recommendations as to selection of profile and area of a hydrofoil [79]

Based on the above presentation recommendations can be offered as to the selection of the shape of a profile and its relative thickness and as to determination of the lift area of a subcavitating hydrofoil.

The profile of a subcavitating hydrofoil must:

- 1) be free of cavitation at the greatest possible velocity and over the greatest possible range of angles of attack;
- 2) prevent the occurrence of stall on the upper surface over the greatest possible range of angles of attack when moving in direct proximity to the surface of the water and when piercing it;
- 3) have the highest possible lift-drag ratio.

The main parameters on which meeting the above demands depends in large measure are the relative thickness and shape of the profile, area of the lift surface (correct selection ensures the proper angle of attack), depth of immersion of the foil beneath the free surface of the water, and sweepback in the plan.

The shape of a profile must ensure the fullest and smoothest (no peaks) possible pressure gradient curve on the upper side (low-pressure side). A Falkner profile or segmental profile that is plano-convex or close to it meets these demands better than others. The shape of Falkner profiles is very

close to that of a theoretical profile with a given constant pressure on the upper side. They are characterized by a flat lower side, a slightly raised and rounded nose, and a maximum thickness near midchord. Their chief advantage over segmental profiles is their more than doubled range of subcavitating angles of attack. Profiles of the Falkner type are recommended only for deeply submerged foils; for depth-effect or surface-piercing foils they are unsuitable since their rounding leading edges engender stall.

It is recommended that sharp-edged profiles with their lower side flat and their maximum thickness located about 0.4 chord back from the nose be used for surface-piercing and depth-effect foils.

Plano-convex segmental profiles can also be used. As tests show, due to the increase in curvature of the camber line at the leading edge the range of angles of stall-free flow around them is greater than around segmental foils.

The relative thickness of a foil is selected based on absence of cavitation. The following formula which was obtained from (I.104) for a velocity corresponding to the onset of cavitation of a foil of finite span rectangular in the plan can be used to make approximate calculations of relative thickness: [80]

$$c \approx \frac{p_a - p_d + \gamma h}{3.4 \rho v_{\max}^2 \cdot \varphi} \quad (\text{I.105})$$

Diagrams of velocity corresponding to the onset of cavitation can also be used for determining the thickness of a profile (Fig. 44).

We will point out that formula (I.105) includes the factor 3.4 in the denominator which allows for the local increase in C_y at midspan on a rectangular foil.

Calculations based on (I.105) yield the greatest permissible profile thickness based on avoidance of cavitation at a given speed. The least possible relative thickness of a foil profile is based on considerations of strength. For the designs and materials now in use this thickness is close to $\bar{c} = 0.04$. At this thickness the greatest permissible velocity of subcavitating flow of a deeply submerged foil is about 60 knots and for a depth-effect foil about 80 knots. It must be remembered that decreasing the relative thickness of a foil for the purpose of increasing the velocity of subcavitating flow leads to a reduction in the range of angles of subcavitating flow and as a result there may be a sharp reduction in seakeeping characteristics of a craft. There is no need to

use profiles thinner than those required based on considerations of cavitation since decreasing the thickness further merely leads to a decrease in the resulting range of angles of attack.

The calculated lift coefficient and therefore the area of the lift surface of a foil is selected based on the requirement that at all operational modes the true angle of attack of any foil section must not lie outside the zone of subcavitating angles of attack. Typical values of these angles and corresponding values of C_y plotted as a function of profile relative thickness (foil of finite span) for an unbounded liquid are shown by the curves in Fig. 43b which were drawn from cavitation diagrams. The angles of attack of subcavitating flow around a profile (when $\lambda = \infty$) for a foil of finite span are determined based on the assumption that they are the same in an unbounded liquid and beneath a free surface. Sequential change in $C_y(\alpha)$ of a profile in an unbounded liquid in transition to a profile beneath a free surface and then to a foil of finite span beneath a free surface is shown in Fig. 45.

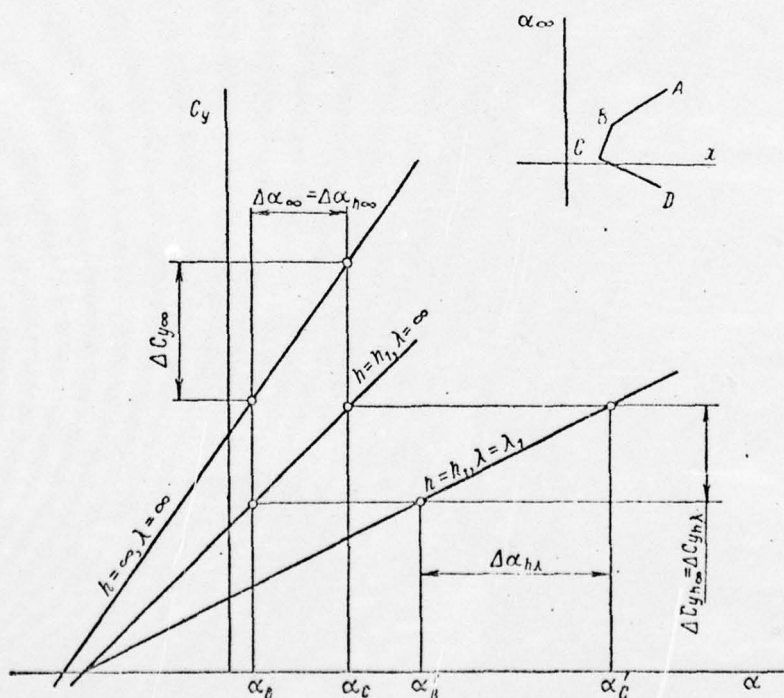


Fig. 45. Change in range of geometric angles of attack of subcavitating flow in transition from a profile in an unbounded liquid to a hydrofoil of finite span.

By assuming equality between angles of attack of a profile in an unbounded liquid and beneath a free surface and using Fig. 45 we can find the relation between angles of attack

∞ and the lift coefficient $C_{y\infty}$ of a profile in an unbounded liquid, on the one hand, and between these same characteristics for a hydrofoil of finite span on the other.

When $\alpha_{h\infty} = \alpha_\infty$

[81]

$$\left. \begin{aligned} C_{y\infty} &= a_\infty (\alpha_\infty + \alpha_0), \\ C_{yh\infty} &= \gamma a_\infty (\alpha_\infty + \alpha_0 - \Delta\alpha_0), \\ C_{yh\infty} &= \gamma C_{y\infty} \left(1 - \frac{\Delta\alpha_0}{\alpha_\infty + \alpha_0}\right). \end{aligned} \right\} \quad (I.106)$$

whence

Based on the hypothesis of flat sections

$$C_{yh\lambda} = C_{yh\infty} \quad \text{when} \quad \alpha_{h\infty} = \alpha_{h\lambda} - \Delta\alpha_{\lambda h}.$$

Since
obtain

$$\Delta\alpha_{\lambda h} = \frac{1}{\pi\lambda} \zeta C_{yh}, \quad \text{taking (I.106) into account we}$$

$$\alpha_{h\lambda} = \alpha_\infty + \gamma \frac{a_\infty}{\pi\lambda} \zeta (\alpha_\infty + \alpha_0 - \Delta\alpha_0). \quad (I.107)$$

The subscripts used for C_y and α have the following meanings: ∞ for a profile in an unbounded liquid ($h = \infty$, $\lambda = \infty$); $h\infty$ for a profile beneath a free surface ($h = h_1$, $\lambda = \infty$); $h\lambda$ for a hydrofoil of finite span ($h = h_1$, $\lambda = \lambda_1$).

[82]

The values of coefficient C_{yh} for $C_{y\infty} = 5$ at different depths of immersion are determined from the graph in Fig. 46 for $C_{yh\infty} = f(\bar{\sigma})$ which was drawn based on calculations made with formula (I.106).

Fig. 47 shows a graph for the relation $C_{yh}/C_{y\infty}$ for $\bar{\sigma} = 0.06$ which shows the free-surface effect on the lift coefficient of a given foil.

The geometric angle of attack of a hydrofoil of finite span is greater compared with that of a profile in an unbounded liquid α_∞ . As calculations made with formula (I.107) show, the change in angle of attack is due mainly to the effect of the finiteness of a span and depends almost not at all on depth of immersion. For example, when $\lambda = 5$ the magnitude of $\gamma \frac{a_\infty}{\pi\lambda} \zeta$ in front of the parentheses in the second term of formula (I.107) in the range $\bar{h} = 0.1--1$ remains practically constant and is equal to about 0.4. The corresponding increase in geometric angle of attack with an aspect ratio of $\lambda = 5$ when $\bar{\sigma} = 0.05$ is about 1° .

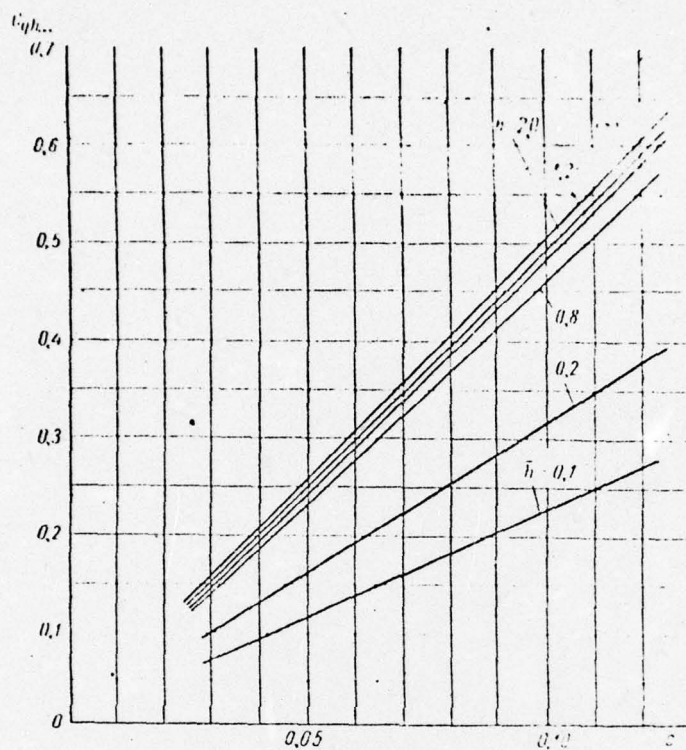


Fig. 46. Effect of free surface on calculated lift coefficient corresponding to the boundary of subcavitating flow around a profile ($\lambda = \infty$).

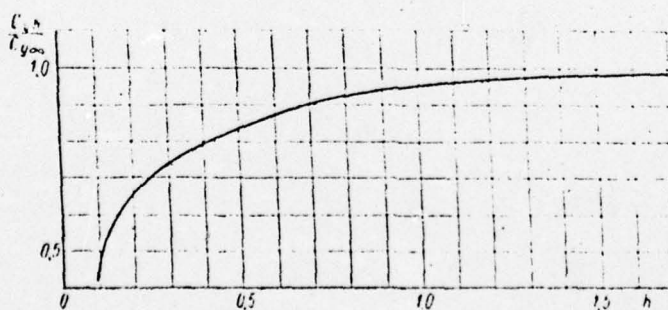


Fig. 47. Relation between calculated lift coefficient and depth of immersion on the boundary of subcavitating flow for a profile with a relative thickness of $\epsilon = 0.06$.

The ratio between the ranges of angles of shock-free entry $\Delta\alpha_{h\lambda}/\Delta\alpha_\infty$ and therefore the ratio $\Delta C_{yh\lambda}/\Delta C_{y\infty}$ for a hydrofoil and profile in an unbounded liquid can be determined from the following relations:

$$\Delta C_{yh\lambda} = \gamma \Delta C_{y\infty}, \quad (I.108)$$

$$\Delta\alpha_{h\lambda} = \Delta\alpha_\infty \left(1 + \gamma \frac{\alpha_\infty}{\alpha_0} \zeta\right). \quad (I.109)$$

As can be seen from (I.108), the range of change in $\Delta C_{yh\lambda}$ within the limits of angles of shock-free entry is less for a hydrofoil than for a profile in an unbounded liquid. The range of angles of attack of shock-free entry is always greater for a hydrofoil of finite span than for a profile in an unbounded liquid. As calculations show, the range of angles $\Delta\alpha_{h\lambda}$ of a foil with an aspect ratio of $\lambda = 5$ at a depth of immersion of $h = 0.1-1$ is approximately 38--43% greater than the range of $\Delta\alpha_\infty$. As a consequence of the fact that the effects of the parameters γ and ζ are mutually exclusive the increment $\Delta\alpha_{h\lambda}$ is practically constant and differs little from the increment when $h \rightarrow \infty$, being equal to about 35° .

By using formula (I.104) for v_{kh} and formulas (I.106) and (I.101) for C_{yh} and $C_{y\infty}$, it is possible to determine the specific load on one square meter of foil lift area corresponding to the limiting velocity of subcavitating flow:

$$\frac{Y}{S} = C_{yh} \frac{1}{2} \rho v_{kh}^2 = \gamma(h) \frac{p_a - p_d + \gamma h b}{1.37 \eta} \left(1 - \frac{\Delta\alpha_0}{\alpha_\infty + \alpha_0}\right). \quad (I.110)$$

Fig. 48 shows a graph of specific load for two values of chord, $b = 1 \text{ m}$ and $b = 2 \text{ m}$, as calculated with formula (I.110).

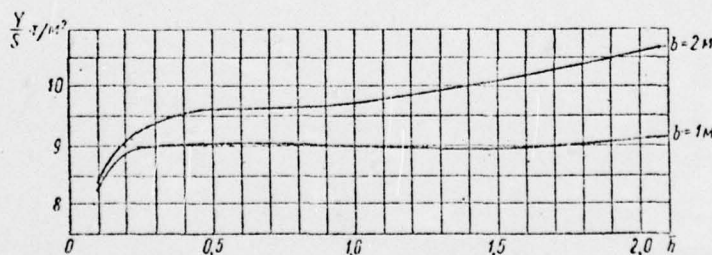


Fig. 48. Greatest permissible specific load of a rectangular hydrofoil corresponding to the limiting velocity of subcavitating flow.

It is interesting to note that at the velocity corresponding to the onset of cavitation at the boundary of cavitation of type δ ($\chi = 6\sigma$) with a lift coefficient corresponding to the calculated point ($C_{y\infty} = 5\sigma$) the permissible specific

load Y/S is the same for profiles of any thickness and depends practically not at all on the relative depth of immersion, while at the same time C_{yh} as the profile draws closer to the free surface is cut in half (Figs. 47 and 48). So, for $b = 1 \text{ m}$ when $0.3 < \bar{h} < 2$ $Y/S \approx 9000 \text{ kgf/m}^2 = \text{const}$ and only when $\bar{h} = 0.1$ does it decrease to 8300 kgf/m^2 . When $b = 2 \text{ m}$ Y/S changes within the limits $9500-10,000 \text{ kgf/m}^2$.

The indicated values of specific load are for that case when the relative thickness is determined for a foil operating at the boundary of cavitation of the second type. Under actual conditions specific loads can differ markedly from what is indicated. For example, the specific load on the bowfoil on the Raketa is only about 2300 kgf/m^2 and on the sternfoil about 3000 kgf/m^2 . This great difference can be explained by the fact that the relative foil thickness of 0.06 which is used is much smaller than what is permissible based on considerations of cavitation which with respect to the cavitation boundary is more than 0.2.

§11. The effect of sweepback on lift and velocity of sub-cavitating flow around a hydrofoil

It was indicated in the preceding section that the use of depth-effect foils makes it possible to greatly increase the velocity of subcavitating flow around a hydrofoil. However, this entails impairment of the seakeeping characteristics of hydrofoil craft.

It is better for seagoing craft to increase the velocity [85] of subcavitating flow by imparting sweepback to the foils, thus improving rather than impairing seakeeping characteristics.

In determining the hydrodynamic characteristics of a sweptback foil a procedure similar to the hypothesis of flat sections is employed.

We will consider the flow around an element of a sweptback foil (Fig. 49a) of rather great span to be identical to the flow around a slant foil (Fig. 49b) which has the same chord and angle of attack and whose angle of slant is the same as the angle of sweepback. The characteristics of a slant foil can be simply and clearly determined from a comparison of the flow around it and the flow around a straight foil.

Let a slant foil move at a velocity v_e at an angle of slant of χ to the direction of movement (Fig. 49b). The velocity of the oncoming flow v_e can be broken down into components--one parallel to the span $v_e \sin \chi$ and one perpendicular to the span $v_e \cos \chi$. The first component does not disrupt boundary conditions on the surface of the foil and its trailing edge and therefore it can be neglected in making calculations of

pressure and lift.

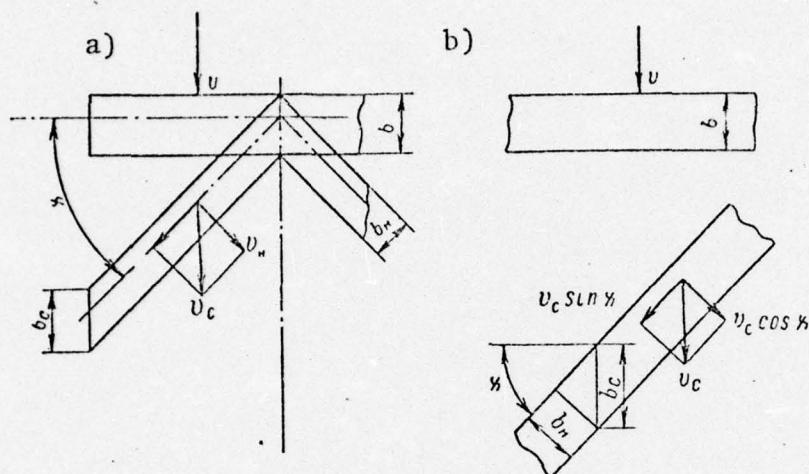


Fig. 49. Geometry of a sweptback foil and breakdown of velocity of flow into components: a--sweptback foil; b--slant foil.

In order to compare the flow around straight and slant foils further it is necessary to stipulate methods for determining the profile of a sweptback foil. The profile of a foil obtained by passing a plane perpendicular to the lift line will be called normal and all elements of it and also the projection of velocity onto this plane will be indicated with the subscript "n." A profile in a plane parallel to the line of movement will be called a flow profile and its characteristics indicated with the subscript "c." The following relations are apparent between the geometric characteristics of the normal and flow profiles: [86]

$$\left. \begin{aligned} b_n &= b_c \cos \chi; & \bar{c}_n &= \frac{\bar{c}_c}{\cos \chi}; & \alpha_n &= \frac{\alpha_c}{\cos \chi}; \\ \bar{l}_n &= \frac{\bar{l}_c}{\cos \chi}; & \alpha_{0n} &= \frac{\alpha_{0c}}{\cos \chi}. \end{aligned} \right\} \quad (\text{I.111})$$

We will consider the flow around a slant foil in the simplest case when the normal profile coincides with the profile of a straight foil.

Postulating that if the angle of attack of a straight foil is equal to the angle of attack of a normal profile of a slant foil, that is, if

$$\alpha = \alpha_n = \frac{\alpha_c}{\cos \chi},$$

then the following relation must hold:

$$\frac{\Delta v_c}{v_c \cos \chi} = \frac{\Delta v}{v}, \quad (\text{I.112})$$

where Δv_c is the increment of velocity of flow around a normal profile of a slant foil coinciding in direction with the normal component of velocity and Δv is the corresponding increment of velocity of flow around a straight foil.

The pressure distribution over the surface of a slant foil of infinite aspect ratio can be determined by using the Bernoulli equation. Despite the fact that the velocity component along a slant foil $v_c \sin \chi$ does not violate boundary conditions on a foil, when writing the Bernoulli equation obviously it must be taken into account:

$$p_0 + \frac{\rho v_c^2}{2} = p_c + \frac{\rho}{2} [(v_c \cos \chi + \Delta v_c)^2 + v_c^2 \sin^2 \chi].$$

Now it is easy to determine the pressure coefficient

$$\begin{aligned} \bar{p}_c &= \frac{p_c - p_0}{\frac{\rho v_c^2}{2}} = 1 - \frac{1}{v_c^2} [(v_c \cos \chi + \Delta v_c)^2 + v_c^2 \sin^2 \chi] = \\ &= -\frac{2\Delta v_c}{v_c} \cos \chi - \left(\frac{\Delta v_c}{v_c}\right)^2. \end{aligned}$$

Using relation (I.112) we obtain

$$\bar{p}_c = -\frac{\Delta v}{v} \left(2 + \frac{\Delta v}{v}\right) \cos^2 \chi. \quad (\text{I.113})$$

Completely analogously, for a straight foil [87

$$\bar{p} = -\frac{\Delta v}{v} \left(2 + \frac{\Delta v}{v}\right). \quad (\text{I.114})$$

Hence,

$$\bar{p}_c = \bar{p} \cos^2 \chi. \quad (\text{I.115})$$

and since the lift coefficient of a profile can be expressed by the integral

$$C_y = \oint \bar{p} d\bar{x},$$

where $\bar{x} = x/b$, consequently,

(I.116)

In this case

$$C_{yc} = C_y \cos^2 \chi.$$

and similarly

$$\left. \begin{aligned} \alpha_c &= \alpha \cos \chi \\ \alpha_{0c} &= \alpha_0 \cos \chi. \end{aligned} \right\}$$

(I.117)

From the last two relations it follows that

$$\left(\frac{\partial C_y}{\partial \alpha} \right)_c = \frac{\partial C_y}{\partial \alpha} \cos \chi. \quad (I.118)$$

By using the relations found it is easy to obtain theoretical formulas for determining lift coefficients and the induced drag for a sweptback hydrofoil of finite span

$$C_{yhc} = \frac{\gamma a_\infty \cos \chi}{1 + \frac{\gamma a_\infty \cos \chi}{\pi \lambda} (1 + \tau) \xi \left(\frac{\bar{h}}{\lambda} \right)} (\alpha + \alpha_{0c} - \Delta \alpha_{0hc}); \quad (I.119)$$

$$C_{xc} = \frac{C_{yhc}^2}{\pi \lambda} (1 + \delta) \xi \left(\frac{\bar{h}}{\lambda} \right), \quad (I.120)$$

where $a_\infty = \left(\frac{\partial C_y}{\partial \alpha} \right)_{\substack{h=\infty \\ \lambda=\infty}}$ for a normal profile; $\gamma(\bar{h})$ is determined from depth of immersion referred to the normal chord; and α_{0c} and $\Delta \alpha_{0hc}$ are found from the corresponding characteristics of a normal profile.

Calculations performed with formula (I.119) yield a somewhat exaggerated effect of sweepback. The experimental value of $(\delta C_{yc} / \delta \alpha)_{h=\infty}$ is somewhat greater than that obtained from calculations.

If the velocity corresponding to the onset of cavitation of a profile (a straight foil) is known, the velocity of onset of cavitation of a slant foil can be determined from the condition of equality between absolute pressures, that is:

$$p_c - p_0 = \bar{p}_c - \frac{\rho v_c^2}{2} = p - p_0 = \bar{p} - \frac{\rho v^2}{2}.$$

Utilizing this equation and relations (I.115) we can express the velocity corresponding to the onset of cavitation of a slant foil in terms of the velocity of the profile

[88]

$$v_{kc} = v_k \sqrt{\frac{\bar{p}}{p_c}} = \frac{v_k}{\cos \chi}. \quad (I.121)$$

We will now consider another case when a flow profile of a slant foil coincides with the profile of a straight foil.

Since the normal profile of a slant foil and its angle of attack will now be different from that of a foil with no slant, in the general case it is impossible to obtain the given characteristics for a slant foil directly from the usual cavitation characteristics of a foil profile. Therefore, it is first necessary to determine by any existing method for any given c_n , f_n , and α_n the induced velocities Δv on a normal profile and then, using the Bernoulli equation, to determine p_c .

Indeed, if Δv is the induced velocity at a certain point on a profile of a straight foil, then $v + \Delta v$ is the total velocity at the given point. Then from the Bernoulli equation

$$p_0 + \frac{\rho v^2}{2} = p + \frac{\rho}{2} (v + \Delta v)^2.$$

After the necessary transformations we obtain a formula for determining the relative excess pressure on a profile of a straight foil

$$\bar{p} = \frac{p - p_0}{\rho \frac{v^2}{2}} = -\frac{\Delta v}{v} \left(2 + \frac{\Delta v}{v} \right) \quad (\text{I.122})$$

and correspondingly for a slant foil

$$\bar{p}_c = -\frac{\Delta v}{v} \left(2 + \frac{\Delta v}{v} \right) \cos^2 \chi. \quad (\text{I.123})$$

The condition for onset of cavitation will be

$$\kappa_k = -\bar{p}_c.$$

If cavitation diagrams are available for a profile coinciding with a normal one, that is, if it is possible to determine the cavitation number κ_k corresponding to the onset of cavitation for this profile for an angle of attack α_n , then the induced velocity in the zone of greatest pressure drop can be found as follows:

$$\bar{p} = -\frac{\Delta v}{v} \left(2 + \frac{\Delta v}{v} \right) = -\kappa_k.$$

Consequently,

$$\frac{\Delta v}{v} = -1 + \sqrt{1 + \kappa_k}. \quad (\text{I.124})$$

Considering that $v = v_c \cos \chi$, we can easily obtain

$$\bar{p}_c = -\left[2 \left(\sqrt{1 + \kappa_k} - 1 \right) (1 - \cos \chi) + \kappa_k \cos \chi \right] \cos^2 \chi. \quad (\text{I.125})$$

In one particular case of interest when the edge angle of [89] attack of a slant foil is close to zero and, consequently, $\alpha_e \approx \alpha$ we can obtain a direct tie between the maximum velocities of subcavitating flow for slant and straight foils if the profile of the latter coincides with the flow profile of the slant foil. The assumption is made that the velocities induced on the surface of two profiles in one and the same family are related by $\Delta v_1/v_1 : \Delta v_2/v_2 = q$, where q is a constant defining the ratio between profile ordinates at equal abscissa \bar{x} ,

$$q = \frac{\bar{y}_1}{\bar{y}_2}.$$

This assumption can be made because, as indicated in §9, regardless of the relative thickness of a profile \bar{c} the ratio x_k/\bar{c} is constant and close to 6. This holds for segmental profiles as well as for Falkner profiles but only at small positive angles of attack when cavitation starts on the back of a profile.

Using formula (I.24) and assuming that $x_k = 6\bar{c}$, we obtain

$$\frac{\Delta v}{v} \approx -1 + \sqrt{1 + 6\bar{c}} \approx 2,5\bar{c}. \quad (\text{I.126})$$

Consequently,

$$\frac{\Delta v_1}{v_1} : \frac{\Delta v_2}{v_2} \approx \frac{\bar{c}_1}{\bar{c}_2}.$$

Calculations of potential flow around profiles for several particular cases also point to the same conclusion. If a normal profile of a slant foil and a profile of an ordinary foil coinciding with a flow profile are regarded as profiles of one family, then

$$\frac{\Delta v_c}{v_c \cos \chi} : \frac{\Delta v}{v} = \frac{\bar{l}}{\bar{l}_n} = q.$$

Since

$$\bar{l} = \bar{l}_n \cos \chi \quad \text{or} \quad q = \frac{1}{\cos \chi},$$

$$\frac{\Delta v_c}{v_c} = \frac{\Delta v}{v},$$

(I.127)

Using this relation and the formulas obtained earlier

$$\bar{p} = -\frac{\Delta v}{v} \left(2 + \frac{\Delta v}{v} \right), \quad \bar{p}_c = -\frac{\Delta v_c}{v_c} \left(2 \cos \chi + \frac{\Delta v_c}{v_c} \right),$$

we can find the tie between maximum velocities of subcavitating [90]

flow around slant and straight foils:

$$\left. \begin{aligned} v_c &= v \sqrt{\frac{p}{p_c}} = v \sqrt{\frac{2 + \frac{\Delta v}{v}}{2 \cos \chi + \frac{\Delta v}{v}}} \\ \text{or} \quad v_c &= v \sqrt{\frac{2 + \frac{\Delta v_c}{v_c}}{2 \cos \chi + \frac{\Delta v_c}{v_c}}} \end{aligned} \right\} \quad (\text{I.128})$$

Considering that at the onset of cavitation at the point of greatest pressure drop $p_c = -\chi k_c$, we can find from the formula for the pressure coefficient

$$\frac{\Delta v_c}{v_c} = -\cos \chi + \sqrt{\cos \chi + \chi_{kc}}.$$

Consequently,

$$v_c \leq v \sqrt{\frac{2 - \cos \chi + \sqrt{\cos \chi + \chi_{kc}}}{\cos \chi + \sqrt{\cos \chi + \chi_{kc}}}}. \quad (\text{I.129})$$

When $\chi = 30^\circ - 50^\circ$ and $\chi_{kc} = 0.10 - 0.40$, that is, in the entire range of change in these magnitudes of interest, we can assume with sufficient accuracy for all practical purposes

$$\left. \begin{aligned} v_c &= v \sqrt{\frac{2 + \chi_{kc}}{2 \cos \chi + \chi_{kc}}} \\ \text{or even} \quad v_c &= \frac{v}{\sqrt{\cos \chi}} \end{aligned} \right\}$$

Above we considered the effect of slant on the cavitation characteristics of an infinite slant foil. But the pressure distribution and consequently the cavitation characteristics of an actual foil are affected also by the finiteness of span and a slant or sweptback foil are affected differently than an ordinary one.

Fig. 50 shows straight, slant, and sweptback foils and also the load distribution over their spans. Obviously the difference in nature of load distribution can be explained by the difference in magnitudes of velocities induced on these foils by the converging vortices. For example, for the slant foil the velocity and downwash angle at point A_1' are less and at point A_2' greater than at corresponding point A_1 on the

straight foil since the adjacent, most intensive tip vortices in the first case begin lower and in the second case higher with respect to the flow than for the straight foil. Vortices converging farther from the tips of the foil have an opposite position with respect to points A_1' and A_2' but the velocity induced by them is opposite in direction and therefore they also contribute to an increase in the load at point A_1' and a decrease at point A_2' . [91]

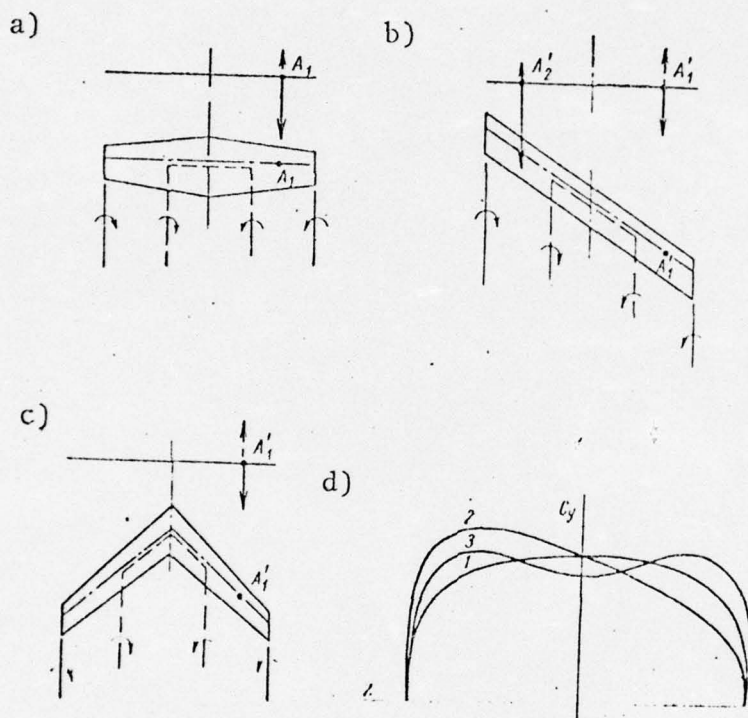


Fig. 50. Effect of sweepback on the flow around a foil of finite span. The induced velocity at corresponding points along the span: a--straight foil; b--slant foil; c--swept-back foil; d--distribution of load along the span of a swept-back and a slant foil.
1--straight foil; 2--slant foil; 3--sweptback foil.

For the same reason as with the slant foil with the swept-back foil the load increases on tips which are deflected rearward and decreases in comparison with the load in the middle of an ordinary foil. The additional increase in downwash in the middle of the sweptback foil is due to the effect of adjoining vortices which is lacking in the case of the straight foil.

The occurrence during tests of a cavitation cavity simultaneously over the entire leading edge of a sweptback foil, in distinction from an ordinary foil where cavitation

starts at midfoil, is apparently due to the strong downwash in the centerline and close-to-centerline sections of a sweptback foil, this kind of downwash compensating for the lack of slant effect, and therefore the sometimes recommended twisting of sweptback foils for the purpose of decreasing the angle of attack at midfoil doesn't appear advisable. [92]

It is natural to expect that at small angles of attack, due to the absence of slant, the middle of a foil will begin to cavitate first. However, in this case twisting a foil will apparently not produce a positive effect and may only contribute to the onset of cavitation at the nose on the high-pressure side of the foil. An increase in the velocity of subcavitating flow around the midpart of a sweptback foil at small angles of attack can be achieved by decreasing the relative thickness or decreasing the relative depth of immersion of the midpart by increasing the chord and simultaneously narrowing the foil tips.

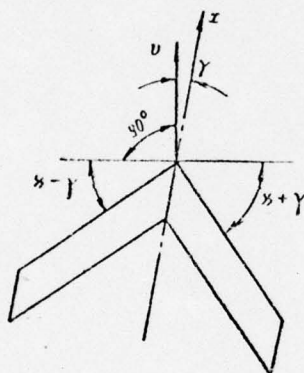


Fig. 51. Movement of a sweptback foil accompanied by drift.

Hence, with the geometric characteristics of the profiles of ordinary and slant or sweptback foils the same, the maximum velocity of subcavitating flow around the latter is significantly greater. If, for example, for ordinary relatively deeply submerged foils having the minimum relative thickness of 4% encountered in practice this velocity reaches 60 knots, the calculated velocity of subcavitating flow around a foil with an angle of slant of 45° , the normal profile remaining the same, may reach 80--85 knots.

Another advantage of a sweptback foil is that in a turn it creates a moment banking the ship in the direction of turn, thereby improving stability. The occurrence of this moment for an angle of drift γ (Fig. 51) is due to the fact that on the half of the foil on the inside of the circle the angle of slant increases from x to $x + \gamma$ and this leads to a drop in lift. On the other half of the foil the angle of slant decreases to $x - \gamma$ and this leads to an increase in lift.

Finally, the advisability of imparting sweepback to foils can be decided only after its effect on the lift-drag ratio and seakeeping characteristics of the craft and foil strength have been determined.

Experimental data show that when the profiling of ordinary and sweptback foils is the same, the lift-drag ratio of the latter is somewhat less.

In practice ordinary and sweptback or slant foils having about the same relative depth of immersion and calculated for the same load and velocity can have different relative thicknesses.

An approximate ratio between relative thicknesses which are the maximum permissible based on absence of cavitation for normal profiles of a slant and an ordinary foil can be found as follows. If $v_c = v$ and $\chi_c = \chi$, then $\bar{p}_c = \bar{p}$. We obtained earlier [93]

$$\bar{p}_c = -\frac{\Delta v_c}{v_c} \left(2 + \frac{\Delta v_c}{v_c} \right) \cos^2 \chi$$

and

$$\bar{p} = -\frac{\Delta v}{v} \left(2 + \frac{\Delta v}{v} \right).$$

Since at high speeds of movement $\Delta v/v$ and $\Delta v_c/v_c$ are small compared with 2, we can obtain

$$\frac{\Delta v_c}{v_c} : \frac{\Delta v}{v} \approx \frac{1}{\cos^2 \chi}.$$

From the ratio presented earlier

$$\frac{\Delta v_1}{v_1} : \frac{\Delta v_2}{v_2} \approx \frac{\bar{c}_1}{\bar{c}_2},$$

and inasmuch as $v = v_c$, it follows that

$$\frac{\bar{c}_2}{\bar{c}_1} = \frac{\Delta v_c}{\Delta v} = \frac{1}{\cos^2 \chi}, \text{ that is, t. e. } \bar{c}_2 = \frac{\bar{c}_1}{\cos^2 \chi}. \quad (1.131)$$

Increasing the relative thickness of sweptback foils is advisable since it makes possible increasing the range of angles of subcavitating flow and this should play a positive role during movement in a seaway and during transitional modes when the angles of attack of foils are variable and differ significantly from those calculated for full speed in calm water.

Decreasing the derivative $\partial C_y / \partial \alpha$ by introducing slant should also have a favorable effect on seakeeping characteristics since the change in angles of attack of foils due to the orbital velocity of waves will lead to a smaller change in lift. Furthermore, the great length of slant foils in the direction of movement makes them less sensitive to short waves which, especially at a small depth of foil immersion, cause sharp rolling.

The lift-drag ratio of the foils on high-speed craft at angles of attack considered permissible from the standpoint of absence of cavitation, usually $1-2^\circ$, is determined mainly by the magnitude of their area or, in other words, by the lift coefficient. As already noted, when the profiling of ordinary and slant foils is the same, the lift coefficient of the latter is smaller, since

$$\alpha_{0c} = \alpha_0 \cos \chi \text{ and } \left(\frac{\partial C_y}{\partial \alpha} \right)_c = \frac{\partial C_y}{\partial \alpha} \cos \chi.$$

If now it is assumed that $\bar{c}_n = \bar{c} / \cos^2 \chi$, then [94]
 $\alpha_{0n} = \alpha_0 / \cos^2 \chi$. Considering that $\alpha_{0c} = \alpha_{0n} \cos \chi$, we obtain

$$\alpha_{0c} = \frac{\alpha_0}{\cos \chi}.$$

Taking into account that $\partial C_y / \partial \alpha$ depends almost not at all on relative foil thickness, we can write

$$C_{yc} = \frac{\partial C_{yc}}{\partial \alpha} (\alpha_{0c} + \alpha_c) = \frac{\partial C_{yc}}{\partial \alpha} (\alpha_0 + \alpha_c \cos \chi). \quad (1.132)$$

Hence, at a zero edge angle of attack ($\alpha_c = 0$) the lift coefficients of slant and ordinary foils coincide if these foils have the same maximum pressure drop coefficient. At the small positive angles of attack which occur in practice C_{yc} can be somewhat smaller than C_y (Fig. 52). Considering that friction drag, which depends on foil area, accounts for the greater part of foil drag at small angles of attack, imparting sweepback to them should not lower the lift-drag ratio appreciably.

Assuming that the lift coefficient, load, span, and distance between supports in a direction perpendicular to the centerline plane are the same for slant and straight foils, it is easy to find the ratio between the stresses arising in them. The relation between distances between supports under these conditions is $l_c = l / \cos \chi$. Since $S_c = S$ then $b_n = b \cos \chi$. Furthermore, in this case $\bar{c}_n = \bar{c} / \cos^2 \chi$.

If $M_{\text{bend}} = K_1 l Y$ and $W = K_2 b c^2 = K_2 b^3 c^2$, where K_1 and [95]

K_2 are coefficients of proportionality, then

$$\frac{\sigma_c}{\sigma} = \frac{l_c b^3 c^2}{l b^3 c^2 n} = 1. \quad (1.133)$$

Therefore, under the same conditions with respect to cavitation, slant and straight foils have about the same bending strength.

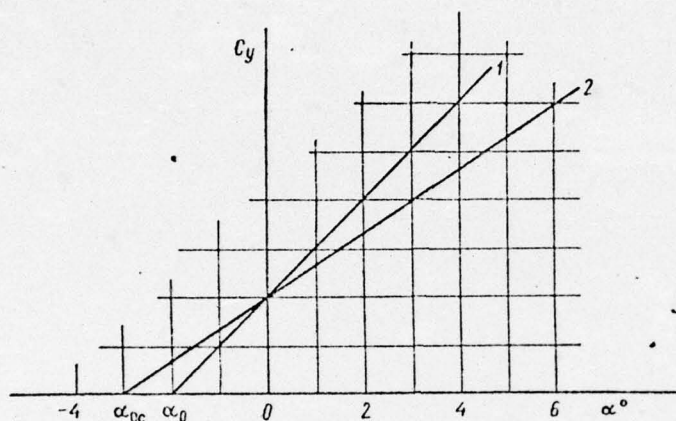


Fig. 52. Lift coefficient of a sweptback foil as a function of angle of attack.

--straight foil; 2--sweptback foil.

Hence, imparting sweepback to foils makes it possible to delay the onset of cavitation and improve seakeeping and also maneuvering capabilities of hydrofoil craft. This can be achieved without significantly changing foil drag or strength characteristics.

§12. Some data on the hydrodynamic characteristics of supercavitating and ventilating profiles

When achieving a given speed of movement with subcavitating flow around the foils becomes impossible for a high-speed craft, it is best to employ foils with supercavitating profiles. By supercavitating is meant profiles in which the low-pressure side is completely covered by a cavitation cavity which extends beyond the trailing edge and the lift is created only by the pressure on the high-pressure side.

The main demands made of supercavitating foil profiles first formulated by Academician V. L. Pozdnyunin [10] in 1945 are the following:

a) they must provide for rapid transition to a supercavitating mode so as to rapidly bypass the first stage of cavitation which is harmful with respect to erosion;

b) their high-pressure side, which is the working side, must not cavitate;

c) the shape of the profile must provide for a high lift-drag ratio under conditions of developed cavitation for cavitation numbers ranging from 0.15 to 0.01.

For the purpose of determining the hydrodynamic characteristics of a supercavitating profile it is necessary to know the cavitation number which defines the pressure in the cavity and the pressure distribution over the high-pressure side. The low-pressure side should be profiled such that it is completely covered by the cavity, provides the required foil strength, and prevents sharp jumps in lift and drag during transition from unseparated flow to developed cavitation. These demands are met[96] by foils with a wedge-shaped profile.

The main problem of the designer is to select an optimal angle of attack and an optimal shape for the high-pressure side of the profile and also to determine the hydrodynamic forces acting on the foil.

Existing domestic and foreign theoretical and experimental research makes it possible to solve many practical problems in designing and calculating supercavitating profiles. In the case of strongly developed cavitation the coefficients of hydrodynamic forces arising on foils do not depend on the absolute pressure in the cavity or on what the cavity is filled with--vapor or air. It is only necessary that the cavitation number calculated from the pressure in the cavity correspond to that given. This makes it possible by delivering air to a cavity to model supercavitating flows at velocities much slower than those corresponding to natural cavitation. The main distinction between such "ventilated" foils and foils operating under natural cavitation is that air delivered to any point on a profile does not spread forward and so the point at which the cavity starts to form can be considered fixed. Delivery of air behind the trailing edge of a wedge-shaped profile at speeds corresponding to pre-cavitating modes of flow, which makes it possible to greatly reduce the drag, has almost no effect on lift, thereby causing a sharp rise in the lift-drag ratio at intermediate modes of movement.

Inasmuch as the main operating mode of supercavitating and ventilating foils corresponds to small cavitation numbers, the theory of jet streams in an ideal liquid can be used with sufficient accuracy to determine the forces acting on the profiles of such foils.

We will consider the flow around a thin foil of infinite span as it moves beneath the free surface of an ideal liquid at depth h and constant velocity v . The flow is accompanied by sep-

aration of the stream at an arbitrary fixed point on the low-pressure side and on the trailing edge of the high-pressure side of the profile (Fig. 53). The cavitation number is infinitesimally small ($\chi \rightarrow 0$) and the relative velocity great ($Fr \rightarrow \infty$). Consequently on the free surface and in the free streams forming the boundaries of the cavity the velocity of flow is equal to v_1 , that is, there are no induced horizontal velocities on the free surface. Such a formulation of the problem means neglecting the effect of the liquid's mass. Assuming that the induced velocities are small and that the conditions on the profile and on the boundaries of the cavity are met on the x axis makes it possible to linearize the problem. Linearizing boundary conditions makes it possible to reduce the problem of seeking velocities of flow to a problem of seeking an analytical function whose values are given at the boundaries (Fig. 54). After the induced velocities have been found it is easy to determine the hydrodynamic characteristics of a profile.

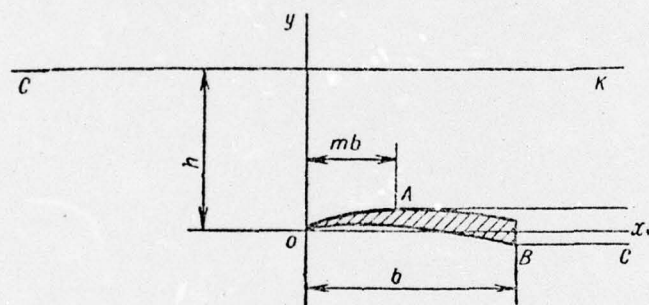


Fig. 53. Movement of a supercavitating profile beneath a free surface.

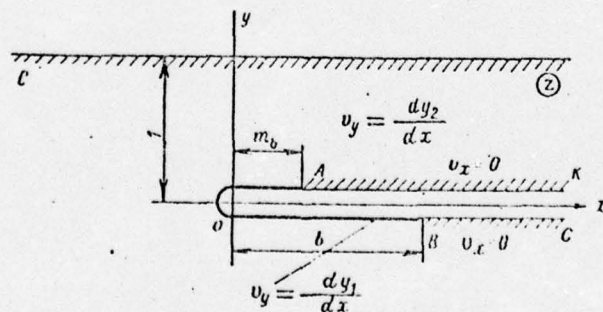


Fig. 54. Hydrodynamic model of a supercavitating hydrofoil.

If the shape of the high-pressure side of a profile, the angle of attack, and the depth of immersion are known, it is possible to determine the lift and drag of a profile operating in a supercavitating mode (Fig. 55b).

[98

We will present formulas which make it possible to determine the hydrodynamic characteristics of a profile on the high-pressure side in the form of a circle arc and a Tulin profile with the shape of the high-pressure side optimal. We will consider the chord of the profile to be the line connecting the forward and rear edges of the high-pressure side of the foil. The angle between it and the oncoming flow is the profile's angle of attack.

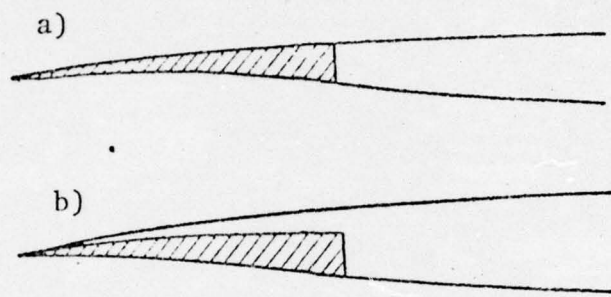


Fig. 55. Flow around a profile: a--ventilated profile with separation occurring at trailing edge; b--supercavitating profile.

Profile with high-pressure side in the form of a circle arc.
The equation for the high-pressure side of the profile is

$$\bar{y} = \frac{\gamma}{2} (\bar{x} - \bar{x}^2) = 4\bar{f}_h (\bar{x} - \bar{x}^2), \quad (I.134)$$

where γ is the central angle of the arc forming the high-pressure side of the profile and $\bar{f}_h = \gamma/8$ the maximum relative camber of the profile's high-pressure side.

For the case of an unbounded liquid

$$\left. \begin{aligned} C_y &= \frac{\pi}{2} (\alpha + 3.5\bar{f}_h), \\ C_{x \text{ cav}} &= \frac{\pi}{2} (\alpha + \bar{f}_h)^2, \end{aligned} \right\} \quad (I.135)$$

where $3.5\bar{f}_h$ is the angle of zero lift.

When $\alpha_{cav} = \gamma/8 = \bar{f}_h$ cavitation theoretically begins on the low-pressure side.

The Tulin profile

$$\bar{y} = 1.6442 \left(\frac{4}{3} \bar{x} + \frac{8}{3} \bar{x}^{3/2} - 4\bar{x}^2 \right), \quad (I.136)$$

$$\left. \begin{aligned} C_y &= \frac{\pi}{2} (\alpha + 3,56 \bar{f}_h), \\ C_x \text{ cav} &= \frac{\pi}{2} (\alpha + 1,09 \bar{f}_h)^2, \\ \alpha_0 &= -3,56 \bar{f}_h; \\ \alpha_{\text{cav}} &\approx 0,55 \bar{f}_h. \end{aligned} \right\} \quad (I.137)$$

Fig. 56 shows curves for the angle of zero lift and $\partial C_y / \partial \alpha$ as a function of the depth of immersion on the high-pressure side of the two types of profile indicated above, making it possible to determine the coefficient of lift of a super-cavitating profile beneath a free surface.

The formulas of linear theory give results close to actual for profile angles of attack up to 8--10°. In the case of large angles of attack the results of nonlinear stream theory must be used to determine hydrodynamic forces. [99]

For a flat plate moving in an unbounded flow the formulas for calculation take the form

$$\left. \begin{aligned} C_y &= \frac{\pi \sin 2\alpha}{4 + \pi \sin \alpha}, \\ C_x &= \frac{2\pi \sin^2 \alpha}{4 + \pi \sin \alpha}. \end{aligned} \right\} \quad (I.138)$$

For a profile with a curved high-pressure side ($\bar{f}_h \neq 0$) the formulas for C_y and C_x can be written in the form

$$\left. \begin{aligned} C_y &= (C_y)_{\bar{f}_h=0} + \left(\frac{\partial C_y}{\partial \bar{f}_h} \right)_{\bar{f}_h=0} \cdot \bar{f}_h, \\ C_x &= (C_x)_{\bar{f}_h=0} + \left(\frac{\partial C_x}{\partial \bar{f}_h} \right)_{\bar{f}_h=0} \cdot \bar{f}_h, \end{aligned} \right\} \quad (I.139)$$

where

$$\left. \begin{aligned} \left(\frac{\partial C_y}{\partial \bar{f}_h} \right)_{\bar{f}_h=0} &\approx -3,5\alpha + 5,5, \\ \left(\frac{\partial C_x}{\partial \bar{f}_h} \right)_{\bar{f}_h=0} &\approx \frac{16\pi \sin \alpha}{(4 + \pi \sin \alpha)^2} \left[1 - \frac{1}{3} \sin^2 \alpha + \right. \\ &\quad \left. + \frac{\pi \sin \alpha \cos^2 \alpha}{4(4 + \pi \sin \alpha)} \right]. \end{aligned} \right\} \quad (I.140)$$

The data presented hold for a zero cavitation number. To obtain more accurate values for hydrodynamic characteristics it is necessary to introduce a correction for the cavitation number:

$$\left. \begin{aligned} C_y \text{ cav} &= (1 + \kappa) C_{y_{\kappa=0}}, \\ C_x \text{ cav} &= (1 + \kappa) C_{x_{\kappa=0}}. \end{aligned} \right\} \quad (I.141)$$

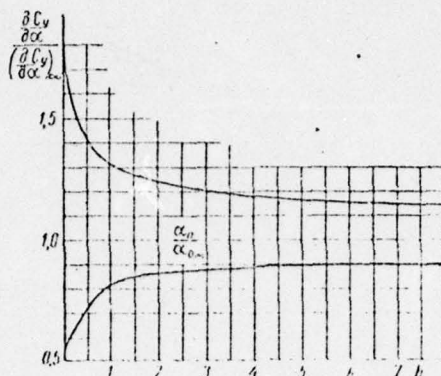


Fig. 56. Effect of free surface on the derivative of C_y with respect to α and the angle of zero lift of a supercavitating profile.

These formulas hold only for low cavitation numbers, for higher χ the relation becoming more complex. However, they are entirely suitable for making practical calculations of supercavitating foils since they provide for adequate accuracy. [100]

In order to calculate the total drag coefficient of a supercavitating profile it is necessary to add to the cavitation drag coefficient a friction drag coefficient for the high-pressure side of the profile which can be set equal to $C_{xpr} = 0.0025$.

Calculations of various profiles show that operative for a supercavitating foil are angles of attack of $\alpha \approx 5$ -- 9 , curvature of the high-pressure side $\bar{f}_h \approx 0.01$ -- 0.03 , and relative profile thickness 5 -- 7% . Corresponding values of C_y are 0.10 -- 0.25 .

References

1. Keldysh, M. V. and Lavrent'yev, M. A. Movement of a foil under the surface of a heavy liquid. In the collection: Trudy konferentsii po teorii volnovogo soprotivleniya. Moscow, 1937, TsAGI.
2. Kochin, N. Ye. Wave drag and lift of bodies immersed in a liquid. In the book by N. Ye. Kochin: Sobraniye sochineniy (Collected works), Vol. 2, AN SSSR, Moscow, 1949.
3. Vladimirov, A. N. Approximate hydrodynamic calculations of a finite-span hydrofoil. Trudy TsAGI, 1937, No. 311.
4. Panchenkov, A. N. Gidrodinamika podvodnogo kryla (Hydrodynamics of a hydrofoil). Kiev, Naukova dumka, 1965.
5. Nishiyama, T. Lift line theory of a submerged hydrofoil of finite span. Institute of American Society of Naval Engineers, 1958, Vol. 70, No. 3.

6. Shuster, S. and Schwaneche, N. Über den Einfluss der Wasseroberfläche auf die Auftriebsverteilung von Tragflügeln-- Schiffstechnik 1957, bd. 4, H. 21, 4 Band.

7. Chudinov, S. D. Lifting force of a hydrofoil of finite span. Trudy VNITOSS, 1955, Vol. 6, No. 2.

8. Multhopp, H. Die Berechnung der Auftriebsverteilung von Tragflügeln. Luftfahrtforschung, 1938, bd. 15.

9. Karafoli, Ye. Aerodinamika kryla samoleta (neszhimayemaya zhidkost') (Aerodynamics of an aircraft wing. (incompressible fluid). Moscow, AN SSSR, 1956.

10. Pozdyunin, V. L. Fundamentals of the theory, design, and behavior of supercavitating propeller screws. Izvestiya AN SSSR, Otdel Tekhnicheskikh nauk, Moscow, 1945, Nos. 10--11.

A. Some results from the theory of a nonstationarily moving thin foil

In the preceding chapter we discussed methods of determining hydrodynamic forces acting on the lift surfaces of high-speed craft during steady movement. The hypothesis of stationarity can be used to determine the forces acting on structures of a ship's hull and also on lift foils mainly under the conditions prevailing in calm water or in a seaway but at low speeds. With an increase in a ship's speed, especially in a seaway, its movement becomes much more dynamic and marked pitching and rolling give rise to impacts against waves. All this means that lift surfaces operate in nonstationary modes. A need therefore arises to study nonstationary hydrodynamic forces acting on the lift structures of craft during unsteady movement.

The lift surfaces of craft, rudders, propeller blades, stabilizers, and other structures are made in the form of foils having one profile and aspect ratio or another depending on their purpose and design peculiarities.

From the standpoint of hydrodynamics the hull of a craft also can be considered to be a foil of small aspect ratio oriented in a certain way with respect to the water's surface. Such an approach finds application in the study of planing, wave drag, controllability, and also many other areas in ship theory. Consequently, in this chapter we will devote principal attention to a consideration of unsteady interaction between a surrounding liquid and the lift surfaces of a craft which take the form of foils or something close to them.

§13. Hydrodynamic patterns of movement of a liquid and hydrodynamic forces acting on a foil during unsteady movement

In the past the principal investigations of nonstationary forces acting on a foil have been based on the concept of a straight-line vortex wake introduced by Prandtl and developed later by Birnbaum [1]. Nevertheless, because of the different approaches which have been used to describe the patterns of formation and development of a vortex wake and also the different methods used to reach analytical conclusions, three identifiable trends of investigation exist.

[102

The first of them is the quasistationary solution of Karman and Sears which is based on a pattern with a vortex wake un-

folding at every instant of time toward an infinitely distant point. The second is the dynamic theory of Birnbaum and Kyussner which is based on the idea of a vortex wake developing continuously and having over a concrete time interval a definite length which increases with the passage of time. The third trend of investigation is illustrated in the works of S. A. Chaplygin, M. V. Keldysh, M. A. Lavrent'yev, and L. I. Sedov in which the intensity of a dynamically developing vortex wake, movement of the liquid, and hydrodynamic forces are found by using functions of a complex variable.

We will not discuss the first two methods of drawing vortex patterns and solving the problem, the reader being invited to read the recognized monograph by A. I. Nekrasov [2], but will proceed to a direct discussion of the results found by the Soviet school. We will consider movement from a state of rest of a thin profile $(-a, a)$ with a rounded leading edge and a sharp trailing edge (Fig. 57). The profile begins its movement at point o_1 which is the origin of a fixed system of $x_1 y_1$ coordinates. We will consider the geometric angle of attack of a profile β_0 formed by the angle between the x axis of the coordinates which is rigidly oriented on the profile and the line oo_1 representing the direction of main forward movement at a velocity of u_0 to be small. Along with velocity u_0 the profile may also have vertical y' and also angular ω_0 velocities whose projections onto a perpendicular to the foil are comparable in magnitude with the product $(u_0 \beta_0)$.

The normal component of the velocity vector for a profile with a flat lower side can be determined from the following equation (Fig. 58):

[103

$$v_n(x, t) = y' - u_0 \beta_0 + \omega_0 x. \quad (II.1)$$

At the instant movement of the foil starts the flow of an ideal liquid around it is characterized by the existence on the profile of two points A and B with a zero velocity and one point C with an infinite velocity (Fig. 59).

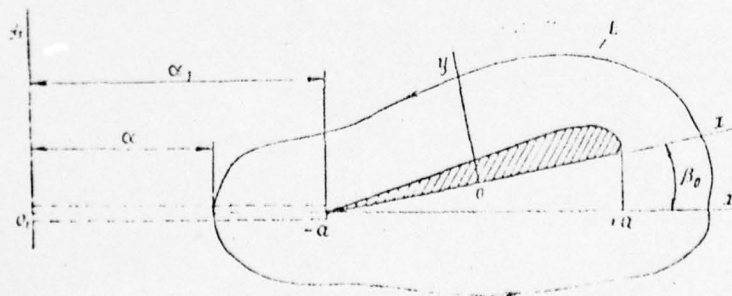


Fig. 57. Unsteady movement of a thin foil in an unbounded liquid (main notation).

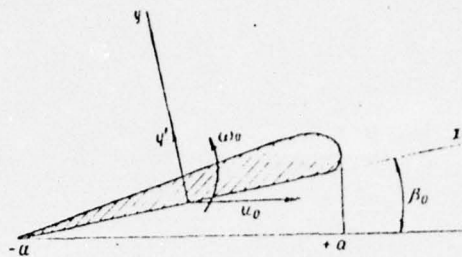


Fig. 58. Positive directions of velocities of foil movement.

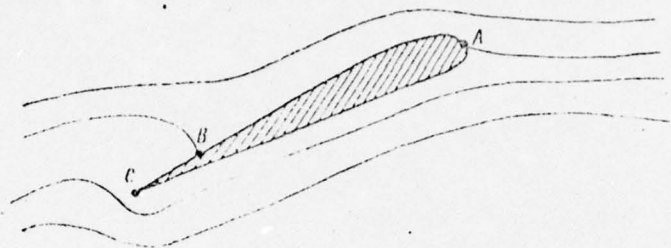


Fig. 59. Critical points on a foil.

In an actual liquid infinite velocity is impossible since, according to the Lagrange integral this would lead to the rise of infinite negative pressures at point C . Therefore, at the initial instant of movement particles of liquid strive to get around the sharp edge of the foil. As a consequence of the reduced pressure created here their movement increases, as a result of which the streams of liquid arriving at the trailing edge from above and below the foil have different velocities. The discontinuity in velocities of liquid flow which occurs is characterized by the fact that on line segment $o_1(-a)$ (see Fig. 57) the normal component of the velocity vector is continuous and the tangential component reflects a discontinuity. The surface of the velocity continuity, as is known, is equivalent to a vortex sheet. In accordance with Thompson's theorem the intensity of the vortex layer trailing from the foil is compensated for by the circulation occurring around the profile. As a result of the gradual increase in circulation the point of zero velocity B shifts toward the trailing edge of the profile; in this process the particles of liquid cease to try to pass around the sharp edge of the foil and smooth flow at a finite velocity begins around the sharp edge of the profile. This flow persists around the profile until a new disturbance to steady movement occurs.

For an analytical study of the phenomenon described above it is assumed that the vortices forming the wake remain unmoving in the liquid. During straight-line forward movement of a foil the vortex wake is considered to be straight-line and the

[104

direction of propagation of the wake to be directly opposite to the velocity vector of the profile [1].

Using the above pattern to describe the phenomenon makes it possible to formulate the following mathematical problem [3].

It is required to find a function for the velocities of flow of a liquid

$$\frac{d\omega}{dz} = u_0 - iv_0, (z = x - iy), \quad (\text{II.2})$$

which will be regular over an entire plane with the exception of a segment $(o_1, +a)$ and equal to zero at infinity. On the line of velocity discontinuity the derivative $d\phi/dy = v_0$ is continuous and the derivative $d\phi/dx = u_0$ finite at point $(-a)$.

The function $d\omega/dz$ is determined based on the following boundary conditions.

On segment $(-a, a)$ the derivative

$$\frac{d\phi}{dy} = v_n \quad (\text{II.3})$$

has given values as calculated from formula (II.1).

If we assume the liquid to be weightless and neglect in the Lagrange integral the squares of the velocities of absolute movement of the liquid, the boundary condition on the real axis outside the segment $(o_1, +a)$ can be written in the form

$$d\phi/dt = 0 \quad \text{when} \quad -\infty \leq x \leq o_1; \quad +a \leq x \leq +\infty.$$

Inasmuch as movement began from a state of rest and at the start of movement we can consider that $\phi = 0$, the boundary condition on the real axis outside segment $(o_1, +a)$ will be

$$\phi = 0. \quad (\text{II.4})$$

For further exposition we will introduce the concept of a velocity discontinuity function $u_2(\alpha)$ or, as its doubled value is called, a function of intensity or density of vortices trailing from the rear edge of a foil. Function $u_2(\alpha)$ is related to circulation Γ along a certain contour L (Fig. 57) by the relation

$$\Gamma = 2 \int_0^a u_2(\alpha) d\alpha \quad (\text{II.5})$$

and is determined from the condition of finiteness of the velocity of flow of the liquid at the rear edge during unsteady movement (the Chaplygin-Zhukovskiy condition).

We will present the function $d\omega/dz$ in the form of a product of two functions

$$\frac{d\omega}{dz} = F(z)g(z). \quad (\text{II.6})$$

We will write the function $g(z)$ in the form [3] [105]

$$g(z) = \sqrt{\frac{z-a}{z+a}}. \quad (\text{II.7})$$

In expression (II.7) when Real $z > a$ the root carries a plus sign, that is $g(z) > 0$.

If the Cauchy formula is applied to (II.6), function $d\omega/dz$ becomes

$$\frac{d\omega}{dz} = \frac{1}{2\pi i} \oint_L F(\xi) \frac{\sqrt{\frac{\xi-a}{\xi+a}}}{\xi-z} d\xi, \quad (\text{II.8})$$

where L is a circle of small radius with its center at point z .

Since $F(\xi) = \frac{d\omega}{d\xi} \sqrt{\frac{\xi+a}{\xi-a}}$, (II.8) can be written in the form

$$\frac{d\omega}{dz} = \frac{1}{2\pi i} \sqrt{\frac{z+a}{z-a}} \oint_L \frac{\frac{d\omega}{d\xi} \sqrt{\frac{\xi-a}{\xi+a}}}{\xi-z} d\xi. \quad (\text{II.9})$$

Deforming circle L into an infinitely distant contour and into the contour of segment $(o_1, +a)$, we obtain

$$\begin{aligned} \frac{d\omega}{dz} = \frac{1}{2\pi i} \sqrt{\frac{z+a}{z-a}} & \left(\oint_{L_1} \frac{\frac{d\omega}{d\xi} \sqrt{\frac{\xi-a}{\xi+a}}}{\xi-z} d\xi \right) \\ & + \left(\int_{L_2} \frac{\frac{d\omega}{d\xi} \sqrt{\frac{\xi-a}{\xi+a}}}{\xi-z} d\xi \right). \end{aligned}$$

In the last expression as contour L_1 tends to infinity the first integral vanishes since

The integral over contour L_2 can be written in the form

$$\int_{\gamma_1} \frac{d\omega}{d\xi} \frac{\sqrt{\xi-a}}{\xi-z} d\xi = \int_0^{\alpha_1} \frac{(u_2 - iv_2) \sqrt{\xi-a}}{\xi-z} d\xi +$$

$$+ \int_{-a}^a \frac{(u_2 - iv_2) \sqrt{\xi-a}}{\xi-z} d\xi + \int_a^0 \frac{(u_1 - iv_1) \sqrt{\xi-a}}{\xi-z} d\xi +$$

$$+ \int_{\alpha_1}^0 \frac{(u_1 - iv_1) \sqrt{\xi-a}}{\xi-z} d\xi,$$

where u_2 and v_2 are the horizontal and vertical components of velocities when approaching the cut $(0, +a)$ from above and u_1 and v_1 from below. [106]

Keeping in mind that $u_2(\alpha) = u_2 - u_1$ and $u_2 = -u_1$ and also $v_1 = v_2 = -v_n$, we obtain

$$\frac{d\omega}{dz} = \frac{1}{\pi i} \sqrt{\frac{z+a}{z-a}} \left[\int_0^{\alpha_1} \frac{u_2(\alpha) \sqrt{\xi-a}}{\xi-z} d\alpha + \right.$$

$$\left. + \int_{-a}^a \frac{v_n(\xi, t) \sqrt{\frac{a-\xi}{a+\xi}}}{\xi-z} d\xi \right]. \quad (\text{II.10})$$

In formula (II.10) the variables α and ξ are related by $\xi = \alpha - \alpha_1 - \alpha$.

On the other hand, the following expansion into a Loran series can be obtained for functions $d\omega/dz$ close to an infinitely distant point:

$$\frac{d\omega}{dz} = \frac{\Gamma_0}{2i} \frac{1}{z} + \frac{iC_2}{z^2} + \frac{iC_3}{z^3} + \dots, \quad (\text{II.11})$$

where Γ_0 is the circulation over an infinitely distant contour which is constant over time.

Coefficients Γ_0 , C_2 , and C_3 are determined by comparing (II.10) and (II.11). For this purpose formula (II.10) can be transformed into

$$\frac{d\omega}{dz} = \frac{1}{\pi i} \sqrt{\frac{1 + \frac{a}{z}}{1 - \frac{a}{z}}} \left[\int_0^{\alpha_1} \frac{u_2(\alpha)}{\xi} \sqrt{\frac{\xi - a}{\xi + a}} d\alpha + \int_{-a}^a \frac{v_n(\xi, t)}{\xi} \sqrt{\frac{a - \xi}{a + \xi}} d\xi \right] \quad (\text{II.12})$$

If in (II.11) and (II.12) the coefficients of $1/z$ are equated, assuming in (II.12) that $z = \infty$, we obtain

$$\Gamma_0 = -2 \left[\int_{-a}^a v_n(\xi, t) \sqrt{\frac{a - \xi}{a + \xi}} d\xi + \int_0^{\alpha_1} u_2(\alpha) \sqrt{\frac{\xi - a}{\xi + a}} d\alpha \right] \quad (\text{II.13})$$

For determining C_2 and C_3 , after expanding (II.10) into a Loran series and comparing the resulting expansion with (II.11), the following relations are found: [107]

$$C_2 = \frac{1}{\pi} \left[\int_{-a}^a v_n(\xi, t) \sqrt{a^2 - \xi^2} d\xi + \int_0^{\alpha_1} u_2(\alpha) \sqrt{\xi^2 - a^2} d\alpha \right]; \quad (\text{II.14})$$

$$C_3 = \frac{1}{2\pi} \left[\int_{-a}^a v_n(\xi, t) [2\xi(\xi + a) + a^2] \sqrt{\frac{a - \xi}{a + \xi}} d\xi + \int_0^{\alpha_1} u_2(\alpha) [2\xi(\xi + a) + a^2] \sqrt{\frac{\xi - a}{\xi + a}} d\alpha \right] \quad (\text{II.15})$$

Expressions for the hydrodynamic forces can be obtained by using formulas [3]:

$$\left. \begin{aligned} Y &= \rho_0 u_0 \Gamma_0 - 2\pi \rho_0 a \frac{dC_2}{dt}, \\ M &= -2\pi \rho_0 u_0 C_2 - \rho_0 \pi a \frac{dC_3}{dt}, \end{aligned} \right\} \quad (\text{II.16})$$

where ρ_0 is the density of the liquid, Y is the lift, and M the moment in the plane of the profile.

After substituting the values of Γ_0 , C_2 , and C_3 into (II.16) the following general formulas are derived for determining Y and M :

$$\begin{aligned} Y &= -\frac{d\rho_0 \pi a^2 V_1}{dt} - 2\pi \rho_0 a u_0 \left(V_1 - \frac{a\omega_0}{2} \right) - \\ &\quad - 2\rho_0 a \left(u_0 + \frac{da}{dt} \right) \int_0^{\alpha_1} \frac{u_2(\alpha) d\alpha}{\sqrt{\xi^2 - a^2}}; \end{aligned} \quad (\text{II.17})$$

$$\begin{aligned}
Y_3 = & -\frac{\rho_0 \pi a^4}{8} \frac{d\omega_0}{dt} - \rho_0 \pi a^2 V_1 \left(u_0 + \frac{da}{dt} \right) - \\
& - \rho_0 a^2 \left(u_0 + \frac{da}{dt} \right) \int_0^{a_1} \frac{u_2(\alpha) d\alpha}{V|\xi^2 - a^2|}.
\end{aligned}
\tag{II.18}$$

The suction force X is found from the formula

$$X = 2\rho_0 \pi a \left[V_1 - \frac{Y_3}{2\rho_0 \pi a \left(u_0 + \frac{da}{dt} \right)} \right]^2.
\tag{II.19}$$

In formulas (II.17) -- (II.19): $V_1 = y' - u_0 \beta_0$, $Y_1 = -\frac{d\rho_0 \pi a^2 V_1}{dt}$

is a force allowing for the effect of adjoining masses,

$Y_2 = -2\rho_0 \pi a u_0 \left(V_1 - \frac{a\omega_0}{2} \right)$ the quasistationary force of N. Ye.

Zhukovskiy, and $Y_3 = -\rho_0 a \left(u_0 + \frac{da}{dt} \right) \int_0^{a_1} \frac{u_2(\alpha) d\alpha}{V|\xi^2 - a^2|}$ the component

of hydrodynamic forces allowing for the effect of trailing vortices whose intensity can be determined from the function $u_2(\alpha)$. [108]

From the expressions obtained it follows that the magnitude of Y , X , and X can be found for a given movement only after determining function $u_2(\alpha)$.

Finding the relation between $u_2(\alpha)$ and the kinematic parameters of profile movement amounts to solving equation (II.13) which for known values of r_0 and $v_n(\xi, t)$ can be regarded as an integral equation with respect to function $u_2(\alpha)$.

Equation (II.13) can be written in the form

$$\begin{aligned}
& 2 \int_0^{a_1} u_2(\alpha) \sqrt{\frac{2a + a_1 - \alpha}{a_1 - \alpha}} d\alpha = \\
& = - \left[\Gamma_0 + 2 \int_{-a}^{+a} v_n(\xi, t) \sqrt{\frac{a - \xi}{a + \xi}} d\xi \right].
\end{aligned}
\tag{II.20}$$

The right side of equation (II.20) which is a Volterra equation of the first order for the given law governing movement of the foil, is a known function of time.

The first solutions to equation (II.20) for movement of a foil from a state of rest at a constant velocity and smoothly accelerating movement were obtained by G. Wagner in [4]. In view of the fact that the particular cases indicated above involved movement of a foil from a state of rest, circulation Γ_0 in equation (II.20) was assumed to be equal to zero and as

a result Wagner solved the following equation:

$$\int_0^s u_2(x) \sqrt{\frac{1+s-x}{s}} dx = \pi v_p \sin \beta_0, \quad (II.21)$$

where v_p and β_0 are given functions of the dimensionless path $s = \alpha_1/2\alpha$ expressed in chords and $x = \alpha/2\alpha$, $0 \leq x \leq s$.

Presenting the solution to equation (II.21) in the form of a series

$$u_2(x) = \sum_{m=0}^{\infty} C_m V \alpha^m, \quad (II.22)$$

and also expanding into a series the known right side of equation (II.21)

$$v_p \sin \beta_0 = \sum_{n=0}^N a_n V s^n, \quad (II.23)$$

Wagner reduced determination of the function $u_2(x)$ to seeking the values of the coefficients C_m in the expansion of (II.22). As a result of numerical calculations he found values for these coefficients for the indicated two types of foil movement. Specifically, for foil movement at a constant velocity Wagner obtained function $u_2(x)$ in the form of the following series: [109]

$$u_2(x) \approx v_0 \left[1.1328 \left(\sqrt{\frac{1}{x}} \right)^3 - 0.4883 \left(\sqrt{\frac{1}{x}} \right)^5 + \dots \right]. \quad (II.24)$$

Later in the text we shall deal with an analysis of these solutions in greater detail.

For determining the function $u_2(\alpha)$ in the case of steady harmonic oscillations of a foil we will transform equation (II.21) to

$$\begin{aligned} \int_0^1 u_2(a + \alpha_1 - as) \left(\sqrt{\frac{s+1}{s-1}} - 1 \right) ds = \\ = \frac{1}{2a} [\Gamma(\alpha_1) - \Gamma_0] + \frac{1}{a} \int_{-a}^{+a} (v_n - v_{n0}) \sqrt{\frac{a-\xi}{a+\xi}} d\xi, \end{aligned} \quad (II.25)$$

where $a + \alpha_1 - \alpha = as$, $\Gamma(\alpha_1)$ is the circulation over the contour of the foil, and v_{n0} is the normal velocity during steady movement.

G. Glauert, M. A. Lavrent'yev, and M. V. Keldysh in the works cited above give solutions to equation (II.21) for simple harmonic oscillations of a rigid thin foil. L. I. Sedov,

presenting the harmonic oscillations of a deformed foil around steady forward movement at a velocity of u_0 in the form

$$v_n(x, t) - v_{n0}(x) = \text{Real} \left[F(x) e^{ik\alpha_1} \right]$$

($F(x)$ is a function giving the form of oscillation and k the frequency), obtained the following solution for equation (II.21):

$$u_2(a + \alpha_1 - as) = \text{Real} \left[\frac{i\mu}{2a} D e^{i\mu} e^{-i\mu s} e^{ik\frac{\alpha_1}{a}} \right], \quad (\text{II.26})$$

where

$$D = \frac{2e^{-i\mu} A}{\pi\mu \left[H_0^{(2)}(\mu) - iH_1^{(2)}(\mu) \right]},$$

$$A = 2 \int_{-a}^a F(\xi) \sqrt{\frac{a-\xi}{a+\xi}} d\xi,$$

$\mu = ka/u_0$; and $H_i^{(2)}(\mu)$ is a second-order Hankel function.

L. I. Sedov obtained a similar solution for steady harmonic oscillations of a foil with a variable chord. He presented his solution in the form

$$u_2(a_0 + \alpha_1 - a_0 s) = -\text{Real} \left[\frac{i\mu}{2a_0} D e^{i\mu} e^{-i\mu s} e^{ik\frac{\alpha_1}{a_0}} \right]; \quad (\text{II.27})$$

his determination of constant D amounting to calculating the integral $\int_{-\infty}^{\infty} \frac{1}{e^{-i\mu s}} \left[\sqrt{\frac{s+1}{s-1}} - 1 \right] ds$ and then solving the resulting algebraic equation. The result of these operations is [110]

$$D = \frac{4e^{-i\mu} A}{\mu \left[H_0^{(2)}(\mu) - iH_1^{(2)}(\mu) \right]},$$

where $\mu = ka_0/u_0$ and $A = A_0 \cos(kt + \epsilon)$, A_0 being the amplitude of oscillation.

In view of the linearity of integral equation (II.12) the formulas obtained can be used for determining $u_2(\alpha)$ for any periodic steady movement of a foil. Direct use of them for calculating velocity discontinuity functions during unsteady aperiodic movement has proved to be ineffective.

One more partial solution of integral equation (II.13) which was obtained during an investigation of self-similar immersion of a step in a liquid is known. However, prior to discussing this solution we will consider the possibilities and conditions under which the solutions presented above can

be applied to nonstationary movement of a foil or plate over the surface of a liquid.

§14. Extending the methods and results of the theory of a thin foil to planing and impact

The formulas of the preceding sections were derived for movement of a thin foil in an unbounded liquid. Despite this, thanks to the above formulation of the problem, the results obtained can be applied to the case of planing and impact [3], [5].

In this section we will discuss the possibility of applying to unsteady movement an analogy between foil movement and planing over the water's surface during steady movement.

As follows from boundary conditions (II.3) and (II.4) the function $d\omega/dz$ on the x_1 axis assumes real values. Over the entire plane, with the exception of the segment $(o_1, +a)$ $d\omega/dz$ is regular and continuous. These circumstances make it possible to apply to this function a known theorem from the principle of symmetry from which it follows that under the indicated conditions ϕ and $d\phi/dt$ above and below the real axis are equal in magnitude and opposite in sign [6].

The conditions of symmetry make it possible to view movement of the liquid in the upper and lower half-spaces independently. Excluding the upper space, we reduce the problem of unsteady movement of a thin foil in an unbounded liquid to a problem of unsteady interaction between it and the surface of the liquid filling the entire lower half-space. It should be kept in mind that the condition on the free surface (II.4) holds only at large relative velocities. Therefore, the indicated transition from an unbounded liquid with a free surface is justified only for conditions corresponding to the assumptions made in the first section. [111]

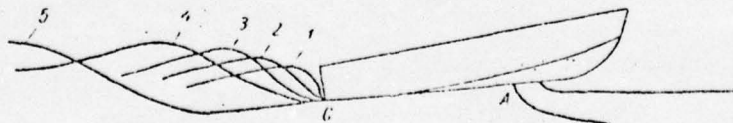


Fig. 60. Flow around the bottom rear edge of a planing hull.

The description presented above of development of lift on a foil is confirmed also for a foil or plate moving over a liquid's surface. This can be seen most clearly in the development of flow around a planing model. Fig. 60 shows the flow around the transom of a model drawn from moving pictures taken at the instant of change from displacement mode to planing mode

as the model picked up speed approximately linearly from a state of rest. It can easily be seen that in this nonstationary process, as in the case of nonstationary movement of a foil from a state of rest, at the initial instant particles of liquid strive to pass around the sharp edge C (curve 1). As the model continues to pick up speed the pressure drop increases at the trailing edge and particles do not succeed in passing around it, as a consequence of which at a sufficiently high speed the liquid separates from the transom (curve 2). The cavity formed behind the model becomes filled with air. As the process continues the flow levels off behind the transom until the stream finally begins to trail from edge C smoothly (lines 3--5). The instant at which smooth flow around the model starts corresponds to the instant when stable movement begins and, consequently, complete development of the forces supporting it, that is, a lifting force.

The pattern presented illustrates the analogy between unsteady movement of a foil and unsteady planing.

On the basis of the foregoing the lift acting on a foil or plate during unsteady movement over a liquid's surface will be equal to half the force obtained from expression (II.17), that is, it will be determined by the formula [7] [112]

$$Y = -\frac{1}{2} \frac{d\rho_0 \pi a^2 V_1}{dt} - \pi \rho_0 a V_1 \left(V_1 - \frac{u_{00}}{2} \right) - \rho_0 a \left(u_0 + \frac{da}{dt} \right) \int_0^{\alpha_1} \frac{u_2(a) da}{V \sqrt{k^2 - a^2}}. \quad (\text{II.28})$$

During steady forward movement over a liquid's surface the first and third components of force Y are equal to zero and therefore

$$Y = Y_2 = \pi \beta_0 (\rho_0 u_0^2) a, \quad (\text{II.29})$$

that is, we obtain the well-known Wagner formula for lift during steady planing.

If unsteady movement occurs without the existence of horizontal velocity ($u_0 = 0$), there is only potential movement of the liquid caused by motion of the plate at velocity y' . The resultant of hydrodynamic pressures on the plate will be due to the effect of the adjoining masses and determined by the first term in formula (II.28), that is,

$$Y = Y_1 = -\frac{d}{dt} \left(\frac{\rho_0 \pi a^2}{2} y' \right). \quad (\text{II.30})$$

Setting in this formula $\Delta m = \rho_0 \pi a^2 / 2$ and $y' = -v$ and differentiating, we transform it into

$$Y_1 = \Delta m \frac{dv}{dt} + v \frac{d\Delta m}{dt}. \quad (\text{II.31})$$

If an initial velocity of v_0 is imparted instantaneously to a body of mass m floating on the surface of a liquid, its speed of movement according to the law governing movement $[(m + \Delta m)v = mv_0]$ will be determined by the formula

$$v = \frac{v_0}{1 + \mu}, \quad (\text{II.32})$$

where $\mu = \Delta m/m$ is the adjoining mass of the liquid.

Substituting (II.32) into (II.31) and differentiating, we obtain the Wagner formula

$$Y_1 = m \frac{v_0}{(1 + \mu)^2} \cdot \frac{d\mu}{dt} \quad (\text{II.33})$$

or

$$Y_1 = m \frac{v_0^2}{(1 + \mu)^3} \cdot \frac{dh}{dt}, \quad (\text{II.34})$$

where $h = -y$ is the displacement of the body and $v = dh/dt$.

Formulas (II.33) and (II.34) were derived by Wagner for a wedge or inclined plate immersed in a liquid. Despite the fact that they were obtained from the theory of potential flow around a flat plate at a zero angle of attack ($\beta_0 = 0$) and extension of them to a wedge is conditional, these formulas cannot be used for calculating hydrodynamic forces on a plate immersed as described. This is due to the fact that during inelastic impact the velocity of the plate and the adjoining mass of liquid changes instantaneously and as a result, as follows from the formulas presented, an infinite hydrodynamic force acts on the plate. [113]

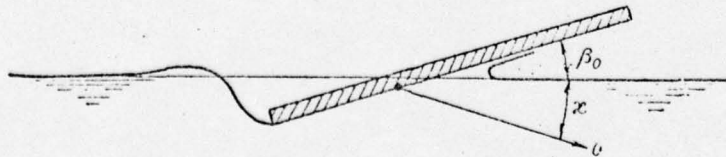


Fig. 61. Landing of a plate.

Using the analogy cited, G. Wagner [5] and L. I. Sedov [7] considered also the problem of interaction between a plate and a liquid's surface in the presence of horizontal velocity ($u_0 \neq 0$). This is the well-known problem of a step landing on an undisturbed surface (Fig. 61). The problem is solved under the assumption that the velocity V remains constant during the

immersion process. During such immersion movement of the liquid at various instants of time is dynamically similar, as a consequence of which the wetted length of plate and circulation of liquid are proportional to time, that is,

$$u_2 = (1/V)(d\Gamma/dt) = \text{const.}$$

This makes it possible to remove function $u_2(\alpha)$ in (II.21) from behind the integration sign and, after simple transformations, write it in the following form:

$$u_2 = \frac{\pi V (\beta + \kappa)}{V s_0^2 - 1 + \ln(s_0 - \sqrt{s_0^2 - 1})}, \quad (\text{II.35})$$

where $s_0 = 1 + \alpha_1/\alpha > 1$ and β and κ are angles as illustrated in Fig. 61.

Substituting (II.35) into (II.28) and integrating, we find the external forces acting on a step upon impact with the water,

$$Y = \rho \pi V^2 h e, \quad (\text{II.36})$$

where h is the depth of immersion of the trailing edge of the step [114]

$$h = \kappa V t; \quad (\text{II.37})$$

and

$$e = \frac{\left(1 + \frac{\beta}{\kappa}\right) (s_0 + 1) \sqrt{s_0^2 - 1}}{(s_0 - 1)^2 \left[\sqrt{s_0^2 - 1} + \ln(s_0 + \sqrt{s_0^2 - 1}) \right]}. \quad (\text{II.38})$$

A curve of function e is shown in Fig. 62.

The moment acting on the step is determined from the relation

$$M = \frac{\rho \pi V^2 a h}{2} \left(1 + \frac{\beta}{\kappa}\right) \frac{(s_0 + 1)}{(s_0 - 1)^2}. \quad (\text{II.39})$$

It follows from Fig. 62 that function e has a minimum. This suggests the existence of a least value of hydrodynamic forces during the landing process.

Solution (II.35) together with those presented in the second section exhaust all the partial solutions to integral equation (II.21) found in the literature.

The general expressions for hydrodynamic forces obtained in the theory of a thin foil and presented above, retaining

the assumptions made, can be used as a basis for determining the external forces acting on the lift surfaces of a ship during unsteady movement. However, prior to using them for this purpose several additional investigations must be carried out, the results of which will make it possible to take into account in these general expressions distinguishing aspects of unsteady movement of the lift surfaces of a craft and, consequently, to adapt them for solving hydrodynamic problems in ship theory.

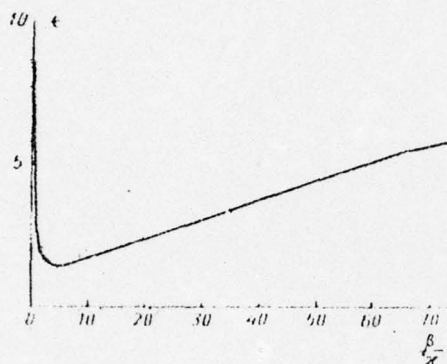


Fig. 62. Curve of function $\epsilon(\beta/\chi)$.

§15. Hydrodynamic forces during arbitrary unsteady movement of a foil in an unbounded liquid

A study of movements of lift surfaces of a craft which are aperiodic with respect to time and space is of great interest in shipbuilding practice. This can be explained first of all by the fact that with existing rates of ship movement most harmonic processes proceed relatively slowly, not extending beyond the framework of the hypothesis of stationarity, but at the same time aperiodic movements of craft lift surfaces proceed very rapidly with abrupt changes in velocity. Impacts of hull, motion stabilizers, or lift foils against the water when moving in a seaway or sudden application of a load above the waterline constitute far from all the hydrodynamic processes illustrating kinematic parameters of movements which are aperiodic functions of time. Therefore a need arises to determine hydrodynamic forces during movements of lift surfaces different from those considered in foil theory. Investigation of these forces, as follows from the preceding section, is limited in the main to steady processes at velocities which are constant or change harmonically over time. [115]

The main difficulty in determining hydrodynamic forces in various types of unsteady movement lies in solving integral equation (II.20). Due to the multiplicity of forms of non-stationary movement of a craft's lift surfaces it becomes necessary to find a general solution to this equation whose

use might in each individual case make it possible to establish the function of velocity discontinuity without solving the integral equation itself. Such a problem has been posed and in this chapter we will present a general solution for equation (II.21) as obtained from nonsymmetric Fourier formulas. The relations found make it possible to determine the velocity discontinuity function, circulation, and hydrodynamic forces when any arbitrary law governs the movement of a foil in an unbounded liquid. By "arbitrary" is meant any movement of a lift surface not transgressing the limitations adopted in the theory of a thin foil [8].

Let us return to a consideration of integral equation (II.20). Using (II.1), we can calculate the integral standing on the right side of this equation:

$$i = \int_{-a}^a v_n(\xi, t) \sqrt{\frac{a}{a-\xi}} d\xi = \pi \left(y' - u_0 \beta_0 + \frac{a}{2} \omega_0 \right). \quad (\text{II.40})$$

The expression in parenthesis in formula (II.40) is the normal velocity of a profile at a point lying at a distance of one-fourth chord from the trailing edge (Fig. 63).

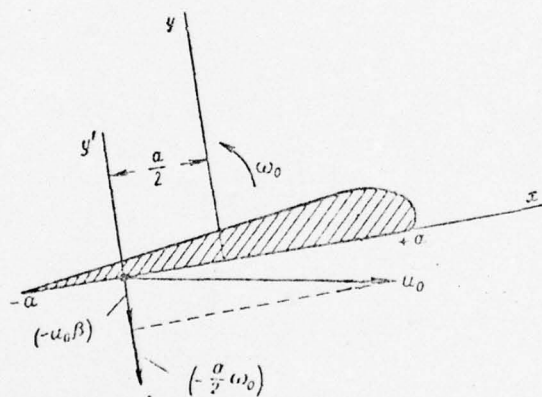


Fig. 63. Normal velocity at rear focal point on a foil.

Consequently, the initial integral equation can be written in the form

$$\int_0^{a_1} u_2(\alpha) \sqrt{\frac{2a + a_1 - \alpha}{a_1 - \alpha}} d\alpha = \pi \left[\frac{1}{2} \Gamma_0 + \pi \left(y' - u_0 \beta_0 + \frac{a}{2} \omega_0 \right) \right]. \quad (\text{II.41})$$

Introducing the notation

[116

$$v_2 = \left[\frac{v_0}{2a\pi} + \left(y' - u_0 \right) - \frac{a}{2} \omega_0 \right], \quad (\text{II.42})$$

we will transform equation (II.41) as follows:

$$\int_0^{a_1} u_2(\alpha) \sqrt{\frac{2a + a_1 - \alpha}{a_1 - \alpha}} d\alpha = -a\pi v_2, \quad (\text{II.43})$$

where v_2 is a known given function of time.

The latter equation can be made dimensionless by making the substitutions $x = \alpha/a$ and $s = a_1/a$:

$$\int_0^s u_2(x) \sqrt{\frac{2 + s - x}{s - x}} dx = -\pi v_2(s). \quad (\text{II.44})$$

Equation (II.44) has a difference kernel and in type resembles an Abel equation. The solution for this equation presented below is based on the use of nonsymmetrical Fourier formulas for solving integral equations [9].

We will multiply equation (II.44) by $\sqrt{\frac{2}{\pi}} e^{i\omega s} ds$ and integrate from 0 to ∞ . In the following discussion in equations containing the complex multiplier $e^{i\omega s}$ only the real part will be of interest.

As a result we obtain

$$\begin{aligned} \sqrt{\frac{2}{\pi}} \int_0^\infty e^{i\omega s} ds \int_0^s u_2(x) \sqrt{\frac{2 + s - x}{s - x}} dx = \\ = -\sqrt{2\pi} \int_0^\infty v_2(s) e^{i\omega s} ds. \end{aligned}$$

By using the Dirichlet formula we will change the order of integration on the left side of the resulting equation: [117]

$$\begin{aligned} \sqrt{\frac{2}{\pi}} \int_0^\infty u_2(x) dx \int_0^\infty \sqrt{\frac{2 + s - x}{s - x}} e^{i\omega s} ds = \\ = -\sqrt{2\pi} \int_0^\infty v_2(s) e^{i\omega s} ds. \end{aligned}$$

Setting

$$G(\omega) = \sqrt{\frac{2}{\pi}} \int_0^\infty v_2(s) e^{i\omega s} ds \quad (\text{II.46})$$

and making the substitution $(s - x) = t$ in equation (II.45) we change it to

$$\sqrt{\frac{2}{\pi}} \int_0^{\infty} u_2(x) e^{i\omega x} dx \int_0^{\infty} \sqrt{\frac{2+t}{t}} e^{t\omega t} dt = -\pi G(\omega). \quad (\text{II.47})$$

If

$$U(\omega) = \sqrt{\frac{2}{\pi}} \int_0^{\infty} u_2(x) e^{i\omega x} dx, \quad (\text{II.48})$$

$$K(\omega) = \sqrt{\frac{2}{\pi}} \int_0^{\infty} \sqrt{\frac{2+t}{t}} e^{t\omega t} dt, \quad (\text{II.49})$$

then equation (II.47) can be written

$$\sqrt{\frac{2}{\pi}} U(\omega) K(\omega) = -\pi G(\omega),$$

whence

$$U(\omega) = -\sqrt{2\pi} \frac{G(\omega)}{K(\omega)}. \quad (\text{II.50})$$

Integral equation (II.48) imposes certain limitations on the behavior of function $u_2(x)$ at infinity. In view of the fact that function $u_2(x)$ is being sought, the question of existence of the integral in (II.48) remains open. Nevertheless, even if the integral in (II.48) doesn't exist for real values of $\omega = u$ it may exist for complex values of $\omega = u + iv$ where v is a certain positive number when $x > 0$.

So that the convergence multiplier e^{-vx} improve the convergence of the integral in (II.48), it must be assumed that function $u_2(x)$ exists only on the half-axis $x > 0$; when $x < 0$ $u_2(x) = 0$ also agrees with the physical conditions of the problem under consideration.

Function $u_2(x)$ can be represented as a Fourier integral [118] as follows:

$$u_2(x) = \frac{1}{\pi} \int_0^{\infty} e^{-i\omega x} d\omega \int_{-\infty}^{\infty} u_2(t) e^{i\omega t} dt.$$

The latter expression, considering that $u_2(t) = 0$ when $t < 0$, can be written in the form

$$u_2(x) = \frac{1}{\pi} \int_0^{\infty} e^{-i\omega x} d\omega \int_0^{\infty} u_2(t) e^{i\omega t} dt. \quad (\text{II.51})$$

Comparing (II.48) and (II.51) we see that $U(\omega)$ is a

Fourier transform of the function $u_2(x)e^{-vx}$ for $x > 0$ and 0 when $x < 0$. Transforming, we obtain the following expression for the sought function $u_2(x)$ [10]:

$$u_2(s) = \frac{1}{\sqrt{2\pi}} \int_{i\alpha+0}^{i\alpha+\infty} U(\omega) e^{-i\omega s} d\omega. \quad (\text{II.52})$$

Here α is a certain positive number in the area $x > 0$.

Bearing (II.50) in mind, we can write (II.52) as follows:

$$u_2(s) = \int_{i\alpha+0}^{i\alpha+\infty} \frac{G(\omega)}{K(\omega)} e^{-i\omega s} d\omega. \quad (\text{II.53})$$

Formula (II.53) yields a general--or as it is sometimes called formal--solution for integral equation (II.44).

Let us consider the term $K(\omega)$ which occurs in (II.53). Using the substitution $t = \mu - 1$ we transform it into

$$K(\omega) = \sqrt{\frac{2}{\pi}} e^{-i\omega} \int_1^{\infty} \sqrt{\frac{\mu+1}{\mu-1}} e^{i\omega\mu} d\mu = \\ = \sqrt{\frac{2}{\pi}} e^{-i\omega} \left[\int_1^{\infty} \frac{\mu}{\sqrt{\mu^2-1}} e^{i\omega\mu} d\mu + \int_1^{\infty} \frac{1}{\sqrt{\mu^2-1}} e^{i\omega\mu} d\mu \right].$$

We will make one more change in variables in the expression obtained. Assuming that $\mu = \text{ch } \kappa$, we find

$$K(\omega) = \sqrt{\frac{2}{\pi}} e^{-i\omega} \left[\int_0^{\infty} e^{i\omega \text{ch } \kappa} \text{ch } \kappa d\kappa + \int_0^{\infty} e^{i\omega \text{ch } \kappa} d\kappa \right].$$

Keeping in mind that

$$\int_0^{\infty} e^{i\omega \text{ch } \kappa} \text{ch } \rho \kappa d\kappa = \frac{\pi i}{2} e^{\rho \frac{\pi i}{2}} H_p^{(1)}(\omega),$$

we obtain the following expression for $K(\omega)$:

[119

$$K(\omega) = \sqrt{\frac{2}{\pi}} e^{-i\omega} [iH_0^{(1)}(\omega) - H_1^{(1)}(\omega)], \quad (\text{II.54})$$

where $H_p^{(1)}(\omega)$ is a first-order Hankel function.

Substituting (II.54) into (II.53) we obtain

$$u_2(s) = - \sqrt{\frac{2}{\pi}} \int_{i\alpha+0}^{i\alpha+\infty} \frac{G(\omega) e^{-i\omega s}}{e^{-i\omega} [iH_0^{(1)}(\omega) - H_1^{(1)}(\omega)]} d\omega. \quad (\text{II.55})$$

In (II.55) we will replace s with η , multiply it by η , and integrate from 0 to s with respect to s :

$$\int_0^s u_2(\eta) d\eta = - \sqrt{\frac{2}{\pi}} \int_{i\alpha+0}^{i\alpha+\infty} \frac{G(\omega)}{e^{-i\omega} [iH_0^{(1)}(\omega) - H_1^{(1)}(\omega)]} \int_0^s e^{-i\eta\omega} d\eta d\omega.$$

Setting

$$u_{21}(s) = \int_0^s u_2(\eta) d\eta \quad (\text{II.56})$$

and considering that

$$\int_0^s e^{-i\eta\omega} d\eta = \frac{(e^{-i\omega s} - 1)}{(-i\omega)},$$

we obtain the expression

$$u_{21}(s) = - \sqrt{\frac{2}{\pi}} \int_{i\alpha+0}^{i\alpha+\infty} \frac{G(\omega) (e^{-i\omega s} - 1)}{(-i\omega) e^{-i\omega} [iH_0^{(1)}(\omega) - H_1^{(1)}(\omega)]} d\omega. \quad (\text{II.57})$$

Taking into account (II.46) and the replacement of s by η , we write (II.57) in the following form:

$$u_{21}(s) = - \frac{2}{\pi} \int_0^\infty v_2(\eta) d\eta \int_{i\alpha+0}^{i\alpha+\infty} \frac{[e^{i\omega(\eta-s)} - e^{i\omega\eta}] d\omega}{(-i\omega) e^{-i\omega} [iH_0^{(1)}(\omega) - H_1^{(1)}(\omega)]}.$$

For future derivations expression (II.58) can be conveniently written in the form

$$u_{21}(s) = - \frac{2}{\pi} \int_0^\infty v_2(\eta) I(\eta, s) d\eta, \quad (\text{II.59})$$

where

$$I(\eta, s) = \int_{i\alpha+0}^{i\alpha+\infty} \frac{[e^{i\omega(\eta-s)} - e^{i\omega\eta}] d\omega}{(-i\omega) e^{-i\omega} [iH_0^{(1)}(\omega) - H_1^{(1)}(\omega)]}. \quad (\text{II.60})$$

It can be demonstrated that the integrand in (II.60), in the interval of change in argument of interest to us, does not contain singularities. For proof of this let us consider the following limits which characterize the denominator of the integrand: [120

$$g(\omega) = (-i\omega) e^{-i\omega} [iH_0^{(1)}(\omega) - H_1^{(1)}(\omega)];$$

$$\lim_{\omega \rightarrow u} g(\omega) = \lim_{u \rightarrow 0} \{(-iu) e^{-iu} [iH_0^{(1)}(u) - H_1^{(1)}(u)]\}.$$

With the help of the asymptotic relations [11]

$$H_0^{(1)}(u) \rightarrow -i \frac{2}{\pi} \ln \frac{2}{u}; \quad H_\nu^{(1)}(u) \rightarrow -i \left(\frac{2}{u}\right)^\nu \frac{\Gamma(\nu)}{\pi}$$

$u \rightarrow 0$ $u \rightarrow 0$ $\nu > 0$

we obtain

$$\lim_{\substack{u \rightarrow 0 \\ v \rightarrow 0}} g(\omega) = \lim_{u \rightarrow 0} \left\{ (-iu) e^{-iu} \left(\frac{2}{\pi} \ln \frac{2}{u} + i \frac{2}{\pi} \frac{1}{u} \right) \right\} = \frac{2}{\pi}.$$

The limit of function $g(\omega)$ when $iv \rightarrow 0$ will be

$$\lim_{\substack{\omega = iv \rightarrow 0 \\ v \rightarrow 0}} g(\omega) = \lim_{v \rightarrow 0} \left\{ ve^v \left[i H_0^{(1)}\left(ve^{i\frac{\pi}{2}}\right) - H_1^{(1)}\left(ve^{i\frac{\pi}{2}}\right) \right] \right\}.$$

Using the formula

$$K_\nu(\omega) = \frac{\pi i}{2} e^{\frac{i\pi\nu}{2}} H_\nu^{(1)}\left(\omega e^{\frac{i\pi}{2}}\right)$$

$$\left(-\pi < \arg \omega < \frac{\pi}{2}\right)$$

(K_ν is a MacDonald function) and also the asymptotic expressions

$$K_0(v) \rightarrow \ln \frac{2}{v}; \quad K_\nu(v) \rightarrow \frac{2^\nu \Gamma(\nu)}{v^\nu}$$

$v \rightarrow 0$ $v \rightarrow 0$ $\nu > 0$

we obtain the limit of interest to us

$$\begin{aligned} \lim_{\substack{v \rightarrow 0 \\ u \rightarrow 0}} g(\omega) &= \lim_{v \rightarrow 0} \frac{2}{\pi} \{ve^v [K_0(v) + K_1(v)]\} = \\ &= \lim_{v \rightarrow 0} \frac{2}{\pi} \left\{ ve^v \left(\ln v + \frac{1}{v} \right) \right\} = \frac{2}{\pi}. \end{aligned}$$

In this way it can be proved that with any approach to zero in the interval of change in the argument ($-\pi < \omega < \pi/2$) function $g(\omega)$ has the limit $\lim_{\omega \rightarrow 0} g(\omega) = 2/\pi$.

When $\omega \rightarrow \infty$ the integrand diminishes monotonically. After analyzing the integrand, we will return again to (II.60). Integrating along the contour (Fig. 64) we can write this equation in the form of a sum: [121]

$$I(\eta, s) = \left\{ \int_{u=0}^{u=R} + \int_{RA} + \int_{CR} + \int_{v=B}^{v=0} + \int_0^{\alpha} \right\}. \quad (\text{II.61})$$

In (II.61) all integrals with $(\eta - s) > 0$ and $\eta > 0$

are equal to zero. The convergence multiplier, in view of the good convergence of the integral in (II.60), can be set equal to unity, that is, $\alpha = 0$.

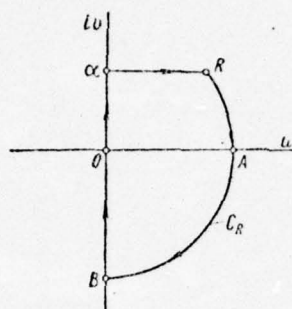


Fig. 64. Contour of integration.

When $R \rightarrow \infty$ the integral over contour C_R vanishes in accordance with the Jordan lemma.

Inasmuch as within the contour of integration under consideration there are no singular points, according to the Cauchy theorem the sum of the integrals remaining in (II.61) is equal to zero. This makes it possible for convenience of subsequent calculations to express the real part of the integral in (II.60), which is of interest to us, in terms of an integral with respect to the imaginary axis.

We will transform the integral in (II.61) on the basis of what we have stated. For this purpose we will first of all write the integrand in polar coordinates

$$I(\eta, s) = \int_{i\alpha}^{i\alpha + \infty} \frac{e^{i(\eta-s)\rho e^{i\varphi}} d(\rho e^{i\varphi})}{(-i\rho e^{i\varphi}) e^{-i\rho e^{i\varphi}} [iH_0^{(1)}(\rho e^{i\varphi}) - H_1^{(1)}(\rho e^{i\varphi})]},$$

where $\rho = \sqrt{u^2 + v^2}$ and $\phi = \arctg v/u - 2k\pi$ (k is a whole number).

Keeping in mind that

$$I(\eta, s) = \int_{u=0}^{u=\infty} = - \int_{v=-\infty}^{v=0},$$

and that for the last integral with respect to the imaginary axis $\rho = v$ and $\phi = -\pi/2$, we will write the integral of interest to us in the form

$$I(\eta, s) = - \int_{-\infty}^0 \frac{e^{I(\eta-s)} e^{I(\eta-s)} e^{-i\pi/2} d(v e^{-i\pi/2})}{(-i v e^{-i\pi/2}) e^{-i v e^{-i\pi/2}} [i H_0^{(1)}(v e^{-i\pi/2}) - H_1^{(1)}(v e^{-i\pi/2})]} =$$

$$= i \int_0^{\infty} \frac{e^{-(\eta-s)} v_0 dv_0}{v_0 e^{v_0} [i H_0^{(1)}(v_0 e^{i\pi/2}) - H_1^{(1)}(v_0 e^{i\pi/2})]},$$

where $v_0 = -v$.

Taking into account the above formula for transition from [122] a Hankel function to a MacDonald function and dropping the subscript of the argument, we transform the last integral as follows:

$$I(\eta, s) = i \int_0^{\infty} \frac{e^{-(\eta-s)} v dv}{v e^v \left[i \frac{2}{\pi i} K_0(v) - \frac{2}{\pi i} e^{i\pi/2} K_1(v) \right]}$$

or

$$I(\eta, s) = i \frac{\pi}{2} \int_0^{\infty} \frac{e^{-(\eta-s)} v dv}{v e^v [K_0(v) + K_1(v)]}. \quad (\text{II.62})$$

Substituting (II.62) into (II.59), we obtain

$$u_{21}(s) = -i \int_0^{\infty} v_2(\eta) d\eta \int_0^{\infty} \frac{e^{-v(\eta-s)}}{v e^v [K_0(v) + K_1(v)]} dv, \quad (\text{II.63})$$

Keeping integral equation (II.56) in mind, we find the following expression for function $u_2(s)$:

$$u_2(s) = -i \frac{d}{ds} \int_0^s v_2(\eta) d\eta \int_0^{\infty} \frac{e^{-v(\eta-s)}}{v e^v [K_0(v) + K_1(v)]} dv.$$

If

$$I_1 = \int_0^{\infty} \frac{e^{-v(\eta-s)}}{v e^v [K_0(v) + K_1(v)]} dv, \quad (\text{II.64})$$

then the function for velocity discontinuity behind a foil is

$$u_2(s) = -i \frac{d}{ds} \int_0^{\infty} v_2(\eta) I_1(\eta-s) d\eta. \quad (\text{II.65})$$

It follows from (II.65) that double integration must be performed in order to determine function $u_2(s)$.

Prior to proceeding to calculation of $I_1(\eta-s)$ we will

analyze its integrand. The denominator of the integrand has the following limits:

$$\lim_{v \rightarrow 0} \frac{1}{ve^v [K_0(v) + K_1(v)]} = \lim_{v \rightarrow 0} \frac{1}{ve^v \left(\ln \frac{2}{v} + \frac{1}{v} \right)} = 1,$$

$$\lim_{v \rightarrow \infty} \frac{1}{ve^v [K_0(v) + K_1(v)]} = \lim_{v \rightarrow \infty} \frac{1}{ve^v \left(\sqrt{\frac{\pi}{2v}} e^{-v} + \sqrt{\frac{\pi}{2v}} e^{-v} \right)} = 0.$$

Consequently the integrand

$$F(\eta - s, v) = \frac{e^{-v(\eta-s)}}{ve^v [K_0(v) + K_1(v)]} \quad (\text{II.66})$$

within the limits of $0 \leq v \leq \infty$ changes monotonically from 1 to 0, and as $(\eta - s)$ increases this function tends to zero exponentially. [123]

Fig. 65 shows curves of function (II.66) for different values of $(\eta - s)$. By measuring the curves of the function $F(\eta - s, v)$ with a planimeter we find numerical values for I_1 which is of interest to us. These values are presented graphically in Fig. 66.

Using a numerical value for I_1 for subsequent determination of function $u_2(s)$ is greatly hindered by the existence behind the integral sign in (II.65) of the arbitrary function $v_2(\eta)$. Therefore in order to pursue an analytical solution to the problem we will find, relying on the numerical solution found, the value of the equation for I_1 . We will represent the integrand in the equation for I_1 in the form of a product of two functions:

$$I_1 = \int_0^{\infty} \frac{e^{-v(\eta-s)}}{\sqrt{v}} \cdot \frac{1}{\sqrt{v} e^v [K_0(v) + K_1(v)]} dv; \quad (\text{II.67})$$

The function

$$A(v) = \frac{1}{\sqrt{v} e^v [K_0(v) + K_1(v)]} \quad (\text{II.68})$$

is constant in sign in the interval $0 < v < \infty$ (Fig. 67).

The remaining part of the integrand in this interval is continuous. This makes it possible to use the second mean value theorem to calculate I_1 :

$$I_1 = A(v_i) \int_0^{\infty} \frac{e^{-v(\eta-s)}}{\sqrt{v}} dv, \quad (\text{II.69})$$

where $0 < v_i < \infty$.

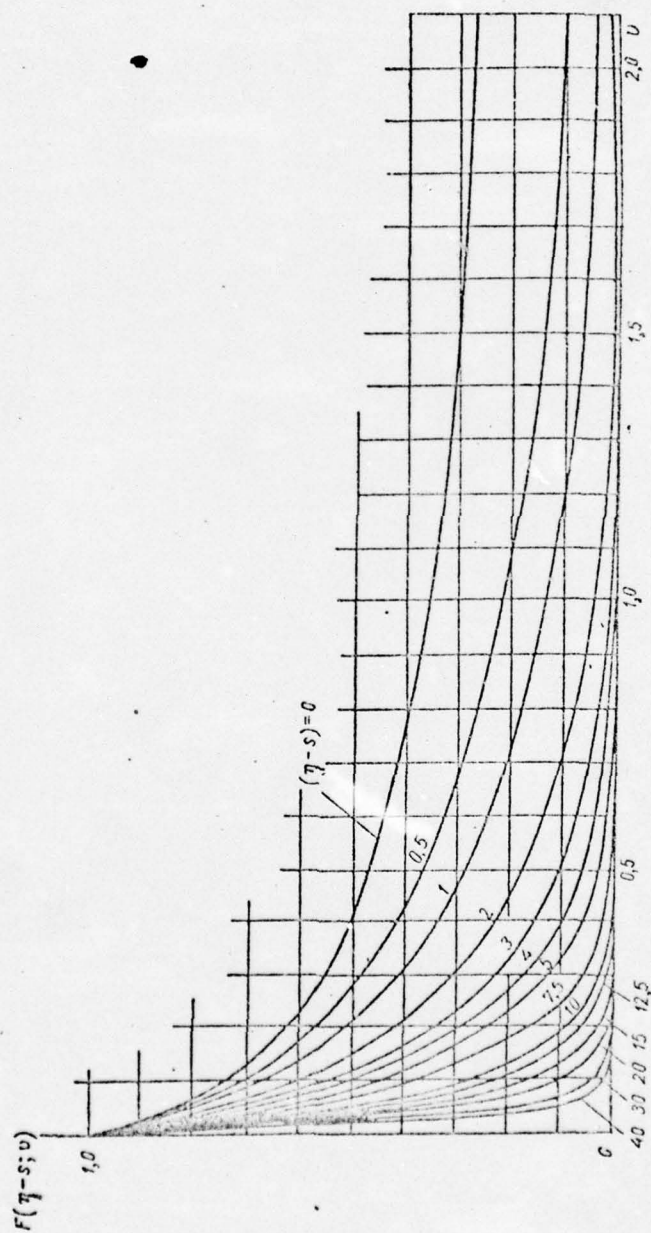


Fig. 65. Curves of function $F(\eta - s; v)$.

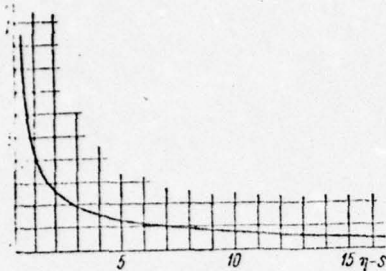


Fig. 66. Values of the equation $I_1(\eta - s) = \int_0^\infty \frac{e^{-v(\eta-s)} dv}{v e^v [K_0(v) + K_1(v)]}$

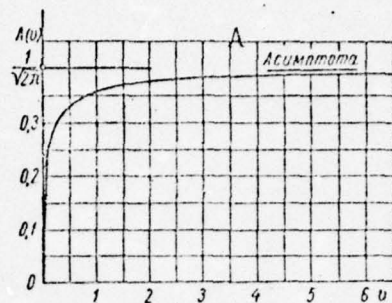


Fig. 67. Curve of the function $A(v)$.
KEY: A--asymptote.

Solving (II.69), we obtain

$$I_1 = \frac{A(v_i) \Gamma\left(\frac{1}{2}\right)}{\sqrt{\eta-s}}, \quad (\text{II.70})$$

where $\Gamma(1/2)$ is an Euler gamma function.

The numerical value found above for I_1 can also be transformed to the same form as (II.70)

$$I_1 = \frac{A_\Gamma(|\eta-s|)}{\sqrt{\eta-s}}. \quad (\text{II.71})$$

A graph of $A_\Gamma(|\eta-s|)$ is shown in Fig. 68. Equating (II.70) and (II.71), we find the condition for determining function $A(v_i)$

$$A(v_i) \Gamma\left(\frac{1}{2}\right) = A_\Gamma(|\eta-s|). \quad (\text{II.72})$$

It follows from identity (II.72) that $A(v_i)$ is a function of the difference $|\eta-s|$. As numerical calculations from zero to rather large values of $|\eta-s|$ show, identity (II.72) is satisfied best when [125

$$A(v_i) = \frac{1}{\sqrt{2\pi} \sqrt{1+|\eta-s|}}. \quad (\text{II.73})$$

At very large asymptotic values of $|\eta-s|$ identity (II.72) is satisfied best by the function

$$A(v_i) = \frac{2}{\sqrt{2\pi} [2+|\eta-s|]}. \quad (\text{II.74})$$

For a comparison with exact values of A_Γ curves of the functions

$$\frac{\Gamma\left(\frac{1}{2}\right)}{\sqrt{2\pi} \sqrt{1+|\eta-s|}} \quad \text{and} \quad \frac{2\Gamma\left(\frac{1}{2}\right)}{\sqrt{2\pi} [2+|\eta-s|]}$$

are presented in Fig. 68.

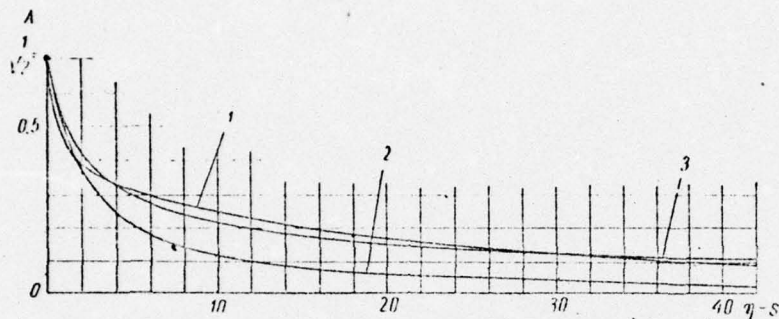


Fig. 68. Approximate and exact values of the function $A(|\eta - s|)$.

1-- A_T ; 2-- $\frac{2\Gamma\left(\frac{1}{2}\right)}{\sqrt{2\pi} (2+|s-\eta|)}$; 3-- $\frac{\Gamma\left(\frac{1}{2}\right)}{\sqrt{2\pi} \sqrt{1+|s-\eta|}}$.

As a result of the analysis performed for determining the value of the integral equation for I_1 , we obtain the following formulas:

a) exact solution

$$I_1 = i \frac{A_T(|\eta-s|)}{\sqrt{s-\eta}}; \quad (\text{II.75})$$

b) approximate solution which holds from zero to rather large values of $|\eta - s|$

$$I_1 = i \frac{\Gamma\left(\frac{1}{2}\right)}{\sqrt{2\pi}} \cdot \frac{1}{\sqrt{s-\eta} \sqrt{1+|s-\eta|}}; \quad (\text{II.76})$$

c) approximate solution for very large and asymptotic values of $|\eta - s|$

$$I_1 = i \frac{2\Gamma\left(\frac{1}{2}\right)}{\sqrt{2\pi}} \cdot \frac{1}{\sqrt{s-\eta}} \cdot \frac{1}{(2+|s-\eta|)}. \quad (\text{II.77})$$

An analogous approximate solution could be found for the entire range of change $0 \leq |\eta - s| \leq \infty$ by presenting graphical function I_1 in the form of the series

[126]

$$I_1 = \sum_{k=0}^{\infty} \frac{A_{2k+1}}{(s-\eta)^{\frac{2k+1}{2}}}$$

or even in the form of a trigonometric series. However, such expansions are not effective for purposes of investigating further.

By substituting (II.75)--(II.77) into (II.65) we obtain the following relations for determining the function $u_2(s)$.

An exact solution to integral equation (II.44) is

(II.78)

or

$$u_2(s) = \frac{d}{ds} \int_0^s \frac{v_2(\eta) A_1(|s-\eta|)}{\sqrt{s-\eta}} d\eta$$

$$u_2(s) = \left[\frac{v_2(\eta) A_1(s)}{\sqrt{s}} + \int_0^s \frac{v_2'(\eta) A_1(|s-\eta|)}{\sqrt{s-\eta}} d\eta \right], \quad (II.79)$$

where

$$v_2'(\eta) = \frac{dv_2(\eta)}{d\eta}$$

An approximate solution to equation (II.44) which holds from zero to rather large values of s is

$$u_2(s) \approx -\frac{\Gamma\left(\frac{1}{2}\right)}{\sqrt{2\pi}} \frac{d}{ds} \int_0^s \frac{v_2(\eta)}{\sqrt{s-\eta} \sqrt{1+|s-\eta|}} d\eta. \quad (II.80)$$

An approximate solution for asymptotic values of s is [127

$$u_2(s) \approx -\frac{2\Gamma\left(\frac{1}{2}\right)}{\sqrt{2\pi}} \frac{d}{ds} \int_0^s \frac{v_2(\eta)}{\sqrt{s-\eta} (2+|s-\eta|)} d\eta. \quad (II.81)$$

It can easily be seen that the expressions obtained for small values of $|s-\eta| \ll 2$ become the well-known solution of an Abel integral equation [12]

$$u_2(s) = -\frac{1}{\sqrt{2}} \frac{d}{ds} \int_0^s \frac{v_2(\eta)}{\sqrt{s-\eta}} d\eta, \quad (II.82)$$

which can be found directly from equation (II.44) if the

kernel $\sqrt{\frac{2+s-x}{s-x}}$ is replaced with its approximate value $\sqrt{\frac{2}{s-x}}$.

By using formulas (II.78)--(II.82) it is possible to find the function $v_2(\eta)$ for a given velocity $u_2(s)$, that is, to find the intensity of the vortex sheet trailing from the sharp edge of a nonstationarily moving foil.

Using the substitutions $x = \alpha/a$ and $s = \alpha_1/a$ to transform (II.5) and also formulas (II.17)--(II.19) to dimensionless form, replacing s in $u_2(s)$ with x , and integrating, we determine for a given value of $v_2(\eta)$ the circulation and hydrodynamic forces acting on a foil during nonstationary movement.

Below we present several examples of computations of $u_2(x)$, $r(s)$, and $\gamma(s)$ for the most typical types of function $v_2(\eta)$. There is also a comparison of data obtained with the results of solutions previously found.

By way of a first and very simple example we will consider the movement of a profile from a state of rest at a constant velocity of $u_0 = \text{const.}$ Inasmuch as in this case movement begins from a state of rest circulation Γ_0 , according to Thompson's theorem, is equal to zero. Function $v_2(\eta)$ in accordance with formula (II.42) will be equal to $v_2(\eta) = -u_0\beta_0$. Using the formulas presented above we obtain for this type of movement the following dimensionless expressions for the velocity discontinuity function $u_2(s) = u_2(s)/u_0\beta_0$:

for $0 \leq s \ll 1$ [formula (II.82)]

$$\bar{u}_2(s) = \frac{1}{\sqrt{2s}}; \quad (\text{II.83})$$

for $0 \leq s \leq 20-30$ [formula (II.80)]

$$\bar{u}_2(s) = \frac{1}{\sqrt{2s} \sqrt{1+s}}; \quad (\text{II.84})$$

for $s \rightarrow \infty$ [formula (II.81)]

[128

$$\bar{u}_2(s) = \frac{1}{\sqrt{2s} \left(1 + \frac{1}{2}s\right)}. \quad (\text{II.85})$$

Fig. 69 shows approximate values of $u_2(s)$ as determined from formulas (II.83)--(II.85) and also the exact value of $u_2(s)$ found from formula (II.79). Here also is the value of $u_2(s)$ as obtained by Wagner [4] for the given type of movement as a result of the above described approximate numerical calculation of integral equation (II.44).

A comparison shows that the exact and approximate values found for $u_2(s)$ agree well with those found for this special case of foil movement using the Wagner numerical method. As

should be expected formula (II.74) gives values of $u_2(s)$ close to the exact ones only up to $s \leq 1$. At greater values of s the results are inflated. The values of $u_2(s)$ obtained with formula (II.80) practically coincide with the exact solution up to $s \leq 20-30$.

Asymptotic formula (II.81) approaches the exact solution in the best possible fashion when $s > 30-40$.

Corresponding dimensionless values of circulation $\bar{\Gamma}(s) = \Gamma(s)/2\pi\alpha u_0 \beta_0$ for a given foil movement are found from formula (II.5) which after transformation to dimensionless form, substitution of formulas (II.83)--(II.85), and integration make it possible to obtain the following expressions:

for $0 \leq s \ll 1$

$$\bar{\Gamma}(s) \approx \frac{\sqrt{2}}{\pi} \sqrt{s}; \quad (\text{II.86})$$

for $0 \leq s \leq 20-30$

$$\bar{\Gamma}(s) \approx \frac{\sqrt{2}}{\pi} \text{Arsh } \sqrt{s}; \quad (\text{II.87})$$

for $s \rightarrow \infty$

$$\bar{\Gamma}(s) \approx \frac{2}{\pi} \text{arctg } \sqrt{\frac{s}{2}}. \quad (\text{II.88})$$

Fig. 70 shows circulation as calculated with approximate formulas (II.86)--(II.88). The figure also shows the exact value of $\bar{\Gamma}(s)$ obtained as a result of numerical integration of the expression

$$\bar{\Gamma}(s) = \frac{1}{\pi} \int_0^s l_1(x) dx. \quad (\text{II.89})$$

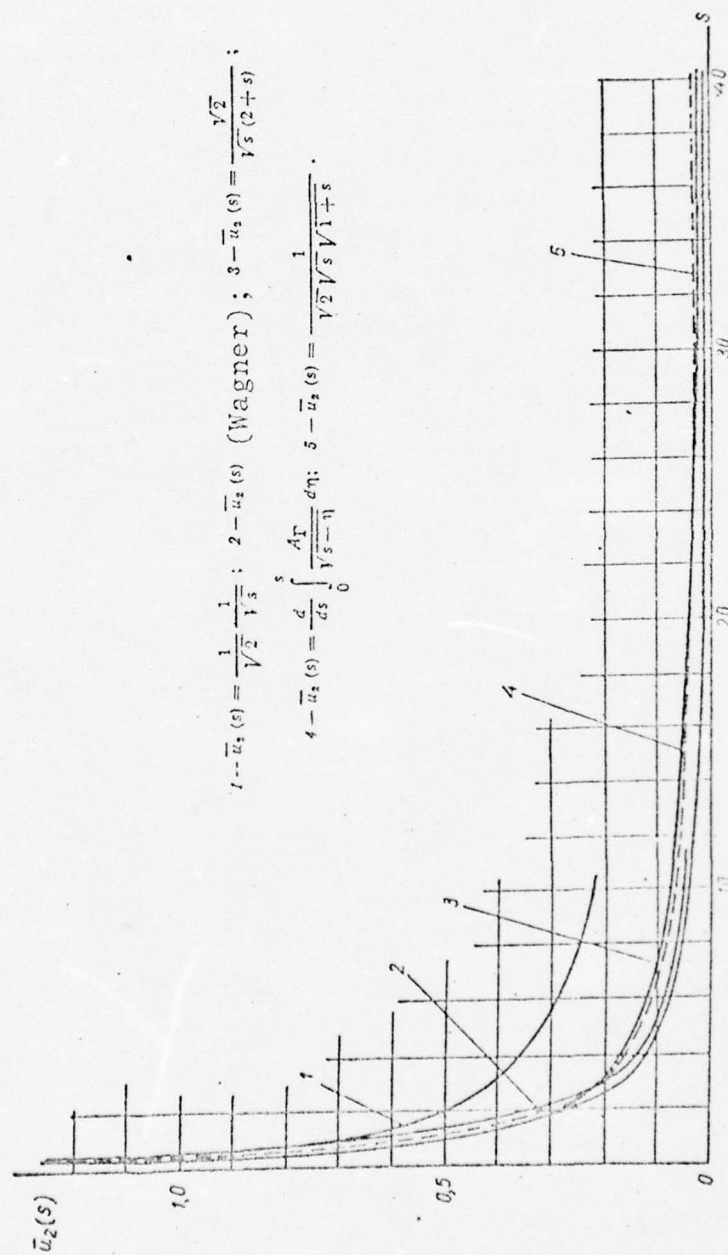
The graph in Fig. 70 makes it possible to trace the development of circulation on a foil in relation to its movement. When $s \rightarrow \infty$ the circulation tends toward its full values $\bar{\Gamma}(s) = 1$.

The lift is determined in the case of foil movement under [130 consideration from the following formulas ($\bar{Y} = \bar{Y}_2 + \bar{Y}_3$):

for $0 \leq s \leq 1$

$$\bar{Y} = \left[1 - \frac{\sqrt{2} K\left(\sqrt{\frac{s}{s+2}}\right)}{\pi \sqrt{s+2}} \right]; \quad (\text{II.90})$$

Fig. 69. Velocity discontinuity function $u_2(s)$ for a thin foil moving from a state of rest at constant velocity



for $0 \leq s \leq 20-30$

$$\bar{\gamma} = \left[1 - \frac{\sqrt{2}}{\pi} \frac{K \left(\sqrt{\frac{s(s+3)}{(s+1)(s+2)}} \right)}{\sqrt{(s+1)(s+2)}} \right]; \quad (\text{II.91})$$

for $s \rightarrow \infty$

$$\bar{\gamma} = \left[1 - \frac{\sqrt{2}}{\pi} \frac{\Pi(n, K)}{\sqrt{s+2}} \right]. \quad (\text{II.92})$$

In the above formulas $\bar{\gamma} = \gamma/\gamma_{st}$ is the dimensionless expression for lift; $\gamma_{st} = 2\pi\rho\beta_0\omega_0 a$ the stationary value of lift; K a total elliptical integral of the first order; [131]

$$\Pi = \int_0^{\pi/2} \frac{d\varphi}{(1+n\sin^2\varphi)\sqrt{1-k^2\sin^2\varphi}}$$

a total elliptical integral of the third order; $n = s/2$; and

$$k = \sqrt{\frac{s}{s+2}}.$$

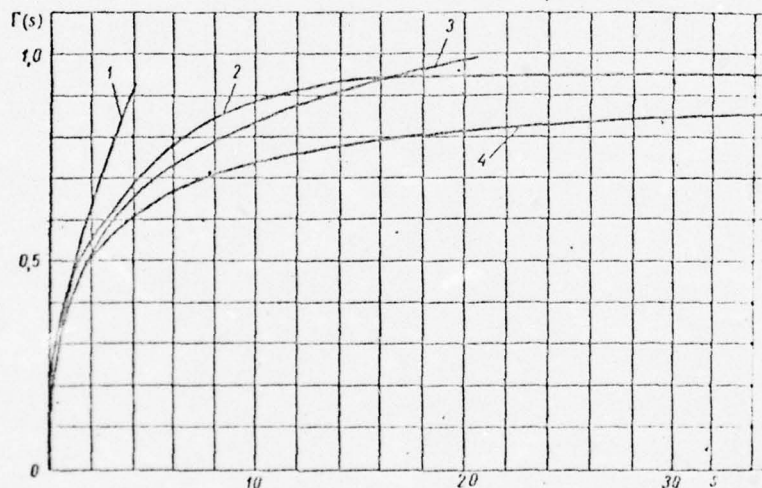


Fig. 70. Circulation $\bar{\gamma}(s)$ for movement of a thin foil from a state of rest at constant velocity.

Fig. 71 shows a graph of the integral equation for
ver the interval $0 \leq s \leq 40$.

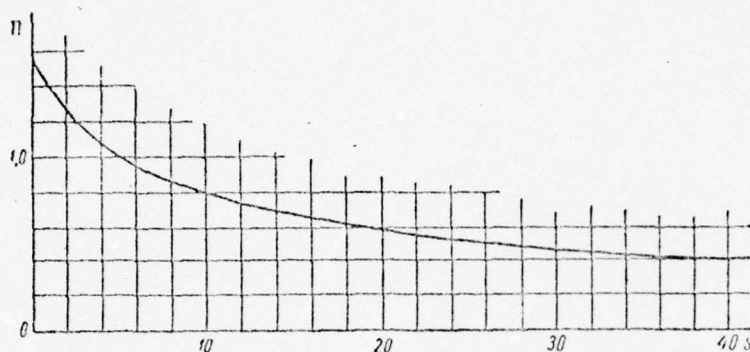


Fig. 71. Total elliptical integral of the third order $\Pi(s)$.

Values found for \bar{Y} using formulas (II.90) -- (II.92) are shown in Fig. 72. For comparison the figure also shows the results of Wagner calculations.

Expressions for determining the function $u_2(s)$ for a linearly changing normal velocity $v_2(\eta) = -k\eta$ can be found similarly. In this case the velocity discontinuity function and circulation around a foil can be found as follows:

for $0 \leq s \leq 1$

$$\left. \begin{aligned} u_2(s) &= \sqrt{2} k \sqrt{s}, \\ \Gamma(s) &= \frac{4}{3} \sqrt{2} (ak) s \sqrt{s}; \end{aligned} \right\} \quad (\text{II.93})$$

for $0 \leq s \gg 1$

$$\left. \begin{aligned} u_2(s) &= \sqrt{2} k \operatorname{Arsh} \sqrt{s}, \\ \Gamma(s) &= 2 \sqrt{2} (ak) \left[\left(\frac{1}{2} + s \right) \operatorname{Arsh} \sqrt{s} - \frac{1}{2} \sqrt{s} \sqrt{1+s} \right]; \end{aligned} \right\} \quad (\text{II.94})$$

for $s \rightarrow \infty$

$$\left. \begin{aligned} u_2(s) &= 2k \operatorname{arctg} \sqrt{\frac{s}{2}}, \\ \Gamma(s) &= 4 (ak) \left[(2+s) \operatorname{arctg} \sqrt{\frac{s}{2}} - 2 \sqrt{\frac{s}{2}} \right]. \end{aligned} \right\} \quad (\text{II.95})$$

In order to determine the exact value of $u_2(s)$ it is necessary to use the second of formulas (II.79), that is, integrate numerically the expression

[132

$$u_2(s) = k \left[2 \sqrt{s} A_R(s) + \int_0^s \frac{A_R(|s-\eta|)}{\sqrt{s-\eta}} d\eta \right]. \quad (\text{II.96})$$

Fig. 73 shows the results of calculations performed with formulas (II.93) -- (II.96).

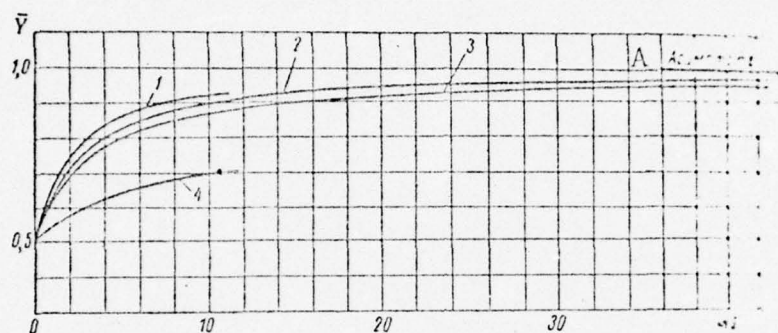


Fig. 72. Lift during movement of a thin foil from a state of rest at constant velocity.

KEY: A--asymptote.

1-- Y according to Wagner; 2-- $Y = 1 - \frac{\sqrt{s}}{\pi} \frac{1}{\sqrt{s+2}} \Pi(nk)$;

$$3--Y = 1 - \frac{\sqrt{s}}{\pi} \frac{1}{\sqrt{(s+1)(s+2)}} K \left[\frac{\pi}{2}, \sqrt{\frac{s(s+3)}{(s+1)(s+2)}} \right];$$

$$4--Y = 1 - \frac{\sqrt{s}}{\pi} K \left(\sqrt{\frac{s}{s+2}} \right).$$

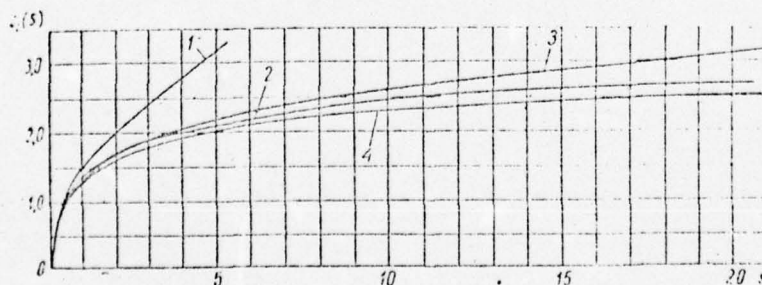


Fig. 73. Velocity continuity function $\bar{u}_2(s) = u_2(s)/k$ when a thin foil builds up velocity linearly from a state of rest.

1-- $\bar{u}_2(s) = \sqrt{2s}$; 2-- $\bar{u}_2(s)$ from formula (II.96); 3-- $\bar{u}_2(s) = \sqrt{2} \operatorname{Arch} \sqrt{s}$; 4-- $\bar{u}_2(s) = 2 \operatorname{arctg} \sqrt{\frac{s}{2}}$.

At velocities of $v_2(\eta) = -(n + k\eta)$ the values of function $u_2(s)$ are equal to the algebraic sum of corresponding solutions presented above.

The value of the velocity discontinuity function in the case of harmonic unsteady movement from a state of rest, that is, $v_2(\eta) = v_0 e^{i\bar{\omega}\eta}$, where $\bar{\omega} = k\alpha/u_0$ and k is the frequency of oscillation, is also of interest.

In §13 we presented values of function $u_2(s)$ for steady harmonic oscillation of a foil.

For small $s \ll 1$ and $v_2(\eta) = -v_0 e^{i\bar{\omega}\eta}$ function $u_2(s)$ can be expressed by the following formula: [133]

$$u_2(s) = v_0 \left\{ \frac{1}{\sqrt{2s}} + \sqrt{\pi\bar{\omega}} i e^{i\bar{\omega}s} \left[C(\sqrt{\bar{\omega}s}) - iS(\sqrt{\bar{\omega}s}) \right] \right\}, \quad (\text{II.97})$$

where C and S are Fresnel integrals.

When $\bar{\omega} \rightarrow 0$ and $v_2(\eta) \rightarrow (-v_0)$ formula (II.97) becomes formula (II.83) which was obtained for unsteady movement of a foil from a state of rest at constant velocity.

Let us assume that a foil moves at a constant velocity with variable angle of attack which obeys the harmonic law $\beta = \beta_0 e^{i\bar{\omega}\eta}$. This movement also starts from a state of rest. Then $v_2(\eta) = -u_0 \beta_0 e^{i\bar{\omega}\eta}$ and $v_0 = u_0 \beta_0$ and, consequently, the intensity of the vortex sheet can be determined from formula (II.97). In the case under consideration there is complex nonstationary movement starting from a state of rest at a constant velocity of u_0 and movement due to harmonic oscillations in the angle of attack $\beta = \beta_0 e^{i\bar{\omega}\eta}$. There is a term in formula (II.97) for each of these two types of nonstationary movement. Of great practical importance is the resulting unique principle of addition of solutions which is a consequence of the linearity of the integral equation considered above. Having a set of formulas for the function $u_2(s)$ for the simplest types of nonstationary movement, it is possible to apply this principle to many of the more complex cases of foil movement in order to find a function for intensity of a vortex sheet and, as a consequence, the hydrodynamic forces.

The total supporting hydrodynamic force ($\bar{Y} = \bar{Y}_2 + \bar{Y}_3$) for the type of foil movement under consideration at large values of ω is [134]

$$\bar{Y} = \left[1 - e^{-i\bar{\omega}s} \frac{\sqrt{2}}{\pi} \cdot \frac{K\left(\sqrt{\frac{s}{s+2}}\right)}{\sqrt{s+2}} - \frac{\Gamma\left(\frac{1}{2}\right)}{4} (1-i) \sqrt{\bar{\omega}} e^{i\bar{\omega}} H_0^{(2)}(\bar{\omega}) \right], \quad (\text{II.98})$$

where $\bar{Y} = Y_1/Y_2$; $Y_2 = 2\rho_0 \pi a u_0 v_0 e^{i\bar{\omega}s}$, and $H_0^{(2)}(\omega)$ is a second order Hankel function.

The following is the limit in formula (II.98):

$$\text{since} \quad \lim_{\bar{\omega} \rightarrow \infty} \bar{Y} = \frac{1}{2},$$

$$\begin{aligned} & \lim_{\bar{\omega} \rightarrow \infty} \text{Real} \left[(1-i) \sqrt{\bar{\omega}} e^{i\bar{\omega}} H_0^{(2)}(\bar{\omega}) \right] \\ &= \lim_{\bar{\omega} \rightarrow \infty} \left\{ \sqrt{\bar{\omega}} \left[I_0(\bar{\omega}) (\sin \bar{\omega} + \cos \bar{\omega}) - N_0(\bar{\omega}) (\cos \bar{\omega} - \sin \bar{\omega}) \right] \right\} \\ &= \lim_{\bar{\omega} \rightarrow \infty} \left\{ \sqrt{\bar{\omega}} \left[\sqrt{\frac{2}{\pi \bar{\omega}}} \cos \left(\bar{\omega} - \frac{\pi}{4} \right) (\sin \bar{\omega} + \cos \bar{\omega}) - \right. \right. \\ & \quad \left. \left. - \sqrt{\frac{2}{\pi \bar{\omega}}} \sin \left(\bar{\omega} - \frac{\pi}{4} \right) (\cos \bar{\omega} - \sin \bar{\omega}) \right] \right\} = \frac{2}{\sqrt{\pi}}. \end{aligned}$$

It follows directly from formula (II.97) that when $\bar{\omega} \rightarrow 0$ the effect of harmonic oscillations on the intensity of the vortex sheet and, consequently, on the force caused by it tends to zero.

All this is evidence that with the occurrence of harmonic unsteady movement of a foil the effect of trailing vortices at large frequencies of oscillations ($\bar{\omega} \rightarrow \infty$) leads, as in the case of steady harmonic oscillations [3], to cutting the quasistationary lift in half. In the case of low frequencies of oscillations $\bar{\omega} \rightarrow 0$ the effect of the vortex sheet tends to zero, that is, the forces supporting the foil are determined by the potential and quasistationary components of external forces.

By using the above general formulas the velocity discontinuity function, circulation, and hydrodynamic forces can also be found analogously for other types of unsteady foil movement in an unbounded liquid.

B. Hydrodynamic forces acting on a hydrofoil during unsteady movement [135]

Having discussed the main results from the theory of a thin foil moving nonstationarily in a flow of unbounded liquid, by using the methods of computation developed in preceding sections for arbitrary nonsteady movement of a foil we will proceed to formulate and solve the problem of determining nonstationary hydrodynamic forces acting on foils moving close to a free water surface.

§16. Formulation of the problem and derivation of integral equation for determining the intensity of the vortex sheet of a foil moving close to the water's surface

Let us consider the movement of a thin profile $(-a, +a)$ immersed beneath the free surface of a liquid to a depth of (Fig. 74). The profile executes movement the normal component of the velocity vector of which can be determined from formula (II.1). As formerly, the geometric angle of attack of the profile is β_0 and the velocity of additional disturbances affecting the foil are small.

Stipulating that movement of the profile begins from a state of rest, assuming the liquid to be weightless, and neglecting in the Lagrange integral squares of absolute velocities of movement of the liquid, we obtain the following boundary condition on the free surface of the liquid:

$$\begin{aligned} \phi &= 0 \text{ when } y_1 = 0; \\ -\infty &< x \leq \infty. \end{aligned} \quad (\text{II.100})$$

Condition (II.100) makes it possible to apply the principle of symmetry and to extend analytically the flow of the liquid to the upper half-plane, as a result of which we obtain a flow equivalent to the disturbance caused in a liquid by unsteady movement of a biplane in an unbounded flow (Fig. 75). The latter holds, as in the case of a hydrofoil during unsteady movement (see §4), only at large relative velocities of the principal movement.

Behind each foil of the biplane, starting immediately at the trailing edge, stretches a two-walled cut which is equivalent to a discontinuity in horizontal velocities or to a vortex wake with a vortex intensity behind upper and lower foils of $u_1(\alpha)$ and $u_2(\alpha)$ respectively. [136]

Let us replace the upper and lower foils of the biplane with vortex wakes of intensities $\omega_1(x)$ and $\omega_2(x)$. The vortex layer $\omega_1(x)$ will induce a normal velocity on the upper foil of [13]

$$\omega_{11} = -\frac{1}{2\pi} \int_{-a}^{+a} \frac{\omega_1(\xi) d\xi}{\xi - x}, \quad (\text{II.101})$$

where ξ is the abscissa of a singularity in moving xy coordinates and x is the abscissa of the point at which the given singularity induces a normal velocity.

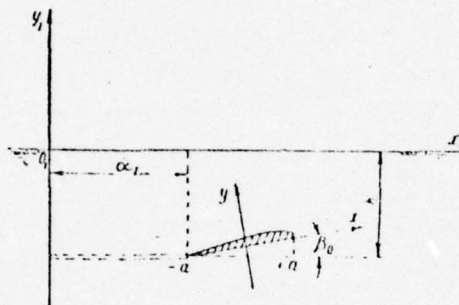


Fig. 74. Nonstationary movement of a foil near the water's surface (main notation).

The upper vortex wake on the upper foil will induce the normal velocity

$$v_{11} = \frac{1}{2\pi} \int_0^{\alpha_1} \frac{u_1(\alpha) d\alpha}{\xi - x}, \quad (\text{II.102})$$

where

$$\xi = \alpha - \alpha_1 - a, \quad -(\alpha_1 + a) \leq \xi \leq -a.$$

The normal velocity induced by the vortices of the lower foil on the upper is

$$\omega_{12} = -\frac{1}{2\pi} \int_{-a}^{+a} \frac{\omega_2(\xi) (\xi - x)}{(2h)^2 + (\xi - x)^2} d\xi. \quad (\text{II.103})$$

The lower vortex induces on the upper foil the normal velocity

$$v_{12} = \frac{1}{2\pi} \int_0^{\alpha_1} \frac{u_2(\alpha) (\xi - x)}{(2h)^2 + (\xi - x)^2} d\alpha. \quad (\text{II.104})$$

The normal velocity induced by all vortices at a certain point $A(x)$ on the upper foil will be

$$W_1(x) = -\frac{1}{2\pi} \int_a^{+a} \frac{\omega_1(\xi) d\xi}{\xi - x} + \frac{1}{2\pi} \int_0^{\alpha_1} \frac{u_1(\alpha) d\alpha}{\xi - x} -$$

$$-\frac{1}{2\pi} \int_{-a}^{+a} \frac{\omega_2(\xi) (\xi - x)}{(2h)^2 + (\xi - x)^2} d\xi + \frac{1}{2\pi} \int_0^{\alpha_1} \frac{u_2(\alpha) (\xi - x)}{(2h)^2 + (\xi - x)^2} d\alpha$$

or

[138

$$W_1(x) = \frac{1}{2\pi} \int_0^{\alpha_1} \left[\frac{u_1(\alpha)}{\xi - x} + \frac{u_2(\alpha) (\xi - x)}{(2h)^2 + (\xi - x)^2} \right] d\alpha -$$

$$-\frac{1}{2\pi} \int_{-a}^{+a} \left[\frac{\omega_1(\xi)}{\xi - x} + \frac{\omega_2(\xi) (\xi - x)}{(2h)^2 + (\xi - x)^2} \right] d\xi. \quad (\text{II.105})$$

By analogy, because of symmetry, the normal velocity induced by all vortices on the lower foil is

$$W_2(x) = \frac{1}{2\pi} \int_0^{\alpha_1} \left[\frac{u_2(\alpha)}{\xi - x} + \frac{u_1(\alpha) (\xi - x)}{(2h)^2 + (\xi - x)^2} \right] d\alpha -$$

$$-\frac{1}{2\pi} \int_{-a}^{+a} \left[\frac{\omega_2(\xi)}{\xi - x} + \frac{\omega_1(\xi) (\xi - x)}{(2h)^2 + (\xi - x)^2} \right] d\xi. \quad (\text{II.106})$$

In view of the fact that separation-free flow around foils is under consideration, normal velocities (II.105) and (II.106) are equal to velocities $v_n(x, t)$ [see formula (II.1)] or upon rise of unsteady movement not from a state of rest are equal to v_2 [see formula (II.42)].

Subjecting (II.105) and (II.106) to one of these conditions we obtain the system of equations

$$\left. \begin{aligned} & \int_0^{\alpha_1} \left[\frac{u_1(\alpha)}{\xi - x} + \frac{u_2(\alpha) (\xi - x)}{(2h)^2 + (\xi - x)^2} \right] d\alpha - \\ & - \int_{-a}^{+a} \left[\frac{\omega_1(\xi)}{\xi - x} + \frac{\omega_2(\xi) (\xi - x)}{(2h)^2 + (\xi - x)^2} \right] d\xi = 2\pi v_n, \\ & \int_0^{\alpha_1} \left[\frac{u_2(\alpha)}{\xi - x} + \frac{u_1(\alpha) (\xi - x)}{(2h)^2 + (\xi - x)^2} \right] d\alpha - \\ & - \int_{-a}^{+a} \left[\frac{\omega_2(\xi)}{\xi - x} + \frac{\omega_1(\xi) (\xi - x)}{(2h)^2 + (\xi - x)^2} \right] d\xi = 2\pi v_n, \end{aligned} \right\} \quad (\text{II.107})$$

from which flow the following relations:

$$u_1(\alpha) = u_2(\alpha) = u(\alpha) \quad \text{and} \quad \omega_1(\xi) = \omega_2(\xi) = \omega(\xi).$$

The above equalities flow from the principle of symmetry.

Thus, in place of system of equations (II.107) we obtain [139]
two identical equations, each of which has the form

$$\begin{aligned} & \int_0^{\alpha_1} \frac{u(\alpha)}{\xi - x} \left[1 + \frac{(\xi - x)^2}{(2h)^2 + (\xi - x)^2} \right] d\alpha - \\ & - \int_{-a}^{+a} \frac{\omega(\xi)}{\xi + x} \left[1 + \frac{(\xi - x)^2}{(2h)^2 + (\xi - x)^2} \right] d\xi = 2\pi v_n. \end{aligned} \quad (\text{II.109})$$

Equation (II.109) contains two unknown functions $u(\alpha)$ and $\omega(\xi)$ which along with (II.109) must satisfy the condition flowing from Thompson's theorem that circulation around a contour enveloping a foil and its vortex wake must always be equal to zero if foil movements start from a state of rest.

It is easy to see that when $h \rightarrow \infty$ equation (II.109) describes the movement of a monoplane in an unbounded liquid. When $h \rightarrow 0$ we obtain the following formula from (II.109):

$$\int_0^{\alpha_1} \frac{u(\alpha)}{\xi - x} d\alpha - \int_{-a}^{+a} \frac{\omega(\xi)}{\xi - x} d\xi = \pi v_n, \quad (\text{II.110})$$

the solution to which should be doubled, having in mind the existence on segment $(-a, a)$ of a monoplane consisting of two combined foils.

In the case of steady movement, that is, $u(\alpha) = 0$, equation (II.109) acquires the form

$$\int_a^{+a} \frac{\omega(\xi)}{\xi - x} \left[1 + \frac{(\xi - x)^2}{(2h)^2 + (\xi - x)^2} \right] d\xi = -2\pi v_n. \quad (\text{II.111})$$

An approximate solution of equation (II.111) for stationary movement of a biplane in an unbounded liquid was obtained by N. F. Sakharnyy [14].

We will transform (II.109) so that we can express the velocity discontinuity function directly in terms of the normal velocities on segment $(-a, a)$. For this purpose we will replace functions $u(\alpha)$ and $\omega(\xi)$ in (II.109) with values of horizontal velocities on the contour of the two-walled cut

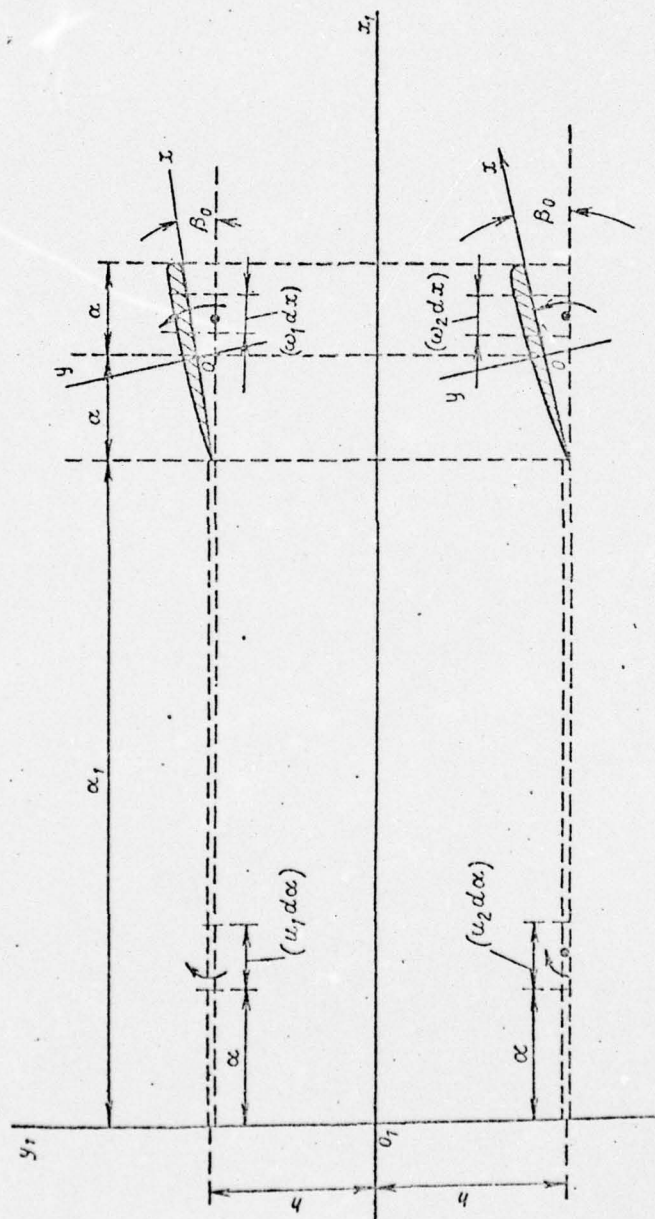


Fig. 75. Nonstationary movement of a biplane.

If $u_{22}(\alpha)$ and $\omega_{22}(\xi)$ are the values of horizontal velocities when approaching the cut from above and $u_{21}(\alpha)$ and $\omega_{21}(\xi)$ are respectively the same velocities when approaching the cut from below, then $u(\alpha) = u_{22}(\alpha) - u_{21}(\alpha)$ and also $\omega(\xi) = \omega_{22}(\xi) - \omega_{21}(\xi)$.

Substituting the latter formulas into equation (II.109), [140] we obtain

$$\begin{aligned} & \int_0^{\alpha_1} \frac{u_{22}(\alpha)}{(\xi - x)} \left[1 + \frac{(\xi - x)^2}{(2h)^2 + (\xi - x)^2} \right] d\alpha - \\ & - \int_0^{\alpha_1} \frac{u_{21}(\alpha)}{(\xi - x)} \left[1 + \frac{(\xi - x)^2}{(2h)^2 + (\xi - x)^2} \right] d\alpha - \\ & - \int_{-a}^{+a} \frac{\omega_{22}(\xi)}{(\xi - x)} \left[1 + \frac{(\xi - x)^2}{(2h)^2 + (\xi - x)^2} \right] d\xi + \\ & + \int_{-a}^{+a} \frac{\omega_{21}(\xi)}{(\xi - x)} \left[1 + \frac{(\xi - x)^2}{(2h)^2 + (\xi - x)^2} \right] d\xi = 2\pi v_n. \end{aligned} \quad (\text{II.112})$$

The left side of equation (II.112) represents a certain function $F(z)$ which is regular over the entire plane with the exception of cuts $(\alpha_1, +a)$ located symmetrically with respect to the real axis at a distance h and which is expressed by a Cauchy formula in terms of its value at the boundary of the cut. This makes it possible to replace (II.112) with the following equation:

$$2\pi i F(z) = 2\pi v_n \quad \text{or} \quad F(z) = -iv_n. \quad (\text{II.113})$$

As in the problem of unsteady movement of a monoplane, we will seek the relation $F(z)$ in a certain class of functions satisfying boundary conditions and conditions on the trailing edges of a biplane. For this purpose we will multiply both sides of (II.113) by the function $g(z)$ which in this case assumes the form

$$g(z) = \sqrt{\frac{z-a}{z+a}} \cdot \sqrt{\frac{z-a-i\tau}{z+a+i\tau}}. \quad (\text{II.114})$$

Function (II.114) can be simplified by assuming that the path traveled by a hydrofoil from the instant of inception of unsteady movement is small as compared with the chord of the foil $2a$ and the distance $2h$. This assumption, which was first used by G. Wagner to solve a similar problem [4], is equivalent to taking into account in a vortex wake trailing from a hydrofoil only those singularities which are located right at the rear

edge of a profile. As experiments show, as a consequence of dissipation of its energy a vortex wake rapidly breaks down and therefore the main influence on the process of unsteady movement of a foil is exerted by singularities located close to the profile.

The function $g(z)$, which can be written in the form

$$g(z) = \sqrt{\frac{2a + \alpha_1 - \alpha}{\alpha_1 - \alpha}} \cdot \sqrt{\frac{2a + \alpha_1 - \alpha + 2h}{\alpha_1 - \alpha + 2h}}$$

under the assumption that $(\alpha_1 - \alpha) \ll 2a$ and $(\alpha_1 - \alpha) \ll 2h$, becomes transformed into the following approximate relation: [141]

$$g(z) \approx \sqrt{\frac{2a}{\alpha_1 - \alpha}} \sqrt{1 + \frac{a}{h}}.$$

The second factor in the latter variation does not depend on the path of integration of α and amounts to a certain additive constant which after substitution of $g(z)$ into (II.113) can be shortened in subsequent operations. This gives a basis, as in the case of unsteady movement of a monoplane, to write function $g(z)$ in the form $g(z) \approx \sqrt{(z - a)/(z + a)}$, not forgetting the assumption made above.

As a result, we can write equation (II.113) in the form

$$F(z) \sqrt{\frac{z - a}{z + a}} = -iv_n \sqrt{\frac{z - a}{z + a}}.$$

Integrating over the contour of the cut $(\alpha_1, +a)$, we obtain

$$\begin{aligned} & \int_0^{\alpha_1} F(\xi) \sqrt{\frac{\xi - a}{\xi + a}} d\alpha + \int_{-a}^{+a} F(\xi) \sqrt{\frac{\xi - a}{\xi + a}} d\xi + \\ & + \int_{+a}^{-a} F(\xi) \left(-\sqrt{\frac{\xi - a}{\xi + a}}\right) d\xi + \int_{\alpha_1}^0 F(\xi) \sqrt{\frac{\xi - a}{\xi + a}} d\alpha = \\ & = -i \int_0^{\alpha_1} v_{22} \sqrt{\frac{\xi - a}{\xi + a}} d\alpha - i \int_{-a}^{+a} v_{22} \sqrt{\frac{\xi - a}{\xi + a}} d\xi - \\ & - i \int_{+a}^{-a} v_{21} \left(-\sqrt{\frac{\xi - a}{\xi + a}}\right) d\xi - i \int_{\alpha_1}^0 v_{21} \sqrt{\frac{\xi - a}{\xi + a}} d\alpha. \end{aligned}$$

Substituting into the latter expression the values of function $F(z)$ at the edges of the cut and also taking into account that $u_{22} = -u_{21}$, $\omega_{22} = -\omega_{21}$, and $v_{22} = v_{21} = -v_n$, we find

$$\begin{aligned}
& \int_0^{\alpha_1} u_{22} K \sqrt{\frac{\xi-a}{\xi+a}} d\alpha - \int_{-a}^{+a} \omega_{22} K \sqrt{\frac{\xi-a}{\xi+a}} d\xi - \\
& - \int_{+a}^{-a} \omega_{22} K \sqrt{\frac{\xi-a}{\xi+a}} d\xi - i \int_{\alpha_1}^0 u_{22} K \sqrt{\frac{\xi-a}{\xi+a}} d\alpha = \\
& = -i \int_0^{\alpha_1} v_{22} \sqrt{\frac{\xi-a}{\xi+a}} d\alpha - i \int_{-a}^{+a} v_{22} \sqrt{\frac{\xi-a}{\xi+a}} d\xi + \\
& + i \int_{+a}^{-a} v_{22} \sqrt{\frac{\xi-a}{\xi+a}} d\xi - i \int_{\alpha_1}^0 v_{22} \sqrt{\frac{\xi-a}{\xi+a}} d\alpha,
\end{aligned}$$

or, shortening, we find

[142

$$\int_0^{\alpha_1} u_{22}(\alpha) K(h, \xi - x) \sqrt{\frac{\xi-a}{\xi+a}} d\alpha = - \int_{-a}^{+a} v_n(x, t) \sqrt{\frac{a-\xi}{a+\xi}} d\xi, \quad (\text{II.151})$$

where

$$K(h, \xi - x) = 1 + \frac{(\xi - x)^2}{(2h)^2 + (\xi - x)^2}.$$

Calculating the integral on the right side of equation (II.115), we obtain

$$\int_0^{\alpha_1} u_{22}(\alpha) K(h, \xi - x) \sqrt{\frac{\xi-a}{\xi+a}} d\alpha = -\alpha v_{22}, \quad (\text{II.116})$$

where

$$v_{22} = y' - u_0 \beta_0 - \frac{a}{2} \omega_0.$$

The singular first order integral equation (II.116) describes the intensity of a vortex sheet trailing from a hydrofoil moving nonstationarily. When $h \rightarrow \infty$ it becomes equation (II.44).

§17. Solution to an integral equation for a hydrofoil. Hydrodynamic forces in the general case of unsteady movement of a profile close to the free surface of the water

The general solution obtained above for integral equation (II.44) can be extended to equation (II.116). Transforming this equation to dimensionless form and expanding the solution into the series described in §15, we obtain the following expression:

$$u_{22}(s) = -\sqrt{\frac{2}{\pi}} \frac{d}{ds} \int_0^s v_{22}(\eta) I(\eta-s, h) d\eta, \quad (II.117)$$

where

$$I(\eta-s, h) = \int_{i\alpha+0}^{i\alpha+\infty} \frac{e^{i\omega(\eta-s)} - e^{i\omega\eta}}{(-i\omega) K(\omega)} d\omega; \quad (II.118)$$

$$K(\omega) = \sqrt{\frac{2}{\pi}} \int_0^\infty \left[1 + \frac{(1+x_0+t)^2}{(2h)^2 + (1+x_0+t)^2} \right] \sqrt{\frac{2+t}{t}} e^{i\omega t} dt; \quad (II.119)$$

$$\omega = u + iv; t = s - x; s = \frac{a_1}{a}; x_1 = \frac{a}{a}; x_0 = \frac{x}{a}; h_1 = \frac{h}{a}.$$

In the following discussion the subscript "1" will be dropped from x_1 and h_1 for simplicity of notation. [143]

It is easy to see that in order to determine the function $u_{22}(s)$ it is necessary to calculate integral equations (II.117) -- (II.119).

Calculation of the indicated integrals is in large measure simplified if it is stipulated that the path traveled by the coil is short. The latter stipulation makes it possible to transform (II.119) to the form

$$K(\omega) \approx \frac{2}{\sqrt{\pi}} \left[1 + \frac{1}{1 + (4h)^2} \right] \int_0^\infty \frac{e^{i\omega t}}{\sqrt{t}} dt$$

or

$$K(\omega) \approx \sqrt{\frac{t}{\pi}} (-i\omega)^{-1/2} \Gamma\left(\frac{1}{2}\right) \left[1 + \frac{1}{1 + (4h)^2} \right]. \quad (II.120)$$

Taking formula (II.120) into account, (II.118) acquires the form

$$I = \frac{\sqrt{\pi}}{2\Gamma\left(\frac{1}{2}\right) \left[1 + \frac{1}{1 + (4h)^2} \right]} \int_{i\alpha+0}^{i\alpha+\infty} \frac{e^{i\omega(\eta-s)} - e^{i\omega\eta}}{(-i\omega)^{1/2}} d\omega.$$

Resolving the above equation and substituting the value obtained into (II.117), we find

$$u_{22}(s) = -\frac{1}{\sqrt{2}} \frac{d}{ds} \int_0^s \frac{f_0(h) v_{22}(\eta)}{\sqrt{s-\eta}} d\eta, \quad (II.121)$$

where

$$f_0(h) = \frac{1 + (4h)^2}{2 + (4h)^2}. \quad (\text{II.122})$$

Formula (II.122) holds in all cases when there are disturbances in the main movement of the foil which are abrupt as to time. For processes closer to stationary the Prandtl hypothesis can be used similarly to obtain the formula

$$f_1(h) = \frac{1 + (2h)^2}{2 + (2h)^2}, \quad (\text{II.123})$$

a comparison of which with test data is shown in Fig. 76.

By comparing (II.121) with $u_2(s)$ for the case of movement of a foil in an unbounded liquid [see formula (II.82)] we see that they differ in the factor $f_i(h)$. Function $f_i(h)$ takes into account the effect of a free surface on the intensity of vortices trailing behind a nonstationarily moving foil. When $0 < h < \infty$ functions (II.122) and (II.123) vary in the range $\frac{1}{2} < f_i(h) < 1$ (Fig. 76).

It follows from (II.121) that when considering the movement of a foil close to a free surface we can arbitrarily replace it with some other foil moving in an unbounded liquid at somewhat different normal velocities. This conclusion follows directly from equation (II.116) if the assumption is made that the path traveled by the foil is short. [145]

As is known, in the case of an unbounded liquid hydrodynamic forces can be expressed in terms of normal velocities on a foil and the intensity of a vortex wake can be expressed by the following equation:

$$\begin{aligned} Y = & -2\rho_0 u_0 \int_{-a}^{+a} v_n(\xi, t) \sqrt{\frac{a-\xi}{a+\xi}} d\xi - \\ & -2\rho_0 \frac{d}{dt} \int_{-a}^{+a} v_n(\xi, t) \sqrt{a^2 - \xi^2} d\xi - \\ & -2\rho_0 a \left(u_0 + \frac{da}{dt} \right) \int_0^{a_1} \frac{u_2(a) da}{V| \xi^2 - a^2 |}. \end{aligned} \quad (\text{II.124})$$

By replacing, in accordance with what has been stated, $v_n(\xi, t)$ with $[f(h)v_n(\xi, t)]$ in formula (II.124) and also taking into account that

$$u_{22}(s)_{h=h_1} = f_i(h) u_2(s)_{h=\infty}, \quad (\text{II.125})$$

and integrating, we obtain an expression for determining the

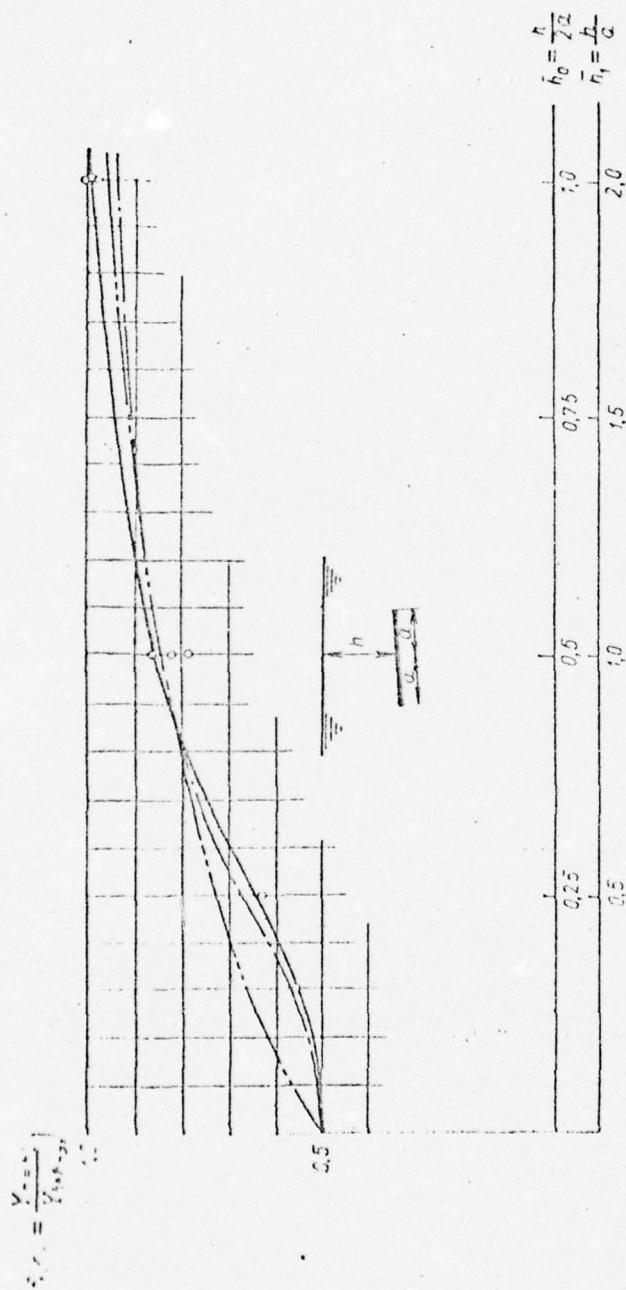


Fig. 76. Graph of function $f_1(h)$ which takes into account the effect of the free surface of the water on the lifting force of a hydrofoil. Circle--results of experiment; --- $f_1(h) = \frac{1 + (2h/a)^2}{2 + (2h/a)^2}$;

--- $f_1(h) = 1 - 0.5e^{-2.5h/a}$.

lift generated by a foil moving close to a free surface:

$$Y = -\frac{d}{dt} [f_i(h) \rho_0 \pi a^2 V_1] - 2\pi \rho_0 a u_0 f_i(h) \left(V_1 - \frac{a}{2} \omega_0 \right) - \\ - 2\rho_0 a \left(u_0 + \frac{da}{dt} \right) f_i(h) \int_0^{a_1} \frac{u_2(\alpha) d\alpha}{V|\xi^2 - a^2|}. \quad (\text{II.126})$$

Here $V_1 = y' - u_0 \beta_0$ and $u_2(\alpha)$ is a function determined from the integral equation for an unbounded liquid.

If it is considered that the force defined by the first and second terms in formula (II.126) is applied at the center of a profile chord and the force due to the effect of trailing vortices (third term) at the forward focal point ($x = \frac{1}{2}a$), a similar formula can be obtained also for the moment in the plane of a foil profile.

It is apparent from formula (II.126) that the effect of a free surface leads to a reduction of $f_1(h)$ in the hydrodynamic forces acting in an unbounded liquid.

Despite the fact that formula (II.126) is approximate, data calculated with it coincide very well with data from tests performed for arbitrary values of s .

If equations (II.118) and (II.119) are calculated without the stated stipulation, we can obtain

$$u_{22}(s) = -\frac{d}{ds} \int_0^s v_{22}(\eta) \frac{A_F(h, |s - \eta|)}{V|s - \eta|} d\eta, \quad (\text{II.127})$$

where A_F is a function analogous to the function represented by formulas (II.73) and (II.74), only in this case A_F depends also on the depth of immersion h of the foil. [146]

Numerical values for the function $A_F(h, |s - \eta|)$ are presented in Table 5. The table also contains values for the approximating function A_F^* which is expressed by the following formula:

$$A_F^* = \frac{1}{V^2} f_i(h) \frac{1}{V|1 + \psi(h)|s - \eta|}, \quad (\text{II.128})$$

where

$$\psi(h) = 1 + 2.84h^{0.23}e^{-0.22h}. \quad (\text{II.129})$$

Substituting into formula (II.127) the exact numerical value of function A_F or its approximation A_F^* and integrating for each given value of normal velocities at the rear focal point of a foil $v_{22}(\eta)$, we find the velocity discontin-

TABLE 5

Numerical Values of the Functions $A_{\Gamma}(h, |s - \eta|)$ and A_{Γ}^*

$\eta - s$	$\bar{h}=0$		$\bar{h}=0.5$		$\bar{h}=1.0$		$\bar{h}=1.5$		$\bar{h}=2.0$		$\bar{h}=3.0$		$\bar{h}=\infty$	
	A_{Γ}	A_{Γ}^*	A_{Γ}	A_{Γ}^*	A_{Γ}	A_{Γ}^*	A_{Γ}	A_{Γ}^*	A_{Γ}	A_{Γ}^*	A_{Γ}	A_{Γ}^*	A_{Γ}	A_{Γ}^*
0	0.354	0.354	0.590	0.590	0.667	0.667	0.688	0.688	0.696	0.696	0.703	0.703	0.707	0.707
0.5	0.264	0.259	0.348	0.407	0.382	0.437	0.410	0.472	0.430	0.483	0.442	0.504	0.528	0.577
1.0	0.225	0.250	0.296	0.331	0.320	0.369	0.350	0.382	0.368	0.392	0.375	0.413	0.450	0.500
2.0	0.191	0.204	0.240	0.254	0.269	0.284	0.283	0.294	0.300	0.302	0.311	0.322	0.382	0.408
3.0	0.175	0.177	0.209	0.214	0.230	0.239	0.231	0.248	0.260	0.255	0.260	0.272	0.350	0.353
4.0	0.164	0.158	0.190	0.189	0.206	0.210	0.207	0.218	0.228	0.225	0.236	0.240	0.328	0.316
5.0	0.155	0.145	0.179	0.170	0.190	0.190	0.180	0.197	0.201	0.203	0.214	0.217	0.311	0.289
7.5	0.137	0.121	0.150	0.141	0.169	0.157	0.150	0.163	0.169	0.168	0.164	0.180	0.274	0.242
10	0.123	0.106	0.126	0.124	0.150	0.137	0.126	0.142	0.158	0.147	0.158	0.158	0.247	0.213
12.5	0.116	0.095	0.118	0.111	0.141	0.123	0.115	0.127	0.143	0.132	0.141	0.142	0.233	0.192
15	0.101	0.089	0.108	0.102	0.132	0.112	0.108	0.117	0.139	0.121	0.135	0.130	0.201	0.177
20	0.085	0.077	0.089	0.088	0.110	0.098	0.103	0.101	0.120	0.105	0.112	0.113	0.170	0.154
30	0.063	0.064	0.077	0.072	0.088	0.080	0.071	0.083	0.104	0.086	0.100	0.093	0.126	0.127
40	0.048	0.055	0.063	0.060	0.070	0.070	0.057	0.072	0.076	0.075	0.073	0.080	0.095	0.110

uity function behind a foil moving close to a free surface in which we are interested.

The general expressions of hydrodynamic forces for a hydrofoil can be represented by the following formulas:

$$Y = -\frac{d}{dt} [f_i(h) \rho_0 \pi a^2 V_1] - 2\pi \rho_0 a u_0 f_i(h) \left(V_1 - \frac{a}{2} \omega_0 \right) - 2\rho_0 a \left(u_0 + \frac{da}{dt} \right) \int_0^{\alpha_1} \frac{u_{22}(\alpha) d\alpha}{\sqrt{|\xi^2 - a^2|}}; \quad (\text{II.130})$$

$$\mathfrak{M} = -f_i(h) \frac{\rho_0 \pi a^4}{8} \frac{d\omega_0}{dt} - \rho_0 \pi a^2 f_i(h) V_1 \left(u_0 + \frac{da}{dt} \right) - \rho_0 a^2 \left(u_0 + \frac{da}{dt} \right) \int_0^{\alpha_1} \frac{u_{22}(\alpha) d\alpha}{\sqrt{|\xi^2 - a^2|}}. \quad (\text{II.131})$$

In formulas (II.130) and (II.131) the coefficients $f_i(h)$ standing in front of the first terms describe the effect of the free surface on the force which takes into account the effect of the adjoining masses. Their magnitude can be determined with sufficient accuracy from formula (II.122), that is,

$$f_0(h) \approx \frac{1 + (4h)^2}{2 + (4h)^2}. \quad (\text{II.132})$$

An empirical formula obtained by the author based on an experiment performed with high-aspect hydrofoils in a test basin can also be recommended for the purpose of determining the values of $f_1(h)$ [15].

$$f_1(\bar{h}) \approx (1 - 0.5e^{-2.5\bar{h}}), \quad (\text{II.133})$$

where $\bar{h} = h/2a$.

The function $u_{22}(\alpha)$ which enters into the third terms of formulas (II.130) and (II.131) can be determined for a hydrofoil from (II.127) or for small ε from formula (II.122). [148]

Formulas (II.130) and (II.131) make it possible to find hydrodynamic forces during unsteady movement of a thin foil for any depth of immersion beneath a free surface. They yield correct limiting processes when the depth of immersion of the foil passes to zero and to infinity.

By way of example we will consider the generation of lift during movement of a hydrofoil from a state of rest at a constant velocity. In this case $v_{22} = -u_0 \delta_0$. After calculating with formula (II.127) we find that

$$u_{22}(x) = \frac{Ar(x, h)}{\sqrt{x}} u_0 \delta_0. \quad (\text{II.134})$$

Substituting (II.134) into (II.130), having preliminarily transformed (II.130) into dimensionless form, we obtain the following formula for lift Y :

$$\bar{Y} = \left\{ 1 - \frac{1}{\pi} \cdot \frac{f(h)}{f_1(h)} \sqrt{\frac{2}{\psi}} \frac{K \left(\sqrt{\frac{s(s+1/\psi+2)}{(s+2)(s+1/\psi)}} \right)}{\sqrt{(s+2)(s+1/\psi)}} \right\}, \quad (\text{II.135})$$

where

$$\bar{Y} = Y/Y_{st}, \quad Y_{st} = 2\pi\rho_0\beta_0 u_0^2 a f_1(h),$$

and K is a total elliptical integral of the first order.

Formula (II.135) describes the development of lift on a foil moving from a state of rest at a constant velocity at depth h under a free surface.

Fig. 77 shows the results of calculations made with formula (II.135) for the case $h_1 = 1$, that is, when the foil is immersed one-half chord beneath a free surface. For comparison the results of calculations for $h = \infty$ are also shown in the figure.

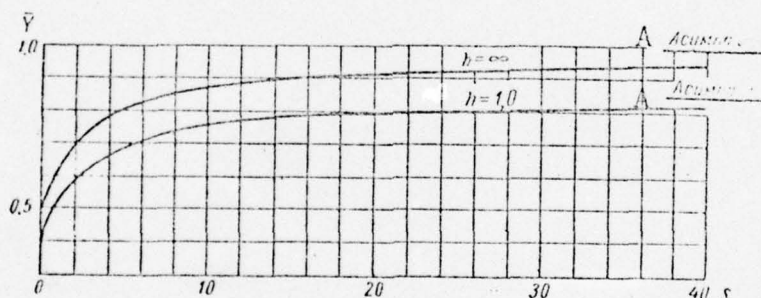


Fig. 77. Lift $Y(s)$ on a thin hydrofoil when it moves from a state of rest at a constant velocity. KEY: A--Asymptote.

We will cover below other special cases of unsteady movement of a hydrofoil when discussing application of the results obtained to practical problems in ship theory. [149]

§18. Experimental investigation of unsteady movement of a hydrofoil

The effect of a free surface on the performance of foils during steady modes of movement has been studied in the principal known experimental investigations into the hydrodynamic forces acting on hydrofoils.

In this section we will present the results of experimental

Investigation in a test basin into unsteady movement of a foil close to the surface of a liquid. The purpose of the tests was to obtain the experimental data needed to verify the results of theoretical investigation. The tests were conducted on a model of a foil with a span of 1.0 m and a chord length of 0.1 m. The relative thickness of the foil profile was 6%. The maximum thickness of the profile was at 40% chord from the nose.

The tests were performed on a setup consisting of a swinging mechanism which made it possible to impart various amplitudes, frequencies, and phases of pitch and heave and also meters and instruments including tensometric force sensors, amplifier, and oscillograph for recording external forces. The foil was attached to the setup at given geometric angles of attack.

Included in the program of tests was first of all determination of the relation between foil lift during steady movement and angles of attack at various depths of immersion. Then a determination was made of the development of lift on the foil at various depths of immersion with a given law governing the velocity of the carriage, beginning from zero. Finally, recordings were made of the lifting force on an oscillating foil at varying speeds of forward movement.

Fig. 78 shows values of the coefficient of stationary lift as a function of angles of attack and relative depth of immersion expressed in terms of chords ($\bar{h} = h/2a$) which satisfy approximate formula (II.133). They are of interest even though in the problems being discussed they have only ancillary significance.

The results of measurements of nonstationary lift on a foil whose velocity was made to vary in accordance with the law illustrated in Fig. 79 are given in Fig. 80 for different depths of immersion ($1.0 \leq \bar{h} \leq 6$) and different angles of attack ($-2^\circ \leq \beta_0 \leq 6^\circ$). The relation between nonstationary lift Y at a given instant of time t and lift Y_{st} during steady movement of the foil traveling at a velocity corresponding to time t are laid off as ordinates in the graph in Fig. 79. The value of Y/Y_{st} is given as a function of time which is laid off on the abscissa axis. Test data are presented in Fig. 80 without breakdown by angle of attack since the difference in Y/Y_{st} for different angles of attack in the indicated range lay within the experimental point spread for one instant of time and for one and the same depth of immersion. Consequently, the law governing the buildup of lift on a foil in the type of movement under consideration appears to depend little on the angle of attack and the depth of immersion has little effect on the law governing the change in lifting force. This shows that the effect of $\psi(\bar{h})$ [see formula (II.129)] on

[150]

the velocity discontinuity function $u_{21}(\alpha)$ is negligible since in this case it is close to unity.

Fig. 80 also shows the results of calculations made with a theoretical formula whose derivation will be covered later. Here we will only note that in this case theoretical data agree well with experimental.

Along with nonstationary movement, measurements were also made of complex movement involving a variable horizontal velocity in the presence of harmonic vertical oscillations. [152] Fig. 81 shows a sample of a recording of forces $Y_0(t)$ generated on an oscillating foil moving at a forward velocity of $u(t)$ varying in accordance with a law close to that shown in Fig. 79. The figure also shows the main parameters characterizing unsteady movement of the foil. Fig. 81 also shows the curve of $Y_p(t)$ representing the change in lifting force in the absence of harmonic oscillations but in the presence of all other conditions affecting foil movement.

An analysis of the curves in Fig. 81 and others like them revealed that at steady movement of a foil in the presence of frequency oscillations ($0.012 \leq \omega \leq 0.050$, where $\omega = ka/u_0$) the magnitude of the lifting force $Y_0(t)$ was no different from the force as calculated based on the hypothesis of stationarity (points in the graph of Fig. 81). The phase shift between displacement of the foil and oscillations in lifting force was about equal to $3\pi/2$. Both these results agree with the known solution for steady harmonic oscillations of a foil (see [3], pp. 85-86).

The graph in Fig. 81 confirms graphically the principle of superposition of solutions as stated above. In this case of foil movement $v_2(\eta) = y' - u(t)\beta_0$ where $y' = -A\omega e^{i\omega t}$.

Prior to occurrence of foil movement at a velocity of $u(t)$ vertical oscillations had already become established. As follows from the graph, over the entire range of change in velocity $0 \leq u(t) \leq u_0$ force $Y_0(t)$ amounts to the algebraic sum of the component of hydrodynamic force $Y_p(t)$ caused by the forward movement of the foil at velocity $u(t)$ and of the hydrodynamic force caused by harmonic oscillations of the foil $y' = -v_0 e^{i\omega t}$. Consequently, in calculations of the external forces acting on a foil during such movement each of the components of external forces can be obtained independently for any given unsteady foil movement. The resulting force acting on the foil will be equal to the algebraic sum of the separate components.

Experiments similar to what has been described but with small oscillations in amplitude were conducted at various

depths of foil immersion. A comparison of results from these experiments during steady movement of the foil made it possible to find experimental values for $f_1(h)$ which took into account the effect of the free surface on the total hydrodynamic force. Fig. 76 shows experimental values of $f_1(h)$ and values found using formula (II.123). A comparison of the experimental and theoretical curves for the function $f_1(h)$ shows good agreement between them.

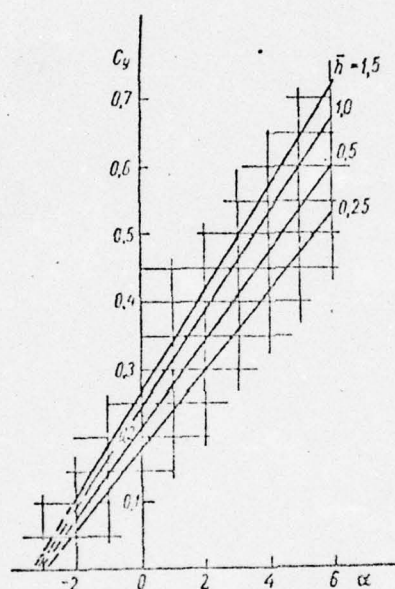


Fig. 78. Effect of immersion on lift coefficient $C_y(\alpha)$ for a segmental profile with $c = 0.05$ during steady movement.

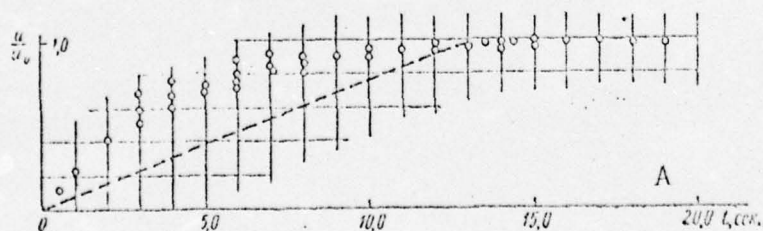


Fig. 79. Buildup in speed of movement of foil during experiment. (The circle shows experimental result.)
KEY: A-- t , sec.

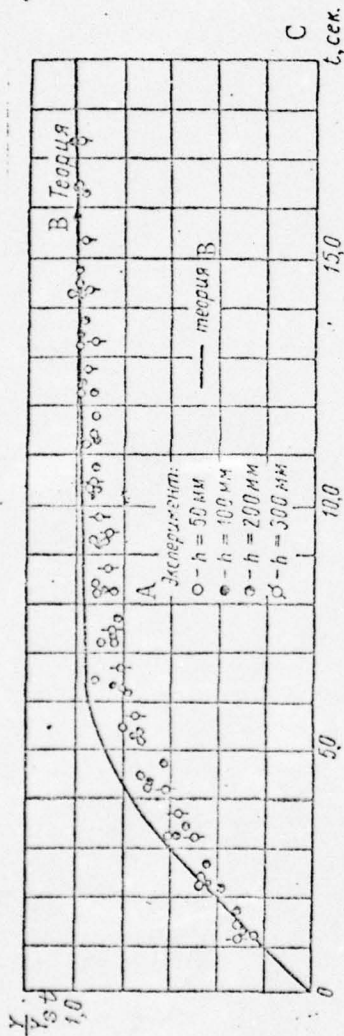


Fig. 80. Change in lift on foil during speed buildup obeying law illustrated in Fig. 79.
KEY: A--experiment; B--theory; C-- t , sec.

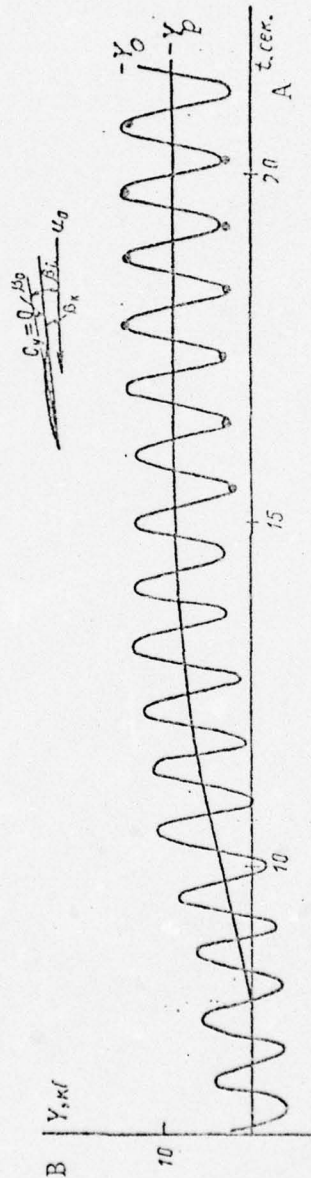


Fig. 81. Change in lift on oscillating hydrofoil during buildup of forward speed obeying the law illustrated in Fig. 79.
The solid line shows experimental results and the heavy dot calculated. Set horizontal velocity $u_0 = 3.97$ m/sec; frequency of oscillation $n = 0.93$ Hz; amplitude of oscillation $A = 50$ mm; depth of immersion $h = 300$ mm; angle of attack $\alpha = 1.1^\circ$.
KEY: A-- t , sec; B-- Y , kgf.

In the preceding sections we investigated unsteady movement of a single profile. The foil systems on high-speed craft constitute complex systems of foils. Therefore, in this section we will determine the effect of a free surface on a foil system.

By way of first example we will discuss unsteady movement of an infinite flat array of profiles. The profiles in the array are flat plates with a chord of $2a$ inclined to the flow at small angles of attack β (Fig. 82). The array moves at velocity u_0 in the positive direction of the real axis and it also has vertical and rotational disturbances with small velocities of y' and ω_0 respectively. We will use the symbol L to designate a contour encompassing cuts of the real axis C_1 and C_2 , each replacing one of the profiles lying on the real axis, and a straight-line vortex wake extending behind this profile. We will select outside contour L and in the plane of the flow a certain point z . We will designate a contour which encompasses the area of cuts C_1 and C_2 and also point z . According to the Cauchy formula we have between contours L and L'

$$\omega(z) = \frac{1}{2\pi i} \int_{L'} \frac{\omega(\xi) d\xi}{\xi - z} - \frac{1}{2\pi i} \int_L \frac{\omega(\xi) d\xi}{\xi - z}, \quad (\text{II.136})$$

where $\omega(z) = d\omega/dz$ is a function of complex velocity and ω is the complex velocity potential.

The integral over the L' contour encompasses the area within which point z lies. The integral over the L contour defines two different analytical functions within and without contour L . We will continue the analytical function expressed by the integral over the L' contour within the L contour which in the process we will deform to cut of the real axis C_1C_2 and the L' contour to an L'' contour and the set of contours $L(-\infty, \dots, L(-2), L(-1), L(1), L(2), \dots, L(n) \dots$

As a result, formula (II.136) can be written in the form

$$\begin{aligned} \omega(z) = & -\frac{1}{2\pi i} \int_L \frac{\omega(\xi) d\xi}{\xi - z} - \frac{1}{2\pi i} \int_{L(1)} \frac{\omega(\xi) d\xi}{\xi - z} - \\ & - \frac{1}{2\pi i} \int_{L(-1)} \frac{\omega(\xi) d\xi}{\xi - z} - \frac{1}{2\pi i} \int_{L(+2)} \frac{\omega(\xi) d\xi}{\xi - z} - \\ & - \frac{1}{2\pi i} \int_{L(-2)} \frac{\omega(\xi) d\xi}{\xi - z} \dots - \frac{1}{2\pi i} \int_{L(n)} \frac{\omega(\xi) d\xi}{\xi - z} - \\ & - \dots - \frac{1}{2\pi i} \int_{L(-n)} \frac{\omega(\xi) d\xi}{\xi - z} + \frac{1}{2\pi i} \int_{L''} \frac{\omega(\xi) d\xi}{\xi - z}, \end{aligned}$$

$$\begin{aligned}
\omega(z) = & -\frac{1}{2\pi i} \int_L \frac{\omega(\xi) d\xi}{z-\xi} - \frac{1}{2\pi i} \int_{L(1)} \frac{\omega(\xi) d\xi}{z-\xi} - \\
& - \frac{1}{2\pi i} \int_{L(-1)} \frac{\omega(\xi) d\xi}{z-\xi} - \frac{1}{2\pi i} \int_{L(2)} \frac{\omega(\xi) d\xi}{z-\xi} - \\
& - \frac{1}{2\pi i} \int_{L(-2)} \frac{\omega(\xi) d\xi}{z-\xi} - \dots - \frac{1}{2\pi i} \int_{L(n)} \frac{\omega(\xi) d\xi}{z-\xi} - \\
& - \frac{1}{2\pi i} \int_{L(-n)} \frac{\omega(\xi) d\xi}{z-\xi} = -\frac{1}{2\pi i} \int_{L''} \frac{\omega(\xi) d\xi}{z-\xi}.
\end{aligned}
\tag{II.137}$$

On contours $L(k)$ the argument ξ assumes the following values:

$$\xi_k = \xi + ik\tau,$$

therefore

$$\int_{L(k)} \frac{\omega(\xi) d\xi}{z-\xi} = \int_L \frac{\omega(\xi) d\xi}{z-\xi - ik\tau}. \tag{II.138}$$

Taking (II.138) into consideration, we will write formula (II.137) in the form

$$\begin{aligned}
\omega(z) = & \frac{1}{2\pi i} \int_L \omega(\xi) \left[\frac{1}{z-\xi} + \sum_{k=1}^{\infty} \left(\frac{1}{z-\xi - ik\tau} + \frac{1}{z-\xi + ik\tau} \right) \right] d\xi \\
= & -\frac{1}{2\pi i} \int_{L''} \frac{\omega(\xi) d\xi}{z-\xi}.
\end{aligned}
\tag{II.139}$$

Keeping in mind that

$$\begin{aligned}
\left[\frac{1}{z-\xi} + \sum_{k=1}^{\infty} \left(\frac{1}{z-\xi - ik\tau} + \frac{1}{z-\xi + ik\tau} \right) \right] = \\
= \left[\frac{\pi}{\tau} \operatorname{cth} \frac{\pi(z-\xi)}{\tau} \right],
\end{aligned}
\tag{II.140}$$

we obtain

$$\omega(z) = \frac{1}{2\pi i} \int_L \omega(\xi) \left[\frac{\pi}{\tau} \operatorname{cth} \frac{\pi(z-\xi)}{\tau} \right] d\xi - \frac{1}{2\pi i} \int_{L''} \frac{\omega(\xi) d\xi}{z-\xi}. \tag{II.141}$$

The integral over the L'' contour is an analytical function which is finite over the entire plane. According to the Louisville theorem such a function is constant. When

$L'' \rightarrow \infty$ and the array starts movement from a state of rest, this constant tends to zero

$$\omega(z) = \frac{1}{2\pi i} \int_L \omega(\xi) \left[\frac{\operatorname{cth} \frac{\pi}{\tau} (z - \xi)}{\frac{\tau}{\pi}} \right] d\xi \quad (\text{II.142})$$

or

[156

$$\frac{d\omega}{dz} = \frac{1}{2\pi i} \int_L \frac{d\omega}{d\xi} \left[\frac{\operatorname{cth} \frac{\pi}{\tau} (z - \xi)}{\frac{\tau}{\pi}} \right] d\xi. \quad (\text{II.143})$$

We will transform function (II.143) to the following form:

$$\frac{d\omega}{dz} = \frac{1}{2\pi i} \int_L \frac{d\omega}{d\xi} \left[\frac{\pi}{\tau} (z - \xi) \operatorname{cth} \frac{\pi}{\tau} (z - \xi) \right] d\xi. \quad (\text{II.144})$$

We will represent the function $d\omega/dz$, as formerly, in the form of a product of two functions [3]

$$\frac{d\omega}{dz} = \frac{df}{dz} \cdot g(z), \quad (\text{II.145})$$

where

$$g(z) = \prod \sqrt{\frac{z - a - ik\tau}{z + a - ik\tau}}, \quad k = 0, 1, 2, \dots$$

As formerly, we will assume that the path traveled by the system of profiles under consideration from the instant of inception of unsteady movement, that is, α_1 , is small compared with chord $2a$ and the spacing of the array. In this case function $g(z)$ which can be written in the form

$$g(z) = \prod \sqrt{\frac{2a + \alpha_1 - \alpha - ik\tau}{\alpha_1 - \alpha - ik\tau}}, \quad k = 0, 1, 2, \dots$$

becomes transformed to the following product of radicals:

$$g(z) \approx \sqrt{\frac{2a}{\alpha_1 - \alpha}} \cdot \sqrt{1 - \frac{2a}{i\tau}} \cdot \sqrt{1 - \frac{2a}{2i\tau}} \dots$$

It is easy to see that all radicals, with the exception of the first, do not depend on the path of integration in (II.144) and when substituted in the latter reduce to additive constants. This justifies writing function $g(z)$, as in the case of unsteady movement of a monoplane, in the form $g(z) \approx \sqrt{(z - a)/(z + a)}$, not forgetting however the assumption that the path traveled by the foil system from the instant of inception of unsteady movement is small. As formerly, on segments $(-a, a)$ $g(x + i0) = -g(x - i0)$ and on segments of the

vortex wake and in front of the foil $\text{Im } g(z) = 0$.

In light of what has been said, we transform (II.144) to the form

$$\frac{d\omega}{dz} = \frac{1}{2\pi i} \sqrt{\frac{z+a}{z-a}} \times \int_L \frac{d\omega}{z-\xi} \left[\frac{\pi}{\tau} (z-\xi) \text{cth} \frac{\pi}{\tau} (z-\xi) \right] \sqrt{\frac{\xi-a}{\xi+a}} d\xi. \quad (\text{II.146})$$

Contracting the L contour to cut in the real axis $C_1 C_2$ [157] and using $u_1 - iv_1$ and $u_2 - iv_2$ to designate values of $d\omega/dz$ when approaching the cut from below and from above respectively and also keeping in mind that $u_2 = -u_1$ and $v_2 = v_1 = -v_n$, we obtain the following expression for determining complex velocity:

$$\begin{aligned} \frac{d\omega}{dz} = \frac{1}{\pi i} \sqrt{\frac{z+a}{z-a}} \times \\ \times \left\{ \int_0^{a_1} \frac{u_2(\alpha) \left[\frac{\pi}{\tau} (x-\xi) \text{cth} \frac{\pi}{\tau} (x-\xi) \right] \sqrt{\frac{\xi-a}{\xi+a}} d\xi}{z-\xi} + \right. \\ \left. + \int_{-a}^{+a} \frac{v_n \sqrt{\frac{\xi-a}{\xi+a}} d\xi}{z-\xi} \right\}. \end{aligned} \quad (\text{II.147})$$

Comparing (II.147) with the expansion of the velocity function $d\omega/dz$ close to an infinitely distant point, we obtain for the case of inception of unsteady movement of a profile array from a state of rest the following integral equation:

$$\begin{aligned} \int_0^{a_1} u_2(\alpha) \left[\frac{\pi}{\tau} (\xi-x) \text{cth} \frac{\pi}{\tau} (\xi-x) \right] \sqrt{\frac{\xi-a}{\xi+a}} d\xi = \\ = -\pi v_2(\alpha_1), \end{aligned} \quad (\text{II.148})$$

where $v_2(\alpha_1) = y' - u_0\beta - a\omega_0/2$.

It is easy to show that the singular integral equation (II.148) when $\tau \rightarrow \infty$ becomes equation (II.21) which was considered above and in the case of an array consisting of two profiles, a biplane, it becomes equation (II.116).

Integral equation (II.148) can be obtained more simply by the method of singularities as was done above in the case of a hydrofoil.

Equation (II.148) is initial for determining the velocity

discontinuity function $u_2(\alpha)$. A solution to equation (II.148) can easily be obtained if the assumption made holds [4], that is, $(s - x) \ll 1$; $s = \alpha_1/\alpha$; $x = \alpha/\alpha$. In this case the equation assumes the form

$$\int_0^s \frac{u_2(x)}{V s - x} dx = -\frac{\pi}{V^2} \frac{\operatorname{th}\left(\frac{\pi}{\tau_0}\right)}{\frac{\pi}{\tau_0}} v_2(s), \quad (\text{II.149})$$

and its solution is

$$u_2(s) = -\frac{1}{V^2} \frac{d}{ds} \int_0^s \frac{f_\infty(\tau_0) v_2(\eta)}{V s - \eta} d\eta, \quad (\text{II.150})$$

where

[158]

$$f_\infty(\tau_0) = \frac{\tau_0}{\pi} \operatorname{th}\left(\frac{\pi}{\tau_0}\right); \quad \tau_0 = \frac{1}{\alpha}. \quad (\text{II.151})$$

Function (II.151) is a known correction for the effect of an array which is obtained for the case of stationary forward movement of an array consisting of thin profiles [16].

When $0 \leq \tau_0 \leq \infty$ function (II.151) changes in the range $0 \leq f_\infty(\tau_0) \leq 1$ (Fig. 83). The fact that formula (II.151) is the same for the start of movement $(s - x) \ll 1$ and also for the steady process makes possible the conclusion that with a certain amount of approximation also during unsteady movement it takes into account the main distinguishing aspects of the effect of an array on the hydrodynamic characteristics of a profile included in it.

It also follows from (II.150) that the effect of an array amounts to a change in the magnitude of normal velocities $v_n(\eta)$. This latter fact makes it possible to use the expression for lift of a profile in an unbounded liquid in calculating the lift of a profile included in an array [see formula (II.124)]. Substituting in this formula the values of normal velocities $v_n(\xi, t)$ in light of correction (II.151), we find the following formula for the lift generated on a profile in an array:

$$Y = -\frac{d}{dt} (f_\infty(\tau_0) \rho_0 \pi a^2 V_1) - 2\pi \rho_0 a u_0 f_\infty(\tau_0) \left(V_1 - \frac{a}{2} \omega_0 \right) - 2\rho_0 a \left(u_0 + \frac{da}{dt} \right) f_\infty(\tau_0) \int_0^{\alpha_1} \frac{u_2(\alpha) d\alpha}{V \sqrt{\frac{1}{4} - \alpha^2}}, \quad (\text{II.152})$$

where $V_1 = y' - u_0 \beta$ and the function $u_2(\alpha)$ is found from the integral equation derived for an isolated profile moving in an unbounded liquid [see formulas (II.78) -- (II.82)]. [159]

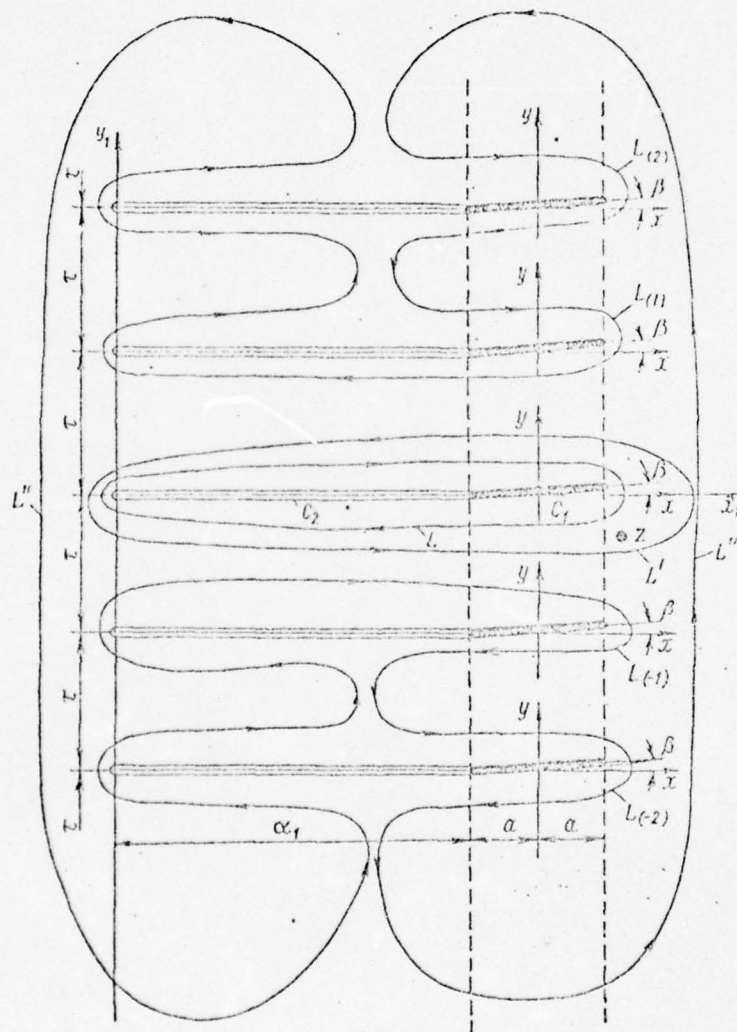


Fig. 82. Nonstationary movement of an infinite array of thin profiles (main notation).

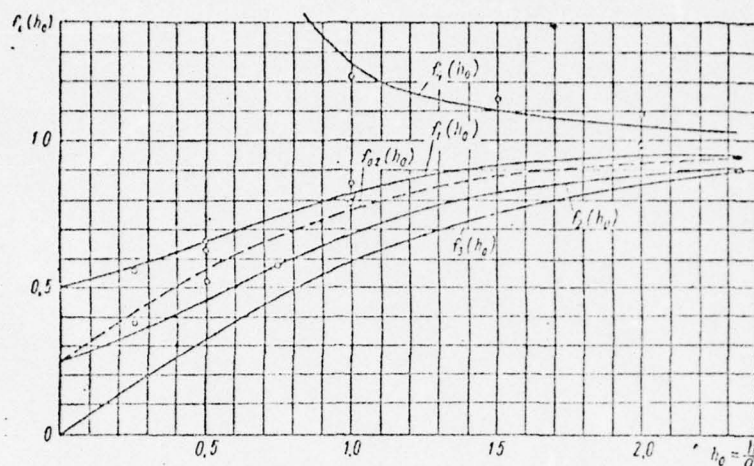


Fig. 83. Values of the coefficients $f_1(h_0)$ taking into account the effect of a free surface on the lift of a system of profiles. The solid line shows calculated results and the small circles experimental.

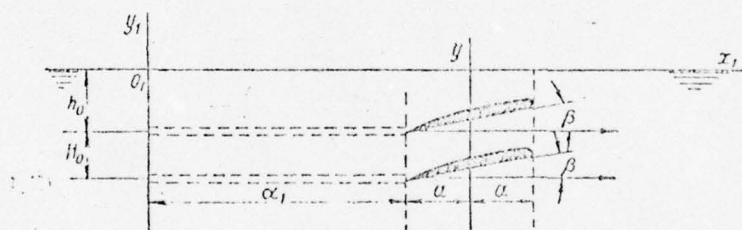


Fig. 84. Unsteady movement of an underwater biplane (main notation).

In calculating the moment of forces acting on a profile it should be kept in mind that when solving the problem in this approximate form the force defined by the first and second terms of formula (II.152) is applied at the center of the chord while the force due to the effect of trailing vortices (the third term) is applied at the forward focal point on the profile [7].

Analogous solutions can be obtained in the case of movement close to the surface for a system consisting of a finite number of profiles. In the case of a system of profiles consisting of two foils (underwater biplane, Fig. 84) the function allowing for nearness of the boundary of the liquid assumes the form:

a) when $H = 2h_0$ for the upper and lower profiles of the biplane respectively

$$f_2(h) = \frac{1 + 20h^3 + 64h^4}{4 + 56h^2 + 64h^4}, \quad (\text{II.153})$$

$$f_{02}(h) = \frac{1 + 56h^3 + 784h^4 + 2304h^6}{4 + 168h^2 + 1568h^4 + 2304h^6}, \quad (\text{II.154})$$

where $h = h_0/a$;

b) when $H \neq 2h_0$ formulas (II.153) and (II.154) become respectively

$$f_2(h, H) = \frac{1}{1 + \frac{1}{1 + (2h)^2} + \frac{1}{1 + H^2} + \frac{1}{1 + (2h + H)^2}}, \quad (\text{II.155})$$

$$f_{02}(h, H) = \frac{1}{1 + \frac{1}{1 + H^2} + \frac{1}{1 + (2h + H)^2} + \frac{1}{1 + (2h + 2H)^2}} \quad (\text{II.156})$$

Here $H = H_0/a$.

Curves for functions (II.153) and (II.154) appear in the graph in Fig. 83.

These methods can be used to solve the problem of unsteady movement of a thin profile traveling close to a wall or above the water's surface at great relative velocities and we will devote particular attention to this later. In the first approximation the value of this function can be calculated from the formula [160]

$$f_H(h) = 1 + \frac{1}{(2h)^2}. \quad (\text{II.157})$$

The function $f_H(h)$ also is shown in the graph in Fig. 83.

Taking into account the formulas presented, the expressions for lift (II.130) and (II.152) can be written for all these cases in the general form

$$\begin{aligned} Y = & -\frac{d}{dt} [f_i(h) \rho_0 \pi a^2 V_1] - \\ & - 2\pi \rho a u_0 f_i(h) \left(V_1 - \frac{a}{2} \omega \right) - \\ & - 2\rho a \left(u_0 + \frac{da}{dt} \right) f_i(h) \int_0^{a_1} \frac{u_z(a) da}{V \sqrt{\xi^2 - a^2}}. \end{aligned} \quad (\text{II.158})$$

Depending on the number of profiles making up a system function $f_1(h)$ assumes values in the range $f_1(h) \leq f_i(h) \leq f_\infty(h)$ when $h = \text{const.}$

In the case of unsteady movement of a profile above the

water's surface

$$f_1(h) = f_1(h).$$

The function $u_2(\alpha)$ in formula (II.158) can be determined from expressions (II.78) -- (II.82).

§20. Method for calculating external forces acting on a hydrofoil in a regular seaway

The formulas presented above can be used for determining the external forces generated on hydrofoils under the conditions prevailing in a regular seaway. In this case use of these formulas is limited by the following assumptions. It is considered that a foil is absolutely inelastic, the seaway harmonic, and the dimensions of the foil small compared with wave dimensions. It is assumed that the foil is immersed to a sufficient depth and during movement oscillates slightly, not piercing the free surface.

When a foil moves under these conditions a disturbance in normal velocities will be harmonic in nature, that is,

$$\delta V_1 = \text{Real } A e^{i\omega t} \quad \text{and} \quad \delta V_2 = \text{Real } B e^{i\omega t}. \quad (\text{II.159})$$

The hydrodynamic forces acting on a foil of finite span [161] can be determined by the following approximate formulas:

$$Y_1 = -\Delta m \omega^2 A e^{i\omega t}, \quad (\text{II.160})$$

where $\Delta m = \rho \pi a^2 k(\lambda) f_1(h)$ is the adjoining mass of the foil and $k(\lambda) = 1.2/(1.2 + \lambda)$ is the Pabst correction;

$$Y_2 - Y_{st} = -\left(\frac{\partial C_{y\lambda}}{\partial \beta}\right) f_1(h) \frac{\rho u_0^2}{2} \frac{B}{u_0} e^{i\omega t} S, \quad (\text{II.161})$$

where the stationary value of the lift is

$$Y_{st} = \left(\frac{\partial C_{y\lambda}}{\partial \beta}\right) f_1(h) (\beta + \beta_0) \frac{\rho u_0^2}{2} S; \quad (\text{II.162})$$

$(\partial C_{y\lambda}/\partial \beta)$ is the derivative of the lift coefficient with respect to the angle of attack when the foil moves in an unbounded liquid; β_0 is the angle of zero lift; and $S = 2a\lambda$ is the foil area.

$$Y_3 = -\left(\frac{\partial C_{y\lambda}}{\partial \beta}\right) f_1(h) \frac{\rho u_0^2}{2} S \frac{vB}{u_0} e^{i(\omega t + \phi)}, \quad (\text{II.163})$$

where v and ϕ are parameters determined from graphs [3] which are presented in Fig. 85 a and b as a function of

$$u = \omega a / u_0.$$

The total value of the nonstationary force acting on the foil will be

$$Y = Y_1 + Y_2 + Y_3. \quad (II.164)$$

The effect of a seaway is reflected in the hydrodynamic forces acting on a hydrofoil in two ways. First, the way the water flows around a foil changes because of the rotational and translational motion of the craft in the seaway. Second, there is a redistribution of velocities in the flow reaching the foil because of the orbital movement of particles in the liquid of a wave.

The following formulas are an approximate representation of heaving and pitching of a craft under conditions prevailing in a regular seaway. The following expression describes heaving:

$$H = H_G + H_a e^{i(\omega_1 t + \chi)}, \quad (II.165)$$

where H is the vertical displacement of the craft; H_G the ascent of the center of gravity of the craft as it moves at a given horizontal velocity u_0 in calm water; H_a the amplitude of heaving measured from H_G ; ω_1 the frequency of heaving; and χ the phase of heaving of the craft with respect to a wave expressed by the equation

$$\zeta = -r_0 \cos 2\pi \left(\frac{\xi}{\lambda_w} + \frac{t}{\tau_w} \right). \quad (II.166)$$

In the formula (II.166) ζ and ξ are coordinates of particles of liquid in a wave at instant of time t ; λ_w the length of the wave; and τ_w the period of oscillation (Fig. 86). [162]

Pitching of a craft can be described by the formula:

$$\varphi = \varphi_0 + \varphi_a e^{i(\omega_1 t + \psi)}, \quad (II.167)$$

where ϕ is the angular displacement of the craft in the centerline plane; ϕ_0 is the initial trim of the craft when moving at a velocity of u_0 in calm water; ϕ_a is the amplitude of pitching of the craft; and ψ is the phase of pitching with respect to the wave (Fig. 87).

When the heaving and pitching of a craft are known, it is not difficult to find the normal velocity of the rear focal point of the foil, that is, velocity v_f [see formula (II.1)]. Considering the dimensions of the foil to be small in comparison with its distance behind the center of gravity and assuming that at high velocities a hydrofoil craft heaves

and pitches with an apparent period, that is,

$$\tau_k = \frac{\lambda_w}{v_w + u_0 \cos \psi_k}; \quad \omega_1 = \omega_2 = \frac{2\pi}{\tau_k}, \quad (\text{II.168})$$

where $v_w \approx 1.25\sqrt{\lambda_w}$ is the velocity of wave movement and ϕ_k is the course angle of the craft. The approximate value of the increment of normal velocity v_2 can be written in the form

$$\delta v_2(t) = \text{Real } B e^{i\omega t}, \quad (\text{II.169})$$

where $B = H_a i \omega e^{i\chi} + r \varphi_a i \omega e^{i\psi} - u_0 \varphi_a e^{i\psi}$.

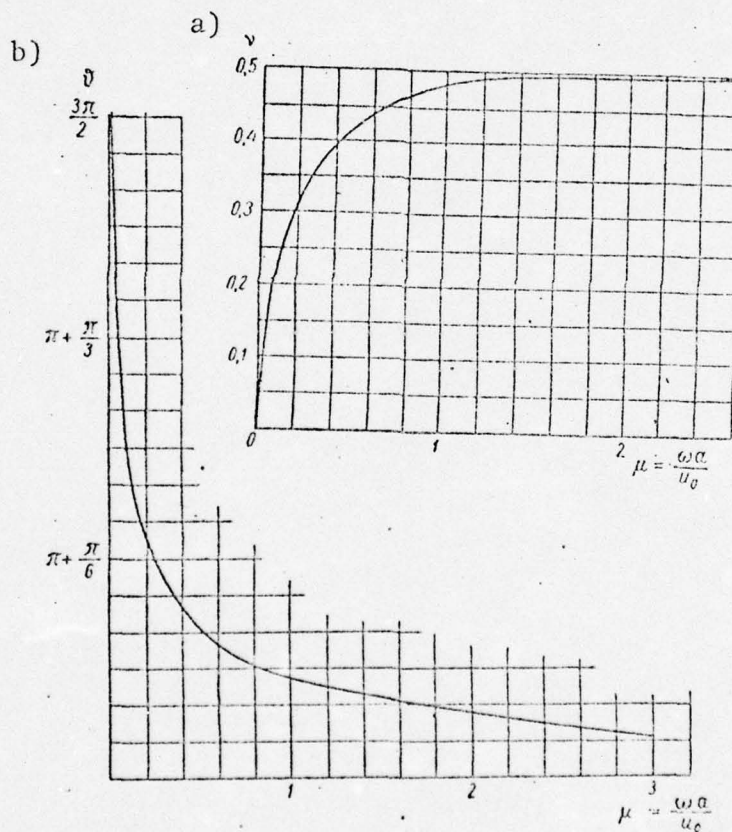


Fig. 85. Graphs of the coefficients v and θ : a-- $v(\mu)$; b-- $\theta(\mu)$.

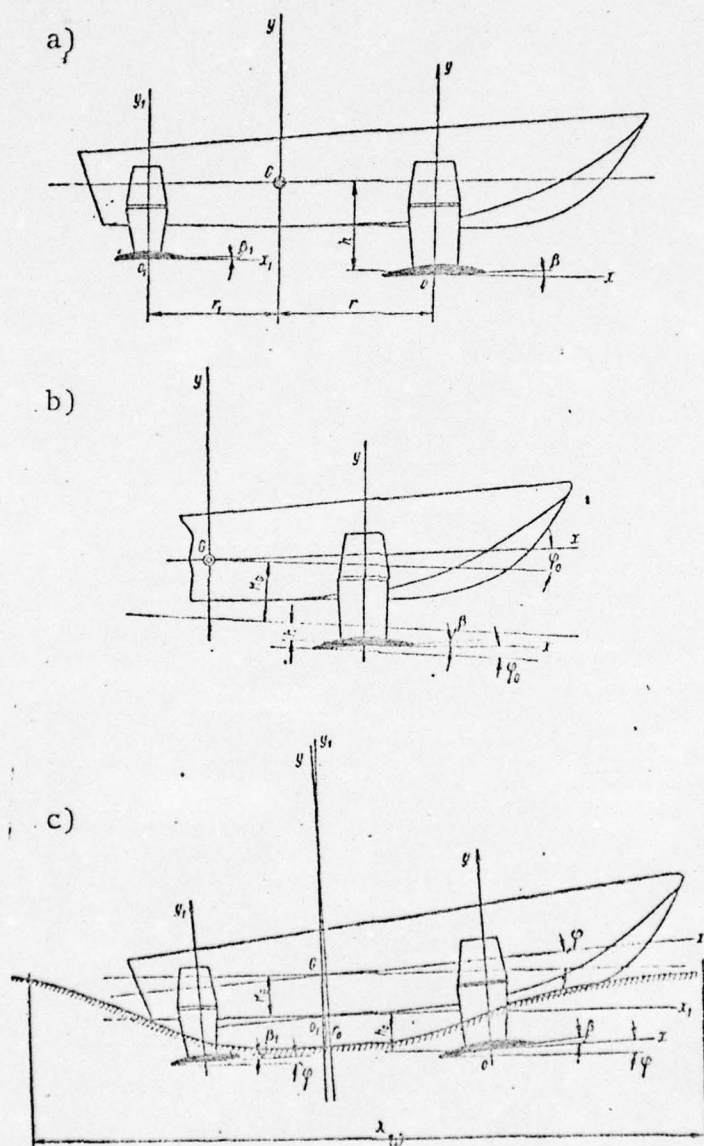


Fig. 86. Attitude of hydrofoil craft with respect to surface of water (main notation): a--when $u_0 = 0$; b-- u_0 calculated for calm water; c-- u_0 calculated for a wave.

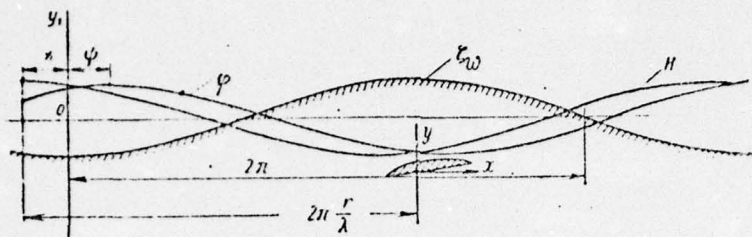


Fig. 87. Functions of heaving \bar{H} and pitching ϕ of a hydrofoil craft.

$$\begin{aligned} \bar{z}_w &= -r_0 \cos 2\pi \left(\frac{x}{\lambda} + \frac{t}{T} \right); \quad \bar{H} = \frac{H - H_0}{H_a} = \cos(\omega t + \chi); \\ \bar{\phi} &= \frac{\phi - \phi_0}{\phi_a} = \cos(\omega t + \psi). \end{aligned}$$

The effect of orbital motion of the water will be manifest in the main in the magnitude of the effective angle of attack of the foil. In a seaway described by formula (II.166) account must be taken of an additional angle of attack

$$\beta_w = \frac{\frac{v_y}{u_0}}{\sqrt{1 + \left(\frac{v_y}{u_0} \right)^2}}. \quad (\text{II.170})$$

Here

$$v_y = r_0 \sigma c^{kY_0} \sin(kx + \sigma t),$$

where $k = 2\pi/\lambda_w$, $\sigma = \sqrt{gk}$, and Y_0 is the depth of immersion of a particle of liquid beneath the free surface ($Y_0 < 0$) and $v_y/u_0 \ll 1$.

Substituting (II.169) and (II.170) into formula (II.164) we obtain the following expression for the external nonstationary hydrodynamic forces acting on a hydrofoil under the conditions prevailing in a regular seaway: [165]

$$\begin{aligned} Y - Y_1 &= \frac{\partial C_{yl}}{\partial \beta} f_l(h) \left\{ (\beta_0 + \beta + \phi_0) - \right. \\ &\quad \left. - \left[\frac{H_0 i \omega e^{i\chi}}{u_0} + \frac{r \phi_0 i \omega e^{i\chi}}{u_0} - \phi_a e^{i\psi} + \right. \right. \\ &\quad \left. \left. + \beta_a e^{i\theta} \right] \left[e^{i\omega t} + v e^{i(\omega t + \theta)} \right] \right\} \frac{\rho u_0^2}{2} S. \end{aligned} \quad (\text{II.171})$$

In formula (II.171) the terms in the braces have the following physical meaning. The term $(\beta_0 + \beta + \phi_0)$ is the sum of static angles of attack of the foil, β_0 being the angle of zero lift, β the set angle of the foil with respect to the base line of the craft (see Fig. 86a), and ϕ_0 the angle of

running trim when the craft is moving at a calculated velocity of u_0 in calm water (see Fig. 86b). In the absence of non-stationary movement the indicated angles of attack impart to the craft the stationary lift:

$$Y_{st} = \frac{\partial C_{y\lambda}}{\partial \beta} \cdot f_i(h) (\beta_0 + \beta + \varphi_0) \frac{\rho u_0^2}{2} \cdot S. \quad (\text{II.172})$$

The first factor in the second term

$$\frac{H_a i \omega e^{i\chi}}{u_0} + \frac{r \varphi_a i \omega e^{i\psi}}{u_0} - \varphi_a e^{i\psi} - \beta_a e^{i\theta}$$

is the sum of kinematic angles of attack of the foil, $\frac{H_a i \omega e^{i\chi}}{u_0}$

being the kinematic angle of attack of the foil due to the existence of vertical displacements resulting from heaving. The term $\frac{r \varphi_a i \omega e^{i\psi}}{u_0}$ also takes vertical displacement into

account but only that due to pitching of the craft; $\varphi_a e^{i\psi}$

is an incremental angle of attack due to pitching; and

$\beta_a e^{i\theta} = \frac{r_0 \sigma_c^k Y_0}{u_0} e^{i\theta}$ is an incremental angle of attack due to the orbital motion of particles of liquid in a wave.

The second pair of brackets in formula (II.171) expresses the law governing the change in kinematic angles of attack over time. The first term gives a quasistationary idea of the change in lift while the second term takes into account the effect of trailing vortices. Therefore, we can write the quasistationary value of lift acting on a foil in the form:

$$= \frac{\partial C_{y\lambda}}{\partial \beta} f_i(h) \left\{ (\beta_0 + \beta + \varphi_0) - \left[\frac{H_a i \omega}{u_0} e^{i(\omega t + \chi)} + \frac{r \varphi_a i \omega}{u_0} e^{i(\omega t + \psi)} - \right. \right. \\ \left. \left. - \varphi_a e^{i(\omega t + \psi)} + \beta_a e^{i(\omega t + \theta)} \right] \right\} \frac{\rho u_0^2}{2} \cdot S. \quad (\text{II.173}) \quad (\text{II.173})$$

The phase angles χ , ψ , and θ can easily be determined [166] if it is accepted that the axes of the fixed system of coordinates are so selected that the trough of a wave coincides in abscissa with the origin of the system (see Fig. 86c). The magnitudes of the phase angles χ and ψ are found from experimental recordings of pitching and heaving. In determining phase angle θ it must be kept in mind that a foil is shifted with respect to the location of the center of gravity of the craft by a distance of r and therefore

$$\theta = \pi/2 + \chi + 2\pi r/\lambda u,$$

where $\chi = 2\pi(x_G/\lambda)$ and x_G is the abscissa of the center of gravity when $t = 0$ (see Fig. 87).

To make future use convenient formula (II.171) can be written in the form:

$$Y = Y_1 + Y_2 \varepsilon(\omega, t), \quad (\text{II.174})$$

where

$$\begin{aligned} Y_1 &= \Delta m \omega^2 A e^{i\omega t}, \\ \Delta m &= \rho \pi a^2 f_i(h) k(\lambda), \\ A &= H_a e^{i\chi} + r \varphi_a e^{i\psi}. \end{aligned} \quad (\text{II.175})$$

The stationary lift can be calculated from the formula

$$Y_{st} = \frac{\partial C_{p\lambda}}{\partial \beta} f_i(h) \beta_{tot} \frac{\rho u_0^2}{2} S, \quad (\text{II.176})$$

where $\beta_{tot} = \beta_0 + \beta + \phi_0$.

The function $\varepsilon(\omega, t)$ in formula (II.174) is equal to

$$\begin{aligned} \varepsilon(\omega, t) = & \left\{ 1 - \left[\frac{H_a i \omega}{u_0 \beta_{tot}} \cdot e^{i\chi} + \frac{r \varphi_a i \omega}{u_0 \beta_{tot}} e^{i\psi} - \right. \right. \\ & \left. \left. - \frac{\varphi_a}{\beta_{tot}} e^{i\psi} + \frac{\beta_0}{\beta_{tot}} \cdot e^{i0} \right] [e^{i\omega t} + v e^{i(\omega t + \theta)}] \right\}. \end{aligned} \quad (\text{II.177})$$

In the formulation of the problem under consideration it was noted that displacements of a foil due to rotational and translational motion of a craft are small. Therefore in the derivation of the formulas presented above it was considered that $H_a \ll h$ and $r\phi_a \ll h$, that is, the change in depth of immersion of a foil is small compared with the depth of immersion itself. This assumption makes it possible in determining function $f_i(h)$ to take for a foil under consideration values of h which neglect the rotational and translational motion of a craft traveling at any given calculated velocity u_0 . If such displacements should be comparable with depth of immersion, the error arising in the formulas presented above could be large. In such a case it would be necessary to use a concrete value for the magnitude of h at each specific instant of time.

In some cases the experimental value of stationary lift Y_{st} may be known and then this value must be substituted in formula (II.174), this formula then being used for calculating only additional components of forces caused by the existence of nonstationarity.

The expressions presented above make it possible to calculate the hydrodynamic forces acting on an isolated hydrofoil on a system of hydrofoils whose planes of span are parallel

to the surface of the water. The foil systems of craft usually [167] have a complex geometric shape in which horizontal elements of a foil are combined with various types of inclined foil (stabilizers, subfoils, inclined struts, etc.). While the formulas presented above can be used directly for foils of types Nos. 1, 2, and 7 (Fig. 88), when calculations are made for foils of types Nos. 3, 4, 5, and 6 an inclined foil must be replaced with a certain horizontal foil which will be equivalent with respect to the effect of external forces. An equivalent foil when the relative thickness is small is a horizontal foil of the same span and angle of attack which is immersed under a free surface of the water to a depth equal to that of span midpoint on the inclined foil (Fig. 88). The lifting forces acting on the foils will be the same and a restoring moment equal to the restoring moment on the inclined foil will act on the horizontal equivalent. As demonstrated by the author, the magnitude of this moment can be determined from the formula

$$\mathfrak{M}_k = C_m \frac{\rho u_0^2}{2} \cdot Sl, \quad (\text{II.178})$$

where

$$C_m = C_{y\infty} K \frac{(2a)^3}{Sl}.$$

Here $C_{y\infty}$ is the coefficient of lift of a given foil of finite span when an unbounded liquid flows around it. The coefficient K is

[168]

$$K = \frac{e^{-2.5\left(\frac{H}{2a}\right)}}{50_k} \left[e^{2.50_k \frac{l}{4a}} \left(\frac{l}{4a} - \frac{1}{2.50_k} \right) + e^{-2.50_k \frac{l}{4a}} \left(\frac{l}{4a} + \frac{1}{2.50_k} \right) \right], \quad (\text{II.179})$$

where θ_k is the angle of inclination of the foil with respect to the free surface of the water and

$$\lim_{\theta_k \rightarrow 0} K = 0; \quad \lim_{H \rightarrow \infty} K = 0.$$

Knowing the magnitude of the moment \mathfrak{M}_k , acting on the equivalent horizontal foil it is easy to find the arm for application of force Y as determined for the equivalent foil and, consequently, for the main foil using formula (II.174). The length of this arm is

$$c = \frac{\mathfrak{M}_k}{Y}; \quad -\frac{l}{2} \leq c \leq \frac{l}{2}. \quad (\text{II.180})$$

The indicated conclusions hold only for small angles of bank θ_k and also, as already indicated above, for thin foils not piercing the water. In the case of deviations from these conditions formulas (II.174)--(II.178) can be used only for an approximate evaluation of the effect of nonstationarity on external forces and force Y_{st} must be determined experimentally or by using the stricter and, naturally, more complex methods of calculation presented above.

In the first chapter data were presented for the effect of cavitation on the hydrodynamic forces on a hydrofoil during steady movement. The probability of occurrence of cavitation is much greater in a seaway because of the large total geometric and kinematic angles of attack. The effect of nonstationarity of flow on the occurrence and development of cavitation is very complex and constitutes a subject for independent investigation. Therefore, here we will limit ourselves to remarks about the need when calculating external forces for making sure that the maximum dynamic angle of attack of a foil for a given cavitation number not exceed a critical angle characterizing the inception of cavitation, that is, it is necessary that the following condition always be met:

$$\beta_{tot}(\omega, t) \leq \beta_{crit}; \quad x = x_{cal}. \quad (II.181)$$

The magnitude of angle β_{crit} for the profile under consideration for a given cavitation number $x = \frac{p - p_d}{\rho u_0^2 / 2}$ must be determined from cavitation diagrams (Fig. 89). In the event inequalities (II.181) do not apply the effect of cavitation on hydrodynamic forces must be taken into account. [169]

Let us now consider an algorithm for calculating nonstationary external forces. The best approach is to follow actual examples.

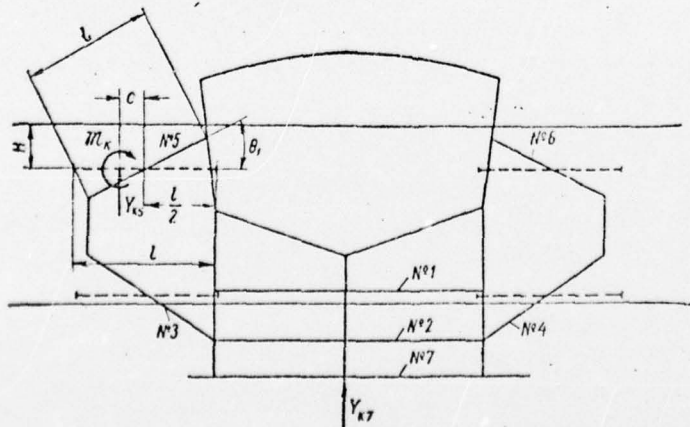


Fig. 88. Diagram giving notation for foil of a hydrofoil craft.

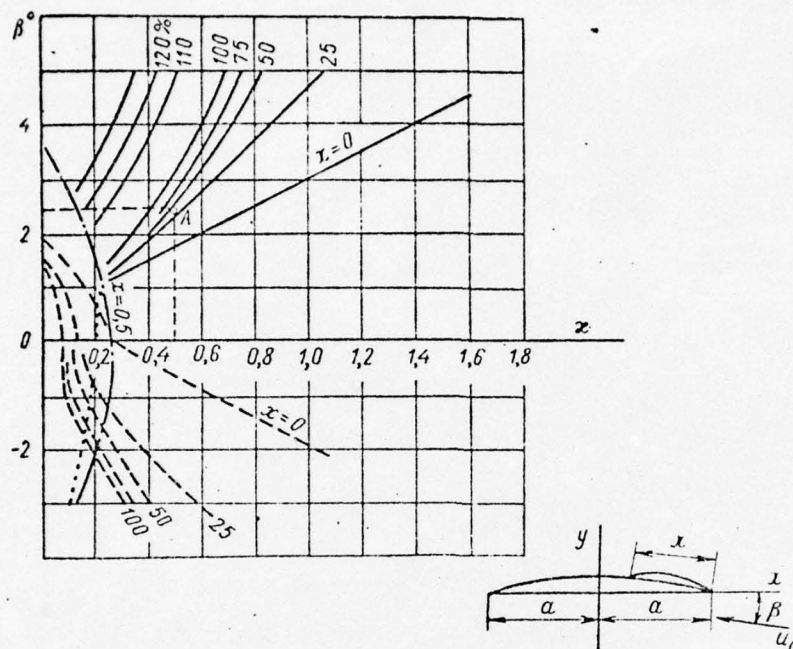


Fig. 89. Cavitation diagram, $\lambda = \infty$.

* * *

Example 1. By way of a first and very simple example we will go through calculations for the hydrodynamic forces acting on a flat foil (Fig. 90) moving at a constant velocity close to a disturbed water surface.

Foil description:

Span $l = 0.5$ m.

Chord $2a = 0.1$ m.

Aspect ratio $\lambda = 5$.

Area $S = 2al = 0.05$ m².

Relative thickness $\delta = 0.05$.

Profile--segmental.

Angle of zero lift $\beta_0 = 0.05$ (3°).

Set angle of attack $\beta = 0.07$ (4°).

Derivative of foil coefficient of lift with respect to angle of attack $\partial C_{y\lambda} / \partial \beta = 4$.

Seaway description:

Wavelength $\lambda_w = 2.9$ m.

Half-height of wave $r_0 = 0.06$ m.

Relative height of wave $2r_0/\lambda_w \approx 1/25$.

Velocity of wave displacement $v_w = 1.25\sqrt{\lambda} = 2.13$ m/sec.

Period of wave $\tau_w = 0.8\sqrt{\lambda} = 1.36$ sec.

Frequency of wave $\omega_w = 2\pi/\tau_w = 4.62$ 1/sec.

[170

Conditions affecting movement:

Velocity of horizontal displacement of foil $u_0 = 5$ m/sec.
 Depth of immersion of foil $h_0 = 0.08$ m..
 Apparent period $\tau_k = \lambda / (v_w + u_0) = 0.41$ sec.
 Rate of foil encounter with waves $\omega = 2\pi / \tau_k = 15.3$ 1/sec.

Calculation of external forces:

1. Since there is no vertical displacement of the foil $y_1 = 0$.
2. Total angle of attack of the foil

$$\beta_{tot} = \beta_0 + \beta = 0.05 + 0.07 = 0.12.$$

3. Coefficient of effect of water's free surface

$$h = \frac{h_0}{a} = \frac{0.08}{0.05} = 1.6; f_1(h) = \frac{1 + (2h)^2}{2 + (2h)^2} = \frac{1 + (3.2)^2}{2 + (3.2)^2} = 0.92.$$

4. Stationary lift of foil

$$Y_{st} = \frac{\partial C_{y\lambda}}{\partial \beta} f_1(h) \beta_{tot} \frac{\rho u_0^2}{2} \cdot S = 4 \cdot 0.92 \cdot 0.12 \cdot 51 \cdot 25 \cdot 0.05 = 28.1 \text{ kg}.$$

5. In this case function $\varepsilon(\omega, t)$ is written in the form

$$\varepsilon(\omega, t) = \left\{ 1 - \frac{\beta_a}{\beta_{tot}} e^{i\theta} [e^{i\omega t} + v e^{i(\omega t - \theta)}] \right\};$$

where

$$k = 2\pi / \lambda_w = 2.17 \text{ 1/m}; \quad \sigma = \sqrt{gk} = 4.62 \text{ 1/sec}; \quad y_0 = -h_0 = -0.08 \text{ m};$$

$$\beta_a = \frac{r_0 \sigma e^{-kh_0}}{u_0} = \frac{0.06 \cdot 4.62 \cdot e^{-2.17 \cdot 0.08}}{5} = 0.047;$$

[171

$$\theta = \frac{\pi}{2}; \quad \mu = \frac{\omega \cdot a}{u_0} = \frac{15.3 \cdot 0.05}{5} = 0.153.$$

From the graph in Fig. 85 we find $v = 0.3$, $v = 219^\circ$ or 3.82 rad. Finally, we write function $\varepsilon(\omega, t)$ in the form

$$\varepsilon(\omega, t) = 1 + 0.39 [\sin 15.4t + 0.3 \sin (15.4t + 3.82)].$$

Substituting the values obtained for functions Y_{st} and $\varepsilon(\omega, t)$ into formula (II.178), we obtain the following final expression for calculating the nonstationary lift of the foil:

$$Y = 28.1 [1 + 0.39 [\sin 15.4t + 0.3 \sin (15.4t + 3.82)]] \text{ kgf}.$$

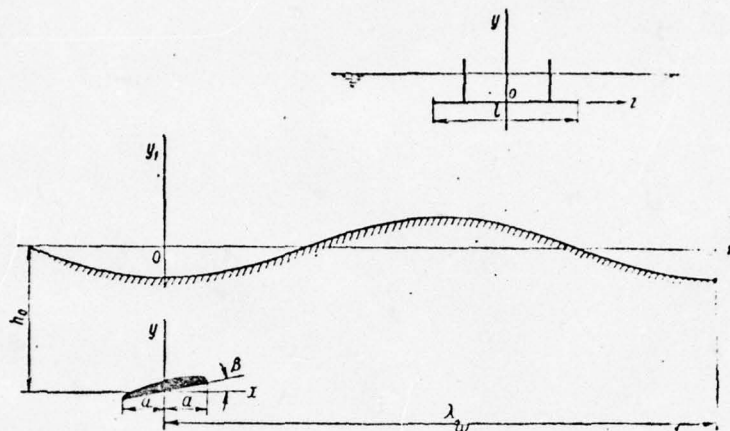


Fig. 90. Nonstationary movement of a foil close to a disturbed water surface.

* * *

The results of calculations using the above formula are shown in Fig. 91. The figure also shows the results of an experimental determination of external forces for the case of foil movement under consideration.

The relations between external forces and time are shown in dimensionless form, that is, the forces are referred to their value during steady movement. The calculated value of Y_{st} is equal to 28.1 kgf and Y_{st} was found by experiment to be 30.2 kgf [12]. As can be seen in Fig. 91 there is good agreement between the calculated and experimental values of nonstationary foil lift. The quasistationary value of lift Y_q presented there [see formula (II.173)] makes it possible to graphically evaluate the effect of nonstationarity. For clarity Fig. 92 shows the position occupied by the foil with respect to the wave as it moves at constant velocity u_0 . Analogous calculations can be carried out for movement of a craft over a wave, that is, when the course angle is $\phi_k = \pi$ and also for other values of course angle [9].

* * *

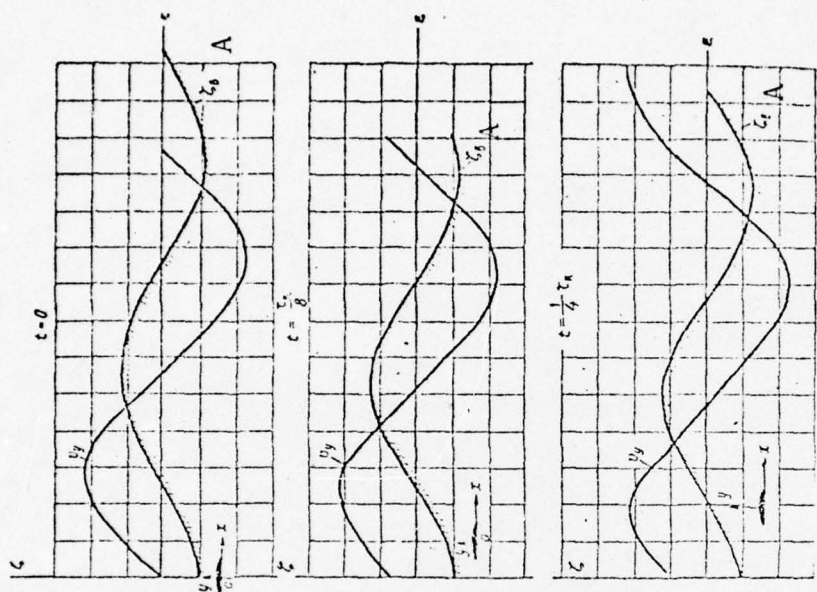


Fig. 92a. Position of foil with respect to wave whose lift is shown in Fig. 91. KEY: A-- z_w .

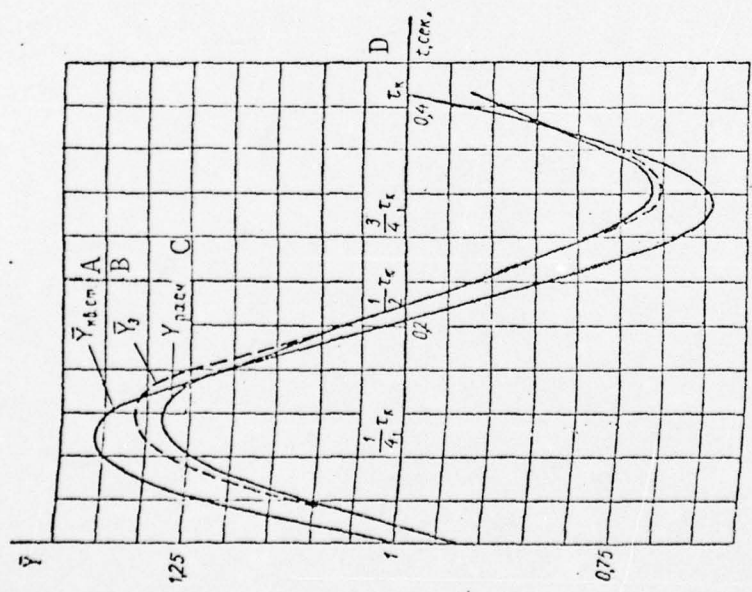


Fig. 91. Lift \bar{Y} acting on a foil moving close to undisturbed surface of water. Calculated and experimental. KEY: A-- \bar{Y}_q ; B-- \bar{Y}_e ; C-- \bar{Y}_{cal} ; D-- t , sec.

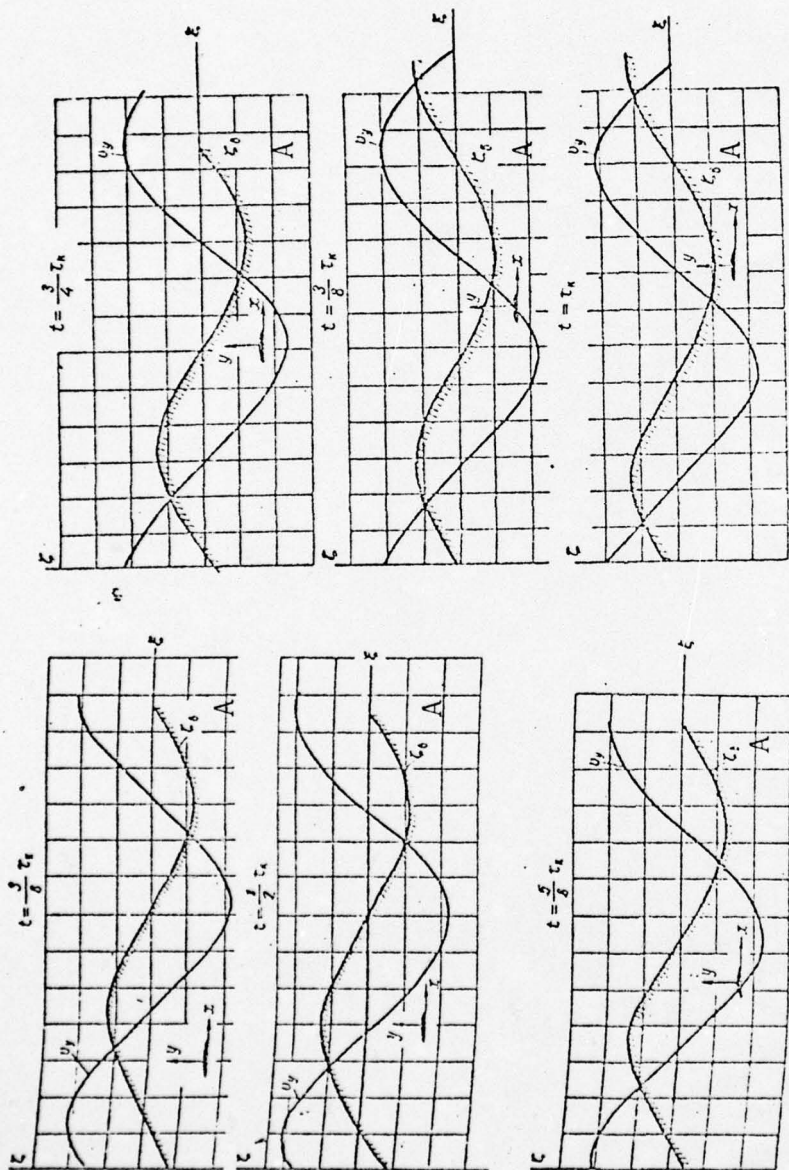


Fig. 92b. Position of foil with respect to wave whose lift is shown in Fig. 91.
KEY: A-- ζ_w .

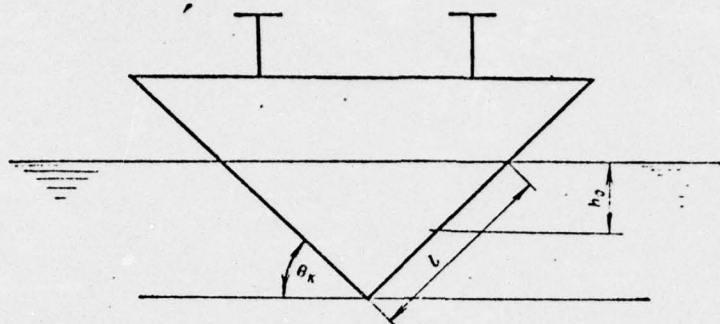


Fig. 93. V-shaped hydrofoil (main notation).

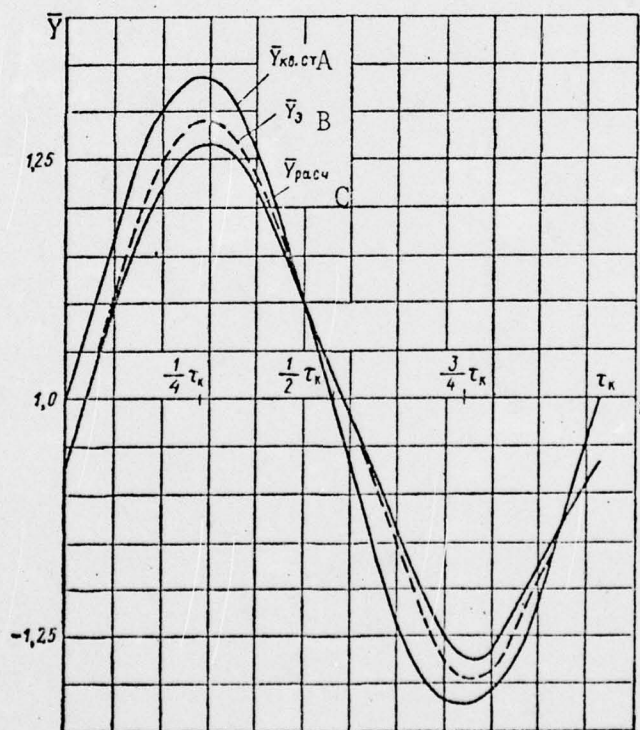


Fig. 94. Lift acting on a V-shaped foil during movement close to a disturbed water surface.
KEY: A-- \bar{Y}_q ; B-- \bar{Y}_e ; C-- \bar{Y}_{cal} .

Example 2. We will calculate nonstationary hydrodynamic forces acting on a V-shaped hydrofoil (Fig. 93) during movement in a regular seaway.

Foil description:

Span of foil element at given depth of immersion $l = 0.3$ m.
 Chord $2a = 0.1$ m.
 Area $S = 0.03$ m².
 Angle of external dihedral $\theta_k = 30^\circ$.
 Profile of foil--segmental.
 Relative thickness $\delta = 0.05$.
 Set angle of attack $\beta = 0.06$ (3.5°).
 Angle of zero lift $\beta_0 = 0.05$.
 Derivative $\partial C_{y\lambda} / \partial \beta = 3.34$.

Seaway description:

Wavelength $\lambda_w = 3.30$ m.
 Half-height of wave $r_0 = 0.05$ m.
 Relative height of wave $h_w / \lambda_w = 1/33$.
 Velocity of wave displacement $v_w = 2.27$ m/sec.

Conditions affecting movement:

Horizontal displacement velocity of foil $u_0 = 5$ m/sec.
 Depth of immersion of midpoint of wetted length of foil element $h_0 = 0.075$ m.
 Apparent period $\tau_k = 0.455$ sec.
 Rate of foil encounter with waves $\omega_k = 13.8$ 1/sec.

[174

Calculation of external forces:

1. $Y_1 = 0$.
2. Total angle of attack of foil

$$\beta_{tot} = \beta_0 + \beta = 0.11.$$

3. Coefficient of effect of water's free surface

$$h = \frac{h_0}{a} = \frac{0.075}{0.05} = 1.5; f_1(h) = \frac{1 + (2h)^2}{2 + (2h)^2} = \frac{10}{11} = 0.91.$$

4. Stationary lift of foil element

$$Y_{st e} = \frac{\partial C_{y\lambda}}{\partial \beta} f_1(h) \beta_{tot} \frac{\rho u_0^2}{2} S = 3.34 \cdot 0.91 \cdot 0.11 \cdot 51 \cdot 25 \cdot 0.03 = 12.8 \text{ kgf.}$$

5. Stationary lift of entire foil

$$Y_{st} = 2Y_{st e} = 25.6 \text{ kgf.}$$

6. Value of the function $\varepsilon(\omega, t)$

$$k = \frac{2\pi}{\lambda_w} = 1,9 \text{ 1/m} \quad \sigma = \sqrt{gk} = 4,32 \text{ 1/sec}; \quad y_0 = -h_0 = -0,075 \text{ m};$$

$$\beta_a = \frac{r_0 \sigma e^{-kh_0}}{u_0} = 0,038; \quad \theta = \frac{\pi}{2}; \quad \mu = \frac{\omega_a}{u_0} = 0,138;$$

$$v = 0,29; \quad \phi = 3,877 = 222^\circ;$$

$$e(\omega, t) = 1 + 0,34 [\sin 13,8t + 0,29 \sin (13,8t + 3,88)] \text{ kgf}.$$

7. Value of nonstationary lift

$$Y = 25,6 \{1 + 0,34 [\sin 13,8t + 0,29 \sin (13,8t + 3,88)]\} \text{ kgf}.$$

Fig. 94 shows in dimensionless form ($\bar{Y} = Y/Y_{st}$) the value of the nonstationary force in this case of movement of a foil close to a disturbed surface. It also shows quasistationary and experimental values of this force. The experimental value of the stationary force is $Y_{st} e = 28 \text{ kgf}$.

8. Along with force Y on each element of the foil there will act a moment, the value of which can be determined from formula (II.178)

$$M_k = C_m \frac{\rho u_0^2}{2} \cdot Sl.$$

We will determine the values of the variables which occur in formula (II.178):

$$C_{y\infty} = \frac{\partial C_{y\lambda}}{\partial \beta} (\beta_0 + \beta) = 3,34 \cdot 0,11 = 0,368;$$

$$K = \frac{e^{-2,5 \left(\frac{0,075}{0,1} \right)}}{2,62} \left[e^{2,5 \cdot 0,524 \frac{0,3}{0,2}} \left(1,5 - \frac{1}{1,31} \right) + e^{-2,5 \cdot 0,524 \cdot 1,5} \left(1,5 + \frac{1}{1,31} \right) \right] = 0,0325;$$

$$C_m = C_{y\infty} \cdot K \frac{(2a)^3}{Sl} = 0,368 \cdot 0,0325 \frac{(0,1)^3}{0,03 \cdot 0,3} = 0,013.$$

It follows from the above that the moment acting on a foil [176 element is

$$M_k = 0,013 \cdot 51 \cdot 25 \cdot 0,009 = 0,153 \text{ kgf} \cdot \text{m}.$$

The point of application of force Y is shifted from the center of span of a foil element in the direction of greater depth of immersion by the magnitude

$$c = \frac{y_{R_k}}{y_{st} e} = \frac{0,153}{12,8} = 0,012 \text{ m.}$$

In view of the fact that the depth of immersion of a foil symmetrical with respect to the centerline plane was considered, the total restoring moment over the entire foil is equal to zero. Calculations for a V-shaped foil when there is an angle of bank can be performed similarly.

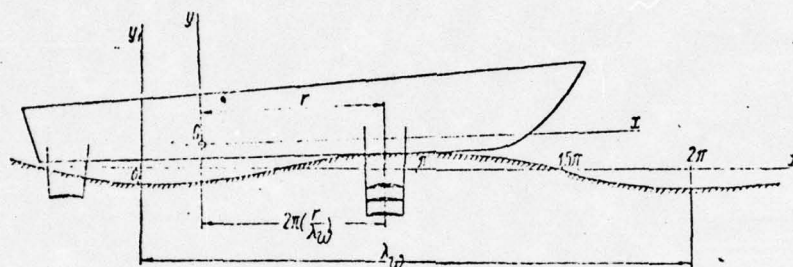


Fig. 95. Position of hydrofoil craft with respect to wave.

Example 3. Finally, we will consider the hydrodynamic forces acting on elements of a foil system (Fig. 88) of a craft in a seaway when bank occurs. The position of the craft with respect to the wave is shown in Fig. 95.

Foil system description:

Span of foil system elements $l_{1,2} = 6 \text{ m}$; $l_3 = 2 \text{ m}$.
 Aspect ratio $\lambda_{1,2} = 3$; $\lambda_3 = 1$.
 Chord $2a_{1,2,3} = 2 \text{ m}$.
 Relative thickness $\delta_{1,2,3} = 0.05$.
 Profile--segmental.
 Angle of zero lift $\beta_0 = 0.05$ (approximately).
 Set angle of attack $\beta_{1,2,3} = -0.0175$ (-1°).
 Derivative $(\partial C_{y\lambda} / \partial \beta)_{1,2} = 3.34$; $(\partial C_{y\lambda} / \partial \beta)_3 = 1.99$.
 Foil located at $r = 10 \text{ m}$ forward of center of gravity toward bow of craft.

Seaway description:

Wavelength $\lambda_w = 30 \text{ m}$.
 Height of wave $h_w = 2 \text{ m}$ ($r_0 = 1 \text{ m}$).
 Curvature of wave $1/15$.
 Velocity of wave displacement $v_w = 6.83 \text{ m/sec}$.

Conditions affecting craft movement:

Velocity of craft movement $u_0 = 25 \text{ m/sec}$ (about 49 knots).
 Apparent period and frequency of encounter with waves $\tau_k = 0.943 \text{ sec}$.

Rise of center of gravity of craft above free surface at velocity of $u_0 H_0 = 1.0$ m.

Initial trim of craft under same conditions $\phi_0 = 0.035$ (2°).

Amplitude and phase (relative to wave) of heaving: $H_a = 0.25$ m, $\chi = 20^\circ$.

Amplitude and phase (relative to wave) of pitching: $\phi_a = 0.026$ (1.5°), $\psi = -15^\circ$ [177]

Depth of immersion of elements of foil system relative to level of undisturbed water surface $h_{01} = 1.6$ m; $h_{02} = 3.2$ m; $h_{03} = 2.7$ m.

Calculation of external forces:

External forces are calculated sequentially for each element of the foil system.

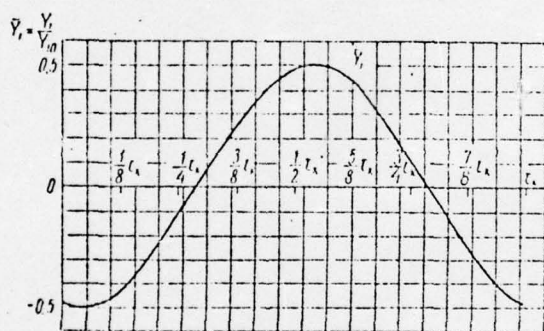


Fig. 96. Force \bar{Y}_1 due to the effect of adjoining masses.

Foil No. 1:

1. The force due to the effect of adjoining masses is calculated using the formula [see formula (II.160)]

$$Y_1 = -\Delta m \omega^2 A \cdot e^{i\omega t}.$$

We will find values for the variables in this formula:

$$h = \frac{h_{01}}{a} = \frac{1.6}{1} = 1.6;$$

$$I_2(h) = \frac{1 + 20h^2 + 64h^4}{4 + 56h^2 + 64h^4} = 0.83;$$

$$K(\lambda) = \frac{1.2}{1.2 + \frac{2a}{l}} = \frac{1.2}{1.533} = 0.783;$$

$$\Delta m = \rho \pi a^2 l \cdot f_2(h) k(\lambda) = 102 \cdot 3,14 \cdot 1 \cdot 6 \cdot 0,83 \cdot 0,783 = 1250 \text{ (kgf} \cdot \text{sec}^2/\text{m});$$

$$Y_1 = 1,25 \cdot 10^3 (6,67)^2 (0,25 e^{i\pi/9} + 10 \cdot 0,026 e^{-i\pi/12}) \cdot e^{i \cdot 6,67t} =$$

$$= 55,6 \cdot 10^3 [0,25 e^{i(6,67t + \pi/9)} + 0,26 e^{i(6,67t - \pi/12)}] \text{ kgf}.$$

The real part of the last expression is

$$Y_1 = 55,6 \cdot 10^3 [0,25 \cos(6,67t + \pi/9) + 0,26 \cos(6,67t - \pi/12)] \text{ kgf}.$$

Function $Y_1(t)$ in dimensionless form (separately for the amplitude value $Y_{10} = 55,6 \cdot 10^3$) is shown in Fig. 96.

2. The total angle of attack of the foil is

$$\beta_{tot} = \beta_0 + \beta + \varphi_0 = 0,050 + 0,018 + 0,035 = 0,067.$$

3. The stationary lift is

$$Y_{st} = \frac{\partial C_{yl}}{\partial \beta} \cdot f_2(h) \beta_{tot} \frac{\rho u_0^2}{2} \cdot S = 3,34 \cdot 0,83 \cdot 0,067 \cdot 51 \cdot 625 \cdot 12 = 71,5 \cdot 10^3 \text{ kgf}.$$

4. The value of function $\epsilon(\omega, t)$ is

[178

$$\epsilon(\omega, t) = \left\{ 1 - \left[\frac{H_a i \omega}{u_0 \beta} e^{i\chi} + \frac{r \eta_{\kappa} i \omega}{u_0 \beta} \cdot \frac{e^{i\psi}}{t o t} - \right. \right.$$

$$\left. - \frac{\eta_a}{\beta_{tot}} e^{i\psi} + \frac{\beta_a}{\beta_{tot}} \cdot e^{i\theta} \right] [e^{i\omega t} + v e^{i(\omega t + \theta)}] \} =$$

$$= 1 - (0,995 i e^{i\chi} + 1,035 i e^{i\psi} - 0,388 e^{i\psi} + 0,612 e^{i\theta}) [e^{i \cdot 6,67t} + 0,37 e^{i(6,67t + 3,66)}];$$

$$k = 0,21 \text{ 1/m}; \sigma = 1/\text{sec}; \beta_a = 0,047;$$

$$\mu = 0,267; \nu = 0,37; \theta = 3,66.$$

The real part of this expression, inasmuch as $\chi = 0,349$, $\psi = -0,262$, and $\theta = 4,01$, will be

$$\epsilon(\omega, t) = 1 + [0,995 \sin(6,67t + 0,349) + 0,368 \sin(6,67t +$$

$$+ 4,01)] + [1,039 \sin(6,67t - 0,262) + 0,383 \sin(6,67t + 3,398)] + [0,388 \times$$

$$\times \cos(6,67t - 0,262) + 0,144 \cos(6,67t + 3,398)] - [0,612 \cos(6,67t + 4,01) +$$

$$+ 0,227 \cos(6,67t + 7,67)].$$

Substituting the values found for functions Y_1 , Y_{st} , and $\epsilon(\omega, t)$ (II.174), we obtain the total value of nonstationary external forces acting on foil No. 1 under the conditions stated above. For convenience of analysis of the relations obtained, Figs. 97--100 show the components of lift: \bar{Y}_H due to heaving of the craft; $\bar{Y}_{r\phi}$ due to vertical displacement of the foil resulting from pitching; \bar{Y}_ϕ the component of lift due to change in angle of attack during pitching; and $\bar{Y}_{\beta a}$ allowing for the effect on lift due to orbital motion of particles of liquid in a wave. For comparison the quasistationary values of these forces are also shown. For this purpose Figs. 102 and 103 show curves for heaving and pitching. Fig. 104 shows the locations of the centers of gravity of the craft and the foil with respect to the wave.

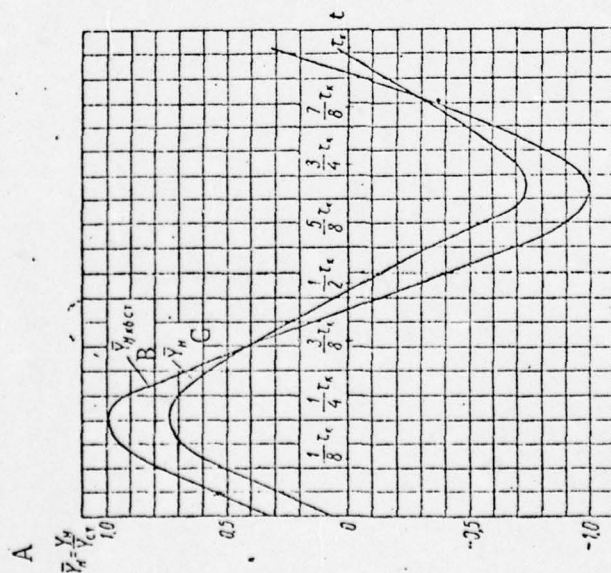


Fig. 97. Lift \bar{Y}_H due to heaving of a craft.
KEY: A-- $\bar{Y}_H = Y_H / Y_{st}$; B-- $\bar{Y}_H q$;
C-- \bar{Y}_H .

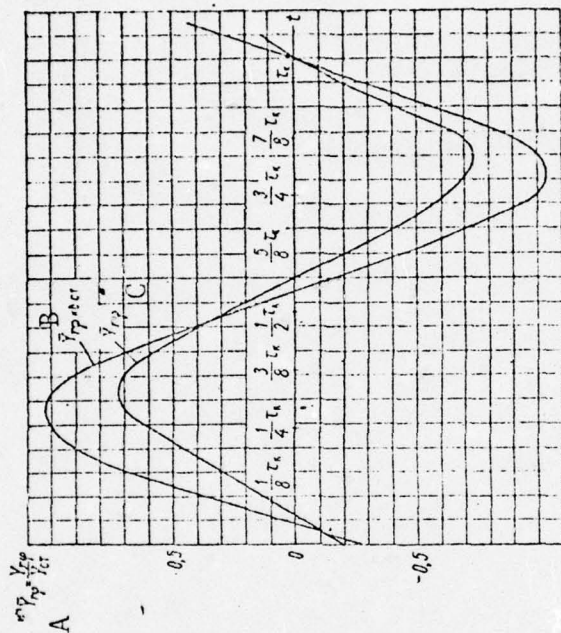


Fig. 98. Lift $Y_{p\phi}$ due to vertical displacements of a foil caused by pitching in a seaway.
KEY: A-- $\bar{Y}_{p\phi} = Y_{p\phi} / Y_{st}$; B-- $\bar{Y}_{p\phi} q$;
C-- $\bar{Y}_{p\phi}$.

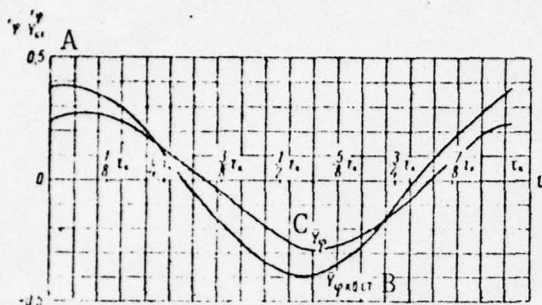


Fig. 99. Lift \bar{Y}_ϕ developing on a foil due to pitching of a craft.

KEY: A-- $\bar{Y} = Y_\phi / Y_{st}$; B-- $\bar{Y}_\phi q$; C-- \bar{Y}_ϕ .

Fig. 100. Comparison of lift on a foil $\bar{Y}_{\beta a}$ arising due to orbital motion of water in a wave.

KEY: A-- $\bar{Y}_{\beta a} = Y_{\beta a} / Y_{st}$; B-- $\bar{Y}_{\beta a} q$; C-- $\bar{Y}_{\beta a}$.

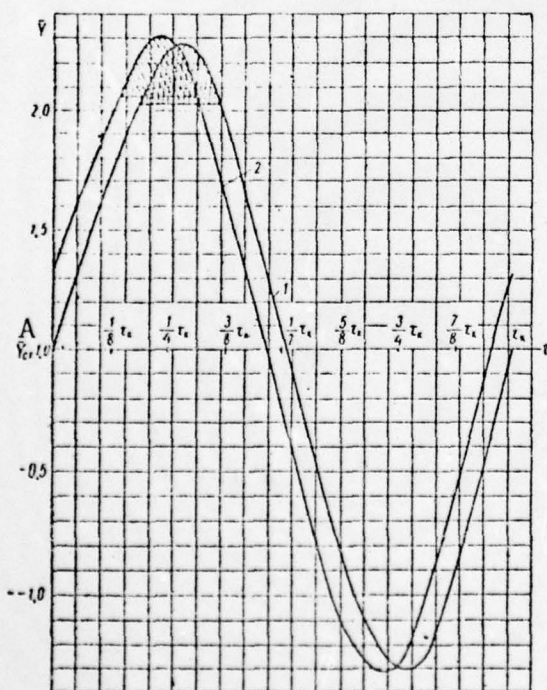
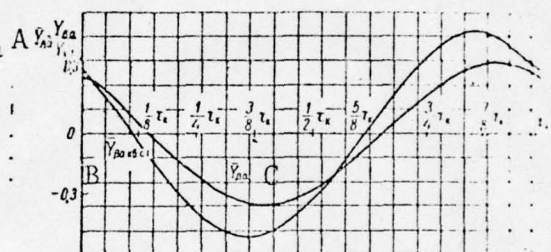


Fig. 101. Total values of lift of nonstationarily moving foil in a seaway.

1-- $\epsilon(\omega, t)$; 2-- $\bar{Y} = Y / Y_{st} = Y_1 / Y_{st} + \epsilon(\omega, t)$. KEY: A-- Y_{st} .

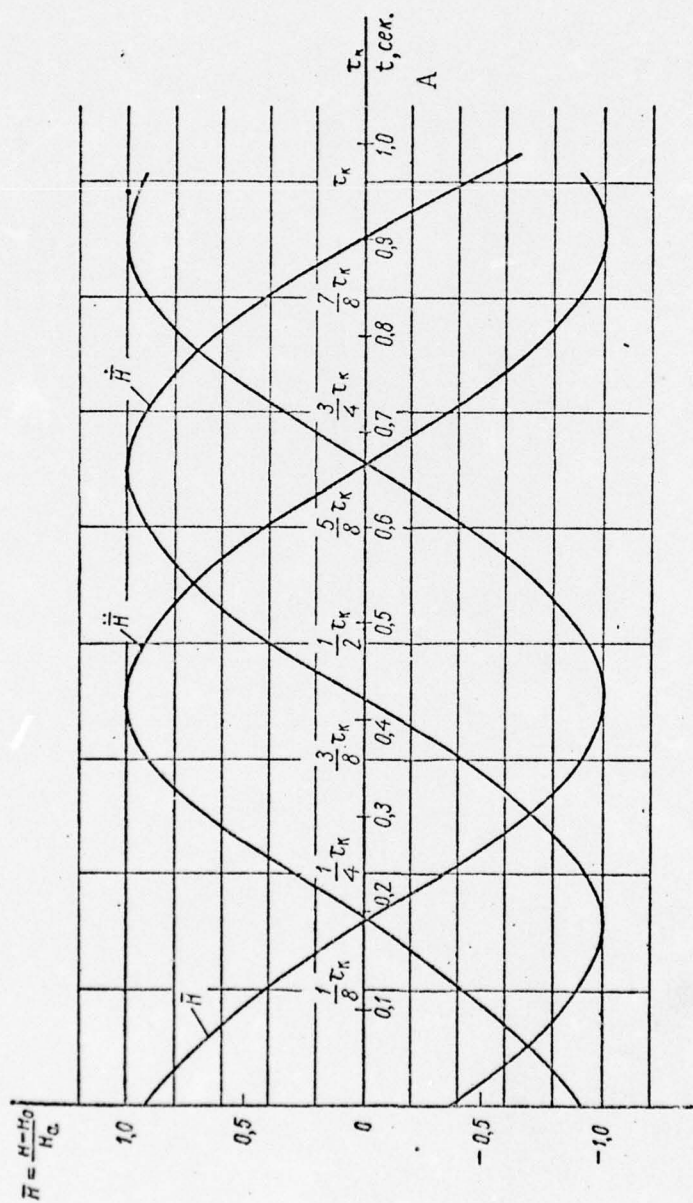


Fig. 102. Curve of craft heaving in a regular seaway.
KEY: A-- t , sec.

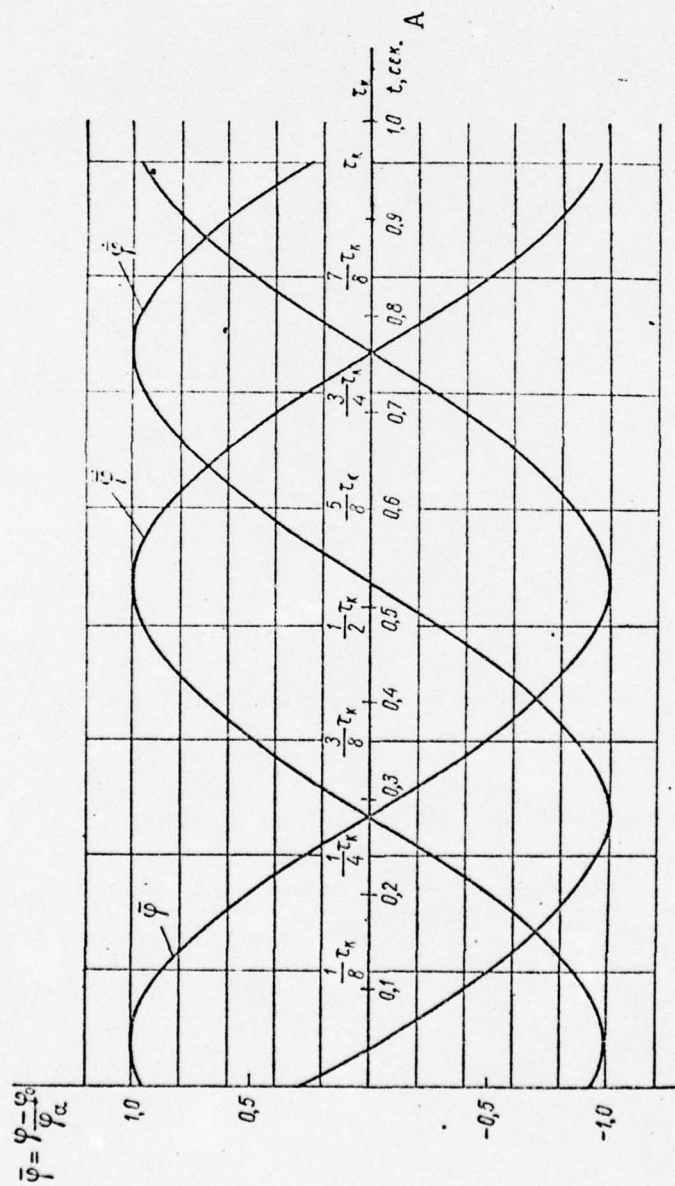


Fig. 103. Curves of craft pitching in regular seaway.
KEY: A-- t , sec.

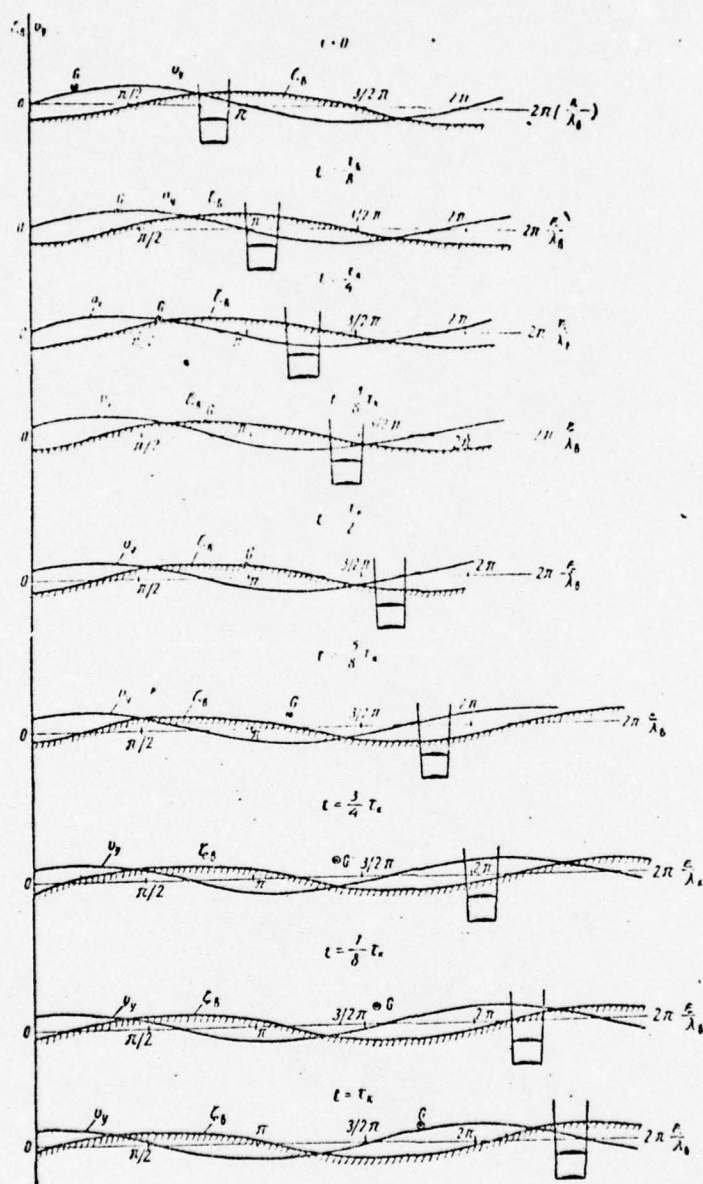


Fig. 104. Position of foil system calculated in example 3 with respect to wave.

KEY: A--The subscript following ζ refers to wave.

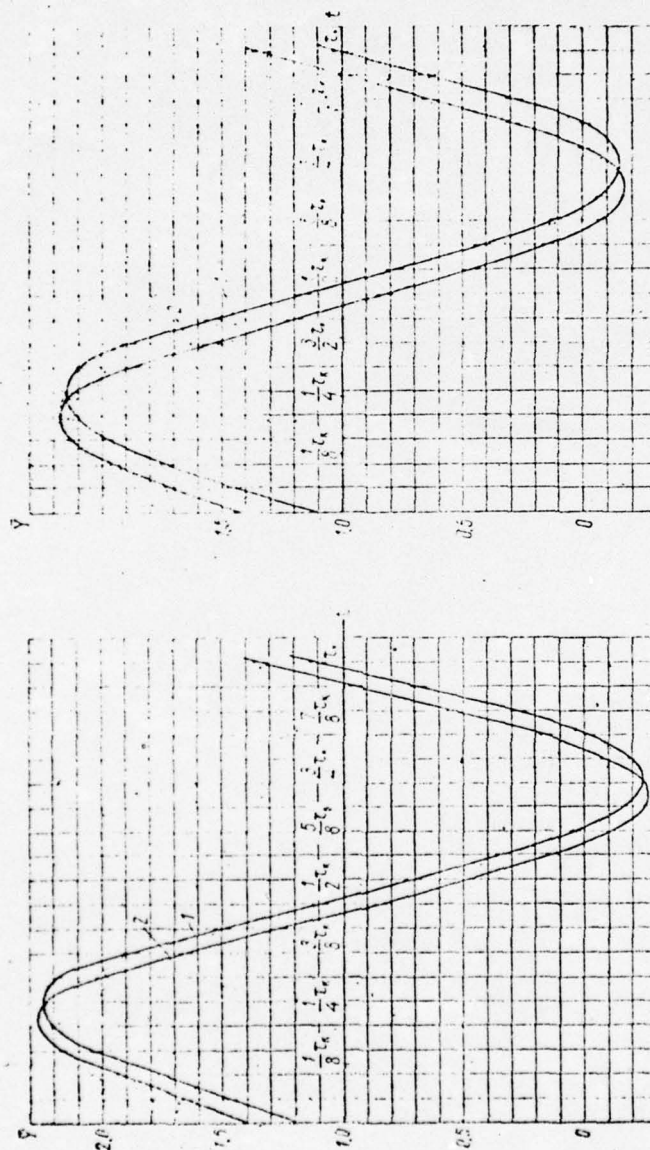


Fig. 105. Nonstationary external forces acting on foil No. 2.
 $1--\bar{Y} = Y/Y_{st}$; $2--\epsilon(\omega, t)$.

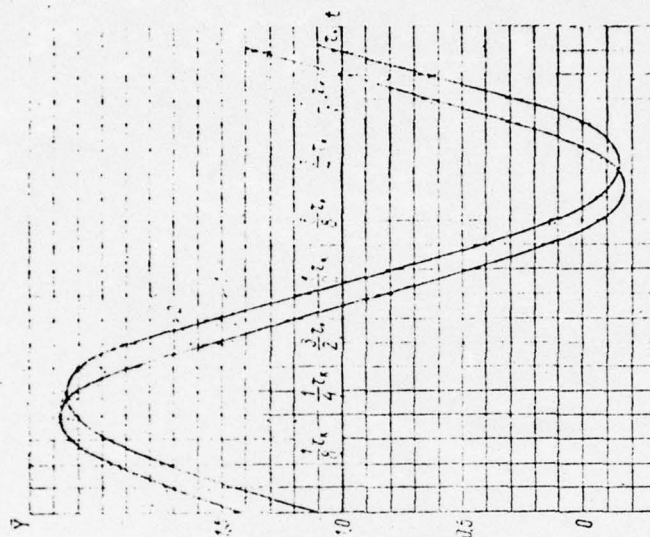


Fig. 106. Nonstationary external forces acting on foil No. 3.
 $1--\bar{Y} = Y/Y_{st}$; $2--\epsilon(\omega, t)$.

As follows from the graph in Fig. 101 the nonstationary external forces acting on a foil in a seaway are approximately ± 2.3 times greater than the stationary external forces which support a craft in calm water. Naturally, the increase pertains to the case at hand only. In other cases its magnitude may be greater or less depending on the nature of movement of the craft and the seaway. It also follows from Fig. 101 that quasistationary values of external forces are much greater than their real values. The conclusion follows that when determining external forces it is necessary to take into consideration the effect of nonstationarity. The difference between quasistationary and nonstationary values of external forces is manifest in their amplitude as well as in their phase. The "inertia" of nonstationary lift is of interest. During accelerated movement of a foil the change in it is delayed with respect to the quasistationary value and during decelerated movement, on the other hand, leads it.

Similar conclusions also follow from calculations for foils Nos. 2 and 3, the total forces acting on which are shown in Figs. 105 and 106 respectively.

It was noted above that such large increments of nonstationary forces cannot be achieved in many cases because of the occurrence of cavitation on the foils. In order to use the cavitation diagram presented in Fig. 89 and determine possible inception of cavitation (for example, on foil No. 1), it is necessary to preliminarily calculate the maximum dynamic angle of attack on the foil:

$$\beta_{\text{dyn}} = \beta_{\text{tot}} \cdot \epsilon(\omega, t) = 0.067 \cdot 2.3 = 0.154 = 8.82^\circ.$$

The angle of attack β for a foil with an aspect ratio of $\lambda = \infty$ is laid off on the ordinate axis in Fig. 89 and therefore

$$\begin{aligned} \beta_{\text{dyn}} &= \beta_{\text{dyn}} - \beta_0 - \beta_{\text{downwash}} = 8.82^\circ - 2.86^\circ - \\ &\quad - 3.5^\circ = 2.46^\circ. \end{aligned}$$

The cavitation number is

[185

$$\sigma = \frac{p - p_d + \gamma h_0}{\frac{\rho v_0^2}{2}} = \frac{10340 - 180 + 1600}{51.625} = 0.37.$$

In view of the fact that the diagram in Fig. 89 was drawn from experimental data for a foil in an unbounded liquid, it can be used for determining cavitation of a hydrofoil only conditionally, changing the cavitation number which, as was indicated above, taking the effect of the free surface into account, is approximately equal to

$$\alpha_h = \frac{\alpha_\infty}{f_i(h)} = \frac{0.37}{0.83} = 0.45.$$

Referring to the diagram in Fig. 89, we see that if a foil were located in a stationary flow of liquid with the given angle of attack and cavitation number, then about 50% of the low-pressure side of the profile (point A) would be covered by cavitation. This would lead to a reduction in lift, the magnitude of which could be determined from a graph for $C_{yh}(\beta)$ when $\chi = 0.45$. It follows from Fig. 107 that the value of the component of nonstationary force $Y_{ste}(\omega, t)$, due to the presence of cavitation, must be decreased by multiplying it by the factor $\mu = \frac{C_{yh} \text{ when } \chi = \chi_h}{C_{yh} \text{ when } \chi = \infty}$. In this given case $\mu = 0.89$. Therefore the maximum value of the total nonstationary force \bar{Y} is reduced in this case from $\bar{Y} = 2.3$ to $\bar{Y} \approx 2.0$ (see Fig. 101).

The method described for taking cavitation into account is sufficiently accurate for a stationarily moving foil. In the case of a foil in a nonstationary flow the question of inception and development of cavitation on it in a concrete small interval of time remains unanswered.

* * *

The method presented above for calculating external forces makes it possible to determine values for nonstationary hydrodynamic forces acting on the lift elements of hydrofoils in a regular seaway. The investigation has showed that the values of external forces acting on hydrofoils in a seaway can greatly surpass these forces in calm water. The method developed makes it possible to evaluate the magnitude of this increment for each particular case of craft movement and seaway. Taking nonstationarity into account is essential when calculating external forces since quasistationary values of these forces yield a greatly inflated impression of their magnitude. A comparison of data from calculations and experiments for isolated foils of very simple form moving in a regular seaway has showed good agreement. The latter fact gives reason to assume that this agreement persists when it comes to foils of more complex form. [186]

§21. Effect of nonstationarity of movement on lift and restoring moment when a craft rises on its foils

In this section we present a method for determining the nonstationary hydrodynamic forces acting on a hydrofoil when a craft rises on its foils. This mode of unsteady movement is of practical interest from the standpoint of ensuring stability of a craft when its hull leaves the water. Initially when a

craft moves from a state of rest its stability depends on hydrostatic forces which are due to the immersion of a certain part of the craft in the water as it banks. As the forward velocity builds up hydrodynamic forces develop on the foils. These forces cause the craft to rise and the hull to leave the water, thus cancelling hydrostatic forces of support and stabilization.

In most types of hydrofoil craft their stability in the main modes of movement depends on the stabilizing effect had on a banked foil by the surface of the water. In investigation of the stability of hydrofoil craft hydrodynamic forces can be found by applying the hypothesis of stationarity. The expressions presented below for nonstationary hydrodynamic forces make it possible to investigate stability without resorting to the hypothesis of stationarity.

For the purpose of determining nonstationary hydrodynamic forces acting on supporting foils in the takeoff mode it is necessary to know in every concrete case the law governing the buildup of velocity of the craft. As a rule, the relation between velocity and time is a curve which with a sufficient degree of accuracy can be approximated by a linear function of time. We will assume that a craft moves at a velocity which varies in accordance with the law shown by the graph in Fig. 79. [187] Linearizing the function $u/u_0 = f(t)$, we obtain

$$u = \frac{u_0}{t_0} t; \quad t \leq t_0. \quad (\text{II.182})$$

In this case the path traveled by the foil over time t will be $z = \frac{1}{2} \frac{u_0}{t_0} t^2$, and its dimensionless expression

$$\eta = \frac{1}{2} \frac{u_0}{u_0 t_0} t^2.$$

Consequently, the velocity as a function of dimensionless path is written in the form

$$u = \frac{2u_0}{t_0} \eta; \quad \eta \leq \frac{1}{2} \frac{u_0 t_0}{a_0}. \quad (\text{II.183})$$

The velocity normal to the foil is

$$v_z(\eta) = -u\beta = -\frac{2a_0\beta}{t_0} \eta. \quad (\text{II.184})$$

The lift on the foil in this particular case according to formula (II.130) will be

$$Y = f_1(h) \rho_0 \pi a^2 \beta \frac{du}{dt} + \frac{\partial C_{u\lambda}}{\partial \beta} f_1(h) \rho_0 a_0 u^2 \beta - 2\rho_0 a_0 u \int_0^{\alpha_1} \frac{u_{z2}(\alpha) d\alpha}{V|\xi^2 - a^2|}. \quad (\text{II.185})$$

The first term in formula (II.185), due to the smallness of acceleration $\frac{du}{dt} \approx \frac{\Delta u_0}{\Delta t_0}$ (in this given case equal to

0.317 m/sec²), is small in comparison with the second and third and therefore in the following discussion, for simplicity of exposition, it will be neglected. As a consequence, formula (II.185) can be written

$$Y = \frac{\partial \psi}{\partial \beta} \cdot \beta f_1(h) \rho_0 a_0 u^2 - 2 \rho_0 a_0 u \int_0^{\alpha_1} \frac{u_{22}(\alpha) d\alpha}{V[\xi^2 - a^2]}. \quad (\text{II.186})$$

Transforming (II.186) we obtain the following expression for the lift acting on a foil:

$$Y = Y_{st} \left\{ 1 - \frac{1}{\pi u \beta} \int_0^{\alpha_1} \frac{u_{21}(\alpha)_{h \rightarrow \infty} d\alpha}{V[\xi^2 - a^2]} \right\}, \quad (\text{II.187})$$

where

$$Y_{st} = 2\pi\beta f_1(h) \rho_0 u^2 a_0.$$

Transforming (II.187) to dimensionless form and substituting in the value of the velocity discontinuity function in accordance with formula (II.94), we find that the lift per unit of foil span in this case will be determined by the following relation: [188]

$$\bar{Y} = 1 - \frac{\sqrt{2}}{\pi} \frac{1}{s} \int_0^s \frac{\text{Arsh } \sqrt{\eta} d\eta}{V[(s-\eta)^2 + 2(s-\eta)]}, \quad (\text{II.188})$$

where $\bar{Y} = Y/Y_{st}$.

The value of the improper integral

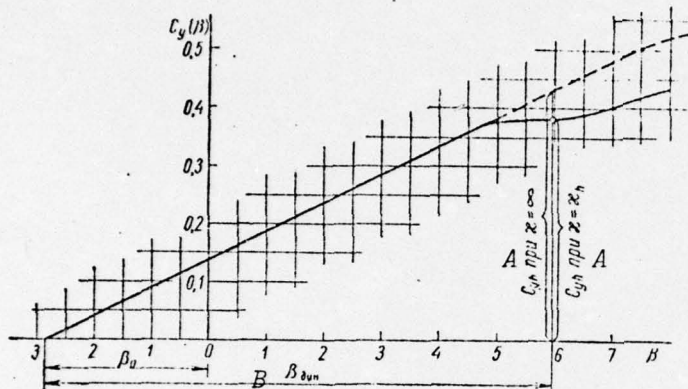
$$I_0(s) = \int_0^s \frac{\text{Arsh } \sqrt{\eta} d\eta}{V[(s-\eta)^2 + 2(s-\eta)]},$$

which is found by numerical methods is shown in the graph in Fig. 108. Graphs of the lift in the form of functions of s/\bar{Y} and t are shown in Figs. 109 and 110. For comparison the curve in Fig. 110 is drawn on the graph used in Fig. 80, from which it is apparent that the results of calculation and experiment agree well.

When a craft moves at a certain angle of bank θ_k , a restoring moment develops on a foil banked close to the free surface of the water, as already stated. The existence of this moment is due to the fact that elements of the foil distant from the free surface produce a greater lift than do those close to the free surface. By applying the hypothesis of flat sections, that is, considering each element of a foil to function independently of any other, it is possible to determine the magnitude of restoring moment. The following lift acts on a foil element (along the span) Δy located beneath

the free surface at a depth h (Fig. 111):

$$\Delta y' = -\frac{\partial C_{yH}}{\partial \beta} \cdot \beta \rho_0 u^2 a_0 f_1(h) \left[1 - \frac{V\sqrt{2}}{\pi} \cdot \frac{I_0(s)}{s} \right] \Delta y.$$



$$\kappa = \frac{\rho - \rho_d + \gamma h_0}{\frac{\rho u_0^2}{2}} = 0.37.$$

Fig. 107. Effect of cavitation on lift of a foil.
KEY: A--when; B-- β_{dyn} .

The moment of this force with respect to point o is (see Fig. 111):

$$\Delta \mathfrak{M}_{res} = -\frac{\partial C_{yH}}{\partial \beta} \cdot \beta \rho_0 u^2 a_0 f_1(h) \left[1 - \frac{V\sqrt{2}}{\pi} \cdot \frac{I_0(s)}{s} \right] y \Delta y.$$

Taking the limit in the latter formula, we obtain

$$\mathfrak{M}_{res} = -\frac{\partial C_{yH}}{\partial \beta} \cdot \beta \rho_0 u^2 a_0 \left[1 - \frac{V\sqrt{2}}{\pi} \cdot \frac{I_0(s)}{s} \right] \int_{-b}^{+b} f_1(h) y dy.$$

Integrating and transforming somewhat, we find the following expression for the restoring moment

$$\mathfrak{M}_{res} = -\frac{1}{4} C_{yH} \frac{\rho_0 u^2}{2} (2a_0)^3 K_1(s) K_2\left(\frac{H}{a}; \frac{b}{a}; 0\right), \quad (\text{II.189})$$

where C_{yH} is the lift coefficient at depth of immersion H ; [190]

$$K_1(s) = 1 - \frac{V\sqrt{2}}{\pi} \cdot \frac{I_0(s)}{s},$$

and, if $\bar{H} = H/a$, $\bar{b} = b/a$; and

$$K_2 = \left(\frac{1}{40}\right)^2 \left\{ \frac{1}{2} \ln \left[\frac{(2 + 16\bar{H}^2) - 32\bar{H}\bar{b} + 160\bar{b}^2}{(2 + 16\bar{H}^2) + 32\bar{H}\bar{b} + 160\bar{b}^2} \right] + \right. \\ \left. + 2\sqrt{2}\bar{H} \operatorname{arctg} \left[\frac{4\sqrt{2}\bar{b}}{1 + 8(\bar{H}^2 - \bar{b}^2)} \right] \right\}.$$

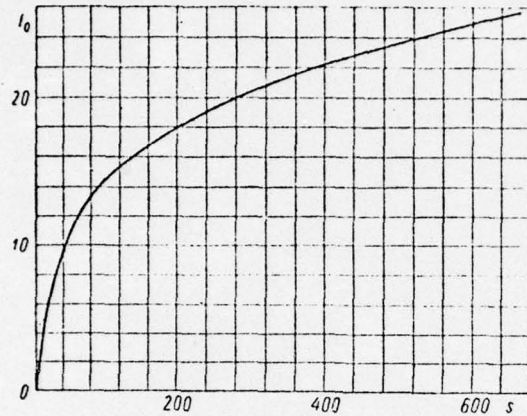


Fig. 108. Graph of the integral equation for $I_0(s)$.

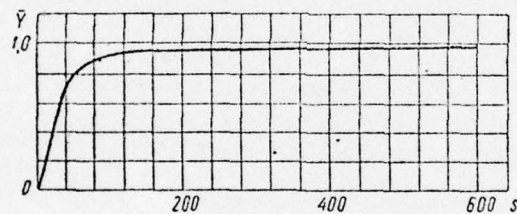


Fig. 109. Graph of lift $\bar{Y}(s)$.

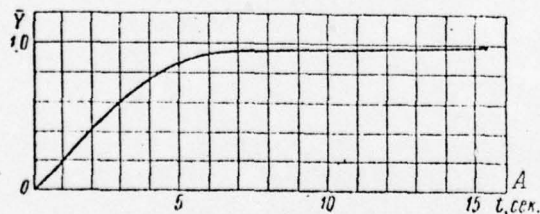


Fig. 110. Graph of lift $\bar{Y}(t)$.
KEY: A--t, sec.

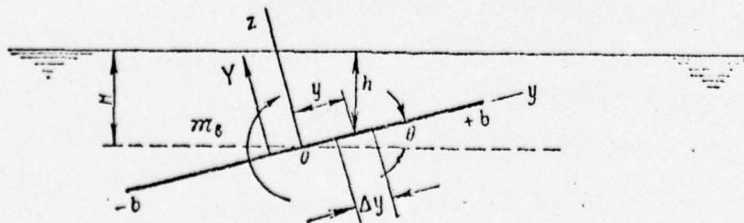


Fig. 111. Restoring moment m_{res} on a banked foil.

The minus sign in (II.189) shows that the moment acts in a direction opposite to that of the angle of bank, that is, it is a restoring moment. The following limits are characteristic of the moment expressed in (II.189):

$$\lim_{H \rightarrow 0} M_{res} = 0; \quad \lim_{\theta \rightarrow 0} M_{res} = 0.$$

The formula for moment (II.189) can also be written in the form

$$M_{res} = - C_m \frac{\rho_0 u^2}{2} S_k l,$$

where

$$S_k = 4ab, \quad l = 2b, \quad (II.190)$$

$$C_m = -\frac{1}{4} C_{yu} K_1(s) K_2 \frac{a^2}{b}, \quad (II.191)$$

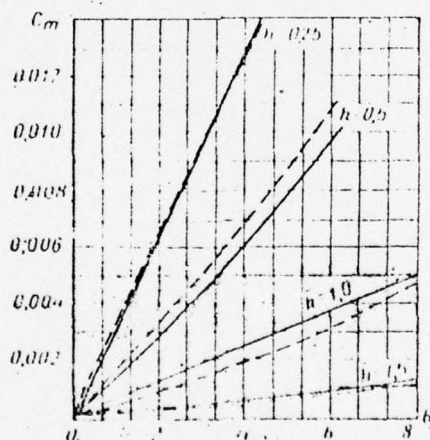


Fig. 112. Coefficient C_m or restoring moment on a rectangular foil close to the water's surface ($\beta_0 = 0$).

The results of experiments and data from calculations of the coefficient of restoring moment C_m made with formula (II.191) for foil angle of attack $\beta_0 = 0$ are shown in Fig. 112.

The formulas presented above for determining the lift and restoring moment are derived assuming absence of cavitation and air entrainment on the foil. These formulas can be used for determining the stability of a hydrofoil craft during takeoff.

References.

[191

1. Birnbaum. Das ebene Problem des schlagenden Flugels. ZAMM, 1924. Be., 4, H. 5.
2. Nekrasov, A. I. Teoriya kryla v nestatsionarnom potoke (Theory of a foil in nonstationary flow). Moscow, AN SSSR, 1947.
3. Sedov, L. I. Ploskiye zadachi gidrodinamiki i aerodinamiki (Two-dimensional problems in hydrodynamics and aerodynamics). Moscow, GITTL, 1950.
4. Wagner, H. Über die Entstehung des dynamischen Auftriebs von Tragflugeln. ZAMM, 1925, bd. 3, H. 5.
5. Wagner, H. Über stob- und Gleitvorgänge an der Oberfläche von Flüssigkeiten. ZAMM, Bd. 12, H. 4, 1932.
6. Smirnov, V. I. Kurs vysshey matematiki (Course in higher mathematics). Vol. 3, Moscow and Leningrad, GITTL, 1949.
7. Sedov, L. I. Theory of nonstationary planing and movement of a foil with trailing vortices. Trudy TsAGI, No. 252, 1936.
8. Jegorow, I. T. Hydrodynamische Kräfte am Tragflugel bei instationärer Bewegung. Schiffbautechnik, H. 6, 1959.
9. Titmarsh, Ye. Vvedeniye v teoriyu integralov Fur'ye (Introduction to the theory of Fourier integrals). OGIZ, 1948.
10. Khaskind, M. D. Acoustical radiation from oscillating bodies in a compressible fluid. ZhTF, 1946, Vol. 16, No. 7.
11. Lebedev, N. N. Spetsial'nyye funktsii i ikh prilozheniya (Special functions and their application). GITTL, 1953.
12. Gursa, E. Kurs matematicheskogo analiza (Course in mathematical analysis). Vol. 3, Part 2, Moscow, AN SSSR, 1956.
13. Karafoli, Ye. Aerodinamika kryla samoleta (Aerodynamics of an aircraft wing). Moscow, AN SSSR, 1956.
14. Sakharnyy, N. F. Separation-free flow around a system consisting of two arcs of given shape. PMM, Vol. 13, No. 4.
15. Voytkunskiy, Ya. I., et al. Spravochnik po teorii korablya (Manual on ship theory). Leningrad, Sudpromgiz, 1960.
16. Kochin, N. Ye. Sobraniye sochineniy (Collected works). Vol. 2, Moscow, AN SSSR, 1949.

CHAPTER III. Nonstationary hydrodynamic forces in interaction between the lift surfaces of craft and the free surface of the water

A. Hydrodynamic forces during impact

In solid mechanics the term impact is used to describe the process of encounter between two or more bodies whose points of contact have at the instant of encounter a relative velocity not lying in a common tangential plane [1]. This means that the mutual reactions occurring at points of contact change the velocity of each body in a very brief interval of time. The interval of time during which these reactions take place is the duration of impact. Despite the brief duration of impact the forces of reaction exceed by many times the other forces acting on the bodies which influence their movement before and after impact. [192]

The physical nature of the bodies has a huge influence on the process of impact. Even Newton, investigating impact between solid bodies, advanced the hypothesis that the relation between absolute magnitude of the normal projection of relative velocity of bodies after impact and the magnitude following impact is a certain physical constant which depends on the nature of the colliding bodies and does not depend on the magnitude of the relative velocity or the mass of the bodies. This constant is called the coefficient of restitution and its numerical value fluctuates between 0 and 1. When the coefficient of restitution is equal to unity the impact is absolutely elastic. If the coefficient of restitution is equal to zero the impact is absolutely inelastic. After such an impact the bodies travel together, losing in the process of impact some of their kinetic energy.

The problem investigated by us amounts to a consideration of the process of impact between a solid body and a liquid. In this process the body impacting on the water will be considered to be absolutely inelastic, deformation of the body on impact being zero. We will consider the liquid to be ideally incompressible, or if compressible then only to an acoustical approximation. When two such bodies collide the coefficient of restitution is equal to zero, that is, the impact is absolutely inelastic.

When a hydrofoil craft moves in an irregular seaway a foil may enter or leave the water. As a rule the process of immersion which follows is accompanied by impact of foil against wave.

Below we present methods for calculating the hydrodynamic forces occurring when a foil or other lift surface of a craft impacts on the water.

§22. Hydrodynamic forces and movement during impact of bodies moving on the surface of the water

The formulas presented in §14 for calculating external forces during impact against water are based on the assumption of incompressibility of water. This assumption can be applied if two conditions are observed: first, the induced velocities of the liquid v are small compared with the velocity c at which sound is propagated in it ($v \ll c$ or mach number $M = v/c \ll 1$); and, second, the inequality $\tau \gg \ell/c$ holds where τ and ℓ are time and distance of such an order that the velocity of the liquid undergoes a detectable change [2].

In the nonstationary processes covered in ship theory [193] the first condition is met in most cases since the mach numbers are almost always less than unity. The effect of compressibility of a liquid on the vortex components of total hydrodynamic force is determined, as is known, by the value of the mach number (for example, $C_{ycom} = C_{yinc}/\sqrt{1 - M^2}$, where C_y is the coefficient of lift).

In view of the smallness of M its effect on the vortex components of hydrodynamic forces in ship theory problems can be neglected, these components being determined from the formulas in §12 which were derived based on the assumption that the liquid is incompressible.

The second condition is determined in the main by the elastic and inertial properties of the liquid and is not always observed in dynamic ship theory problems. Therefore, in those cases when τ is comparable with ℓ/c a nonstationary process must be considered in light of the elasticity of the liquid which in the last analysis must affect the magnitude and nature of change over time of the potential component of hydrodynamic forces. An example is the problem presented below of hydrodynamic forces during direct impact on a plate floating on the surface of a compressible liquid.

It follows from the general expression for hydrodynamic forces (see formula II.17) and also directly from formula (II.33) that in a direct impact involving a floating plate the force of impact which is determined by the potential component of Y_1 is equal to infinity and the duration of its action to zero. The latter results are, as already stated, a consequence of the assumption of incompressibility of the liquid. In view of the instantaneous propagation of disturbances in an incompressible liquid and instantaneous change in speed of movement of the plate the second inequality presented above is

not satisfactory. Therefore, in order to obtain finite values for the forces acting in an actual liquid elasticity of the liquid must be taken into consideration.

When a plate floating on the surface impacts on an actual liquid the resulting hydrodynamic pressures spread from the surface of contact within both media at a finite velocity due to the elasticity of the liquid and the plate. We will consider the velocity of elastic disturbances in the plate to be infinitely great compared with the velocity of propagation in the liquid, that is, we will consider the plate to be absolutely inelastic. In this event the total velocity of movement lost by the plate will be absorbed by the liquid. The hydrodynamic phenomena occurring on the wetted surface of the plate develop so rapidly that the liquid does not manage to part due to their effects, as a consequence of which at the first instant of impact compression occurs in the layers of liquid adjacent to the plate. The resulting wave of compression spreads within the liquid at the speed of sound and gradually becomes damped. After the impact pressures dissipate and flow starts around the plate, hydrodynamic pressures due to movement of the plate remain in the liquid. [194]

The idea of studying impact of a solid body against water while taking into account the elasticity of the latter is attributed to L. Prandtl who proposed studying this phenomenon in the same way as hydraulic hammer in a pipe [3]. Below we present a solution for the two-dimensional problem of direct impact of a plate floating on the surface of a compressible liquid [4], [5] which was found using the apparatus of Mat'ye functions [6]. The expressions found for the external forces around a flat plate are extended using Wagner's hypothesis to the case of impact of an inclined plate and a wedge against the surface of a compressible liquid.

Let a certain elastic ideal liquid fill a lower half-space. The solid body on the surface of the liquid is a flat plate in the shape of a strip $2a_0$ wide. At a certain instant of time $t = 0$ the plate instantaneously acquires a velocity v_0 . We will consider movement of the liquid caused by displacement of the body in a system of xy coordinates oriented on the body (Fig. 113). Prior to taking up movement of the liquid we will describe distinguishing aspects in the formulation of the problem which are due to compressibility of the liquid.

The main distinction between movement of a compressible liquid and movement of an incompressible one is that small changes in pressure spread instantaneously in an incompressible one and in an elastic one at a finite velocity equal to the speed of sound ([12], Chapter II):

$$c = \sqrt{\frac{dp}{d\rho}}, \quad (\text{III.1})$$

where $p = p(x, y, t)$ is the pressure at a given point in the liquid and $\rho = \rho(x, y, t)$ is the density of the liquid.

In an incompressible liquid the field of velocities and pressures caused by movement of the body is established instantaneously while in an ideal compressible medium it becomes established gradually as the elastic disturbances caused by changes in the pressure on the body spread in the liquid.

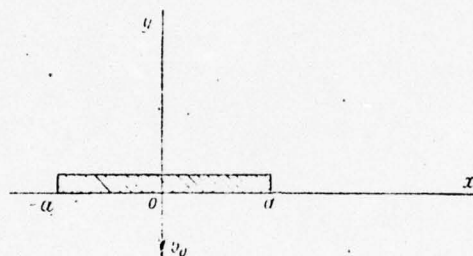


Fig. 113. Impact on a plate floating on the surface of water (main notation).

As a consequence of the fact that the density of an elastic liquid is a function of coordinates and time, the condition of continuity for it takes the following form [7]: [195]

$$\frac{1}{\rho} \frac{d\rho}{dt} + \frac{\partial v_x}{\partial x} + \frac{\partial v_y}{\partial y} = 0, \quad (\text{III.2})$$

where v_x and v_y are components of the velocity vector on the axis of a normal system of coordinates.

Equation (III.2) can be transformed and written in the form

$$\frac{\partial \rho}{\partial t} + \frac{\partial (\rho v_x)}{\partial x} + \frac{\partial (\rho v_y)}{\partial y} = 0. \quad (\text{III.3})$$

The equation derived by I. S. Gromeko for the movement of an ideal compressible liquid when body forces are neglected can be written [8]:

$$\left. \begin{aligned} \frac{1}{\rho} \frac{\partial p}{\partial x} + \frac{1}{2} \frac{\partial v^2}{\partial x} + \frac{\partial v_x}{\partial t} &= 0, \\ \frac{1}{\rho} \frac{\partial p}{\partial y} + \frac{1}{2} \frac{\partial v^2}{\partial y} + \frac{\partial v_y}{\partial t} &= 0, \end{aligned} \right\} \quad (\text{III.4})$$

where $v^2 = v_x^2 + v_y^2$.

In the following discussion we will investigate impact spreading at subsonic velocities and therefore movement of the liquid everywhere in the flow can be considered to be potential. Keeping this in mind and also assuming that the medium is barotropic, that is, $\rho = f(p)$ holds, it can easily be shown that the general integral equation for system (III.4) is

$$P + \frac{1}{2} v^2 + \frac{\partial \phi}{\partial t} = c_0. \quad (\text{III.5})$$

Here $P = \int \frac{dp}{\rho} = \int \frac{dp}{f(p)}$, ϕ is the potential of velocities of movement of the liquid, and c_0 is an arbitrary constant of integration.

Formula (III.5) is a generalization of the Lagrange integral for the case of a potential barotropic flow of an ideal weightless liquid.

Considering the process of impact to be isothermic (change in pressure directly proportional to change in density) we obtain the following relation for P :

$$P = \int \frac{dp}{\rho} = c^2 \int \frac{d\rho}{\rho} = c^2 \ln \rho + c_1,$$

substituting which in the Lagrange integral we find

$$c^2 \ln \rho + \frac{1}{2} v^2 + \frac{\partial \phi}{\partial t} = c_2. \quad (\text{III.6})$$

In view of the fact that at infinity the liquid is at rest, we can write (III.6) in the form

$$\ln \rho + \frac{1}{2} \frac{v^2}{c^2} + \frac{1}{c^2} \frac{\partial \phi}{\partial t} = 0. \quad (\text{III.7})$$

Equation (III.7) can be simplified. In view of its smallness in comparison with the other two terms we can neglect the term containing the ratio between the squares of the induced velocities and the speed of sound. This makes it possible to write (III.7) in the form

$$\ln \rho + \frac{1}{c^2} \frac{\partial \phi}{\partial t} = 0,$$

whence it follows that

$$\rho = e^{-\frac{1}{c^2} \frac{\partial \phi}{\partial t}}. \quad (\text{III.8})$$

Substituting (III.8) into (III.3) and making several simple transformations we obtain the condition of continuity in the following form:

$$\frac{\partial^2 \varphi}{\partial x^2} + \frac{\partial^2 \varphi}{\partial y^2} = \frac{1}{c^2} \cdot \frac{\partial^2 \varphi}{\partial t^2}, \quad (\text{III.9})$$

Equation (III.9) is of the hyperbolic type and is known in acoustics under the name of wave equation. By assuming that in it $c = \infty$ we obtain the Laplace equation expressing the conservation of mass for an incompressible liquid.

Along with equation (III.9) the velocity potential being sought $\phi(x, y, t)$ must satisfy boundary and initial conditions in keeping with the physical essence of the problem.

On the free surface the change in density of the liquid during the process of impact is negligible. Therefore, taking into account the linearized formulation of the problem and also the fact that movement begins from a state of rest, we obtain the following boundary condition at the free surface:

$$\phi = 0 \text{ when } |x| > a_0, y = 0. \quad (\text{III.10})$$

We have the following condition of impermeability on the surface of the plate:

$$\partial \phi / \partial y = y' \text{ when } |x| < a_0, y = 0. \quad (\text{III.11})$$

In the following discussion we will be interested in solutions to a wave equation vanishing at infinity as $z^{-\frac{1}{2}}$ where $z^2 = x^2 + y^2$. Therefore, to avoid ambiguity in the solution we must add a condition at infinity to the boundary conditions listed above. We will use the principle of propagation which expresses the condition of nonpropagation of waves from infinity to within a flow; in other words, disturbances arising upon impact become dissipated at infinity.

The mathematical formulation of this principle of propagation involves the following limits ([10], Chap. 11):

$$\lim_{r \rightarrow \infty} V \bar{r} \left(\frac{\partial \varphi}{\partial r} + i v \varphi \right) = 0; \quad \lim_{r \rightarrow \infty} |V \bar{r} \varphi| = \text{const.} \quad (\text{III.12})$$

At the instant of start of impact movement of the plate [197 is defined by the conditions

$$y_1 = 0; y_1' = -v_0 \text{ when } t = 0, \quad (\text{III.13})$$

where y_1 is the ordinate in a fixed system of $x_1 y_1$ coordinates, the axis of abscissas (x_1 axis) coinciding with the free surface of the liquid and the y_1 axis being directed upward.

The conditions presented define uniquely the function sought for the velocity potential ϕ in the lower half-plane.

For the purpose of solving the problem function ϕ should be continued into the upper part of the xy plane. The real boundary conditions (III.10) and (III.11) make it possible to use the principle of symmetry for this purpose. As a result of the continuation we obtain the function $\phi(x, y, t)$ which is analytical over the entire plane with the exception of the segment $|x| \leq a_0, y = 0$ and, as formerly, $\phi(x, y, t) = -\phi(x, -y, t)$.

Comparing the problem of impact of a solid body against a compressible liquid with the problem of inelastic impact, we see that in distinction from the latter for the former it is necessary to find the solution to a wave equation instead of a Laplace equation when a boundary condition in the form of the principle of propagation is in effect at infinity.

A general solution for the posed mixed problem for an equation of the hyperbolic type cannot be obtained in the form of a simple, finite formula as for example in the Cauchy problem for a three-dimensional wave equation whose solution in closed form can be expressed by the Poisson formula. Solving equation (III.9) by the Fourier method is the most effective. The theoretical basis of this method for solving a mixed problem in the case of a linear hyperbolic equation is explained in the works of S. L. Sobolev [9] and O. A. Ladyzhenskaya [10].

Using the Fourier method Sommerfeld and Lamb [11] obtained a solution to the problem with homogeneous boundary conditions of propagation of elastic disturbances from an unbounded plane located on the surface of a compressible medium filling a lower half-space. M. D. Khaskind [12] solved the problem of acoustical propagation in the flutter of a thin foil moving in a flow of compressible liquid at a constant horizontal velocity and executing additional small oscillations in the plane of the foil profile in accordance with a simple harmonic law.

In the problems cited there is no solution for propagation in a liquid of a disturbance which at the initial instant is localized in a certain way, only the phase of a certain sinusoidal solution satisfying limiting conditions being propagated.

Using the Fourier method we will make the assumption that the function ϕ being sought represents a product of the two functions

$$\phi(x, y, t) = \psi(x, y) T(t), \quad (\text{III.14})$$

of which ψ depends on the variables x and y and T only on time t .

Substituting this proposed solution into equation (III.9) [198] and dividing both sides of the equation by the product ψT , we obtain on the left side a function depending only on coordinates x and y and on the right side a magnitude not depending on them. The equation obtained holds only in that case when there are constants on both the right and left sides. As a result we arrive at a system consisting of two equations

$$\frac{d^2 T}{dt^2} + \lambda^2 T = 0, \quad (\text{III.15})$$

$$\frac{\partial^2 \psi}{\partial x^2} + \frac{\partial^2 \psi}{\partial y^2} + \frac{\lambda^2}{c^2} \psi = 0, \quad (\text{III.16})$$

where λ is a certain constant.

In the case of simple harmonic displacements λ is a real number describing the frequency of natural oscillations. In the more general case simple movements can be expressed by an exponential expansion, the superscript indicating the power of which λ can assume any value in the complex plane $\lambda = \alpha + i\beta$ ([2], Chap. II).

Finding partial solutions in the form of simple harmonic oscillations $\lambda = \alpha$ makes it possible in principle to arrive at a general solution to the problem for arbitrary complex movements of a plate since any function of movement of velocity of movement satisfying the Dirichlet conditions can be represented in the form of sums of simple harmonics, that is, by a Fourier series or integral equation. The idea behind the Fourier method lies essentially herein.

However, the use of this method under the conditions prevailing in the problem posed is difficult due to the cumbersome mathematical computations involved.

In order to arrive at expressions for the force of an impact and movement of a plate in finite form we will note that the process of impact has a clearly expressed aperiodic nature damping over time and we will set $\lambda = i\beta$, thereby limiting the problem posed by the condition that the velocity of disturbed movement of the liquid be damped exponentially over time. One example of such movement is that of the impact of a plate floating freely on the surface of a compressible liquid.

With this approach to the problem the Fourier method is used only in that part which pertains to separation of the variables in the initial wave equation.

From the general integral of the ordinary differential equation

$$T = c_1 e^{i\lambda t} + c_2 e^{-i\lambda t} \quad (\text{III.17})$$

only the first partial integral satisfies the physical conditions of the problem and therefore we present the sought solution to equation (III.9) in the following form:

$$\psi(x, y, t) = \psi(x, y) e^{-i\lambda t} \quad (\text{III.18})$$

The function $\psi(x, y)$ must be determined by solving an incomplete wave equation (III.16). Assuming in this equation $x = ax_1$ and $y = ay_1$, we reduce it to the form [199

$$\frac{\partial^2 \psi}{\partial x^2} + \frac{\partial^2 \psi}{\partial y^2} + v^2 \psi = 0 \quad \left(v^2 = -\frac{a^2 \beta^2}{c^2} \right). \quad (\text{III.19})$$

Here and in the following discussion for simplicity of notation we omit the subscript "1" of the variables x_1 and y_1 .

Along with equation (III.19) function $\psi(x, y)$ must satisfy the boundary conditions:

$$\psi = 0 \quad \text{when} \quad |x| > 1, y = 0, \quad (\text{III.20})$$

$$\frac{\partial \psi}{\partial y} = av \quad \text{when} \quad |x| < 1, y = 0, \quad (\text{III.21})$$

and also the conditions from the principle of propagation

when $r \rightarrow \infty$

$$\lim_{r \rightarrow \infty} V \sqrt{r} \left(\frac{\partial \psi}{\partial r} + iv\psi \right) = 0, \quad \lim_{r \rightarrow \infty} |V \sqrt{r} \psi| = \text{const.} \quad (\text{III.22})$$

It is desirable to seek further solution to the problem in elliptical coordinates, transition to which can be accomplished by conformal transformation of the plane $z = x + iy$ onto the plane $\zeta = \xi + i\eta$ using the relations [6]:

$$z = \text{ch } \zeta, \quad x = \text{ch } \xi \cos \eta, \quad y = \text{sh } \xi \sin \eta. \quad (\text{III.23})$$

Transforming these relations, we obtain two equations:

$$\frac{x^2}{\text{ch}^2 \xi} + \frac{y^2}{\text{sh}^2 \xi} - \cos^2 \eta + \sin^2 \eta = 1,$$

$$\frac{x^2}{\cos^2 \eta} - \frac{y^2}{\sin^2 \eta} = \text{ch}^2 \xi - \text{sh}^2 \xi = 1,$$

from which it follows that a family of cofocal ellipses in

the z plane corresponds to the lines $\xi = \text{const}$ in the ζ plane and a family of cofocal hyperbolas which are orthogonal to the family of ellipses to the lines $\eta = \text{const}$ (Fig. 114). The segment of the real axis of interest to us $|x| < 1$, $y = 0$ is a confluent ellipse $\xi = 0$, $|\eta| < \pi$. The confluent hyperbola $\eta = 0$, $\xi > 0$ corresponds to the free surface of the liquid which is represented by the sector of the real axis $x > 1$ and the confluent hyperbola $\eta = \pm\pi$, $\xi > 0$ to $x < -1$.

Translating in (III.19) to elliptical coordinates, using the Lamé relation [13]

$$\frac{\partial^2 \psi}{\partial x^2} + \frac{\partial^2 \psi}{\partial y^2} = \left(\frac{\partial^2 \psi}{\partial \xi^2} + \frac{\partial^2 \psi}{\partial \eta^2} \right) \left| \frac{d\xi}{dz} \right|^2, \quad (\text{III.24})$$

where $\frac{d\xi}{dz} = \frac{1}{\sqrt{\text{ch}^2 \xi - \cos^2 \eta}}$, we obtain an incomplete wave equation in the form

$$\frac{\partial^2 \psi}{\partial \xi^2} + \frac{\partial^2 \psi}{\partial \eta^2} + v^2 (\text{ch}^2 \xi - \cos^2 \eta) \psi = 0. \quad (\text{III.25})$$

Assuming the solution to equation (III.25) to be in the form of a product of two functions, one of which depends only on ξ and the other only on η [200]

$$\psi(\xi, \eta) = F(\xi) G(\eta), \quad (\text{III.26})$$

that is, resorting for a second time to the method of separation of variables, we find the equation

$$\frac{d^2 F}{d\xi^2} G + \frac{d^2 G}{d\eta^2} F + v^2 (\text{ch}^2 \xi - \cos^2 \eta) GF = 0,$$

from which follows the following equation:

$$\frac{1}{F} \frac{d^2 F}{d\xi^2} + v^2 \text{ch}^2 \xi = - \frac{1}{G} \frac{d^2 G}{d\eta^2} + v^2 \cos^2 \eta.$$

Since the left side in the latter expression does not depend on η and the right side does not depend on ξ , each side must be equal to a certain separation constant, for example $\alpha + v^2/2$.

As a result of separation we obtain a system consisting of two ordinary equations

$$\left. \begin{aligned} \frac{d^2 G}{d\eta^2} + \left(\alpha - \frac{v^2}{2} \cos 2\eta \right) G &= 0, \\ \frac{d^2 F}{d\xi^2} - \left(\alpha - \frac{v^2}{2} \text{ch} 2\xi \right) F &= 0. \end{aligned} \right\} \quad (\text{III.27})$$

Setting $\theta^* = \frac{1}{4} v^2$, $\theta^* = -0$, $\theta = \frac{a^2 \beta^2}{4c^2}$, we obtain equation (III.27) in the form

$$\left. \begin{aligned} \frac{d^2 G}{d\eta^2} + (\alpha - 2\theta^* \cos 2\eta) G &= 0, \\ \frac{d^2 F}{d\xi^2} - (\alpha - 2\theta^* \operatorname{ch} 2\xi) F &= 0. \end{aligned} \right\} \quad (\text{III.28})$$

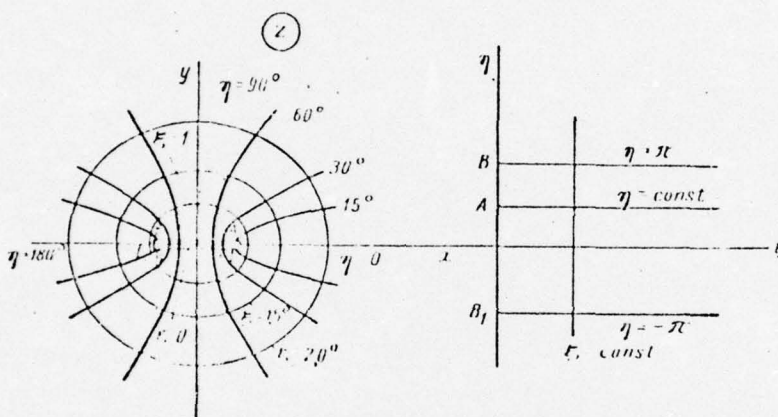


Fig. 114. Elliptical system of coordinates.

The equations of system (III.28) represent canonical forms [201] of the Mat'ye equation. The second of them is often called a modified Mat'ye equation. If in it we replace ξ with $\pm i\eta$ it becomes the first equation and, conversely, if we replace $\pm i\eta$ with $\pm i\xi$ in the first, we get the modified equation.

The solution (III.26) being sought contains the product of two functions, each of which is a solution of one of the equations in system (III.28) having the same values for parameters α and θ^* .

As a consequence of the fact that α can assume any value, for uniqueness of solution the function $G(\eta)$ must be periodic in the z plane and have a period of 2π . A set of eigenvalues $\alpha_{2n+1}(\theta^*)$ where $n = 0, 1, 2, \dots$ defines this condition. The family of fundamental functions of an integral order which correspond to these values forms a complete orthogonal system. Function $F(\xi)$ must be expressed in terms of modified Mat'ye functions satisfying the principle of propagation. Of all the possible solutions to the second equation in system (III.28) combined functions conformable with Hankel functions satisfy this principle.

Products of pairs of functions representing a solution to system (III.28) must also satisfy the condition of symmetry flowing from the physical conditions of the problem. In our case movement of the liquid is symmetrical with respect to the minor axis of cofocal ellipses (see Fig. 114). Representation of the potential $\psi(\xi, \eta)$ in the form of an expansion with respect to odd Mat'ye functions having an odd subscript corresponds to this condition of symmetry.

The following form of the function $\psi(\xi, \eta)$ satisfies the demands listed above:

$$\psi(\xi, \eta) = \sum_{n=0}^{\infty} a_{2n+1} Ne_{2n+1}^{(1)}(\xi, -0) se_{2n+1}(\eta, -0). \quad (\text{III.29})$$

In formula (III.29) $se_{2n+1}(\eta, -0)$ is an odd periodic Mat'ye function which is a solution to the first equation in (III.28) and is expressed in terms of trigonometric functions in the form of the series

$$se_{2n+1}(\eta, -0) = (-1)^n \sum_{r=0}^{\infty} (-1)^r A_{2r+1}^{2n} \sin(2r+1)\eta, \quad (\text{III.30})$$

where A_{2r+1}^{2n+1} are coefficients of expansion of a function of r ;

$Ne_{2n+1}^{(1)}(\xi, -0)$ is a combined odd Mat'ye function of the first order which is expressed in terms of second solutions of a modified equation by the following relation:

$$Ne_{2n+1}^{(1)}(\xi, -0) = 2i Gek_{2n+1}(\xi, -0). \quad (\text{III.31})$$

In turn the function $Gek_{2n+1}(\xi, -0)$ can be expressed in terms of a product of Bessel functions of an imaginary argument in the form of the following series:

[202

$$Gek_{2n+1}(\xi, -0) = \frac{p_{2n+1}}{\pi A_1^{2n+1}} \sum_{r=0}^{\infty} A_{2r+1}^{2n+1} [I_r(v_1) K_{r+1}(v_2) + I_{r+1}(v_1) K_r(v_2)]. \quad (\text{III.32})$$

In the last formula

$$p_{2n+1} = \frac{(-1)^{n+1}}{k A_1^{2n+1}} ce_{2n+1}(0, 0) ce_{2n+1}\left(\frac{\pi}{2}, 0\right), \quad k^2 = 0;$$

$ce_{2n+1}(\xi, 0)$ is an even periodic Mat'ye function with an odd subscript; $I_m(v_1)$ is a Bessel function of the imaginary argument; $K_m(v_2)$ is a MacDonald function; $v_1 = ke^{-\xi}$; and $v_2 = ke^{\xi}$.

The function $Ne_{2n+1}^{(1)}(\xi, -0)$ has the following asymptotic representation:

$$Ne_{2n+1}^{(1)}(\xi, -0) \approx p_{2n+1}' \frac{e^{-v}}{\sqrt{2\pi v}}, \quad (\text{III.33})$$

where $v = 2kch\xi$, whence it is apparent that when $\xi \rightarrow \infty$ function (III.33) passes monotonically to zero. Consequently, expression for potential (III.29) satisfies the principle of propagation.

Function (III.20) expressing the potential satisfies the first boundary condition (III.20) since on a free surface [$\eta = 0$, $\eta \neq \pi$ when $\xi > 0$] the function $se_{2n+1}(\eta, -0)$ vanishes which follows directly from expression (III.30).

For the purpose of determining the arbitrary constant of integration a_{2n+1} , we will use the boundary condition on a plate (III.21) which can be written in elliptical coordinates in the form

$$\frac{d\psi}{d\xi} = av \sin \eta \quad \text{when } |\eta| < \pi, \xi = 0. \quad (\text{III.34})$$

Requiring (III.29) to meet boundary conditions (III.34), we obtain

$$av \sin \eta = \sum_{n=0}^{\infty} a_{2n+1} Ne_{2n+1}^{(1)'}(0, -0) se_{2n+1}(\eta, -0), \quad (\text{III.35})$$

where

$$|\eta| < \pi, Ne_{2n+1}^{(1)'}(0, -0) = \left[\frac{\partial Ne_{2n+1}^{(1)}(\xi, -0)}{\partial \xi} \right]_{\xi=0}.$$

By multiplying the equation obtained by $se_{2n+1}(\eta, -0)d\eta$ and integrating from $-\pi$ to $+\pi$ we find

$$\begin{aligned} av \int_{-\pi}^{\pi} se_{2n+1}(\eta, -0) \sin \eta d\eta &= \\ &= \sum_{n=0}^{\infty} a_{2n+1} Ne_{2n+1}^{(1)'}(0, -0) \int_{-\pi}^{\pi} se_{2n+1}^2(\eta, -0) d\eta. \end{aligned} \quad (\text{III.36})$$

Due to the orthogonality of a Mat'ye function the integral [203 on the left side of equation (III.36) is equal to

$$\int_{-\pi}^{\pi} se_{2n+1}(\eta, -0) \sin \eta d\eta = (-1)^n \pi A_1^{2n+1}.$$

According to the second condition for normalizing the Mat'ye functions we have

$$\int_{-\pi}^{+\pi} se_{2n+1}^2(\eta, -0) d\eta = \pi.$$

Substituting the values found for the integrals into equation (III.36) and solving with respect to a_{2n+1} , we obtain

$$a_{2n+1} = (-1)^n \frac{A_1^{2n+1}}{Ne_{2n+1}^{(1)'}(0, -0)} av. \quad (\text{III.37})$$

Substituting in turn (III.37) into (III.29) we find the following solution for incomplete wave equation (III.25):

$$\psi(\xi, \eta) = av \sum_{n=0}^{\infty} (-1)^n A_1^{2n+1} \frac{Ne_{2n+1}^{(1)}(\xi, -0)}{Ne_{2n+1}^{(1)'}(0, -0)} se_{2n+1}(\eta, -0). \quad (\text{III.38})$$

Taking formula (III.18) into account and also the initial conditions (III.13) we will represent the velocity potential of the liquid movement under consideration in the form

$$\varphi(\xi, \eta, t) = a \sum_{n=0}^{\infty} (-1)^n A_1^{2n+1} \frac{Ne_{2n+1}^{(1)}(\xi, -0)}{Ne_{2n+1}^{(1)'}(0, -0)} se_{2n+1}(\eta, -0) ve^{-\beta t}. \quad (\text{III.39})$$

The expression found for the velocity potential is a partial integral of wave equation (III.9) satisfying the boundary conditions and the initial conditions established for the surface of the plate. Function (III.39) is written in elliptical coordinates. Relations (III.23) must be used to translate to a cartesian plane.

The solution obtained, just as those noted above [11] and [12], do not express the law governing propagation in a liquid of a locally concentrated disturbance induced at the initial instant by a plate since potential (III.39) represents a continuous function of coordinates and time with continuous derivatives with respect to these arguments. Therefore formula (III.39) should be regarded as a function characterizing the movement of a liquid only between a plate and the front of a sound wave and this makes it possible to write it in the following form:

$$\varphi = a \sum_{n=0}^{\infty} (-1)^n A_1^{2n+1} \frac{Ne_{2n+1}^{(1)}(\xi, -0)}{Ne_{2n+1}^{(1)'}(0, -0)} se_{2n+1}(\eta, -0) ve^{-2\beta s_0}, \quad (\text{III.40})$$

where

$$s_0 = \frac{ct}{u} \quad \text{wherein } r = \sqrt{x^2 + y^2} \leq s_0.$$

[204

Function (ξ, η, t) satisfies the condition when $t < 0$, $= 0$ since $v = 0$; when $t = 0$ it satisfies the initial condition on the plate; and when $t > 0$ the plate moves in a flow of liquid whose velocity field is established by a sound wave regardless of the plate movement at the given instant. In this connection the circumstances listed above do not limit the use of the potential (III.39) for determining the hydrodynamic pressures and forces acting on the plate in the case of impact under consideration.

The data obtained in preceding sections on the flow of a liquid during impact make it possible to proceed to a determination of hydrodynamic pressures and forces. Limiting the problem to a consideration of impact against a slightly compressible liquid, a change in the density of which can be neglected in generalized Lagrange integral equation (III.5), we obtain the following linearized relation between pressure and velocity potential:

$$p - p_0 = -\rho_0 \frac{\partial \phi}{\partial t}. \quad (\text{III.41})$$

Differentiating (III.39) over time and substituting $\partial \phi / \partial t$ into (III.41), we find the formula

$$p - p_0 = a_0 \rho_0 \beta \sum_{n=0}^{\infty} (-1)^n A_1^{2n+1} \frac{Ne_{2n+1}^{(1)}(\xi, -0)}{Ne_{2n+1}^{(1)}(0, -0)} se_{2n+1}(\eta, -0) v e^{-\beta t}, \quad (\text{III.42})$$

for the hydrodynamic pressures in the flow of liquid behind the front of a sound wave.

Assuming in formula (III.42) that $\xi = 0$, $|\eta| < \pi$, we obtain the excess pressure on a plate

$$p - p_0 = a_0 \rho_0 \beta \sum_{n=0}^{\infty} (-1)^n A_1^{2n+1} \frac{Ne_{2n+1}^{(1)}(0, -0)}{Ne_{2n+1}^{(1)}(0, -0)} \times \\ \times se_{2n+1}(\eta, -0) v_0 e^{-\beta t} \quad \text{npn } |\eta| < \pi. \quad (\text{III.43})$$

It follows from formula (III.43) that the pressure, in light of the law governing movement of the plate, will be maximum at the instant of start of impact.

The odd periodic Mat'ye function $se_{2n+1}(\eta, -0)$ when $\theta \rightarrow 0$ degenerates into the trigonometric function $\sin \eta$. Inasmuch as when $\xi = 0$ $\eta = \arccos x$ [see (III.23)], that is,

$\sin \eta = \sin(\arccos \frac{x}{a}) = \sqrt{1 - (\frac{x}{a})^2}$, we see convincingly that the law governing pressure distribution over the surface of a plate during impact against a slightly compressible liquid is close to the elliptical observed during inelastic impact. [205]

Formula (III.43) can be transformed as follows. Multiplying and dividing the right side of (III.43) by $|c/a|$, we obtain

$$p - p_0 = \rho_0 c v_0 \sum_{n=0}^{\infty} (-1)^n A_1^{2n+1} \frac{N e_{2n+1}^{(1)}(0, -0)}{N e_{2n+1}^{(1)'}(0, -0)} s e_{2n+1}(\eta, -0) \times \\ \times \frac{d}{ds_0} e^{-2 \sqrt{0} s_0}. \quad (\text{III.44})$$

It follows from formula (III.44) that the amplitude of hydrodynamic pressures expressing that component of formula (III.44) which does not depend on the kinematics of plate movement, is equal to

$$p - p_0 = \rho_0 c v_0 \sum_{n=0}^{\infty} (-1)^n A_1^{2n+1} \frac{N e_{2n+1}^{(1)}(0, -0)}{N e_{2n+1}^{(1)'}(0, -0)} s e_{2n+1}(\eta, -0). \quad (\text{III.45})$$

When $\theta \rightarrow 0$ the sum standing on the right side of the last equation, as will be shown below, tends to the value of the first term in the series $A_1^{(1)} \frac{N e_1^{(1)}(0, -0)}{N e_1^{(1)'}(0, -0)} s e_1(\eta, -0)$ which in turn tends to $\sin \eta = \sqrt{1 - (\frac{x}{a})^2}$. From this we obtain for the amplitude of hydrodynamic pressures acting in the center-line plane of a plate [$x = 0$] the expression

$$p - p_0 = \rho_0 c v_0. \quad (\text{III.46})$$

The latter agrees with the known solution from the theory of two-dimensional waves arising during instantaneous communication of velocity to the infinite plane delimiting the lower half-space [11] and [14].

The total hydrodynamic force acting on a unit of plate width during impact can be obtained by integrating pressures over the contour of a plate s

$$Y_1^* = -\rho_0 \int_s \frac{\partial \varphi}{\partial t} dx \Big|_{y=0} = -\rho_0 a \int_{s_1} \frac{\partial \varphi}{\partial t} dx_1 \Big|_{y_1=0} = \rho_0 a \int_{-\pi}^{+\pi} \frac{\partial \varphi}{\partial t} \sin \eta d\eta \Big|_{\xi=0};$$

$$\begin{aligned}
Y_1 &= \rho_0 a^2 \left(\frac{d}{dt} v_0 e^{-\beta t} \right) \int_{-\pi}^{\pi} \sum_{n=0}^{\infty} (-1)^n A_1^{2n+1} \frac{N_{e,2n+1}^{(1)}(0, -0)}{N_{e,2n+1}^{(1)}(0, -0)} \times \\
&\quad \times s_{e,2n+1}(\eta, -0) \sin \eta d\eta = -\rho_0 a^2 \left(\frac{d}{dt} v_0 e^{-\beta t} \right) \times \\
&\quad \times \sum_{n=0}^{\infty} (-1)^n A_1^{2n+1} \frac{N_{e,2n+1}^{(1)}(0, -0)}{N_{e,2n+1}^{(1)}(0, -0)} \int_{-\pi}^{\pi} s_{e,2n+1}(\eta, -0) \sin \eta d\eta; \\
Y_1 &= \rho_0 \pi a^2 \sum_{n=0}^{\infty} \frac{N_{e,2n+1}^{(1)}(0, -0)}{N_{e,2n+1}^{(1)}(0, -0)} (A_1^{2n+1})^2 \frac{d}{dt} v_0 e^{-\beta t}.
\end{aligned} \tag{III.47}$$

Formula (III.47) was derived for the case of movement of a plate in an unbounded liquid.

According to the principle of symmetry ϕ and $d\phi/dt$ above and below the real axis are equal in magnitude and opposite in sign. It follows from this that the force acting on a plate when it impacts on the free surface of a liquid is equal to half the force developing on a plate which executes the same movement in a flow of unbounded liquid, that is,

$$Y_1 = \frac{\rho_0 \pi a^2}{2} \sum_{n=0}^{\infty} \frac{N_{e,2n+1}^{(1)}(0, -0)}{N_{e,2n+1}^{(1)}(0, -0)} (A_1^{2n+1})^2 \frac{d}{dt} (v_0 e^{-\beta t}) \tag{III.48}$$

or

$$Y_1 = \frac{\rho_0 \pi a^2}{2} Le(0) \frac{d}{dt} (v_0 e^{-\beta t}), \tag{III.49}$$

where

$$Le(0) = \sum_{n=0}^{\infty} \frac{G_{e,k,2n+1}(0, -0)}{G_{e,k,2n+1}(0, -0)} (A_1^{2n+1})^2. \tag{III.50}$$

In order to use the general expressions presented above for determining concrete forces it is necessary to know the dependence of functions and coefficients of the Mat'ye function on the parameter θ included in them. In [4] the value of the function $Le(\theta)$ for $0 \leq \theta \leq 16$ is found. A graph of function $Le(\theta)$ is shown in Fig. 115. At small values of θ ($\theta \leq 0.2$) the following asymptotic formula can be recommended for calculating the function $Le(\theta)$:

$$Le(\theta) = \frac{1 + \frac{1}{8}\theta + \frac{1}{192}\theta^2}{1 + \frac{7}{8}\theta + \frac{1}{2}\theta \ln \frac{2}{\sqrt{\theta}}}, \tag{III.51}$$

which was found from (III.50) by replacing the functions in it with their asymptotic values when $\theta \rightarrow 0$. The behavior of function $Le(\theta)$ close to $\theta = 0$ and $\theta = \infty$ is in keeping with the following two limits:

$$\left. \begin{aligned} \lim_{\theta \rightarrow 0} Le(\theta) &= -1, \\ \lim_{\theta \rightarrow \infty} Le(\theta) &= 0. \end{aligned} \right\} \quad (\text{III.52})$$

The first limit in (III.52) determines the value of function $Le(\theta)$ on transition to an incompressible liquid ($c = \infty$).

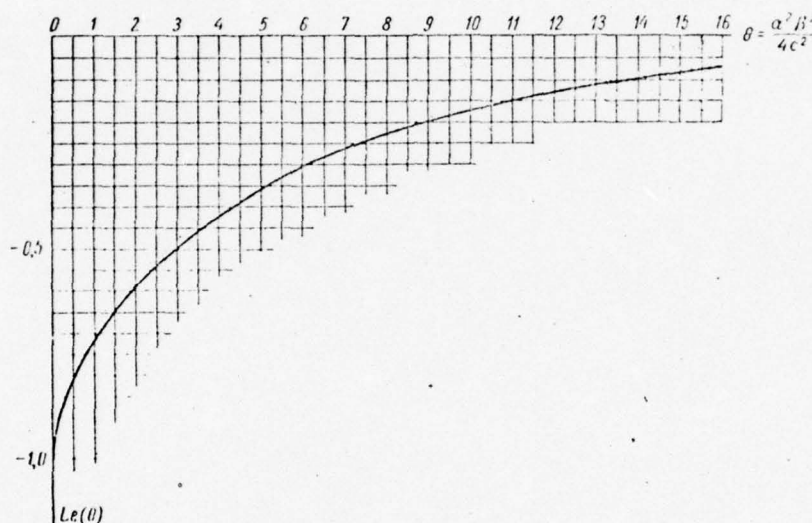


Fig. 115. Graph of function $Le(\theta)$.

Formula (III.49) was derived under the assumption of exponential damping over time of the velocities induced in the liquid. Therefore it holds during movements of a plate during which movement of the liquid at an arbitrary point with coordinates (ξ, η) takes place in accordance with formula (III.49) at a velocity which obeys the law

$$v_{\xi} = \frac{\partial \Psi}{\partial \xi} e^{-\mu t} \quad \text{and} \quad v_{\eta} = \frac{\partial \Psi}{\partial \eta} e^{-\mu t}.$$

We will assume that for a certain particular case of impact of a plate against a liquid we know the value of exponent β . Then using the formula $\theta = \alpha^2 b^2 / 4 c^2$ we can calculate the value of parameter θ and then using the graph in Fig. 115 find the value of function $Le(\theta)$. By substituting the data obtained into formula (III.49) we can determine force Y_1 .

For liquids with a different speed of sound the force of impact, all other things remaining equal, according to formula (III.49) will be greatest where the speed of sound is greatest. In the case of an incompressible liquid when $c \rightarrow \infty$ and $\theta \rightarrow 0$, $Le(\theta) \rightarrow (-1)$ and formula (III.49) becomes formula (II.30). As a consequence of the instantaneous change in velocities which takes place in an incompressible liquid the exponent β must be equal to infinity and therefore from formula (II.30) as well as from formula (III.49) we obtain for the movement under consideration infinitely large values for force Y_1 .

[208

Having determined the external forces, we will now discuss the movement of an absolutely inelastic plate floating on a free surface which results from instantaneous communication to it of an initial velocity v_0 and continues on due to forces of inertia and the hydrodynamic force of impact. We will consider all remaining forces to be small as compared with the two categories indicated, their effect on movement of the plate during the time of impact being ignored. As experience shows, the latter assumption is valid for the entire process of impact with the exception of the final stage when impact is replaced with flow around a plate.

In accordance with what has been stated the differential equation of plate movement can be written in the following form:

$$m \frac{dv}{dt} = -Y_1, \quad (III.53)$$

where $v = -y'$ and m is the mass of the plate.

After substituting into equation (III.53) the value of force Y_1 from (III.49), preliminarily having differentiated, we find

$$m \frac{dv}{dt} = \frac{\rho_0 \pi a^2}{2} Le(0) \beta v_0 e^{-\beta t} \quad \text{or} \quad \frac{dv}{dt} = \mu Le(0) \beta v_0 e^{-\beta t}, \quad \mu = \frac{\rho_0 \pi a^2}{2m}. \quad (III.54)$$

Integrating the latter expression and imposing the initial condition (when $t = 0$, $v = v_0$) on the result, we obtain the following expression for the velocity of the plate

$$v = v_0 [1 + \mu Le(0) - \mu Le(0) e^{-\beta t}], \quad (III.55)$$

Formula (III.55) uniquely describes plate velocity since the unknown function $Le(\theta)$ is included in it. For the purpose of determining $Le(\theta)$ we use the condition of equality between the work of the forces of pressure and the kinetic energy lost by the plate during the time of impact. The energy lost by the plate is known:

$$T_0 - T_k = \frac{1}{2} m v_0^2 \left[1 - \frac{1}{(1 + \mu)^2} \right], \quad (\text{III.56})$$

where $T_0 = \frac{1}{2} m v_0^2$ is the kinetic energy of the plate prior to impact and $T_k = (\frac{1}{2} m v_0^2) (1 / (1 + \mu)^2)$ is the kinetic energy of the plate following impact.

As will be indicated below, energy $(T_0 - T_k)$ is expended [209] on the formation of a sound wave and imparting to the adjoining mass of liquid ($\Delta m = \frac{1}{2} \rho_0 \pi a^2$) the velocity $v_0 / (1 + \mu)$.

The work of the forces of pressure during the time of impact can be expressed by the integral equation

$$W = \int_0^t Y_1 v dt. \quad (\text{III.57})$$

Substituting into (III.57) the values found from Formulas (III.49) and (III.55), we obtain

$$W = -\Delta m v_0^2 \beta Le(0) \int_0^t [1 + \mu Le(0) - \mu Le(0) e^{-\beta t}] e^{-\beta t} dt.$$

Integrating the last expression, assuming the upper limit of integration to be $t = \infty$, we obtain the following expression for function W :

$$W = -\Delta m v_0^2 \left[Le(0) + \frac{1}{2} \mu Le^2(0) \right]. \quad (\text{III.58})$$

Equating formulas (III.56) and (III.58) in accordance with what has been stated, we obtain for determining the function $Le(\theta)$ the equation

$$Le^2(0) + \frac{2}{\mu} Le(0) + \frac{1}{\mu^2} \left[1 - \frac{1}{(1 + \mu)^2} \right] = 0, \quad (\text{III.59})$$

by solving which we find that the first root of equation (III.59) is

$$Le(0) = -\frac{1}{1 + \mu}. \quad (\text{III.60})$$

The second root of equation (III.59) does not satisfy the physical conditions of the problem.

Equation (III.60) expresses the condition from which the value of parameter θ can be found for the case of plate movement under consideration. Knowing the dimensions and mass of the plate, we will then calculate the value of coefficient μ and the entire right side of equation (III.60) from which we find the function $Le(\theta)$. Laying off the value obtained for $Le(\theta)$ on the approximate axis of the graph in Fig. 115, we use the curve to find parameter θ . If the values of $Le(\theta)$ are close in absolute value to unity, which does happen during impact of heavily loaded plates, the following approximate formula can be used for determining θ :

$$\theta \approx -8 \left[\frac{1 + Le(0)}{1 + 7Le(0)} \right], \quad (\text{III.61})$$

This formula was derived directly from the asymptotic expression for the function $Le(\theta)$.

The final expression for the velocity of a plate in the given case of movement can be found by substituting (III.60) into (III.55): [210]

$$v = \frac{v_0}{1 + \mu} (1 + \mu e^{-\beta t}), \text{ where } \beta = \sqrt{\bar{0}} \frac{2c}{a}. \quad (\text{III.62})$$

Differentiating (III.62) with respect to time and substituting the result into initial equation (III.54), we see that the movement equation is satisfied when the condition described by (III.60) is met.

Displacement of the plate during the time of impact is determined by the equation

$$h = \frac{v_0}{1 + \mu} \left[t + \frac{\mu}{\beta} (1 - e^{-\beta t}) \right], \quad (\text{III.63})$$

which is obtained by integrating (III.62) over time and fitting the result of integration to the condition when $t = 0$, $h = 0$. The result makes it possible to write the total hydrodynamic force of impact per unit length of plate in the following form:

$$Y_1 = \frac{\frac{\rho_0 \pi a^2}{2}}{1 + \mu} \beta v_0 e^{-\beta t}. \quad (\text{III.64})$$

Proceeding to an incompressible liquid, that is, assuming in formula (III.62) that $c = \infty$, we obtain formula (II.32) which defines the velocity of a plate after an inelastic impact.

The displacement of the plate during impact can be found from the equation

$$\lim_{t \rightarrow \infty} v = \lim_{t \rightarrow \infty} \left(\frac{v_0}{1 + \mu} \right) (1 + \mu e^{-\beta t}) = \frac{v_0}{1 + \mu}. \quad (\text{III.65})$$

We will multiply the right and left sides of (III.64) by dt and integrate from 0 to t , as a result of which we find

$$\int_0^t Y_1 dt = -\frac{\frac{\rho_0 \pi a^2}{2}}{1 + \mu} \int_0^t d(v_0 e^{-\beta t}).$$

Setting $P = \int_0^t Y_1 dt$ and integrating, we obtain the following formula for determining impulse P :

$$P = \frac{\frac{\rho_0 \pi a^2}{2}}{1 + \mu} v_0 (1 - e^{-\beta t}). \quad (\text{III.66})$$

When $\beta = \infty$ ($\beta = \infty$) the latter formula becomes the well-known expression for impulse force during inelastic impact [16]

$$P = \frac{\rho_0 \pi a^2}{2} \frac{v_0}{1 + \mu}. \quad (\text{III.67})$$

The kinetic energy of a plate during impact can be determined from the equation [211

$$T = \frac{1}{2} \frac{mv_0^2}{(1 + \mu)^2} (1 + \mu e^{-\beta t})^2, \quad (\text{III.68})$$

which yields limiting processes, one for $t \rightarrow 0$ and one for $t \rightarrow \infty$, determining respectively the kinetic energy of the plate prior to impact $T_0 = \frac{1}{2}mv_0^2$ and its energy at the end of impact $T_k = \frac{1}{2}mv_0^2/(1 + \mu)^2$. As already indicated, during the time of impact the plate transmits to the liquid energy equal to the difference ($T_0 - T_k$) [see formula (III.56)].

It is easy to show that the energy lost by the plate is equal in magnitude to the work of the forces of pressure during the time $0 \leq t \leq \infty$.

Calculating integral equation (III.57), or Y_1 and v which are determined respectively from formulas (III.62) and (III.64), we obtain

$$W = \int_0^\infty Y_1 v dt = \left[\frac{\Delta m_1}{(1 + \mu)^2} v_0^2 \beta \right] \int_0^\infty e^{-\beta t} (1 + \mu e^{-\beta t}) dt$$

or, using formula (III.58) in light of condition (III.60),

we find the following expression for the work of the forces of pressure:

$$W = \frac{\Delta m v_0^2}{(1 + \mu)^2} \left(1 + \frac{1}{2} \mu \right), \quad (\text{III.69})$$

where

$$\Delta m = \rho_0 \pi \frac{a^2}{2}, \quad \mu = \frac{\Delta m}{m}.$$

Formula (III.69) can be transformed as follows:

$$\begin{aligned} W &= \frac{m v_0^2}{2} \cdot \left[\frac{2 \frac{\Delta m_1}{m} + \frac{\Delta m_1}{m} \mu}{(1 + \mu)^2} \right] = \\ &= \frac{m v_0^2}{2} \frac{2\mu + \mu^2}{(1 + \mu)^2} = \frac{m v_0^2}{2} \left[\frac{2\mu + \mu^2 + 1}{(1 + \mu)^2} - \frac{1}{(1 + \mu)^2} \right] \end{aligned}$$

or

$$W = \frac{m v_0^2}{2} \left[1 - \frac{1}{(1 + \mu)^2} \right]. \quad (\text{III.70})$$

By comparing (III.56) and (III.70) we see justification for what has been stated.

Formula (III.70) can be transformed to read:

$$W = \frac{m v_0^2}{2} \left[\frac{\mu}{(1 + \mu)^2} + \frac{\mu}{1 + \mu} \right]. \quad (\text{III.71})$$

The first term in formula (III.71) expresses the work done, or the part of the kinetic energy lost, by the plate on imparting to the adjoining mass of liquid Δm the velocity $v_0/(1 + \mu)$. The second term represents the total energy of the sound wave [15].

Taking into account the fact that $T_0 - T_k = W$, on the basis of formula (III.71) we can write the equation [212]

$$T_0 = T_k + \frac{\Delta m v_0^2}{2} \left(\frac{1}{1 + \mu} \right)^2 + \frac{\Delta m v_0^2}{2} \frac{1}{1 + \mu}. \quad (\text{III.72})$$

It follows from (III.72) that the energy of the plate at the start of impact is equal to the sum of the energy of the plate after impact and the energy lost on imparting to the adjoining mass of liquid a velocity of $v_0/(1 + \mu)$ and on forming a shock sound wave.

Equation (III.72) does not hold for the case of impact against an incompressible liquid since with inelastic impact there is no third term. The kinetic energy lost by the plate upon inelastic impact is described by formula (III.56). At the same time the energy carried off by the liquid which is lost on imparting to the adjoining mass Δm a speed of $v_0/(1 + \mu)$ is equal to only

$$T_m = \frac{\Delta m v_0^2}{2} \frac{1}{(1 + \mu)^2}.$$

Therefore in the theory of impact against an incompressible liquid the energy balance is upset.

The idea of an adjoining mass which is usually applied to an ideal incompressible liquid can be extended to the case of an ideal compressible liquid. In a compressible liquid an adjoining mass is dependent not only on the shape of the body but is a function of time and movement of the body. For the purpose of determining this function in the problem under consideration we will use an amount of movement theorem and an impulse theorem.

From the condition of constancy of amount of movement in the process of impact we get the following equation:

$$(m + \Delta m) v = m v_0 = \text{const.} \quad (\text{III.73})$$

The adjoining mass of liquid is

$$\Delta m = m \left(\frac{v_0}{v} - 1 \right). \quad (\text{III.74})$$

Applying the theorem of impulses, we obtain

$$m (v_0 - v) = \int_0^t Y_1 dt. \quad (\text{III.75})$$

Taking into account formula (III.49) and integrating, we transform (III.75) to the form

$$m \left(\frac{v_0}{v} - 1 \right) = \frac{v_0}{v} \frac{\rho_0 \pi a^2}{2} L e(0) (e^{-\beta t} - 1). \quad (\text{III.76})$$

It follows from formulas (III.74) and (III.76) that

$$\Delta m = (-1) \frac{\rho_0 \pi a^2}{2} L e(0) \frac{v_0}{v} (1 - e^{-\beta t}).$$

The expression obtained describes the development of an adjoining mass of liquid during the time of impact. In

[213

the case of free immersion of a plate, when its velocity is determined by formula (III.62) and function $Le(\theta)$ by formula (III.60), the expression for the adjoining mass assumes the form

$$\Delta m = \frac{\rho_0 \pi a^2}{2} \cdot \frac{1 - e^{-\beta t}}{1 + \mu e^{-\beta t}}. \quad (\text{III.77})$$

Formula (III.77) has the following limits:

$$\lim_{t \rightarrow 0} \Delta m = 0; \quad \lim_{t \rightarrow \infty} \Delta m = \frac{\rho_0 \pi a^2}{2}; \quad \lim_{c \rightarrow \infty} \Delta m = \frac{\rho_0 \pi a^2}{2}.$$

Consequently, the adjoining mass in the case under consideration of movement of a liquid changes from zero at the start of impact to a constant value of $\rho_0 \pi a^2 / 2$ at the end of impact.

Taking formula (III.77) into account, the expression for velocity of a plate during impact against a compressible liquid can be written in the same form as for an incompressible liquid [see formula (II.32)],

$$v = \frac{v_0}{1 + \frac{\Delta m(t)}{m}}. \quad (\text{III.78})$$

Only in the given case the adjoining mass Δm is not constant in magnitude but variable, its dependence on time being described by formula (III.77). By substituting (III.77) into (III.78) we obtain formula (III.62).

Analyzing the latter formulas and the limiting processes when $c \rightarrow \infty$, we can conclude that the new solutions agree with the theory of impact against an incompressible liquid.

The solutions obtained in accordance with the principle of symmetry also hold in the case of occurrence of sudden movement of a plate in an unbounded liquid at a normal velocity of v_0 . In this case the values of the adjoining mass $\Delta m = \rho_0 \pi a^2 / 2$ in all the preceding formulas must be doubled.

The solutions describing impact against water of a plate on a liquid's surface at a zero geometric angle of attack can be extended to the case of impact of a plate floating on the surface at an angle of attack β_0 somewhat different from zero (Fig. 116) and also impact of a wedge (Fig. 117). The two latter phenomena are also accompanied by the formation of sound waves in the interface between body and liquid although the effect of compressibility of the liquid in these cases is more weakly manifest. This can be explained first of all by the fact that the impermeable inclined walls which serve as guides

for the flow of liquid contribute to the rapid establishment of flow around the plate or wedge and hinder compression in the layers of liquid adjacent to them, that is, the formation of sound waves. Nevertheless, in the cases of a plate whose angles of attack are small or a wedge whose dihedral is small acoustical phenomena have a significant effect on the course of the impact process.

[214

The second distinguishing aspect of this type of impact is that the wetted surface of the body is variable and depends on the nature of movement of the body and also on the stream effects on the surface of the liquid.

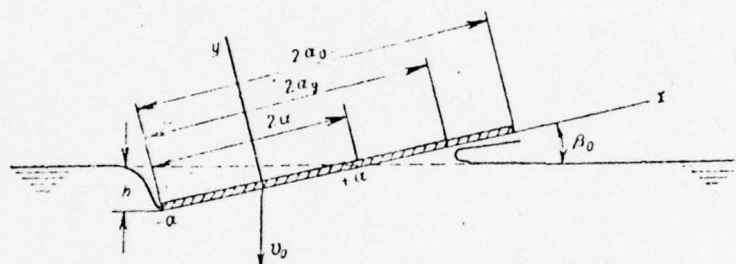


Fig. 116. Impact on inclined plate floating on the surface of the water (main notation).

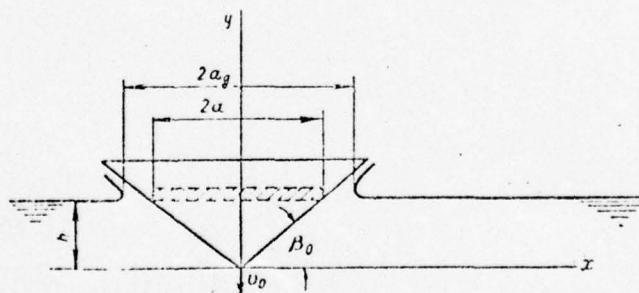


Fig. 117. Impact on a wedge floating on the surface of the water (main notation).

The work by G. Wagner mentioned in Chapter II is a study of hydrodynamic forces during direct immersion of a wedge (and with a certain accommodation this pertains to immersion of a plate at an angle of attack) in an incompressible liquid. Wagner's theory of vertical impact is based on the hypothesis that the adjoining mass of a wedge or a plate being immersed at an angle of attack is equal at every instant of time to the adjoining mass of a flat plate whose width is equal to the projection of the wetted surface on the horizontal axis. In this way, according to this hypothesis, the actual picture of

flow around a wedge or some other body is replaced with flow around a continuously expanding flat plate whose rate of expansion is equal to the rate of increase in wetted surface of the body and the rate of flow to the rate of immersion.

[215

Despite the fact that this hypothesis should be applicable only to cases of small angles of attack or dihedral, tests show that the results obtained with the Wagner theory agree well with experiments for large angles of attack also [16].

As already stated, a study of impact taking into account elasticity of a liquid is of interest mainly when the angles of attack are small. Therefore, in the problem under consideration there is even more reason for using the Wagner hypothesis for investigating hydrodynamic forces.

Formula (II.32) which is derived in Chapter II based on the amount of movement theorem holds for immersion in a liquid of a body of any arbitrary shape. For a flat plate in contact with an incompressible liquid over all its surface the adjoining mass $\Delta m = \rho_0 \pi a^2 / 2$ entering into this formula is constant. In the identical case for a compressible liquid Δm is variable and, as already stated, is determined by formula (III.77). When a wedge or inclined plate is immersed in an incompressible liquid the velocity of movement, according to Wagner's hypothesis, will also be determined by formula (II.32) but the adjoining mass $\Delta m = \rho_0 \pi a^2(t) / 2$ will become variable since the wetted surface $a(t)$ will vary. When extending Wagner's hypothesis to the case of immersion of an inclined plate or wedge in a compressible liquid we will assume that their adjoining mass is defined by the following formula:

$$\Delta m = \frac{\rho_0 \pi a^2}{2} \frac{1 - e^{-\beta t}}{1 + \mu e^{-\beta t}}, \quad (\text{III.79})$$

which differs from (III.77) only in that the variables a , μ , and β in it are functions of time.

Substituting formula (III.79) into the expression for velocity (II.32) or, what is the same thing, in (III.78), we obtain an expression describing the rate of immersion of an inclined plate or wedge in a compressible liquid:

$$\begin{aligned} \text{or} \quad v &= \frac{v_0}{1 + \frac{\Delta m}{m}} = \frac{v_0}{1 + \mu \frac{1 - e^{-\beta t}}{1 + \mu e^{-\beta t}}} \\ v &= \frac{v_0}{1 + \mu} (1 + \mu e^{-\beta t}). \end{aligned} \quad (\text{III.80})$$

In formula (III.80), in distinction from (III.62), μ and β are functions of time t .

Differentiating (III.80) with respect to time we find the acceleration to be

$$\frac{dv}{dt} = -\frac{v_0}{(1+\mu)^2} \left[(1 - e^{-\beta t}) \frac{d\mu}{dt} + \mu e^{-\beta t} (1 + \mu) \left(\beta + \frac{d\beta}{dt} t \right) \right]. \quad (\text{III.81})$$

Substituting the acceleration (III.81) into the equation for plate movement $m \frac{dv}{dt} = -Y_1$ we obtain for force Y_1 the following formula [216

$$Y_1 = m \frac{v_0}{(1+\mu)^2} \left[(1 - e^{-\beta t}) \frac{d\mu}{dt} + (1 + \mu) \left(\beta + \frac{d\beta}{dt} t \right) \mu e^{-\beta t} \right]. \quad (\text{III.82})$$

Formula (III.82) can also be obtained directly from (II.31) or (II.33) if the value for adjoining mass determined from (III.77) is substituted in the latter. Taking into account the fact that during impact against a compressible liquid the coefficient of adjoining masses is

$$\mu(t) = \frac{\Delta m(t)}{m} = \mu \frac{1 - e^{-\beta t}}{1 + \mu e^{-\beta t}}, \quad \mu = \frac{\rho_0 \pi a^2}{m},$$

and substituting it into formula $Y_1 = m \frac{v_0}{[1 + \mu(t)]^2} \cdot \frac{dv(t)}{dt}$ or

$$Y_1 = \frac{d}{dt} \Delta m \frac{v_0}{1 + \frac{\Delta m}{m}} \quad [\text{see (II.30)}] \quad \text{we obtain following differentia-}$$

tion the formula presented above (III.82).

Formula (III.82) determines the force of impact during immersion in a compressible liquid of an inclined plane or wedge and is more general than the relations expressed by (II.33) and (II.74) which were obtained earlier.

Writing (III.82) in the form

$$Y_1 = m \frac{v_0}{(1+\mu)^2} \frac{d\mu}{dt} (1 - e^{-\beta t}) + \Delta m \frac{v_0}{1+\mu} \left(\beta + \frac{d\beta}{dt} t \right) e^{-\beta t}, \quad (\text{III.83})$$

we see that the first term in this formula represents the force due to the effect of adjoining masses. The factor $(1 - e^{-\beta t})$ in the first term takes into account the effect of change in adjoining mass over time on this component of force Y_1 . The second term represents the component of force Y_1 due to the formation of adjoining mass and also acoustical phenomena taking place in the liquid during the time of impact. The second term in the factor $\beta + \frac{d\beta}{dt} t$ takes into

account the effect on the acoustical component of force of impact of a change in the dimensions of a plate or wedge as it becomes immersed in the liquid.

Formula (III.83) agrees with the formulas for force Y_1 (II.33) and (III.64). If the geometric wetted length of the body is constant ($a = \text{const}$), then $da/dt = 0$, $\beta = \text{const}$, and $d\beta/dt = 0$, as a result of which (III.83) becomes formula (III.64), namely,

$$Y_1 = \frac{\frac{\rho_0 \pi a^2}{2}}{1 + \mu} \beta v_0 e^{-\beta t}.$$

Changing in formula (III.83) to an incompressible liquid, that is, assuming in it $c = \infty$ ($\beta = \infty$), we obtain the Wagner formula presented above [see (II.33)]

[217]

$$Y_1 = m \frac{v_0}{(1 + \mu)^2} \frac{du}{dt}.$$

When determining the force of impact the variables u and du/dt entering into formula (III.83) and also β and $d\beta/dt$, in distinction from immersion in a liquid of a plate with angle of attack $\beta_0 = 0$, must be determined in light of the oncoming stream motion of the liquid displaced by the immersed body which serves to increase the wetted surface and change its rate of spread. Later we will discuss methods for taking these aspects into account.

As is known, formula (II.33), on the basis of the same Wagner hypothesis, is also used in practice for determining the force of impact when a wedge with a varying dihedral, such as the transverse sections of a craft or a V-shaped foil are taken to be, is immersed in a liquid. On the same basis formula (III.83) can also be used for determining the force of impact of these bodies. This makes it possible, on one hand, to calculate the values of hydrodynamic forces while taking elasticity of the liquid into account and, on the other hand, to find values for external forces in case of immersion in a liquid of bodies with complex cross sections having flat horizontal line sectors to which formula (II.33) is inapplicable.

§23. Some information about hydrodynamic forces which arise when bodies fall on the surface of a liquid

The problem of determining hydrodynamic forces and characteristics of movement when bodies fall vertically onto the surface of a liquid is similar to that discussed in the preceding section. The main difference between them is that in the latter case the process of impact takes place when

there is air between the body and the liquid at the instant they come in contact.

Finding a theoretical solution to this problem in a strict formulation is exceedingly difficult. Therefore the phenomenon is investigated experimentally.

Fig. 118 shows an oscillogram of vertical displacement, rate of acceleration, and pressure as a plate falls onto an undisturbed water surface. The four main modes of movement of the model are recorded on the oscillogram. The first mode is acceleration when the increase in rate experienced by the plate is due to the energy of compressed springs. After cessation of the action of the springs the plate changes to a mode of free fall, the rate of movement during which increases due to the force of gravity. The mode of free fall is replaced by impact against the water as the plate becomes freely immersed in the water. In the initial stage of impact there is an abrupt drop in vertical velocity which, as impact becomes damped, changes much more slowly over time. Free immersion of the plate ceases as a result of landing on limiters. [219]

An analysis of such oscillograms shows that prior to the instant of contact between plate and water due to displacement of the plate an air flow is established which exerts a pressure on the water's surface. Due to the excess air pressure particles of water on the free surface directly under the plate and close to it acquire a certain initial velocity appreciably ahead of the instant of contact. As a result, the surface of the liquid becomes deformed and a cavity forms, one possible shape of which is shown in Fig. 119. The existence of the cavity leads to two distinguishing aspects of such an impact. First, the plate in falling flat on the surface of the water doesn't come in contact with the water instantly but becomes immersed gradually. Second, the transmission of energy from plate to liquid during impact doesn't take place directly but through a layer of air. As special tests have proved, the first of these distinguishing aspects doesn't have any great effect on the process of impact but the effect of the air is important.

We will point out that according to data from theoretical investigation in the case of impact of a plate floating on the surface of an incompressible liquid a change in rate of movement occurs in jumps, that is, instantaneously from v_0 to $v_0/(1 + \mu)$ (Fig. 120). In the case of a plate floating on the surface of an elastic liquid, the change in velocity from v_0 to $v_0/(1 + \mu)$ takes place gradually and is an exponential function of time (Fig. 120). But in both cases the velocity following impact is a constant magnitude and equal to $v_0/(1 + \mu)$. [220]

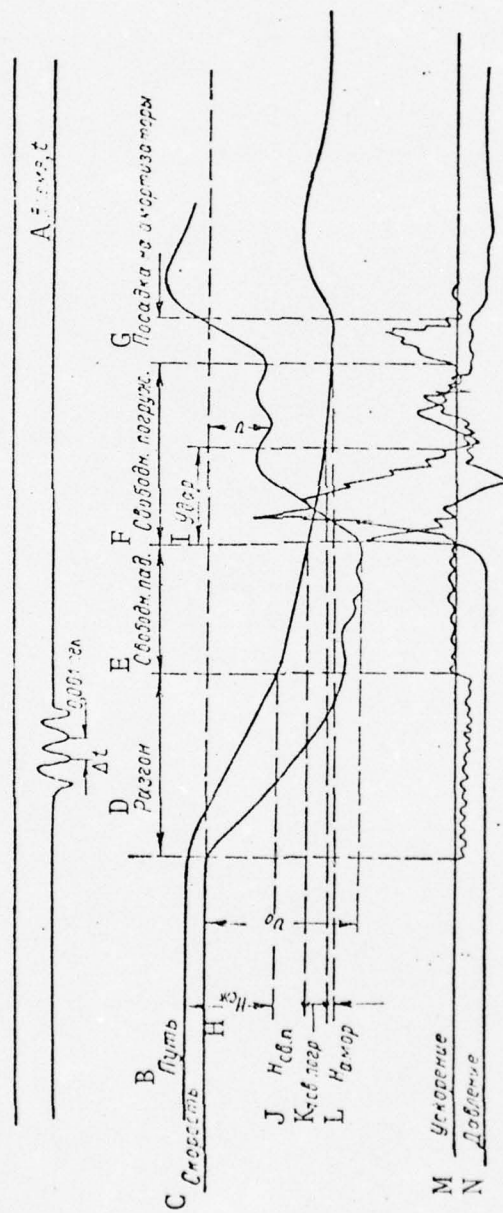


Fig. 118. Oscillogram of kinematics of movement when a plate falls on a free water surface.

KEY: A--time, ; B--Path; C--Rate; D--Acceleration; E--Free fall; F--Free immersion; G--Landing on shock absorbers; H--Hspr; I--Impact; J--Hfrfall; K--Hfrimm; L--Habs; M--Acceleration; N--pressure.

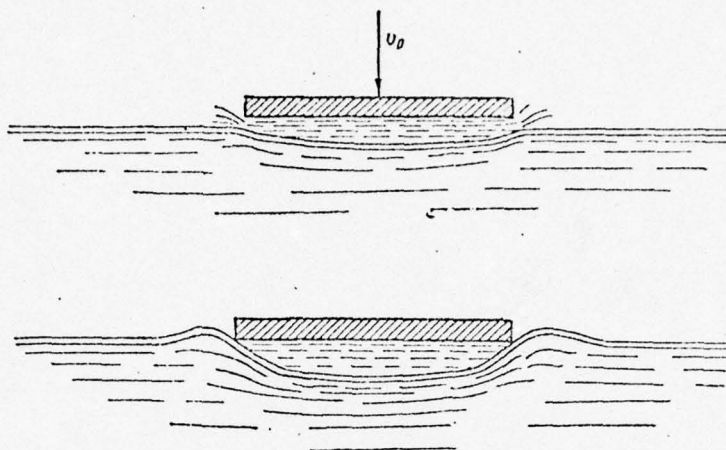


Fig. 119. Phenomenon occurring when a plate falls onto water.

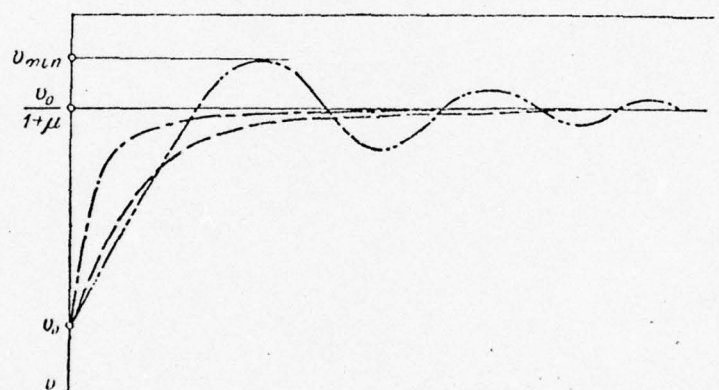


Fig. 120. Change in velocity of plate movement when impacting against water.

— impact of plate floating on surface of incompressible liquid;
 - - - impact of plate floating on surface of elastic liquid;
 impact when a plate falls flat on the water's surface in the presence of air; - - - approximating function of velocity during fall on water.

From the oscillogram shown in Fig. 118 and others similar to it it follows that the velocity of a plate falling flat on the water at the end of an impact after a series of oscillations also tends to a certain constant magnitude greater than zero. If in the cases of impact recorded on the oscillograms the effect of aspect ratio of a plate on the coefficient of adjoining mass as proposed by Pabst is taken into account and the corrected value of the coefficient of adjoining mass substituted into formula (II.32), then the calculated values of velocity v and the

Experimental value of plate velocity following impact practically coincide [see formula (III.160)]. This shows that both in the case of a plate falling flat onto the water and in the case of impact of a plate floating on the free surface of a compressible or incompressible liquid the final value of drop in velocity of plate movement is the same and, consequently, the magnitudes of impulse, work, and kinetic energy transmitted by the plate to the liquid and also the final value of the adjoining mass of liquid are the same.

The difference between the three types of impact lies in the law governing the change over time of velocity of plate movement in the interval $v_0 \geq v \geq v_0/(1 + \mu)$.

In distinction from theoretical investigation into types of impact when a plate falls flat onto the water's surface in the presence of air, oscillograms show that the velocity of plate movement diminishes relatively slowly in the initial stage of impact and prior to reaching $v_0/(1 + \mu)$ goes through several damping oscillations. Both these circumstances are due to the existence of an air cavity which at a certain instant closes and becomes immersed in the liquid along with the plate (Fig. 119b). The process continues almost to the end of impact as evidenced by the bubbles of air rising to the surface of the liquid after the process of immersion of the plate is complete (under test conditions after landing on limiters). Thus, in the case of impact under consideration transmission of energy from plate to liquid takes place through a layer of air entrapped in the cavity between body and liquid. The air in the cavity is elastic. Under pressure from the plate the volume of the cavity is reduced and as a consequence the air contained in it becomes compressed. But since the walls of the cavity are formed in part by the surface of the water which amounts to a kind of elastic base, compression of the air in the cavity is accompanied by continuous transmission of pressure from the liquid. [221]

The energy transmitted by the plate to the liquid in this case is dissipated not only on imparting to the adjoining mass of liquid a velocity of $v_0/(1 + \mu)$ and forming a sound wave field, but on compressing the air in the cavity. Therefore, the velocity of the plate in the initial stage of the process under consideration changes from v_0 to v_{min} , a magnitude less than $v_0/(1 + \mu)$ (Fig. 120). The velocity difference $v_0/(1 + \mu) - v_{min}$ is expended by the plate on compressing the air in the cavity.

To the extent the impact pressures become dissipated and spread within the liquid in the form of a sound wave, pressure drops replace the pressures on the interface between air and water and, consequently, in the cavity. As a result, the vel-

velocity of plate movement is somewhat increased and this continues until the pressure in the cavity, due to the action of the plate, again becomes positive. An increase in pressure in the cavity leads to a new decrease in velocity. In this way a certain oscillatory mode becomes established in the movement of the plate. It continues until damping of the pulsating of pressures in the cavity itself and on the boundary with the liquid occurs and until smooth flow around the plate at a velocity of $v_0/(1 + \mu)$ under the influence of which the cavity is washed away becomes established.

All this is evidence that impact in this case takes place in a medium with the inertial properties of water while at the same time its elastic properties are determined for all practical purposes by the compressibility of the air. Mechanical mixtures of undissolved gases in a liquid have analogous properties. As is known, these mixtures also possess the inertial properties of a liquid and the elastic properties of the contained gases. The rate at which elastic disturbances spread in such mixtures depends on the concentration of gases in them and can be much less than the rate at which pressures spread in each medium. For this reason in the case of impact under consideration there is an increase in the interval of time needed for transmission of pressure from plate to liquid which in the final analysis is expressed in a slower change in velocity during impact and the entire process is accompanied by slower accelerations.

For our present investigation the greatest hydrodynamic forces acting on a plate during impact are of principal interest. As can be seen from the oscillograms presented the greatest accelerations are experienced by a plate when the velocity drops from v_0 to v_{min} , that is, when an adjoining mass is formed in a liquid a sound wave is formed and the air in the cavity becomes compressed. [222]

The preceding section contained a theoretical investigation of the formation of an adjoining mass of liquid and development of a sound wave during impact which omitted the effect of air on these processes. But in both cases the final value of the adjoining mass and also that of the energy carried away by the sound wave are the same. Naturally therefore a question arises as to whether it is possible to use the solutions obtained in §22, after correction of them based on experimental data, for the purpose of gaining an approximate idea of the phenomenon occurring when a plate falls flat onto a surface. Calculations which have been performed and comparisons of experimental results have showed that for taking into account the effect of air on the formation of a pressure field in a liquid it suffices to change the value of parameter B , decreasing it in accordance with the decrease in rate of spread of elastic dis-

turbances in the case under consideration. The relation $\beta = f(1/(1 + \mu))$ which makes it possible to find parameter β while taking the cited distinguishing aspects into account has been established experimentally. Fig. 120 shows a theoretical relation characterizing the change in velocity when a plate falls flat on the water's surface. The curve was drawn from formula (III.62) taking into account experimental values of parameters β and μ .

As follows from the figure, the approximating function coincides with the experimental curve in the sector of maximum acceleration and at the end of impact. It does not reflect processes which occur as a consequence of pulsation of the cavity but since these phenomena occur in the second stage of impact, they have practically no influence on the maximum values of effective forces.

After transforming formula (III.62) to the form

$$\beta = -\frac{1}{t} \ln \left[\frac{\frac{v(t)}{v} - 1}{\frac{v_0}{v} - 1} \right],$$

it is not difficult using the experimental relation $v(t)$ to find the value of function $\beta = f(1/(1 + \mu))$ and then the value of the parameter $\theta = \beta^2 a^2 / 4c^2$.

Preliminary approximate results of an experiment conducted to find θ are given in the graph in Fig. 121. The caption contains empirical formulas for the cases $1/(1 + \mu) \rightarrow 0$ and $1/(1 + \mu) \rightarrow -1$.

Comparing the graphs in Figs. 115 and 121 we see that there is complete qualitative agreement between the curves. [223

Knowing the magnitude of parameter θ , it is possible by using the formulas in the preceding section to find the hydrodynamic forces acting on a plate and to trace its movement during the process of impact when it falls on the surface of water with air present.

Tests involving dropping inclined plates on the surface of water have made it possible to find the value of parameter β as a function of angle of attack β_0 . The results of tests show that with an increase in angle β_0 the magnitude of parameter β increases and this means that the effect of the air on the external forces acting during the time of impact decreases. The tests yielded the following empirical relation for small angles of attack:

$$\beta = \beta_T - (\beta_T - \beta_e) \cos \beta_0, \quad (\text{III.84})$$

where β_T is the value of parameter β according to theoretical data (Fig. 115) and β_e is the value of β obtained from an experiment involving dropping a plate flat onto the water's surface (Fig. 121).

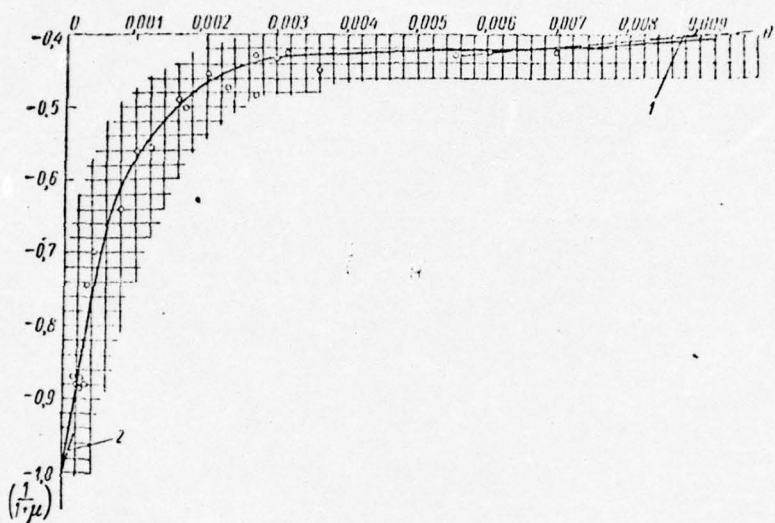


Fig. 121. Experimental curve of the function $Le(\theta)$ when a plate falls on water.
Circle--experimental points; Broken line--empirical formulas.

$$1-- \theta = \left[\frac{1}{2} \ln \frac{1}{1+\mu} \right]^6 \quad \text{when} \quad \frac{1}{1+\mu} < 0.5; \quad ; \quad 2-- \theta = -\frac{1}{406} \ln \frac{1}{1+\mu} \quad \text{when} \quad 0.9 < \frac{1}{1+\mu} < 1.$$

By substituting in this way the value obtained for into formula (III.83) we can find the external forces which act when inclined plates fall onto water. In this process it should be borne in mind that in that case when $\beta_0 > 0$ the effective wetted length of plates $2a_{eff}$ at each instant of time is somewhat greater than the geometric length $2a_g$ (see Fig. 116). According to Wagner [5] for a plate becoming immersed in water this relation is equal to $v = a_{eff}/a_g = \pi/2$. When a plate is actually dropped into water parameter v depends on the rate of landing as well as on the relative dimensions of the plate and differs somewhat from $\pi/2$.

§24. Nonstationary forces acting on lift foils of high-speed craft during impact against waves [224]

The formulas presented in §22--23 can be used for calculating the hydrodynamic forces acting on hydrofoils during impact against waves. For this purpose it is first necessary to establish initial conditions, that is, the position of the

foil and the velocity at the instant of contact.

Knowing the movement of the craft in a given seaway [under conditions prevailing in a regular seaway (II.166) this movement is given by formulas (II.165) and (II.167)], it is possible to determine in each particular case whether the lift foils pierce the surface of a wave and also determine the instant of time and the kinematics of movement of foils on entering the water. For this purpose we will write an equation expressing the movement of the leading edge of a foil [point A (x_A, y_A)] and its trailing edge [point B (x_B, y_B)]. It is easy to show that (Fig. 122):

$$(III.85)$$

and

$$\begin{aligned} x_A &= x_G + \rho_{Ax}, y_A = y_G - \rho_{Ay} \\ x_B &= x_G + \rho_{Bx}, y_B = y_G - \rho_{By} \end{aligned}$$

$$(III.86)$$

where ρ_{Ax} , ρ_{Ay} , ρ_{Bx} , and ρ_{By} are projections onto fixed axes of the radius vectors ρ_A and ρ_B .

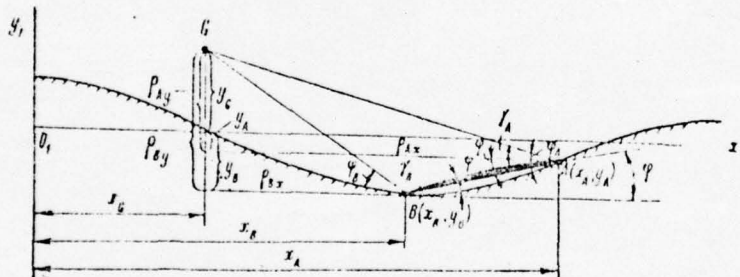


Fig. 122. Position of foil with respect to wave during impact against water. KEY: Subscript "B" refers to wave.

At given magnitudes of these vectors and also design angles γ_A and γ_B these projections can be defined as (Fig. 122)

$$\begin{aligned} \rho_{Ax} &= \rho_A \cos \varphi_A, \rho_{Ay} = \rho_A \sin \varphi_A, \\ \rho_{Bx} &= \rho_B \cos \varphi_B, \rho_{By} = \rho_B \sin \varphi_B, \end{aligned} \quad (III.87)$$

where $\varphi_A = \gamma_A - \phi$, $\varphi_B = \pi - (\gamma_B + \phi)$.

Angle ϕ is considered positive when measured counterclockwise from the horizontal.

After determining the coordinates of points A and B in fixed coordinates (Fig. 122) we can write the following equation for \overline{AB} , that is, the equation for the line of the foil: [225

$$y = y_A + \left(\frac{y_B - y_A}{x_B - x_A} \right) (x - x_A). \quad (\text{III.88})$$

The points of intersection of the line of the foil and the surface of the wave can be found by solving the transcendental equation

$$y = \zeta_w, \quad (\text{III.89})$$

where $\zeta_w = r_0 \cos 2\pi \left(\frac{x}{\lambda_w} - \frac{t}{\tau_w} \right)$. In this process it should be borne in mind that the actual piercing of the wave by the foil at points $C_i (x_i, y_i)$ (Fig. 123) occurs only when the following inequalities are met:

$$x_B \leq x_i \leq x_A; \quad y_B \leq y_i \leq y_A.$$

The lengths of wetted sectors of the foil can be calculated from the formula

$$a = \frac{1}{2} \sqrt{(x_B - x_i)^2 + (y_B - y_i)^2}$$

or

$$a = \frac{1}{2} \sqrt{(x_A - x_i)^2 + (y_A - y_i)^2}. \quad (\text{III.90})$$

Depending on the velocity of craft movement, the nature of the seaway, and also the design of the foil system the following variations may occur in the way a foil impacts against a wave. At a relatively slow velocity of craft movement impact of a flat foil against the water may come at an instant of time immediately following the instant the foil emerges from a wave (Fig. 124a). This type of impact is possible when a foil broaches the surface either totally or partially. With an increase in the velocity or with a change in parameters of the seaway the second, third, and fourth types of foil impact against the water can occur (Fig. 124 b, c, and d). In these cases the foil impacts against the trough of a wave or against the crest of the next wave.

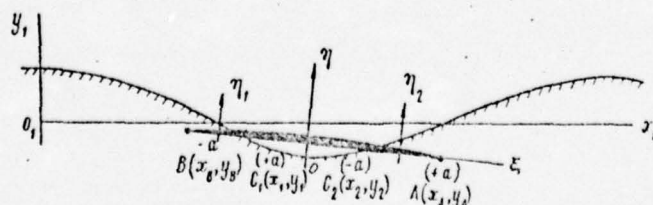


Fig. 123. Foil piercing surface of water. (Subscript "B" is wave.)

If the foil chord is small compared with the length of the wave, that is, when $2a \ll \lambda_w$, with accuracy adequate for all practical purposes we can replace the profile of the wave with

the line kk' (see Fig. 124) tangent to its surface at the point of contact between foil and wave and replace the wave with the tangent plane. The angle at which the foil lands β_{tot} must be selected in light of the angle of inclination of this tangent plane, that is,

[226

$$\beta_{tot} = \alpha_w + \phi, \quad (\text{III.91})$$

where $\alpha_w = -\frac{2\pi a}{\lambda_w} \sin\left(2\pi \frac{x}{\lambda_w}\right)$ is the angle of wave inclination; x the abscissa of the point of contact between foil and wave; and ϕ the angle of attack which is equal to the algebraic sum of the trim angle of the craft and the set angle of the foil.

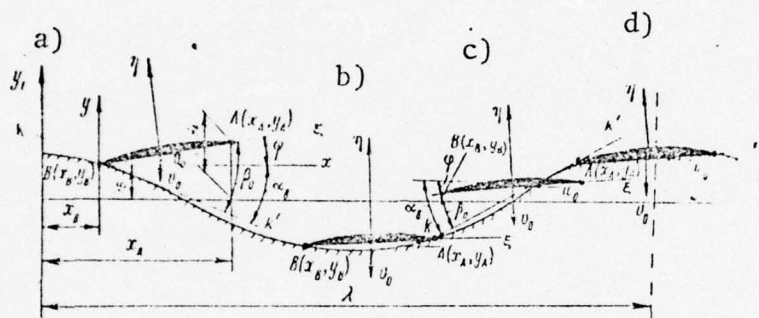


Fig. 124. Variations in foil impact against a wave (a--d).
KEY: The subscript "B" refers to wave.

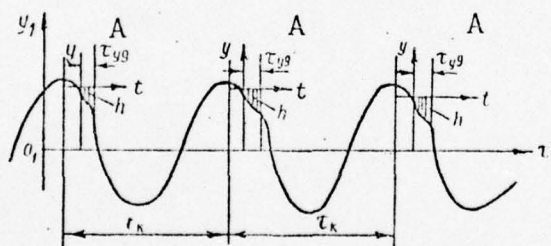


Fig. 125. Recording of heaving of hydrofoil craft taking impact of foil against the water into account.
KEY: A-- τ_{im} .

Replacing the profile of the wave at the area of impact with the tangent plane made it possible to use the formulas presented in §22-23 for determining the force of impact between foil and wave.

Assuming that $\beta = \beta_{tot}$ and determining from the curves in Figs. 115 and 121 for each concrete type of foil the values of parameters β_T and β_e , we can find β and θ by using formula (III.84). Further, using either formula (II.33) or (III.83)

Depending on the type of impact, we can find the hydrodynamic forces acting on the foil.

Vertical movement of a foil in the process of impact can be determined from formulas (III.62) and (III.63). The general picture of foil movement in light of heaving and movement in the process of impact as determined from formula (III.63) is shown in Fig. 125 where τ_{zm} is the duration of impact.

By way of example illustrating the application in practice [227] of the formulas presented above, we will consider the impact against the water of a foil with a chord of $2a_0 = 0.960$ m and a span of $l = 5.2$ m. The reduced mass of the craft for the given foil is $m = 3.5 \cdot 10^3$ kg·sec²/m.

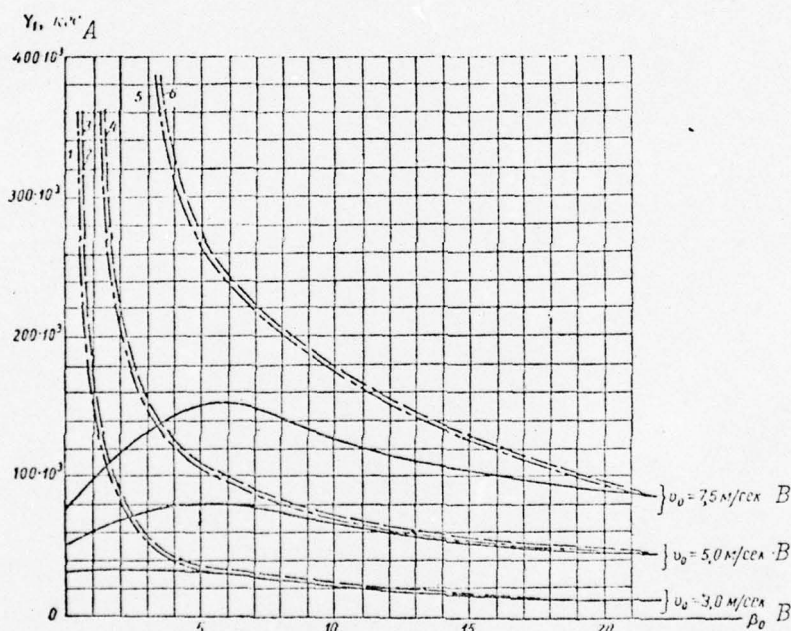


Fig. 126. Hydrodynamic forces during impact of a plate against water when the rate of fall is $v_0 = 3, 5$, and 7.5 m/sec.

KEY: A--kgf; B--m/sec.

— — — force during impact for a plate floating on the surface of an incompressible liquid; — — — force during impact for a plate floating on the surface of a compressible liquid; — force during fall of a plate onto the surface of water in the presence of air. Asymptotic values of Y when $\beta_0 \rightarrow 0$: 1-- $Y_1 \rightarrow 776 \cdot 10^3$; 2, 4, 6-- $Y_1 \rightarrow \infty$ when $c = \infty$; 3-- $Y_1 \rightarrow 1294 \cdot 10^3$; 5-- $Y_1 \rightarrow 1940 \cdot 10^3$.

The results of calculations of hydrodynamic forces for different types of foil landing $0 \leq \beta_{tot} \leq 20^\circ$ and $0.5 \leq v_0 \leq 7.5$ m/sec are shown in Figs. 126 and 127. These figures show the maximum external forces when a foil is immersed in incompressible and compressible liquids without taking the

effect of the air into account and also the external forces when a foil falls on the surface of the water.

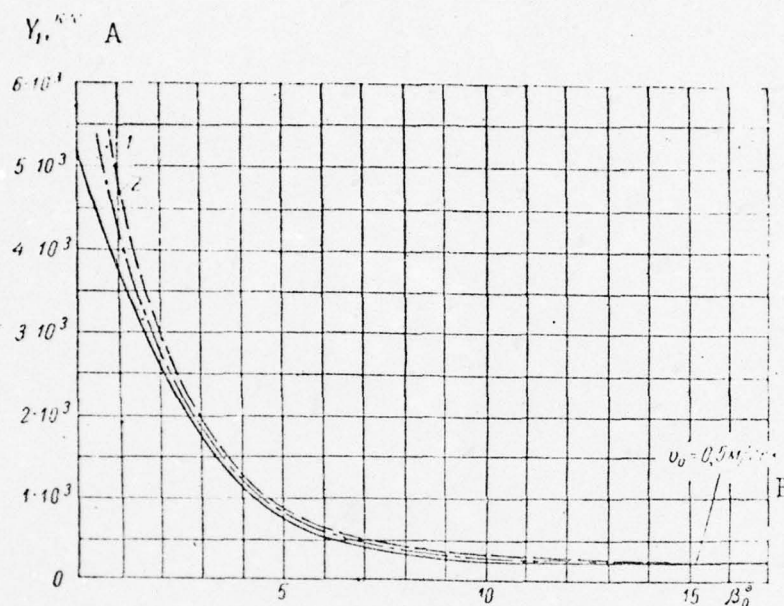


Fig. 127. Hydrodynamic forces when a plate impacts on water falling at a rate of $v = 0.5 \text{ m/sec.}$

KEY: A--kgf; B--m/sec.

--- force during impact for a plate floating on the surface of an incompressible liquid; -.-.- force during impact for a plate floating on the surface of a compressible liquid; — force during fall of a plate onto the surface of water in the presence of air. Asymptotic values of Y_1 when $\beta_0 \rightarrow \infty$: 1-- $Y_1 = 129.4 \cdot 10^3$; 2-- $Y_1 \rightarrow \infty$ when $c = \infty$.

The curves in the figures make it possible to trace the effect of compressibility of a liquid and the presence of air on the maximum value of the force of impact. The effect of compressibility of a liquid is important at small angles of impact β_0 and large values of initial velocities v_0 . A layer of air between plate and liquid during impact has an important effect on the maximum value of the force of impact. The greatest effect of an air layer, as of compressibility of a liquid, occurs at small angles of attack and large landing velocities. This can lead to the maximum force of impact occurring when angle of attack β_{tot} is not equal to zero (see Fig. 126). When such plates land on the water the component of hydrodynamic forces due to acoustical phenomena may, because of the effect of the air, be small as compared with the component due to a change in shape (du/dt). Therefore, if it is considered that in the case $\beta_{tot} = 0$ when $t = 0$ and $du/dt = 0$,

[228

At large landing velocities the force of impact will be greatest at a certain small angle of attack different from zero. In the case of an exceedingly small initial velocity v_0 the effect of the air layer becomes so small that the maximum value of the force of impact may occur when $\beta_{tot} = 0$ (see Fig. 127).

With an increase in the angle β_{tot} the curves of force of impact for identical conditions approach one another, the less velocity v_0 is the earlier they meet. This is evidence of the fact that the effect of the air layer decreases with an increase in angle β_{tot} and with a decrease in v_0 . These distinguishing aspects agree with physical notions about the phenomenon and the mathematical description presented above in the theoretical part of the investigation. [229]

At large horizontal foil movement velocities vortex components of hydrodynamic forces will act on the foil along with the potential component in the process of impact under certain flow conditions. From the instant the trailing edge of a foil enters the water and streamline flow becomes established around it a circulation flow will become established around the foil as it completes its entry into the water. In the case of incomplete entry of a foil into the water a flow is established as in planing, that is, there is a back stream at the nose on the lower side of the foil.

Development of lift on a foil due to circulation movement of the liquid can be expressed in the form of a function of the path traveled by the foil.

In the case of entry of a foil at a constant rate the lift is expressed by the formula

$$Y_2 = C_y \frac{\rho u_0^2}{2} S \psi(\bar{s}). \quad (\text{III.92})$$

Here

$$C_y = \frac{dC_{y\lambda}}{d\beta} f_1(h) \beta_{tot},$$

S is the foil area; $\bar{s} = s/a$ the path traveled by the foil from the instant the trailing edge enters the water; and $\psi(\bar{s})$ is a function determined from analytical expressions (II.90)--(II.92) or determined graphically from Fig. 128 (a Kyussner function [17]).

When the path traveled by the foil during impact is great and the necessary conditions stipulated above for rise of circulation apply, the force acting on the foil is

$$Y = Y_1 + Y_2. \quad (\text{III.93})$$

Foil movement in this case can no longer be determined by formulas (III.62) and (III.63). A detailed investigation of such modes of movement is contained in [18].

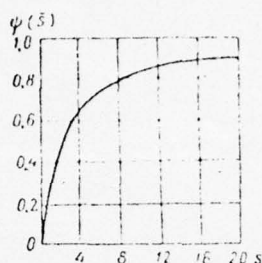


Fig. 128. The Kyussner function $\psi(\bar{s})$.

The method explained in this section for calculating nonstationary hydrodynamic forces acting on the lift surfaces of high-speed craft (specifically hydrofoils) under conditions of nonstationary movement can be used to determine movement of a craft in a seaway and also to evaluate the strength of lift surfaces. In the latter case it should be kept in mind that the expressions presented for the external forces were obtained while assuming the lift surfaces to be absolutely inelastic. At the same time, as is known, the effect of elasticity on the magnitude of the external forces and on the nature of changes in them over time is very great. Taking into account the effect of elasticity of a structure on the external nonstationary forces is a separate and distinct problem and lies outside the framework of this book.

[230]

B. Planing in a seaway

Planing over the surface of calm water has been studied rather thoroughly [19]. The results of theoretical investigation into movement of planing craft in a seaway have not yet gone beyond formulation of the problem and this is due primarily to its complexity. In [20] a first attempt is made at a theoretical approach to the problem. Below we set forth the main results of this investigation.

§25. Hydrodynamic forces during unsteady planing

A two-dimensional problem in unsteady planing of a thin profile over the surface of a weightless liquid has been considered by G. Wagner [5] and L. I. Sedov [21].

As indicated above, the total hydrodynamic force acting on a planing plate can be represented in the following form [see formula (II.28)]:

$$Y = -\frac{1}{2} \cdot \frac{d}{dt} (\rho_0 \pi a^2 V_1) - \pi \rho_0 a u_0 \left(V_1 - \frac{a \omega_0}{2} \right) - \\ - \rho_0 a \left(u_0 + \frac{da}{dt} \right) \int_0^{\alpha_1} \frac{u_2(\alpha) d\alpha}{V \sqrt{\xi^2 - a^2}}.$$

In the above formula $V_1 = y' - u_0 \beta$; $u_2(\alpha)$ is a horizontal velocity discontinuity function behind a planing plate which depends on the nature of movement of the plate and can be found by solving integral equation (II.43); $\xi = \alpha - \alpha_1 - a$ (Fig. 129); α_1 is the path traveled by a plate from the instant of rise of unsteady movement, $0 \leq \alpha \leq \alpha_1$; a is the wetted half-length of a plate; y' the velocity of vertical displacements of a profile; u_0 the horizontal velocity of a plate; β_0 the angle of attack [23] of a plate; ω_0 the velocity of angular displacements of a plate; and ρ the density of the liquid.

Formula (II.28) can be extended to the case of planing of a plate of finite span [21] in which case it can be written in the form

$$Y = Y_1 + Y_2 + Y_3, \quad (\text{III.94})$$

where

$$Y_1 = -B \xi_1(\beta_k) \frac{d}{dt} \left[\frac{\rho_0 \pi l^2}{8} k_1(\lambda) V_1 \right]; \quad (\text{III.95})$$

$$Y_2 = -B \xi_1(\beta_k) k_2(\lambda) \frac{\rho_0 \pi l}{2} u_0 \left(V_1 - \frac{a \omega_0}{2} \right); \quad (\text{III.96})$$

$$Y_3 = -B \xi_2(\beta_k) k_3(\lambda) \frac{\rho_0 l}{2} \left(u_0 + \frac{1}{2} \frac{dl}{dt} \right) \int_0^{\alpha_1} \frac{u_2(\alpha) d\alpha}{V \sqrt{\xi^2 - \left(\frac{l}{2} \right)^2}}. \quad (\text{III.97})$$

Here l is the length of the plate; B the width of the plate; and $k_1(\lambda)$ correctional coefficients allowing for the effect of finiteness of the span of the planing plate.

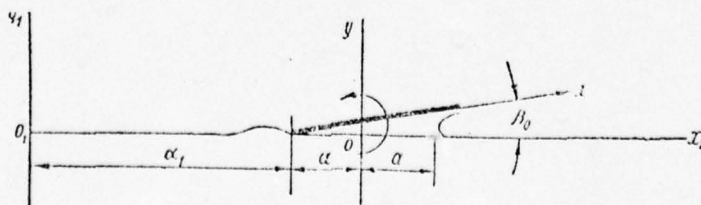


Fig. 129. Nonstationary planing of a plate (main notation).

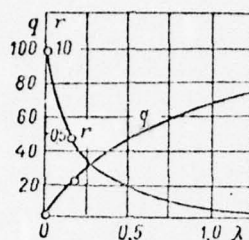


Fig. 130. Graph of the functions $r(\lambda)$ and $q(\lambda)$.

The Pabst coefficient is $k_1(\lambda) = \frac{1}{\sqrt{1+\lambda^2}} \times \left(1 - 0.425 \frac{\lambda}{1+\lambda^2}\right)$
or $k_1(\lambda) \approx \frac{1.2}{1.2+\lambda}$.

Coefficients $k_2(\lambda) = 0.7/(1 + 1.4\lambda)$ and $k_3(\lambda) = re^{iq}$ where r and q are functions of aspect ratio $\lambda = l/B$ as shown in Fig. 130 [22].

The correctional coefficient $\xi_1(\beta_k)$ takes into account the effect of plate dihedral (β_k)

$$\xi_1(\beta_k) = \frac{2 \operatorname{tg} \beta_k}{\pi} \left[\frac{\Gamma\left(\frac{3}{2} - \frac{\beta_k}{\pi}\right) \Gamma\left(\frac{\beta_k}{\pi}\right)}{\Gamma\left(\frac{1}{2} + \frac{\beta_k}{\pi}\right) \Gamma\left(1 - \frac{\beta_k}{\pi}\right)} - 1 \right]$$

or approximately $\xi_1(\beta_k) = 1 - \beta_k/\pi$ and $\Gamma(x)$ is an Euler gamma function.

Formulas (III.94) and (III.97) make it possible to calculate the approximate value of hydrodynamic forces acting on the bottom of a craft during unsteady planing in a seaway if the kinematic parameters of this movement are known. The latter can be determined experimentally or by solving equations describing the movement of a planing craft. [232]

§26. Differential equations describing movement of a planing craft in a seaway

The movement of a planing craft over the surface of a disturbed liquid represents an unsteady process of interaction between a craft as a certain solid body and the surrounding mass of water. The mode of interaction changes continuously. If when sliding from the crest of a wave a craft is in a planing mode, on encounter with the following wave this mode is replaced by a mode of impact against a liquid. Since both modes are nonstationary, a mathematical description of them in general form presents great difficulty. This gives rise to a need to create an approximate pattern of the phenomenon which will lend itself to analytical investigation and differ

from the actual phenomenon in the following ways:

- 1) a craft is considered to be an absolutely solid body;
- 2) when calculating hydrodynamic forces components of velocity and acceleration due to orbital movement of liquid particles in a wave are ignored in view of their smallness as compared with the velocity of the craft;
- 3) horizontal movement of the craft is assumed to be at constant velocity;
- 4) in view of the relatively small frequencies of forced oscillations of the craft and also the smallness of the aspect ratio of the lift surface [$k_3(\lambda)$ is small] in considering the problem in the first approximation the third term in the expression for hydrodynamic forces (III.94) is neglected, that is, the problem is considered in its quasistationary formulation.

We will select the following system of coordinates for the purpose of comparing differential equations of movement. The x axis lies in the direction of movement of the craft (Fig. 131) and in the plane of undisturbed liquid and the y axis is directed vertically upward. The origin of the fixed system of coordinates is selected so that it coincides with the crest of a wave whose profile in a given system of coordinates is described by the equation

$$\xi_w = r_0 \cos 2\pi \frac{x}{\lambda_w}, \quad (\text{III.98})$$

where r_0 is the radius of an orbit which is traced by particles [233] of the free surface of the water and which is equal to half the height of the wave, and λ_w is the wavelength.

We will consider the movement of a craft in relative coordinates, that is, in coordinates oriented on a wave. In so doing we will consider the wave to be fixed and the craft to be moving through a section of the wave at a relative velocity of

$$x' = v_k + v_w, \quad (\text{III.99})$$

where v_k is the absolute horizontal velocity of craft movement and v_w is the velocity of forward movement of the wave,

$$v_w = \sqrt{\frac{g}{2\pi} \lambda_w} \approx 1.25 \sqrt{\lambda_w}.$$

Neglecting the hydrostatic forces and considering the angular displacements of the craft to be small, we can write the differential equation for movement of the craft in the form

$$\left. \begin{aligned} mx'' &= W_x - Y\varphi - T, \\ my'' &= Y + W_y + T\varphi - G, \\ I\varphi'' &= Yc + W_x b\varphi - W_y b, \end{aligned} \right\} \quad (\text{III.100})$$

where m is the mass of the craft; G the force due to its weight; x'' , y'' , and ϕ'' the accelerations of the horizontal, vertical, and angular displacements of the craft; Y the total hydrodynamic force determined from formulas (III.94) -- (III.96); T the force of friction; W_x and W_y the horizontal and vertical components of the force of thrust from the propellers (W); I the moment of inertia of the mass of the craft with respect to the transverse axis; ϕ the angular displacements of the craft; and b and c the arms of application of forces W and Y with respect to the center of gravity (Fig. 132).

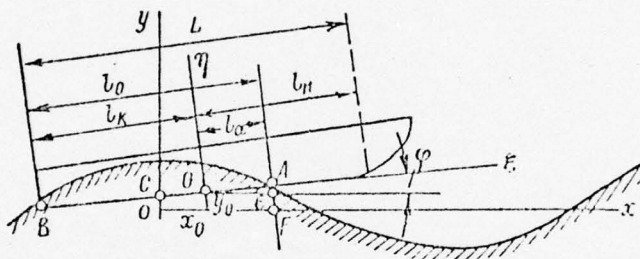


Fig. 131. Position of planing craft in a seaway (main notation).

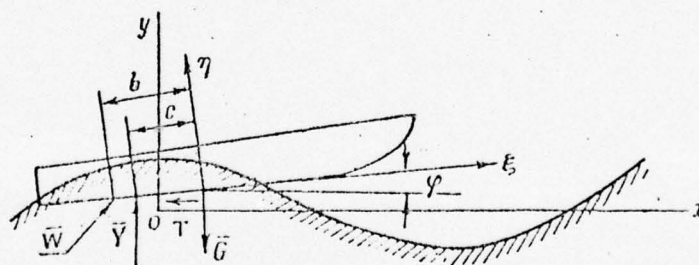


Fig. 132. Diagram of external forces acting on a planing craft in a seaway.

Considering in system of equations (III.100) due to the assumption of constancy of velocity that $x' = \text{const}$ and that forces W_x , W_y , and $T\phi$ are small compared with forces Y and G , we reduce system of equations (III.100) to the simpler form:

$$\left. \begin{aligned} x'' &= 0, \\ my'' &= Y - G, \\ I\varphi'' &= Yc. \end{aligned} \right\} \quad (\text{III.101})$$

Solving even this very simple system of inhomogeneous differential equations with variable coefficients which are squared in the general form is practically impossible. In the following discussion we will consider an approximate numerical solution of the problem based on an artificial division of the process of movement of the craft as it crosses one wave into three characteristic modes. However, before turning to a discussion of these modes of movement it is necessary for solving system of equations (III.101) to explain the initial conditions determining the position of the craft in the selected system of coordinates for a specific instant of time which is taken to be initial.

As a consequence of the impossibility of specifying exact initial conditions on the basis of any theoretical premises in the problem being solved by way of first approximation we will limit ourselves to a static setting of the craft on the wave, that is, we will start from the condition that when $t = 0$ ($Y' = 0$; $\phi' = 0$) the craft is on the apex of a wave. Taking into account that the stationary value of lift of a planing plate is

$$Y = \pi \rho_0 k_z(\lambda) \frac{\rho_0 \mu_0^2}{2} l_0 B \quad (\text{III.102})$$

and the center of pressure of the flow around a planing plate is at a point three-fourths the wetted length l_0 from the aft edge of the plate, by using equations (III.101) we can find [235] the following initial conditions (Fig. 133). When $t = 0$

$$\left. \begin{aligned} x &= \frac{l_0}{4}; \quad x' = \text{const}; \\ y &= r \cos\left(\pi \frac{l_0}{\lambda_n}\right) - \frac{l_0}{4} \varphi_0; \quad y' = 0; \\ \varphi &= \frac{2G}{B\pi\rho_0\mu_0^2 k_z l_0}; \quad \varphi' = 0. \end{aligned} \right\} \quad (\text{III.103})$$

Naturally the initial conditions determined from statistical premises will differ from the dynamic position which a craft may assume at instant $t = 0$. However, by employing the method of successive approximations and viewing movement of the craft on a series of waves it is possible to adjust conditions (III.103) and establish the exact position of the craft at instant $t = 0$.

§27. Main modes of movement of a planing craft in a seaway

Planing over the surface of disturbed water, a craft encounters waves at an interval equal to the apparent period

$$\tau_k = \frac{\lambda \omega}{v_w - v_k \cos \psi}, \quad (\text{III.104})$$

where ψ is the angle between the directions of craft velocity and that of the run of the wave.

When a craft moves in a head sea ($\psi = 180^\circ$) this formula becomes

$$\tau_k = \frac{\lambda \omega}{v_w + v_k}. \quad (\text{III.105})$$

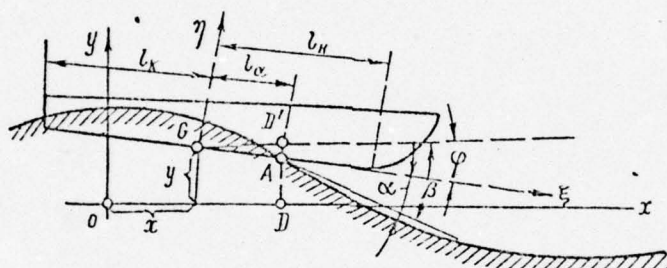


Fig. 133. Wetted length of bottom of planing craft in a seaway (main notation).

Within the limits of one apparent period a craft experiences modes of interaction with the liquid. When moving off the crest of a wave a craft is in a mode of unsteady planing until its bow lines encounter the next wave. At this point a new mode of interaction begins between craft and liquid--impact against the liquid. After completion of the impact process the craft rises on the wave and this is also an unsteady planing mode but different from the first in the magnitude and nature of application of the effective forces. All these modes are mutually related and affect each other, representing a continuous process of craft movement in a seaway. Differential equations (III.101), due to their generality, hold for all the indicated modes of movement. However, since the expressions needed to describe the parameters of external forces are highly complex if written to suit all modes of movement, different formulas are used for the different modes. [236]

Thus, in the first mode of movement--from the initial position described by conditions (III.103) until the instant the craft encounters the next wave--the wetted length of the bottom lines of the craft are determined by formula (Fig. 133)

$$l = l_k + l_a, \quad (\text{III.106})$$

where l_k is the distance from the transom to the center of gravity of the craft and l_a is found from the equation

$$l_a = \frac{1}{q} \left[y - r \cos 2\pi \left(\frac{x + l_a}{\lambda} \right) \right]. \quad (\text{III.107})$$

Included in the expression for force Y along with l_a is its derivative with respect to time

$$\frac{dl_a}{dt} = -\frac{\alpha}{\beta_0} x' + \frac{1}{\beta_0} y' - \frac{l_a}{\beta_0} q'; \quad (\text{III.108})$$

and also $\beta_0 = \phi + \alpha$, where α is the angle of wave slope,

$$\alpha = \frac{2\pi r_0}{\lambda_w} \sin 2\pi \left(\frac{x + l_a}{\lambda_w} \right). \quad (\text{III.109})$$

In order to determine l_a and dl_a/dt it is necessary to solve transcendental equation (III.107) or a differential equation of the first order with variable coefficients (III.108). Neither equation can be solved in final form. This forces us to find approximations for l_a and dl_a/dt . Thus, by way of first approximation for large velocities of craft movement we can write

$$\frac{dl_a}{dt} \approx -x' \quad \text{and} \quad l \approx l_0 - x'l.$$

In the first approximation we can also write $V_l \approx y'$.

The indicated assumptions somewhat simplify the problem but they don't enable us to obtain a general solution for system of equations (III.101).

In the work cited [19] an approximate solution is obtained [237] for this system by representing the sought functions in the form of an exponential series. Because they are so cumbersome they are not presented here.

The first mode of craft movement ends when the bow of the craft comes in contact with the profile of an oncoming wave. At certain combinations of length of craft and wavelengths there is a sharp increase in the wetted surface of the bottom accompanied by an abrupt increase in the hydrodynamic forces characteristic of impact processes. The second mode of craft movement begins. The instant of impact is easy to establish if the movement of the craft and movement of the wave are known. As already remarked, expressions defining hydrodynamic forces (III.94) and equations of movement (III.101) continue to hold for this mode of movement.

Termination of the process of impact is established by equating to zero the velocities of vertical and angular

displacement of the craft. After this comes the third mode of movement--rise of the craft on a wave. A theoretical analysis of movement of a craft in this mode is additionally complex in that at small velocities it is necessary in many cases to consider the hydrostatic forces which contribute to rise of the craft on the wave.

Having considered the craft movement over one period we find a value for all kinematic parameters of this movement and the effective forces. Having determined the movement of the craft over a series of waves, in view of the convergence of the process we can establish the actual initial conditions.



Fig. 134. Parameters of heaving for movement of a planing craft in a seaway.

KEY: A--Vertical movement; B--Period; C--Mode.

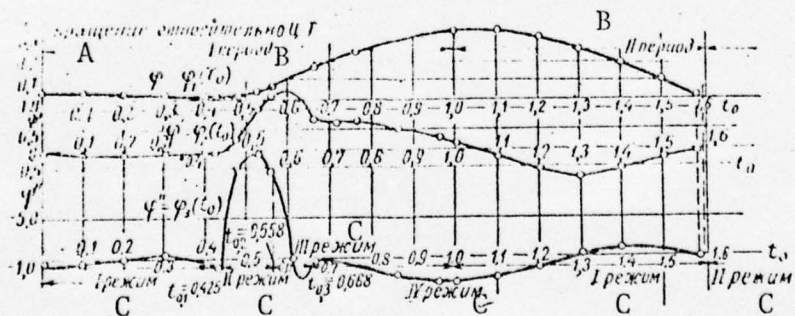


Fig. 135. Parameters of pitching for a planing craft in a seaway.

KEY: A--Rotation relative to center of gravity; B--Period; C--Mode.

Figs. 134 and 135 show by way of example the result of a solution to system (III.101) found by the described method for a craft having the following characteristics: weight--22,000 kg; abscissa of center of gravity--1.34 m, and radius of inertia of the mass--4.45 m. The bottom lines of the craft are

placed with two plates equivalent as to hydrodynamic forces and intersecting at an external angle of 60° . The dimensions of the plates are: length of bottom plate 15.8 m, length of bow portion of bottom plate--6.6 m. Width of plate--2.85 m. The velocity of relative movement is 30 m/sec. The wavelength is 30 m and the height of wave 2 m.

[238

The mathematical difficulty cited above which arises when solving this problem prevents obtaining any simple analytical relations for evaluating the movement of a planing craft in a seaway. Therefore, the results presented can be considered only as a method for formulating the problem and deciding the approach to it. The decision itself in each particular case must be found numerically.

Having found the movement of a planing craft in a seaway it is easy to use formula (III.94) to determine the value of the hydrodynamic forces acting on the craft in all modes of movement, including impact against the water.

References

1. Roze, N. V. Dinamika tverdogo tela (Dynamics of a solid body). Leningrad, KUBUCH Press, 1932.
2. Landau, L. D. and Livshits, Ye. M. Mekhanika sploshnykh sred (Mechanics of continuous media). Moscow, GITTL, 1954.
3. Prandtl, L. Gidroaeromekhanika (Hydroaerodynamics). Moscow, IL, 1949.
4. Yegorov, I. T. Impact against a compressible liquid. PMM, 1956, Vol. 20, No. 1.
5. Wagner, H. Uber stob--und Gleitvorgange an der Oberflache von Flussigkeiten. ZAMM, 1932, Bd. 12, H. 4.
6. Mak--Lakhlani, N. Teoriya i prilozheniya funktsiy Mat'ye (Theory and application of Mat'ye functions). Moscow, IL, 1953.
7. Fabrikant, N. Ya. Aerodinamika (Aerodynamics). T. I. M., GITTL, 1949.
8. Golubev, V. V. Lektsii po teorii kryla (Lectures on foil theory). Moscow, GITTL, 1949.
9. Sobolev, S. L. Uravneniya matematicheskoy fiziki (Equations of mathematical physics). Moscow, GITTL, 1954.
10. Ladyzhenskaya, O. A. Smeshannaya zadacha dlya giperbolicheskogo uravneniya (Composite problem for a hyperbolic equation). Moscow, GITTL, 1953.
11. Frank, F. and Mizes, R. Differentsial'nyye integral'nyye uravneniya matematicheskoy fiziki (Differential integral equations of mathematical physics). Moscow, ONTI, 1937.
12. Khaskind, M. D. Oscillations of a foil in a subsonic flow of gas. PMM, 1947, Vol. 11, No. 1.
13. Untteker, Ye. T. and Vatson, G. N. Kurs sovremennogo analiza (Course in modern analysis). Part 2. Moscow, GITTL,

1934.

14. Lamb, G. *Gidrodinamika* (Hydrodynamics). OGIZ, 1947. [239
15. Logvinovich, G. V. Impact of a solid body against a compressible liquid. *Trudy TsAGI*, 1956, No. 688.
16. Povitskiy, A. S. Landing of hydroplanes. *Trudy TsAGI*, 1939, No. 423.
17. Bisplinghoff, R. L., et al. *Aerouprugost'* (Aeroelasticity). Moscow, IL, 1958.
18. Yegorov, I. T. Oblique impact against a liquid. *Izvestiya AN SSSR, OTN*, 1957, No. 8.
19. Sedov, L. I. *Ploskiye zadachi gidrodinamiki i aerodinamiki* (Two-dimensional problems in hydrodynamics and aerodynamics). Moscow, GITTL, 1950.
20. "Schip en Werf", No. 4, februari, 1962, s. 113 (I. T. Yegorow, Planing of a Ship in Waves, *Trudy Nauchno--Isse. Inst. A. N. Krylov*, vip. 114, 1957).
21. Sedov, L. I. Theory of nonstationary planing and movement of a foil with trailing vortices. *Trudy TsAGI*, 1936, No. 252.
22. Enshteyn, L. A. Stability of planing of hydroplanes and skimmers. *Trudy TsAGI*, 1941, No. 500.

CHAPTER IV. Hydrodynamic calculations for a hydrofoil craft

A. Hydrodynamic calculations for foil systems

§28. Foil arrangements along the length and width of a craft. Distribution of load between bow- and sternfoils

Longitudinal stability is imparted to a craft by using two or three foils positioned along the length of the hull fore and aft from the center of gravity. The system now most widespread is the tandem pattern consisting of two foils, one behind the other. In the tandem pattern there may be two flat surface-effect foils, two deeply submerged foils, two V-shaped foils, a bow V-shaped foil and a flat sternfoil, or some other arrangement. Examples of tandem arrangements are provided by the domestically produced Raketa and Meteor, American craft with their deeply submerged foils, and craft of the Supramar concern with their V-shaped foils.

The relative distance the foils are from the center of gravity of a craft determines the load distribution between bow- and sternfoils. Based on load distribution foil systems are identified as tandem, airplane type, and canard (Fig. 136). In a normal tandem pattern each foil carries about half (40--60%) the displacement by weight of the craft. In the airplane and canard types the more heavily loaded foil is the main lift foil. The main foil carries about 80--90% of the load (displacement by weight). The other foil, which is lightly loaded, acts as a stabilizer. In the airplane pattern the bowfoil is the main foil and in the canard pattern the sternfoil. [240]

It is completely evident that the hydrodynamic forces developed by a system of tandem foils must differ from the simple sum of the forces developed by the separate foils since the sternfoil of a tandem system moves in a flow disturbed by the bowfoil. The effect of interaction among the foils in a tandem system leads to the rise of an additional horizontal force which, depending on velocity, can vary not only in magnitude but also in sign. In the case of depth-effect tandem foils their interaction also causes additional trim by the stern. [241]

In those cases when interaction in a tandem system proves to be unfavorable and also for the purpose of increasing transverse stability of a craft it may be advisable to split one of the foils (usually the bowfoil) so that it will consist of two symmetrical parts located outboard from the centerline plane. Usually the transverse gap between the half-foils is no greater than the width of the other foil. Such a three-foil pattern can be formed from any of the three methods named for distributing the load between bow- and sternfoils.

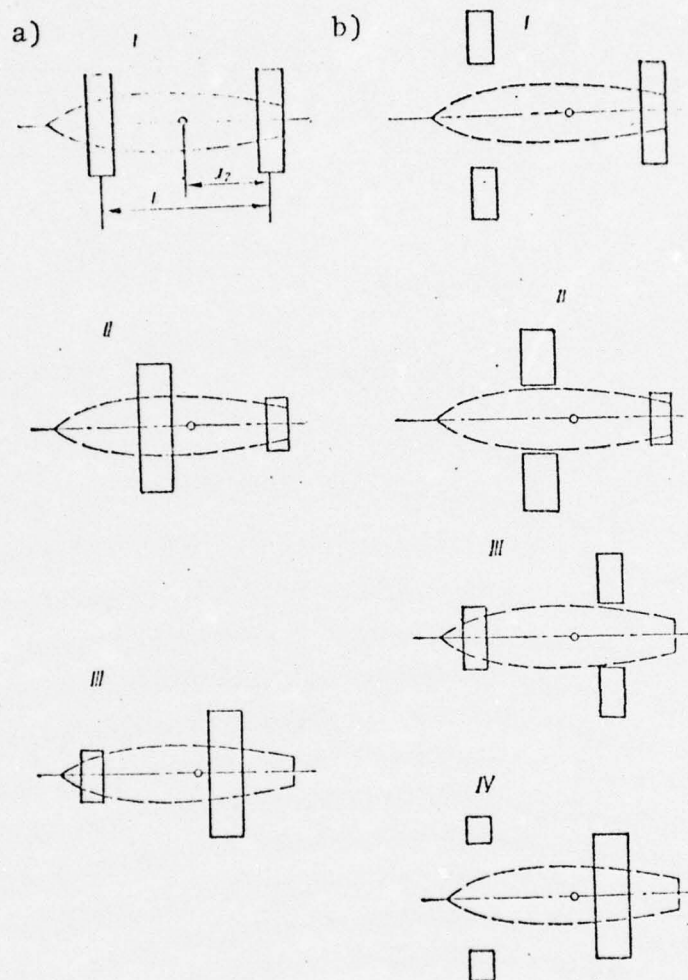


Fig. 136. Foil arrangements.

a--continuous foils: I--tandem; II--airplane; III--canard;
b--split foils (three-foil pattern): I, II, IV--split bowfoil;
III--split sternfoil.

As to nature of hydrodynamic interaction the main foil system patterns can be relegated to one of the types considered, that is, to either a tandem type or a three-foil type with a split foil.

As of the present time there are no general theoretical solutions to the problem of movement of a system of foils of finite span beneath the water's surface. The results obtained by solving a two-dimensional problem involving movement beneath the surface of a system of foils of finite span cannot be used for determining their characteristics since the nature and parameters of a wave behind a foil of finite span differs

importantly from two-dimensional waves. Consequently, an approximate method of making hydrodynamic calculations based on experimental investigation of the deformation in a free surface caused by a hydrofoil moving at a great relative velocity is recommended for the purpose of making a practical determination of the characteristics of a tandem system.

At the same time, in order to establish a connection between the shape of a free surface and induced velocities and to evaluate the role of separate components of the induced velocities in determining the effect of interaction among foils, it is advisable to consider a theoretical solution to the two-dimensional problem of waves induced by a foil of finite span.

§29. Waves excited by a hydrofoil of finite span. Effect of interaction in tandem systems

On actual craft the sternfoil is located 10--20 chords behind the bowfoil. Therefore, when determining the disturbance caused by the bowfoil at the location of the sternfoil the immediate vicinity of the bowfoil is not of direct interest. This approach to the problem of wave formation caused by a foil of finite span makes it possible to replace the foil with an infinite straight-line vortex whose intensity is equal to the velocity circulation around the foil.

[242

The conditions of movement, notation, and coordinate axes will be the same as in §3 of Chap. I. In [1] the following formula is derived for the ordinates of the profile of two-dimensional waves caused by a vortex:

$$y_0 = \frac{c}{g} \operatorname{Re} \left[\frac{dW}{dz} \right]_{y=0} \quad (\text{IV.1})$$

It follows from (IV.1) that far to the front of a foil the liquid is at rest, that is, $\lim_{x \rightarrow \infty} y_0 = 0$, and far to the rear of the foil sinusoidal waves form which can be described by the asymptotic formula

$$y_0 = -\frac{2\Gamma}{v} e^{-\frac{gh}{v^2}} \sin \frac{g}{v^2} x \quad (\text{IV.2})$$

or

$$y_0 = -a \sin \frac{2\pi}{\lambda^*} x, \quad (\text{IV.3})$$

where λ^* is the wavelength and a the amplitude,

$$\left. \begin{aligned} \lambda^* &= \frac{2\pi v^2}{g}, \\ a &= \frac{2V}{v} e^{\frac{gh}{v^2}} \end{aligned} \right\} \quad (\text{IV.4})$$

The induced velocities, horizontal component u , and vertical component w , on the basis of the formula for complex velocity $dW/dz = u - iw$, also can be expressed in terms of a derivative of complex potential

$$\left. \begin{aligned} u &= \text{Real} \left[\frac{dW}{dz} \right], \\ w &= \text{Im} \left[\frac{dW}{dz} \right]. \end{aligned} \right\} \quad (\text{IV.5})$$

A comparison of (IV.1) and (IV.5) makes it possible to write an equation relating the ordinate of the wave profile and the induced horizontal velocity u_0 of surface particles of the liquid

$$y_0 = -\frac{v}{g} u_0 \quad (\text{IV.6})$$

or

$$\frac{u_0}{v} = -\frac{y_0 g}{v^2}, \quad (\text{IV.7})$$

Considering the contour of the free surface in steady movement to be a line of flow, we can express the induced vertical relative velocity (downwash) in terms of a derivative of the ordinate of the wave profile [243

$$\frac{w_0}{v} \approx \frac{w_0}{v + u_0} = \frac{dy_0}{dx}. \quad (\text{IV.8})$$

Differentiating equation (IV.3) and substituting it into (IV.8) we obtain an expression for the angle of inclination of a wave profile far behind a vortex

$$\frac{w_0}{v} = -a \frac{2\pi}{\lambda^*} \cos \frac{2\pi}{\lambda^*} x. \quad (\text{IV.9})$$

Expressions (IV.7) and (IV.9) hold for induced velocities of surface particles. Assuming that particles of the liquid follow circular orbits, we will determine the induced velocities at a depth of h by using the known relations

$$\left. \begin{aligned} u &= u_0 e^{-\frac{gh}{v^2}}, \\ w &= w_0 e^{-\frac{gh}{v^2}}. \end{aligned} \right\} \quad (\text{IV.10})$$

Hence, knowing the circulation and rate of movement of an infinite vortex, it is possible to determine the parameters of a sinusoidal wave and the ordinate of the wave profile and then, by using formulas (IV.7), (IV.9), and (IV.10), to find the induced horizontal velocity and downwash at any point in the disturbed liquid.

Let us now proceed from a vortex to a foil of infinite span with chord b . We substitute into formulas (IV.2) and (IV.4) the equation for circulation $\Gamma = \frac{1}{2} C_y b v$. At the same time we introduce dimensionless magnitudes referred to the chord of the foil b :

$$\bar{x} = \frac{x}{b}; \quad \bar{y}_0 = \frac{y_0}{b}; \quad \bar{\lambda}^* = \frac{\lambda^*}{b}; \quad \bar{a} = \frac{a}{b}; \quad \bar{h} = \frac{h}{b} \quad \text{и} \quad \text{Fr} = \frac{v^2}{g b}.$$

As a result of the substitution we obtain expressions for the ordinates of a wave profile and wave parameters in dimensionless form

$$\bar{y}_0 = -C_y e^{-\frac{\bar{h}}{\text{Fr}^2}} \sin \frac{\bar{x}}{\bar{\lambda}^*} \quad (\text{IV.11})$$

or

$$\frac{\bar{y}_0}{C_y} = -e^{-\frac{\bar{h}}{\text{Fr}^2}} \sin \frac{2\pi}{\bar{\lambda}^*} \bar{x}, \quad (\text{IV.12})$$

$$\bar{\lambda}^* = 2\pi \text{Fr}^2, \quad (\text{IV.13})$$

$$\bar{a} = C_y e^{-\frac{\bar{h}}{\text{Fr}^2}}, \quad (\text{IV.14})$$

$$\frac{\bar{a}}{C_y} = e^{-\frac{\bar{h}}{\text{Fr}^2}}. \quad (\text{IV.15})$$

From equations (IV.11) -- (IV.14) flows the following condition of similitude for dimensionless parameters of a profile of waves caused by a foil of infinite span: [244

$$\left. \begin{aligned} \bar{\lambda}^* &= \bar{\lambda}^*(\text{Fr}), \\ \bar{a} &= \bar{a}(C_y, \text{Fr}), \\ \bar{y}_0 &= \bar{y}_0(C_y, \bar{h}, \text{Fr}), \\ \frac{\bar{y}_0}{C_y} &= f(\bar{h}, \text{Fr}). \end{aligned} \right\} \quad (\text{IV.16})$$

It is apparent from (IV.15) that

$$\bar{a}/C_y \rightarrow 1 \text{ when } Fr \rightarrow \infty.$$

Therefore, when $Fr \rightarrow \infty$ $\bar{a} = \bar{a}(C_y)$, that is, for large Froude numbers wave amplitude does not depend on velocity. For all practical purposes what has been stated holds even for $Fr > 4$ since if $Fr = 4$ $\bar{a}/C_y = 0.97$, that is, it is 3% less than the limiting value which is 1.

Fig. 137 shows curves of a wave profile in the form \bar{y}_0/C_y as a function of \bar{x}/Fr^2 for various values of \bar{h}/Fr^2 drawn based on the results of numerical integration of (IV.1).

It is apparent from a consideration of these curves that only in direct proximity to a vortex does a wave profile deviate noticeably from a sinusoid, but even when $\bar{x} > \lambda^*/8$ it practically coincides with a sinusoid.

The graph of ordinates of a wave profile (see Fig. 137), taking the change in sign to its opposite into account, can also serve as a graph of induced horizontal velocity, the scale of which can be established based on relation (IV.6).

Fig. 138 shows curves for the angle of inclination ω_0/v drawn to meet the same conditions as the graph in Fig. 137.

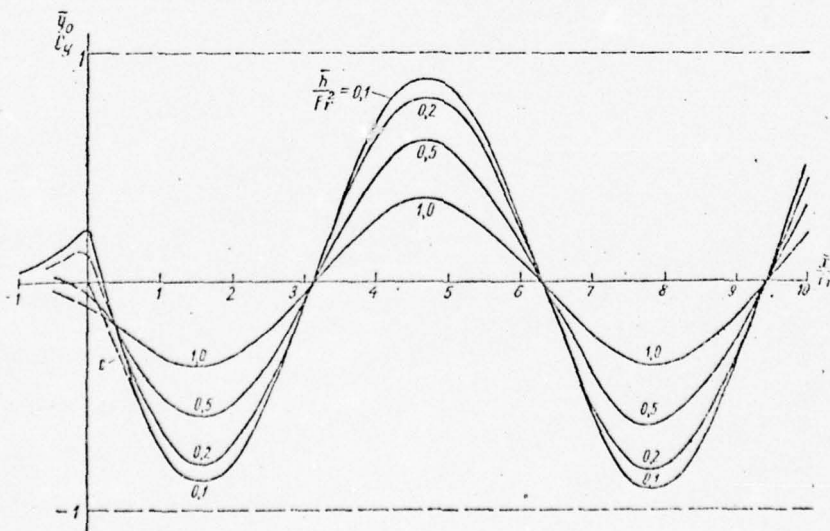


Fig. 137. Profile of two-dimensional waves caused by an infinite vortex. c--sinusoid.

Calculations for a foil with a chord of $b = 0.8 \text{ m}$ moving

at velocities of 22 and 44 knots when $Fr = 4$ and 8 were performed using formulas (IV.7) and (IV.9) in order to evaluate the magnitude of induced velocities far to the rear of a foil. Three values of the lift coefficient, $C_y = 0.15$, 0.3 , and 0.6 were used in the calculations. The results of calculations in the form of u_0/v and w_0/v curves as a function of \bar{x}/Fr^2 are shown in Fig. 139.

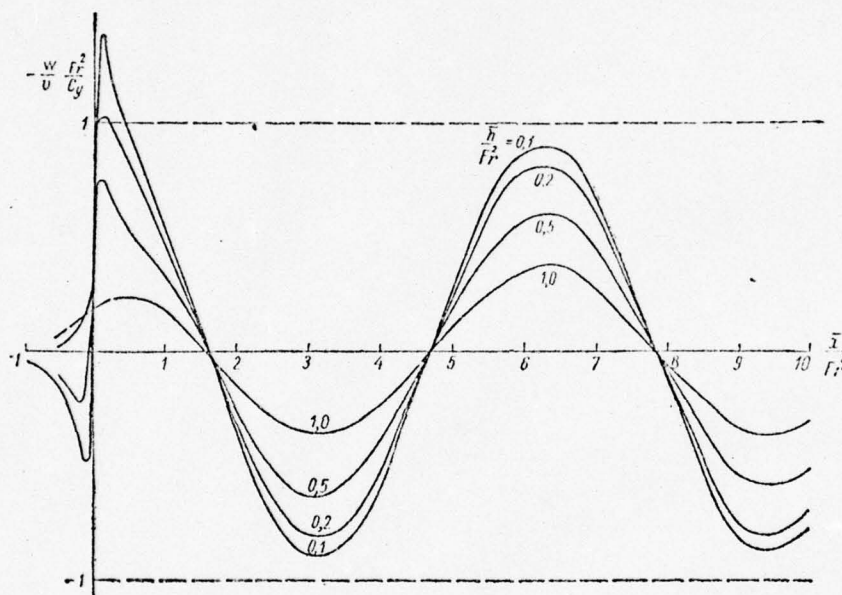


Fig. 138. Angle of inclination of wave profile behind an infinite vortex.

The curves of u_0/v and w_0/v are sinusoids with the same amplitudes and a phase displacement of $3/2\pi$. The amplitudes of induced velocities for $v = 44$ knots and $C_y = 0.15$ come to only 0.002 . On the steeper wave, when $v = 22$ knots and $C_y = 0.3--0.6$, the induced velocities reach $0.018--0.035$ of the velocity of foil movement. With such small induced velocities the change in magnitude of effective velocity of flow can be neglected and only the downwash which has a significant effect on the hydrodynamic characteristics of a foil taken into account. For example, when $w_0/v = 0.018$ the downwash is about 1° which with an initial value of $C_y = 0.38$ causes a change in C_y of up to 25% .

For making practical calculations for depth-effect foils traveling at high velocities, that is, when $\bar{h} = 0.2--1$ and $Fr = v/\sqrt{gb} > 4--5$, when $\bar{h}/Fr^2 = 0.95--0.98$, we can set

$$u = u_0 \text{ and } w = w_0.$$

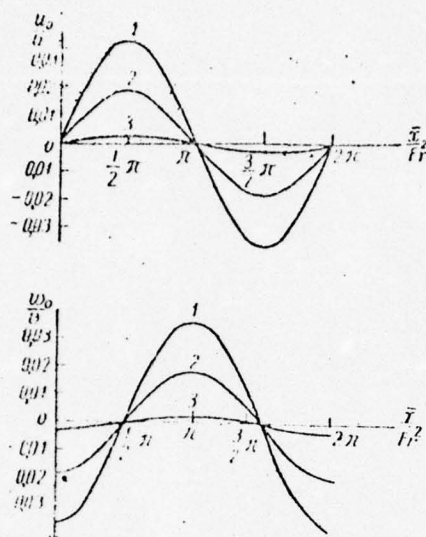


Fig. 139. Induced velocities far to the rear of a foil of infinite span (chord $b = 1$ m).

1 - $Fr = 1$, $C_y = 0.6$; 2 - $Fr = 1$, $C_y = 0.3$;
3 - $Fr = 8$, $C_y = 0.15$.

The results presented above for determining forces, wave profile, and velocities induced by a vortex moving under a free surface make it possible to show that the effect of interaction of a tandem system of foils of infinite span amounts to a change in the hydrodynamic characteristics of the sternfoil as a result of wave disturbances caused by the bowfoil and also that this effect can be negative (additional increase in total wave drag) as well as positive (decrease in wave drag of system).

By way of example we will discuss movement beneath the water's surface of two vortices of the same intensity at a distance of L from one another so as to simulate a system of tandem foils of infinite span. We will compare the wave drag of the system of tandem vortices with the sum of the wave drags of two isolated vortices and show that the excess drag, or thrust of the system, is equal to a projection of the lift of the rear vortex which is deflected from the vertical by an angle equal to the downwash at its location.

As is known, the wave drag of a vortex can be expressed in terms of the amplitude of the waves induced by it by means of the following formula:

$$R_w = \frac{1}{4} \rho g a^2. \quad (\text{IV.17})$$

The amplitude of a wave far to the rear of a tandem system can be determined by adding the profiles of the waves caused by each vortex separately and shifted one with respect [247

to another along the horizontal axis by a magnitude equal to the distance between foils. This procedure is possible due to the linearity of a complex potential, thanks to which the potential of a system of tandem vortices is equal to the sum of the potentials of isolated vortices, that is,

$$W_T = W_1 + W_2, \quad (\text{IV.18})$$

whence on the basis of formula (IV.1)

$$y_{0T} = y_{01} + y_{02}$$

or, considering (IV.3),

$$y_{0T} = -a \left[\sin \frac{2\pi}{\lambda^*} x + \sin \left(\frac{2\pi}{\lambda^*} x - \beta \right) \right], \quad (\text{IV.19})$$

where β is the phase of the wave of the forward vortex at the location of the aft vortex.

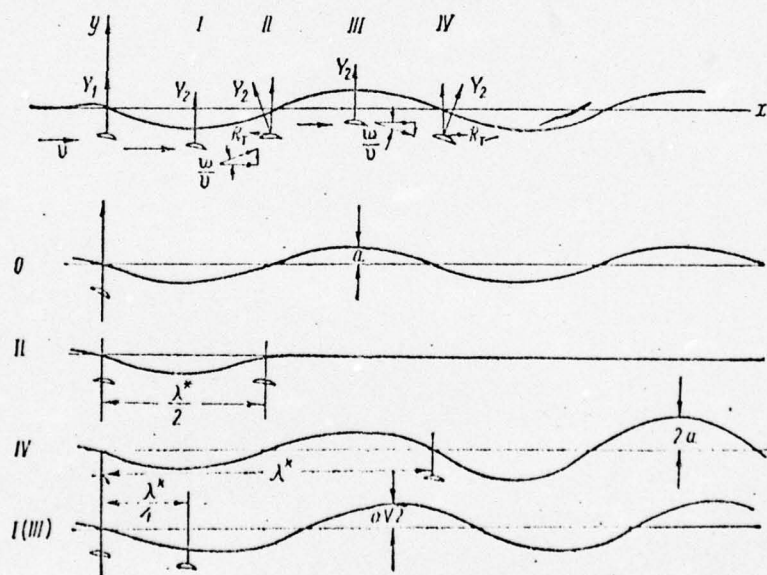


Fig. 140. Wave profiles behind a tandem system of foils of infinite span having the same lifting force at various phases of displacement of the sternfoil. (The large circle pertains to the wave profile behind a single foil.)
 I-- $\beta = \pi/2$ trough of wave; II-- $\beta = \pi$ rise from trough of wave to crest; III-- $\beta = 3\pi/2$ crest of wave; IV-- $\beta = 2\pi$ slope from crest of wave to trough.

Fig. 140 shows the wave profiles behind a tandem system

obtained graphically by adding the profiles of waves caused by two isolated vortices. By way of example we have considered limiting cases to which correspond the existence of one horizontal or one vertical induced velocity, that is, when the downwash is either equal to zero or is maximum in magnitude and either negative or positive in sign. [248]

Table 6 gives a summary of the amplitudes of waves, induced velocities, and also the total wave drag of a system and interaction drag or added "induced" drag of the aft foil. Line 5 in the table also gives the horizontal projection of the lift of the aft foil.

It follows from an analysis that the added force of interaction in a tandem system of foils of infinite span is determined entirely by the magnitude and sign of downwash at the location of the sternfoil. Downwash downward leading to an increase in the drag of the tandem system is considered to be positive. The phase of the wave and consequently the effect of interaction depend on the relative velocity, or the Froude number. In that case when the aft vortex is located under a wave trough or crest the downwash and force of interaction are equal to zero. The greatest interaction drag is observed when the aft vortex is at a distance of $L = \lambda^*$ from the forward vortex where the maximum downwash is directed downward. In this case the amplitude of a wave in the system is doubled and the wave drag quadrupled as compared with an isolated vortex.

The most favorable effect of interaction is achieved when the distance of the aft vortex from the forward one is $L = 0.5\lambda^*$ when the downwash is directed upward and is equal in magnitude to the maximum downwash downward. The waves from the vortices are in antiphase and, therefore, behind the system of vortices the water's surface remains undisturbed. The wave drag of the system is correspondingly equal to zero and the drag of interaction negative, that is, on the aft vortex a thrust develops in the direction of movement.

It is apparent from a comparison of lines 5 and 8 in the table that the interaction drag of the system is equal to the horizontal projection of the lift of the aft vortex on condition that the lift is deflected from the vertical by an angle equal to the downwash. All the results obtained remain unchanged when the phase β is changed by an integral multiple of 2π .

We will point out that the system investigated consisted of two infinite vortices of identical intensity and that the circulation of the aft vortex remained unchanged when located at any phase of the wave. Furthermore, it was assumed that the forward vortex in a system of tandem vortices was in no way affected by the aft vortex and its wave drag always remained unchanged.

TABLE 6

Amplitude of Waves Behind a System of Tandem Vortices,
Induced Velocities at the Location of the Aft Foil,
and the Wave Drag of a System

Phase of wave at location of the aft
vortex (see Fig. 140)

Parameters of the
system

	$\beta = \frac{\pi}{2}$ $\beta = \frac{3}{2}\pi$	$\beta = \pi$	$\beta = 2\pi$
1. Distance between vortices (in wave-lengths)	$\frac{1}{4}\lambda^*$ $\frac{3}{4}\lambda^*$	$\frac{1}{2}\lambda^*$	λ^*
2. Amplitude of wave far to rear of the system	$a\sqrt{2}$	0	2a
3. Horizontal induced velocity u_0/v	$\pm 2 \frac{\rho g \Gamma^2}{v^3} e^{-\frac{2h}{Fr^2}}$	0	0
4. Downwash w_0/v	0	$-2 \frac{\rho g \Gamma^2}{v^3} e^{-\frac{2h}{Fr^2}}$	$2 \frac{\rho g \Gamma^2}{v^3} e^{-\frac{2h}{Fr^2}}$
5. Horizontal projection of lift of aft vortex - $(w_0/v)(Y_2)$	0	$2 \frac{\rho g \Gamma^2}{v^3} e^{-\frac{2h}{Fr^2}}$ $-2R_w$	$-2 \frac{\rho g \Gamma^2}{v^3} e^{-\frac{2h}{Fr^2}}$ $+2R_w$
6. Wave drag of system $R_{wT} = R_w(\alpha_T/a)^2$	$2R_w$ iso	0	$4R_w$
7. Sum of drags of two isolated vortices $R_{w1} + R_{w2}$	$2R_w = 2 \frac{\rho g \Gamma^2}{v^3} e^{-\frac{2h}{Fr^2}}$		
8. Interaction drag of tandem system R_T	0	$-2R_w$ (thrust)	$2R_w$

30. Practical calculations of hydrodynamic characteristics of foils of finite span in a tandem system [250]

Finding approximate solutions to the problem of interaction between foils of finite span in a tandem system is based on experimental investigation of deformation in a free surface caused by a hydrofoil. It is considered, as demonstrated in the preceding section, that there is a direct relation between the induced velocities and the shape of the wave surface.

Measurements of the deformation in a surface show that in front of a foil wave disturbances are completely damped at a distance of 3--5 chords. Inasmuch as the distance between foils is usually more than 10 chords it can be safely assumed that the sternfoil has no effect on the flow around the bowfoil. But then the problem of interaction between foils in a tandem system reduces to determining the hydrodynamic characteristics of the sternfoil working in a flow disturbed by the bowfoil. In connection with the fact that movement of foils at great speed ($Fr > 4$ --5) is under consideration, it appears possible to neglect the curvature of flow and the horizontal induced velocity.

Thus, it is considered that the bowfoil in a tandem system works in an undisturbed flow and a skewed plane-parallel flow with a velocity equal to that of the craft impinges on the sternfoil.

Under these assumptions the lift of the sternfoil in a tandem system will vary in proportion to the true angle of attack which changes by the magnitude of the downwash

$$Y_{2r} = Y_2 \left(1 - \frac{\Delta\alpha_r}{\alpha + \alpha_0} \right). \quad (IV.20)$$

The drag of the sternfoil in a tandem system also changes. The added drag is equal to the horizontal projection of the lift which is deflected from the vertical by the angle of downwash, that is,

$$R_{2r} = R_2 + \Delta\alpha_r Y_{2r}. \quad (IV.21)$$

In formulas (IV.20) and (IV.21) $\Delta\alpha_r$ is the downwash caused by the bowfoil at the location of the sternfoil, downwash downward being considered positive.

For determining the total lift and drag of a tandem foil system the following relations hold:

$$\left. \begin{aligned} Y_r &= Y_1 + Y_{2r} \\ R_r &= R_1 + R_2 + \Delta\alpha_r Y_{2r} \end{aligned} \right\} \quad (IV.22)$$

in dimensionless form

[251

$$C_{y2r} = C_{y2} \left(1 - \frac{\Lambda a_r}{a + a_0} \right) = C_{y2} - \Delta \alpha_r \frac{\partial C_{y2}}{\partial \alpha}, \quad (\text{IV.23})$$

$$C_{yT} = C_{y1} + C_{y2r}, \quad (\text{IV.24})$$

$$C_{AT} = C_{A1} + C_{A2} + \Delta \alpha_r C_{y2r}. \quad (\text{IV.25})$$

The lift and drag of bow- and sternfoils in a tandem system and also their coefficients which do not have the subscript "T" in formulas (IV.20)--(IV.25) are determined from their characteristics in isolation. The geometric angle of attack of the isolated bowfoil should be set equal to the angle of attack of the tandem system foil measured with respect to the direction of movement and the geometric angle of attack of the sternfoil should be measured from the direction of downwash. So that the sternfoil of a tandem system develop the required lift, the angle at which it is set must be increased ahead of time by the angle of downwash. Furthermore, it must be taken into account that the true depth of immersion of the sternfoil should be measured not from the horizontal undisturbed surface but from the level of the wave depression which the bowfoil would cause in the absence of the sternfoil. Lowering of the actual level of free surface for a stern (depth-effect) foil would lead to an increase in trim which would cause a corresponding increase by the same amount in the angles of attack of both foils. Therefore, in order to obtain calculated angles of attack for the foils of an actual craft, the angles at which they are set must be decreased by the angle of added trim caused by the lowering in the level of the water at the location of the sternfoil.

Finally, in this way the problem presented by a tandem system reduces to determining the downwash and the drop in the level of the water's surface behind a hydrofoil of finite span.

At a great relative speed of movement ($Fr > 3$) the wave surface behind a foil of finite span has the shape of a trough-shaped depression whose transverse sections have almost flat bases and vertical sides (Fig. 141). The depression, whose width is at first somewhat less than the span of the foil, gradually becomes constricted and then at a certain distance behind the foil its sides merge, forming a rooster tail. When the foil is immersed to a depth greater than 1.0--1.2 chord the sharp lines of the depression begin to smooth out.

A longitudinal wave profile constitutes something like a

half-wave and can with sufficient accuracy be replaced with a sinusoid. Then the ordinate of greatest lowering in the wave profile a and its distance from the foil $\lambda^*/4$ will represent respectively the amplitude and a quarter of a sinusoidal wavelength. These two parameters completely determine the longitudinal wave profile. The dimensionless wave profile ordinate $\bar{y}_0 = y_0/b$, depending on the distance $\bar{x} = x/b$ from the bowfoil, [252] can be expressed by the formula

$$\bar{y}_0 = \bar{a} \sin \frac{2\pi}{\bar{\lambda}^*} \bar{x}, \quad (\text{IV.26})$$

where $\bar{\lambda}^*$ is the relative wavelength (in foil chords).

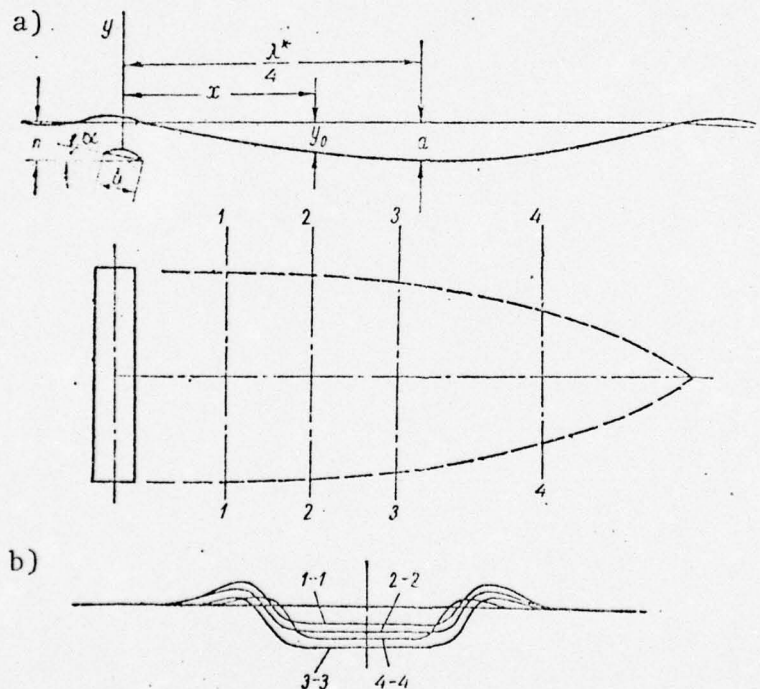


Fig. 141. Wave depression behind a foil of finite span: a--longitudinal wave profile; b--transverse profiles.

The downwash of a foil at a depth of up to one chord can be taken as equal to the inclination of the tangent to the wave profile, that is,

$$\frac{w}{v} = -\frac{d\bar{y}_0}{d\bar{x}}. \quad (\text{IV.27})$$

The following empirical formulas have been obtained for $\bar{a} = a/b$ and $\bar{\lambda}^*/4$:

$$\frac{\bar{\lambda}^*}{4} = \frac{\pi}{2} Fr^{2v}, \quad (IV.28)$$

$$\frac{\bar{a}}{C_y} = e^{-\frac{\bar{h}}{Fr^{2v}}} + \frac{0.5}{\lambda} (Fr^{2v} - 2), \quad (IV.29)$$

where

[253

$$v = e^{-\frac{0.73}{\lambda^{0.2}}}, \quad (IV.30)$$

and λ is the aspect ratio of the wave-forming (bow) foil.

Formula (IV.29) for \bar{a}/C_y holds for depths of immersion of the wave-forming foil to 1.0-1.2 chord. In the indicated range of depths of immersion \bar{a}/C_y depends practically not at all on \bar{h} .

For convenience of use Figs. 142 and 143 show curves of $\lambda^*/4$ and \bar{a}/C_y as a function of Fr_b in terms of λ .

Substituting the expressions for \bar{a} and $\bar{\lambda}^*/4$ into formulas (IV.26) and (IV.27), we obtain formulas for calculating the ordinates and angles of inclination of the tangent of the wave profile:

$$\bar{y}_0 = C_y \left[e^{-\frac{\bar{h}}{Fr^{2v}}} + \frac{0.5}{\lambda} (Fr^{2v} - 2) \right] \sin \frac{\bar{x}}{Fr^{2v}}; \quad (IV.31)$$

$$\frac{w}{v} = \frac{C_y}{Fr^{2v}} \left[e^{-\frac{\bar{h}}{Fr^{2v}}} + \frac{0.5}{\lambda} (Fr^{2v} - 2) \right] \cos \frac{\bar{x}}{Fr^{2v}}. \quad (IV.32)$$

The average downwash along the span of the sternfoil differs from the downwash in the centerline plane since its span is usually greater than the width of the flat part of the wave depression. At the usual ratios of foil dimensions when the span of the sternfoil is about 0.8 times the span of the bowfoil, the average downwash, as experimental data show, is equal to approximately 75% of maximum.

In light of what has been said the following approximate formula can be recommended for downwash in an ordinary tandem system:

$$\Delta\alpha_r = 0.75 \frac{C_y}{Fr^{2v}} \left[e^{-\frac{\bar{h}}{Fr^{2v}}} + \frac{0.5}{\lambda} (Fr^{2v} - 2) \right] \cos \frac{\bar{L}}{Fr^{2v}}, \quad (IV.33)$$

where $\bar{L} = L/2$ is the distance between foils in chords of the bowfoil.

By using the formulas presented it is easy to determine the lift and drag of a tandem system of foils for which the

geometric dimensions of the foils, the distance between them, the angles of attack, and the speed of movement are given. The lift and drag of the bow- and sternfoils (foil systems) are determined preliminarily depending on the angle of attack and relative depth of immersion. For the purpose of calculating the characteristics of a tandem system consisting of complex foils the latter are replaced with monoplane's equivalent to them. When determining the characteristics of a sternfoil, included in the calculations should be the actual depth of immersion as measured from the level of the depression, taking into account its lowering by y_0 , and the actual angle of attack, taking into account the downwash from the bowfoil. [255]

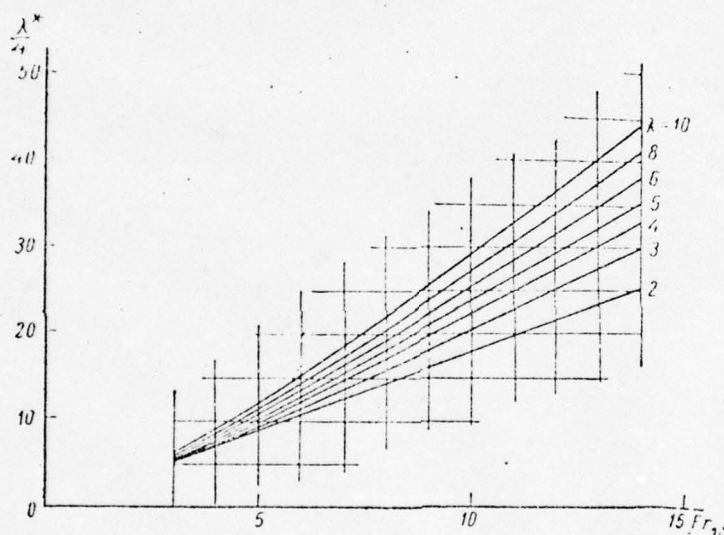


Fig..142. Graph of length of wave depression as a function of $Fr_w = v/\sqrt{gb}$.

The arrangement of the foils and also the angles of attack and depths of immersion corresponding to the calculated speed of movement are given. The angles of attack and depths of immersion of the foils in all intermediate modes are determined from calculations of craft attitude.

§31. Comparative description of main patterns of foil arrangement

The results of interaction in a tandem foil system presented in the preceding section make it possible to evaluate the effect of foil arrangement on the lift-drag ratio and attitude of a craft in various modes of movement.

The downwash and added drag of the sternfoil in a tandem system depend on the ratio between the distance between foils

and the length of the wave depression (Fig. 144).

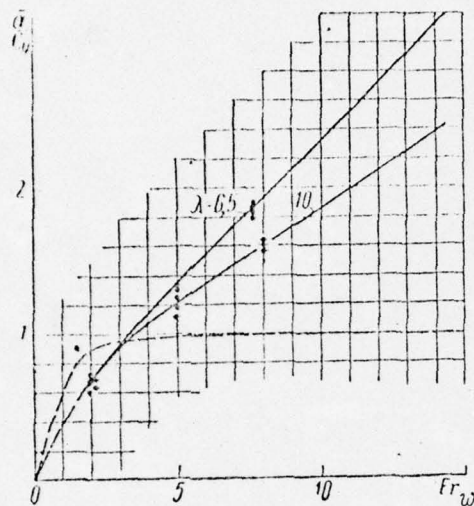


Fig. 143. Graph of ordinates of maximum lowering (amplitude) of wave profile.

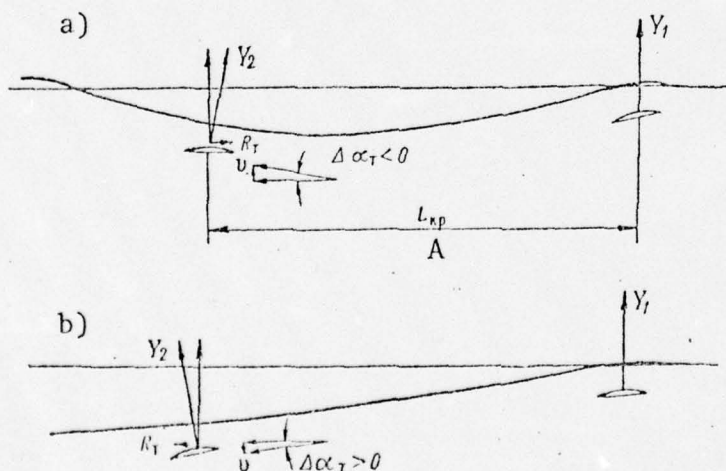


Fig. 144. Effect of length of wave profile on the nature of interaction in tandem systems: a--relatively slow craft for which $Fr < 4-6$; $\lambda^*/4 < L_f$; interaction drag negative (thrust); b--high-speed craft for which: $Fr > 8-10$; $\lambda^*/4 > L_f$; interaction drag occurs.

KEY: A-- L_f .

When $L = \lambda^*/4$, that is, when the sternfoil is under the trough of a wave profile, there is no downwash ($\Delta \alpha_T = 0$) and the drag caused by interaction in the system is also equal to zero.

When $L < \lambda^*/4$ a downwash directed downward ($\Delta\alpha_T > 0$) causes added drag; when $L > \lambda^*/4$ the downwash is directed upward ($\Delta\alpha_T < 0$) and therefore the added drag is negative, that is, "thrust" directed forward and decreasing the overall drag of the system occurs. A decrease in the drag of a tandem system accompanying a relative decrease in the wavelength has been confirmed experimentally.

[256

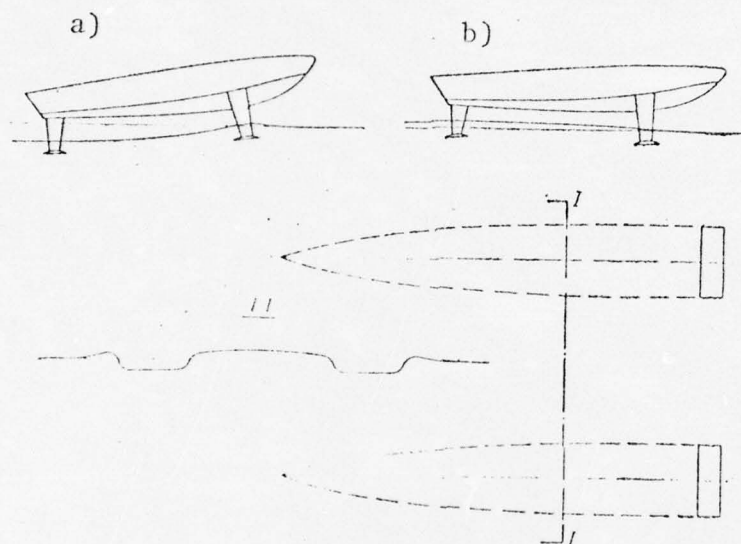


Fig. 145. Wave profile behind a split foil: a--attitude of a craft with tandem foils; b--attitude of a craft with a split bowfoil.

However, under actual conditions the distance between foils cannot be chosen arbitrarily and therefore the positive effect of interaction in a tandem system can be utilized only at moderate speeds of movement characterized by a Froude number of 4--6. For high-speed craft when $Fr > 8$ --10 interaction in a tandem system produces a negative effect since $L < \lambda^*/4$.

In the latter case dividing the bowfoil into two half-foils and moving them outward so that the gap between the inner edges is no greater than the span of the sternfoil may prove to be advisable. Behind the split bowfoil there form two wave depressions with a wave hump between them (Fig. 145) under which the sternfoil moves. There are no data from direct measurements of the wave profile or velocity field behind a split foil. However visual observations of the flow [257 around a sternfoil in a model of a three-foil system (split foil) suggest that transverse sections of a wave hump are not flat but slightly convex.

The centerline section of the wave hump along the entire length of the wave depression behind each of the half-foils

rises above the level of the undisturbed water, forming a smooth maximum close behind the foil. Judging by the longitudinal profile of the wave hump and also by the increase in drag of a three-foil system, as the distance between foils decreases (when $Fr = \text{const}$) it can be supposed that the small downwash upward immediately behind the foil gradually decreases with increasing distance from the foil and then changes sign, remaining small in magnitude. The ideas presented above permit the assertion that with respect to interaction a three-foil pattern with a split bowfoil is undoubtedly preferable to a tandem system for large values of Fr . However, implementing this advantage is in practice difficult since design considerations dictate the use of separate foils of small aspect ratio, the additional induced losses of which exceed the gain in drag resulting from their interaction.

A three-foil system with a split bowfoil can prove to be a better design for small high-speed craft inasmuch as the foils of such craft are relatively small compared with the foils of large craft designed to travel at moderate speeds.

If based on the condition of cavitation-free flow it is accepted that the absolute speeds of a large and a small craft are the same, then the specific load per one square meter of foil must also be the same. Indeed, since the area of a foil S is proportional to the displacement in the first power of D and the width of the hull B proportional to raised to the one-third power, then

$$\frac{S}{B^2} \sim \frac{D}{D^{2/3}} \sim D^{1/3} \text{ when } v = \text{const}$$

or

$$\frac{S_1}{B_1^2} : \frac{S_2}{B_2^2} = k,$$

that is, with a decrease in the displacement of a craft the ratio S_f/B^2 does not remain constant but decreases proportionally to the linear scale of k .

For any speed this ratio is equal to

$$\frac{S_f}{B^2} = \frac{2C_D^{2/3}}{C_{yf}} \cdot \frac{1}{Fr_D^2},$$

where

$$C_D = \frac{D}{\gamma B^3}; \quad ; Fr_D = \text{see (IV.34)}.$$

Based on the condition of transverse stability the angle of a foil cannot be decreased arbitrarily and therefore for high-speed and small craft the chord of a foil turns out to be small. In this case separating the foil into two parts may prove to be advisable based on design considerations. It is also desirable to split the bowfoil based on considerations of seakeeping characteristics when making way at acute course angles or beam to the sea. The latter recommendation applies no matter what method is used to distribute the load between the bow- and sternfoils.

B. Drag and attitude of hydrofoil craft

§32. Modes of movement of hydrofoil craft. Components of craft drag

A craft at rest is subjected by the water to hydrostatic pressure which is spread over the entire wetted surface of its immersed parts. The resulting hydrostatic surface forces constitute an archimedean supporting force which is directed upward. The archimedean force in this case is exactly equal to the weight of the craft

$$D = \gamma V_0,$$

where $V_0 = V_{0h} + V_{0f}$ is the volume of the underwater part of the craft in a static state, V_{0h} is the underwater volume of the hull, and V_{0f} is the underwater volume of the foils.

When a craft moves on the surface the underwater part of its hull and the foils are subjected to additional forces exerted by the liquid, or hydrodynamic forces. The total force supporting the craft consists of hydrostatic, or archimedean, forces and hydrodynamic forces and the equation expressing the forces supporting a moving craft assumes the form

$$D = \gamma V + Y,$$

where

$$V \neq V_0.$$

In the general case during acceleration of a craft

$$V = V_h + V_f,$$

$$Y = Y_h + Y_f.$$

For a craft without foils three modes of movement can be distinguished depending on the relative magnitude of the hydrodynamic force of support:

1. Floating, when the hydrodynamic force of support is [259]

negligible, for which

$$Y \approx 0,$$

$$D \approx \gamma V_0.$$

2. Transitional mode of movement characterized by the rise of a significant hydrodynamic force. The total supporting force is then

$$D = \gamma V + Y.$$

3. Planing or skimming of the craft when 90--95% of the supporting force is due to hydrodynamic forces, that is, for all practical purposes $D \approx Y$.

With further increase in speed planing becomes ricocheting.

A change in the mode of movement is accompanied by a change in the mean draft and trim of the craft and by an increase in its drag (Fig. 146).

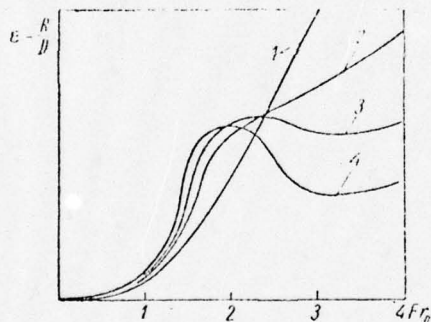


Fig. 146. Nature of change in drag as a function of Fr_D for various types of craft.

1--displacement craft; 2--stepless planing hull; 3--stepped planing hull; 4--hydrofoil craft.

The following values of relative speed expressed in terms of displacement Froude numbers are usually used by way of arbitrary boundaries for making an approximate evaluation of modes of craft movement:

- a) floating mode $Fr_D < 1$;
- b) transitional mode $1 < Fr_D < 3$;
- c) planing mode $Fr_D > 3$.

Here

$$Fr_D = \frac{v}{\sqrt{g \left(\frac{D}{\gamma} \right)^{1/3}}} = Fr_L \sqrt{\bar{L}}, \quad (IV.34)$$

where

$$\bar{L} = L : \left(\frac{D}{\gamma} \right)^{1/3}, \quad (IV.35)$$

$$Fr_L = \frac{V}{\sqrt{gL}}.$$

Three modes of movement are also identified in the case of hydrofoil craft based on the physical nature of the supporting forces:

- a) floating mode when $D = \gamma(V_{0h} + V_{0f})$.
- b) transitional mode when $D = (V_h + V_f)\gamma + Y_h + Y_f$. (IV.35)
- c) foilborne mode when the hull leaves the water entirely [260]

$$D = \gamma V_f + Y_f.$$

For all practical purposes in the foilborne mode $D \approx Y_f$ inasmuch as the volume of the foils displacing water is small. The relative speed on the boundary of the displacement mode is the same as for a craft without foils and the relative speed of takeoff depends on the design of the foil system. For all practical purposes for most craft already built foilborne movement begins at $Fr_D = 2.7--3$.

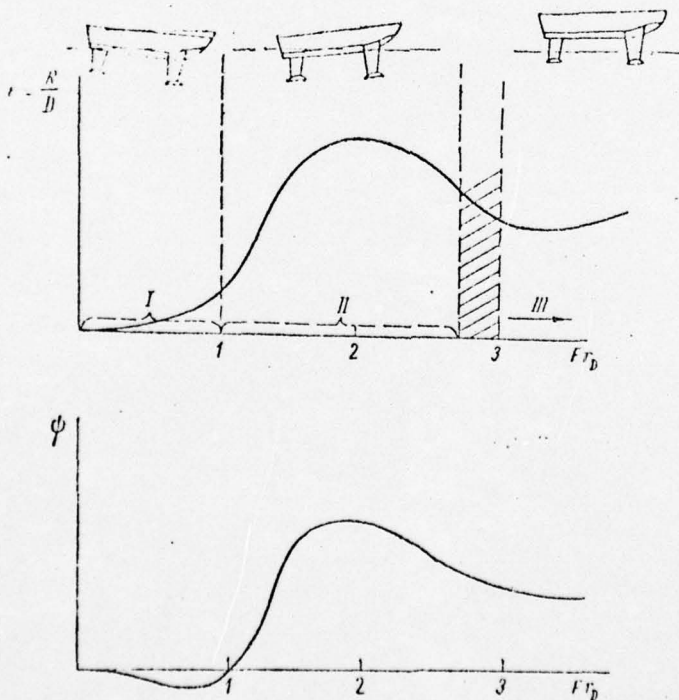


Fig. 147. Modes of movement of a hydrofoil craft.
I--floating; II--transitional mode; III--foilborne.

Operationally the first and second modes of movement constitute the period of start or acceleration of a craft and the third is the mode of normal operation.

Fig. 147 shows the change in trim and drag depending on Fr_D and attitude of a hydrofoil craft.

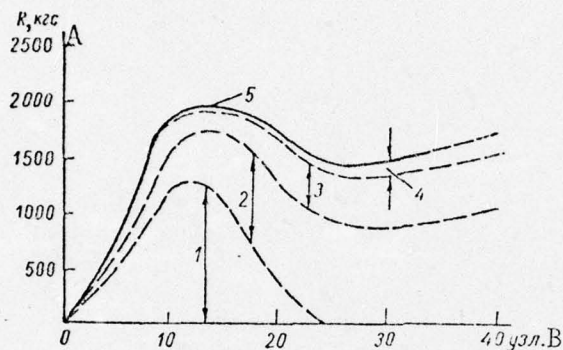


Fig. 148. Drag components for the hydrofoil craft Aquastroll. 1--hull resistance; 2--foil resistance; 3--propeller shaft, rudder, strut, and bracket resistance; 4--air resistance; 5--total drag.

KEY: A-- R , kgf; B--knots.

The total drag of a hydrofoil craft is the sum of the following components: [261

a) during acceleration

$$R = R_h + R_f + R_{app} + R_a, \quad (IV.36)$$

b) foilborne

$$R = R_f + R_{app} + R_a, \quad (IV.37)$$

where R_h is the hull resistance; R_f the resistance of the foil system; R_{app} the resistance of all non-lift members of the craft, including shafts, brackets, fairings, rudders, and foil struts; and R_a is the air resistance.

Fig. 148 shows a graph of total drag and its components for the hydrofoil craft Aquastroll.*

* The Marine Engineer and Naval Architect, 1957, VI, No. 6, p. 207.

§33. Distinguishing aspects of the hydrodynamics of hydrofoil craft in the transitional mode

In the displacement mode the attitude of a hydrofoil craft is no different from that of a craft with no hydrofoils since the hydrodynamic forces supporting the foils are small. Almost all elements of the foil system, including the lift foils and their struts, and also all appendages are immersed in the water and experience strong resistance to movement from the water. Therefore the drag on a hydrofoil craft in the displacement mode is greater than for a craft without foils. However, almost no attention is paid to evaluating the drag on a hydrofoil craft in a displacement mode inasmuch as in magnitude it is [262] a fraction of the maximum at the drag hump and has almost no effect on attaining the main mode of movement. At the same time during acceleration the transitional mode is of great importance when at a speed of 0.5--0.7 times the speed of takeoff the drag on the craft reaches a maximum which usually greatly exceeds the drag on the craft in the foilborne mode. During foilborne movement the lift-drag ratio is 10--14 or higher; at the hump it is equal to 7--8 and rarely reaches 10. Overcoming the drag hump when the propellers on the craft are fixed pitch can subject the engines to an intolerable overload. If "light" propellers are used to avoid overload on the engines, then maximum speed is reduced due to nonuse of full power. Hence the importance of correctly determining the drag hump and reducing it as much as possible is obvious. Correct selection of hull lines in light of the flow around them during the transitional mode plays a large role in reducing the drag hump.

A supporting force of the foils which increases with increasing speed of movement and a concomitant decrease in the share of the load carried by the hull and also a reduction in lift-drag ratio of the hull are characteristic of the transitional mode. Calculations show that at a speed of movement corresponding to the drag hump the support offered by the hull is 25--35% of the weight displacement of the craft and at the same time hull drag is 0.4--0.6 times the total craft drag.

At the hump the flow around the hull is very complex in nature. The bow extremity of the craft rises sharply so that the forward boundary of the wetted surface on the bottom approaches the bowfoil. But continuous flow does not stretch to the stern as in a planing craft. It separates from the hull behind the bowfoil as a result of the formation of the wave depression behind the bowfoil. Continuous flow again washes the hull aft of the hull midpoint. The bottom is washed by a fine sheet of spray from the point of separation of the main flow and upward from this boundary at the bow. Distinguishing the boundary where the main flow turns into spray is diffi-

cult. An additional difficulty is related to the indefinite nature of the flow in the boundary layer and the inapplicability of ordinary methods of determining the friction drag in the zone of fine spray. The degree of turbulence in the flow caused by a foil close to the hull is also unknown. All this makes it practically impossible to calculate theoretically the friction drag on a hull or to scale the drag from a model to a full-scale craft.

The supporting force generated by a hull at drag hump speeds is made up of hydrostatic and hydrodynamic forces. Calculating the hydrodynamic lift is also precluded in practice due to lack of methods for calculating the flow over the bottom in the transitional mode. Therefore in practice the lift and drag on the hull of a hydrofoil craft in the takeoff mode are determined from experimental diagrams drawn based on the results of tests of model hulls in the absence of foils but with a variable load and with the hull centered. The diagrams are drawn in the form of dimensionless coefficients of drag $C_R = R/\gamma B^3$ as a function of the Froude number with respect to the width of the hull $Fr_B = V/\sqrt{gB}$. The parameters used are the coefficient of static load

[263

$$C_D = \frac{D}{\rho g B^3}$$

and the coefficient of center of pressure \bar{x}_g which is a ratio between hull length and the distance the point of application of the supporting force is removed from Sta. 20.

The attitude of a craft is determined from graphs of trim and relative draft \bar{y}_{20} drawn for a point on the base line at Sta. 20 as a function of Fr_B . The curves for $\psi(Fr_B)$ and $\bar{y}_{20}(Fr_B)$ are drawn from the same parameters, C_D and \bar{x}_D . [267

Figs. 150--152 show the curves calculated for the model whose lines are shown in Fig. 149. By using such graphs for models with different lines, after calculating the attitude of several variations, optimal elements of the hull can be selected so as to provide minimum drag on a hydrofoil craft in the transitional mode.

An analysis of the characteristics of way-making ability and seakeeping characteristics based on the results of model and full-scale tests of ships already built makes it possible to offer the following recommendations as to the selection of lines for the hulls of hydrofoil craft.

In most cases encountered in practice it is advisable to employ hard chines with a deadrise in the bow and a lift in the buttocks at the stern. The lift at the stern on slow

craft should be greater and on faster craft less.

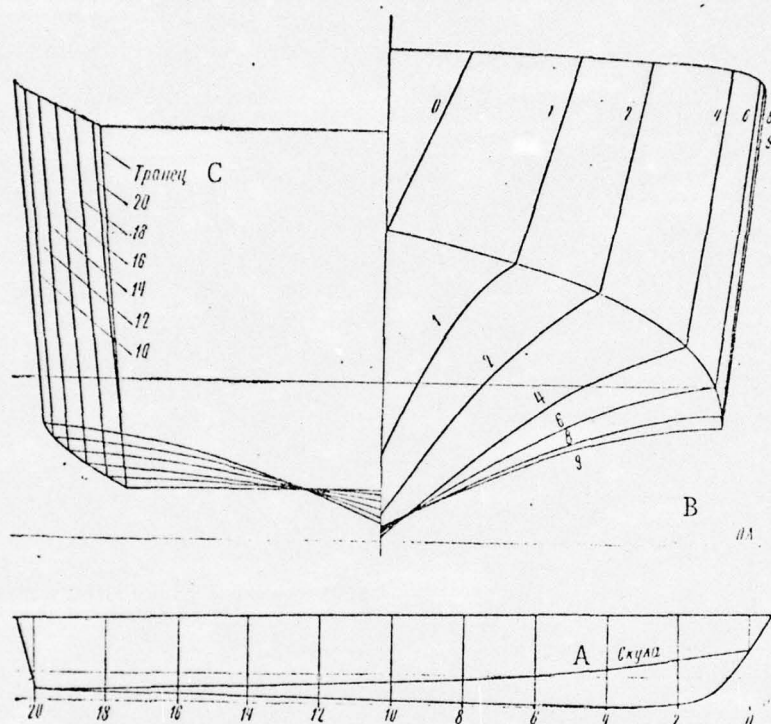


Fig. 149. Lines of model of a craft hull.
KEY: A--Bilge line; B--Base line; C--transom.

For values of the coefficient of static load of a hull at the drag hump equal to 0.1--0.2, it is advisable to use a step located in the area Sta. 14--16. The optimal trim with respect to hull drag in the transitional mode in most cases is 2--4. To improve seakeeping characteristics in the displacement mode the volume of the bow above the waterline should be increased as compared with ordinary craft.

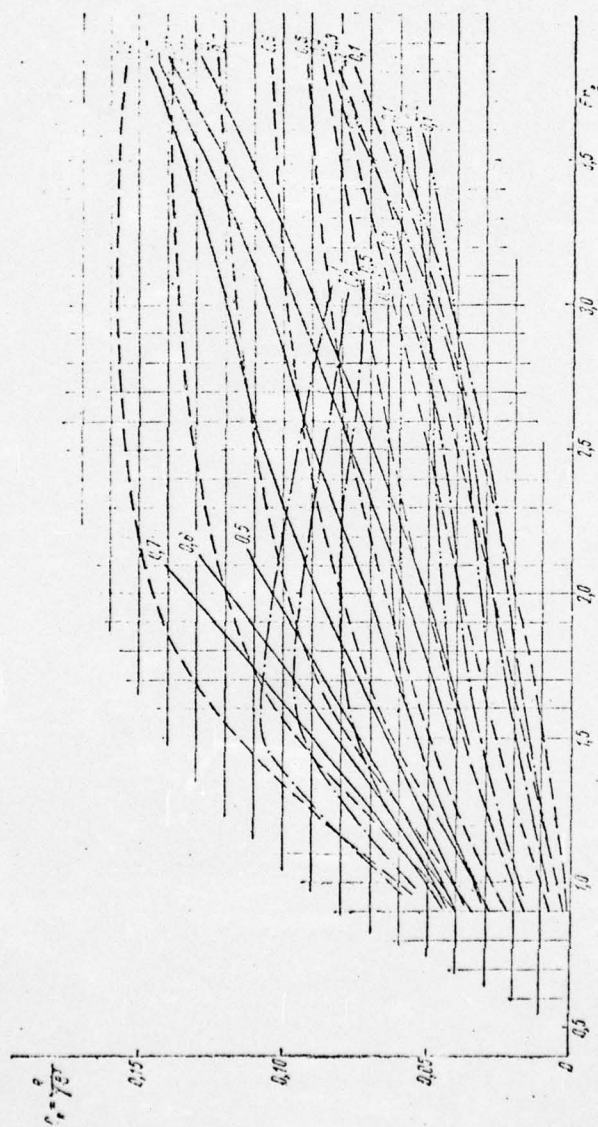


Fig. 150. Diagram of drag coefficient of hull model unloaded.
 — $x_d = 0.5$; - - - $x_d = 0.4$; - · - · - $x_d = 0.3$; - · - · - $x_d = 0.2$.

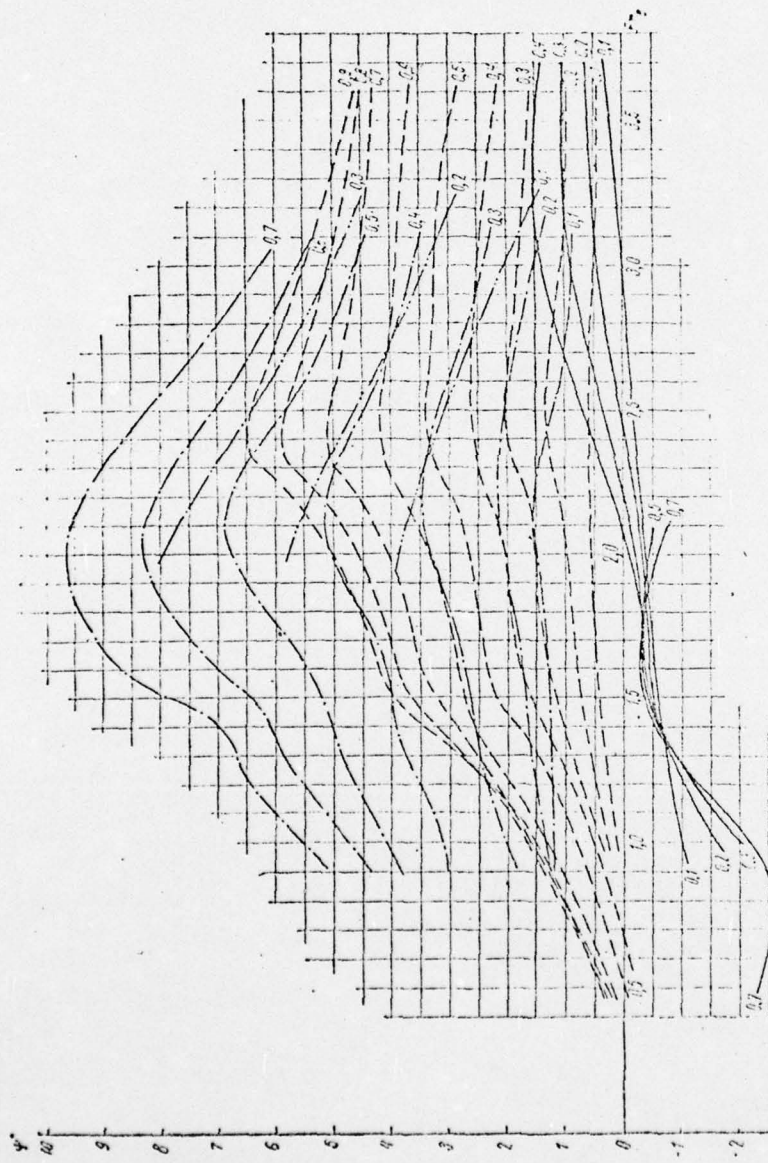


Fig. 151. Diagram of trim angles of hull model.
 — $x_d = 0.5$; - - $x_d = 0.4$; - · - · $x_d = 0.3$; - · - · - $x_d = 0.2$.

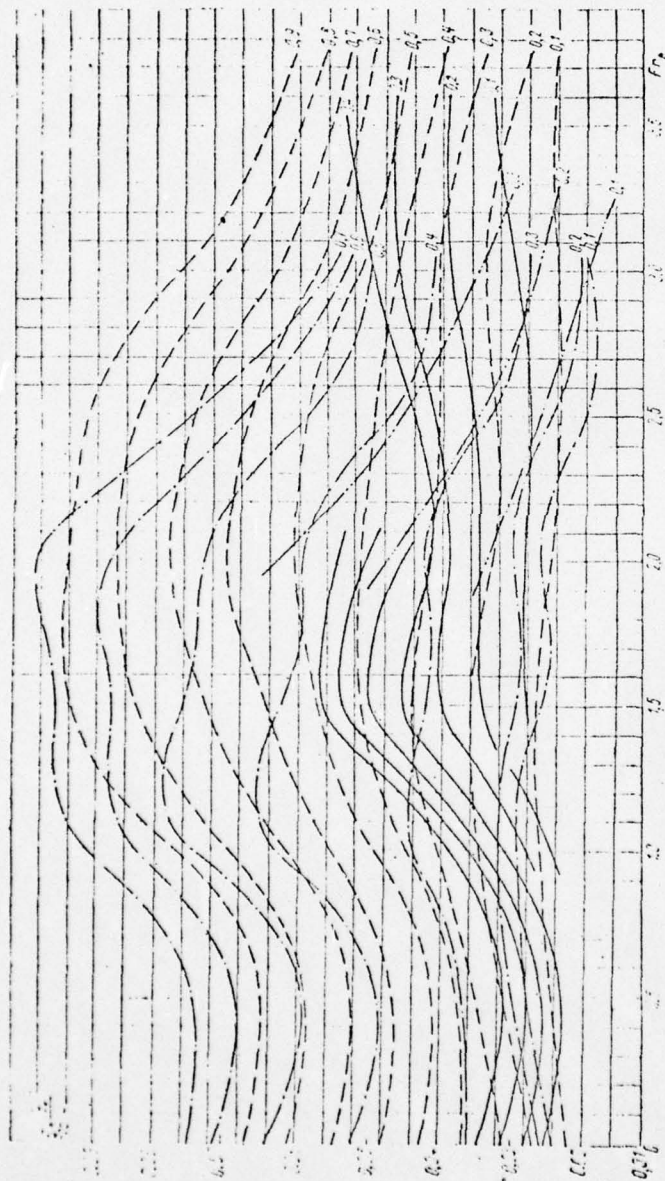


Fig. 152. Diagram of draft of hull model for point on base line at Sta. 20.
 — $x_d = 0.5$; - - $x_d = 0.4$; - · - · $x_d = 0.3$; - · - · - $x_d = 0.2$.

§34. Calculating the attitude of a hydrofoil craft

Since the drag generated on a hydrofoil craft depends on its attitude, the first step in making hydrodynamic calculations must be to calculate attitude.

Attitude is determined by solving a system of equations expressing the condition of equilibrium among the forces acting on a craft during steady, straight-line movement. The shape and geometric dimensions of the hull, foils, and appendages and their mutual arrangement and also the weight and location of the center of gravity are considered to be given.

Fig. 153 shows a diagram of the forces acting on a craft and their coordinates. The equations of equilibrium take the form:

$$\left. \begin{aligned} \sum Y_i &= D - \sum (P_{\phi i} \sin \varphi_i + Q_i \cos \varphi_i), \\ \sum R_i &= \sum X_i - \sum (P_{\phi i} \cos \varphi_i - Q_i \sin \varphi_i), \\ \sum Y_i (\xi_i - \eta_i \psi) + \sum X_i (\xi_i \psi + \eta_i) - \\ &- D (\xi_g - \eta_g \psi) - \sum (P_{\phi i} l_{Pi} + Q_i l_{Qi}), \end{aligned} \right\} \quad \text{[IV.38]}$$

here Y_i is the lift acting on a given element of a craft around which water flows; $R_i = X_i$ the drag on the given element; D the displacement of the craft; $P_{\phi i}$ the thrust (along the axis) of one propulsor; Q_i the transverse force developed by one propulsor; ψ the trim angle of the craft ($\psi > 0$ for trim by the stern); $\phi_i = \gamma_i + \psi$ the angle between the direction of thrust of a propulsor and the direction of movement; γ_i the angle between the direction of thrust of a propulsor and the base line of the craft; ξ_g and η_g the coordinates of the center of gravity of the craft; ξ_i and η_i coordinates of the lift elements of the craft in a system of coordinates oriented on the craft; and l_{Pi} and l_{Qi} are arms of the forces $P_{\phi i}$ and Q_i measured from the origin of the coordinates which is considered to be the moment pole.

[268]

In equation (IV.38) due to the smallness of the trim angle it was assumed that $\sin \psi = \psi$ and $\cos \psi = 1$.

Equation (IV.38) can conveniently be represented in dimensionless form for which purpose all forces are referred to the product of the velocity head and the "main" area (for example of the bowfoil) $\frac{1}{2} \rho v^2 S_1$ and the moments divided by the same product and additionally by the length of the craft $\rho (v^2/2) S_1 L$. Then, in light of what has been stated, the equations of equilibrium assume the form:

$$\left. \begin{aligned} \sum C_{yi} \bar{S}_i &= \frac{D - \sum (P_{qi} \sin \varphi_i + Q_i \cos \varphi_i)}{\frac{\rho v^2 \bar{S}_1}{2}}, \\ \sum C_{xi} \bar{S}_i &= \frac{\sum (P_{qi} \cos \varphi_i - Q_i \sin \varphi_i)}{\frac{\rho v^2 \bar{S}_1}{2}}, \\ \sum C_{yi} \bar{S}_i (\bar{\xi}_i - \bar{\eta}_i \psi) + \sum C_{xi} \bar{S}_i (\bar{\xi}_i \psi + \bar{\eta}_i) &= \\ &= \frac{D (\bar{\xi}_g - \bar{\eta}_g \psi) - \sum (P_{qi} \bar{l}_{pi} + Q_i \bar{l}_{qi})}{\frac{\rho v^2 \bar{S}_1}{2}}, \end{aligned} \right\}$$

where

$$\bar{S}_i = \frac{S_i}{S_1}, \quad \bar{\xi}_i = \frac{\xi_i}{L}, \quad \bar{\eta}_i = \frac{\eta_i}{L}, \quad \bar{l}_i = \frac{l_i}{L}.$$

[269

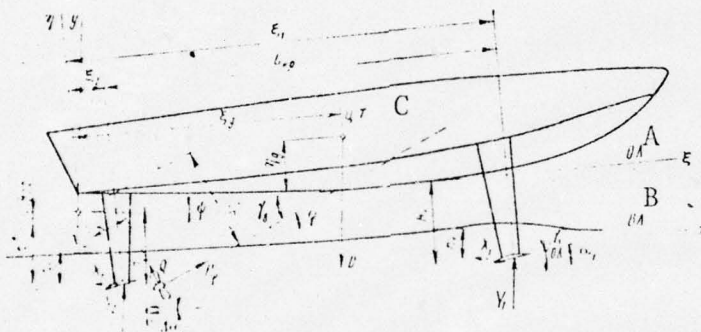


Fig. 153. Diagram of the forces acting on a hydrofoil craft.
KEY: A--base line; B--wave line; C--CG.

The coefficients of dynamic forces C_x and C_y on the left side of equations (IV.39) are functions of depth of immersion and angle of attack. Inasmuch as the location of all parts of the craft with respect to the base line is fixed, the angle of attack and depth of immersion of each of these elements with respect to the undisturbed surface can be expressed by two coordinates defining the location of the base line itself, for example, in terms of the trim angle ψ and draft y_{20} of a point on the base line at Sta. 20. In order to determine the reduction in level and the angle of downwash caused by the bow-foil the speed of movement of the craft must be given.

Thus, the left side of all three equations can be expressed in terms of three variables y_{20} , ψ , and v . In other words, very definite values of hydrodynamic coefficients of elements immersed in the water can be given for every position of the waterline and speed of movement. Since the purpose of solving is to determine the dependence of y_{20} and ψ on v , we will consider the speed to be known and y_{20} and ψ the variables being sought. The three available equations for the system make it possible to find three unknowns depending on the magnitude of v included in them, that is, one more unknown can be introduced, but several unknowns of propulsor thrust and transverse force enter into the right side of the equations

(when there are several propulsors). It is clear that in the general form system of equations (IV.39) has no determinate solution. It has a unique solution when only one (the second) equation of the system is used for matching the forces of thrust and transverse forces developed by all propulsors. Then the remaining two equations will suffice for determining the two unknowns y_{20} and ψ as a function of speed v . In order to realize these conditions the magnitudes of thrust and transverse forces of all propulsors must be expressed in terms of one of the propulsors which is taken as the main one. If the propulsors differ only in the inclination of their axes, the mean angle of inclination must be used and if they differ as to power the thrust ratio must be given.

In the case of n identical propulsors with axes inclined at the same angle and developing the same thrust, it suffices to use a constant ratio at all speeds $Q_i/P_{\phi i} = q = \text{const}$. Then the second equation in (IV.39) will assume the form

$$\sum C_{xi} \bar{S}_i = \frac{n P_{\phi} [\cos(\gamma_n + \psi) - q \sin(\gamma_w + \psi)]}{\frac{\rho v^2 S_1}{2}} \quad (\text{IV.39})$$

After eliminating P_{ϕ} and substituting the expression for [270] it into the remaining equations of system (IV.39), we obtain the following system of two equations not containing P_{ϕ} :

$$\left. \begin{aligned} \sum C_{xi} \bar{S}_i + \sum C_{xi} \bar{S}_i k_1 &= \frac{D}{\frac{\rho v^2 S_1}{2}}, \\ \sum C_{yi} \bar{S}_i (\bar{\xi}_i - \eta_i q) + \sum C_{xi} \bar{S}_i (\bar{\xi}_i \psi + \bar{\eta}_i + k_2) &= \frac{D(\bar{\xi}_g - \bar{\eta}_g \psi)}{\frac{\rho v^2 S_1}{2}}, \end{aligned} \right\} \quad (\text{IV.40})$$

where

$$k_1 = \frac{\lg(\gamma_w + \psi) + q}{1 - q \lg(\gamma_w + \psi)}, \quad \text{and} \quad k_2 = \frac{\bar{l}_p + q \bar{l}_q}{\cos(\gamma_w + \psi) - q \sin(\gamma_w + \psi)}.$$

In that case when there is no interaction among the lift elements of the craft and the effect of interaction can be neglected, solving system of equations (IV.40) doesn't entail any fundamental difficulty although calculations become very cumbersome. It is recommended that the equations be solved graphically. The procedure is as follows.

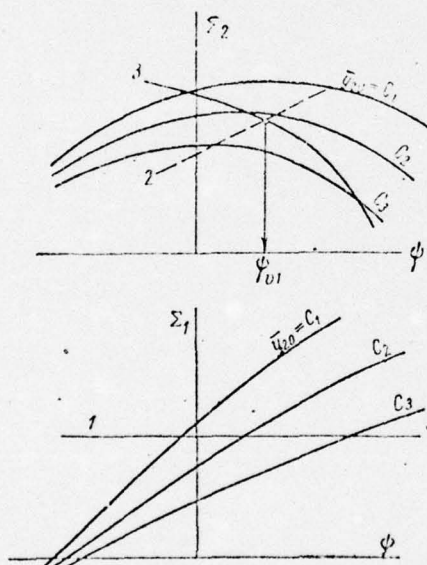
A series of values is given for the draft \bar{y}_{20} and for each draft the left side of the first equation Σ_1 and the second equation Σ_2 (IV.40) are calculated depending on the angle of trim. Each of these relations is drawn on a graph in the form

In order to determine the attitude of the craft at a given speed $v = v_1$, it is necessary to calculate the right side of each equation and enter their dependence on ψ on the graphs of ε_1 and ε_2 respectively (Fig. 154). In this process $D/\frac{\rho v^2 S_1}{2}$

line 1 and the curves of Σ_1 constitute the solution of the first equation in (IV.40) expressing the condition of equilibrium of vertical forces and the intersection of straight line 2 and the curves of Σ_2 gives the solution to the equation of moments.

Fig. 154. Graphical solution to system of equations for craft equilibrium.

- 285 -



ψ coordinates. The intersection of line 2 with curve 3 also yields the sought solution. The procedure described for solving equation (IV.40) can be used for determining the attitude of a craft in the transitional mode.

For the purpose of reducing the volume of calculations it is recommended that the system of equations be simplified, making the assumption that the drag on the craft and the horizontal projection of thrust are completely balanced (not yielding a force couple) and the weight displacement D^* is decreased by a constant value equal to the unloading $\Delta D = \Sigma (P_i \sin \phi_i + Q_i \cos \phi_i)$ and corresponding to the foilborne mode. It is also assumed that $\psi \approx 0$.

After simplifying the equations of equilibrium assume the form:

$$\left. \begin{aligned} \Sigma C_{yi} \bar{S}_i &= \frac{D^*}{\frac{\rho v^2 S_1}{2}}, \\ \Sigma C_{yi} \bar{S}_i \bar{x}_i &= \frac{D^* \bar{x}_g}{\frac{\rho v^2 S_1}{2}}. \end{aligned} \right\} \quad (IV.41)$$

The coefficients of lift entering into systems of equations (IV.40) and (IV.41) and the foil drag are determined by methods set forth in Chap. I and the supporting force and hull drag with unloading taken into account from the experimental diagrams described in the preceding section. When determining the attitude of a craft with tandem foils consideration must be given to the drop in the level of y_0 and the downwash $\Delta \alpha_T$ at the location of the sternfoil.

When making calculations for a tandem system an additional assumption must be made concerning the constancy of the arms of the vertical forces. This makes it possible to consider the loading on each tandem foil to be independent of speed.

The steps in calculating the attitude of a tandem hydrofoil craft moving with its hull above the water are as follows.

1. The methods described in Chap. I are used to make hydrodynamic calculations of the bow- and sternfoils separately. The results are used to draw graphs of the coefficients of lift for the bowfoil $C_{y1} = f_1(\psi, h_1)$ (Fig. 155a) and the sternfoil $C_{y2} = f_2(\psi, h_2)$ (Fig. 155b). It should be remembered that the depth of immersion of a sternfoil is measured not from the horizontal undisturbed surface of the water but from the surface of the wave depression formed by the bowfoil. When progressing from angle of attack to angle of trim consideration is given to the angles at which the foils are set γ_1 and γ_2 [272]

with respect to the base line of the craft and the angle of downwash for the sternfoil $\Delta\alpha_1$. The relation between the craft's angle of trim and the angle of attack of each foil is determined from the equations:

$$\left. \begin{aligned} \alpha_1 &= \psi + \gamma_1, \\ \alpha_2 &= \psi + \gamma_2 - \Delta\alpha_1 = \psi^* + \gamma_2, \end{aligned} \right\} \quad (\text{IV.42})$$

whence

$$\begin{aligned} \psi &= \alpha_1 - \gamma_1, \\ \psi^* &= \alpha_2 - \gamma_2. \end{aligned}$$

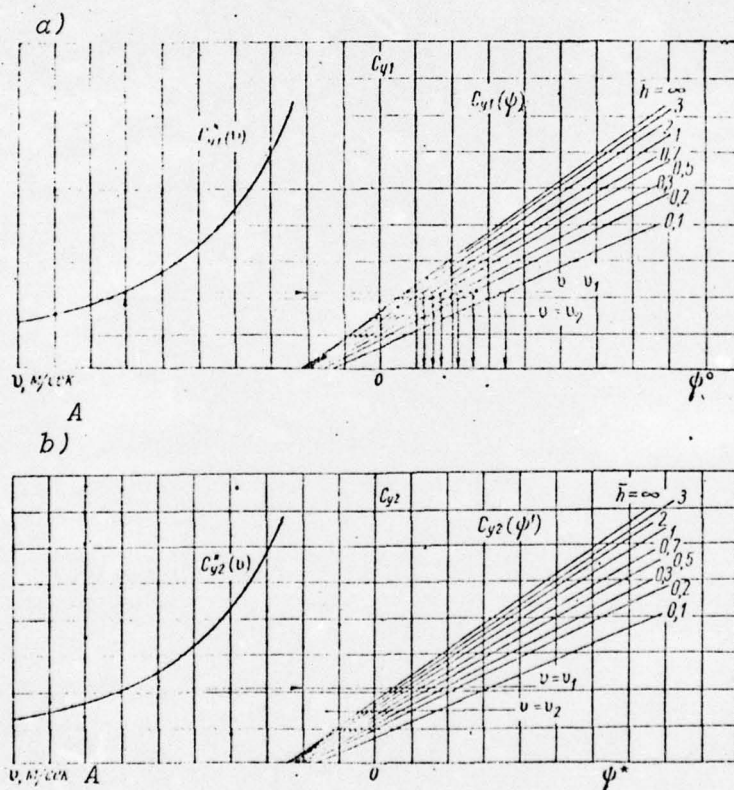


Fig. 155. Graphs of coefficients of lift as a function of \bar{h} and ψ and the required coefficients as a function of speed: a--bowfoil; b--sternfoil. KEY: A-- v , m/sec.

2. The depth of immersion of the sternfoil beneath the level of the undisturbed surface $h_2^* = f(h_1)$ is determined depending on the depth of immersion of the bowfoil, using in the process an expression for the angle of trim of the craft obtained from obvious relations among geometric elements and parameters of attitude.

[273]

$$\psi \approx \lg \psi = \frac{(H_1 - h_1) - (H_2 - h_2 - y_0)}{L_f} = \frac{h_2 - h_1 + y_0 + (H_1 - H_2)}{L_f}$$

or

$$\psi = \frac{(h_2^* - h_1) + (H_1 - H_2)}{L_f}, \quad (\text{IV.43})$$

where L_f is the distance between foils; H_1 and H_2 are the distances of the foils from the base line; and h_1 and h_2 are the actual depths of immersion of the foils.

The following expression for depth of immersion of the sternfoil measured from the level of the undisturbed (horizontal) surface of the water is obtained from (IV.43):

$$h_2^* = h_2 + y_0 = h_1 + \psi L_f + (H_2 - H_1). \quad (\text{IV.44})$$

Relation (IV.44) is drawn graphically in Fig. 156.

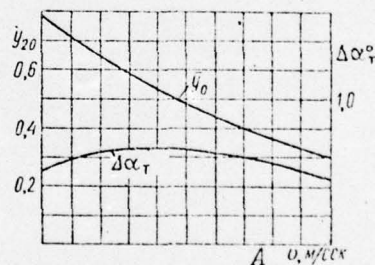
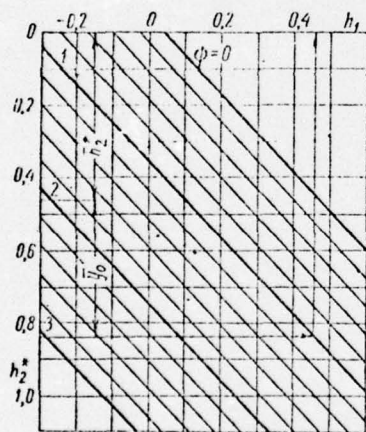


Fig. 156. Graph of $h_1 = f(h_2^*)$. Fig. 157. Graph of ordinates y_{20} and angles of downwash $\Delta\alpha_T$ of a wave profile.
KEY: A - $v/m/sec$.

3. The coefficients of required lift of foils as a function of speed of movement are found as follows:

$$\left. \begin{aligned} C_{y1}^* &= \frac{Y_1}{\rho v^2 S_1} = \frac{mD}{\rho S_1} \cdot \frac{1}{v^2}, \\ C_{y2}^* &= \frac{Y_2}{\rho v^2 S_2} = \frac{(1-m)D}{\rho S_2} \cdot \frac{1}{v^2}, \end{aligned} \right\} \quad (\text{IV.45})$$

where

$$m = -\frac{\xi_2 - \xi_1}{L f} \quad (IV.46)$$

4. The lowering in level $y_{20}(v)$ and downwash $\Delta\alpha_T$ caused by the bowfoil at the location of the sternfoil are determined as a function of speed (Fig. 157). [274]

The parameters $(\alpha/C_{y1})(Fr_1)$ and $(\lambda^*/4)(Fr_1)$ for a bowfoil are found from the formulas in §30.

The values of \bar{C}_{y1} needed for calculating $\bar{\alpha}$ are taken from the graph in Fig. 155.

5. The attitude is determined by means of a graphical solution to the equations of equilibrium for the craft.

The initial data for this are the calculations performed in steps 1--4. These data can conveniently be presented in the form of graphs: $C_{y1}(\psi)$ with the parameter h_1 ; $C_{y2}(\psi^*)$ with the parameter h_2 ; $C_{y1}^*(v)$, $C_{y2}^*(v)$, and $h_2^*(h_1)$ with the parameter ψ and also $y_0(v)$ and $\Delta\alpha_T(v)$ (Figs. 155-158).

Further calculations go as follows.

a) A series of values is given for the speed and for each speed values for C_{y1}^* , C_{y2}^* , and y_0 are taken from the appropriate graphs.

b) In accordance with the values found for C_{y1}^* and C_{y2}^* for each speed, using the graphs for $C_{y1}(\psi)$ and $C_{y2}(\psi)$ relations $h_1 = f_1(\psi)$ when $C_{y1} = \text{const}$ (Fig. 158a) and $h_2 = f_2(\psi)$ when $C_{y2} = \text{const}$ (Fig. 158b) are drawn. When drawing the curve of $h_2(\psi)$ the downwash should be taken into account and the trim determined from the formula $\psi = \psi^* + \Delta\alpha_T$.

c) Using the graph of $h_2^*(h_1)$ and considering the lowering in level from formula $h_2^* = h_2 + y_0$ from the graph of $h_2^*(h_1)$ a determination is made of $h_1(\psi)$ corresponding to the relation $h_2(\psi)$ when $C_{y2} = \text{const}$ as obtained in "b" above and this curve is drawn on the combined graph. In this way two curves for $h_1(\psi)$ are drawn on a common graph (Fig. 158a).

The first of them (see "b" above) expresses the possible combinations of h_1 and ψ at which the required coefficient of lift C_{y1}^* corresponding to the speed under consideration is developed on the bowfoil. The second curve $h_1(\psi)$ obtained as a result of redrawing $h_2(\psi)$ expresses possible combinations of h_1 and ψ at which the required magnitude of C_{y2} is generated on the sternfoil. The intersection of these curves yields a solution to the problem of craft attitude at a given speed since the values of C_{y1}^* and C_{y2}^* required for supporting [275]

the craft are obtained simultaneously.

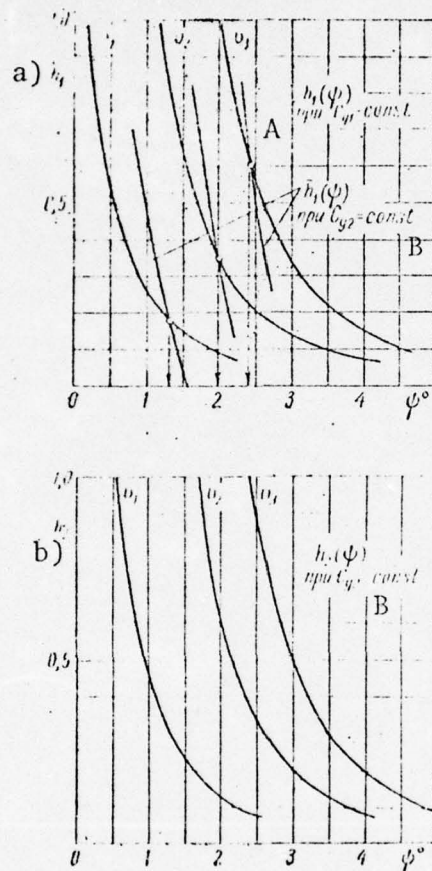


Fig. 158. Graphs of $h_1(\psi)$ and $h_2(\psi)$:
a--for bowfoil; b--for sternfoil.
KEY: A-- $C_{y1} = \text{const}$; B-- $C_{y2} = \text{const}$.

§35. Method of calculating the components of drag on a hydrofoil craft

Calculations of the drag generated on a hydrofoil craft in the main mode of movement yield rather reliable results. Furthermore, for determining the drag on the lift foils themselves determination by calculation is even preferable to scaling the drag from a model to a full-scale craft using the cubic law. In the takeoff mode calculations are much less accurate since the drag on the hull, which constitutes a large part of the overall drag, is calculated based on model tests without taking the scale effect into account when scaling to a full-scale craft.

1. The drag of a foil system is determined as the following

$$R_f = \sum C_{xi} \frac{\rho v^2}{2} S_i + C_{xin} \frac{\rho v^2}{2} S_{st}, \quad (\text{IV.47})$$

where $C_x = C_{xp} + C_{xi} + C_{xw}$ is the coefficient of drag of a separate foil; C_{xp} , C_{xi} , and C_{xw} are the profile, induced and wave drag coefficients respectively; and C_{xin} is the drag coefficient due to the interaction between lift surfaces.

For tandem systems

$$C_{xin} = \Delta C_{xT} = \Delta \alpha_T C_{y2},$$

where $\Delta \alpha_T$ is the downwash caused by the bowfoil of the tandem system.

For a system consisting of three foils (one continuous and one split),

$$C_{xin} \approx 0.$$

Profile drag:

$$C_{xp} = 2\zeta_p \left\{ 1 + \left[(m + 0.5) \frac{\varphi}{k_\phi} - 0.5 \right] C_{ph} \right\},$$

where $\phi(h) = \xi_h / \xi_{h\infty}$ is the coefficient of reduction in pressure drop (on the upper side); $k_\phi = \alpha_h / \alpha_\infty$ is the coefficient of reduction in the derivative of C_y with respect to α close to the free surface; [276]

$$\begin{aligned} m &= 0.5 & \text{when } C_y &= 0.15--0.20; \\ m &= 0.75 & \text{when } C_y &= 0.5--0.6. \end{aligned}$$

Induced drag:

$$C_{xi} = \frac{C_{ph}^2}{\pi \lambda} \zeta (1 + \delta),$$

where $\lambda = \ell^2 / S$ is the aspect ratio of the foil; $\zeta = f(\bar{h} / \lambda)$ is a function taking into account the effect of the free surface on the induced downwash (as determined from the graph in Fig. 19); and δ is an increment allowing for the planform of the foil.

In the case of a complex foil the mean values of aspect ratio and depth of immersion of an equivalent monoplane as calculated from the formulas in Chap. I should be included in the calculations.

Wave drag:

$$C_w = \frac{C_{w0}^2}{2Fr^2} e^{-\frac{2h}{Fr}} \left(1 - \frac{2\pi}{Fr} e^{-\frac{2h}{Fr}} \right).$$

2. The hull drag is

$$R_h = C_R \gamma B^3, \quad (IV.48)$$

where $C_R = f(Fr_B, y_{20}, \psi)$ is determined from experimental diagrams (see Fig. 150); B is the width of the hull; y_{20} and ψ are variables for the draft of the base line at Sta. 20 and the trim angle which are obtained from calculations of attitude.

The diagram of $C_R(Fr_B)$ includes all types of drag on the hull (friction, wave, spray) and is determined from the results of model tests without correction for the scale effect. Consequently, for a full-scale craft C_R is somewhat high.

3. The resistance of appendages is determined as the sum:

$$R_{app} = R_{sh} + R_{br} + R_{st} + R_r. \quad (IV.49)$$

The drag of an inclined propeller shaft is

$$R_{sh} = C_{xsh}(\rho v^2 S_{sh}/2), \quad (IV.50)$$

where $C_{xsh} = 0.2$ and S_{sh} is the area of the projection of the shaft onto the plane of the frame.

The drag on the shaft brackets, foil struts, and rudders is [277] determined from the single-type formula

$$R_{st} = C_{xst}(\rho v^2 S/2), \quad (IV.51)$$

where S is the area of the lateral projection.

The drag coefficient of a foil strut, bracket, or rudder in separation-free flow is

$$C_{xst} = 2k_s \zeta_{pl} + C_{xspray}, \quad (IV.52)$$

In the case of separation in the flow around a wedge-shaped strut

$$C_{xst} = 2k_s \zeta_{pl} + C_{xcav} + C_{xspray}, \quad (IV.53)$$

where ζ_{pl} is the coefficient of friction of a smooth plate and C_{xcav} is a coefficient taking into account the curvature of the

surface, for struts and rudders k_s being 1.1 and for brackets .2;

$$C_{x\alpha v} = \frac{\pi}{8} \bar{c}^2 \left(1 + \frac{\lambda}{Fr_m^2} \right); \quad (IV.54)$$

$$C_{x spr} \approx \frac{0.24 \bar{c}^2}{\lambda}, \quad (IV.55)$$

where $\lambda = h/b$ is the wetted aspect ratio of a strut (rudder or bracket).

The air drag is

$$R_a = C_{xa} (\rho v^2 \Omega / 2), \quad (IV.56)$$

where Ω is the area of the projection of the craft onto the transverse plane and $C_{xa} = 0.5--0.6$.

§36. Methods of determining drag on a hydrofoil craft experimentally

Despite significant progress in creating methods for calculating the drag and attitude of a hydrofoil craft, model tests are still the main means used for developing foil systems and determining drag. When test models of hydrofoil craft are towed the experimental means and methods used are the same as for models of high-speed craft without foils.

Modeling in tow tests involves the Froude number and therefore the load of the model (displacement by weight) is taken to be inversely proportional to the cube of the scale. When $Fr_m = Fr_{fs}$ with an accuracy to the scale effect there is similarity in wave formation and pressure forces, that is, there is agreement in attitude and interaction between foils on model and full-scale craft and also equality between the coefficients of lift and wave and induced drag on the foils. [278]

The coefficient of drag of a model is different from that of a full-scale craft due to lack of sameness in the Reynolds and cavitation numbers. In order to obtain full-scale values for the cavitation numbers a speed close to full-scale must be imparted to the model.

The scale effect in model tests is most significant in regard to friction drag on foils. However, as calculations show, the value of the coefficient of profile drag of hydrodynamically smooth full-scale foils with a negligible error on the safe side can be accepted as the same as those obtained in model tests which must be produced at Reynolds numbers not less than $5 \cdot 10^5$. If the full-scale foils are

If hydrodynamically smooth, a correction must be made for roughness. Accordingly, the scale selected for a model must be based on the need for providing a Reynolds number of $Re \geq 5 \cdot 10^5$. It should be kept in mind that based on the condition of similitude in planing the width of the model's hull should be not less than 0.3 m.

As applicable to the indicated conditions, scaling of drag to full-scale should follow a cubic law approximately. As practice shows, such scaling yields satisfactory results for the foilborne mode but results in a drag inflated by 10--20% at the hump in the $R(v)$ curve.

C. Transverse stability of hydrofoil craft

One of the most important seakeeping characteristics of any craft is its stability. For craft in a displacement mode stability is provided by hydrostatic forces arising as a result of immersing a certain volume of the craft in the water when the craft rolls.

When determining the stability of a craft in the displacement mode the hydrodynamic forces developed on its wetted surface during movement are usually neglected because of their smallness as compared with the hydrostatic forces. Therefore in existing methods of determining stability of craft in a displacement mode speed of movement is neglected.

The picture changes radically for craft moving at great relative speeds. As a craft progresses from the displacement mode through takeoff to the foilborne mode, hydrostatic forces are replaced by hydrodynamic ones, as a consequence of which pressure becomes redistributed over the hull and this in turn affects the stability of the craft. [279]

At low speeds of movement transverse stability is ensured, as was indicated, by the restoring moment of hull volume entering and leaving the water, that is, by hydrostatic forces. In the case of a hydrofoil craft moving at high speeds stability is ensured in the main by the hydrodynamic restoring moment resulting from the effect of the water's free surface on the hydrodynamic characteristics of the lift foils. At intermediate speeds of movement in many cases the hull almost completely leaves the water at a time when the foils are not yet adequately effective. Inasmuch as stability in this mode is not ensured in due measure by any of the factors named above, it is regarded as the most dangerous.

By way of a measure of stability we will take the arbitrary magnitude h which is the ratio between the restoring moment of all hydrodynamic forces M_{res} acting on the craft and the initial displacement D_0 multiplied by the angle of bank θ_k ($h = M_{res}/D_0\theta_k$).

At slow speeds the magnitude of h is nothing other than the metacentric height and therefore at high speeds we will call it the conditional metacentric height in the following discussion.

For convenience in determining the conditional metacentric height we will divide the entire process of build-up in speed from zero to the maximum into three modes. In the first mode which is characterized by constancy in craft displacement the magnitude of h is determined by methods known from ship statics [2].

We will not discuss this mode. The second mode of movement begins at the instant of decrease in the volumetric displacement of the craft due to the developing hydrodynamic forces on the lift surfaces of the craft and ending with complete separation of the hull from the water. It is characterized by combined action of hydrostatic and hydrodynamic forces and therefore we will call it the intermediate mode.

The third mode begins at the instant of complete separation of the hull from the water. All motion of the craft in this mode is due to hydrodynamic forces. A subject for further investigation by the author is determining the stability of a hydrofoil craft in the second and third modes. Initial stability will be discussed since large angles of bank in hydrofoil craft in these modes are impermissible

§37. Hydrodynamic forces, attitude, and drift of a banked hydrofoil craft

[280]

The complexity of the problem at hand does not permit investigating craft stability in the foilborne mode in a nonstationary formulation. Therefore in the following discussion we will view the static problem under the assumption of constancy in the speed of movement of the craft. This condition from the standpoint of stability is in many cases more rigid than in a nonstationary treatment of the problem since in the case of rapid change in speed of movement a craft does not succeed in a brief period of time in deviating significantly from its state of equilibrium in zones of reduced stability.

In the second and third modes of movement, in distinction from the first, stability of a craft must be determined for each value of speed since the position of the craft with respect to the free surface of the water changes with the speed of movement.

In Sect. B of this chapter we considered methods of calculating the attitude of a hydrofoil craft. Assuming the angles of bank to be small, the methods presented above for calculating the attitude can be extended to a banked craft. By applying

[281]

these methods to each particular case we can determine the attitude of a craft for a given constant speed of movement. We will consider as known the relations between craft trim and speed of movement $\phi(v)$ and between the wetted length and the speed of movement $L(v)$ and depth of immersion of the foils $h(v)$.

A banked craft, as a consequence of lack of symmetry in the flow around its lift surfaces, is subjected to drift. In order to determine the drift it is necessary to determine the components of hydrodynamic forces acting on the craft in a horizontal plane and solve jointly the equation for projections of these forces on the G_y axis (Fig. 159) and the equation for moments of the given forces with respect to the vertical axis G_z which passes through the center of gravity of the craft.

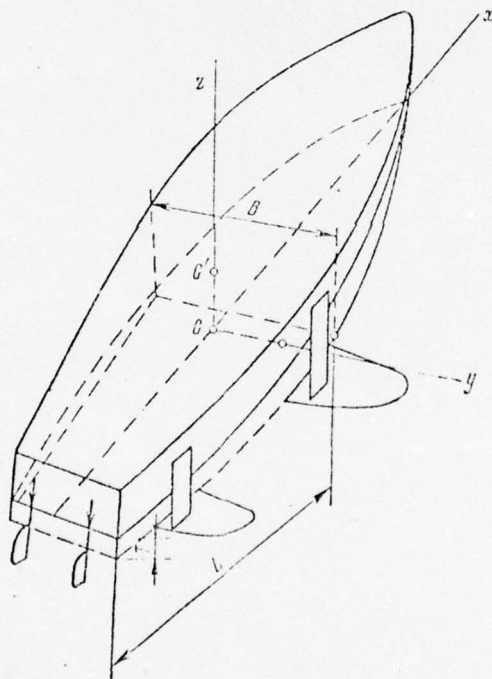


Fig. 159. Notation for coordinate axes.

The equation for the projections of all external forces acting on a craft in the horizontal plane can be written in the following form (Fig. 160):

$$R_h^* + \sum_{k=1}^n R_f^* + \sum_{k=1}^n R_B + \sum_{k=1}^n R_P + R_h = 0, \quad (\text{IV.57})$$

where R_h^* is the hydrodynamic force of drift acting on the immersed portion of the craft's hull; R_f^* the force of drift arising on a banked foil; R_B the hydrodynamic lateral forces

acting on the craft's struts during drift; R_r the force acting on the rudders; and R_h the resistance of the craft's hull to drift.

The magnitudes of the external forces entering into equation (IV.57) are determined as follows:

The force

$$R_h^* = \frac{\partial C_{y\lambda}}{\partial \phi} \psi \frac{\rho u_0^2}{2} BL k_1 k_2 \theta_k, \quad (\text{IV.58})$$

where $\partial C_{y\lambda}/\partial \phi$ is the derivative of the coefficient of lift of the bottom with respect to angle of trim ϕ .

Bearing in mind that approximately $\partial C_{y\lambda}/\partial \phi = \pi$, we can set $\partial C_{y\lambda}/\partial \phi = \pi k_1(\lambda) k_2(\lambda)$, where $k_1(\lambda) = 1.2/(1.2 + \lambda)$; $k_2(\lambda) = 0.7/(1 + 1.4\lambda)$; $\lambda = L/B$, B and L being respectively the width and length of the lift surface of the bottom; and θ_k is the bank angle of the craft.

The forces of drift acting on each lift foil are

$$R_f^* = C_{yk} F(h) \frac{\rho u_0^2}{2} \theta_k. \quad (\text{IV.59})$$

Here C_{yk} is the coefficient of lift of the part of the foil immersed in the water when the flow around the foil is unbounded; $F(h) = f_i(h) S(\phi, h)$ where $f_i(h)$ is a function taking into account the effect of the free surface of the water on the hydrodynamic forces; and S is a function characterizing the change in area of the lift elements of a foil depending on the trim angle of the craft and the depth of immersion.

The struts, which serve to join the foils to the craft, [282 from a hydrodynamical standpoint also constitute foils oriented in a certain way with respect to the free surface. The projection of the hydrodynamic forces acting on the struts onto the Oy axis is

$$R_s = n C_{ys} \frac{\rho u_0^2}{2} S_s, \quad (\text{IV.60})$$

where $C_{ys} = (\partial C_{ys}/\partial \phi) \psi$ and $\partial C_{ys}/\partial \phi$ are found from the results of tests of struts close to the water's surface; ψ the angle of drift; S_s the area of the wetted surface of a strut; and n the number of struts.

The hydrodynamic forces generated on the rudders are [283

$$R_r = m C_{yr} \frac{\rho u_0^2}{2} S_r, \quad (\text{IV.61})$$

where m is the number of rudders; $C_{YR} = (\partial C_{YR} / \partial \beta_R) (\beta_R - \psi)$; the coefficient $\partial C_{YR} / \partial \beta_R$ is found from the results of wind tunnel tests; and β_R is the angle at which the rudders are set.

The approximate value of the force of resistance offered by a side of the craft to drift can be found from the formula

$$R_h \approx \pi \psi \frac{\rho u_0^2}{2} B_0 L k^*, \quad (\text{IV.62})$$

where $B_0 = L\phi/2$; $k^* = 0.7/(1 + 1.4\lambda^*)$; and $\lambda^* = L/B_0 = 2/\phi$.

Substituting the expressions presented above for external forces into equation (IV.57), we transform it to the form

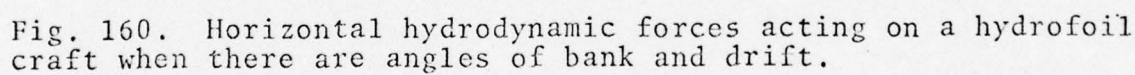
$$\begin{aligned} & \frac{\partial C_{Y\lambda}}{\partial \psi} \psi \frac{\rho u_0^2}{2} L B k_1 k_2 \theta_k + \sum_{k=1}^n C_{Yk} F_k(h) \frac{\rho u_0^2}{2} \theta_k + \\ & + \sum_{p=1}^m \frac{\partial C_{Yp}}{\partial \beta} (\beta_p - \psi) \frac{\rho u_0^2}{2} S_p - \sum_{c=1}^n \frac{\partial C_{Yc}}{\partial \psi} \psi \frac{\rho u_0^2}{2} S_c \\ & - \pi \psi k^* B_0 L \frac{\rho u_0^2}{2} = 0. \end{aligned} \quad (\text{IV.63})$$

The equation for moments of external forces with respect to the Gz axis, the moment being considered positive when it increases the angle of drift, that is, rotates the craft clockwise, is written in the following form:

$$\begin{aligned} & \frac{\partial C_{Y\lambda}}{\partial \psi} \psi L B k_1 k_2 \theta_k \frac{\rho u_0^2}{2} \left(\frac{3}{4} L - x_G \right) - \pi k^* L B_0 \frac{\rho u_0^2}{2} \times \\ & \times \left(\frac{3}{4} L - x_G \right) \psi - \sum_{k=1}^n (-1)^k C_{Yk} F_k(h) l_k \theta_k \frac{\rho u_0^2}{2} + \\ & + \sum_{c=1}^n (-1)^c \frac{\partial C_{Yc}}{\partial \psi} S_c l_c \frac{\rho u_0^2}{2} \psi - \sum_{p=1}^m \frac{\partial C_{Yp}}{\partial \beta} S_p l_p (\beta_p - \psi) \frac{\rho u_0^2}{2} = 0, \end{aligned} \quad (\text{IV.64})$$

where x_G is the distance from the craft's center of gravity to the transom. The meaning of all other symbols is clear from Fig. 160.

According to the directions of forces shown in Fig. 160 the bowfoils and stern struts create positive moments and the sternfoil, bow struts, and rudders negative moments.


$$\psi_0 = \frac{\sum_{k=1}^n C_{pK} F_K(\eta, h) [(I_p - (-1)^K I_K)] + \frac{3}{4} \left(\frac{\partial C_{pK}}{\partial \rho} \right) \eta L^2 B k_1 k_2}{\sum_{s=1}^n \frac{\partial C_{qs}}{\partial \psi} S_s [(I_p - (-1)^s I_s)] + \frac{3}{4} \pi k^* L^2 B_0}, \quad (\text{IV.65})$$

- 299 -

In equations (IV.65) and (IV.66)

$$\beta_0 = \beta_r / \theta_k \text{ and } \psi_0 = \psi / \theta_k. \quad (\text{IV.67})$$

When the lift elements of a craft are known it is possible to use these formulas to establish the angle of drift of a craft ψ and the angle at which the rudder is set β_r for straight ahead movement of the craft at a bank angle of θ_k .

§38. Determination of restoring moment and conditional metacentric height of a hydrofoil craft

The relations obtained above make it possible to proceed to a determination of craft stability, that is, to a determination of the restoring moment when a craft banks at a given angle at a constant speed. For this purpose we will consider the moments of each of the effective forces with respect to the longitudinal axis Gx passing through the center of gravity (Fig. 161).

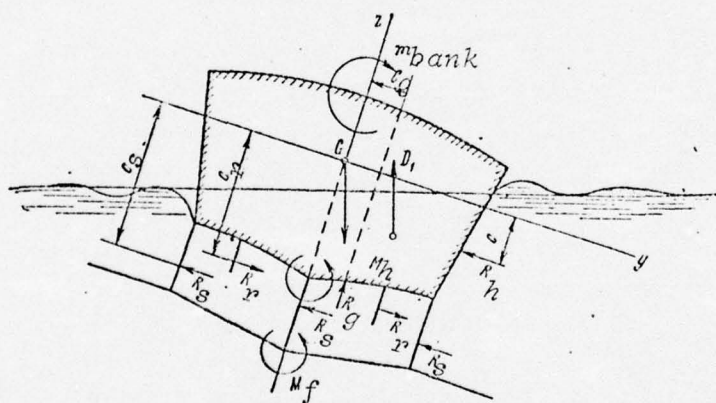


Fig. 161. Moments of external forces acting in the midframe plane of a banked hydrofoil craft.

The restoring moment of hydrostatic forces M_D , which provides for craft stability at low speeds in the first mode of movement, is determined from the well-known formula from ship statics [2]

$$M_D = D_1 h_1 \theta_k, \quad (\text{IV.68})$$

where D_1 is the displacement corresponding to the attitude of the craft at a given speed of movement and h_1 is the transverse metacentric height corresponding to displacement D_1 .

The metacentric height h_1 is found from the formula [2] [285]

$$h_1 = \rho - \alpha = \frac{I_x}{V_1} - (z_G - z_C), \quad (\text{IV.69})$$

where ρ is the metacentric radius; I_x the moment of inertia of the waterline area with respect to the longitudinal axis; V_1 the volume of that part of the hull immersed in the water; and $\alpha = (z_G - z_C)$ is the rise of the center of gravity above the center of buoyancy.

Parameters I_x , V_1 , and z_G in formula (IV.69) are found from ship statics for each speed of movement in the first and second modes of movement.

The following approximate formula can be recommended for a preliminary evaluation of h_1 :

$$h_1 \approx \frac{B^2}{6L_{\psi}} - \left(z_G - \frac{1}{3} L_{\psi} \right). \quad (\text{IV.70})$$

As the speed of craft movement increases in the second mode of movement the magnitudes of I_x and V_1 in formula (IV.69) decrease. In the process displacement V_1 decreases much more rapidly than the moment of inertia of the waterline area I_x , as a consequence of which the metacentric height h_1 increases with an increase in speed of craft movement. The magnitude of the restoring moment M_D decreases with an increase in speed of movement. Therefore the metacentric height h_1 cannot be used in this mode of movement to characterize even that part of the stability of a hydrofoil craft which is provided by hydrostatic forces. The coefficient of stability (D_{ih}) serves as such a characteristic in this particular mode.

In the third mode of movement the magnitude of the restoring moment M_D can be neglected.

The moment acting on the hull of a craft due to hydrodynamic forces R_h^* and R_h can be written in the following form: [286]

$$\begin{aligned} M_h &= R_h^* \cdot c_g + R_h \cdot c_s = \\ &= \frac{\partial C_{y2}}{\partial \psi} \psi \frac{\rho u_0^2}{2} B L k_1 k_2 \eta_c c_g - \pi \psi \frac{\rho u_0^2}{2} B_0 L k^* c_s, \end{aligned} \quad (\text{IV.71})$$

where c_g and c_s are respectively the arms of the hydrodynamic forces developing on the bottom and side of a banked craft, and $c_g = z_G$, $c_s = z_G - L\phi/4$.

The moment due to the effective forces on the struts is

$$M_s = \sum_{i=1}^n \frac{\partial C_{y3}}{\partial \psi} \psi \frac{\rho u_0^2}{2} S_s c_s, \quad (\text{IV.72})$$

where $c_s = z_G + (H_0 - h_s/2)$ are the arms of application of the resultant external forces on the struts (Fig. 162). Here h_s is the depth of immersion of a foil. If $h_s > H_0$, the second term in the last formula should be set equal to $H_0/2$.

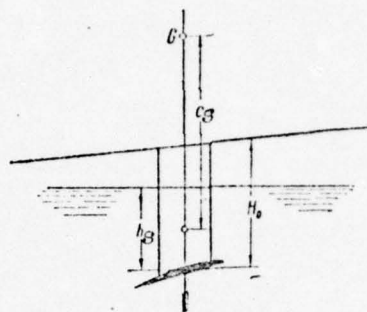


Fig. 162. Approximate location of point of application of hydrodynamic forces acting on the strut of a hydrofoil during drift.

The moment due to the forces acting on the rudders with respect to longitudinal axis Gx are (see Fig. 159):

$$M_r = \sum_{p=1}^n \frac{\partial C_{xp}}{\partial \beta_p} (\beta_p - \varphi) \frac{\rho u_0^2}{2} S_p c_p, \quad (IV.73)$$

where $c_p = z_G + l_p/2$ (l_p is the distance from the base line to the center of pressure on the rudder).

The total restoring moment of the hydrofoils is written in the form

$$M_k = \sum_{k=1}^n \frac{\partial C_{mk}}{\partial \theta_k} \theta_k \frac{\rho u_0^2}{2} S_k L_k, \quad (IV.74)$$

where L_k is the foil span.

The derivative of the coefficient of restoring moment of a foil with respect to the angle of bank $\partial C_{mk}/\partial \theta_k$ must be determined from experimental data. The approximate formula (II.178) -- (II.179) can be recommended as a first approximation for the coefficient of restoring moment of flat foils.

The algebraic sum of all the listed moments constitutes the restoring moment due to the action of the entire complex of lift surfaces, the magnitude of which is

$$M = M_D + M_h + M_s + M_p + M_k. \quad (IV.75)$$

Substituting the value of each moment into the last

[287

expression, we obtain

$$\begin{aligned}
 M = & D_1 h_1 \theta_k + \frac{\partial C_{y\lambda}}{\partial \psi} \varphi \frac{\rho u_0^2}{2} L B k_1 k_2 \theta_k z_G - \pi \psi \frac{\rho u_0^2}{2} B_0 L k^* \psi c_s - \\
 & - \sum_{c=1}^n \frac{\partial C_{y_{cs}}}{\partial \psi} \psi \frac{\rho u_0^2}{2} S_s c_s + \sum_{p=1}^n \frac{\partial C_{y_{pr}}}{\partial \beta} (\beta_r - \psi) \frac{\rho u_0^2}{2} S_r c_r + \\
 & + \sum_{k=1}^n \frac{\partial C_{mk}}{\partial \theta_k} \cdot \frac{\rho u_0^2}{2} S_k L_k \theta_k.
 \end{aligned} \quad (IV.76)$$

Representing moment M in the form $M = D_0 h \theta_k$, we obtain for the arm of the restoring moment--the conditional metacentric height--the following formula:

$$\begin{aligned}
 h = & h_1 \frac{D_1}{D_0} + \frac{1}{D_0} \left[\sum_{k=1}^n \frac{\partial C_{mk}}{\partial \theta_k} \cdot \frac{\rho u_0^2}{2} S_k L_k + \frac{\partial C_{y\lambda}}{\partial \psi} \varphi \frac{\rho u_0^2}{2} \times \right. \\
 & \times L B k_1 k_2 z_G + \sum_{p=1}^n \frac{\partial C_{y_{pr}}}{\partial \beta} (\beta_r - \psi_0) \frac{\rho u_0^2}{2} S_r c_r - \\
 & \left. - \sum_{c=1}^n \frac{\partial C_{y_{cs}}}{\partial \psi} \psi_0 \frac{\rho u_0^2}{2} S_s c_s - \pi \psi_0 \frac{\rho u_0^2}{2} B_0 L k^* c_s \right] \\
 & h = h_1 \frac{D_1}{D_0} + \frac{1}{D_0} \left(\sum_{k=1}^n \frac{\partial C_{mk}}{\partial \theta_k} S_k L_k \right) \frac{\rho u_0^2}{2} K,
 \end{aligned} \quad (IV.77)$$

or

where

$$\begin{aligned}
 K = & 1 + \frac{\frac{\partial C_{y\lambda}}{\partial \psi} \varphi L B k_1 k_2 z_G}{\sum_{k=1}^n \frac{\partial C_{mk}}{\partial \theta_k} S_k L_k} + \frac{\sum_{p=1}^n \frac{\partial C_{y_{pr}}}{\partial \beta} S_r c_r}{\sum_{k=1}^n \frac{\partial C_{mk}}{\partial \theta_k} S_k L_k} (\beta_0 - \psi_0) - \\
 & - \frac{\sum_{c=1}^n \frac{\partial C_{y_{cs}}}{\partial \psi} S_s c_s}{\sum_{k=1}^n \frac{\partial C_{mk}}{\partial \theta_k} S_k L_k} \psi_0 - \frac{\pi B_0 L k^* c_s}{\sum_{k=1}^n \frac{\partial C_{mk}}{\partial \theta_k} S_k L_k} \psi_0.
 \end{aligned} \quad (IV.78)$$

Formula (IV.77) makes it possible to determine the conditional metacentric height depending on the speed of craft movement and the hydrodynamic characteristics of the elements of its lift surfaces.

An analysis of (IV.77) shows that at a speed of movement of $u_0 = 0$ or close to it, that is, in the first mode of movement, stability of the craft is ensured by hydrostatic forces and the conditional metacentric height is equal to the meta-

centric height of the craft

$$h = h_1 \quad \text{when} \quad D_1 = D_0. \quad (\text{IV.79})$$

In the third mode of movement $D_1 \rightarrow 0$ and therefore the conditional metacentric height is determined by only the second term in formula (IV.77), that is, [288

$$h = \frac{1}{D_0} \cdot \frac{\rho u_0^2}{2} K \sum_{k=1}^n \frac{\partial C_{mk}}{\partial \beta_k} S_k L_k. \quad (\text{IV.80})$$

It follows from (IV.77) and (IV.78) that the total moment due to the above listed forces can be positive, equal to zero, and even negative, that is, banking. Usually, as calculations show, function $h(v)$, or the stability of a hydrofoil craft, has a clearly expressed minimum at intermediate speeds of movement. After a craft has risen on its foils its stability increases abruptly. In some cases the curve of $h(v)$ has several extrema.

The existence of a zone with minimum stability is undoubtedly a disadvantage. However, if this zone is small and its boundaries known ahead of time, it is always possible to control a craft in the takeoff mode so as to maintain stability.

The formulas presented above make it possible to evaluate the effect of separate elements of a craft on its initial stability and also to clarify the interrelations among all the lifting surfaces as a kind of hydrodynamic complex.

§39. Problems in standardizing the stability of a hydrofoil craft. Results of calculations and experiments

As with any floating structure a hydrofoil craft, depending on its type and purpose, must satisfy the requirements of stability when afloat. As is known, the initial metacentric height and, in the case of large angles of bank, the diagrams of static and dynamic stability, serve as a measure of stability in any given mode. When a craft moves in the takeoff or foilborne mode only small inclinations in a transverse plane are possible, that is, banks of not more than $5-10^\circ$, since larger deviations of the craft from a state of equilibrium are dangerous at such high speeds of movement. In this connection it is advisable to consider only the initial stability in these modes of movement.

The best way in this case would be to investigate the dynamic stability of hydrofoil craft in a transverse plane. However, the formulation and solution of this problem in

view of its complexity which is due to the absence of standard shapes for foil systems and also to the absence of the necessary hydrodynamic characteristics of craft hulls and devices, entail great difficulty. For this reason it is necessary to resort to a static formulation of the problem using the formulas [290] presented in the preceding sections.

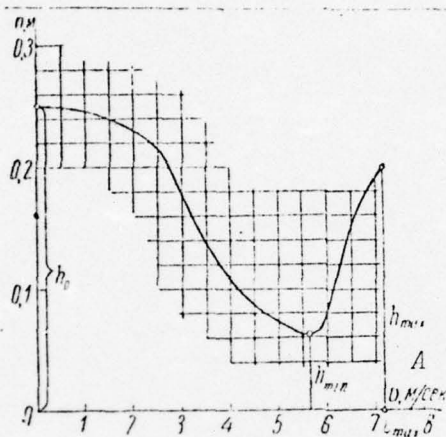


Fig. 163. Main characteristic points on a curve of conditional metacentric height plotted against speed of craft movement.
KEY: A-- v , m/sec.

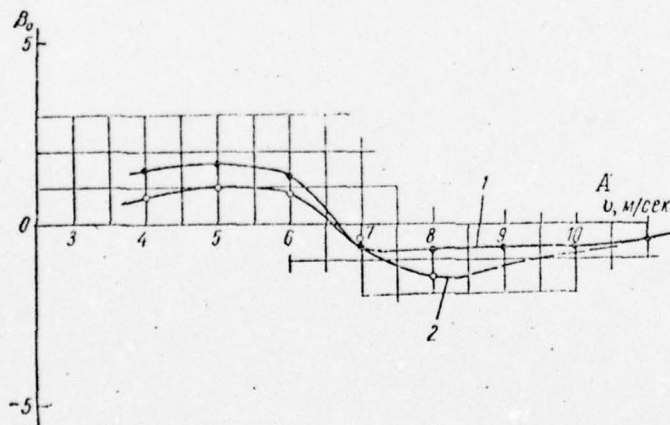


Fig. 164. Relation between angle at which rudders of a hydrofoil craft are set and speed of movement.
1--calculated; 2--experiment.
KEY: A-- v , m/sec.

In standardizing the transverse stability of hydrofoil craft it seems hardly advisable to give all values of the function $h = h(v)$ in the form of a certain limiting curve (Fig. 163).

Apparently it would be better (as is done in statics for large angles of inclination) to standardize individual points which are most characteristic of the function of interest. Among such points in this case are the values of the initial metacentric height h_0 , speeds at which the function $h = h(v)$ reflects minima, the value of conditional metacentric height h_{\min} , and also the value of this magnitude at the maximum speed of movement of a hydrofoil craft (Fig. 163). For an evaluation of the static stability the indicated magnitudes yield a sufficiently complete idea.

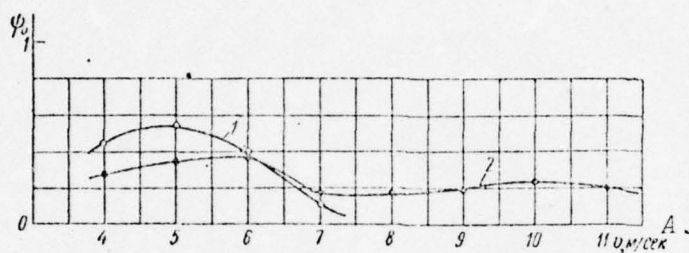


Fig. 165. Relation between angle of drift of hydrofoil craft and speed of movement.

1--calculated; 2--experiment.

KEY: A-- v , m/sec.

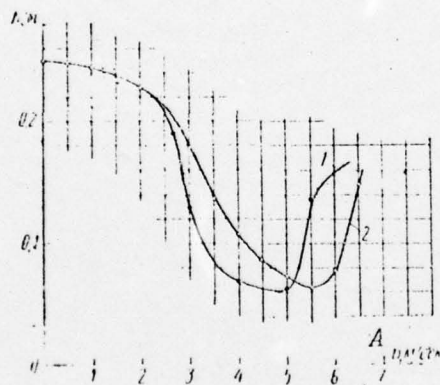


Fig. 166. Conditional metacentric height h as a function of the speed of movement of a hydrofoil craft.

1--calculated; 2--experiment.

KEY: A-- v , m/sec.

Fitting the cited magnitudes into a system will make it possible in the future to introduce standardization in the transverse stability of hydrofoil craft.

For the purpose of illustrating the main relations obtained with the formulas presented above which characterize the transverse stability of a hydrofoil craft and of comparing data from

Calculations with those from experiments Figs. 164--166 show respectively calculated and experimental values for the functions $\beta_0(v)$; $\psi_0(v)$; and $h(v)$. A comparison of calculated and experimental data reveals satisfactory agreement.

D. Translational and rotational motion of hydrofoil craft in an irregular seaway

§40. Investigation into statistical characteristics of translational and rotational motion of hydrofoil craft

Until recently in theoretical investigations and model tests of the seakeeping characteristics of hydrofoil craft an actual seastate was replaced with a regular seaway which amounted to a system of progressive sinusoidal waves of constant period and [291] amplitude. However, in order to make an objective evaluation of the seakeeping characteristics of hydrofoil craft under actual conditions it is necessary to study their behavior and analyze their parameters of movement in an irregular seaway.

In view of the random nature of a seaway the resulting processes which affect a craft (change in hydrodynamic forces acting on foils, translational and rotational motion, stresses in hull members, etc.) studying them and arriving at a quantitative evaluation must be based on probability methods.

In works [10], [11], [12], [14], [16], and [17] probability methods are extensively used to investigate and calculate the characteristics of a seaway and the rotational and translational motion of displacement craft.

During the past few years, thanks to the accumulation and analysis of experimental data from full-scale tests of hydrofoil craft in a seaway, investigations have been made into the characteristics of irregular motion of these craft which make it possible to establish several important results in this area.

The main approaches followed in investigating the motion of hydrofoil craft in an irregular seaway amount to studying the statistical, correlation, and spectral characteristics of various kinds of rotational and translational motion and also establishing the nature of their interaction.

The statistical properties of processes of translational and rotational motion are described completely by laws governing the distribution of the main parameters--wave ordinates, amplitudes, and periods--and are established by analyzing data from statistical processing. The degree of relation among the oscillations of a craft during translational and rotational

tion at various instant of time is described by autocorrelation functions of the motion.

The physical properties of translational and rotational motion which are determined by the distribution of energy of oscillations by frequency are characterized by energy spectra of motion and can be found by the method of spectral analysis.

The mutual correlation functions and mutual spectral densities which are also determined from recordings of translational and rotational motion are the main characteristics of correlation among the various types of motion in an irregular seaway.

Below we set forth the main results of investigation of statistical, correlation, and spectral characteristics of translational and rotational motion of craft on fixed (not controllable) hydrofoils.

1. A statistical analysis of translational and rotational motion of several craft with fixed hydrofoils showed that during movement of the craft in the foilborne mode in a seaway of moderate intensity (sea state of 3--5) the distribution of angles of rolling and pitching and ordinates of heaving are satisfactorily described by a normal gaussian law. Based on the condition of normalcy of the processes of these motions it has been established that pitching occurs with respect to a position determined by the underway trim of the craft in calm water.

[292

The law governing distribution of amplitudes of oscillations of a craft is an important probability characteristic of translational and rotational motion of hydrofoil craft.

In describing the statistical distribution of the amplitudes of translational and rotational motion of displacement craft as well as of hydrofoil craft the law which has been most widely used up to the present time is the Rayleigh law, the probability density of which is expressed by (IV.81) and the likelihood function by (IV.82):

$$f(H) = \frac{H}{4D_x} e^{-\frac{H^2}{8D_x}}; \quad (IV.81)$$

$$P(H) = e^{-\frac{H^2}{8D_x}}, \quad (IV.82)$$

where D_x is the variance of the process and H the amplitude of oscillations. This law holds for processes with the narrowest possible spectrum ($0 \leq \epsilon \leq 0.4$). However, as A. I. Voznesenskiy

has showed, the use of the Rayleigh law for describing the distribution of amplitudes of translational and rotational motion of displacement craft leads in many cases to significant deviation on the unsafe side. Therefore, it has been proposed that use be made of a more universal, general law governing the distribution which takes into account the width of the spectrum of processes. This general law is characterized by a probability density of

$$f(x) = n \left[\Gamma \left(1 + \frac{1}{n} \right) \right]^n \frac{x^{n-1}}{x^n} e^{-\left[\Gamma \left(1 + \frac{1}{n} \right) \right]^n \left(\frac{x}{x} \right)^n}; \quad (\text{IV.83})$$

and a likelihood function of

$$P(x) = e^{-\left[\Gamma \left(1 + \frac{1}{n} \right) \right]^n \left(\frac{x}{x} \right)^n} \quad (\text{IV.84})$$

and has two independent parameters, a mean value for the random magnitude \bar{x} and a parameter n reflecting the effect of spectrum width.

The results of statistical analysis of data from full-scale tests show that deviations in the distribution of amplitudes of translational and rotational motion from the Rayleigh law are observed also in the motion of hydrofoil craft. Since the motion processes of hydrofoil craft have a relatively wide spectrum ($0.4 \leq \epsilon \leq 0.9$) such deviations from the Rayleigh law should be expected.

A comparison of empirical distributions of the amplitudes of translational and rotational motion of hydrofoil craft with theoretical relations for probability density (IV.81) and (IV.82) shows that when the mentioned general law is applied to processes having very many "secondary" oscillations (that is, processes with a wide spectrum) better agreement is achieved with experimental data than when the Rayleigh law is applied. At the same time it should be noted that in order to identify exactly the limits of application of the Rayleigh law more experimental data for statistical investigation of translational and rotational motion of hydrofoil craft must be gathered.

The above noted properties of statistical distributions of translational and rotational motion of hydrofoil craft justify applying the theory of normal random functions to these processes and also using relations established during investigation of translational and rotational motion of displacement craft.

2. On the basis of a calculated verification performed

for numerous recordings of translational and rotational motion of hydrofoil craft it was established that when a craft moves in the foilborne mode at constant speed under unchanging (or slightly changing) conditions of wave formation this motion can be viewed as a stationary and ergodic function of time. It is thus possible to analyze this motion based on separate recordings of sufficient duration with the help of the mathematical apparatus of that part of random theory which has been most fully developed--correlation theory.

Within the framework of correlation theory a stationary and normal random process $x(t)$, as is known, is completely described statistically by mathematical expectation \bar{x} and a correlation function $R_x(\tau)$ which in this case does not depend on the selection of specific instants of time t_1 and t_2 at which the ordinates of the process are read but is only a function of their difference, $\tau = t_2 - t_1$.

Determination of the mean value and correlation function of the process of motion for a given run of duration T is accomplished using the known relations:

$$\bar{x} \approx \frac{1}{T} \int_0^T x(t) dt, \quad (\text{IV.85})$$

$$R_x(\tau) \approx \frac{1}{T-\tau} \int_0^{T-\tau} x(t)x(t+\tau) dt. \quad (\text{IV.86})$$

The correlation function of a stationary random process describes the probability tie between the ordinates of the process taken at different instants of time. The main parameters of a correlation function are:

a) the value of $R_x(0)$ when $\tau = 0$ representing the maximum value of the function and numerically equal to the variance of the process D_x ;

b) the time of correlation τ_k during which the correlation function becomes damped; with an increase in τ the probability tie between the ordinates of the process weakens and when $\tau > \tau_k$ the ordinates of the process are uncorrelated;

c) coefficients α and β describing respectively the degree of damping and the mean frequency of the correlation function.

As a result of an analysis of correlation functions calculated from recordings of translational and rotational motion it has been established that the motion processes of craft with fixed hydrofoils, as compared with displacement craft, are characterized by a much weaker correlation tie among ordinates as evidenced by the short time of correlation 5--20 sec for hydrofoil craft as compared with 20--60 for

ordinary craft).

With a decrease in speed of movement and also transition from a head seaway to a following one, the mean frequency of correlation function β and its coefficient of damping α decrease and the time of correlation τ_k increases. Consequently, movement in a following seaway is characterized by a stronger correlation tie among the ordinates of translational and rotational motion. If parameters α and β are known, the correlation functions of the processes of translational and rotational motion can be satisfactorily approximated by exponential-cosine relations of the type:

$$\left. \begin{aligned} R(\tau) &= e^{-\alpha|\tau|} \cos \beta\tau, \\ R(\tau) &= e^{-\alpha|\tau|} \left(\cos \beta\tau + \frac{\alpha}{\beta} \sin \beta|\tau| \right), \\ R(\tau) &= e^{-\alpha|\tau|} \left(\cos \beta\tau - \frac{\alpha\beta}{2\alpha^2 + \beta^2} \sin \beta|\tau| \right). \end{aligned} \right\} \quad (\text{IV.87})$$

Examples of experimental correlation functions approximated by relations (IV.87) are shown in Fig. 167.

3. The spectral density $S_x(\sigma)$ of the process $x(t)$ can be determined using a Fourier cosine transform based on the correlation function of a stationary random process:

$$S_x(\sigma) = \frac{2}{\pi} \int_0^{\infty} R_x(\tau) \cos \sigma\tau d\tau. \quad (\text{IV.88})$$

The first three even spectral moments are important numerical characteristics of a random process:

$$m_k = \int_0^{\infty} \sigma^k S_x(\sigma) d\sigma, \quad k = 0; 2; 4, \quad (\text{IV.89})$$

using which a determination can be made of the frequency of zeroes $\bar{\sigma}$ and maxima $\bar{\sigma}'$ in the process:

$$\bar{\sigma} = \sqrt{\frac{m_2}{m_0}}, \quad \bar{\sigma}' = \sqrt{\frac{m_4}{m_2}} \quad (\text{IV.90})$$

and the width of the spectrum of the process:

$$\Delta = \sqrt{1 - \frac{m_2^2}{m_0 m_4}}. \quad (\text{IV.91})$$

Functions of spectral density $S_x(\sigma)$, or energy spectra,

characterize the distribution of energy of translational and rotational motion based on the frequencies of separate components of a process. The shape of a spectrum of motion, [296] its length along the frequency axis, and the number and location of the maxima are determined by type and mutual arrangement as to frequency of the seaway spectrum and the amplitude-frequency characteristic of the craft and depend on the craft's speed and direction of movement. With transition from a head seaway to a following one the maximum ordinates of all types of translational and rotational motion increase greatly and shift to the zone of lower frequencies. This situation is clearly illustrated for the process of pitching in Fig. 168.

With an increase in speed of movement there is a shift in the maxima of motion spectra in the direction of the higher frequencies which is related to the increase in frequency of disturbances during movement in a seaway (Fig. 169) and the maximum ordinates of the spectra decrease. According to the relation [298]

$$D_x = \int_0^{\infty} S_x(\sigma) d\sigma, \quad (\text{IV.92})$$

the variance of the process D_x is numerically equal to the area delimited by the graph of the spectrum. As an analysis of spectra has showed the variances (and consequently the amplitudes) of pitching and heaving reach maximum values in a following seaway and the maximum variances of rolling occur when moving beam to the sea. These conclusions, which were obtained from spectral analysis data, are completely confirmed by the results of statistical processing.

V. A. Abramovskiy and Yu. K. Usachev calculated values for the width of a spectrum over a wide range of modes of craft movement in a sea state of 3 or 4 for numerous recordings of processes of translational and rotational motion of several Soviet hydrofoil craft. As a result of their calculations they established that the width of the spectrum for all types of motion varies over rather wide limits, namely:

$$0.4 \leq \epsilon \leq 0.9.$$

The observed values of width of spectrum exceed $\epsilon = 0.4$ with a probability of 97%, the most probable values falling within the limits $0.6 \leq \epsilon \leq 0.8$.

On the basis of the same experimental data the following tendencies for parameter ϵ to vary depending on speed (Fr_D) and the direction of craft movement can be noted:

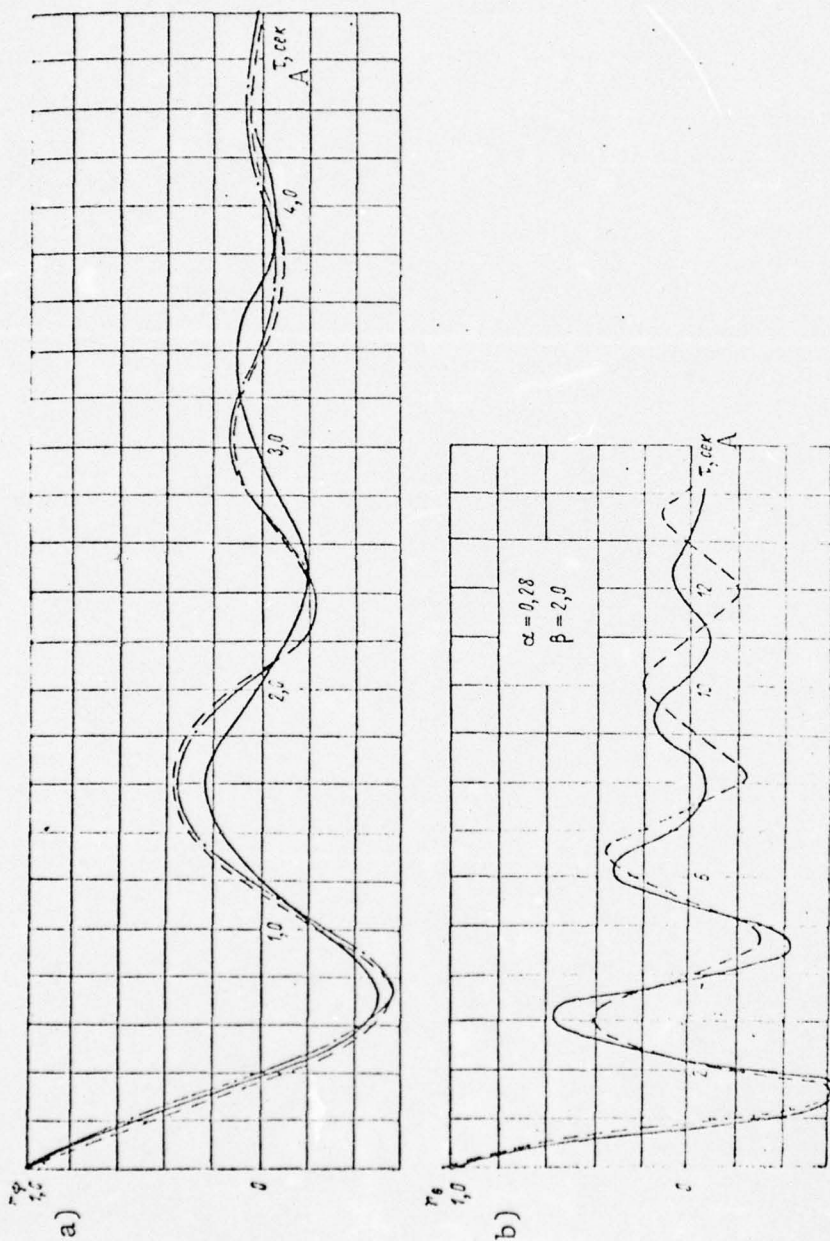


Fig. 167. Approximation of experimental correlation functions:
a-pitching, $\alpha = 0.87$; $\beta = 3.14$; b-rolling, $\alpha = 0.28$, $\beta = 2$.
— experiment; - - $\cos \beta t \cdot e$; - . . . $e^{-\alpha \beta} (\cos \beta t + \sin \alpha / \beta)$.
KEY: A— τ , sec.

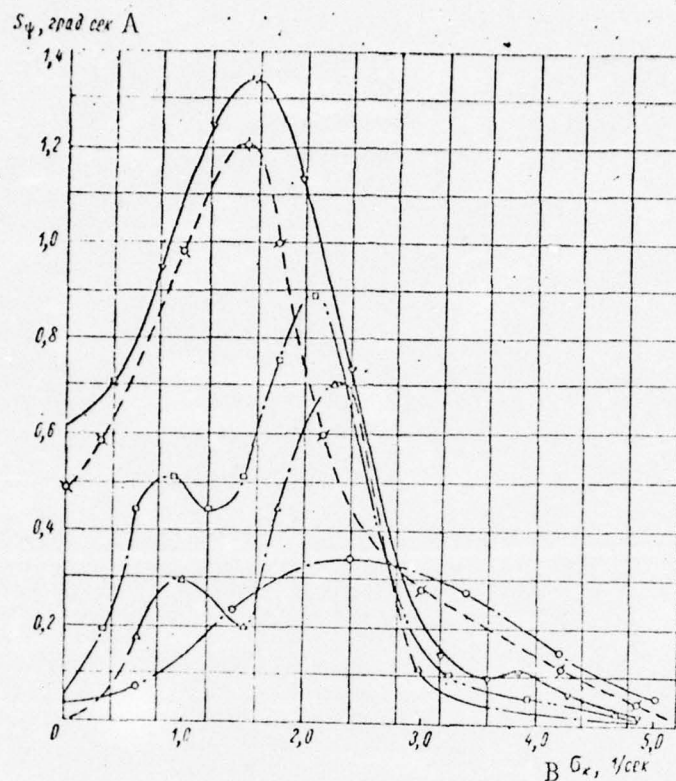


Fig. 168. Experimental spectra of pitching as a function of course angle. Sea state of 4, $Fr_D = 3.2$. Course angles: 1) $\chi = 0^\circ$; 2) $\chi = 45^\circ$; 3) $\chi = 90^\circ$; 4) $\chi = 135^\circ$; 5) $\chi = 180^\circ$.

KEY: A-- S_ψ , deg sec; B-- σ_k , 1/sec.

a) when movement is at acute course angles to the sea ($\chi = 0^\circ, 45^\circ$) with an increase in speed of movement the width of spectrum of the processes of motion increases (in the interval $2 \leq Fr_D \leq 4$ the parameter ϵ varies from 0.4--0.6 to 0.6--0.8 respectively);

b) when movement is at oblique course angles to the sea ($\chi = 135^\circ, 180^\circ$) an increase in speed of movement leads to a decrease in the width of spectrum (in the interval $2 \leq Fr_D \leq 4$ the parameter ϵ decreases from 0.6--0.9 to 0.4--0.7 respectively);

c) when movement is beam to the sea ($\chi = 90^\circ$) the width of spectrum of the processes of motion which is equal to $\epsilon = 0.6--0.8$ varies practically not at all with a change in relative speed (in the interval under consideration $2 \leq Fr_D \leq 4$).

The results of spectral processing presented above make it possible to recommend for calculating the amplitude characteristics of translational and rotational motion of hydrofoil craft formulas which take into consideration the width of spectrum developed for displacement craft. Specifically recommended are formula (V.93) which expresses the relation between the mean amplitudes

of pitching and rolling (\bar{H}) and the corresponding variances (D_x) and formula (IV.94) for the relation between the maximum (H_{\max}) and mean (\bar{H}) amplitude of motion.

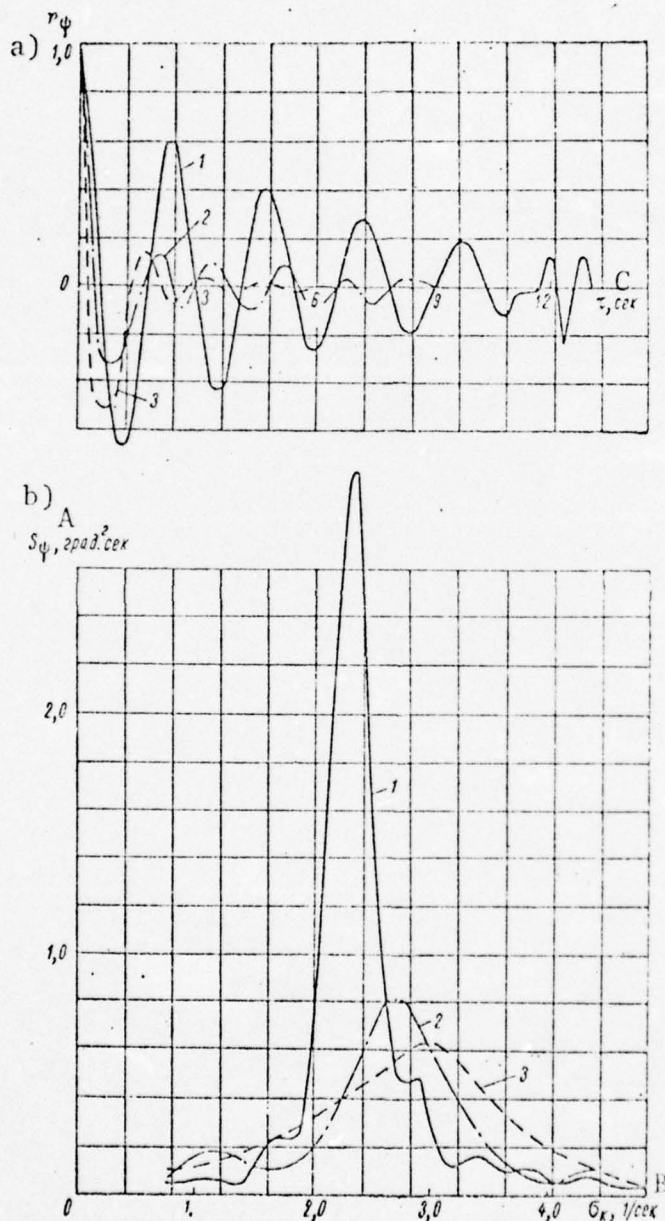


Fig. 169. Experimental correlation functions and spectra of pitching as a function of the speed of movement. Sea state of 4. a--correlation functions; b--spectra.

1--displacement mode ($Fr_D = 1.7$); 2--takeoff mode ($Fr_D = 2.4$); 3--foilborne mode ($Fr_D = 3.3$).

KEY: A-- S_ψ , deg^2/sec ; B-- σ_k , $1/\text{sec}$; C-- τ , sec.

A. G. Stepanov's formula is:

$$\frac{\bar{H}}{\sqrt{D_x}} = \sqrt{2\pi(1-\epsilon^2)}; \quad (\text{IV.93})$$

and A. I. Voznesenskiy's is:

[299

$$\frac{H_{\max}}{H} = \frac{2}{\sqrt{2\pi(1-\epsilon^2)}} \left(\sqrt{2 \ln N \sqrt{1-\epsilon^2}} + \frac{0.577}{\sqrt{2 \ln N \sqrt{1-\epsilon^2}}} \right), \quad (\text{IV.94})$$

where ϵ is the width of spectrum and N the number of amplitudes (size of statistical sample).

4. For calculating the shifts in speed and acceleration in the general case of movement of a hydrofoil craft in an irregular seaway it is necessary to know the statistical characteristics of the mutual relation among various types of translational and rotational motion.

Within the framework of correlation theory the mutual correlation functions and mutual spectral densities, for determining which from the recordings of processes of duration T the following relations serve, are the main statistical characteristics relating the various random processes:

$$R_{xy}(\tau) = \frac{1}{T-\tau} \int_0^{T-\tau} x(t)y(t+\tau) dt, \quad (\text{IV.95})$$

$$S_{xy}(\sigma) = \frac{1}{\pi} \int_{-\infty}^{\infty} e^{-j\sigma\tau} R_{xy}(\tau) d\tau. \quad (\text{IV.96})$$

The mutual spectral density of two stationary and stationary-related processes $x(t)$ and $y(t)$ can be represented in the form of a sum of real and imaginary terms (Fig. 170) using the formulas:

$$S_{xy}(\sigma) = S_{xy}''(\sigma) + jS_{xy}'(\sigma), \quad (\text{IV.97})$$

$$S_{xy}''(\sigma) = \frac{1}{\pi} \int_0^{\infty} [R_{xy}(\tau) + R_{yx}(\tau)] \cos \sigma\tau d\tau, \quad (\text{IV.98})$$

$$S_{xy}'(\sigma) = \frac{1}{\pi} \int_0^{\infty} [R_{xy}(\tau) - R_{yx}(\tau)] \sin \sigma\tau d\tau, \quad (\text{IV.99})$$

where $R_{xy}(\tau)$ is a mutual correlation function of processes

which is related with the function $R_{xy}(\tau)$ by the relation

$$R_{xy}(\tau) = R_{xy}(-\tau).$$

For making calculations of total shifts of a craft during translational and rotational motion it is important to know the magnitude of mutual coefficient of correlation which is equal to the normalized mutual coefficient function at zero shift $\tau = 0$:

$$K_{xy} = r_{xy}(0) = \frac{R_{xy}(0)}{\sqrt{R_x(0)R_y(0)}}. \quad (\text{IV.100})$$

The correlation coefficient of two random processes can also be found from their mutual spectrum by means of the relation [300]

$$K_{xy} = \frac{m_{xy}^{xy}}{\sqrt{m_x^x m_y^y}} = \frac{\int_0^\infty \text{Re} S_{xy}(\sigma) d\sigma}{\sqrt{\int_0^\infty S_x(\sigma) d\sigma \int_0^\infty S_y(\sigma) d\sigma}} = \frac{D_{xy}}{D_x D_y}, \quad (\text{IV.101})$$

where m_{xy}^{xy} is a mixed spectral moment of zero order equal to the mutual variance D_{xy} of the processes under consideration and m_x^x and m_y^y are spectral moments of zero order equal to the respective variances D_x and D_y .

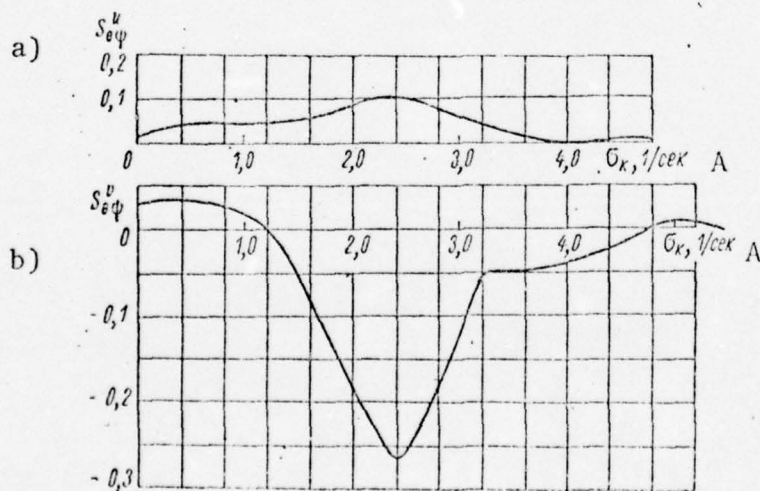


Fig. 170. Mutual spectral density of rolling and pitching:
a--real part; b--imaginary part.
KEY: A--1/sec.

Actual calculations of the statistical characteristics of mutual relation among the various types of translational and rotational motion of hydrofoil craft using relations

(IV.95) -- (IV.101) were carried out on electronic computers based on recordings of these processes during full-scale tests. On the basis of such calculations performed for several craft with fixed foils, V. A. Abramovskiy investigated the characteristics of mutual relation between rolling and pitching ($\theta - \psi$) and also pitching and vertical accelerations at the center of gravity of a craft ($\psi - z_v$) and at the bowfoils ($\psi - z_b$).

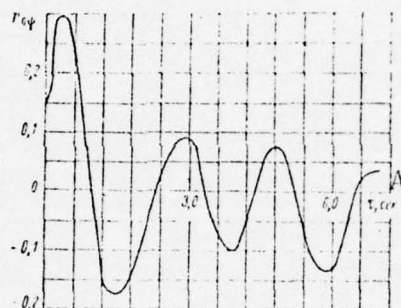


Fig. 171. Mutual correlation function of rolling and pitching ($Fr_D = 3.3$, $\chi = 0^\circ$).
KEY: A-- τ , sec.

As a result of his investigation he established the following distinguishing aspects of relations among processes of translational and rotational motion for these particular hydrofoil craft:

[301

a) processes of translational and rotational motion of hydrofoil craft can be viewed as stationary-related functions of time;

b) the maximum values of correlation coefficients for rolling and pitching in head and following seaways do not exceed (Fig. 171):

$$|r_{\theta\psi}(0)| \approx 0.05 \div 0.10.$$

which gives sufficient basis in the case of a craft moving in a head or following seaway to regard the processes of rolling and pitching as independent;

c) when a craft moves at oblique angles to the sea

$$|r_{\theta\psi}(0)| \approx 0.3 \div 0.5,$$

that is, in this case rolling and pitching are correlation-wise related;

d) processes of pitching and normal accelerations in all directions of movement have a rather high degree of relation which is characterized by the magnitudes

$$|r_{\psi\ddot{z}}(\tau)| \approx 0.5 \div 0.7; \quad |r_{\psi\ddot{z}}(0)| \approx 0.2 \div 0.5,$$

here the lower limits of change in correlation coefficient correspond to the case of movement broadside to the sea. The data presented on the characteristics of mutual relation of the types of translational and rotational motion considered, after they have been supplemented with mutual characteristics of other processes, will make it possible to calculate more accurately the overall shifts of a hydrofoil craft in an irregular seaway.

§41. Approximate method of making practical calculations of pitching and heaving of hydrofoil craft

The longitudinal movement of a hydrofoil craft moving in a regular seaway at a constant horizontal speed is considered with the following assumptions in mind:

- a) the hull does not come in contact with the waves and the lift surfaces of the foils do not broach the surface;
- b) the effect on pitching of the forces of drag, non-stationarity of lifting forces, and adjoining masses of the foils and interaction among them is negligible and therefore not considered; [302]
- c) the shifts in craft position are small and the changes in hydrodynamic characteristics of the foils caused by them obey a linear law.

The movement being considered can be described by a system of linear differential equations with constant coefficients of the type:

$$\left. \begin{aligned} \ddot{z} + a_{11}\dot{z} + a_{10}z - b_{11}\dot{\psi} - b_{10}\psi &= \frac{1}{2} \zeta_0 (A \sin \sigma_k t + B \cos \sigma_k t); \\ \ddot{\psi} + b_{21}\dot{z} + b_{20}\psi + a_{21}\dot{z} + a_{20}z &= \frac{1}{2\sigma_k^2} \zeta_0 (C \sin \sigma_k t + D \cos \sigma_k t), \end{aligned} \right\} \quad (\text{IV.102})$$

where ζ_0 is the half-height and σ_k the apparent frequency of a regular wave and r is the radius of inertia of the craft with respect to the transverse axis.

The coefficients a_{ij} and b_{ij} entering into system of equations (IV.102) are determined by the design and kinematic parameters of the ship and the hydrodynamic characteristics of the foils, and the variables in the expressions for disturbing forces and moments depend, furthermore, on the parameters of the seaway.

Since system of equations (IV.102) is linear its general integral will consist of the general integral of a homogeneous system (natural oscillations) and the solution of an inhomogeneous system (forced oscillations).

As revealed by calculations, electronic modeling, and model tests for actual hydrofoil craft possessing significant longitudinal stability natural oscillations, due to the strong

Damping during foilborne movement, rapidly become damped and the translational and rotational motion of such craft in a regular seaway will be determined only by the forced oscillations.

Solution to equations for pitching of craft equipped with the common types of foil systems and also investigation into stability of movement of such craft in calm water and a regular seaway are examined in detail in many works (see for example [13]). The relations obtained in these works for the characteristics of pitching are very complex and utilization of them requires the employment of electronic computers or modeling equipment.

At the same time in the early stages of designing a need often arises for an approximate evaluation of the characteristics of translational and rotational motion of hydrofoil craft using a relatively simple approach. An approximate calculation method which was proposed by V. A. Abramovskiy can be used for this purpose. The method is based on the assumption that a craft has a symmetrical foil system in which the bow- and sternfoils are equidistant from the center of gravity and have the same (with an accuracy to mutual effect) hydrodynamic characteristics. In this case in the initial equations (IV.102) [303 coefficients b_{11} , a_{20} , and a_{21} become equal to zero, the expressions for the remaining coefficients become much simpler, and the moment equation becomes unrelated to the equation for normal forces. After transferring in the latter the terms containing the variable ψ to the right side and combining it with the disturbing force of the seaway, the equations for pitching can be written in the following (dimensional) form:

$$\left. \begin{aligned} \ddot{z} + 2v_z \dot{z} + n_z^2 z &= \xi_0 \tilde{A}_1 \sin(\sigma_k t + \tilde{e}_1); \\ \ddot{\psi} + 2v_\psi \dot{\psi} + n_\psi^2 \psi &= \xi_0 \tilde{A}_2 \sin(\sigma_k t + \tilde{e}_2). \end{aligned} \right\} \quad (\text{IV.103})$$

The structure of the differential equations (IV.103) and the physical meaning of the coefficients included in them are the same as for displacement craft; the specific nature of hydrofoil craft lies in the structure of the coefficients which are expressed in terms of craft parameters by the following relations.

The relative drag coefficients for heaving and pitching are:

$$v_z = \frac{q C_p^{\alpha} S}{m v}; \quad v_\psi = \frac{q C_p^{\alpha} S l^2}{4 I v} \quad (1/sec). \quad (\text{IV.104})$$

The frequency of natural oscillations of a hydrofoil craft during heaving and pitching is

$$n_z = \sqrt{\frac{2qK^2}{m}}; \quad n_\psi = \sqrt{\frac{qK^2 l^2}{2I}} \quad (1/sec). \quad (IV.105)$$

The dimensionless relative drag coefficients are:

$$\mu_z = \frac{v_z}{n_z} = \frac{C_y^\alpha S}{v} \sqrt{\frac{2q}{mK^2}}; \quad \mu_\psi = \frac{v_\psi}{n_\psi} = \frac{C_y^\alpha S l}{2v} \sqrt{\frac{q}{2IK^2}}. \quad (IV.106)$$

The coefficients of disturbing forces and moments and the shifts in phase between the forces and moments on the foils and a wave take the form:

$$\left. \begin{aligned} \tilde{A}_1 &= [A_{1z}^2 + A_{1\psi}^2 + 2A_{1z}A_{1\psi} \cos(\varepsilon_\psi - \tilde{\varepsilon}_1)]^{1/2}; \\ \tilde{A}_2 &= \frac{q l |\sin \gamma|}{I} \left[\left(\frac{C_y^\alpha S \sigma l^{kz_0}}{v} \right)^2 + (K^2)^2 \right]^{1/2}; \end{aligned} \right\} \quad (IV.107)$$

$$\tilde{\varepsilon}_1 = \arctg \frac{A_{1z} \sin \varepsilon_1 + A_{1\psi} \sin \varepsilon_\psi}{A_{1z} \cos \varepsilon_1 + A_{1\psi} \cos \varepsilon_\psi}; \quad \varepsilon_2 = \arctg \frac{C_y^\alpha S l^{kz_0}}{K^2 v}, \quad (IV.108)$$

where

[304

$$\left. \begin{aligned} A_{1z} &= \frac{2q |\cos \gamma|}{m} \left[\left(\frac{C_y^\alpha S \sigma l^{kz_0}}{v} \right)^2 + (K^2)^2 \right]^{1/2}, \\ A_{1\psi} &= \frac{2\tilde{A}_2 q C_y^\alpha S}{m \sqrt{(n_\psi^2 - \sigma_K^2)^2 + 4v_\psi^2 \sigma_K^2}}, \\ \varepsilon_\psi &= \varepsilon_2 - \delta; \quad \delta = \arctg \frac{2v_\psi \sigma_K}{n_\psi^2 - \sigma_K^2}; \quad \varepsilon_1 = \frac{\pi}{2} - \varepsilon_2, \\ \gamma &= \frac{kl}{2} \cos \chi; \quad K^2 = \frac{\partial}{\partial z} [C_y S]; \quad k = \frac{2\pi}{\lambda}; \quad C_y^\alpha = \frac{\partial C_y}{\partial \alpha}. \end{aligned} \right\} \quad (IV.109)$$

In formulas (IV.104) -- (IV.109) the following symbols are used:

m, I	mass and moment of inertia of mass of a craft with respect to the transverse axis;
S, l, z_0	area, distance between foils, and their depth of immersion when moving in calm water;
σ, λ	the frequency and length of a regular wave;
$q = \rho v^2/2$	velocity head;
χ	course angle with respect to wave.

Solving system of equations (IV.103) yields the following final relations for the parameters of pitch of a craft equipped with symmetrical foils:

a) equations of forced pitch and heave oscillations:

$$\begin{aligned}\psi(t) &= A_\psi \sin(\sigma_\kappa t + \epsilon_\psi), \\ z(t) &= A_z \sin(\sigma_\kappa t + \epsilon_z); \end{aligned} \quad (\text{IV.110})$$

b) amplitude of pitching and heaving:

$$\begin{aligned}A_\psi &= \frac{\xi_0 \tilde{A}_2}{\sqrt{(n_\psi^2 - \sigma_\kappa^2)^2 + 4\nu_\psi^2 \sigma_\kappa^2}} \quad (\text{rad}), \\ A_z &= \frac{\xi_0 \tilde{A}_1}{\sqrt{(n_z^2 - \sigma_\kappa^2)^2 + 4\nu_z^2 \sigma_\kappa^2}} \quad (m); \end{aligned} \quad (\text{IV.111})$$

c) shifts in phase between wave and pitching and heaving:

$$\begin{aligned}\epsilon_\psi &= \epsilon_z - \delta; \quad \epsilon_z = \tilde{\epsilon}_1 - \beta; \\ \beta &= \arctg \frac{2\nu_z \sigma_\kappa}{n_z^2 - \sigma_\kappa^2}. \end{aligned} \quad (\text{IV.112})$$

The relations presented for a regular seaway are also used to determine the statistical characteristics of pitching in an irregular seaway. For such calculations, along with the seaway [305] spectrum, it is necessary to know the relations for the amplitude-frequency characteristics of the ship.

The latter are found from formulas (IV.111) in which we must set $\xi_0 \equiv 1$.

The amplitude-frequency characteristics for pitching and heaving can be written in the form:

$$\begin{aligned}\Phi_{\psi}(\sigma_\kappa) &= \frac{\tilde{A}_2}{\sqrt{n_\psi^4 \left[\left(1 - \frac{\sigma_\kappa^2}{n_\psi^2} \right)^2 + 4\nu_\psi^2 \frac{\sigma_\kappa^2}{n_\psi^2} \right]}}, \\ \Phi_z(\sigma_\kappa) &= \frac{\tilde{A}_1}{\sqrt{n_z^4 \left[\left(1 - \frac{\sigma_\kappa^2}{n_z^2} \right)^2 + 4\nu_z^2 \frac{\sigma_\kappa^2}{n_z^2} \right]}}. \end{aligned} \quad (\text{IV.113})$$

The probability properties of a seaway are determined by its energy spectrum for representing which in shipbuilding practice use is usually made of relations established by G. A. Firsov and N. N. Rakhmanin. Specifically, the empirical spectrum is expressed by the formula

$$S_\zeta(\sigma) = \frac{4}{\pi} D_\zeta \frac{a b^2}{\beta^2 + 2a^2} \cdot \frac{\sigma^2 + a^2}{\sigma^4 + 2a^2 \sigma^2 + b^4}, \quad (\text{IV.114})$$

where $\alpha^2 = \alpha^2 - \beta^2$ and $b^2 = \alpha^2 + \beta^2$.

Parameters α and β are determined in accordance with the recommendations given in work [10].

Inasmuch as the expressions for amplitude-frequency characteristics are obtained in a system of coordinates oriented on the craft and are functions of the apparent frequency, the spectral density of the seaway (IV.114) also must be transformed into a function of apparent frequency. Such a transformation is accomplished by the formula [16]:

$$S_{\zeta}(\sigma_k) = S_{\zeta}(\sigma) \frac{d\sigma}{d\sigma_k}, \quad (\text{IV.115})$$

where the derivative $d\sigma/d\sigma_k$ is determined from the known relation

$$\sigma_k = \sigma + \frac{\sigma^2}{g} v \cos \chi, \quad (\text{IV.116})$$

which must be preliminarily solved for σ .

When a craft moves in a following seaway the relation between σ and σ_k , generally speaking, is not unique. When $0 < \sigma_k < g/4v$ three values of σ correspond to one value of σ_k : two of them correspond to the case when waves overtake the craft and one to the case when the craft overtakes the waves. However, due to the high speeds of movement of the craft when foilborne, as a rule, the condition $\sigma_k > g/4v$, which provides for uniqueness of the relation between σ and σ_k , is met.

In light of the remark made above, for transformation of a seaway spectrum into a function of apparent frequencies the derivatives included in (IV.115) should be determined depending on the course with respect to the wave from the formulas: [306]

a) for a head seaway ($\chi = 0^\circ$)

$$\left(\frac{d\sigma}{d\sigma_k}\right)^0 = \left[1 + \frac{4v}{g} \sigma_k\right]^{-\frac{1}{2}}; \quad (\text{IV.117})$$

b) for a following seaway ($\chi = 180^\circ$)

$$\left(\frac{d\sigma}{d\sigma_k}\right)^{180} = \left[1 - 4 \frac{v}{g} \sigma_k\right]^{-\frac{1}{2}}; \quad (\text{IV.118})$$

c) for an arbitrary course angle with respect to the wave

$$\left(\frac{d\sigma}{d\sigma_k}\right)^2 = \left[1 + \frac{4v}{g} \sigma_k \cos \chi\right]^{-\frac{1}{2}} \quad (\text{IV.119})$$

After transformation of the seaway spectrum the spectral densities of translational and rotational motion can be calculated from the known formulas:

$$\begin{aligned} S_{\psi}(\sigma_k) &= |\Phi_{\psi}(\sigma_k)|^2 S_z(\sigma_k); \\ S_r(\sigma_k) &= |\Phi_r(\sigma_k)|^2 S_z(\sigma_k). \end{aligned} \quad (\text{IV.120})$$

In concluding this section we will briefly formulate the sequence of steps followed in calculating the pitch of craft equipped with fixed hydrofoils.

1. Initial data are determined for calculations, including:

a) main elements of a craft and the geometric parameters of foils:

$m = D/g \cdot T \cdot \text{sec}^2/m$	mass of the craft;
$I, T \cdot \text{sec}^2 \cdot m$	moment of inertia of the mass relative to the transverse axis;
H_b, s, m	rise of center of gravity above the lower planes of the bow- and sternfoils;
l, m	distance between foils;
x_b, s	distance of foils from center of gravity;
α_b, s	set angles of attack of the foils.

The parameters in this group are determined from the appropriate design documents (calculations of load and location of center of gravity, drawings of general layout, etc.).

b) parameters describing steady movement of the craft in calm water:

$v_0, m/\text{sec}$	speed of movement;
ψ_0, rad	trim under way;
z_b, s, m^2	depth of immersion of foils;
S_b, s, m^2	wetted area of foils.

The parameters in this group are given for several speeds [307 corresponding to the calculated modes of movement. They are determined either from calculations for steady movement of the craft or from tests of a model in a tank.

c) hydrodynamic parameters characterizing the intensity of change in lift acting on foils depending on their depth of immersion and angle of attack:

$C_{yb}^{\alpha}, s = (\partial C_y / \partial \alpha)_b, s$	derivative of coefficient of lift with respect to angle of attack for calcu-
--	--

$K_{b, s}^z = \frac{\partial (C_y S)_{b, s}}{\partial z, m}$ lated depths of immersion of foils;
derivative of product of coefficient
of lift on wetted area with respect to
depth of immersion of foils.

These parameters are determined by the methods described in Chap. I.

d) parameters of the seaway:

h, m calculated height of regular wave;
 λ, m length of regular wave;
 $S_\zeta(\sigma)$ spectral density of irregular seaway
(detailed recommendations for determining
it are given in work [10]).

2. Calculations are performed for pitching in a regular seaway, for which purpose a determination is made of:

a) relative coefficients of drag of heaving and pitching v_ϕ and v_z using formulas (IV.104);

b) frequency of natural oscillations n_ψ and n_z using formulas (IV.105);

c) dimensionless relative coefficients of drag μ_ψ and μ_z using formulas (IV.106);

d) coefficients of disturbing forces and moments \tilde{A}_1 and \tilde{A}_2 and phase angles $\tilde{\epsilon}_1$ and $\tilde{\epsilon}_2$ using formulas (IV.111)--(IV.112).

3. Calculations are performed for the statistical characteristics of pitching in an irregular seaway in the following sequence:

a) amplitude-frequency characteristics of pitching and heaving $\Phi_\psi(\sigma_k)$ and $\Phi_z(\sigma_k)$ are calculated from formulas (IV.113);

b) the seaway's variance is determined for a given sea state; and from formula (IV.114), taking into account the recommendations indicated in [10] and [11] for selecting parameters α and β , calculations are performed for the spectral density of the seaway $S_\zeta(\sigma)$;

c) formulas (IV.116)--(IV.119) are used depending on the course angle to transform the spectral density of the seaway into a function of apparent frequency $S_\zeta(\sigma_k)$;

d) transformation (IV.120) is used to calculate the spectral densities of pitching $S_\psi(\sigma_k)$ and heaving $S_z(\sigma_k)$;

e) variances D_ψ and D_z (or standard deviations σ_ψ and σ_z) for pitching and heaving are determined by integrating frequency spectra in accordance with the formula (IV.92);

f) the recommendations contained in §40 are applied to determine the amplitudes of translational and rotational motion for different values of the likelihood function.

[308

References

1. Keldysh, M. V. and Lavrent'yev, M. A. Movement of a foil beneath the surface of a heavy liquid. In the collection: Trudy konferentsii po teorii volnovogo soprotivleniya. Moscow, 1937, TsAGI.
2. Semenov-Tyan-Shanskiy, V. V. Statika korablya (Ship statics). Leningrad, Sudpromgiz, 1940.
3. Pugachev, V. N. Teoriya sluchaynykh funktsiy i eye primeneniye k zadacham avtomaticheskogo upravleniya (Theory of random functions and its application to problems of automatic control). Moscow, GITTL, 1957.
4. Venttsel', Ye. S. Teoriya veroyatnostey (Theory of probability). Gosizdat, 1967.
5. Sveshnikov, A. A. Prikladnyye metody teorii sluchaynykh funktsiy (Applied methods in the theory of random functions). Leningrad, Sudpromgiz, 1961.
6. Solodovnikov, V. V. and others. Vychislitel'naya tekhnika v primenении dlya statisticheskikh issledovaniy i raschetov sistem avtomaticheskogo upravleniya (Application of computer technology to statistical investigation and calculation of automatic control systems). Moscow, GONTI, 1963.
7. Bendat, Dzh. Osnovy teorii sluchaynykh shumov i eye primeneniya (Fundamentals of the theory of random noises and its application). Moscow, "Nauka," 1965.
8. Kharkevich, A. A. Spektry i analiz (Spectra and analysis). GONTI, 1957.
9. Yekimov, V. V. Veroyatnostnyye metody v stroitel'noy mekhanike korablya (Probability methods in structural mechanics of a ship). Leningrad, "Sudostroyeniye," 1965.
10. Boroday, I. K. and Netsvetayev, Yu. A. Kachka sudov na morskoy volnenii (Translational and rotational motion of craft in a seaway). Leningrad, "Sudostroyeniye," 1969.
11. Rakhmanin, N. N. Spectral properties of a seaway used in investigating the seakeeping characteristics of ships. Trudy okeanograficheskoy komissii AN SSSR, 1960, Vol. 9.
12. Girs, I. V., et al. Ispytaniya morekhodnykh kachestv sudov (Tests of seakeeping characteristics of craft). Leningrad, "Sudostroyeniye," 1965.
13. Izvol'skiy, Ye. G. Differential equations of pitching of a hydrofoil ship as an object of control. Trudy MAI, 1961, No. 139.
14. Cartwright, D. and Longuet-Higgins, M. The statistical distribution of the maxima of a random function, Proceedings of the Royal Society, London, 1956.
15. Krylov, Yu. M. Spektral'nyye metody issledovaniya vetrovykh voln (Spectral methods of investigating waves caused by winds). Leningrad, Gidrometeoizdat, 1966.
16. Neumann, G. On ocean spectra and a new method of forecasting wind generated sea. T. M. No. 43, Beach Erosion

Board, 1953.

17. St. Denis, M. and Pierson, W. I. On the motion of ships in confused seas. Trans. SNAME, Vol. 63, 1953.
18. Ogilvie, T. Ye. Theoretical prediction of hydrofoil craft. Journal of Ship Research, 1959, Vol. 3, No. 3.

On high-speed craft, either planing or hydrofoil, the propulsors are usually propellers. In most cases inclined shafts are used to transmit power to the propellers but lately attempts have been made to use zee drives which are often referred to as angled columns.

Because of the high speeds reached by craft of this kind their propellers, as a rule, cavitate. The oblique flow around propellers mounted on inclined shafts and also the work of propellers mounted on angled columns in close proximity to reduction gear fairings and struts lead to unevenness in the flow and this intensifies cavitation.

In order to decrease overall draft partially immersed propellers which pierce the free surface of the water are used. In distinction from completely immersed propellers, the work of such propellers is accompanied by many unfavorable phenomena, including nonstationarity of flow.

Below we analyze the main distinguishing features of calculations made for the way-making ability of high-speed craft due to the noted conditions under which their propellers work.

§42. Action of a blade element on a cavitating propeller

We will consider the forces arising on an element of a propeller blade located at radius r . The velocity triangle of the element with the propeller rotating at n revolutions and the craft moving ahead at a forward speed of v_p is shown in Fig. 172. Here $\beta = \arctg \lambda_p / \pi \bar{r}$ is the advance angle; $\lambda_p = v_p / nD$ the relative advance of the propeller; $D = 2R$ the diameter of the propeller; $\bar{r} = r/R$ the relative radius; $\Delta\beta$ the induced angle of downwash; w_a and w_t respectively the axial and tip induced velocities in the plane of the propeller; α_i the angle of attack of the element; Y and X the lift and drag of the element corresponding to angle of attack α_i ; Y^* and X^* the same, allowing for induced losses; $\epsilon = \arctg X/Y$; $\mu = \arctg X^*/Y^* = \epsilon + \Delta\beta$; and $\Delta\beta = \arctg X/Y^*$.

The relations among forces acting on the element take the following form: [310]

$$\left. \begin{aligned} Y^* &= (Y - X \operatorname{tg} \Delta\beta) \cos \Delta\beta, \\ X^* &= (Y - X \operatorname{tg} \Delta\beta) \sin \Delta\beta + \frac{X}{\cos \Delta\beta}, \\ \Delta X &= (Y - X \operatorname{tg} \Delta\beta) \sin \Delta\beta. \end{aligned} \right\} \quad (V.1)$$

The thrust created by the element is

$$dP = \frac{Y^*}{\cos \mu} \cos(\beta + \mu), \quad (V.2)$$

and the tangential force

$$dT = \frac{Y^*}{\cos \mu} \sin(\beta + \mu). \quad (V.3)$$

The efficiency of the blade element is

$$\eta_r = \frac{dP v_p}{2\pi r n dT},$$

that is,

$$\eta_r = \frac{\operatorname{tg} \beta}{\operatorname{tg}(\beta + \mu)}. \quad (V.4)$$

Transforming (V.4), we obtain [1]

$$\eta_r = \frac{k^* - \operatorname{tg} \beta}{k^* + \operatorname{ctg} \beta}, \quad (V.5)$$

where $k^* = Y^*/X^*$ is the reduced lift-drag ratio of the element.

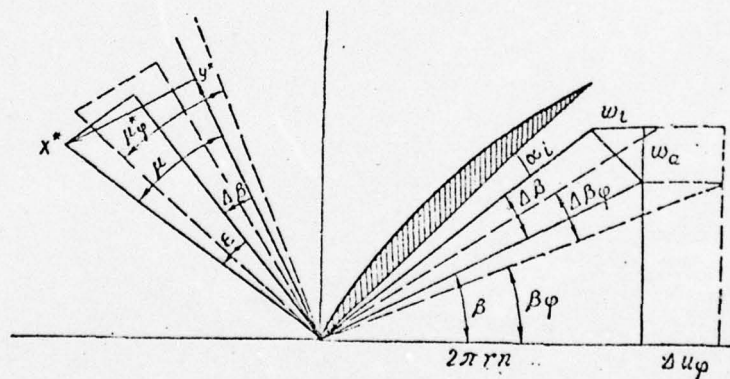


Fig. 172. Velocity triangle of a propeller blade element.

By analogy with k^* we write $k = Y/X$ and $k^{**} = Y^*/\Delta X$, the relation among k , k^{**} , and k^* being

$$k^* = \frac{k k^{**} - 1}{k + k^{**}}. \quad (V.6)$$

Using (V.5) we can obtain an optimal relation between the reduced lift-drag ratio of element k^* and the advance angle β . From the equation

[311

$$\frac{\partial \eta_r}{\partial (\operatorname{tg} \beta)} = \frac{\operatorname{ctg}^2 \beta (k^* - \operatorname{tg} \beta) - (k + \operatorname{ctg} \beta)}{(k^* + \operatorname{ctg} \beta)^2} = 0$$

we find

$$k^* = \operatorname{tg} 2\beta_{\text{opt}}, \quad (\text{V.7})$$

whence

$$\beta_{\text{opt}} = \frac{1}{2} \operatorname{arctg} k^*; \quad (\text{V.8})$$

$$\left(\frac{\lambda_p}{\pi r} \right)_{\text{opt}} = \frac{\sqrt{1+k^{*2}}-1}{k^*}. \quad (\text{V.9})$$

After substituting (V.8) and (V.9) into (V.5) we obtain

$$\eta_{r \text{ opt}} = \operatorname{tg}^2 \beta_{\text{opt}} = \operatorname{tg}^2 \left(\frac{1}{2} \operatorname{arctg} k^* \right) = 1 - \frac{2}{k^{*2}} (\sqrt{1+k^{*2}} - 1). \quad (\text{V.10})$$

The results of calculations made with formulas (V.5) and (V.10) are shown in Fig. 173.

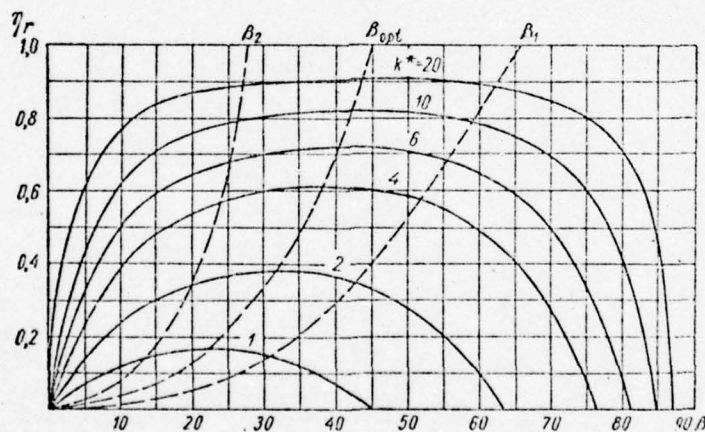


Fig. 173. Results of calculations using formulas (V.5) and (V.10).

An analysis shows that a deviation in the advance angle from optimal in the range $0.31 \operatorname{arctg} k^* < \beta_{\text{opt}} < 0.68 \operatorname{arctg} k^*$ leads to a drop in element efficiency which is slight compared with $\eta_{r \text{ opt}}$. Consequently, with a decrease in k^* the range of permissible change in β also decreases. This has been confirmed by experiment.

Thus, for cavitating propellers whose elements have relatively low values of k^* the optimal modes of work must be established with greater accuracy than in the case of non-cavitating propellers. In addition, it is necessary to improve

in all possible ways the lift-drag ratio of blade elements of [312]
propellers operating in a deep stage of cavitation.

Let us discuss qualitative changes in the efficiency of a cavitating propeller, making use of formula (V.4) which we will write in the form

$$\eta_r = \frac{\operatorname{tg} \beta}{\operatorname{tg} (\beta + \Delta\beta + \epsilon)}. \quad (\text{V.11})$$

It is plain from (V.11) that in order to raise the efficiency of a propeller it is necessary to decrease the magnitude of $\Delta\beta + \epsilon$ with respect to β .

The induced angle of downwash decreases with a decrease in the angle of attack and therefore in order to attain a high efficiency it is necessary to have each element of a blade work at the least possible angle of attack at which the lift-drag ratio remains sufficiently high.

Under conditions of cavitation these requirements are satisfied by wedge-shaped profiles which possess at a given maximum thickness the least possible entry angle γ_{en} which is formed by a chord and a tangent to the low-pressure side of a profile at the leading edge.

Under conditions of developed cavitation the characteristics of profiles in a cavitating propeller array and not the isolated ones of individual blades are determining. Indeed, the existence of cavitation cavities in the space between blades (Fig. 174) can greatly change the nature of flow around the profiles in an array. The latter is expressed in a decrease in the hydrodynamic angle of attack and the more intensive development of cavitation due to constriction of the flow caused by the existence of cavitation cavities between blades. This adverse effect of a cavitating array is intensified with an increase in the thickness of the cavitation cavities and a decrease in the spacing of the array.

It can be considered with a sufficient degree of accuracy [314] that at angles of attack characteristic of elements of propeller blades the thickness of a cavitation cavity of a profile is proportional to the entry angle γ_{en} . For example, of the three profiles in Fig. 175--aviation, segmental, and wedge-shaped--whose maximum thickness is the same, the profile exhibiting the greatest thickness of cavitation cavity is the aviation type and the one exhibiting the least, the wedge-shaped one.

Thus, for profiling the blades of propellers intended for work in a deep stage of cavitation it is best to use the wedge-shaped profile with the smallest possible relative thickness in keeping with strength requirements. Propellers

with the blades profiled in this way were called supercavitating
by V. L. Pozdyunin [2].

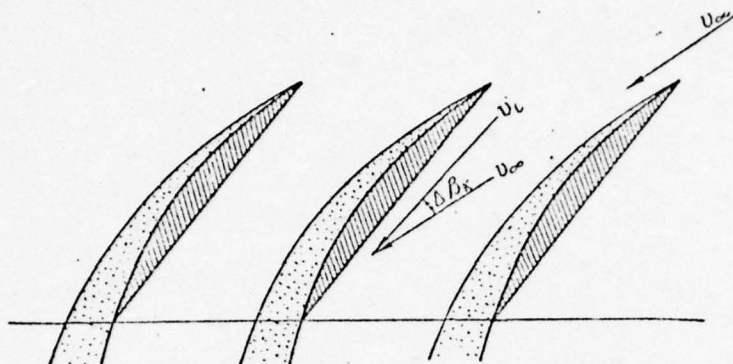


Fig. 174. Nature of flow in a cavitating propeller array.

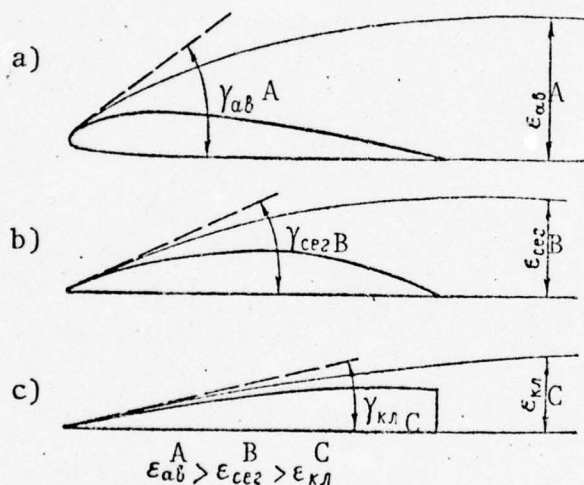


Fig. 175. Dimensions of cavitation cavities of various profiles (a--c).

KEY: A--aviation; B--segmental; C--wedge-shaped.

By way of illustration Fig. 176 shows curves depicting the behavior of ordinary and supercavitating propellers having the same main geometric elements: $A/A_d = 0.80$, $H/D = 1.4$, $z = 3$. It follows from the figure, for example, that the nature of the change in propeller efficiency differs qualitatively. Specifically, the efficiency of a supercavitating propeller reflects no drop over a wide range of change in mode of work as cavitation develops compared with subcavitating flow as is the case for ordinary propellers but, on the contrary, increases.

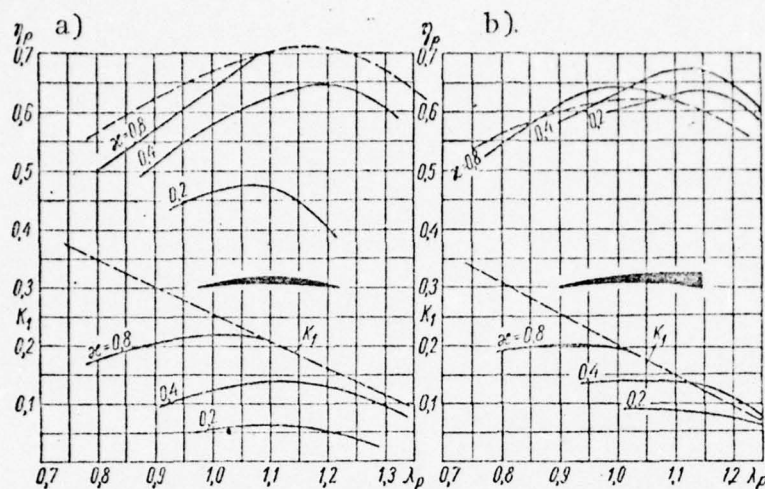


Fig. 176. Running curves showing action of propellers with the elements $A/A_d = 0.80$, $H/D = 1.4$, $z = 3$. a--segmental profile; b--supercavitating profile.

§43. Solution to the problem of cavitation flow around a flat profile array

Methods for calculating subcavitating propellers based on vortex theory are now well developed. Investigations conducted by N. N. Polyakov proved that methods derived from vortex theory can also be used to make calculations for cavitating propellers. Analogous results were obtained later by Tachmindzhi and Morgan [3].

When vortex theory methods are used to calculate cavitating propellers the hydrodynamic characteristics of blade sections must be determined with cavitation and array effect taken into account. The effect of a propeller array, as shown by N. N. Polyakov [4], can be taken into account based on data for flat profile arrays.

Since for cavitating propellers the array effect is decisive, below we present the solution to a problem of cavitating flow around a flat profile array.

The method of hydrodynamic singularities was used to solve the problem. The boundaries of the cavitation cavity representing lines of discontinuity in the tangential components of velocities were replaced with continuously distributed vortices. A profile was considered to be thin and as in thin foil theory was replaced with a vortex layer. Based on the pattern of the flat array of cavitating profiles shown in Fig. 177, the boundary condition on a profile in the array can be written in the form [315]

$$\alpha + \frac{v_\eta}{v} = \eta'_1(\xi), \quad (V.12)$$

where $\eta'_1(\xi) = \partial \eta_1 / \partial \xi$, $\eta_1(\xi)$ being the equation for the profile skeleton; v is the mean velocity in the array; v_η the vertical component of the velocity on a profile chord induced by the system of singularities replacing the profile and the cavitation cavities in an infinite flat array.

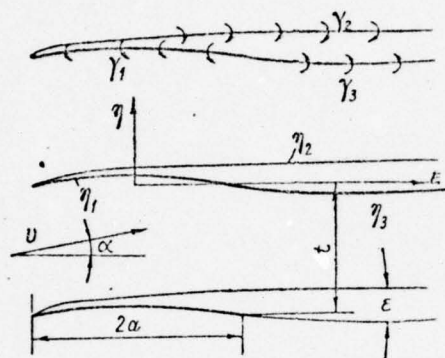


Fig. 177. Diagram of a flat array of cavitating profiles.

The expression for velocity v_η takes the following form:

$$v_\eta = -\frac{1}{2i} \sum_{n=1}^3 \int_p^q \gamma_n \operatorname{cth} \frac{\pi}{l} (\xi_0 - \xi) \times \\ \times \frac{1 + \operatorname{ctg}^2 \frac{\pi}{l} \eta_n(\xi)}{\operatorname{cth}^2 \frac{\pi}{l} (\xi_0 - \xi) + \operatorname{ctg}^2 \frac{\pi}{l} \eta_n(\xi)} \sqrt{1 + \left(\frac{\partial \eta_n}{\partial \xi} \right)^2} d\xi. \quad (V.13)$$

In (V.13) the limits of integration p and q should be $p = -a$ and $q = a$ for a profile, $p = -a$ and $q = \infty$ for the upper boundary of a cavitation cavity, and $p = a$ and $q = \infty$ for the lower boundary.

Substituting (V.13) into boundary condition (V.12), we obtain the following integral equation for determining the intensity function of the vortices replacing a cavitating profile in an array:

$$\int_{-a}^a \frac{\gamma^*(s)}{s_0 - s} ds = \frac{B}{1 - B^2 s_0^2} \left[2tv \left(\frac{\partial \eta_1}{\partial \xi_0} - \alpha + \frac{\Delta v}{v} \right) - B s_0 \Gamma \right]. \quad (V.14)$$

In equation (V.14) $\gamma^* = \gamma_1 + \gamma_2$, $s = \frac{a}{\operatorname{th} \frac{\pi}{l} a} \operatorname{th} \frac{\pi}{l} \xi$ is a new [316

variable, $B = \frac{1}{a} \ln \frac{\pi}{t} a$, $\Gamma = \int_{-a}^a \gamma^*(\xi) d\xi$ is the circulation of a cavitating profile in an array; and Δv is the velocity induced by parts of the cavitation cavities lying outside the limits of profile chords in an array.

In the derivation of equation (V.14) it was assumed that within the limits of a profile chord a cavitation cavity is thin and this made it possible to arrange the vortices replacing the upper boundary of the cavity along the length of a chord on the chord itself. The term $\Delta v/v$ (we will designate it $\Delta\alpha$) entering into the right side of (V.14) is equivalent to the angle of downwash caused by the effect of the cavitation cavities. The following expression has been derived for determining the angle of downwash:

$$\Delta\alpha = \alpha - \frac{\partial \eta_1}{\partial \xi_0} - \frac{C_{y0}}{2\pi} + \frac{\sigma}{4\pi} \left[1 - \frac{1}{2} \int_{-1}^1 \frac{1 - \left(\frac{\xi}{a}\right)}{\left(\frac{\xi_0}{a}\right) - \left(\frac{\xi}{a}\right)} d\left(\frac{\xi}{a}\right) \right], \quad (V.15)$$

where $C_{y0} = f(\alpha, \sigma)$ is the coefficient of lift of a cavitating profile in an unbounded liquid; $\sigma = \frac{p_0 - p_d}{\frac{\rho v^2}{2}}$ is the cavitation

number; p_0 the static pressure; p_d the vapor pressure of the liquid; and ρ the mass density of the liquid.

The expression for the vortex intensity function of a cavitating profile in an array can be written in the form

$$\gamma^*(s) = \left[A_0 v \alpha \psi(s) - \frac{1}{4} v \sigma \mu(s) \right] \frac{t}{\pi} B + \sum_{n=1}^{\infty} A_n \sin \left(n \arccos \frac{s}{a} \right), \quad (V.16)$$

where

$$\psi(s) = \sqrt{\frac{a - \frac{t}{\pi} \operatorname{Arth} Bs}{a + \frac{t}{\pi} \operatorname{Arth} Bs}} \cdot \frac{1}{1 - B^2 s^2},$$

$$\mu(s) = \frac{1 - \frac{t}{a\pi} \operatorname{Arg} Bs}{1 - B^2 s^2}, \quad A_0 = \frac{\sigma}{2} - \frac{C_{y0}}{\pi\alpha}.$$

As a result of solving the initial integral equation (V.14) the following formula was obtained for determining the circulation of a cavitating profile located in a system of an infinite flat array: [317]

$$\Gamma = \frac{1}{1 + \frac{(aB)^2}{\pi} I_4} \left\{ -a v C_{y0} + a B v \frac{t}{\pi^2} \left[A_0 \alpha I_1 - \right. \right. \\ \left. \left. - \frac{\sigma}{4} \left(I_2 - B \frac{t}{\pi} I_3 \right) + \left(C_{y0} - \frac{\sigma}{2} \right) I_5 \right] \right\}. \quad (V.17)$$

The following notation is used in (V.17):

$$I_1 = \int_0^\pi \int_0^\pi \frac{\psi(0) \sin \theta \cos \theta_0}{\cos \theta - \cos \theta_0} d\theta d\theta_0; \quad (V.18)$$

$$I_2 = \int_0^\pi \int_0^\pi \frac{\mu(0) \sin \theta \cos \theta_0}{\cos \theta - \cos \theta_0} d\theta d\theta_0; \quad (V.19)$$

$$I_3 = \int_0^\pi \int_0^\pi \frac{\mu(\theta) \sin \theta \cos \theta_0 d\theta d\theta_0}{\frac{t}{a} \pi (\text{Arth } Ba \cos \theta - \text{Arth } Ba \cos \theta_0) [1 - (Ba \cos \theta_0)^2]}; \quad (V.20)$$

$$I_4 = \int_0^\pi \frac{\cos^2 \theta_0 d\theta_0}{1 - (Ba \cos \theta_0)^2}; \quad (V.21)$$

$$I_5 = \int_0^\pi \frac{\cos \theta_0 d\theta_0}{1 - (Ba \cos \theta_0)^2}. \quad (V.22)$$

The variable θ in integral equations (V.18) -- (V.22) can be expressed in terms of the variable s by means of the relation $\theta = \arccos s/a$.

After calculating integral equations (V.18) -- (V.22) the following final formula was obtained based on (V.17) for determining the coefficient of lift of a cavitating profile in an array:

$$C_y(\sigma) = \frac{1}{\text{ch } \frac{\pi}{t} a} \left\{ C_{y0}(\sigma') \left[1 + \frac{k_0}{\pi^2} I_1 \right] - \right. \\ \left. - k_0 \frac{\sigma'}{2\pi} \left[\frac{1}{\pi} I_1 - \frac{1}{2} (I_2 - k_0 I_3) \right] \right\}, \quad (V.23)$$

where $k_0 = \frac{t}{a\pi} \text{th } \frac{\pi}{t} a$; and I_1 , I_2 , and I_3 are improper integrals whose values are shown in Fig. 178. On the right side of (V.23) is the cavitation number σ' which is determined in light of the change in rate of flow in an array caused by the effect of finiteness of the thicknesses of the cavitation cavities and related to the cavitation number σ by

$$\sigma' = \sigma \left(1 - \frac{k_0}{t} \right)^2, \quad (V.24)$$

Here ϵ_k is the thickness of a cavitation cavity whose magnitude can be determined either from experiment or from calculations.

[318

The following formula can be used for an approximate determination of ϵ_k :

$$\frac{\epsilon_k}{a} = \frac{2C_x}{1 + \sigma - \sqrt{1 + \sigma}}, \quad (V.25)$$

It was derived based on research conducted by N. N. Polyakov on the pressure drag of a cavitating profile.

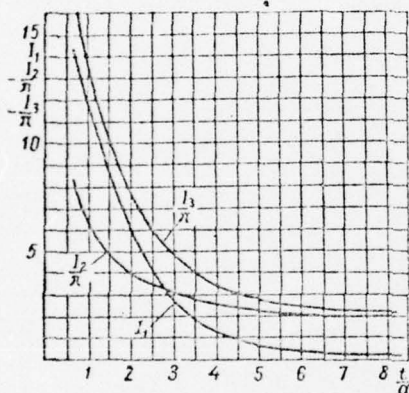


Fig. 178. Values of the integrals I_1 , I_2 , and I_3 .

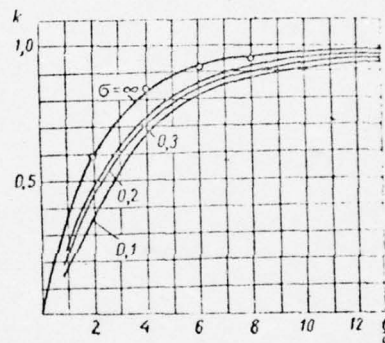


Fig. 179. Results of calculations performed with formula (V.23).

By way of example formula (V.23) was used to make calculations for a flat plate with an angle of attack of $\alpha = 4^\circ$ and cavitation numbers of $\sigma = 0.10$, 0.20 , and 0.30 .

The results of calculation are shown in Fig. 179 in the form of curves of the coefficient $k(t/a) = C_y(\sigma)/C_{y0}(\sigma)$ where $\sigma = \text{const}$.

§44. Verifying calculations of cavitating propellers

The hydrodynamic characteristics of propellers are generally represented in the form of dimensionless coefficients of thrust and moment. The latter are usually expressed in terms of the coefficient of lift and the drag-lift ratio of blade elements C_y and C_x/C_y . If, as in §42, an additional function of the drag-lift ratio $\mu = \arctg C_x/C_y$ is introduced and the coefficients of lift of elements on the basis of the results of the preceding section are expressed in terms of analogous characteristics of profiles in an unbounded liquid, $C_y = kC_{y0}$, then the formulas for the coefficients of thrust and moment of a propeller will take the

[319

form:

$$K_1 = \frac{z}{4} \int_{r_h}^1 k C_{\nu 0} \bar{b} \left(\frac{w_l}{nD} \right)^2 \frac{\cos(\beta_l + \mu)}{\cos \mu} d\bar{r}; \quad (V.26)$$

$$K_2 = \frac{z}{8} \int_{r_h}^1 k C_{\nu 0} \bar{b} \bar{r} \left(\frac{w_l}{nD} \right)^2 \frac{\sin(\beta_l + \mu)}{\cos \mu} d\bar{r}, \quad (V.27)$$

where z is the number of propeller blades; n the number of revolutions of the propeller; coefficient k is determined from formula (V.23); $D = 2R$ is the diameter of the propeller; $\bar{b} = b/D$ is the relative width of chord of an element; $r_h = r_h/R$ is the relative radius of the hub; β_l the induced angle of advance of the propeller; and w_l the velocity with which the flow impinges on an element of the propeller blade.

Thus, if the hydrodynamic characteristics of cavitating profiles are known, computation of the coefficients of thrust and moment of a cavitating propeller from formulas (V.26) and (V.27) doesn't entail any fundamental difficulty and the induced velocities can be calculated by the methods of vortex theory. The form and sequence used to make calculations will depend on the method used to determine the induced velocities of the propeller.

Calculations which have been performed show that the distribution of circulation along the blades of cavitating propellers which possess a high efficiency is close to optimal. Therefore in the following discussion for the purpose of determining the induced velocities we will use vortex theory for a propeller with the least possible induced losses.

The purpose of making verifying calculations is to determine the running curves of a propeller with given geometric characteristics. The following must be given to perform these calculations:

a) the main geometric elements of the propeller--disk ratio A/A_d , number of blades z and the pitch ratio distribution, and the relative width and thickness of blades over the radius of the propeller

$$\frac{H}{D}(\bar{r}), \bar{b}(\bar{r}) \text{ and } \delta(\bar{r});$$

b) the shape of blade cross sections and their hydrodynamic characteristics;

c) the cavitation number of the propeller $\kappa = \frac{p_0 - p_d}{\frac{\rho w_p^2}{2}}$, where

is the translational velocity of propeller movement.

Calculations for the running curves of a cavitating propeller [320] are performed by element, for this purpose breaking the blades down into several sections. For each section located at a relative radius of \bar{r} the calculations are performed in the following sequence:

1. Several values of induced angle of attack of an element relative to its chord α are given.

2. The angles of induced advance are determined using the formula

$$\beta_i = \operatorname{arctg} \frac{\frac{H}{D}}{2\pi r} - \alpha.$$

3. On the basis of work [4] the relative spacing of an equivalent hydrodynamic array is calculated

$$\bar{t} = \frac{t}{a} = \frac{2\pi}{z} \cdot \frac{\bar{r}}{b} \sin \beta_i.$$

4. The local cavitation number of an element is found from the formula

$$\sigma_i = \frac{p_0 - p_d}{\frac{\rho \omega_i^2}{2}} = \kappa \frac{\cos^2 \beta_i}{\left(\frac{\pi r}{\lambda_p} - \frac{v_t}{v_p} \right)}.$$

At the start of calculations when determining σ_i the value of relative induced tip velocity in the plane of the propeller v_t/v_p can be set equal to zero and the relative advance to

$$\lambda_p^0 = \frac{\pi r}{1.1} \operatorname{tg} \beta_i.$$

5. Formula (V.23) is used to calculate coefficient k which characterizes the drop in lift of a cavitating profile in an array.

6. The Prandtl-Goldshteyn correction which takes into account the finiteness of the number of blades $\bar{k}(\bar{r}, z, \beta_i)$ is determined.

7. The coefficients of induced velocities

$$a_1 = \frac{v_a}{v_p} \quad \text{and} \quad a_2 = \frac{v_t}{2\pi r n},$$

where v_a is the axial induced velocity in the plane of the propeller are found.

8. The values of relative advance

$$\lambda_p = \frac{1-a_2}{1+a_1} \pi \bar{r} \operatorname{tg} \beta_i,$$

and also the relative induced tip velocity

$$\frac{v_i}{v_p} = a_2 \frac{\pi \bar{r}}{\lambda_p}.$$

are calculated in the first approximation.

9. The values of λ_p and v_i/v_p from the above step are used to determine the local cavitation number σ_i in the second approximation. The calculations called for in 1--8 above are repeated until the required degree of closeness is found between the results of a preceding and a following approximation.

10. After establishing the induced velocities in accordance with formulas (V.26) and (V.27) the elementary coefficients of thrust and moment of the propeller referred to $d\bar{r}$ are calculated using the formulas

$$\frac{dK_1}{d\bar{r}} = C_y \bar{b} \left(\frac{w_i}{nD} \right)^2 \frac{\cos(\beta_i + \mu)}{\cos \mu}; \quad \frac{dK_2}{d\bar{r}} = C_y \bar{b} \bar{r} \left(\frac{w_i}{nD} \right)^2 \frac{\sin(\beta_i + \mu)}{\cos \mu},$$

here

$$\frac{w_i}{nD} = \lambda_p \frac{1+a_1}{\sin \beta_i}.$$

Analogous calculations are made for other blade sections.

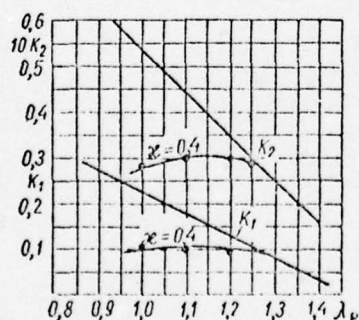


Fig. 180. Running curves of wide-blade propeller. Solid line--experiment; heavy dots--calculations.

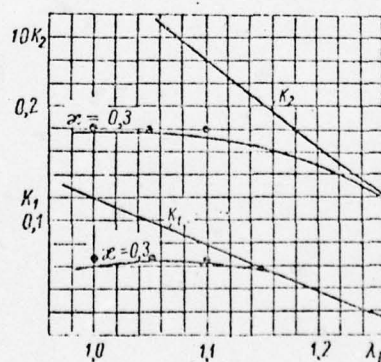


Fig. 181. Running curves of super-cavitating propeller. Solid line--experiment; heavy dots--calculations.

Having the relations $dK_1/d\bar{r}$ and $dK_2/d\bar{r}$ expressed as functions of relative radius \bar{r} by integrating we can find the coefficients of thrust and moment for a propeller as a whole

$$K_1 = \frac{z}{4} \int_{\bar{r}_h}^1 \frac{dK_1}{d\bar{r}} d\bar{r}, \quad K_2 = \frac{z}{8} \int_{\bar{r}_h}^1 \frac{dK_2}{d\bar{r}} d\bar{r}.$$

The above method was used to calculate the running curves of a propeller with segmental blade profiling at a cavitation number of $\chi = 0.4$ and a supercavitating propeller at $\chi = 0.3$. By way of illustration Table 7 shows calculations for a relative radius of $\bar{r} = 0.8$ of the propeller with segmental blade profiling.

Figs. 180 and 181 show a comparison of the results of calculations and experimental data, showing the satisfactory accuracy of the method described.

TABLE 7

Example of Calculations of a Cavitating Propeller

Initial data:

$$\frac{A}{A_d} = 0.80, \quad \chi = 0.4, \quad \bar{r} = 0.8, \quad \frac{H}{D} = 1.4, \quad \bar{b} = 0.565, \quad \delta = 0.024,$$

$$v = \arctg \frac{H}{\pi r} = 0.509, \quad z = 3, \quad \bar{r}_{cr} = 0.165$$

1	α (задано) А	-0,014	0,020	0,056	0,125
2	$\beta_i = v - \alpha$	0,523	0,489	0,453	0,384
3	$\sin \beta_i$	0,499	0,470	0,438	0,374
4	$\bar{r} = \frac{2\pi}{z} \frac{\bar{r}}{\bar{b}} \sin \beta_i$	1,48	1,39	1,30	1,11
5	λ_p^0	1,342	1,201	1,080	0,830
6	$\cos \beta_i$	0,870	0,883	0,899	0,927
7	$\frac{\pi r}{\lambda_p}$	1,892	2,085	2,320	3,025
8	$\sigma_i = \chi \frac{\cos^2 \beta_i}{\left(\frac{\pi r}{\lambda_p} - \frac{v_i}{v_p}\right)^2}$	0,1595	0,1496	0,1394	0,1136
9	$C_{p0}(\alpha, \sigma_i)$	0,121	0,194	0,223	0,307
10	k [по формуле (V.23)] В	0,457	0,363	0,342	0,315
11	$C_y = k C_{p0}$ C	0,055	0,070	0,076	0,097
12	Поправка Прандтля-Гольдштейна $\bar{k}(z, \bar{r}, \beta_i)$	0,59	0,61	0,64	0,69

TABLE 7 (Cont)

13	$\operatorname{tg} \beta_i$	0,576	0,532	0,487	0,403
14	$x = \frac{zb}{4\pi r} \cdot \frac{C_y}{k} \sqrt{1 + \operatorname{tg}^2 \beta_i}$	0,0184	0,0221	0,0224	0,0254
15	$y = x : \operatorname{tg}^2 \beta_i$	0,0553	0,0779	0,0944	0,1564
16	$a_1 = y : (1 - y)$	0,0587	0,0845	0,1042	0,1855
17	$a_2 = x : (1 + x)$	0,0180	0,0216	0,0214	0,0248
18	$(1 - a_2) : (1 + a_1)$	0,930	0,902	0,887	0,823
19	$\lambda_p = \frac{1 - a_2}{1 + a_1} \pi r \operatorname{tg} \beta_i$	1,342	1,201	1,080	0,830
20	$a_2' = a_2 \frac{\pi r}{\lambda_p}$	0,0338	0,0451	0,0498	0,0750
21	$C_x(a; \sigma_i)$	0,0059	0,0089	0,0120	0,0209
22	$\mu = \operatorname{arctg} \frac{C_x}{C_y}$	0,107	0,125	0,156	0,212
23	$\frac{w_i}{nD} = \lambda_p \frac{1 + a_1}{\sin \beta_i}$	2,864	2,780	2,720	2,630
24	$\beta_i + \mu$	0,630	0,614	0,609	0,596
25	$\cos(\beta_i + \mu)$	0,808	0,817	0,820	0,828
26	$\cos \mu$	0,994	0,992	0,988	0,977
27	$\cos(\beta_i + \mu) : \cos \mu$	0,813	0,823	0,830	0,847
28	$\frac{dK_1}{dr} = C_y \bar{b} \left(\frac{w_i}{nD} \right)^2 \frac{\cos(\beta_i + \mu)}{\cos \mu}$	0,209	0,264	0,290	0,330
29	$\sin(\beta_i + \mu)$	0,589	0,576	0,572	0,561
30	$\sin(\beta_i + \mu) : \cos \mu$	0,592	0,580	0,580	0,574
31	$\frac{dK_2}{dr} = C_y \bar{b} r \left(\frac{w_i}{nD} \right)^2 \frac{\sin(\beta_i + \mu)}{\cos \mu}$	0,121	0,148	0,150	0,173

KEY: A--given; B--from formula (V.23); C--Prandtl-Goldshteyn correction.

§45. Hydrodynamic characteristics of cavitating propellers working in a uniformly skewed flow [323]

Let us discuss the movement of a propeller (Fig. 182) with the inclination of its axis of rotation held constant with respect to the direction of motion. Employing the theory of quasi-stationarity, we will analyze the flow around a blade element located at a radius of r on the propeller which rotates at a constant number of revolutions n and moves with a translational velocity of v . The direction of velocity v forms an angle ϕ with the axis of rotation of the propeller. The vector of velocity v for each turn of the blade describes the surface of a circular cone. The angle at the apex of the cone which lies in the plane of the blade element under consideration is equal to twice the angle of downwash ϕ . The axial component of the velocity of the on-

[324]

incoming flow $v_p = v \cos \vartheta$ serves as the height of the cone and is constant in magnitude. As for a propeller working in a uniform flow, v_p is taken to be the characteristic velocity determining the hydrodynamic characteristics of a propeller in an oblique flow. The transverse velocity v_q serves as the radius of the cone base and its projections onto the radial direction and a direction normal to the radius of the propeller are respectively

$$v_r = v_p \operatorname{tg} \varphi \cos \vartheta; \quad \Delta u_\varphi = v_p \operatorname{tg} \varphi \sin \vartheta.$$

Thus, the radial and tip components of velocity change periodically during one revolution of the propeller and consequently the elements of the blades work in a variable velocity field.

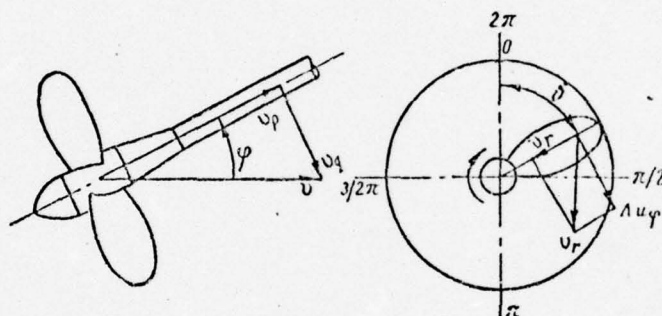


Fig. 182. Directions of propeller velocities in an oblique flow.

In theories of a propeller working in a uniform flow usually the effect of the radial component of velocity on the forces arising on elements of the propeller blades is neglected. In our study of the hydrodynamic characteristics of propellers in an oblique flow we will also neglect the effect of the radial component of velocity and the change in it during one revolution of the blade and we will consider the effect of tip losses, the finiteness of the number of blades, and other factors to be the same as in axial flow.

With these assumptions the distinguishing aspect of the conditions under which a propeller works in an oblique flow will lie in the existence of an additional tangential component of velocity due to the downwash which changes periodically during one revolution of the propeller.

For the purpose of studying the hydrodynamic characteristics of a cavitating propeller in an oblique flow we will introduce a local cavitation number for a blade element

$$\sigma_{\varphi} = \frac{p_0 - p_d}{\frac{\rho}{2} w_{\varphi}^2},$$

where

$$w_{\varphi} = \sqrt{v_p^2 + (2\pi r n + v_p \lg \varphi \sin \theta)^2}$$

takes into account the change in tangential velocity of a propeller in an oblique flow, that is,

$$\sigma_{\varphi} = \frac{\kappa}{1 + \left(\lg \varphi \sin \theta + \frac{\pi r}{\lambda_p} \right)^2}. \quad (\text{V.28})$$

If in (V.28) we set $\phi = 0$, we obtain the well-known [325] expression for the cavitation number of an element of a propeller blade in a uniform flow

$$\sigma = \frac{\kappa}{1 + \left(\frac{\pi r}{\lambda_p} \right)^2}. \quad (\text{V.29})$$

I. Ya. Miniovich showed that in determining the hydrodynamic characteristics of a propeller in a nonuniform flow it is possible to proceed from its characteristics in a uniform flow, considering them to be given.

From the velocity triangle (Fig. 183) it follows that meeting the condition

$$\sigma = \sigma_{\varphi} \quad (\text{V.30})$$

with the same axial component of velocity v_p of, what is the same thing, at equal cavitation numbers κ , ensures equality between angles of attack of corresponding elements of propeller blades in oblique and axial flows. Consequently, the indicated elements are subjected to equal conditions and according to the assumptions made the hydrodynamic forces acting on the elements must be equal in both cases. In order to determine the hydrodynamic characteristics of a cavitating propeller in an oblique flow from its given characteristics in an axial flow it suffices to carry out double integration of forces with respect to the radius of the propeller and the angle of pitch of the blade:

$$K_{1\varphi}(\lambda_p, \kappa) = \frac{1}{2\pi} \int_0^{2\pi} \int_{r_h}^1 \frac{dK_1(\lambda_p', \kappa)}{dr} \left(\frac{\lambda_p}{\lambda_p'} \right)^2 dr d\theta; \quad (\text{V.31})$$

$$K_{2\varphi}(\lambda_p, \kappa) = \frac{1}{2\pi} \int_0^{2\pi} \int_h^1 \frac{dK_2(\lambda'_p, \kappa)}{d\bar{r}} \left(\frac{\lambda_p}{\lambda'_p} \right)^2 d\bar{r} d\vartheta, \quad (\text{V.32})$$

where $dK_1/d\bar{r}$ and $dK_2/d\bar{r}$ are determined on the basis of calculations by element of the running curves of a given propeller under conditions of axial flow. The instantaneous value of the relative advance λ' which for given λ_p and ϕ is a unique function of the angle of rotation of the blade ϑ and relative radius \bar{r} must be determined from equation (V.30) which in light of (V.28) and (V.29) can be transformed to the following form:

$$\lambda'_p = \frac{\pi \bar{r}}{\lg \varphi \sin \vartheta + \frac{\pi \bar{r}}{\lambda_p}}. \quad (\text{V.33})$$

The factor $(\lambda_p/\lambda'_p)^2$ in formulas (V.31) and (V.32) takes into account the difference in propeller revolutions at λ_p and λ'_p . [326]

For calculating the running curves of a cavitating propeller in an oblique flow from formulas (V.31) and (V.32) it is necessary preliminarily to take into account the characteristics of the same propeller in a uniform flow by element. The indicated calculations of running curves of a cavitating propeller in a uniform flow can be carried out by the method described in §44.

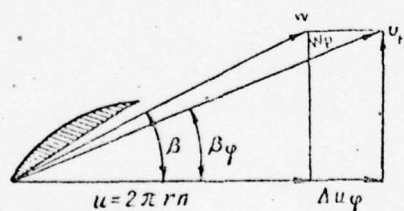


Fig. 183. Velocity triangle of a blade element of a propeller in an oblique flow.

For the purpose of simplifying the calculations of the running curves of a propeller the action of a propeller blade is replaced with the action of an element located in the center of pressure of the blade at a certain radius r_0 . However, as applicable to a propeller working in an oblique flow, this means that the effect of an oblique flow on the propeller as a whole is the same as for an element at radius r_0 while at the same time it is different for each radius. Indeed, in this case condition (V.30) will be satisfied ($\vartheta \neq 0 \neq \pi$) only when $\bar{r} = \bar{r}_0$ (Fig. 184).

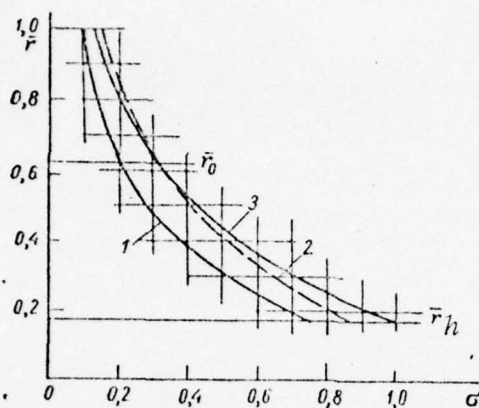


Fig. 184. Change in local cavitation number at instantaneous relative advance λ_p' .

$$1 - \sigma(\bar{r}, \lambda_p); \quad 2 - \sigma(\bar{r}, \lambda_p'); \quad 3 - \sigma_\psi(\bar{r}, \lambda_p, v)$$

$$3 - \sigma_\psi(\bar{r}, \lambda_p, v)$$

For the propeller as a whole meeting this condition strictly is impossible. However, for an approximate solution to the problem propositions can be found such that (V.30) will be satisfied in the best possible way for all elements of the blade. Apparently there must be equality among areas delimited by the curves $\sigma_\phi(\lambda_p, r, \phi, \theta)$ and $\sigma(\lambda_p^*, r)$ drawn as functions of relative radius and by the coordinate axes when $\theta = \text{const}$. Analytically this condition can be expressed by the integral equation

$$\int_{\bar{r}_h}^1 \sigma_\psi(\lambda_p, \bar{r}, \phi, \theta) d\bar{r} = \int_{\bar{r}_h}^1 \sigma(\lambda_p^*, \bar{r}) d\bar{r}. \quad (\text{V.34})$$

Calculating the integrals in (V.34) and taking (V.28) and (V.29) into consideration, we obtain

$$\lambda_p^* \text{arctg} \frac{(1 - \bar{r}_h) \pi \lambda_p^*}{\lambda_p^{*2} + \pi^2 \bar{r}_h^2} = \Phi = \lambda_p \text{arctg} \frac{(1 - \bar{r}_h) \pi \lambda_p}{\lambda_p^2 (1 + \text{tg}^2 \varphi \sin^2 \theta) + (1 + \bar{r}_h^2) \pi \lambda_p \text{tg} \varphi \sin \theta + \pi^2 \bar{r}_h^2}. \quad (\text{V.35}) \quad [327]$$

Calculations which have been performed show that satisfying (V.35) is not only necessary but also for all practical purposes sufficient since in this case the curves of $\sigma_\phi(\lambda_p, r, \phi, \theta)$ and $\sigma(\lambda_p^*, r)$ at corresponding values of θ , λ_p , and λ_p^* are close (Fig. 185).

Based on what has been stated simpler expressions than (V.31) and (V.32) can be written for coefficients of thrust

and moment of a cavitating propeller in an oblique flow:

$$K_{1\varphi}(\lambda_p, \kappa) = \frac{1}{2\pi} \int_0^{2\pi} K_1(\lambda_p^*, \kappa) \times \left(\frac{\lambda_p}{\lambda_p^*} \right)^2 d\theta, \quad (V.36)$$

$$K_{2\varphi}(\lambda_p, \kappa) = \frac{1}{2\pi} \int_0^{2\pi} K_2(\lambda_p^*, \kappa) \times \left(\frac{\lambda_p}{\lambda_p^*} \right)^2 d\theta, \quad (V.37)$$

where the values of K_1 and K_2 in the integrand are determined from corresponding curves for the action of a propeller in an axial flow and λ_p^* from equation (V.35).

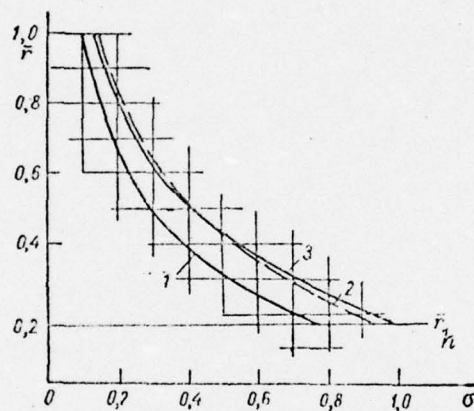


Fig. 185. Change in local cavitation number at instantaneous relative advance λ_p^* .

$$1 - \sigma(\bar{r}, \lambda_p); \quad 2 - \sigma(\bar{r}, \lambda_p^*); \\ 3 - \sigma_{\varphi}(\bar{r}, \lambda_p, \varphi).$$

Formulas (V.36) and (V.37), in distinction from (V.31) and (V.32), make it possible to calculate the running curves of cavitating propellers in an oblique flow from their overall hydrodynamic characteristics for axial flow which can be obtained by means of tests in cavitation tunnels.

In order to determine the values of λ_p^* equation (V.35) should be solved graphically. Ancillary graphs for finding the indicated solution for angles of downwash $\phi = 12^\circ$ and 14° are shown in Figs. 186 and 187 respectively.

In order to check the reliability of the theoretical method of calculating the running curves of cavitating propellers in an oblique flow using formulas (V.36) and (V.37), appropriate calculations were performed for propellers, models of which were tested in cavitation tunnels in axial and oblique [330

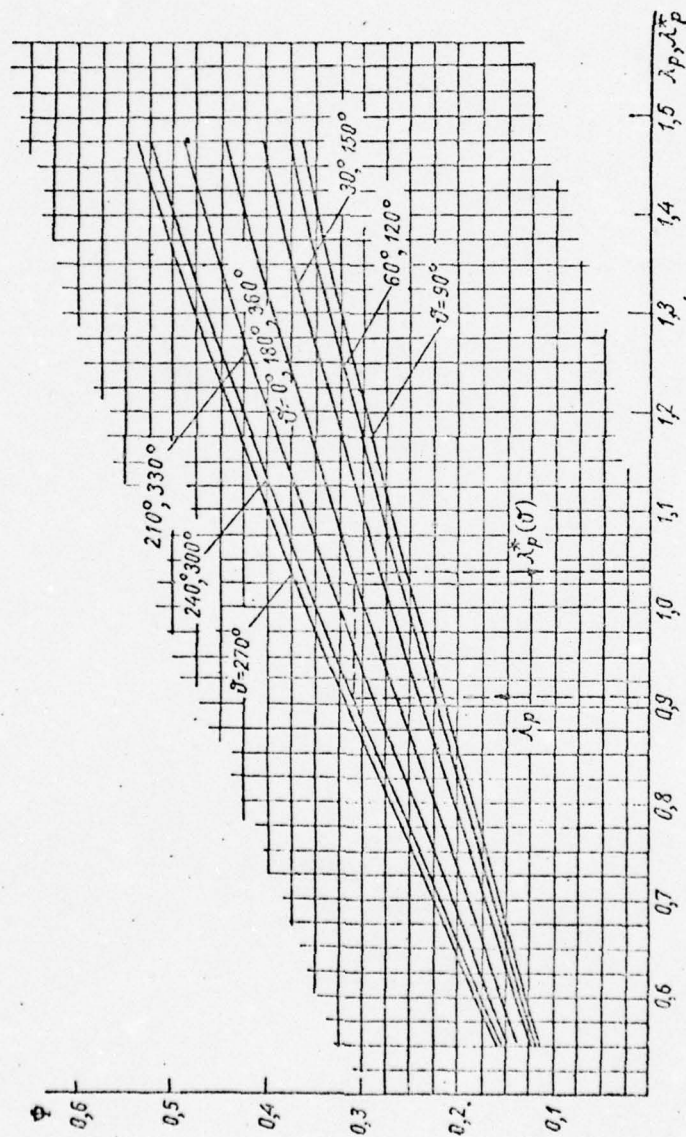


Fig. 186. Graph for determining λ_p^* when $\phi = 12^\circ$.

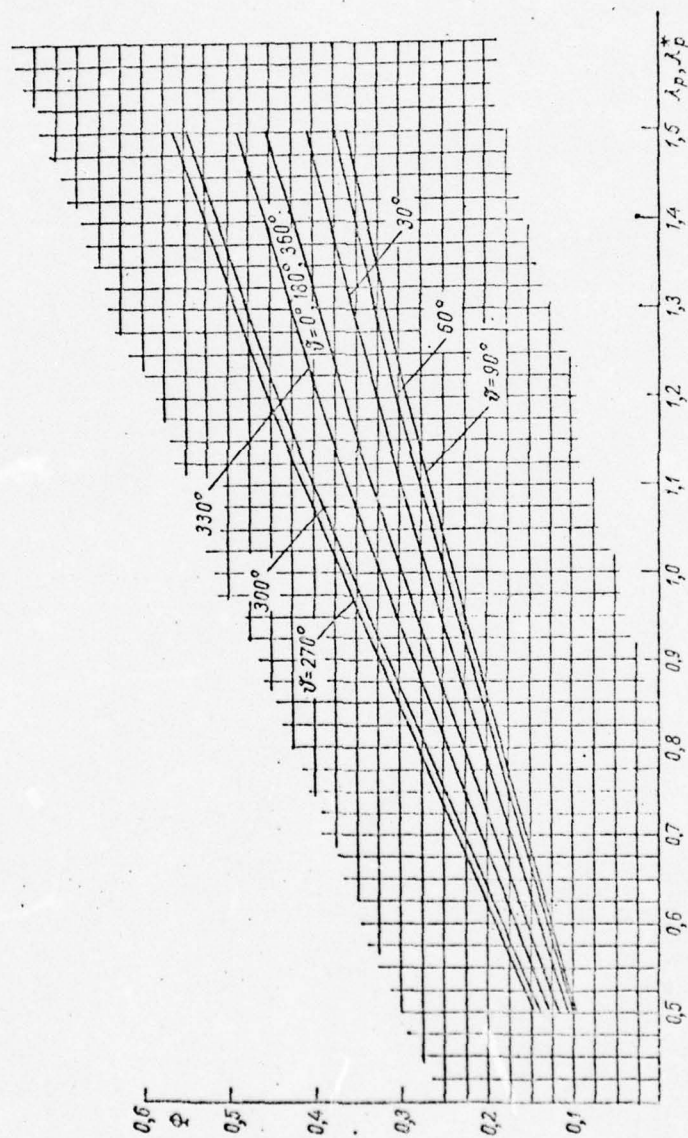


Fig. 187. Graph for determining λ_p^* when $\phi = 14^\circ$.

flows. The comparison of calculations and experiment (from Shirsberg) shown in Fig. 188 is evidence of satisfactory agreement.

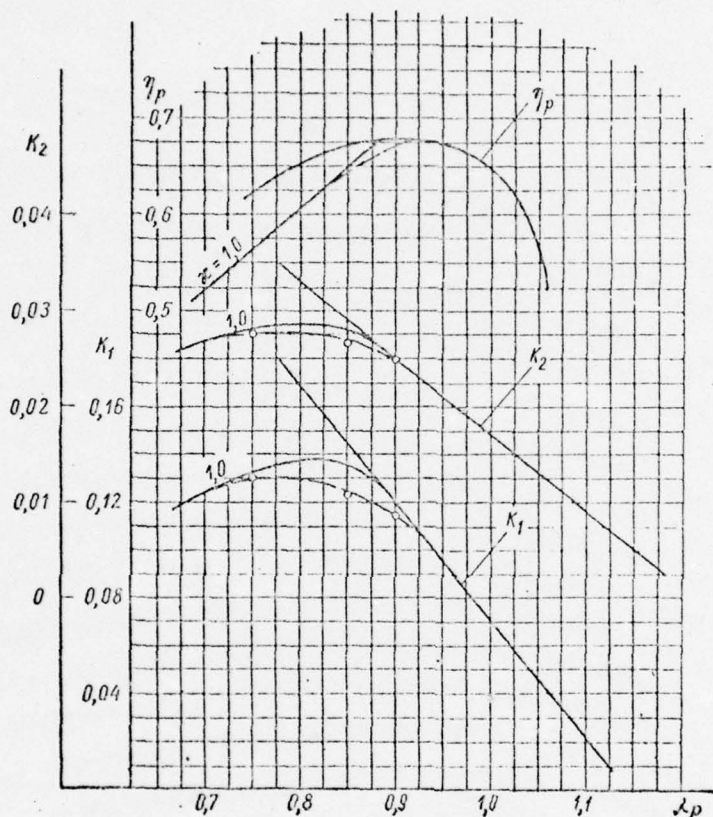


Fig. 188. Running curves of propeller in an oblique flow.
— experiment in axial flow; - - - experiment in oblique flow.
The circles indicate values obtained using formulas (V.36) and (V.37).

Below we discuss in greater detail an investigation of the effect of oblique flow on the efficiency of a propeller.

Usually coefficient η_y characterizing the effect of the conditions under which a propeller works on its efficiency is customarily represented in the form $\eta_y = i_1/i_2$ where i_1 and i_2 are coefficients taking into account the unevenness of flow on thrust and moment respectively of a propeller. By analogy, using formulas (V.31) and (V.32) the indicated coefficients for a propeller working in an oblique flow can be represented in the following form:

[331

$$i_1 = \frac{1}{2\pi K_1} \int_0^{2\pi} \int_{r_h}^1 \frac{dK_1(\lambda_p', \chi)}{d\bar{r}} \left(\frac{\lambda_p}{\lambda_p'} \right)^2 d\bar{r} d\vartheta; \quad (V.38)$$

$$i_2 = \frac{1}{2\pi K_2} \int_0^{2\pi} \int_{r_h}^1 \frac{dK_2(\lambda_p', \chi)}{d\bar{r}} \left(\frac{\lambda_p}{\lambda_p'} \right)^2 d\bar{r} d\vartheta, \quad (V.39)$$

where $dK_1/d\bar{r}$, $dK_2/d\bar{r}$, K_1 , and K_2 are determined from data for the propeller under discussion in an axial flow and λ_p' from formula (V.33).

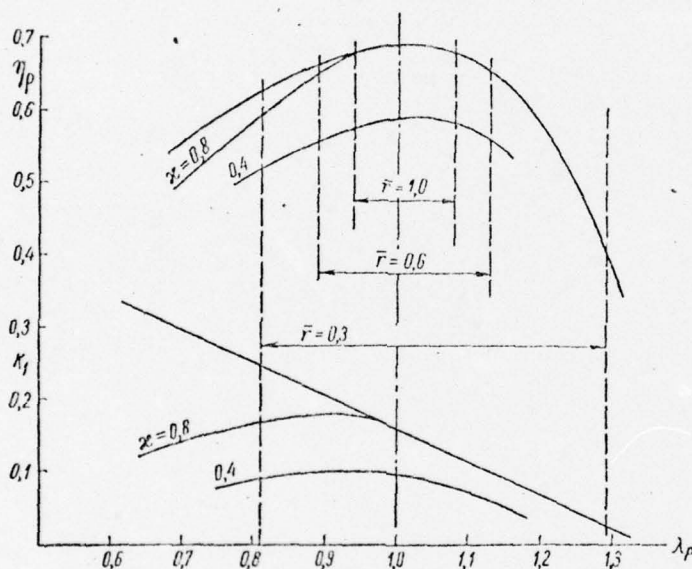


Fig. 189. Change in efficiency of a propeller depending on the relative advance: when $\phi = 12^\circ$ and $\lambda_p = 1.0$, $r = 1.0$; when $\lambda_p' = 0.94-1.08$ and $r = 0.6$; and when $\lambda_p' = 0.89-1.13$ and $r = 0.3$.

Calculations made with (V.38) and (V.39) show that at angles of downwash not exceeding $10-12^\circ$ $i_1 \approx i_2$. Consequently, under the indicated conditions an oblique flow leads to practically no change in the efficiency of a propeller as compared with axial flow. At the same time the instantaneous work modes of elements of a propeller in an oblique flow may change rather significantly during one revolution. Indeed, it follows from (V.33) that the instantaneous advance varies in the range

$$\frac{\lambda_p}{1 + \frac{\lambda_p}{\pi r} \operatorname{tg} \varphi} < \lambda_p' < \frac{\lambda_p}{1 - \frac{\lambda_p}{\pi r} \operatorname{tg} \varphi},$$

[332]

that is, for example, when $\lambda_p = 1.0$ and $\phi = 12^\circ$ for $\bar{r} = 0.3$ we have $\lambda_p' = 0.81--1.29$; for $\bar{r} = 0.6$ $\lambda_p' = 0.89--1.13$; and for $\bar{r} = 1.0$ $\lambda_p' = 0.94--1.08$. For the indicated limits of change in λ_p the efficiency of a propeller changes significantly (Fig. 189) which at first glance contradicts the conclusion reached above. Therefore it is necessary to discuss this matter in greater detail, concentrating on its physical significance. It follows from formula (V.4) that when a propeller works in a uniform flow always $\epsilon > 0$, $\Delta\beta > 0$, and $\eta < 1$. However, we can imagine an external flow for which $\Delta\beta < 0$ and $\mu < 0$. In this case $\eta > 1$, that is, the propeller uses the energy of the external flow and develops useful power, in this case the propeller working as a turbine.

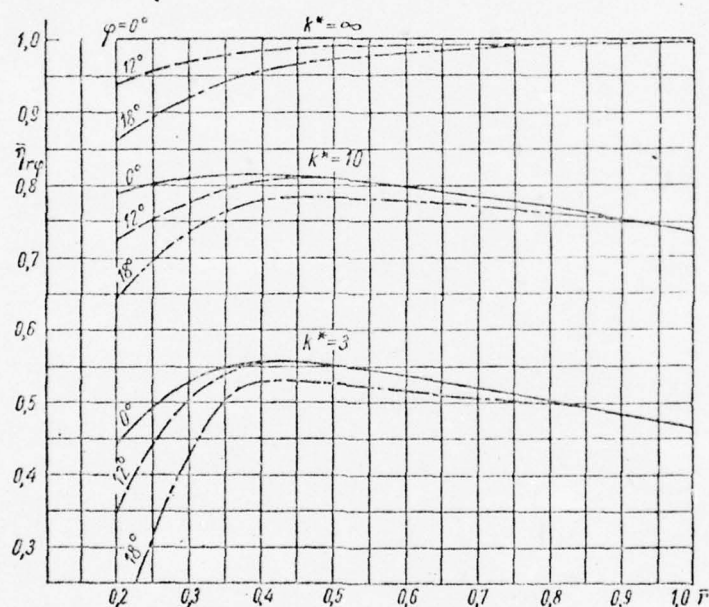


Fig. 190. The relation $\eta_{r\phi}(\bar{r})$ for different values of ϕ when $\lambda_p = 1$.

For a propeller in an oblique flow the external flow creates an additional tangential component of velocity equal to $\Delta u_\phi = v_p \text{tg} \phi \sin \theta$. In this way in that part of a propeller disk where $\Delta u_\phi > 0$, the value of μ can decrease and the efficiency increase and, on the other hand, when $\Delta u_\phi < 0$ the efficiency will decrease in comparison with uniform flow. In this event in the general case the values of ϵ , $\Delta\beta$, and μ will also change and we will designate them ϵ_ϕ , $\Delta\beta_\phi$, and μ_ϕ .

[333]

In light of what has been stated we will represent the efficiency of an element of a propeller blade in an oblique flow in the form

$$\eta_{r\varphi} = \frac{\operatorname{tg} \beta}{\operatorname{tg} (\beta + \mu_{\varphi})}. \quad (\text{V.40})$$

But

$$\mu_{\varphi} = \varepsilon_{\varphi} + \Delta\beta_{\varphi}, \quad \Delta\beta_{\varphi} = \Delta\beta + \beta_{\varphi} - \beta,$$

that is,

$$\eta_{r\varphi} = \frac{\operatorname{tg} \beta}{\operatorname{tg} (\beta_{\varphi} + \varepsilon_{\varphi} + \Delta\beta)}.$$

If we neglect the change in ε_{φ} as compared with ε in the case under consideration, we will have

$$\eta_{r\varphi} = \frac{\operatorname{tg} \beta}{\operatorname{tg} (\beta_{\varphi} + \mu)}. \quad (\text{V.41})$$

We will determine the mean efficiency of an element during one revolution for the purpose of evaluating the change in efficiency of a propeller in an oblique flow. For this purpose we calculate the integral

$$\frac{1}{\pi} \int_{-\pi/2}^{\pi/2} \operatorname{tg} (\beta_{\varphi} + \mu) d\varphi = \operatorname{tg} \mu + \frac{\lambda_p (1 + \operatorname{tg}^2 \mu)}{V(\pi^2 - \lambda_p \operatorname{tg} \mu)^2 - \lambda_p^2 \operatorname{tg}^2 \varphi}. \quad (\text{V.42})$$

Consequently, the mean value for the efficiency of one element during one revolution of a propeller can be represented in the form

$$\begin{aligned} \bar{\eta}_{r\varphi} &= \frac{1}{2\pi} \int_0^{2\pi} \eta_{r\varphi} d\varphi = \\ &= \operatorname{tg} \beta : \left[\operatorname{tg} \mu + \frac{\lambda_p (1 + \operatorname{tg}^2 \mu)}{V(\pi^2 - \lambda_p \operatorname{tg} \mu)^2 - \lambda_p^2 \operatorname{tg}^2 \varphi} \right]. \end{aligned} \quad (\text{V.43})$$

By analogy with (V.43) for an element of a propeller in a uniform flow we can write

$$\eta_r = \operatorname{tg} \beta : \left[\operatorname{tg} \mu + \frac{\lambda_p (1 + \operatorname{tg}^2 \mu)}{V(\pi^2 - \lambda_p \operatorname{tg} \mu)^2} \right]. \quad (\text{V.44})$$

From a comparison of (V.43) and (V.44) it follows that the efficiency of an element of a propeller in an oblique flow due to the existence of the term $\lambda_p \operatorname{tg} \phi$, all other conditions remaining equal, will always be less than in a uniform flow.

For a quantitative evaluation of this effect formulas (V.43) and (V.44) were used to make calculations, the results of which are shown in Fig. 190 in the form of the relations $\eta_{r\phi}(\bar{r})$ for different values of ϕ and k^* for $\lambda_p = 1$. It follows from the figure that, all other conditions remaining the same, the efficiency of elements decreases as the elements become closer to the hub. For relatively small angles of downwash the effect of nonuniformity in flow for the most part begins to become manifest when $\bar{r} < 0.4$ and this explains the weak effect of an oblique flow on the efficiency of a propeller as a whole when $\phi < 12^\circ$. When the angles of downwash increase to $\phi = 18^\circ$ [334] such an effect becomes manifest on practically all elements. Therefore in the indicated case the effect of oblique flow on the efficiency of propellers must be considered. Calculations show that at angles of downwash on the order of $\phi = 18^\circ$ -- 20° the change in propeller efficiency will be significant (10--15%).

§46. Hydrodynamic characteristics of propellers piercing the free surface of the water

Due to design peculiarities it is sometimes advisable to use on hydrofoil craft propellers which pierce the free surface of the water. In this case the conditions affecting a propeller's work differ greatly from those affecting a fully submerged propeller. First of all, the hydraulic section of the propeller is reduced since part of the blades is always out of the water. Unwetting of blades causes nonstationary development of lift on the elements of each blade and entrainment of air around the propeller disk.

The work of a propeller which pierces the free surface or is located close to it, in distinction from a deeply submerged propeller, is accompanied by wave phenomena on the surface. All this leads to a change in the hydrodynamic characteristics of partially immersed propellers as compared with those which are deeply submerged. The results of known experimental investigation into the hydrodynamic characteristics of propellers piercing the free surface show that the thrust exerted by propellers under goes an especially great change. Their efficiency is reduced to a much less degree [5].

Because of the special conditions under which partially immersed propellers work generally accepted methods of making calculations cannot be used for determining their hydrodynamic characteristics. As a consequence of this fact a need arises to study phenomena arising in the work of a propeller at the boundary of a liquid or close to it and to create new methods for determining their characteristics [6].

Work [7] is devoted to a study of a propeller rotating close to the free surface of the water. It sets forth justi-

fication of a method for calculating the hydrodynamic characteristics of completely submerged propellers.

In this section we will investigate the effect of a decrease in hydraulic section and nonstationarity on the work of a propeller whose blades pierce the free surface of the water. As a comparison of the results of calculations performed by the method developed in the course of this investigation and the results of experiment shows, the effect of these latter two factors is manifest in the main in the hydrodynamic characteristics of a partially immersed propeller. [335]

In distinction from deeply immersed propellers the coefficient of thrust of a propeller piercing the free surface of the water can be written as follows:

$$\bar{K}_1 = \frac{\bar{P}}{\rho n^2 D^4} = \frac{z}{8\pi} \int_{\bar{x}}^{\frac{R}{\bar{x}}} \int_{\vartheta_1}^{\vartheta_2} C_y \frac{b}{D} \left(\frac{w_i}{nD} \right)^2 \cos \beta_i (1 - \bar{\varepsilon} \operatorname{tg} \beta_i) d\vartheta d\bar{r}, \quad (\text{V.45})$$

where

$$\bar{P} = \frac{z}{2\pi} \int_{\bar{x}}^{\frac{R}{\bar{x}}} \int_{\vartheta_1}^{\vartheta_2} \frac{\rho}{2} C_y b \omega_i^2 \cos \beta_i (1 - \bar{\varepsilon} \operatorname{tg} \beta_i) d\vartheta d\bar{r} \quad (\text{V.46})$$

expresses the mean value per revolution of the thrust of a partially immersed propeller; z is the number of propeller blades; R and D are the radius and diameter of the propeller; \bar{x} the least possible value of effective radius per revolution of the propeller; $\bar{x} = \bar{x} R$; ϑ_1 and ϑ_2 are respectively the angles of entry into the water and exit from it for a blade element at a given radius r measured clockwise from the vertical (Fig. 191); ρ is the density of the water; C_y the coefficient of lift of a blade element at radius \bar{r} ($\bar{r} = r/R$); b the chord of the blade section corresponding to this radius; w_i and β_i the induced velocity and angle of advance; $\bar{\varepsilon}$ the drag-lift ratio of the profile; and n the number of revolutions of the propeller.

If h_0 is the distance from the axis of a propeller to the free surface of the water, its deformation being taken into account (see Fig. 191), then for angles of entry and exit of each radius when $r \geq |h_0|$ the following relations hold:

$$\left. \begin{aligned} \vartheta_1 &= \frac{\pi}{2} + \operatorname{arcsin} \frac{h_0}{r}, \\ \vartheta_2 &= \frac{3}{2} \pi - \operatorname{arcsin} \frac{h_0}{r}. \end{aligned} \right\} \quad (\text{V.47})$$

Radii satisfying the inequality $r \leq |h_0|$ do not pierce the free surface and therefore for them $\vartheta_1 = 0$ and $\vartheta_2 = 2\pi$. It [336]

should be noted that when $h_0 > 0$ the lower limit of integration $= h_0$ and when $h_0 < 0$ the radius of the hub ($\bar{r}_h = r_h/R$) should be used for x .

Coefficient C_y in this case is a complex function of the path covered by the blade element under consideration from the start of entry into the water. As follows from formula (II.91) the lift on a foil moving in a liquid from a state of rest at a constant rate is the following function of path traveled:

$$\bar{Y} = \left[1 - \frac{\sqrt{2}}{\pi} \cdot \frac{1}{V(s+1)(s+2)} \times K\left(\frac{\pi}{2}; \sqrt{\frac{s(s+3)}{(s+1)(s+2)}}\right) \right], \quad (V.48)$$

where $s = \alpha_l/b/2$; α_l is the path traveled by the foil or, in the given case, the blade element from the instant of entry into the water; K a total elliptical integral of the first order; $\bar{Y} = Y/Y_h$; Y is the current value of lift; $Y_h = C_{y0} \frac{\rho v_l^2}{2} b$ is the stationary lift on the blade element. Taking formula (V.48) into account coefficient C_y can be written in the form

$$C_y = C_{y0} F(s), \quad (V.49)$$

where

$$F(s) = \left[1 - \frac{\sqrt{2}}{\pi} \cdot \frac{1}{V(s+1)(s+2)} K\left(\frac{\pi}{2}; \sqrt{\frac{s(s+3)}{(s+1)(s+2)}}\right) \right].$$

A graph of function $F(s)$ is presented in Fig. 192. The path traveled by a blade element during an increase in angle of rotation from $\vartheta = \vartheta_1$ to $\vartheta = \vartheta_2$, taking into account the forward movement of the propeller, can be calculated from the formula

$$\alpha_1 = \frac{v_p \Delta \vartheta}{2\pi n} \sqrt{1 + \left(\frac{\pi r}{\lambda_p}\right)^2}, \quad (V.50)$$

where v_p is the translational velocity of the propeller; $\Delta \vartheta = \vartheta_2 - \vartheta_1$; and $\lambda_p = v_p/nD$ is the relative advance of the propeller.

Accordingly the dimensionless expression for the path takes the following form: [337

$$s = \frac{\lambda_p \Delta \vartheta}{b\pi} \sqrt{1 + \left(\frac{\pi r}{\lambda_p}\right)^2}, \quad \left(b = \frac{b}{D}\right). \quad (V.51)$$

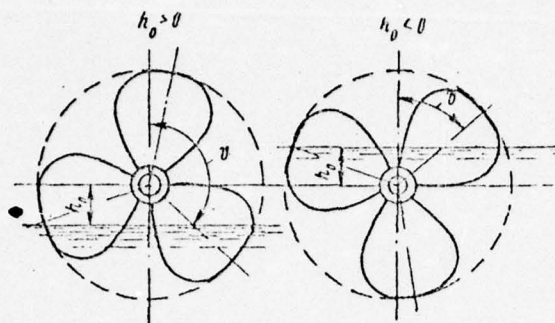


Fig. 191. Diagram showing location of partially immersed propeller with respect to surface of water.

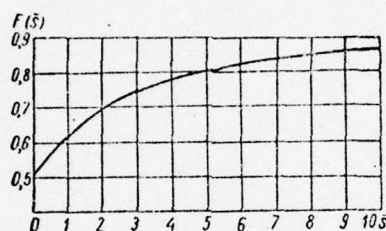


Fig. 192. Determining the effect of nonstationarity on the lift of a propeller blade element.

Substituting (V.49) into (V.45), we obtain for the coefficient of thrust the following relation:

$$\bar{K}_1 = \frac{z}{2\pi} \int_{\bar{x}}^{\frac{1}{x}} \int_{\phi_1}^{\phi_2} \left[\frac{1}{4} C_{y0} \bar{b} \left(\frac{w_t}{nD} \right)^2 \cos \beta_t (1 - \bar{\epsilon} \lg \beta_t) d\bar{r} \right] F(s) d\phi. \quad (\text{V.52})$$

Observing that in this formula the expression in brackets is the differential of coefficient of thrust of a propeller blade element when movement is steady, that is, dK_1 , we transform it into:

$$\bar{K}_1 = \frac{z}{2\pi} \int_{\bar{x}}^{\frac{1}{x}} \int_{\phi_1}^{\phi_2} F(s) \frac{dK_1}{d\bar{r}} d\bar{r} d\phi. \quad (\text{V.53})$$

For a propeller whose axis is above the surface of the water formula (V.53) is written in the following form:

$$\bar{K}_1 = \frac{z}{2\pi} \int_{\bar{h}_0}^{\frac{1}{h_0}} \int_{\phi_1}^{\phi_2} F(s) \frac{dK_1}{d\bar{r}} d\bar{r} d\phi, \quad \bar{h}_0 = \frac{h_0}{K}. \quad (\text{V.54})$$

When $h_0 < 0$, that is, in that case when the axis is below

water level,

$$\bar{K}_1 = \frac{z}{2\pi} \int_{|\bar{h}_0|}^1 \int_{\phi_1}^{\phi_2} F(s) \frac{dK_1}{dr} d\bar{r} d\phi + z \int_{\bar{h}}^{\bar{h}_0} \frac{dK_1}{dr} d\bar{r}. \quad (\text{V.55})$$

In the particular case of a half-immersed propeller when $h_0 = 0$ we have the following formula:

$$\bar{K}_1 = \frac{z}{2\pi} \int_{\bar{r}_h}^1 \int_{\phi_1}^{\phi_2} F(s) \frac{dK_1}{dr} d\bar{r} d\phi. \quad (\text{V.56})$$

Substituting the values of the derivative $dK_1/d\bar{r}$, which is calculated taking into account all changes which the free surface causes in the work of the propeller, into formulas (V.53)--(V.56) and integrating we find the coefficient of thrust for a partially immersed propeller.

By way of example we will calculate the value of the coefficient of thrust for a half-immersed propeller having the following elements: $D = 0.20$ m, disk ratio $A/A_d = 0.65$, pitch ratio $H/D = 1.0$, number of blades $z = 3$. The given propeller [338] was tested in open water and at $h_0 = 0$. The results of the tests are presented in Fig. 193.

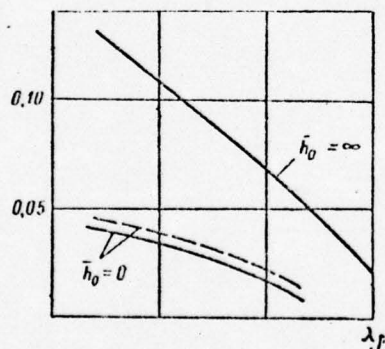


Fig. 193. Change in coefficient of thrust of half-immersed propeller.
— experiment;
— — — calculated.

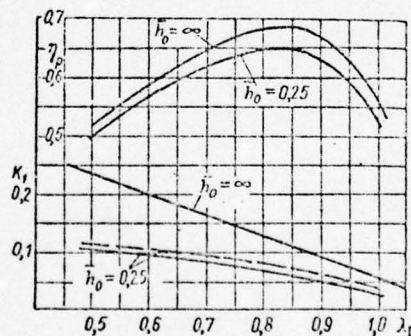


Fig. 194. Running curves of partially immersed propeller.
— experiment;
— — — calculated.

For the purpose of simplifying calculations we will assume that the value of the parameters C_{y0} , v_i , β_i , and ϵ do not depend on the depth of immersion of the propeller and we will replace the effect of the propeller as a whole with the effect of an equivalent section located at a radius r_0 which coincides with the center of gravity of a straightened blade surface (in the case under consideration $r_0 = 0.6$,

$$\bar{b} = 0.486).$$

These assumptions make it possible to write (V.56) in the form:

$$\bar{K}_1 = \frac{K_1}{2\pi} \int_{\pi/4}^{3\pi/4} F(s) d\vartheta = \frac{K_1}{2} \bar{F}(s),$$

where K_1 is the coefficient of thrust of the propeller in open water.

Using formula (V.51) to redraw the graph of function $F(s)$ as a function of ϑ and integrating numerically in the last expression we obtain the values for coefficient of thrust as a function of relative advance shown in Table 8 and in the graph in Fig. 193.

TABLE 8

Values of Coefficient of Thrust

λ_p	0,86	0,92	1,00
$\bar{F}(s)$	0,682	0,685	0,686
\bar{K}_1	0,043	0,034	0,023

Calculations were performed analogously for a propeller with the specifications $D = 0.2$ m; $A/A_d = 0.382$; $H/D = 1.0$; and $z = 3$ immersed to a depth of $h = -0.25$. The results of these calculations are compared in Fig. 194 with the results of tests of the same propeller according to Kempf. [339]

A comparison of test and calculated data confirms that the main factors determining the hydrodynamic characteristics of a partially immersed propeller are the decrease in its hydraulic section and nonstationarity in the development of lift on its blades. The method of calculation developed makes it possible to take into account the effect of these factors and this gives good reason to recommend the method for determining the hydrodynamic characteristics of propellers whose blades pierce the free surface of the water.

§47. Calculation of the way-making ability of planing and hydrofoil craft

The distinguishing aspects of the work of propellers on planing and hydrofoil craft were noted above. We will discuss in greater detail (Fig. 195) the system of forces acting on a propeller working in an oblique flow.

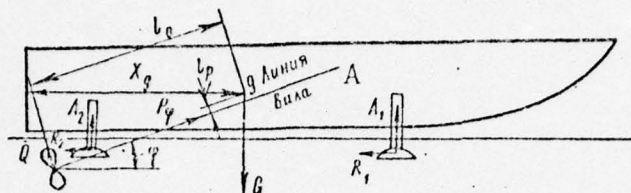


Fig. 195. Diagram of forces acting on a moving hydrofoil craft.
KEY: A--line of shaft.

It is known that on propellers in an oblique flow, in addition to the force acting along the axis of the propeller P_ϕ , there arises a transverse force Q directed perpendicularly to the propeller shaft. Obviously the forces developed by propellers in an oblique flow will change the attitude of a craft and consequently its drag. The attitude of a particular craft is determined by its weight and location of the center of gravity and therefore the effect of the propellers on the drag of hydrofoil craft can conveniently be reduced to a change in the magnitude of these characteristics [8].

Let us assume that a hydrofoil craft has n propellers. Then the correction for the weight of the craft will be determined completely by the sum of the vertical projections of the forces generated by the propellers (Fig. 195)

$$\Delta G = \sum_{i=1}^n P_{\phi i} \left(\sin \varphi_i + \frac{Q_i}{P_{\phi i}} \cos \varphi_i \right). \quad (V.57)$$

The effect of moment $\Delta M = \sum_{i=1}^n (P_{\phi i} l_{pi} + Q_i l_{qi})$ created by the [340]
propellers with respect to the center of gravity of the craft is equivalent to a change in the location of the latter along the length by the magnitude

$$\Delta x_g = \frac{1}{G} \sum_{i=1}^n (P_{\phi i} l_{pi} + Q_i l_{qi}), \quad (V.58)$$

where G is the weight of the craft. In this event the moment is considered to be positive if it causes the craft to be trimmed by the bow.

Thus, when determining the drag on hydrofoil craft instead of the actual values of the weight G and the location of the center of gravity along the length x_g their reduced values which take into consideration the effect of the propellers should be used. They are respectively:

$$G^* = G - \Delta G = G - \sum_{i=1}^n P_{qi} \left(\sin \varphi_i + \frac{Q_i}{P_{qi}} \cos \varphi_i \right), \quad (V.59)$$

$$x_g^* = x_g + \Delta x_g = x_g + \frac{1}{G} \sum_{i=1}^n P_{qi} \left(l_{pi} + \frac{Q_i}{P_{qi}} \right) l_{qi}. \quad (V.60)$$

If the relations between the drag R of the type of craft under consideration as a function of the velocity v , weight G , and location of center of gravity x_g without propellers

$$R = f(v, G, x_g), \quad (V.61)$$

are known from calculations or model tests, then drag R^* of a craft working with propellers can be found on the basis of these same relations (V.61). For this purpose instead of the actual weight and location of the center of gravity G and x_g use can be made of their reduced values G^* and x_g^* as determined from formulas (V.59) and (V.60), that is,

$$R^* = f(v, G^*, x_g^*). \quad (V.62)$$

Let us assume that each propeller must overcome part of the drag on a craft R_i^* , where $R^* = \sum_{i=1}^n R_i^*$. Then the propeller under consideration must develop in the direction of the axis of its rotation the thrust

$$P_{qi} = \frac{R_i^*}{\cos \varphi_i} + Q_i \operatorname{tg} \varphi_i. \quad (V.63)$$

Let us now continue on to a determination of the propulsive efficiency of the craft which we will write in the form [341

$$\eta = \frac{Rv}{N_e} = \frac{v \sum_{i=1}^n R_i}{\sum_{i=1}^n N_{ei}}, \quad (V.64)$$

where $R = \sum_{i=1}^n R_i$ is the towed drag of the craft without taking

into consideration the effect of the propellers; $N_e = \sum_{i=1}^n N_{ei}$

the total power of the mechanical installation; and R_i and N_{ei} are respectively those parts of towed drag and power attributed to the i -th propeller.

We will determine preliminarily the value of the propulsive efficiency provided by the i -th propeller. Obviously,

$$\eta_i = \frac{R_i v}{N_{ei}}.$$

We will express R_i in terms of the characteristics of a propeller. Setting $R_i^* = R_i - \Delta R_i$, we obtain from formula (V.63)

$$R_i = P_{\varphi i} \cos \varphi_i + \Delta R_i - Q_i \sin \varphi_i.$$

In light of what has been stated, defining the efficiency of a propeller in an oblique flow $\eta_{\phi i}$ as

$$\eta_{\phi i} = \frac{P_{\varphi i} v_{pi}}{N_{ei}},$$

where $v_{pi} = v \cos \phi_i$, we finally obtain

$$\eta_i = \eta_{\phi i} \left(1 + \frac{\Delta R_i}{P_{\varphi i} \cos \varphi_i} - \frac{Q_i}{P_{\varphi i}} \operatorname{tg} \varphi_i \right). \quad (\text{V.65})$$

In deriving formula (V.65) the power loss from engine to propeller was not taken into account.

Thus, if a planing or hydrofoil craft has n engine-driven propellers, then its overall propulsive efficiency can be determined as follows:

$$\begin{aligned} \eta &= \frac{v \sum_{i=1}^n R_i}{\sum_{i=1}^n N_{ei}} = \frac{R_1 v}{N_{e1}} \frac{N_{e1}}{N_e} + \dots + \frac{R_n v}{N_{en}} \frac{N_{en}}{N_e} = \\ &= \eta_1 \frac{N_{e1}}{N_e} + \dots + \eta_n \frac{N_{en}}{N_e} = \frac{1}{N_e} \sum_{i=1}^n \eta_i N_{ei}. \end{aligned} \quad (\text{V.66})$$

For practical use of the results obtained it is necessary to be able to determine the transverse force of a propeller in an oblique flow Q . Below we show the reasons for the rise of a transverse force and we present formulas for calculating it. [342]

Let us consider a propeller whose axis of rotation forms the angle ϕ with its direction of movement. We will break the velocity vector of forward movement v of the propeller down into two components: one we will direct along the axis $v_p = v \cos \phi$ and the second we will direct perpendicular to the axis of rotation of the propeller $v_q = v \sin \phi$. The second component of the velocity will lie in the plane of the propeller disk and be directed downward. We will show that in this case a transverse force will arise which will be directed upward regardless of the direction of propeller rotation.

Fig. 196 shows right- and left-rotating propellers and also a velocity triangle of an element of a propeller blade in an oblique flow.

It follows from Fig. 196 that as a blade passes through sector I the flow around it will cause greater angles of attack than in sector II ($\alpha_1 > \alpha_2$). Therefore the tangential force acting on the blade in sector I will always be greater than in sector II. This circumstance will lead to the rise of a transverse force which will be equal to the resulting vertical projections of the tangential forces of the blades in one revolution of the propeller. As follows from Fig. 196 the transverse force will be directed upward regardless of the direction of propeller rotation.

Let us proceed to establish an analytical relation for determining the transverse force.

The component of transverse force at a certain position of the blade characterized by angle of rotation ϑ is

$$Q_\vartheta = T_\vartheta \sin \vartheta, \quad (\text{V.67})$$

where T_ϑ is the instantaneous tangential force determined from the formula

$$T_\vartheta = \frac{M_\vartheta}{r_0} = \frac{\rho n^{*2} D^5}{2\pi r_0} K_2(\lambda_p^*, \kappa). \quad (\text{V.68})$$

In formula (V.68) M_ϑ is the instantaneous value of the moment of the propeller at angle of blade rotation ϑ ; r_0 the propeller radius corresponding to the location of the center of pressure of the blade; $n^* = n\lambda_p/\lambda_p^*$ the reduced number of revolutions of the propeller; and λ_p^* is found from equation (V.35). [343]

By integrating expression (V.67) in light of formula (V.68) with respect to the angle of blade rotation ϑ from 0 to 2π we find the mean value per revolution of transverse force rising on a propeller in an oblique flow

$$Q = \frac{1}{2\pi} \int_0^{2\pi} Q_\vartheta d\vartheta = \frac{\rho n^{*2} D^5}{2\pi r_0} \int_0^{2\pi} K_2(\lambda_p^*, \kappa) \left(\frac{\lambda_p}{\lambda_p^*} \right)^2 \sin \vartheta d\vartheta. \quad (\text{V.69})$$

We will introduce a dimensionless coefficient of transverse force from the formula

$$K_q = \frac{Q}{\rho n^{*2} D^5} = \frac{1}{\pi r_0} \int_0^{2\pi} K_2(\lambda_p^*, \kappa) \left(\frac{\lambda_p}{\lambda_p^*} \right)^2 d\vartheta. \quad (\text{V.70})$$

The following approximate formula can be recommended along with (V.70) for the purpose of determining the coefficient of transverse force K_q :

$$K_q = 1,11 \int_{-\pi/2}^{\pi/2} K_2(\lambda_p', \kappa) \left(\frac{\lambda_p}{\lambda_p'} \right)^2 \sin \vartheta d\vartheta, \quad (V.71)$$

where the value of instantaneous relative advance is

$$\lambda_p' = \frac{\lambda_p}{1 + 0,67 \lambda_p \operatorname{tg} \psi \sin \vartheta}. \quad (V.72)$$

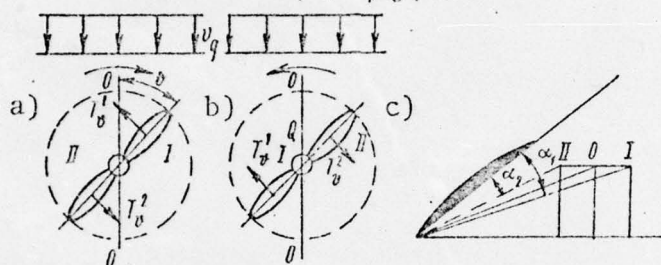


Fig. 196. Rise of transverse force on a propeller.

The above results can be used for calculating way-making ability, that is, for determining the elements of propellers and the propulsive qualities of planing and hydrofoil craft.

We will introduce approximate formulas for evaluating the effect of propellers on the drag and propulsive qualities of planing and hydrofoil craft. To this end we will introduce lift-drag ratios of a craft both without taking the propeller effect into account ($k = G/R$) and with it ($k^* = G^*/R^*$). Considering that foil systems calculated for loads G and G^* can have the same ratio, we will assume that $k = k^*$. We will also consider that all propeller-driving machinery is identical, that is,

$$R^* = \sum_{i=1}^n R_i^* = nR_i^*,$$

$$P_\psi = \sum_{i=1}^n P_{\psi i} = nP_{\psi i}, \quad Q = \sum_{i=1}^n Q_i = nQ_i. \quad (V.73)$$

Then by using formulas (V.59) and (V.63), which in this case assume the form: [344

$$G^* = G - P_\psi \left(\sin \psi + \frac{Q}{P_\psi} \cos \psi \right), \quad P_\psi = \frac{R^*}{\cos \psi} + Q \operatorname{tg} \psi, \quad (V.74)$$

we obtain

$$R^* = \frac{G^*}{k} = \frac{1}{k} \left(G - R^* \operatorname{tg} \psi - Q \frac{\sin^2 \psi}{\cos \psi} - Q \cos \psi \right)$$

or after transforming

$$R^* = \frac{1}{k} \left(G - R^* \operatorname{tg} \psi - \frac{Q}{\cos \psi} \right). \quad (V.75)$$

Solving (V.75) for R^* , we find

$$R^* = R \left(1 - \frac{Q}{G} \cos \varphi \right) \cdot \frac{k}{k + \operatorname{tg} \varphi}. \quad (\text{V.76})$$

Assuming further that $q = Q/P_\phi$ and using formula (V.74), we determine

$$Q = q \left(\frac{R^*}{\cos \varphi} + Q \operatorname{tg} \varphi \right),$$

whence

$$Q = \frac{q}{1 - q \operatorname{tg} \varphi} \cdot \frac{R^*}{\cos \varphi}. \quad (\text{V.77})$$

Substituting (V.77) into (V.76) and substituting at the same time $G = kR$, we have

$$R^* = R \left(1 - \frac{q}{1 - q \operatorname{tg} \varphi} \cdot \frac{R^*}{kR} \right) \frac{k}{k + \operatorname{tg} \varphi}. \quad (\text{V.78})$$

Solving (V.78) for R^* , we finally obtain

$$R^* = \frac{kR}{k + \operatorname{tg} \varphi + \frac{q}{1 - q \operatorname{tg} \varphi}}. \quad (\text{V.79})$$

In the case considered the formula for propulsive efficiency will take the following form:

$$\eta = \eta_\varphi \left(1 + \frac{\Delta R}{P_\phi \cos \varphi} - q \operatorname{tg} \varphi \right). \quad (\text{V.80})$$

Inasmuch as $\Delta R = R - R^*$, then on the basis of formula (V.79) we have

$$\Delta R = R \left(1 - \frac{k}{k + \operatorname{tg} \varphi + \frac{q}{1 - q \operatorname{tg} \varphi}} \right). \quad (\text{V.81})$$

Taking into account (V.81), (V.79), (V.77), and (V.74), [345] we transform the term $\Delta R/P_\phi \cos \varphi$ in formula (V.80) to

$$\frac{\Delta R}{P_\phi \cos \varphi} = \frac{1}{k} (q + \operatorname{tg} \varphi - q \operatorname{tg}^2 \varphi). \quad (\text{V.82})$$

After substituting (V.82) into (V.80) and transforming slightly we finally obtain

$$\eta = \eta_\varphi \left[1 + \frac{1}{k} (q + \operatorname{tg} \varphi) - q \operatorname{tg} \varphi \left(1 + \frac{\operatorname{tg} \varphi}{k} \right) \right]. \quad (\text{V.83})$$

Fig. 197 shows the results of calculations made with formulas (V.79) and (V.83) for the ratios R^*/R and η/η_0 as a function of the lift-drag ratio of a craft when the angle of downwash is $\phi = 14^\circ$ and $q = 0.2$.

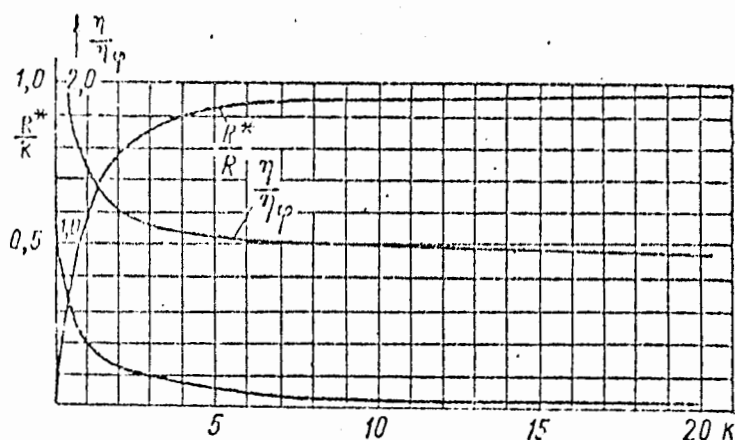


Fig. 197. Results of calculations made with formulas (V.79) and (V.83) when $\phi = 14^\circ$ and $q = 0.2$.

It follows from a consideration of Fig. 197 that propellers working in an oblique flow have a significant effect on the drag and propulsive efficiency of planing and hydrofoil craft which is greater, the less the lift-drag ratio of the craft.

Calculations of the way-making ability of planing and hydrofoil craft, as for ordinary craft, should be performed by the method of successive approximations.

Below by way of example we present calculations of the way-making ability of a hydrofoil craft.

* * *

Propeller Calculations and Determination of the Characteristics of a Mechanical Plant

Initial data. A hydrofoil launch weighs 20 T. The relation $(R/\Lambda)(v_k)$ is shown in Fig. 198. The launch is equipped with $z_p = 1$ propeller.

Maximum speed of movement $v_k = 86.5$ km/hr. Diameter of propeller $D = 0.65$ m. Angle of downwash $\phi = 14^\circ$. Depth of immersion of propeller axis $h = 0.5$ m.

Calculations.

1. Calculated velocity of propeller

$$v_p = 0.278 v_k \cos \phi = 0.278 \cdot 86.5 \cdot 0.97 = 23.2 \text{ m/sec.}$$

[346

2. Cavitation number

$$\kappa = \frac{\rho_0 + \gamma h - p_d}{\frac{\rho v_p^2}{2}} = 0.39.$$

3. General diagrams of the running curves of cavitating propellers are used to determine the optimal elements of the propellers. By way of illustration for this example, Fig. 199 shows such a diagram for several cavitating propellers with a disk ratio of $A/A_d = 0.80$ and number of blades $z = 3$. The diagram shows for propellers with different pitch ratios varying within the limits $H/D = 1.0--2.2$ the relations $K_I(\lambda_p)$ and $\eta_p^{\max}(\lambda_p)$ in various cavitation modes.

As applicable to the given conditions it is possible to establish on the basis of the diagram in Fig. 199 that a propeller with a pitch ratio of $H/D = 1.4$ is close to optimal. The curves for this propeller in a uniform flow are shown in Fig. 200 (solid lines).

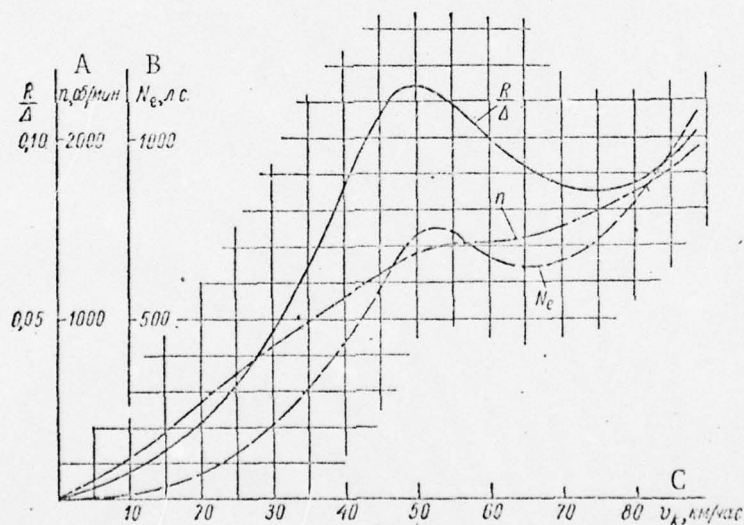


Fig. 198. Relations $R(v_k)$, $N_e(v_k)$, and $n(v_k)$ of a hydrofoil craft.

KEY: A-- n , rev/min; B-- N_e , HP; C-- v_k , km/hr.

4. Scaling the running curves from axial to oblique flow when $\phi = 14^\circ$ using formulas (V.36) and (V.37) is shown in Table 9.

Similar calculations are performed for several values of λ_p .

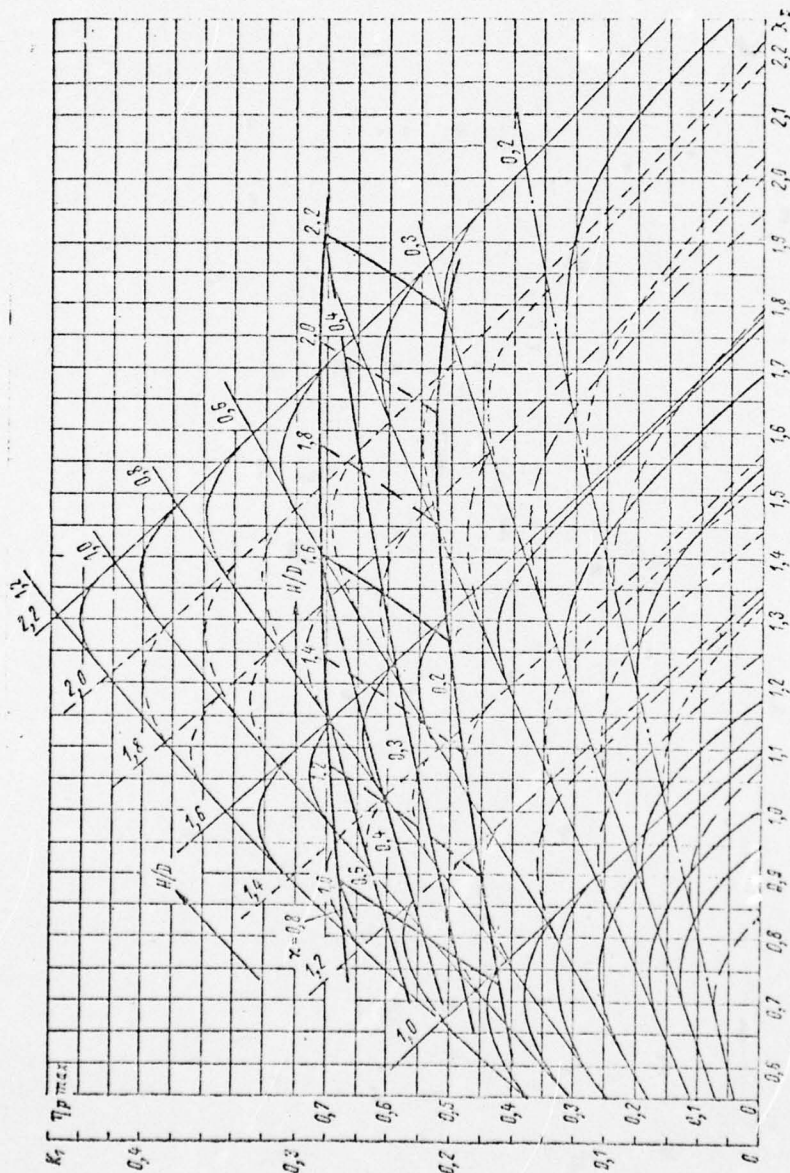


Fig. 199. Diagram of characteristics of cavitating propellers: K_T and η_p max as a function of λ_p and x .
 $z = 3$; $A/A_d = 0.8$; $d/D = 0.165$.

TABLE 9

Initial data: Running curves of propeller in axial flow (Fig. 200). Propeller elements: $A/A_d = 0.80$; $H/D = 1.4$; $s = 3$; $\phi = 14^\circ$; $\lambda_p = 1.15$; $K1\phi$, $K2\phi$, and Kq are determined by numerical integration using formulas (V.36), (V.37), and (V.70)

ϕ	270	300	330	0	30	60	90
λ_p (no pnc. 187) A	1.475	1.385	1.235	1.150	1.04	0.970	0.94
$K_1 (z = 0.3; \lambda_p^*)$	0.015	0.040	0.092	0.100	0.100	0.0900	0.085
$K_1 (z = 0.4; \lambda_p^*)$	0.035	0.062	0.122	0.138	0.132	0.122	0.115
$K_1 (z = 0.6; \lambda_p^*)$	0.055	0.077	0.141	0.183	0.185	0.172	0.165
$K_2 (z = 0.3; \lambda_p^*)$	0.0155	0.0215	0.0325	0.0328	0.0300	0.0280	0.0265
$K_2 (z = 0.4; \lambda_p^*)$	0.0240	0.0272	0.0372	0.0395	0.0368	0.0340	0.0325
$K_2 (z = 0.6; \lambda_p^*)$	0.0248	0.0287	0.0407	0.0477	0.0485	0.0455	0.0438
$\left(\frac{\lambda_p}{\lambda_p^*}\right)^2$	0.640	0.690	0.865	1.000	1.220	1.410	1.500
$K_1 (0.3; \lambda_p^*) \left(\frac{\lambda_p}{\lambda_p^*}\right)^2$	0.0096	0.0276	0.0796	0.100	0.122	0.127	0.1275
$K_1 (0.4; \lambda_p^*) \left(\frac{\lambda_p}{\lambda_p^*}\right)^2$	0.0224	0.0428	0.1055	0.138	0.161	0.172	0.1725
$K_1 (0.6; \lambda_p^*) \left(\frac{\lambda_p}{\lambda_p^*}\right)^2$	0.0352	0.0531	0.122	0.183	0.226	0.242	0.248

TABLE 9 (Cont)

$K_2(0.3; \lambda_p^*) \left(\frac{\lambda_p^*}{\lambda_p} \right)^2$	0.0099	0.0148	0.0281	0.0323	0.0366	0.0395	0.0397
$K_2(0.4; \lambda_p^*) \left(\frac{\lambda_p^*}{\lambda_p} \right)^2$	0.0153	0.0188	0.0322	0.0395	0.449	0.048	0.0488
$K_2(0.6; \lambda_p^*) \left(\frac{\lambda_p^*}{\lambda_p} \right)^2$	0.0159	0.0198	0.0352	0.0477	0.0592	0.0642	0.0657
$\sin \theta$	-1	-0.866	-0.5	0	0.5	0.866	1
$K_2(0.3; \lambda_p^*) \sin \theta \left(\frac{\lambda_p^*}{\lambda_p} \right)^2$	-0.0099	-0.0128	-0.0140	0	0.0183	0.0342	0.0397
$K_2(0.4; \lambda_p^*) \sin \theta \left(\frac{\lambda_p^*}{\lambda_p} \right)^2$	-0.0153	-0.0163	-0.0161	0	0.0224	0.0416	0.0488
$K_2(0.6; \lambda_p^*) \sin \theta \left(\frac{\lambda_p^*}{\lambda_p} \right)^2$	-0.0159	-0.0172	-0.0176	0	0.0296	0.0556	0.0657
$K_{1p}(z) = \frac{1}{12} [2 \sum_{K_1} - (y^{270} + y^{90})];$	$K_{1p}(0.3) = 0.0875; K_{1p}(0.4) = 0.119; K_{1p}(0.6) = 0.161;$						
$K_{2p}(z) = \frac{1}{12} [2 \sum_{K_2} - (y^{270} + y^{90})];$	$K_{2p}(0.3) = 0.0294; K_{2p}(0.4) = 0.0359; K_{2p}(0.6) = 0.0445;$						
$K_c(z) = \frac{1}{12} [2 \sum_{K_3} - (y^{270} + y^{90})];$	$K_c(0.3) = 0.0068; K_c(0.4) = 0.0081; K_c(0.6) = 0.0125.$						

KEY: A--(from Fig. 187).

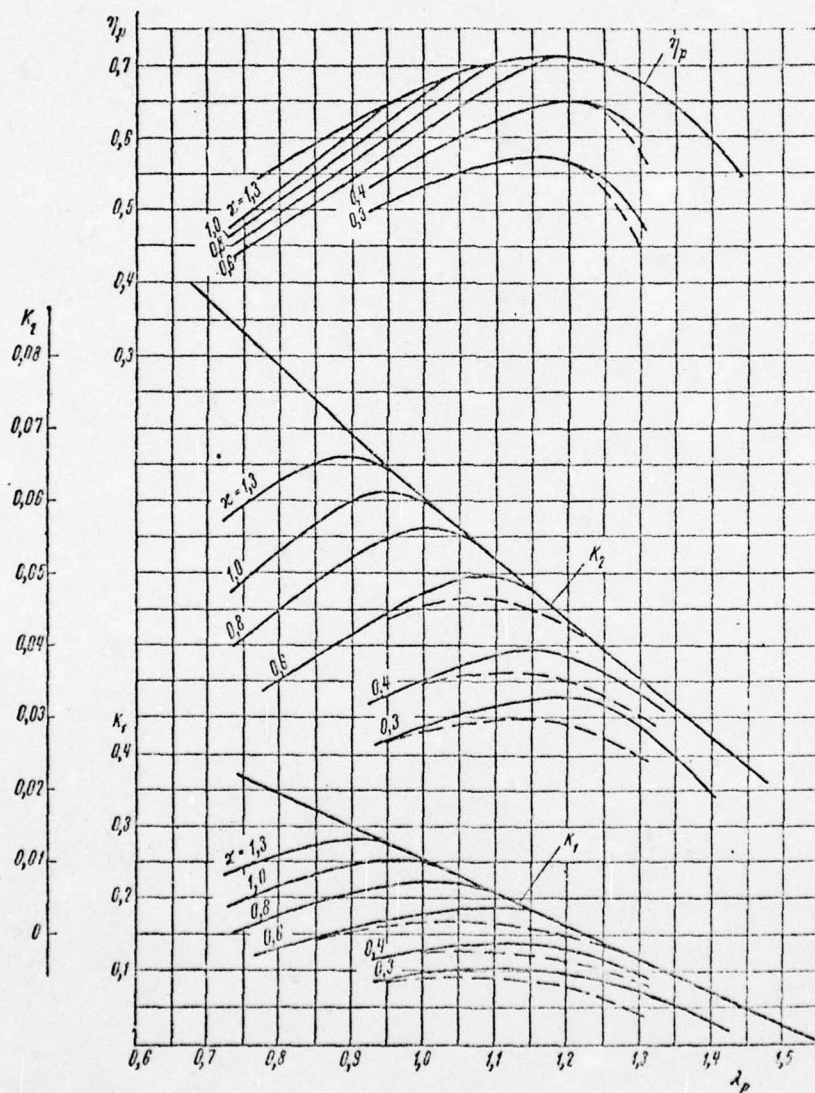


Fig. 200. Running curves of propeller on a hydrofoil craft.

TABLE 10

Calculations of Way-Making Ability of a Hydrofoil Craft

$v_k, \text{ km/hr}$ A	86,5	70,0	60,0	50,0	40,0	20,0
$v_p = 0,278 v_k \cos \varphi$	23,2	18,9	16,2	13,5	10,8	5,4
$\alpha = 210 : v_p^2$	0,39	0,59	0,80	1,15	1,80	7,20
$k = \frac{\Delta}{R}$ (no pnc. 198) B	10,3	11,5	10,0	8,7	11,6	45,5
$q = \frac{K_q}{K_1}$	0,070	0,068	0,069	0,071	0,070	0,065
R^* [no formula (V.79)] C	1880	1690	1930	2220	1680	440
$P_\varphi = R^* \left(\frac{1}{\cos \varphi} + q \lg \varphi \right)$	1970	1770	2020	2320	1760	460
$K_d = D v_p \sqrt{\frac{\rho}{p_\varphi}}$	3,43	2,95	2,36	1,84	1,70	1,65
λ_p (no pnc. 200) D	1,150	1,155	1,050	0,900	0,900	0,900
η_p (no pnc. 200) D	0,635	0,700	0,670	0,590	0,610	0,610
$\eta = 0,98 \eta_p \left[1 + \frac{1}{k} q + \right.$ $\left. + \lg \varphi \right] - q \lg \varphi \times$ $\times \left(1 + \frac{\lg \varphi}{k} \right)$	0,63	0,690	0,660	0,580	0,600	0,600
$n = \frac{v_p}{D \lambda_p}$ (no об/мин) E	1860	1510	1420	1320	1100	555
$N_e = \frac{\Delta 0,278 v_k}{75 k \eta}$ л. с. F	985	655	675	735	425	54

KEY: A-- v_k , km/hr; B--(from Fig. 198); C--[according to formula (V.79)]; D--(from Fig. 200); E--rev/min; F--HP.

5. Table 9 also shows calculations of the coefficient of transverse force K_q made with formula (V.70). When $\lambda_p = 1.15$ [348]

$$q = \frac{K_q}{K_1} = 0,07.$$

6. Considering that $v_k = 86.5$ km/hr and $k = \Delta/R = 10.3$, we find from formula (V.79) the drag of the launch

$$R^* = \frac{kR}{k + \lg \varphi + \frac{q}{1 - q \lg \varphi}} = 1880 \text{ kgf.}$$

7. The thrust which the propeller must develop at a given speed is determined from formula (V.74)

$$P_\varphi = R^* \left(q \lg \varphi + \frac{1}{\cos \varphi} \right) = 1970 \text{ kgf.}$$

8. Further the auxiliary coefficient is determined to be

$$K_d = Dv_p \sqrt{\frac{\rho}{P_\Phi}} = 3.43.$$

9. Entering the function $K_1 = \lambda_p^2 / K_d^2$ on the propeller running curves in Fig. 200, we determine its calculated mode of operation

$$\lambda_p = 1.15, \eta_p = 0.635.$$

10. Taking shaft efficiency to be $\eta_M = 0.98$, we use formula (V.83) to calculate the propulsive coefficient of the launch under consideration

$$\eta = 0.98\eta_p \left[1 + \frac{q + \lg q}{k} - q \lg q \left(1 + \frac{\lg q}{k} \right) \right] = 0.63.$$

11. We determine the revolutions of the propeller to be

$$n = \frac{v_p}{Dk_p} 60 = 1800 \text{ rev/min.}$$

12. The required power is

$$N_e = \frac{0.278 \Delta v_k}{75k\eta} = 985 \text{ HP.}$$

* * *

Similar calculations for other values of speed of movement are shown in Table 10.

The results of calculations of the way-making ability of a hydrofoil launch are shown in Fig. 198 in the form of a relation between the required power and the number of revolutions on one hand and speed of movement on the other, $N_e(v_k)$ and $n(v_k)$.

References

[352

1. Donovan, A. F. and Lawrence, G. R. Aerodinamika chastey samoleta pri bol'shikh skorostyakh (Aerodynamics of parts of an airplane at high speeds). Moscow, IL, 1959.
2. Pozdnyunin, V. L. Supercavitating propellers. Izvestiya AN SSSR, ONT, 1944, Nos. 1--2.
3. Tachmingji, A. I. and Morgan, W. V. The design and estimated performance of a series of supercavitating propellers. Symposium on Naval Hydrodynamics, 2d., Washington, 1958.
4. Polyakhov, N. N. Vertex theory of a propeller from the standpoint of array theory. Trudy LPI im. M. I. Kalinin. 1953, No. 3.

5. Pappel', E. E. Prakticheskiy raschet grebnogo vinta (Practical calculations of a propeller). NIVK, 1936.
6. Yegorov, I. T. and Sadovnikov, Yu. M. Effect of nonstationarity on the hydrodynamic characteristics of semi-immersed propellers. "Sudostroyeniye," 1961, No. 1.
7. Basin, A. M., and Miniovich, I. Ya. Teoriya i raschet grebnogo vinta (Theory and calculations of a propeller). Leningrad, Sudpromgiz, 1963.
8. Sadovnikov, Yu. M. Several distinguishing aspects in calculating the way-making ability of hydrofoil craft. "Sudostroyeniye," 1962, No. 11.